https://ntrs.nasa.gov/search.jsp?R=19870002268 2020-03-20T14:01:51+00:00Z

GRANT /LEWIS

IN-02-37561

RF Project 712620/762009
Interim Technical Report

AN EXPERIMENTAL STUDY OF THE AERODYNAMICS OF A NACA 0012 AIRFOIL WITH A SIMULATED GLAZE ICE ACCRETION

Michael B. Bragg
Department of Aero and Astro Engineering

(NASA-CR-179897) AN EXPERIMENTAL STUDY OF THE AERODYNAMICS OF A NACA 0012 AIRFOIL WITH A SIMULATED GLAZE ICE ACCRETION Interim Technical Report (Ohio State Univ.) 318 p CSCL 01A G3/02 N87-11701 Unclas 44889

NASA-LEWIS RESEARCH CENTER
21000 Brookpark Road
Cleveland, Ohio 44135

Grant No. NAG 3-28

November 1986

The Ohio State University Research Foundation
1314 Kinnear Road
Columbus, Ohio 43212

AN EXPERIMENTAL STUDY OF THE AERODYNAMICS OF A NACA 0012 AIRFOIL WITH A SIMULATED GLAZE ICE ACCRETION

M. B. Bragg

The Ohio State University

Columbus, Ohio

AARL TR 8602

ABSTRACT

An experimental study has been conducted in the Ohio State University subsonic wind tunnel to measure the detailed aerodynamic characteristics of an airfoil with a simulated glaze ice accretion. A NACA 0012 model with interchangeable leading edges and pressure taps every one percent chord was used. Surface pressure and wake data were taken on the airfoil clean, with forced transition and with a simulated glaze ice shape. Lift and drag penalties due to the ice shape were found and the surface pressure clearly showed that large separation bubbles were present. Both total pressure and split-film probes were used to measure velocity profiles, both for the clean model and for the model with a simulated ice accretion. A large region of flow separation was seen in the velocity profiles and was correlated to the pressure measurements. Clean airfoil data were found to compare well to existing airfoil analysis methods.

PRECEDING PAGE BLANK NOT FILMED

TABLE OF CONTENTS

PRECEDING PAGE BLANK NOT FILMED

NOMENCLATURE

Symbol	Description
c	Airfoil chord length
C_d	Airfoil drag coefficient, Drag/$q_\infty c$
C_l	Airfoil lift coefficient, Lift/$q_\infty c$
C_m	Airfoil moment coefficient about $x=c/4$, Moment/$q_\infty c^2$
C_p	Pressure coefficient, $P-P_\infty/q_\infty$
$\bar{d}$	Volume median diameter
E_1, E_2	Hot film output voltage
k	E_1/E_2
LWC	Liquid water content
m	Mach number
P	Pressure
q	Dynamic pressure
R_e	Reynolds number
u,v	Streamwise and normal velocity components
V_{tot}	Total velocity measured by hot film probe
x,y	chordwise and normal coordinate, or y can be the boundary layer coordinate
Y-SEP	Y location of separation streamline
Y-STAG	Y location of u component stagnation streamline
α	Angle of attack
δ^*	Boundary layer displacement thickness
Θ	Boundary layer momentum thickness

Subscripts

l	lower surface
u	upper surface
∞	freestream condition

PRECEDING PAGE BLANK NOT FILMED

I. INTRODUCTION

Ice formation on an airfoil often leads to a sizeable leading edge protuberance. This protuberance causes a leading edge separation bubble to form, thus reducing the lift and increasing the drag. As the angle of attack is increased, the bubble will eventually fail to re-attach causing a reduction in airfoil stall angle and maximum lift. For unprotected airfoils, these aerodynamic penalties are important and further research is needed before they can be accurately predicted.

Airfoil aerodynamic penalties have been investigated by other researchers, primarily by making lift and drag measurements. Jacobs [1] in 1932 measured the lift, drag and moment change due to various protuberances on a NACA 0012 airfoil. While these protuberances were not specifically ice simulations, the data show the sensitivity of the airfoil to any leading edge disturbance. In the 1950's the NACA investigated the effects of ice on airfoil performance. Some of these results can be found in the work of Gray [2,3], on the NACA 65-212 and NACA 65A004 airfoil with actual ice accretions. These data show the adverse effects of ice on airfoil performance, but report only the integrated lift, drag and moment data. More recent studies such as that by Korkan, et. al. [4], Lee [5] and Flemming [6] have also reported lift, drag and moment effects on airfoils with simulated ice shapes.

In an attempt to obtain more detailed flowfield data, Bragg et.al. [7,8] have obtained surface pressures on airfoils with simulated rime and glaze ice shapes. These data give not only the integrated lift, drag and moment data, but provide information on the length of the bubble, re-attachment and trailing edge separation. Flow visualization data reported by Bragg [9], give the first information about the glaze ice separation bubble geometry. Approximate bubble shapes reduced from photographs of oil flow on a splitter plate are presented for two different glaze ice shapes at two angles of attack.

Recently sophisticated computational tools have begun to be applied to the problem of an airfoil with leading edge ice accretion. Potapczak [10] used a parabolized Navier-Stokes code to predict the aerodynamic characteristics of an airfoil with and without ice. Cebeci [11] has modified his interactive boundary layer technique to make similar calculations. The results of these calculations are encouraging, but more experimental data are needed to fully develop and validate these methods.

This report presents the initial results of a detailed experiment to study the effect of a particular glaze ice shape on a NACA 0012 airfoil. Part of this work has been published previously by Bragg and Coirier [12,13] in summary form. The purpose of this report is to present a single report with as much of the detailed data as possible. It should be noted that this work is continuing and more and better data are currently being acquired, and plans for more tests are being made. It was, however, felt that a report presenting the data gathered to date would be valuable at this time.

II. EXPERIMENTAL APPARATUS

Wind Tunnel and Model

These tests were conducted in the Ohio State University's subsonic wind tunnel located at the Aeronautical and Astronautical Research Laboratory. The tunnel is of conventional design with approximately a three-by-five foot test section, eight feet in length. The tunnel operates at speeds from zero to 220 feet per second at Reynolds number of up to 1.3×10^6 per foot. The tunnel is of open return type and uses four turbulence screens and honeycomb in the settling chamber to reduce the tunnel turbulence. The tunnel will accommodate airfoils mounted vertically in the test section or three-dimensional models, strut mounted using an internal strain gauge balance. Tunnel speed, Reynolds number and Mach number are measured through facility transducers.

Standard wind tunnel instrumentation was used for this test. Pressure measurements were made using a Scanivalve system. Two scanivalves capable of measuring 48 pressures each were used. The valves were connected in series sharing one pressure transducer to reduce calibration time and improve the accuracy of the measurements. No cut-off valves were used for this test. A single traversing total pressure probe was used to measure the airfoil wake. The probe was located approximately one chord length downstream of the model trailing edge and was traversed automatically by the computer system.

Two different NACA 0012 models were used for this test. Both models were 21 inches in chord and had a span of 39 inches. The models were mounted vertically in the tunnel providing a height (actually width since the model was mounted vertically) to chord ratio of 2.62. Simulated ice shapes were used with both models which were constructed to approximately duplicate an actual measured ice accretion. The ice was accreted in the NASA Lewis Research Center's Icing Research Tunnel on a NACA 0012 airfoil, also of 21 inch chord [14]. In Figure 1. the measured ice shape, as recorded from an actual tracing, compared to the one used in this test.

Data were first taken on NACA 0012 Model No. 1 while construction was continuing on the more complex model. This model was made from a section of a UH1H helicopter rotor blade. Since the model had twist, all data were taken and the angle of attack was reported on the model center line. The model used external one-eighth inch tubing to provide surface pressure information (pressure belts) and the wooden ice shape was internally tapped. Although pressure data and wake data were acquired on this model, see reference 12, it is considered preliminary and will not be presented here. Split film measurements of the separation bubble were taken using this model and will be presented. NACA 0012 airfoil coordinates clean (i.e. no ice shape attached) are given in Table 1. The coordinates of the airfoil plus ice shape for Model No. 1 are given in Table 2.

NACA Model No. 2 was built for this experiment with some special features. The model has a 21-inch chord and was cut from mahogany using a numerical control machine and laminated together to form the 39-inch span. A unique feature of this model is its interchangeable leading edges. Past experiences using simulated ice on airfoils has identified a problem with the proper placement of the ice shape over the clean leading edge. To avoid this problem, the current model has the ice shape as an integrable part of the first 15 percent of the model (about 3 inches). In this way, the first 15 percent of the model could be attached precisely to the main model section, and the exact airfoil plus ice shape geometry would be accurately known. Experience with earlier simulated models demonstrated the need for a very dense placement of surface pressure taps. The current model was internally tapped with approximately 90 surface pressure ports. The upper surface was instrumented with a tap every one percent (0.21 inches) surface length back to the forty percent chord station. Another 40 taps were located around the rest of the airfoil, on the model centerline. Eight taps were located spanwise at the five percent station to ensure the two-dimensionality of the flow. The entire ice shape was also instrumented with internal pressure taps every one percent surface length resulting in 19 taps ahead of the five percent chord station.

The basic airfoil coordinates for Model No. 2 are the same as those in Table 1. The ice shape is also basically the same, although due to the construction technique some slight differences do exist from the ice shape of Model No. 1. Therefore, the ice shape plus airfoil coordinates for Model No. 2 can be found in Table 3. All the force and surface pressure data shown in this report will be from Model No. 2.

Velocity Profile Measurements

In order to measure the velocity profiles in the separation bubble, a probe capable of determining flow reversal must be accurately positioned in the model boundary layer. A split film probe, TSI model 1288, was chosen. Here two separate films are placed, front and back, on the same 0.006 inch diameter rod. The plane of the split is parallel to the axis of the probe, perpendicular to the freestream flow, thus allowing for the determination of flow reversal. The probe was modified by incorporating a special shield [10]. The shield was set so that it touched the model before the probe, allowing probe protection and setting the probe a known distance off the surface of the model to start each run. This system worked well and prevented damaging the very delicate probe. The hot film data channels were both taken using TSI 1053B anemometers with TSI 1057 signal conditioners.

The entire tunnel set-up is shown in Figure 2. A close-up of the traverse system is shown in Figure 3. A two-dimensional traversing system was used to position the probe in the horizontal plane, containing the airfoil section on the tunnel centerline. The bottom traverse positioned the probe axially from a position approximately 15 percent chord ahead of the model to a point at the airfoil 65 percent chord station. A L.C. Smith BBR30180 traverse was placed on this traverse and provided the probe positioning out from the model. The hot-film probe was supported through a TSI probe support and shield which slid through an airfoil shaped strut extending into the tunnel. This steel strut was rigidly mounted to the fixed end of the top traverse and moved chordwise (along the tunnel axis) through a sealed slide arrangement.Both traverses were driven by d.c. motors and may be either positioned locally or through the computer system. Probe position was determined using standard potentiometers. Using this system probe positioning tolerance including all errors through digitizing, was no more than +0.003 inches or +0.00014 chord-lengths out from the model and no more than +0.010 inches or +0.00048 chord-lengths in the chordwise direction.

On the airfoil without ice, boundary layer profiles were measured using a traversed total pressure probe. The traversing system, and therefore positioning tolerances, were the same as that used for the split film measurements. The probe was constructed of 1/32-inch stainless steel tubing compressed at the tip to reduce its height to approximately 0.020 inches. The probe was positioned on the surface by hand, then traversed out from the wall by the computer controlled traversing system.

Data Acquisition and Reduction

The data were gathered online by the in-house Digital Computer and Data Acquisition System. The system currently based on a Harris H100 computer, a 48-bit machine expandable to 768 K bytes internal memory, with virtual memory address space to 12 M bytes. Two analog-to-digital (A/D) systems were used to acquire these data. A high speed Datel model 256 system with a throughput rate exceeding 100 kHz was used to acquire the hot film data. A medium speed RTP system with 8 kHz throughput was used to sample tunnel conditions and probe position. The system was operated through a CRT terminal with disk and tape data storage, as well as printed and plotted data hardcopy, all were available through the laboratory's computer facility.

III. DATA REDUCTION

Pressure Data

The pressure data, both model surface pressures and wake data were reduced in the usual way. Models pressures were converted into pressure coefficients using the expression

$$C_p = \frac{P - P_\infty}{1/2\rho_\infty U^2} \tag{1}$$

Here all pressure differences were measured directly from the Scanivalve. The pressure coefficients were then integrated to obtain the lift and moment coefficients. It should be noted that since no cut-off valves were used, as much as 90 seconds could elapse between the time the first and last surface pressures were measured. Therefore, the tunnel dynamic pressure was sampled simultaneously with each surface pressure to provide the correct dynamic pressure to be used in eq. (1).

Airfoil drag was obtained from the total pressure survey made in the airfoil wake. Since the survey was made one chord-length downstream of the model, the static pressure was assumed to be just the free stream value. The airfoil drag was then found from the following expression

$$C_d = 2\int\sqrt{\frac{P_{tw} - P_\infty}{q_\infty}}\left(1 - \sqrt{\frac{P_{tw} - P_\infty}{q_\infty}}\right)d\left(\frac{y}{c}\right) \tag{2}$$

In the implementation of this equation allowances were made for any tunnel speed variation which occurred during the traverse. The variation in tunnel speed across the tunnel due to model and wake blockage at high angles of attack was also incorporated.

The lift, drag and moment coefficients, as well as the model angle of attack, have been corrected for tunnel wall interference. These corrections used the procedures outlined by Rae and Pope [15]. The coefficients and angle of attack were corrected for solid blockage, streamline curvature and wake blockage; due to the test section design, no buoyancy corrections were made. The primary effect of these corrections was a reduction in the airfoil lift curve slope on the order of ten percent. Both the corrected and uncorrected values are given in the data tables. No attempt has been made in this report to correct the measured surface pressure distributions.

Velocity profiles were obtained from the boundary layer total pressure probe by assuming a constant static pressure across the boundary layer. Using a surface static pressure tap at the same chordwise location as the boundary layer total probe, the dynamic pressure as each location in the boundary layer was measured. For incompressible flow this was easily converted into a boundary layer velocity using the Bernouilli equation. Probe wall proximity and probe Reynolds number correction were found to be small, therefore, all total pressure probe boundary layer velocity profiles are reported uncorrected.

Split Film Data

The split film probe data reduction utilized calibration data of voltage versus velocity for a range of 0-300 ft/sec and several flow angles. The total velocity sensed by the probe was determined from

$$V_{tot} = f[(E_1 + E_2)^2] \tag{3}$$

Here E_1 and E_2 are the voltages from the front and back of the film, respectively, both corrected for ambient temperature effects. The function f is a fourth order polynomial. The streamwise velocity component, u, and the perpendicular component, v, could be determined knowing the flow angle, Θ . Where Θ is 90 degrees in the free stream. Using the expression for sin Θ given in reference 16,

$$\sin\Theta = \left[\frac{E_1^{\ 2} - k^2 E_2^{\ 2}}{(E_1^{\ 2} - k^2 E_2^{\ 2})_{max}} \right]^{h(V_{tot})} \tag{4}$$

The constant k is the ratio of E_1, to E_2 at Θ = 0 degrees and is a function of velocity. The denominator is the value of $E_1^{\ 2} - k^2 E_2^{\ 2}$ at Θ = +90 degrees depending on the sign of the numerator.

The term $h(V_{tot})$ was assumed to be one, independent of velocity. This was curve fit based on the calibration data as a polynomial in V. Then u and v are

$$v = V_{tot} \sin\Theta, \qquad u = \sqrt{V_{tot}^{2} - v^{2}} \tag{5}$$

with u greater than zero if $E_1^{2} - k^{2}E_2^{2}$ is greater than zero. Note that with a two element split film probe the flow angle can at best be determined only in the range $-90^{o} \leq \Theta \leq 90^{o}$. Therefore, the sign of the v component cannot be determined. When using many samples to determine a time averaged velocity, only the average u component can be calculated. The average v component and average total velocity are unknown. Therefore all velocity data presented here are the average streamwise component, u. RMS values were calculated but are not discussed, since no attempt was made to document the split film frequency response. Note that each split film velocity value presented in this report is really an average of 2048 data samples. These data were taken at a rate of 5 KHz using a 10 KHz low pass filter.

IV. RESULTS AND DISCUSSION

In this section some of the more important results obtained from these tests are summarized. All of the data, except the split film measurements, were obtained on the NACA 0012 Model No. 2. A more complete set of data is presented in the appendices.

Pressure and Force Measurements

Initial tests were conducted on the NACA 0012 Model No. 2 without the ice shape. This is usually referred to as the clean configuration. Due to the slight seam in the model at the 15 percent chord location where the leading edge section meets the main model body, there was some question regarding its affect on the boundary layer transition location. To remove this question, and for ease in comparing these measurements to the computational results, tests were run with the boundary layer tripped at the five percent chord location on the upper and lower surface. The trip strip used was carborundum grit, nominally 0.009 inches in diameter, attached to the model using double-sided tape. The trip was approximately 0.25 inches in the chordwise direction with the back edge at the 0.05, x/c location. Only results from measurements at positive angles of attack are shown for the clean airfoil, with or without trip. Negative angles to stall were tested, but were similar to those at positive angles of attack. All data presented here have been corrected for tunnel wall effects by applying the correction method of Rae and Pope [15].

In Figure 4, the lift as a function of angle of attack for the clean model is shown. Presented are the data for a Reynolds number of 1.5×10^6 and Mach number of 0.12. Also shown are the theoretical predictions from the airfoil analysis codes of Eppler [17] and Smetana [18]. The lift curve slope compares well to the results of Smetana since this code iterates on the displacements thickness to include the decambering of the airfoil due to boundary layer growth.

Eppler merely assumes a lift curve slope of 2Π per radian and this overpredicts these data. The Eppler code does contain a simple $C_{l,max}$ prediction which predicts a maximum lift of approximately 1.12 at 1.5×10^6 Reynolds number. Using the plot of reference 15, a $C_{l,max}$ of 1.22 occurs at an effective Reynolds number of approximately 2×10^6. Tests were also run at 0.9 and 2.0×10^6 in Reynolds number with little affect on the lift.

The drag performance of this airfoil was measured and presented in Figure 5. Here the experiment as well as the theories of references [17] and [18] are shown with natural transition and fixed transition. Both theories show more of a drag bucket than is reflected in the experiment, although some bucket is also seen in the data. At zero degrees angle of attack the experimental data have a drag coefficient of 0.0075 with 0.0070 and 0.0067 predicted by [17] and [18], respectively. This is probably due to some early transition on the wind tunnel model since the data with the boundary layer tripped compare very well to theory. With transition fixed at the 5 percent station, the measured drag rises to 0.0106 with the theories only 2 or 3 drag counts higher. The comparison remains excellent until the theories fail to predict the large drag rise associated with separation at high angle of attack. Experimental and theoretical results were also obtained at 0.9 and 2.0×10^6 in Reynolds number. The drag increased with decreasing Reynolds number as expected.

The measured and predicted pitching moment about the quarter chord location is shown in Figure 6. For the natural transition case, the experimental data show a slightly positive C_m which becomes larger with increasing angle of attack due to the boundary layer growth. The theory due to Smetana reflects this trend but underpredicts its magnitude. Near stall, Smetana's C_m prediction is poor as would be expected. Eppler predicts the C_m trend near stall, but since it includes no boundary layer effects, it does poorly at low angle of attack. Fixed transition had little affect on the C_m in the experimental or theoretical data. Changing the Reynolds number from 0.9 to 2.0 x 10^6 also had little affect on C_m.

In Figure 7, the measured pressures are compared to those predicted by the Smetana code. Comparisons were made at matched lift coefficient since the pressure coefficient data has not been corrected for the tunnel wall interference. The experimental data are for uncorrected angles of attack of 2 and 6 degrees. The comparisons are excellent with only some small deviation near the 15 percent chord location. This is probably due to the slight discontinuity where the model leading edge joins the main element. Note that with the very dense distribution of measured pressures near the leading edge, every symbol represents a measured pressure, the peak pressure was obtained in good agreement to the theory. Changes in C_p with Reynolds number and with the boundary layer trip were small as expected.

After completing the clean NACA 0012 Model No. 2 tests just described the ice shape shown in Figure 1 was installed. The ice shape was tested with no transition strip and with no distributed roughness. Since the airfoil was symmetric, the clean NACA 0012 performed the same at positive and negative angles of attack. However, with the ice shape, the airfoil was no longer symmetric and this was reflected in its aerodynamic characteristics. The ice shape was then tested to $C_{l,max}$ for both positive and negative angles of attack. For ease in data presentation, the negative angles of attack are plotted as positive in Figures 8 and 9 and labelled, "Ice - Lower Horn". In this way, the data are presented as if the ice shape was removed and then inverted, upper and lower surfaces, for these tests. Five pressure taps were located, equally spaced spanwise, on both the upper and lower surfaces at an x/c of 0.05. These taps were compared to ensure the two-dimensionality of the flow, particularly when large separation zones were present. These taps compared well across the span and indicated that the flow was indeed two-dimensional at all conditions examined.

In Figure 8, the lift coefficient as a function of angle of attack for the NACA 0012 clean and with the glaze ice shape is shown. A large $C_{l,max}$ penalty is seen for the airfoil with glaze ice due to either the upper or lower surface horn. The maximum lift decreased from the clean value of over 1.2, to the iced value of about 0.55, over a 50 percent decrease. The angle of attack for stall was also reduced about 50 percent. It is interesting that while the upper and lower surface horns were quite different in shape and location, their affect on the airfoil lift was remarkably similar. Stall for the airfoil with ice shape was due to the failure of the leading edge separation bubble to re-attach at the higher angles of attack. This will be seen more clearly when the pressure distributions are examined. These data were also duplicated at Reynolds numbers of 0.9 and 2.0×10^6 with little affect on the lift.

The effect of the ice accretion on drag is shown in Figure 9. As expected, the drag increase due to the ice was significant, from 0.0075 at $\alpha = 0$ degrees clean to 0.0260 with the glaze ice shape. The drag rose quickly with angle of attack for the glaze shape since it stalled at only seven degrees angle of attack. The drag rise corresponding to the lower surface horn (negative angles of attack) was slightly larger than that from the upper surface horn (positive angles of attack), although the trend was very similar. While this ice shape did not correspond directly to any of those measured by Olsen [17], it was quite similar to one of the shapes reported there and the drag values reported by Olsen compare well to those in Figure 9. Again, these data were repeated at .9 and 2.0×10^6 Reynolds number and no significant effects were noted.

Figure 10 shows the pitching moment coefficient measured on the clean and iced airfoil. The ice shape cambers the airfoil which can be seen by noting the pitching moment at zero degrees angle of attack. The upper horn ice shape data indicate a positive cambering since the C_m here is less than zero. As the angle of attack was increased, the separation bubble on the upper surface grew, thickening the boundary layer and decambering the airfoil causing a positive increase in the moment coefficient. This continued until the airfoil started to stall and the moment becomes a large negative, nose down, value. The affect of the ice shape on the pitching moment, even at the low angles of attack, may be significant in rotorcraft applications. No significant Reynolds number effects were seen on the measured pitching moment coefficient.

Pressure distributions for the airfoil with simulated ice are shown in the next four figures. These pressure distributions have not been corrected for wind tunnel wall effects. As seen in Figure 7, these corrections are not necessary. Therefore, the C_p's here are uncorrected and the angle of attack and lift coefficient indicated on the figures for each distribution are also uncorrected values.

In Figure 11, the pressure distributions for the NACA 0012 clean and with simulated ice are shown at an angle of attack of four degrees. Note first the zone of almost constant pressure occurring on the iced pressure distribution at a C_p level of approximately -1.4 . This is the separation bubble aft of the upper surface horn. The flow accelerated from the stagnation point as it moved toward the upper surface horn and separated as it attempts to flow over the tip of the ice horn. The separation zone was characterized by fairly constant but slightly falling pressure (C_p was decreasing as the flow accelerated) for approximately ten percent chord; then the pressure rose rapidly and ultimately returned to the clean value at about the 40 percent chord station. Hot-film measurements indicated re-attachment somewhat downstream of the minimum pressure point. At a C_p of approximately -0.4 a constant pressure region corresponding to the lower surface bubble was seen. This also occurred at a much lower pressure than the clean airfoil experienced at this same location since the flow accelerated rapidly toward the lower surface horn before separation occurred. The uncorrected lift coefficient at four degrees angle of attack dropped from 0.439 clean to 0.376 iced, due to the separation.

The measured pressure distributions for the airfoil with simulated glaze ice are shown for various angles of attack in Figures 12 and 13. In Figure 12, pressures for 0, 2 and 4 degrees angle of attack are shown. The circles represent the zero angle of attack measured pressures. Here the lower and upper surface separation zones were at C_p's of approximately -0.9 and -0.7, respectively. As the angle of attack was increased, these constant pressure zones occurred at decreasing pressures for the upper surface separation and increasing pressures for the lower. Note also that at $\alpha = 0$ degrees the upper surface separation occurred at a higher pressure than the lower surface separation. At 2 and 4 degrees, this was reversed with the upper surface separation zone occurring at a lower pressure level.

In Figure 13, the pressure distributions for angles of attack of 4, 6 and 8 degrees are shown. Here, as the airfoil begins to approach stall, the upper surface separation bubble grew rapidly in length and the constant pressure zone occurred at higher pressures. Remember that the airfoil stalled at approximately seven degrees angle of attack. As the angle of attack increased the trailing edge pressure is seen to fall, as do the pressures on the entire aft portion of the airfoil. At eight degrees angle of attack, the airfoil has stalled and the scatter in the leading edge, upper surface measured pressures was an indication of the unsteadiness of the flow in this region.

A comparison of the 4 and -4 degree pressure distributions are shown in Figure 14 so that the relative affect of the two ice horns on the pressure distribution may be more easily compared. The suction side separation zone can be seen, as discussed earlier, to be slightly longer and to have a more gentle pressure recovery for the -4 degree case. Both suction and pressure side separation occurred at lower pressures for the positive 4 degree measurements. The constant pressure separation zones all started at the leading edge of the particular ice horn concerned. These plots show that the lower surface horn does, indeed, cause a more severe aerodynamic penalty at negative angles of attack than the upper surface horn does at positive angles. This is an interesting result since these negative angle of attack cases are not usually considered. This finding would be important for any surface which must operate at both positive and negative angles of attack, such as the horizontal stabilizer. It may also have application to airfoils which operate at lower angles of attack than that at which the ice is accreted.

Velocity Profile Measurements

Velocity profile data were taken using a total pressure probe on the NACA 0012 Model No. 2 and a split film probe using Model No. 1. The purpose of these data was to measure the detailed boundary layer and separation zone mean velocity profiles for comparison to the computational results.

Total pressure boundary layer surveys were taken on the model with the trip strip installed and at a Reynolds number of 1.5×10^6. The surveys were reduced in the standard way by assuming no pressure gradient through the boundary layer and, therefore, applying the measured surface static pressure through the boundary layer. Using the measured total pressure, the velocity profile in the boundary layer was determined. In Figure 15, a sample of the measured profiles are shown. The profiles shown are the measured velocity divided by the local edge velocity. The vertical lines are 1.25 U/U_e apart. The y/c location, measured above the surface, of 0.02 is shown which corresponds to 0.42 inches. Profiles at several chordwise locations are shown at an angle of attack of four degrees in Figure 15. Since the boundary layer was tripped at x/c = .05, all of the measured profiles are turbulent. The boundary layer displacement thickness, δ^*/c, calculated from the measured profiles versus x/c for both the $\alpha = 0$ and $\alpha = 4$ degree cases, are shown in Figure 16. Also shown are the predicted values from the Smetana analysis. Overall, the comparisons are quite good except at the 10 and 20 percent stations where the experiment showed a much larger displacement thickness. This was probably due to the trip strip initially increasing the displacement thickness more than would be due to transition alone. Further downstream of the trip the measurements and theory compared very well.

Whenever a separation zone is being probed, as with the split-film probe used in this test, the problem of probe interference must be considered. In Figure 17 a sketch of the NACA 0012 airfoil and the traversing system used for these experiments is shown. While the traversing mechanism itself was outside of the tunnel, a substantial probe support strut was required to properly position the probe. The entire traverse system consisted of the traversing mechanism (not shown), the strut, sleeve and the probe itself.

Surface pressures were measured on the airfoil with the probe at various locations to quantify the affect of the probe on the separation bubble. In Figure 18 the pressure distribution on the airfoil with simulated glaze ice is compared with and without the probe present. The probe and support system when located at the x/c = 0.03 location was seen to lower the pressure in the bubble. If pressure level can be used as a basis for flow re-attachment, the probe and support moved the point of bubble re-attachment forward. The lower surface and the aft part of the upper surface did not appear to be significantly affected by the presence of the probe. The position of the probe in the bubble was shown to be important, Figure 19. Here the probe and support were positioned at three different chordwise locations and the surface pressures recorded. The probe at x/c = 0.11 had the largest affect on bubble re-attachment which occurred around x/c = 0.20. Only the x/c = 0.19 position had little affect on the pressure level in the relatively constant pressure region of the bubble. Tests were also made by positioning the strut and sleeve but not placing the probe in the bubble. These tests showed that the strut and sleeve could be modified so as not to affect the separation zone pressures, however, once the probe was inserted into the bubble the pressures were always affected.

The interference studies showed that the presence of the probe affected the bubble in all cases tested. The primary results were a decreased plateau pressure in the bubble, and an increased pressure in the re-attachment region. The probe appeared to cause early bubble re-attachment, shortening the bubble by a few percent chord. Therefore, all the split-film data where the probe was in the separation bubble included this probe interference error for which no correction has been made.

In Figures 20 through 22, the velocity profiles are shown for the NACA 0012 Model No. 1, upper surface, in the vicinity of the glaze ice shape. All runs were made at a Reynolds number based on chord of 1.5×10^6 and a Mach number of 0.12. Note that the velocity shown was actually the streamwise component of the total boundary layer velocity and was nondimensionalized by the edge velocity. The edge velocity was defined as the maximum velocity measured for each profile. The vertical lines on the plot are the zero velocity reference line for each profile. So points to the left indicate negative velocity or reversed flow. These vertical lines are spaced a distance apart of 1.25 times the local edge velocity. The height scale nondimensionalized by the airfoil chord of 21 inches and is measured from the airfoil surface. All airfoil angles of attack are uncorrected.

The bubble shapes are also represented in Figures 20 through 22. The dashed lines are the stagnation streamline and are merely taken from the point above the surface where the measured streamwise velocity zero (i.e. the velocity changes from negative to positive). The solid lines are the dividing stream lines. These were found by integrating the mass flow in the streamwise direction. The point above the surface where the net mass flow is zero defines the dividing streamline.

The profiles for the -0.15 degree case are shown in Figure 20. If it is assumed that separation occurred at the leading edge of the upper surface horn, x/c = -.0225, then the first profile was only -.0025c downstream. Therefore a relatively large reversed flow region developed very quickly. The reversed flow region grew initially, then decreased until the bubble re-attached around an x/c of .08. The last profile is a fairly characteristic turbulent profile. From the streamline plot it is clear that the reversed flow region was relatively thick and slow moving. Conversely, the shear layer was thin and rapidly accelerated to the edge velocity.

Figure 21 is similar but for the the 1.85 degree angle of attack case. Here, as expected, the bubble was thicker and larger than the previous case. Re-attachment occurred around the 12 percent chord location. Note in the x/c = .14 profile a change in second derivative that occurred about one-fifth of the way up on the profile. This appears to be characteristic of all the re-attached profiles measured to date.

In Figure 22 the profiles are shown for a model angle of attack of 3.85°. Here the bubble was extremely large as shown. In Figure 22, re-attachment occurred around the 18 percent airfoil station.

Note that for this bubble, reversed flow extended up from the airfoil over one-half inch in some cases. Figure 22 also shows three profiles further downstream, aft of re-attachment. Note that here the height scale is different from the other plots. These were clearly turbulent profiles. Re-attachment appeared to be at approximately 18 percent chord for the 3.85 degree case. Note that this was uncorrected and probe interference has probably shortened all the bubble length measurements.

Data Presentation

The detailed results, run by run, are given in the appendices. In Appendix A the wind tunnel run summaries are tabulated. The runs are listed in order by run number and separated into groups according to the model and configuration. For example, NACA 0012 Model No. 2 with Glaze Ice appears as one of the group headings. For the runs where pressure data were taken, both the uncorrected or raw data, and the corrected values are given for the angle of attack; lift, drag and pitching moment coefficients. Mach number and Reynolds number are also given. For the data runs where velocity profile data were taken, no force coefficient data are available. In this case the uncorrected angle of attack, tunnel velocity, Reynolds number, Mach number, and calculated boundary layer thicknesses are given. In the tables AOA is just the angle of attack in degrees and VEL and U-EDGE are the tunnel velocity and boundary layer edge velocity, respectively, in feet per second.

It should be noted that many run numbers are missing. Blocks of run numbers are often missing which represent tunnel runs on other models and projects. In some instances one or two runs may be omitted when the data is bad or questionable due to an equipment or software problem.

In Appendix B the pressure coefficient plots are given in run number order. Each symbol represents a measured pressure with the apex of the triangular symbol up, for upper surface taps, and down, for lower surface taps. Some taps were removed from the plots due to blockage in the pressure lines. Tabulated on each plot are the tunnel conditions and the corrected angle of attack and corrected integrated force coefficients. The nomenclature is straight-forward with the possible exception of the term CDW. Since the OSU software is also capable of calculating and outputting the integrated pressure drag coefficient, the total airfoil corrected drag coefficient obtained from the wake survey probe is given as CDW. This corresponds to the CD value in the table of Appendix A.

The model construction did cause some inconsistencies in the data which should be explained. The model was constructed with a removable leading edge which caused a spanwise seam in the model at the 15 percent chord location. This slight discontinuity in the airfoil surface can be seen in the pressure distribution plots, particularly on the upper surface where taps were located every one percent chord. Some asymmetry, about zero degrees angle of attack, was also seen in the integrated coefficients due to this model seam, since it was slightly smoother on one side than the other. Although an effort was made to smooth the seams, this was not completely successful. This asymmetry was most evident in the drag data on the clean model. Due to what is thought to be different laminar boundary layer transition points, the drag was somewhat asymmetric about zero degrees angle of attack. Also contributing to this was the surface pressure tap installation. From previous experience at OSU it is known that the presence of these taps increases the airfoil drag since they act as boundary layer trips and as surface roughness. This model has many more taps on the upper surface than on the lower, which may explain in part why the drag was higher at negative angles of attack. Even when the boundary layer trip was installed at the five percent chord location, this asymmetry was present. On the runs of the NACA 0012 Model No. 2 with boundary layer trip, a small discontinuity was seen in the pressure plots near the forty percent chord station on the upper surface. This was the point where the pressure measurement was switched to a second Scanivalve. Apparently some small deviation in transducer reference pressure was present. Unfortunately, this was not discovered until after the experiment was completed, but the data are still of acceptable quality and are included here.

In Appendix C selected wake traces are presented. It was not felt that these data would be useful to most readers, so only a representative sample of these plots are presented here. In these figures the dynamic pressure in the wake, assuming that the wake static is just the tunnel freestream static pressure, were plotted versus the position in the wake. Since only the relative positions of the data are used in the data reduction, no attempt has been made to maintain a common coordinate system for all runs. The wake deficit is then a measure of the total airfoil drag. Since, as in the integration of the pressure distributions of Appendix B, the tunnel dynamic pressure is measured to correspond to each wake point, integrating these plots alone will not give the exact drag value reported here. The tunnel speed variation correction is, however, small and the two values should be very close.

The detailed velocity measurements are presented in Appendix D. Two sets of measurements are found here; the split-film results on Model No. 1 with glaze ice and the total probe boundary layer measurements on Model No. 2 with the trip strip. These runs can be easily distinguished by the plot title or run number. In addition to the data listed for each run in the table of Appendix A, the important parameters are gives on each plot. These include run number, uncorrected angle of attack in degrees, the probe chordwise location, the freestream velocity in ft/sec and the model chord Reynolds number in millions. Each symbol represents the measured velocity at a particular height above the model where Y is always zero on the surface. The total pressure data has somewhat more scatter than the split-film data since each total probe data point represents only one data sample instead of the 2048 samples averaged for each split-film velocity.

SUMMARY

An experimental program has been conducted to document the aerodynamic characteristics and flow field about a NACA 0012 airfoil with simulated glaze ice. Two different NACA 0012 models were used for the tests.

NACA 0012 Model No. 2 was instrumented with an extremely dense distribution of surface pressure taps to provide additional details concerning the large separation zones aft of the ice horns. Airfoil

lift and drag were severely affected by the ice shape as was expected. However, the surface pressure provided additional information about the separation bubbles. The bubbles are characterized by a region of almost constant, but slightly falling pressure, followed by a region of pressure recovery. Work on Model No. 1 has shown that re-attachment occurred in this pressure recovery region. The lower surface horn caused a larger separation zone and a more severe aerodynamic penalty when tested at negative angles of attack than did the upper surface horns at positive angles of attack. This is an interesting result which should be studied further. Model No. 2 was also used to document the baseline performance of the NACA 0012 airfoil. These tests were conducted with natural transition and transition fixed at the five percent chord location on both surfaces. The forced transition data compared well to theoretical results in all aerodynamic quantities including the measured boundary layer parameters.

Velocity profile measurements were performed in the separated flow region behind the upper surface glaze ice horn. Using split-film anemometry on the NACA 0012 Model No. 1, streamwise velocity profiles have been measured at several chordwise locations and angles of attack. These profiles have shown the bubble extent and the large regions of reversed flow.

Much of the detailed data from these experiments can be found in the appendices. In addition to the run summary tables, plots of surface pressures, wake total pressure profiles and velocity profiles are also in the appendices. It is hoped that these data will be useful in testing and developing airfoil performance in icing computer codes and providing a better understanding of the flow field.

REFERENCES

1. Jacobs, E. N.,"Airfoil Section Characteristics as Affected by Protuberances", NACA Report No. 446,1932.

2. Gray, V. H. and Von Glahn, Uwe H., "Effects of Ice and Frost Formations on Drag of NACA 65-212 Airfoil for Various Modes of Thermal Ice Protection", NACA TN 2962, 1953.

3. Gray, V. H. and Von Glahn, Uwe H., "Aerodynamic Effects Caused by Icing of an Unswept NACA 65A004 Airfoil", NACA TN 4151, 1957.

4. Korkan, K. D., Cross, E. J. Jr., and Cornell, C. C., "Experimental Study of Performance Degradation of a Model Helicopter Main Rotor with Simulated Ice Shape", AIAA Paper No. 84-0184, presented at the 22nd Aerospace Sciences Meeting, Reno, Nevada, Jan. 9-12, 1984.

5. Lee, J. D. and Shaw, R. J., "The Aerodynamics of Rotor Blades with Ice Shapes Accreted in Hover and in Level Flight", paper presented at the 41st Annual Forum of the American Helicopter Society, Ft. Worth, Texas, May, 1985.

6. Flemming, R. J., Shaw, R. J. and Lee, J. D., "The Performance Characteristics of Simulated Ice on Rotor Airfoils", paper presented at the 41st Annual Forum of the American Helicopter Society, Ft. Worth, Texas, May 1985.

7. Bragg, M. B., Zaguli, R. J., and Gregorek, G. M., "Wind Tunnel Evaluation of Airfoil Performance Using Simulated Ice Shapes", NASA CR 167960, 1982.

8. Bragg, M. B. and Gregorek, G. M.,"Wind Tunnel Investigation of Airfoil Performance Degradation Due to Icing", AIAA Paper No. 82-0582, presented at the 12th Aerodynamic Testing Conference, Williamsburg, Virginia, March 22-24, 1982.

9. Bragg, M. B., "Predicting Airfoil Performance with Rime and Glaze Ice Accretions", AIAA Paper No. 84-0106, presented at the 22nd Aerospace Sciences Meeting, Reno, Nevada, Jan. 9-12, 1984.

10. Potapczuk, M. G. and Gerhart, P. M. "Progress in the Development of a Navier-Stokes Solver for Evaluation of Iced Airfoil Performance", AIAA Paper No. 85-0410, presented at the 23rd Aerospace Sciences Meeting, Reno, Nevada, Jan. 14-17, 1985.

11. Cebeci, T., "Interactive Boundary-Layer Analysis of Iced Airfoils", Airfoil Performance-in-Icing Workshop, NASA Lewis Research Center, July 17-18, 1986.

12. Bragg, M. B. and Coirier, W. J., "Detailed Measurements of the Flowfield in the Vicinity of an Airfoil with Glaze Ice", AIAA Paper No. 85-0409, presented at the 23rd Aerospace Sciences Meeting, Reno, Nevada, Jan. 14-17, 1985.

13. Bragg, M. B., and Coirier, W. J., "Aerodynamic Measurements of an Airfoil with Simulated Glaze Ice", AIAA-86-0484, paper presented at the 24th Aerospace Sciences Meeting, Reno, NV, Jan. 6-9, 1986.

14. Shaw, R. J., private communication, March 1982.

15. Rae, W. H., Jr. and Pope, A., Low-Speed Wind Tunnel Testing, 2nd ed., John Wiley and Sons, New York, 1984.

16. Boerner, Th. and Leutheusser, H. J., "Calibration of Split-Fibre Probe for Use in Bubbly Two-Phase Flow", DISA Information, No. 29, January 1984.

17. Eppler, Richard and Somers, Dan M., "A Computer Program for the Design and Analysis of Low-Speed Airfoils", NASA TM 80210, August 1980.

18. Smetana, F. O., Summey, D. C., Smith, N. S. and Carden, R .K., "Light Aircraft Lift, Drag, and Moment Prediction - A Review and Analysis", NASA CR-2523, May 1975.

19. Olsen, W., Shaw, R. and Newton, J., "Ice Shapes and the resulting Drag Increase for a NACA 0012 airfoil", NASA TM 83556, 1983.

TABLE 1. COORDINATES FOR THE NACA 0012 MODEL NO. 2 - CLEAN CONFIGURATION

No.	X_u	Y_u	X_l	Y_l
1	0.00000	0.00000	0.00000	0.00000
2	0.00309	0.00967	0.00309	-0.00967
3	0.00621	0.01356	0.00621	-0.01356
4	0.01380	0.01984	0.02230	-0.02481
5	0.02230	0.02481	0.04080	-0.03256
6	0.03140	0.02899	0.08000	-0.04307
7	0.04080	0.03256	0.12000	-0.04988
8	0.05000	0.03555	0.16000	-0.05442
9	0.06000	0.03838	0.20000	-0.05738
10	0.07000	0.04086	0.24000	-0.05913
11	0.08000	0.04307	0.28000	-0.05993
12	0.09000	0.04505	0.32000	-0.05993
13	0.10000	0.04683	0.36000	-0.05926
14	0.11000	0.04843	0.40000	-0.05803
15	0.12000	0.04988	0.44000	-0.05631
16	0.13000	0.05119	0.50000	-0.05294
17	0.14000	0.05238	0.56000	-0.04878
18	0.15000	0.05345	0.60000	-0.04563
19	0.16000	0.05442	0.65000	-0.04132
20	0.17000	0.05529	0.70000	-0.03664
21	0.18000	0.05607	0.75000	-0.03160
22	0.19000	0.05676	0.80000	-0.02623
23	0.20000	0.05738	0.85000	-0.02053
24	0.21000	0.05792	0.90000	-0.01448
25	0.22000	0.05839	0.95000	-0.00807
26	0.23000	0.05879	0.97500	-0.00471
27	0.24000	0.05913	1.00000	0.00000
28	0.25000	0.05941		
29	0.26000	0.05864		
30	0.27000	0.05981		
31	0.28000	0.05993		
32	0.29000	0.06000		
33	0.30000	0.06002		
34	0.31000	0.05999		
35	0.32000	0.05993		
36	0.33000	0.05982		
37	0.34000	0.05967		
38	0.35000	0.05949		
39	0.36000	0.05926		
40	0.37000	0.05900		
41	0.38000	0.05871		
42	0.39000	0.05839		
43	0.40000	0.05803		
44	0.42000	0.05723		
45	0.44000	0.05631		

TABLE 1. (continued)

No.	X_u	Y_u
46	0.47000	0.05473
47	0.50000	0.05294
48	0.53000	0.05095
49	0.56000	0.04878
50	0.60000	0.04563
51	0.65000	0.04132
52	0.70000	0.03664
53	0.75000	0.03160
54	0.80000	0.02623
55	0.85000	0.02053
56	0.90000	0.01448
57	0.95000	0.00807
58	0.97500	0.00471
59	1.00000	0.00000

TABLE 2. COORDINATES FOR THE NACA 0012
MODEL NO. 1 - GLAZE ICE CONFIGURATION

No.	X_u	Y_u	X_l	Y_l
1	-0.02557	0.02729*	-0.02557	0.02729
2	-0.02501	0.02877*	-0.02000	0.00621
3	-0.02445	0.02922*	-0.01800	0.00097
4	-0.02389	0.02945*	-0.01200	-0.01151
5	-0.02333	0.02952*	-0.00600	-0.02115
6	-0.00305	0.02632	0.00000	-0.02907
7	0.01857	0.02263	0.00600	-0.03577
8	0.03140	0.02899	0.01200	-0.04155
9	0.05000	0.03555	0.02166	-0.05215*
10	0.06000	0.03838	0.02278	-0.05283*
11	0.08000	0.04307	0.02333	-0.05290*
12	0.10000	0.04683	0.02389	-0.05283*
13	0.12000	0.04988	0.04798	-0.04683
14	0.14000	0.05238	0.06952	-0.04026
15	0.16000	0.05442	0.09900	-0.04700
16	0.18000	0.05607	0.12000	-0.04988
17	0.20000	0.05738	0.16000	-0.05442
18	0.22000	0.05839	0.20000	-0.05738
19	0.24000	0.05913	0.24000	-0.05913
20	0.26000	0.05864	0.28000	-0.05993
21	0.28000	0.05993	0.32000	-0.05993
22	0.30000	0.06002	0.36000	-0.05926
23	0.32000	0.05993	0.40000	-0.05803
24	0.34000	0.05967	0.44000	-0.05631
25	0.36000	0.05926	0.50000	-0.05294
26	0.38000	0.05871	0.56000	-0.04878
27	0.40000	0.05803	0.60000	-0.04563
28	0.42000	0.05723	0.65000	-0.04132
29	0.44000	0.05631	0.70000	-0.03664
30	0.47000	0.05473	0.75000	-0.03160
31	0.50000	0.05294	0.80000	-0.02623
32	0.53000	0.05095	0.85000	-0.02053
33	0.56000	0.04878	0.90000	-0.01448
34	0.60000	0.04563	0.95000	-0.00807
35	0.65000	0.04132	0.97500	-0.00471
36	0.70000	0.03664	1.00000	0.00000
37	0.75000	0.03160		
38	0.80000	0.02623		
39	0.85000	0.02053		
40	0.90000	0.01448		
41	0.95000	0.00807		
42	0.97500	0.00471		
43	1.00000	0.00000		

* NOTE: Upper and lower surface horn radius of curvature, r/c = 0.002232 .

TABLE 3. COORDINATES FOR THE NACA 0012
MODEL NO. 2 - ICED CONFIGURATION

No.	X_u	Y_u	X_l	Y_l
1	-0.02660	0.01690*	-0.02660	0.01690
2	-0.02450	0.02870*	-0.02220	0.00390
3	-0.02080	0.03060*	-0.01750	-0.00700
4	-0.01000	0.02880	-0.01070	-0.01840
5	-0.00010	0.02680	-0.00360	-0.02840
6	0.01000	0.02500	0.00590	-0.03930
7	0.02210	0.02670	0.01500	-0.04740
8	0.03110	0.03000	0.02580	-0.05330**
9	0.04070	0.03330	0.03000	-0.05300**
10	0.04910	0.03610	0.03970	-0.05030
11	0.05950	0.03900	0.04950	-0.04730
12	0.06940	0.04140	0.06000	-0.04410
13	0.07940	0.04350	0.06950	-0.04210
14	0.08910	0.04550	0.07930	-0.04360
15	0.09900	0.04720	0.10940	-0.04870
16	0.10970	0.04870	0.11930	-0.05000
17	0.11970	0.05000	0.12900	-0.05110
18	0.12969	0.05140	0.14000	-0.05200
19	0.14000	0.05240	0.16000	-0.05442
20	0.16000	0.05442	0.20000	-0.05738
21	0.17000	0.05500	0.24000	-0.05913
22	0.18000	0.05607	0.28000	-0.05993
23	0.19000	0.05676	0.32000	-0.05993
24	0.20000	0.05738	0.36000	-0.05926
25	0.21000	0.05792	0.40000	-0.05803
26	0.22000	0.05839	0.44000	-0.05631
27	0.23000	0.05879	0.50000	-0.05294
28	0.24000	0.05913	0.56000	-0.04878
29	0.25000	0.05941	0.60000	-0.04563
30	0.26000	0.05864	0.70000	-0.03664
31	0.28000	0.05993	0.75000	-0.03160
32	0.30000	0.06002	0.85000	-0.02053
33	0.32000	0.05993	0.90000	-0.01448
34	0.34000	0.05967	0.95000	-0.00807
35	0.36000	0.05926	0.97500	-0.00471
36	0.38000	0.05871	1.00000	0.00000
37	0.40000	0.05800		
38	0.42000	0.05700		
39	0.44000	0.05631		
40	0.47000	0.05473		
41	0.50000	0.05294		
42	0.53000	0.05095		
43	0.56000	0.04878		
44	0.60000	0.04563		
45	0.70000	0.03664		

TABLE 3. (continued)

No.	X_u	Y_u
46	0.75000	0.03160
47	0.80000	0.02623
48	0.85000	0.02053
49	0.90000	0.01448
50	0.95000	0.00807
51	0.97500	0.00471
52	1.00000	0.00000

* NOTE: Upper surface horn radius of curvature, $(r/c)_u = 0.00595$.

** NOTE: Lower surface horn radius of curvature, $(r/c)_l = 0.01042$.

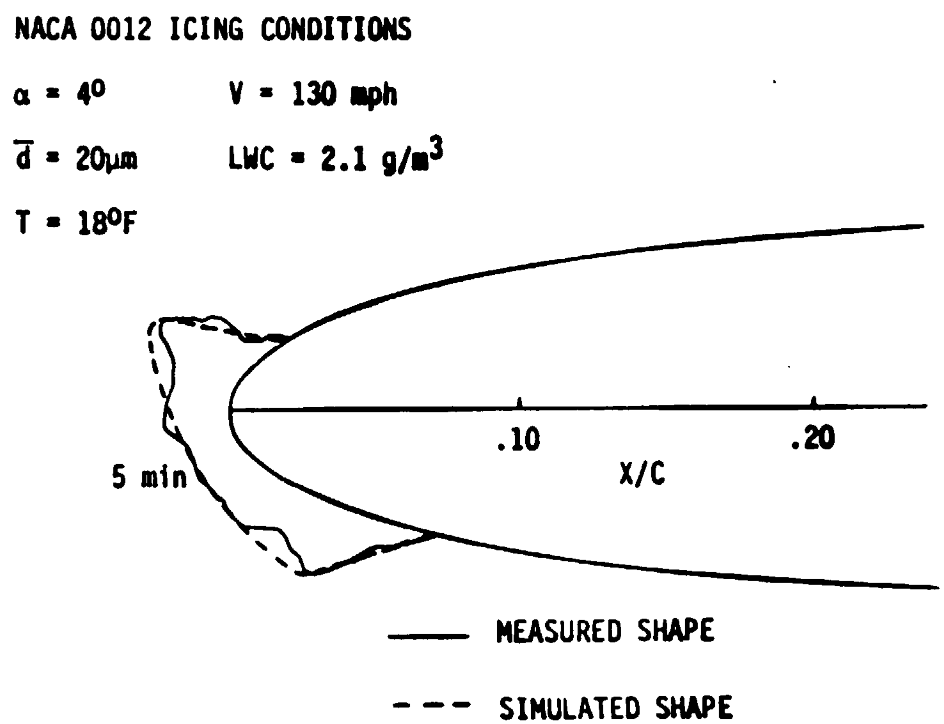

FIGURE 1. COMPARISON OF THE MEASURED AND SIMULATED ICE SHAPE.

ORIGINAL PAGE IS
OF POOR QUALITY

FIGURE 2. OHIO STATE UNIVERSITY SUBSONIC WIND TUNNEL.

OF PC...

ORIGINAL PAGE IS
OF POOR QUALITY

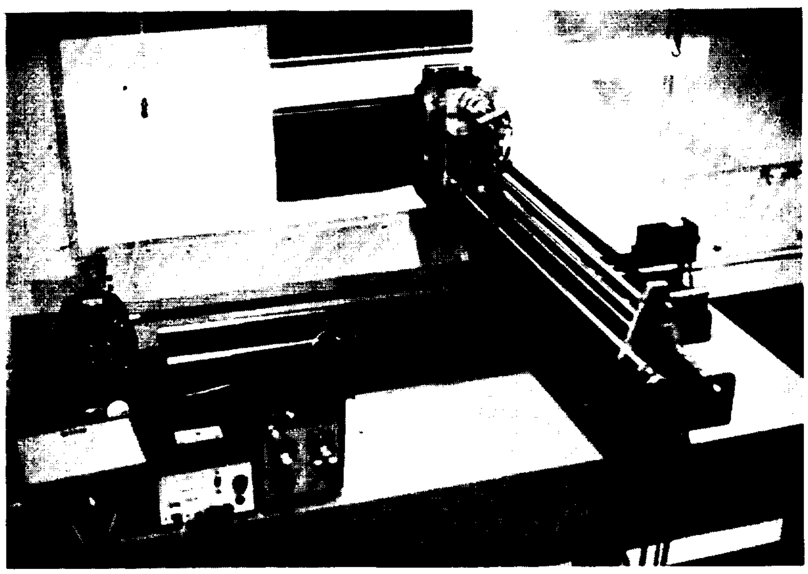

FIGURE 3. TWO-DIMENSIONAL TRAVERSE SYSTEM.

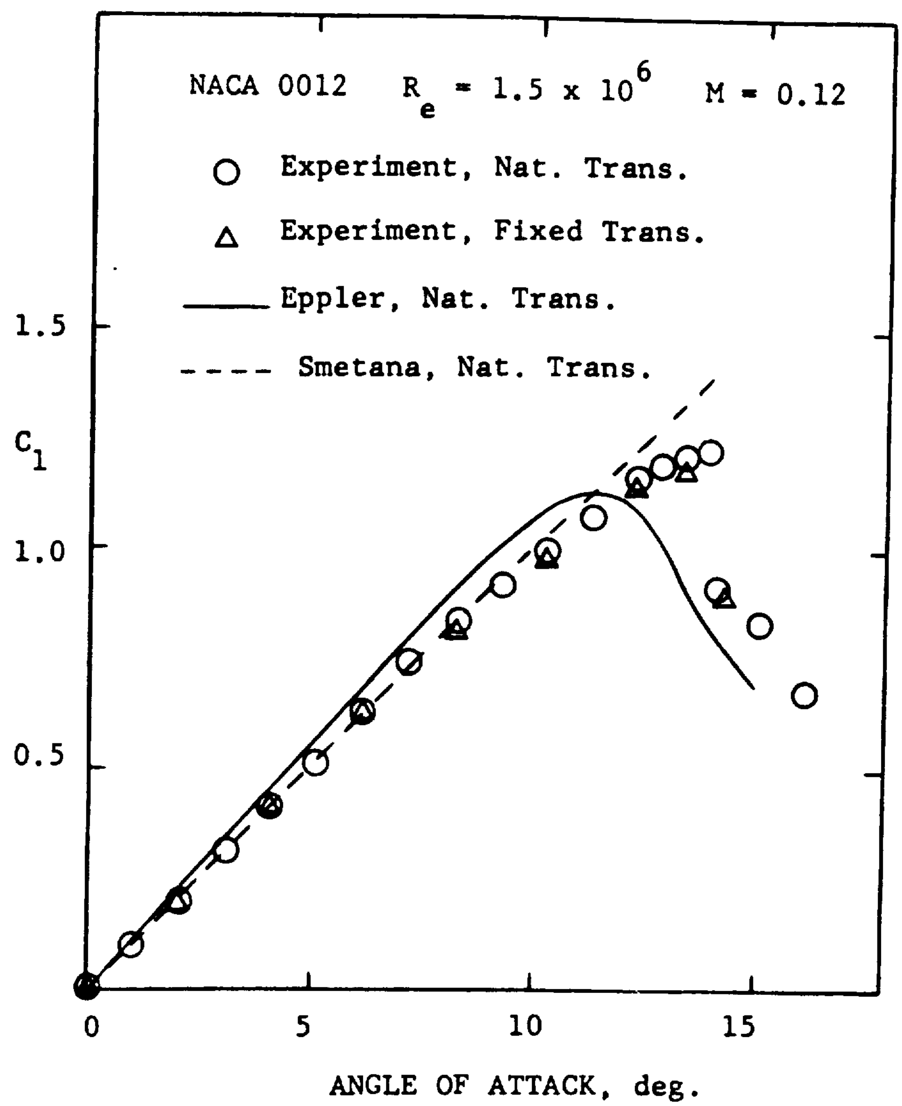

FIGURE 4. COMPARISON OF MEASURED LIFT WITH NATURAL AND FIXED TRANSITION TO THEORY.

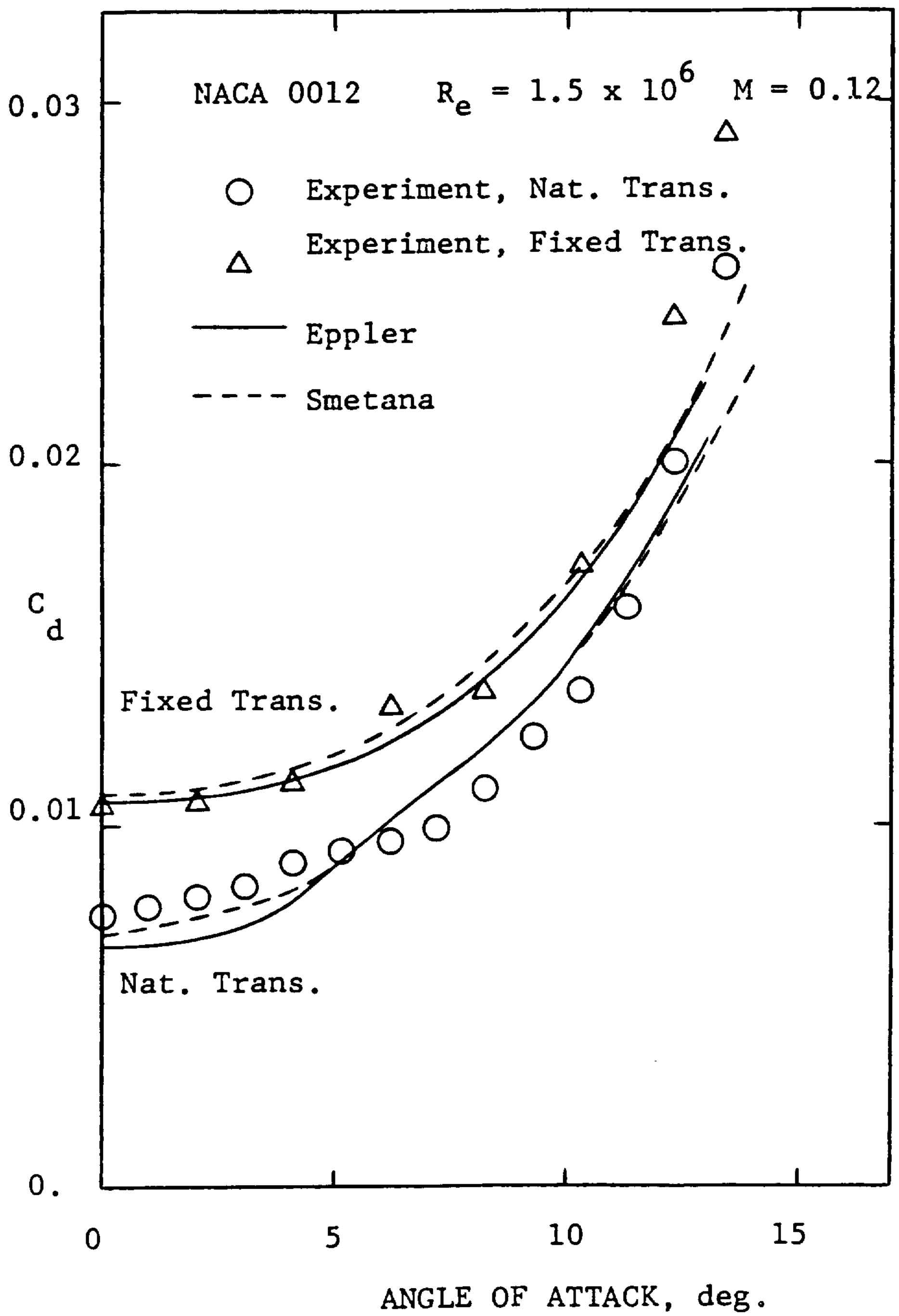

FIGURE 5. COMPARISON OF MEASURED DRAG WITH NATURAL AND FIXED TRANSITION TO THEORY.

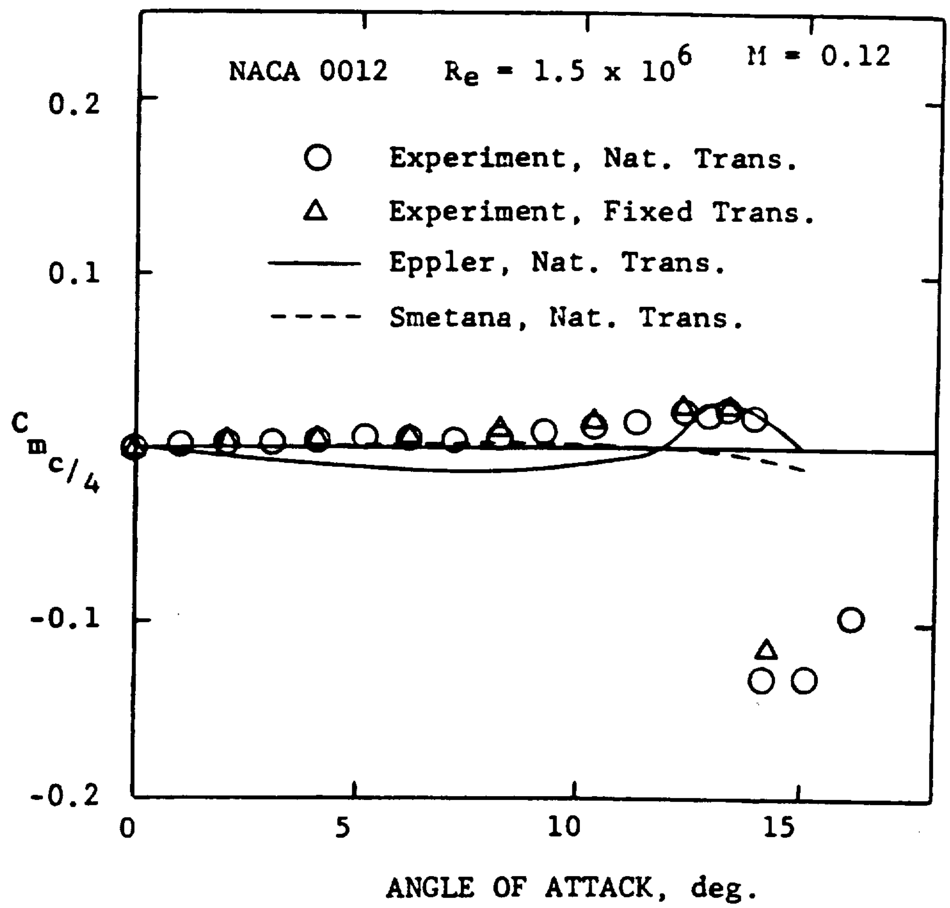

FIGURE 6. MEASURED AIRFOIL PITCHING MOMENT WITH AND WITHOUT SIMULATED GLAZE ICE.

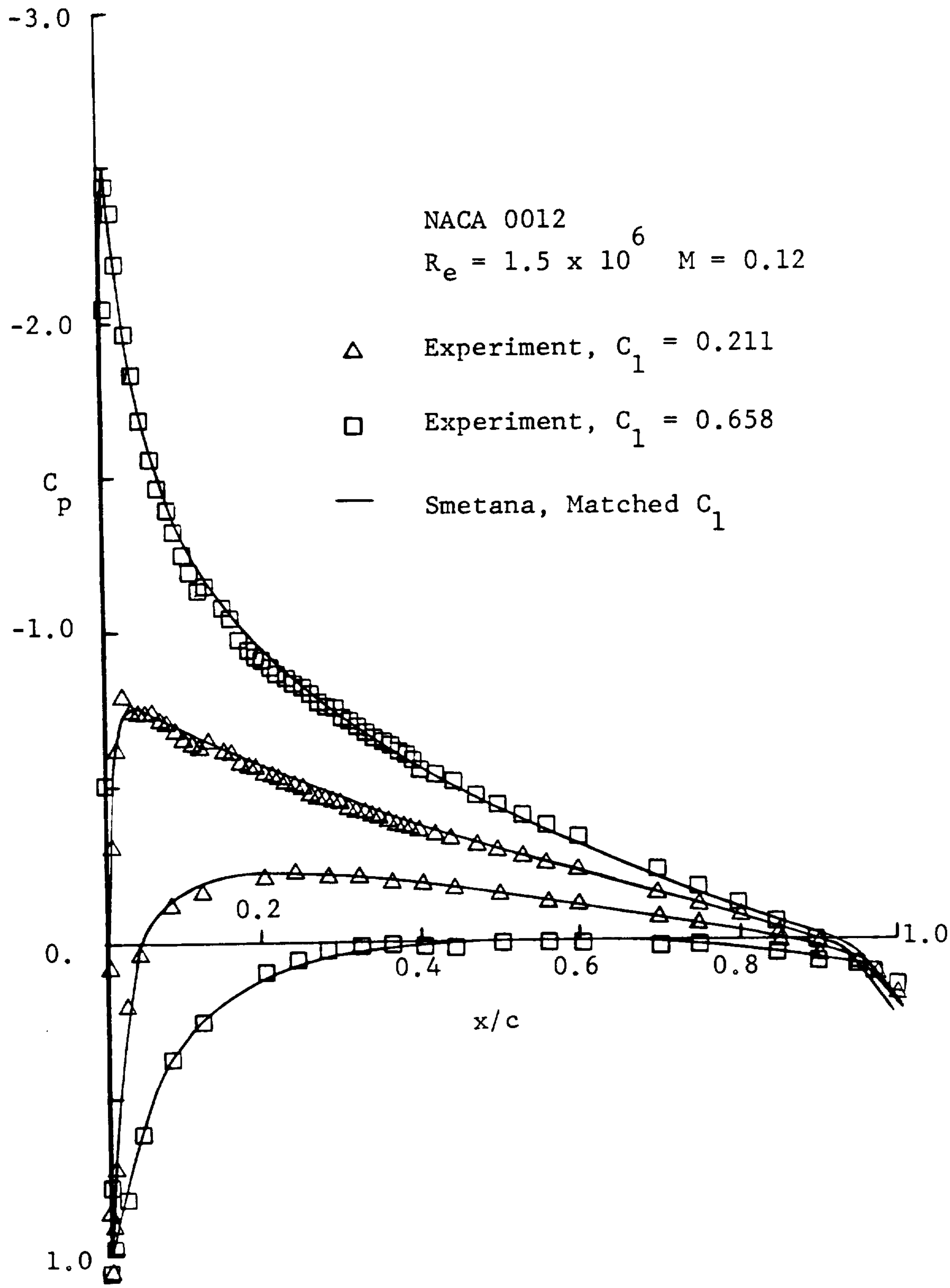

FIGURE 7. MEASURED SURFACE PRESSURES COMPARED TO THEORY AT TWO ANGLES OF ATTACK.

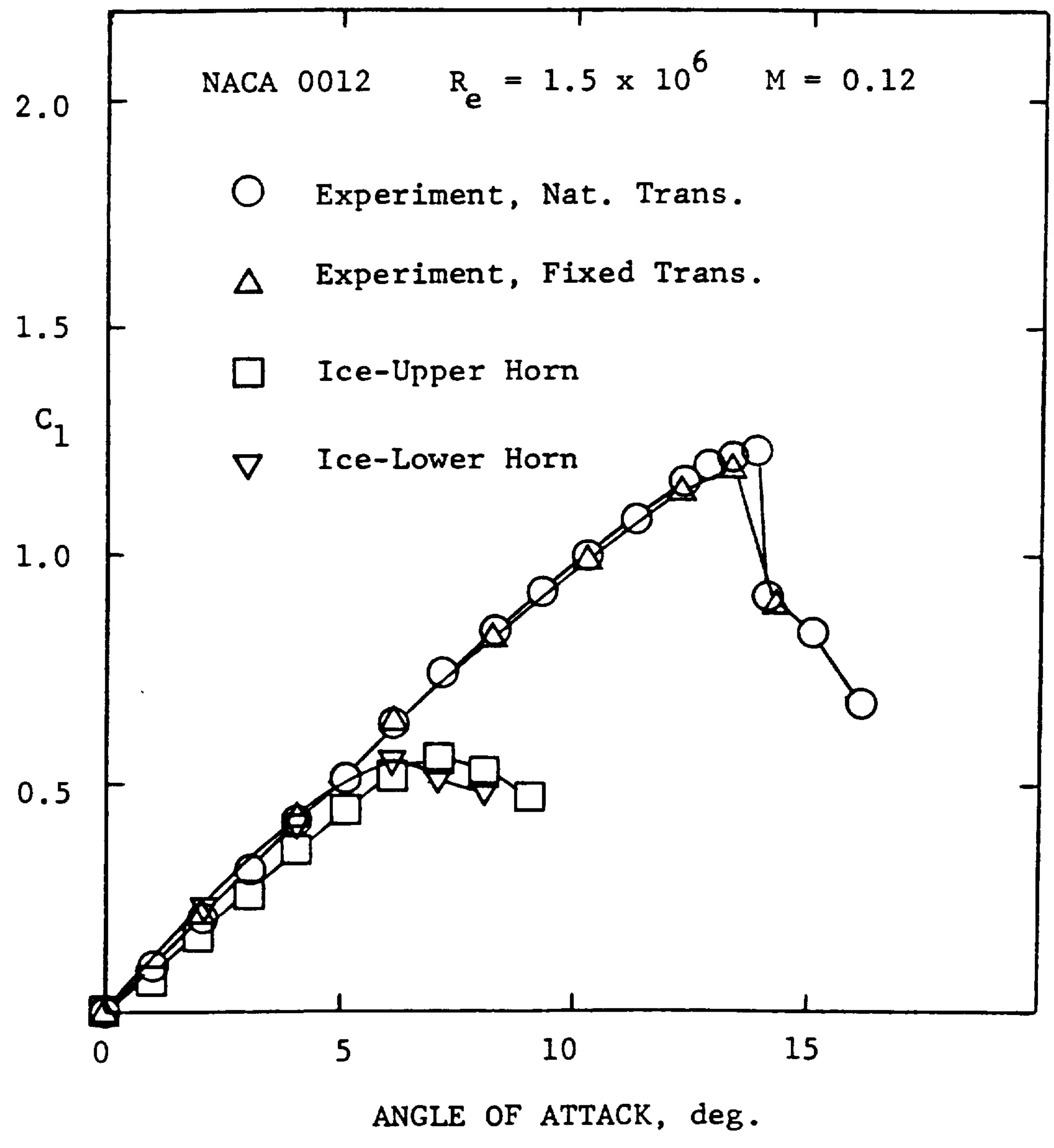

FIGURE 8. MEASURED AIRFOIL LIFT WITH AND WITHOUT SIMULATED GLAZE ICE.

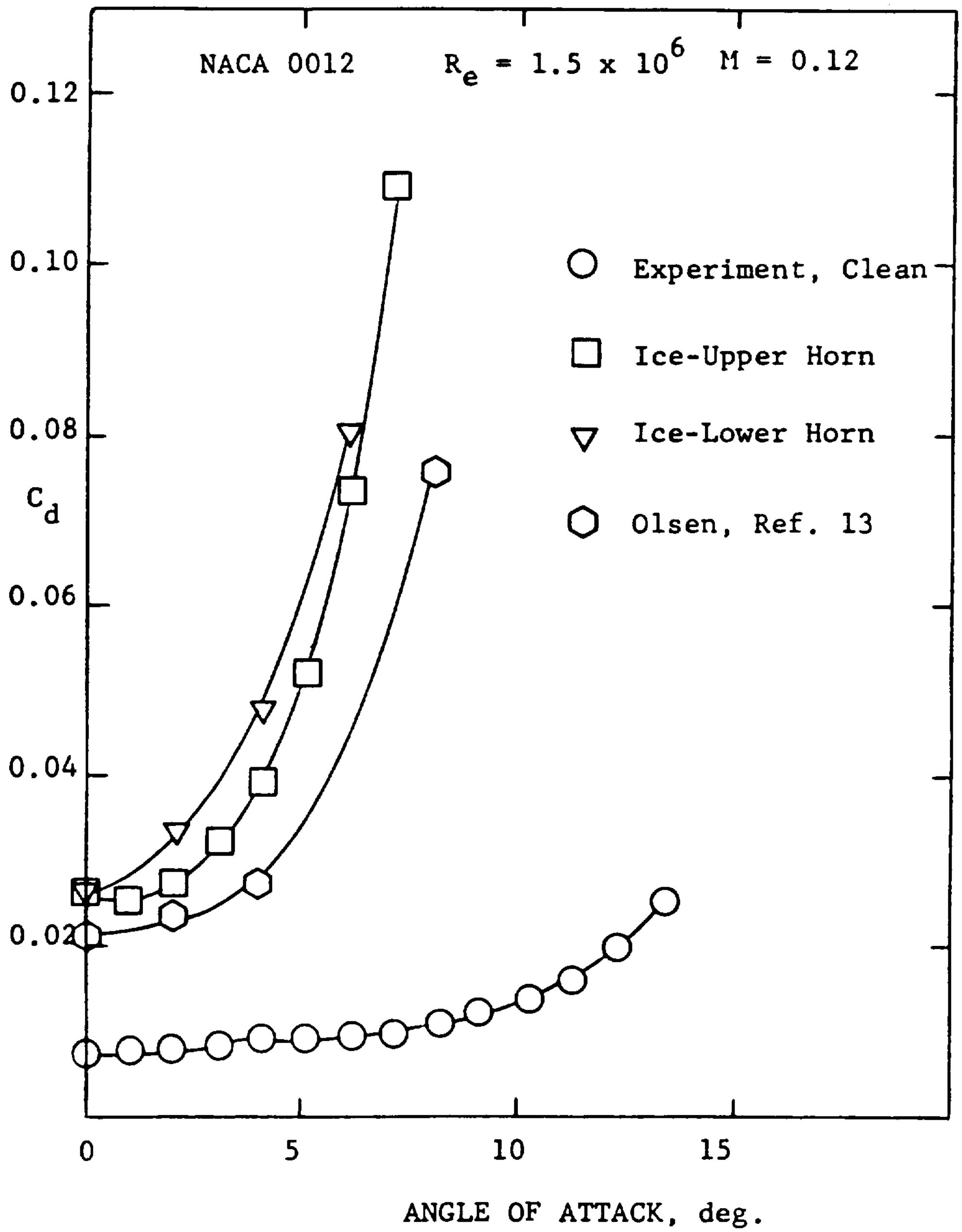

FIGURE 9. MEASURED AIRFOIL DRAG WITH AND WITHOUT SIMULATED GLAZE ICE.

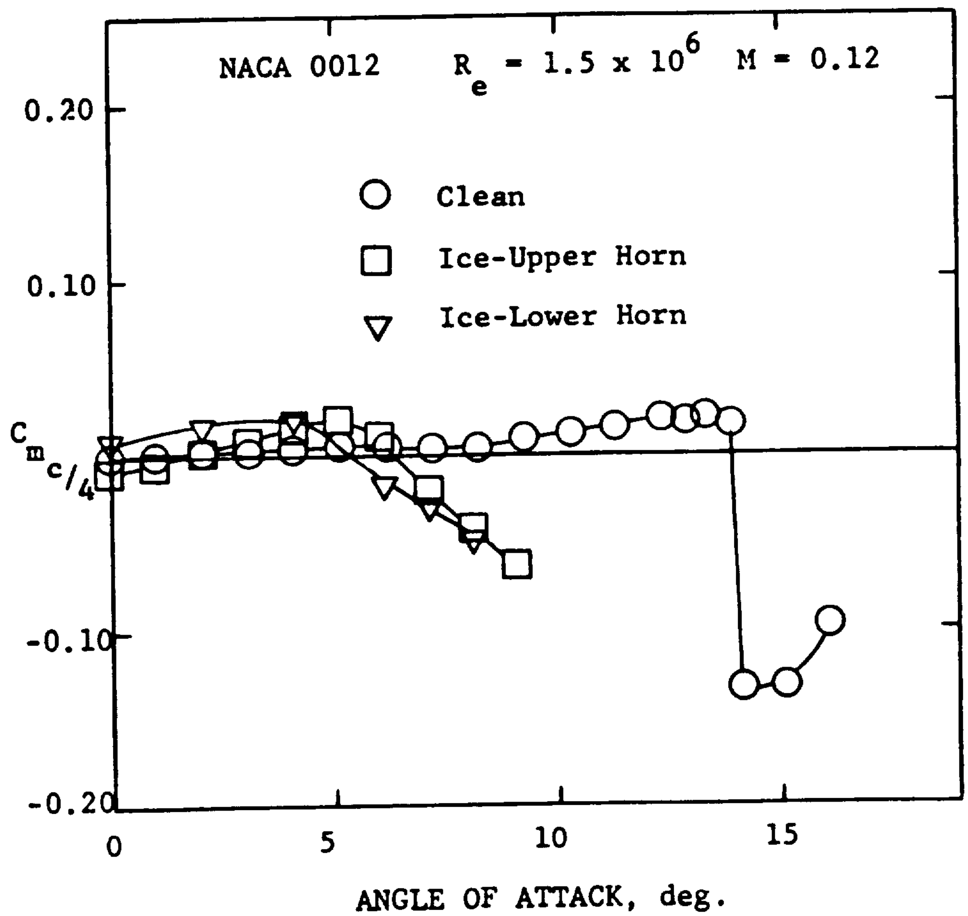

FIGURE 10. COMPARISON OF MEASURED PITCHING MOMENT WITH NATURAL AND FIXED TRANSITION TO THEORY.

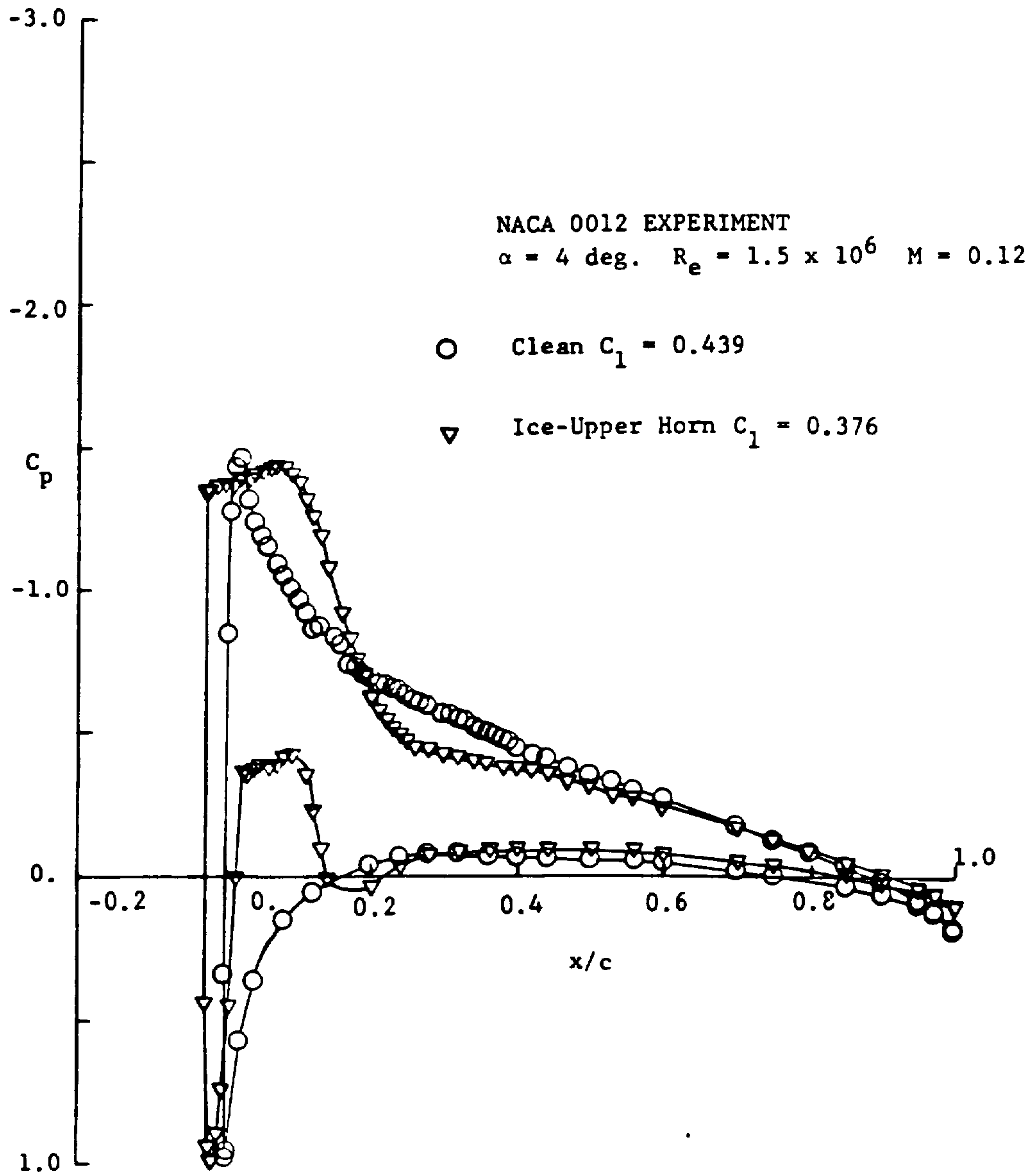

FIGURE 11. MEASURED SURFACE PRESSURES WITH AND WITHOUT SIMULATED GLAZE ICE AT α = 4 DEG.

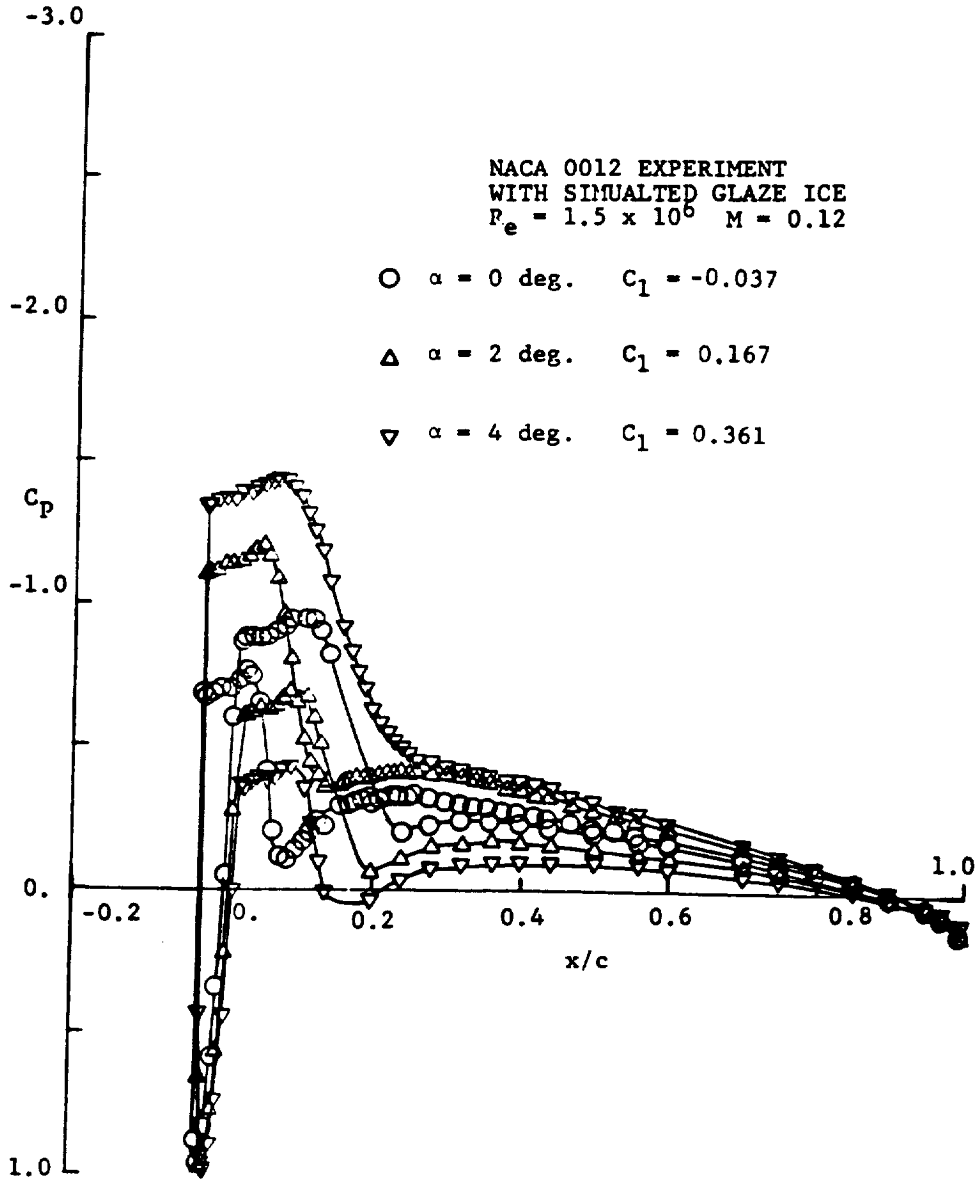

FIGURE 12. MEASURED SURFACE PRESSURES WITH SIMULATED ICE AT LOW ANGLES OF ATTACK.

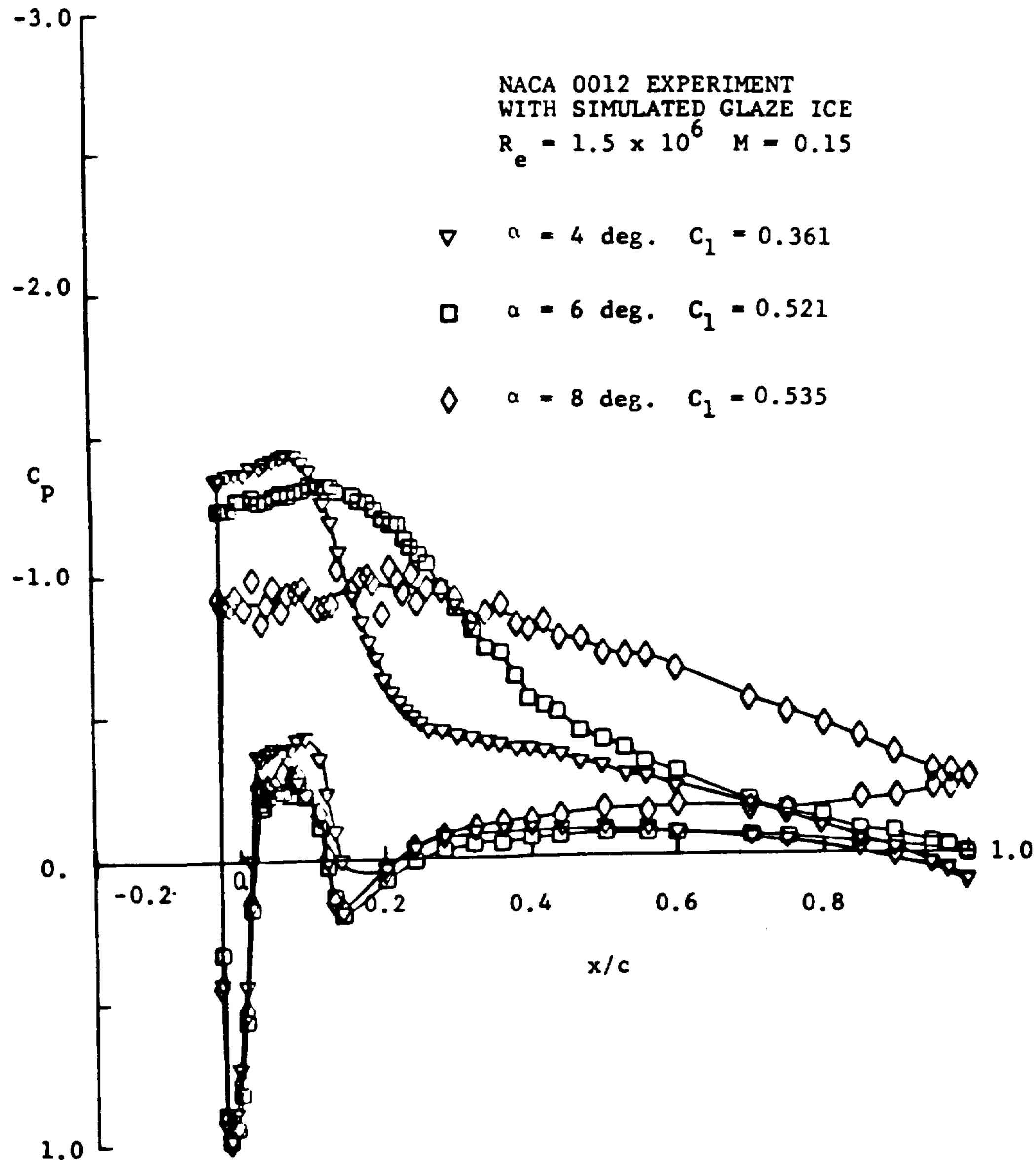

FIGURE 13. MEASURED SURFACE PRESSURES WITH SIMULATED ICE AT HIGH ANGLES OF ATTACK.

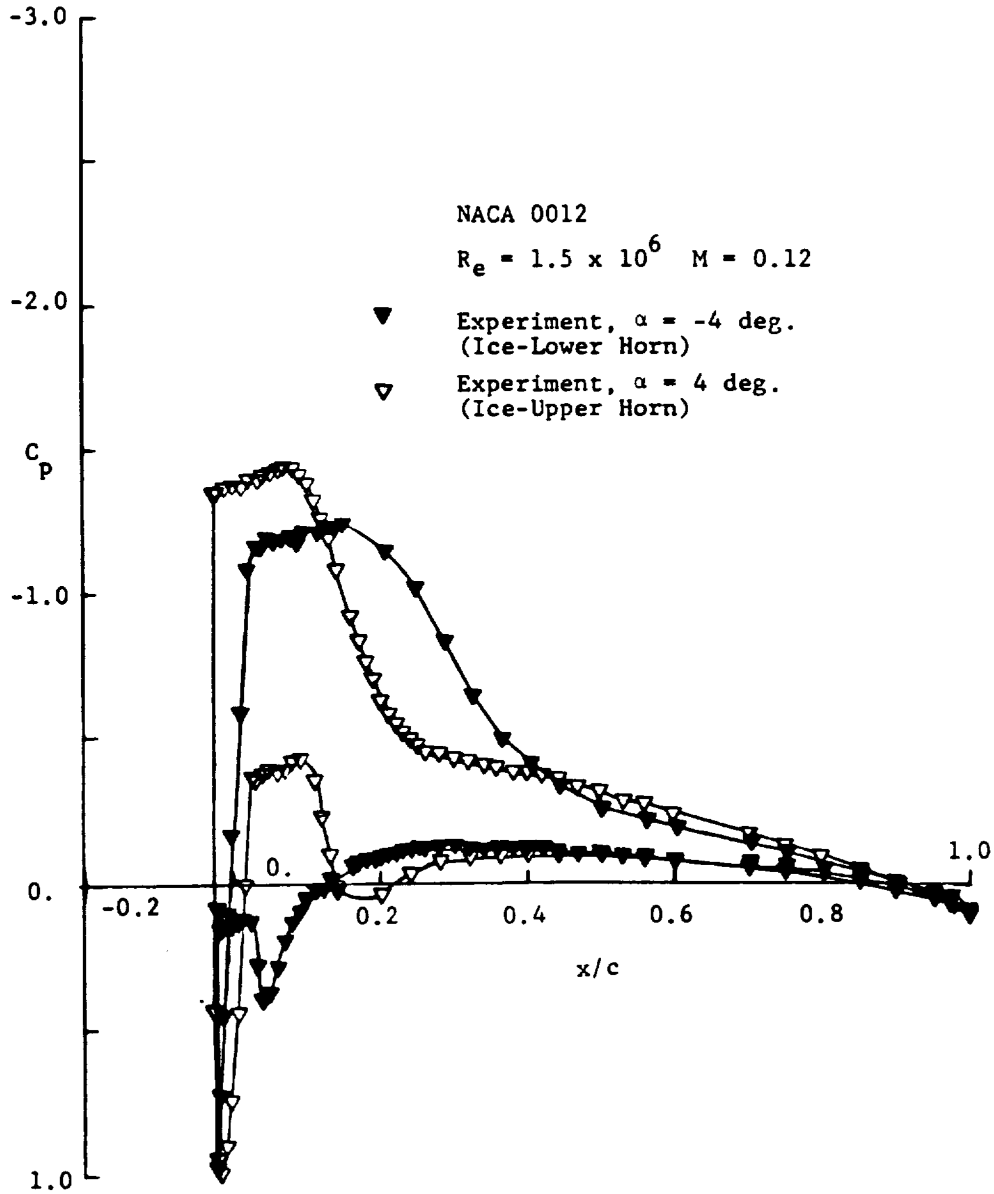

FIGURE 14. MEASURED SURFACE PRESSURES WITH SIMULATED ICE AT α = -4 and 4 DEG.

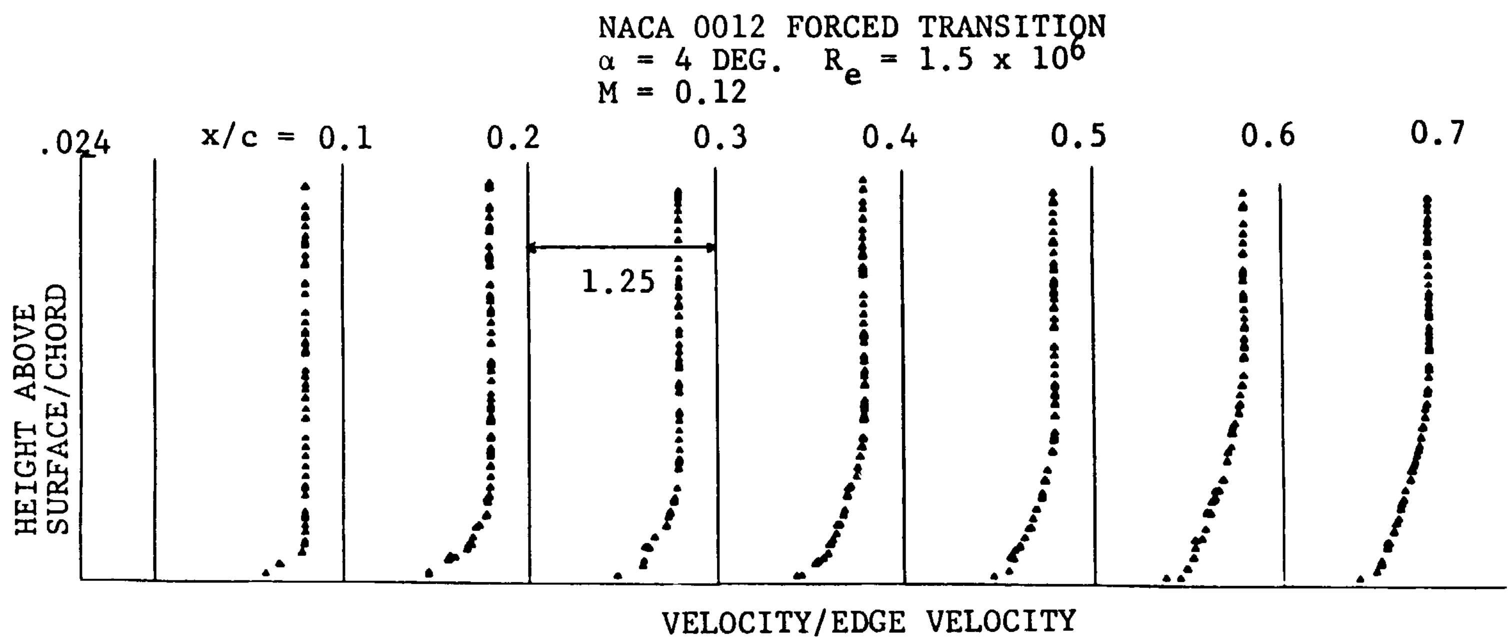

FIGURE 15. MEASURED BOUNDARY LAYER VELOCITY PROFILES ON A NACA 0012 AT α = 4 DEG. WITH FIXED TRANSITION.

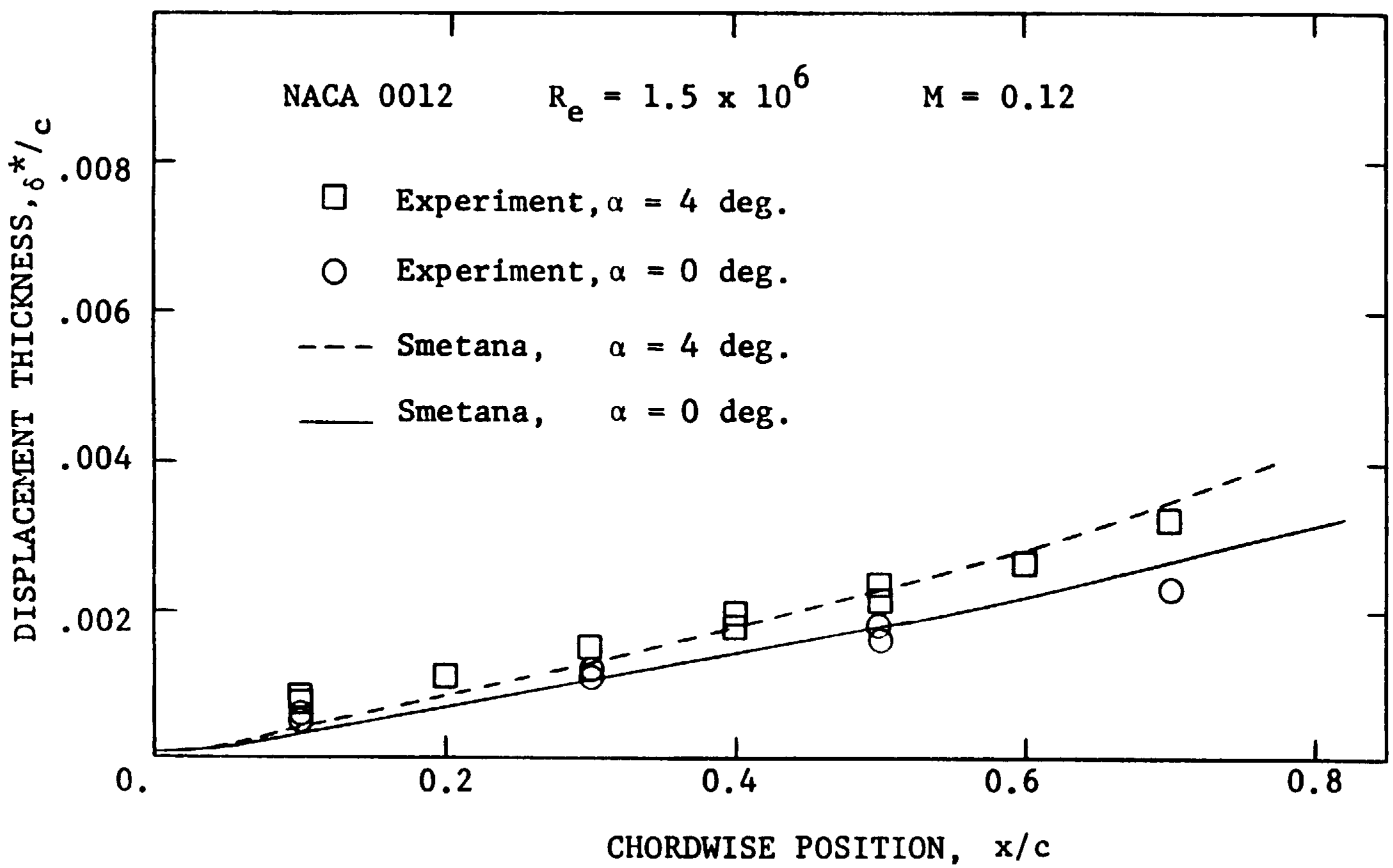

FIGURE 16. EXPERIMENTAL AND THEORETICAL BOUNDARY LAYER DISPLACEMENT THICKNESSES FOR A NACA 0012 WITH FIXED TRANSITION.

EXISTING HOT FILM SUPPORT SYSTEM

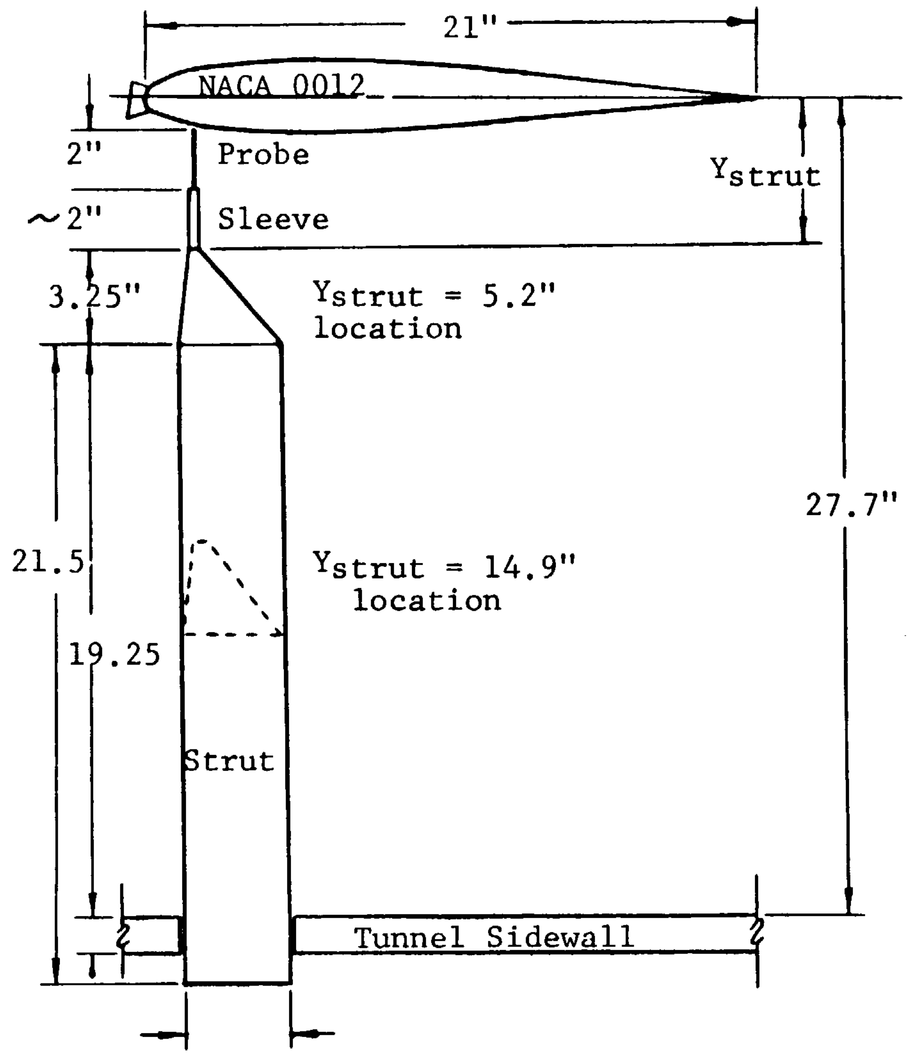

FIGURE 17. HOT FILM SUPPORT SYSTEM

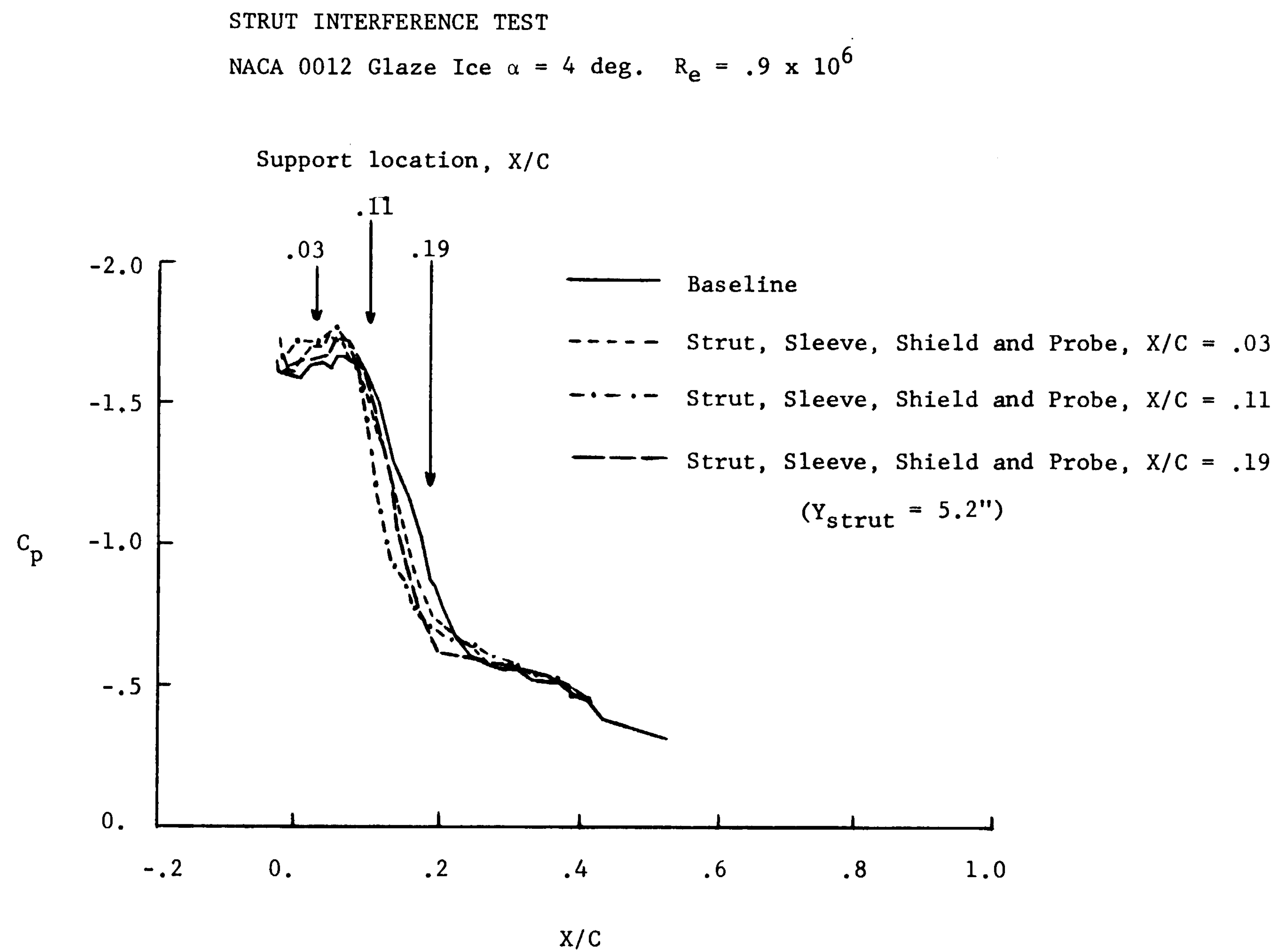

FIGURE 19. EFFECT OF PROBE ON AIRFOIL PRESSURE DISTRIBUTIONS FOR VARIOUS CHORDWISE LOCATIONS.

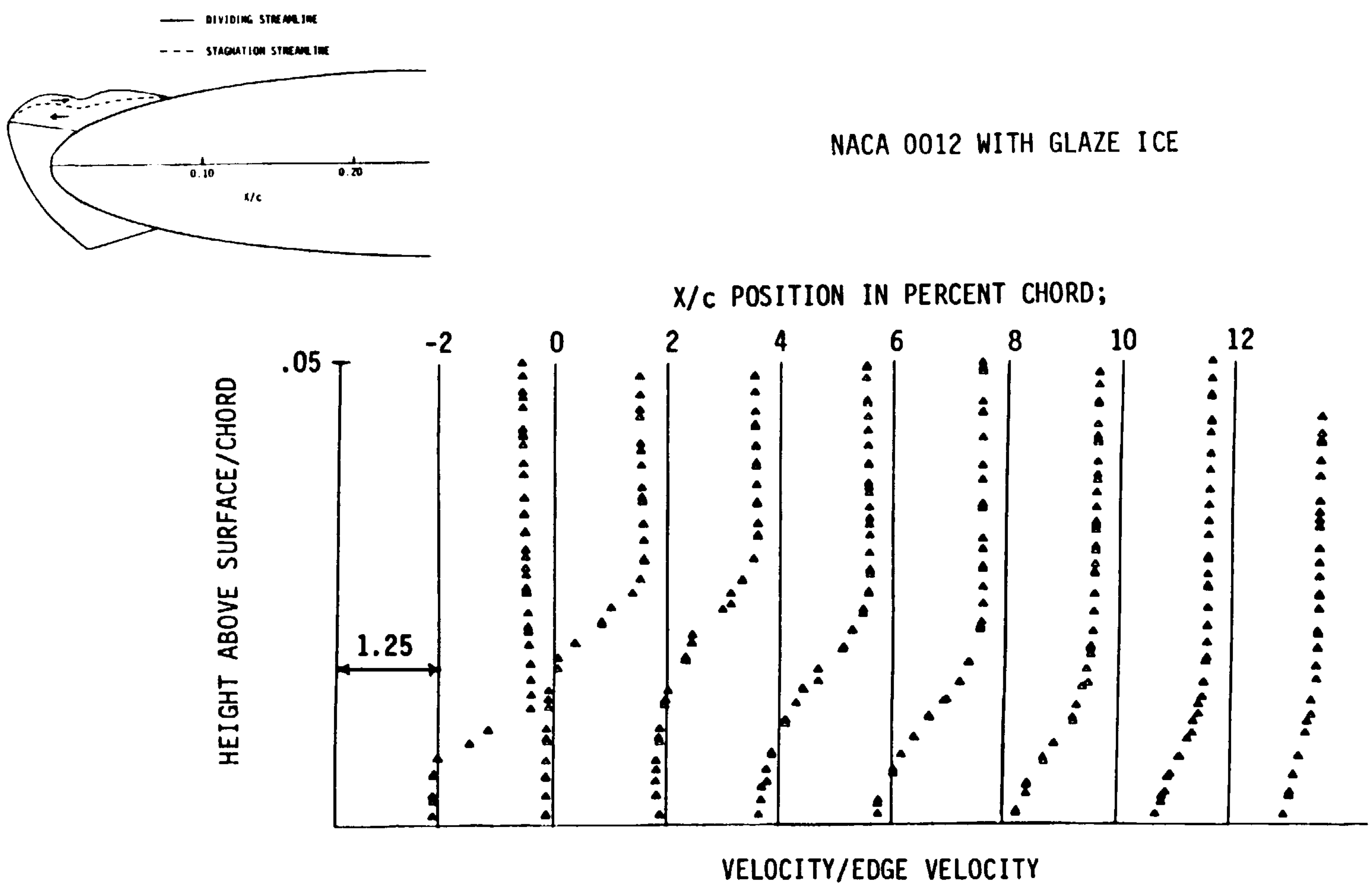

FIGURE 20. STREAMWISE COMPONENT OF VELOCITY PROFILES FOR A NACA 0012 AIRFOIL AT AN ANGLE OF ATTACK OF -0.15 DEG., Re = 1.5×10^6, AND M = 0.12.

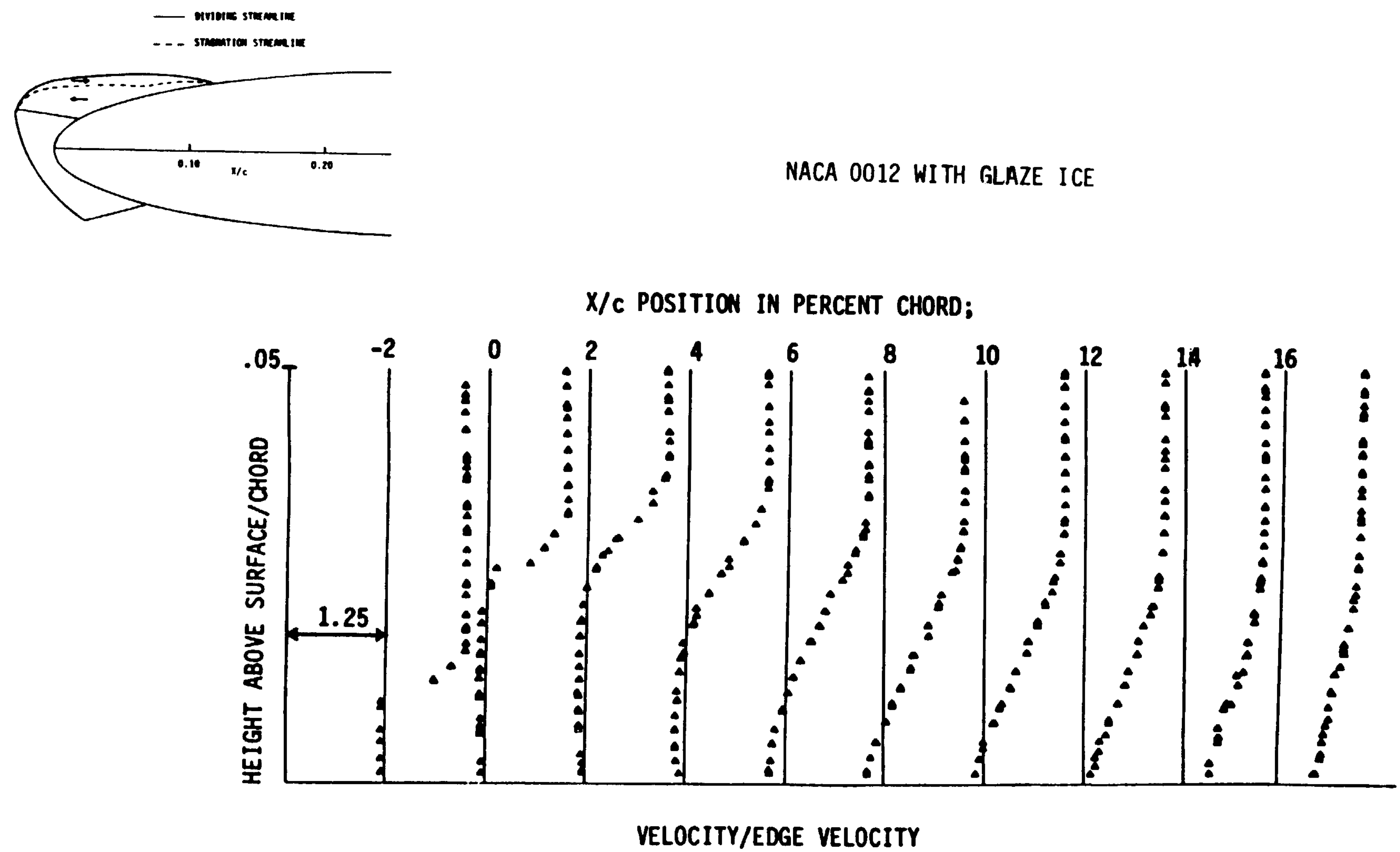

FIGURE 21. STREAMWISE COMPONENT OF VELOCITY PROFILES FOR A NACA 0012 AIRFOIL AT AN ANGLE OF ATTACK OF 1.85 DEG., Re = 1.5 x 10^6, AND M = 0.12.

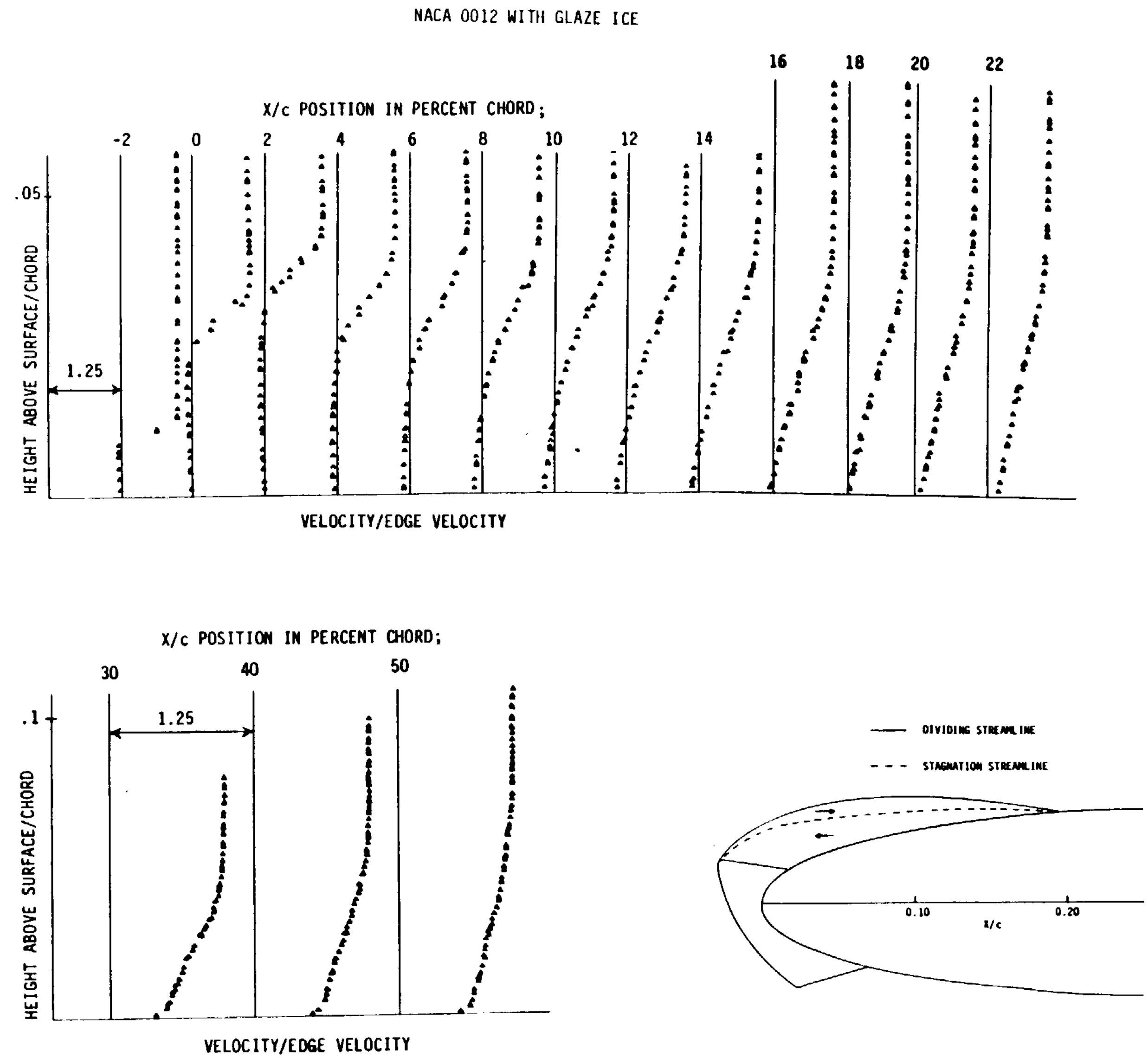

FIGURE 22. STREAMWISE COMPONENT OF VELOCITY PROFILES FOR A NACA 0012 AIRFOIL AT AN ANGLE OF ATTACK OF 3.85 DEG., Re = 1.5×10^6, AND M = 0.12.

APPENDIX A

RUN SUMMARIES

NACA 0012 MODEL NO. 1 - GLAZE ICE CONFIGURATION
SPLIT FILM VELOCITY PROFILES

RUN	AOA	X/C	Re	VEL	U-EDGE	δ^*/C	Θ/C	Y-STAG/C	Y-SEP/C
	(deg)		$x10^{-6}$	(ft/s)	(ft/s)	$x10^3$	$x10^3$		
236	-0.15	0.00	1.46	131.7	171.7	0.02146	0.42626	0.014721	0.020143
238	-0.15	-0.02	1.46	131.7	166.9	0.00950	0.35212	0.006662	0.008399
239	-0.15	0.02	1.46	131.7	170.0	0.02144	1.07510	0.012993	0.018715
240	-0.15	0.04	1.46	131.7	167.4	0.01697	0.77877	0.008640	0.014875
241	-0.15	0.06	1.42	133.5	176.1	0.01214	1.79805	0.004461	0.008394
242	-0.15	0.08	1.42	133.5	169.2	0.00737	3.05670	--	--
243	-0.15	0.10	1.44	132.7	160.6	0.00489	2.90518	--	--
244	-0.15	0.12	1.44	132.7	160.7	0.00375	2.56528	--	--
245	1.85	-0.02	1.44	132.7	184.2	0.01161	0.21754	0.008947	0.010372
246	1.85	0.00	1.44	132.7	200.5	0.01265	-0.17896	0.020703	0.025558
247	1.85	0.02	1.44	132.7	201.7	0.03009	0.46930	0.021808	0.028466
248	1.85	0.04	1.44	132.7	201.8	0.02606	0.91716	0.016222	0.023689
249	1.85	0.06	1.44	132.9	199.4	0.02066	1.88002	0.009068	0.016413
250	1.85	0.08	1.44	132.5	191.8	0.01703	2.68549	0.006024	0.011304
251	1.85	0.10	1.44	132.5	185.3	0.01478	3.49155	0.004404	0.006891
252	1.85	0.12	1.44	132.5	176.7	0.01116	4.33792	--	--
254	1.85	0.14	1.51	130.0	167.3	0.00835	4.28289	--	--
255	1.85	0.16	1.51	130.0	165.5	0.00704	4.42153	--	--
257	3.85	-0.02	1.51	130.0	180.0	0.01041	0.27493	0.008068	0.009076
258	3.85	0.00	1.51	130.0	202.4	0.02907	0.14864	0.022242	0.027926
262	3.85	0.02	1.54	129.0	200.0	0.03682	0.57272	--	--
263	3.85	0.04	1.53	129.3	197.9	0.03195	1.15141	0.019096	0.029356
264	3.85	0.06	1.53	129.3	197.6	0.03110	1.91804	0.018119	0.027221
265	3.85	0.08	1.53	129.3	198.2	0.02875	2.72787	0.012555	0.022697
267	3.85	0.10	1.49	130.6	212.3	0.02849	3.10515	0.012515	0.021727
268	3.85	0.12	1.49	130.6	208.9	0.02717	3.90636	0.009639	0.018506
269	3.85	0.14	1.49	130.6	205.6	0.02418	4.80094	0.007583	0.012813
270	3.85	0.16	1.49	130.6	197.4	0.02072	5.57149	0.002420	0.004897
271	3.85	0.18	1.49	130.6	192.9	0.01939	6.21330	--	--
272	3.85	0.20	1.49	130.6	186.8	0.01797	6.96573	--	--
273	3.85	0.22	1.49	130.6	183.3	0.01687	7.44755	--	--
274	3.85	0.30	1.49	130.6	175.4	0.01279	7.94107	--	--
275	3.85	0.40	1.49	130.6	169.5	0.01223	8.40160	--	--
276	3.85	0.50	1.49	130.6	166.5	0.01297	9.47147	--	--

NACA 0012 MODEL NO. 2 - CLEAN CONFIGURATION

RUN	$ALPHA_u$ (deg)	ALPHA (deg)	CL_u	CL	CD_u	CD	CM_u	CM	MACH	Re $x10^{-6}$
364	0.00	0.00	-0.005	-0.005	0.0080	0.0078	0.0004	0.0003	0.126	1.465
365	0.00	0.00	-0.003	-0.003	0.0078	0.0076	0.0006	0.0005	0.126	1.484
366	1.00	1.03	0.101	0.096	0.0080	0.0078	0.0010	0.0017	0.126	1.484
367	2.00	2.06	0.208	0.198	0.0083	0.0081	0.0010	0.0025	0.126	1.489
368	3.00	3.09	0.318	0.303	0.0085	0.0083	0.0011	0.0034	0.126	1.506
369	4.00	4.12	0.434	0.414	0.0092	0.0090	0.0023	0.0053	0.126	1.507
370	5.00	5.15	0.535	0.511	0.0095	0.0093	0.0027	0.0065	0.126	1.499
371	6.00	6.18	0.652	0.622	0.0098	0.0096	0.0010	0.0056	0.126	1.500
372	7.00	7.21	0.774	0.738	0.0101	0.0099	-0.0014	0.0041	0.126	1.499
373	8.00	8.24	0.870	0.829	0.0114	0.0111	0.0004	0.0066	0.126	1.500
374	9.00	9.27	0.962	0.917	0.0127	0.0124	0.0036	0.0105	0.126	1.501
375	10.00	10.29	1.052	1.003	0.0142	0.0139	0.0058	0.0132	0.125	1.493
376	11.00	11.32	1.134	1.080	0.0165	0.0161	0.0088	0.0168	0.126	1.497
377	12.00	12.35	1.217	1.159	0.0205	0.0200	0.0127	0.0212	0.125	1.494
378	13.00	13.37	1.279	1.216	0.0261	0.0254	0.0152	0.0240	0.125	1.494
379	14.00	14.10	0.908	0.862	0.0317	0.0308	-0.1319	-0.1228	0.118	1.407
380	15.00	15.10	0.876	0.831	0.0373	0.0362	-0.1310	-0.1220	0.117	1.388
381	16.00	16.09	0.713	0.676	0.0429	0.0416	-0.0959	-0.0887	0.117	1.394
382	12.50	12.86	1.256	1.194	0.0233	0.0227	0.0146	0.0233	0.126	1.500
384	13.50	13.87	1.298	1.234	0.0289	0.0281	0.0179	0.0268	0.126	1.497
385	4.00	4.12	0.423	0.403	0.0092	0.0090	0.0021	0.0051	0.126	1.469
386	0.00	0.00	-0.007	-0.006	0.0072	0.0070	0.0004	0.0004	0.125	1.455
387	-2.00	-2.06	-0.228	-0.217	0.0078	0.0076	-0.0005	-0.0021	0.126	1.463
388	-4.00	-4.12	-0.437	-0.417	0.0075	0.0073	-0.0037	-0.0067	0.125	1.452
389	-6.00	-6.18	-0.681	-0.650	0.0067	0.0065	0.0011	-0.0038	0.125	1.459
390	-8.00	-8.24	-0.900	-0.857	0.0127	0.0124	0.0009	-0.0055	0.126	1.469
391	-6.00	-6.19	-0.683	-0.651	0.0069	0.0067	0.0010	-0.0039	0.126	1.462
392	-5.00	-5.16	-0.563	-0.537	0.0077	0.0075	-0.0031	-0.0070	0.125	1.455
393	-10.00	-10.30	-1.084	-1.032	0.0170	0.0166	-0.0061	-0.0137	0.127	1.478
394	-10.00	-10.30	-1.077	-1.025	0.0170	0.0166	-0.0063	-0.0139	0.125	1.458
395	-12.00	-12.35	-1.240	-1.178	0.0272	0.0265	-0.0114	-0.0200	0.125	1.458
396	-14.00	-14.16	-1.015	-0.963	0.0374	0.0363	0.1055	0.0960	0.116	1.353
397	-15.00	-15.17	-1.057	-1.002	0.0425	0.0412	0.1087	0.0987	0.115	1.333
398	-13.00	-13.37	-1.299	-1.233	0.0323	0.0314	-0.0159	-0.0248	0.125	1.455
399	-13.50	-13.87	-1.191	-1.129	0.0349	0.0339	-0.0445	-0.0520	0.117	1.360
400	0.00	0.00	-0.015	-0.014	0.0087	0.0085	0.0003	0.0002	0.168	2.018
401	1.00	1.03	0.097	0.093	0.0081	0.0079	0.0002	0.0008	0.168	2.025
402	2.00	2.06	0.203	0.194	0.0083	0.0081	0.0006	0.0020	0.168	2.017
403	3.00	3.08	0.301	0.287	0.0086	0.0084	0.0002	0.0024	0.168	2.022
404	4.00	4.11	0.407	0.388	0.0087	0.0085	0.0008	0.0037	0.168	2.016
405	5.00	5.14	0.523	0.499	0.0098	0.0096	0.0017	0.0054	0.167	2.011
406	6.00	6.17	0.622	0.594	0.0099	0.0097	0.0004	0.0048	0.168	2.016
407	7.00	7.20	0.742	0.708	0.0099	0.0097	-0.0009	0.0045	0.167	2.009
408	7.00	7.20	0.744	0.710	0.0089	0.0087	-0.0010	0.0044	0.166	1.964
409	5.00	5.14	0.523	0.499	0.0087	0.0085	0.0012	0.0050	0.166	1.964
410	3.00	3.08	0.300	0.286	0.0083	0.0081	0.0001	0.0023	0.165	1.955
412	0.00	0.00	-0.004	-0.004	0.0076	0.0074	0.0004	0.0004	0.167	1.980
413	8.00	8.23	0.843	0.803	0.0112	0.0109	0.0001	0.0062	0.166	1.959

RUN	ALPHA$_u$ (deg)	ALPHA (deg)	CL$_u$	CL	CD$_u$	CD	CM$_u$	CM	MACH	Re x10^{-6}
414	-2.00	-2.06	-0.224	-0.213	0.0071	0.0069	0.0000	-0.0016	0.167	1.970
415	-2.00	-2.06	-0.222	-0.212	0.0076	0.0074	0.0000	-0.0016	0.166	1.960
416	-4.00	-4.12	-0.420	-0.401	0.0082	0.0080	-0.0014	-0.0044	0.167	1.970
417	-6.00	-6.18	-0.646	-0.616	0.0085	0.0083	-0.0015	-0.0061	0.168	1.981
418	-8.00	-8.24	-0.868	-0.827	0.0114	0.0111	0.0003	-0.0059	0.167	1.974
420	9.00	9.26	0.929	0.886	0.0119	0.0116	0.0023	0.0089	0.165	1.948
421	10.00	10.28	1.014	0.967	0.0140	0.0137	0.0048	0.0120	0.165	1.948
422	11.00	11.31	1.098	1.046	0.0158	0.0154	0.0069	0.0146	0.164	1.942
423	12.00	12.33	1.184	1.127	0.0184	0.0179	0.0093	0.0176	0.164	1.940
425	13.00	13.36	1.254	1.193	0.0220	0.0214	0.0116	0.0204	0.163	1.935
426	14.00	14.15	0.965	0.917	0.0256	0.0249	-0.1052	-0.0963	0.148	1.749
427	13.50	13.68	1.034	0.983	0.0238	0.0232	-0.0942	-0.0850	0.151	1.788
428	-10.00	-10.29	-1.035	-0.986	0.0165	0.0161	-0.0040	-0.0113	0.166	1.958
429	-10.00	-10.29	-1.034	-0.985	0.0165	0.0161	-0.0036	-0.0109	0.166	1.960
430	-12.00	-12.34	-1.201	-1.142	0.0227	0.0221	-0.0100	-0.0183	0.166	1.957
431	-14.00	-14.20	-1.110	-1.054	0.0289	0.0281	0.0919	0.0822	0.153	1.800
432	-13.00	-13.36	-1.267	-1.205	0.0258	0.0251	-0.0120	-0.0208	0.166	1.955
433	-13.50	-13.87	-1.292	-1.228	0.0274	0.0267	-0.0129	-0.0218	0.165	1.951

NACA 0012 MODEL NO. 2 - ICED CONFIGURATION

RUN	ALPHA$_u$ (deg)	ALPHA (deg)	CL$_u$	CL	CD$_u$	CD	CM$_u$	CM	MACH	Re x10^{-6}
434	0.00	-0.02	-0.039	-0.037	0.0282	0.0274	-0.0106	-0.0106	0.127	1.476
435	4.00	4.12	0.381	0.361	0.0399	0.0387	0.0134	0.0158	0.127	1.467
436	4.00	4.12	0.385	0.364	0.0401	0.0389	0.0140	0.0164	0.123	1.421
437	4.00	4.12	0.380	0.361	0.0401	0.0389	0.0147	0.0171	0.123	1.420
438	4.00	4.12	0.380	0.361	0.0390	0.0379	0.0135	0.0159	0.123	1.421
439	0.00	-0.02	-0.043	-0.041	0.0258	0.0251	-0.0103	-0.0104	0.124	1.428
440	1.00	1.01	0.070	0.066	0.0261	0.0254	-0.0056	-0.0050	0.124	1.429
441	2.00	2.05	0.176	0.167	0.0283	0.0275	0.0007	0.0019	0.124	1.426
442	3.00	3.08	0.274	0.260	0.0333	0.0324	0.0066	0.0084	0.124	1.457
443	4.00	4.12	0.380	0.360	0.0405	0.0393	0.0144	0.0167	0.123	1.455
444	5.00	5.15	0.478	0.452	0.0537	0.0520	0.0177	0.0207	0.123	1.452
445	6.00	6.16	0.553	0.521	0.0763	0.0735	0.0075	0.0112	0.122	1.443
446	7.00	7.14	0.601	0.561	0.1141	0.1092	-0.0252	-0.0201	0.121	1.431
447	8.00	8.10	0.577	0.535	0.1519	0.1442	-0.0549	-0.0485	0.121	1.438
448	9.00	9.07	0.521	0.479	0.1897	0.1787	-0.0704	-0.0633	0.120	1.429
449	0.00	-0.02	-0.038	-0.036	0.0270	0.0263	-0.0095	-0.0096	0.124	1.483
450	-2.00	-2.09	-0.251	-0.238	0.0345	0.0335	-0.0172	-0.0187	0.124	1.482
451	-4.00	-4.14	-0.444	-0.420	0.0494	0.0479	-0.0194	-0.0220	0.123	1.477
452	-4.00	-4.14	-0.443	-0.420	0.0503	0.0487	-0.0203	-0.0230	0.123	1.406
453	-6.00	-6.13	-0.577	-0.544	0.0649	0.0627	0.0218	0.0171	0.121	1.392
454	-8.00	-8.08	-0.516	-0.486	0.0798	0.0769	0.0553	0.0500	0.120	1.379
455	-7.00	-7.11	-0.547	-0.515	0.0724	0.0698	0.0332	0.0284	0.120	1.377
456	-6.00	-6.13	-0.580	-0.547	0.0649	0.0627	0.0232	0.0185	0.121	1.389
457	-5.00	-5.15	-0.536	-0.505	0.0686	0.0662	-0.0043	-0.0079	0.122	1.402
458	0.00	-0.02	-0.043	-0.041	0.0272	0.0265	-0.0101	-0.0102	0.161	1.883
459	2.00	2.05	0.167	0.159	0.0287	0.0279	0.0008	0.0020	0.161	1.880
460	4.00	4.11	0.364	0.345	0.0417	0.0405	0.0135	0.0158	0.160	1.870

RUN	ALPHA$_u$ (deg)	ALPHA (deg)	CL$_u$	CL	CD$_u$	CD	CM$_u$	CM	MACH	Re x10^{-6}
461	6.00	6.15	0.535	0.504	0.0769	0.0741	0.0052	0.0088	0.157	1.840
462	8.00	8.11	0.575	0.537	0.1121	0.1073	-0.0443	-0.0387	0.154	1.798
463	7.00	7.12	0.568	0.532	0.0945	0.0908	-0.0294	-0.0244	0.155	1.815
464	9.00	9.06	0.489	0.455	0.1297	0.1237	-0.0679	-0.0618	0.152	1.775
465	-2.00	-2.08	-0.238	-0.226	0.0342	0.0332	-0.0178	-0.0192	0.160	1.875
466	-2.00	-2.09	-0.239	-0.227	0.0342	0.0332	-0.0181	-0.0194	0.161	1.904
467	-4.00	-4.14	-0.424	-0.401	0.0506	0.0490	-0.0199	-0.0225	0.160	1.890
468	-6.00	-6.15	-0.546	-0.513	0.0837	0.0806	0.0038	-0.0002	0.157	1.858
469	-8.00	-8.16	-0.644	-0.601	0.1168	0.1117	0.0187	0.0135	0.154	1.826
470	-9.00	-9.16	-0.688	-0.640	0.1334	0.1271	0.0280	0.0221	0.153	1.806
471	-10.00	-10.16	-0.729	-0.676	0.1499	0.1424	0.0360	0.0294	0.150	1.777
472	-10.00	-10.05	-0.414	-0.384	0.1499	0.1424	0.0549	0.0496	0.152	1.794
473	-8.00	-8.10	-0.545	-0.508	0.1168	0.1117	0.0491	0.0435	0.153	1.814
474	-6.00	-6.13	-0.537	-0.504	0.0900	0.0865	0.0144	0.0101	0.157	1.859
475	-4.00	-4.14	-0.426	-0.403	0.0506	0.0490	-0.0185	-0.0211	0.160	1.894
476	-7.00	-7.13	-0.582	-0.546	0.0947	0.0909	0.0261	0.0211	0.156	1.840
477	0.00	-0.02	-0.048	-0.046	0.0250	0.0243	-0.0104	-0.0106	0.075	0.848
478	2.00	2.05	0.182	0.173	0.0278	0.0271	0.0002	0.0015	0.075	0.853
479	4.00	4.12	0.396	0.375	0.0392	0.0381	0.0143	0.0168	0.075	0.849
480	6.00	6.17	0.575	0.542	0.0718	0.0693	0.0122	0.0160	0.074	0.844
481	8.00	8.11	0.596	0.558	0.1044	0.1001	-0.0490	-0.0432	0.073	0.830
482	9.00	9.08	0.571	0.533	0.1210	0.1156	-0.0735	-0.0668	0.073	0.826
483	7.00	7.14	0.624	0.586	0.0880	0.0846	-0.0243	-0.0192	0.074	0.836
484	-2.00	-2.09	-0.269	-0.256	0.0302	0.0294	-0.0187	-0.0203	0.075	0.849
485	-4.00	-4.15	-0.470	-0.445	0.0477	0.0462	-0.0208	-0.0237	0.075	0.845
486	-6.00	-6.14	-0.603	-0.566	0.0839	0.0807	0.0216	0.0167	0.074	0.834
487	-8.00	-8.07	-0.528	-0.494	0.1044	0.1001	0.0651	0.0592	0.073	0.826
488	-7.00	-7.10	-0.581	-0.546	0.0880	0.0846	0.0527	0.0470	0.074	0.833
489	-5.00	-5.17	-0.567	-0.535	0.0669	0.0646	-0.0094	-0.0132	0.074	0.842
490	0.00	-0.03	-0.050	-0.047	0.0250	0.0243	-0.0105	-0.0107	0.075	0.862
491	2.00	2.05	0.177	0.169	0.0278	0.0271	0.0011	0.0023	0.075	0.861
492	4.00	4.12	0.398	0.378	0.0392	0.0381	0.0143	0.0168	0.074	0.857
493	6.00	6.17	0.583	0.549	0.0718	0.0693	0.0117	0.0155	0.074	0.851
494	-4.00	-4.15	-0.469	-0.444	0.0477	0.0462	-0.0210	-0.0238	0.074	0.856
495	-2.00	-2.09	-0.258	-0.245	0.0302	0.0294	-0.0196	-0.0211	0.075	0.861
500	0.00	0.00	-0.011	-0.010	0.0078	0.0076	0.0006	0.0005	0.075	0.872
501	2.00	2.06	0.213	0.203	0.0077	0.0075	0.0013	0.0028	0.075	0.873
502	4.00	4.12	0.435	0.415	0.0088	0.0086	0.0030	0.0060	0.076	0.875
503	6.00	6.19	0.691	0.659	0.0089	0.0087	-0.0026	0.0024	0.076	0.876
504	8.00	8.24	0.888	0.846	0.0129	0.0126	0.0021	0.0084	0.076	0.875
505	10.00	10.30	1.061	1.010	0.0165	0.0161	0.0086	0.0160	0.076	0.876
506	10.00	10.30	1.061	1.010	0.0169	0.0165	0.0092	0.0166	0.076	0.876
507	12.00	12.34	1.189	1.131	0.0244	0.0238	0.0166	0.0247	0.075	0.873
508	14.00	14.12	0.842	0.800	0.0319	0.0310	-0.1027	-0.0946	0.072	0.832
509	13.00	13.32	1.166	1.108	0.0282	0.0274	0.0011	0.0094	0.075	0.871
510	12.50	12.84	1.188	1.129	0.0263	0.0256	0.0170	0.0251	0.075	0.872
511	-2.00	-2.06	-0.233	-0.222	0.0082	0.0080	-0.0010	-0.0026	0.076	0.879
512	-4.00	-4.13	-0.452	-0.431	0.0100	0.0098	-0.0035	-0.0067	0.076	0.896
513	-6.00	-6.19	-0.714	-0.681	0.0137	0.0134	0.0061	0.0009	0.076	0.899
514	-6.00	-6.19	-0.710	-0.677	0.0133	0.0130	0.0060	0.0008	0.076	0.895

RUN	$ALPHA_u$ (deg)	ALPHA (deg)	CL_u	CL	CD_u	CD	CM_u	CM	MACH	Re $x10^{-6}$
515	4.00	4.12	0.433	0.413	0.0080	0.0078	0.0024	0.0055	0.076	0.901
516	-8.00	-8.25	-0.909	-0.866	0.0146	0.0142	-0.0029	-0.0093	0.076	0.900
517	-10.00	-10.31	-1.093	-1.040	0.0192	0.0187	-0.0097	-0.0173	0.076	0.902
518	-12.00	-12.35	-1.210	-1.150	0.0269	0.0262	-0.0163	-0.0246	0.076	0.894
519	-14.00	-14.12	-0.847	-0.804	0.0346	0.0336	0.1031	0.0949	0.073	0.858
520	-13.00	-13.32	-1.164	-1.105	0.0308	0.0300	0.0005	-0.0078	0.076	0.895
521	-12.50	-12.85	-1.197	-1.138	0.0288	0.0280	-0.0191	-0.0272	0.076	0.900

NACA 0012 MODEL NO. 2 - CLEAN CONFIGURATION
TRIP AT X/C = 0.05 (BOTH UPPER AND LOWER SURFACES)

RUN	$ALPHA_u$ (deg)	ALPHA (deg)	CL_u	CL	CD_u	CD	CM_u	CM	MACH	Re $x10^{-6}$
748	0.00	0.00	-0.006	-0.006	0.0081	0.0079	-0.0025	-0.0025	0.116	1.387
749	8.00	8.25	0.875	0.832	0.0108	0.0105	-0.0015	0.0051	0.116	1.386
750	8.00	8.25	0.880	0.837	0.0111	0.0108	-0.0025	0.0042	0.116	1.387
751	0.00	0.00	-0.006	-0.006	0.0109	0.0106	-0.0001	-0.0002	0.116	1.374
* 752	2.00	2.06	0.217	0.207	0.0111	0.0108	0.0007	0.0023	0.117	1.384
* 753	4.00	4.13	0.438	0.417	0.0115	0.0112	0.0004	0.0037	0.116	1.380
* 754	2.00	2.06	0.208	0.198	0.0110	0.0107	-0.0013	0.0003	0.117	1.385
* 755	4.00	4.12	0.430	0.409	0.0116	0.0113	-0.0012	0.0021	0.117	1.391
* 756	6.00	6.19	0.653	0.620	0.0136	0.0133	0.0006	0.0055	0.116	1.381
* 757	8.00	8.25	0.849	0.806	0.0139	0.0135	0.0045	0.0109	0.117	1.390
* 758	10.00	10.31	1.038	0.986	0.0176	0.0171	0.0083	0.0161	0.115	1.370
* 759	12.00	12.36	1.198	1.136	0.0247	0.0240	0.0139	0.0226	0.116	1.373
760	14.00	14.13	0.932	0.882	0.0318	0.0309	-0.1248	-0.1151	0.109	1.293
761	13.00	13.38	1.247	1.181	0.0299	0.0290	0.0167	0.0257	0.116	1.375
762	-4.00	-4.14	-0.463	-0.440	0.0125	0.0122	-0.0030	-0.0065	0.117	1.394
763	-8.00	-8.26	-0.856	-0.812	0.0173	0.0168	-0.0055	-0.0119	0.116	1.380
764	-13.00	-13.37	-1.190	-1.127	0.0283	0.0275	-0.0184	-0.0270	0.109	1.295
765	-14.00	-14.19	-0.939	-0.889	0.0318	0.0309	0.0728	0.0641	0.113	1.337
766	-12.00	-12.36	-1.174	-1.112	0.0285	0.0277	-0.0160	-0.0246	0.116	1.376

* NOTE: Pressure difference between transducers.

NACA 0012 MODEL NO. 2 - CLEAN CONFIGURATION
TRIP AT X/C = 0.05
TOTAL BOUNDARY LAYER PROBE VELOCITY PROFILES

RUN	AOA (deg)	X/C	Re $\times 10^{-6}$	VEL (ft/s)	U-EDGE (ft/s)	δ^*/C $\times 10^3$	Θ/C $\times 10^3$
788	3.85	0.03	1.43	131.8	151.8	3.20166	2.10189
789	3.85	0.03	1.41	130.7	151.1	3.21301	2.10328
790	3.85	0.02	1.42	131.6	163.9	2.15226	1.42940
791	3.85	0.02	1.42	131.1	163.3	2.33087	1.50410
792	3.85	0.02	1.42	131.3	162.9	2.37040	1.57792
793	3.85	0.02	1.41	130.8	162.8	2.76799	1.79168
794	3.85	0.01	1.42	131.2	162.7	1.53397	0.93361
795	3.85	0.01	1.42	131.0	163.9	1.69846	1.02513
796	3.85	0.00	1.42	131.3	194.0	0.77307	0.43989
797	3.85	0.00	1.43	132.5	194.8	0.88946	0.55715
798	-0.15	0.03	1.43	131.1	148.0	2.30661	1.57829
799	-0.15	0.03	1.43	132.4	147.9	2.28867	1.52718
801	-0.15	0.02	1.44	132.0	155.8	1.58051	1.03879
802	-0.15	0.02	1.43	130.4	155.5	1.80664	1.17000
803	-0.15	0.01	1.44	131.8	159.4	1.10019	0.67952
804	-0.15	0.01	1.44	131.6	159.4	1.24502	0.77926
805	-0.15	0.00	1.44	131.5	159.2	0.53174	0.24111
807	-0.15	0.00	1.44	131.6	159.8	0.62718	0.33051
808	-0.15	0.01	1.49	132.9	179.8	1.12362	0.65278
811	-0.15	0.02	1.48	132.8	168.2	1.72779	1.12934
812	-0.15	0.02	1.48	132.3	168.0	1.95480	1.22531
813	-0.15	0.03	1.48	132.2	155.4	2.63122	1.74612

APPENDIX B

PRESSURE DISTRIBUTIONS

PRECEDING PAGE BLANK NOT FILMED

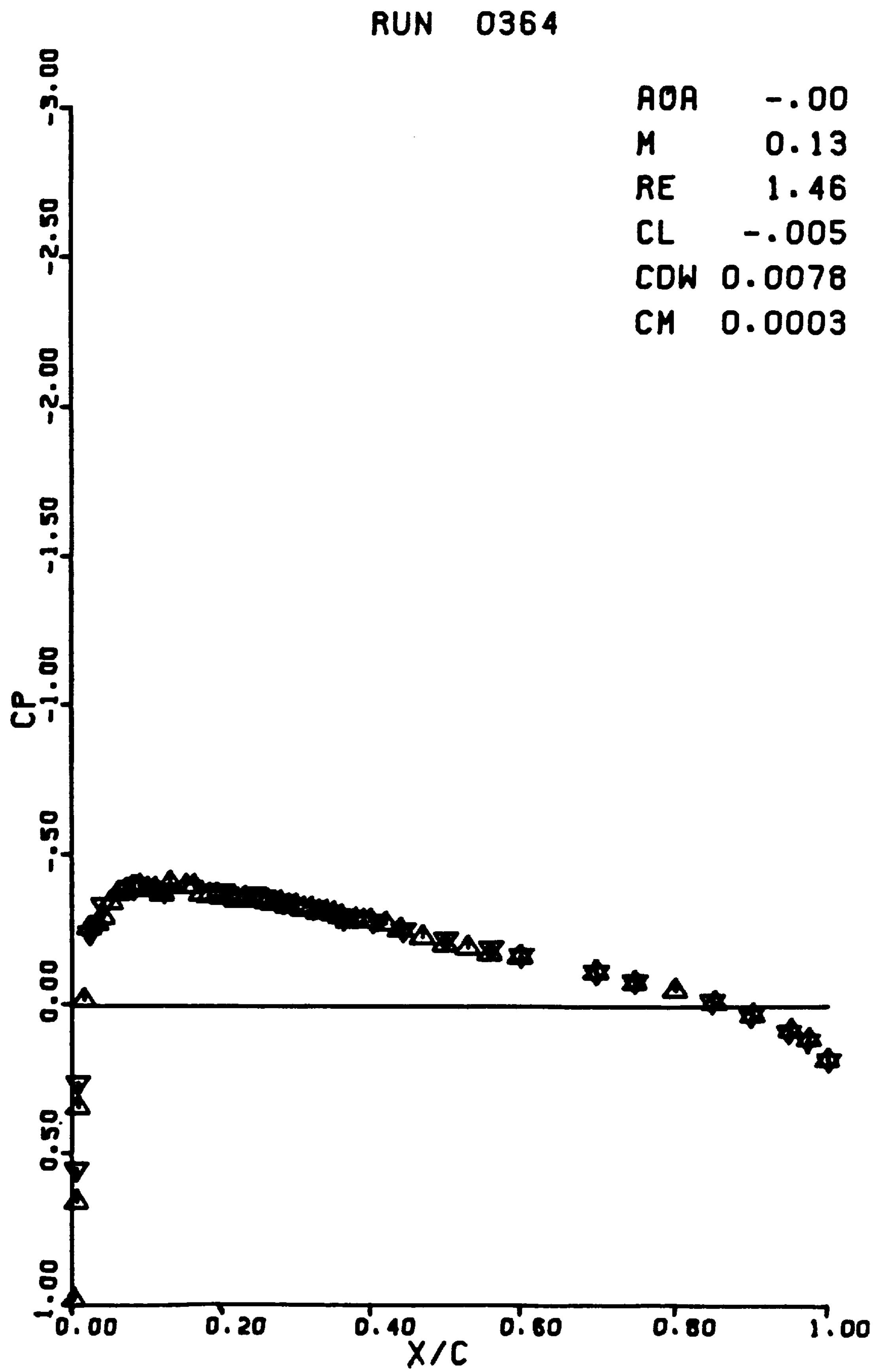

PAGE BLANK NOT FILMED

PRECEDING PAGE BLANK NOT FILMED

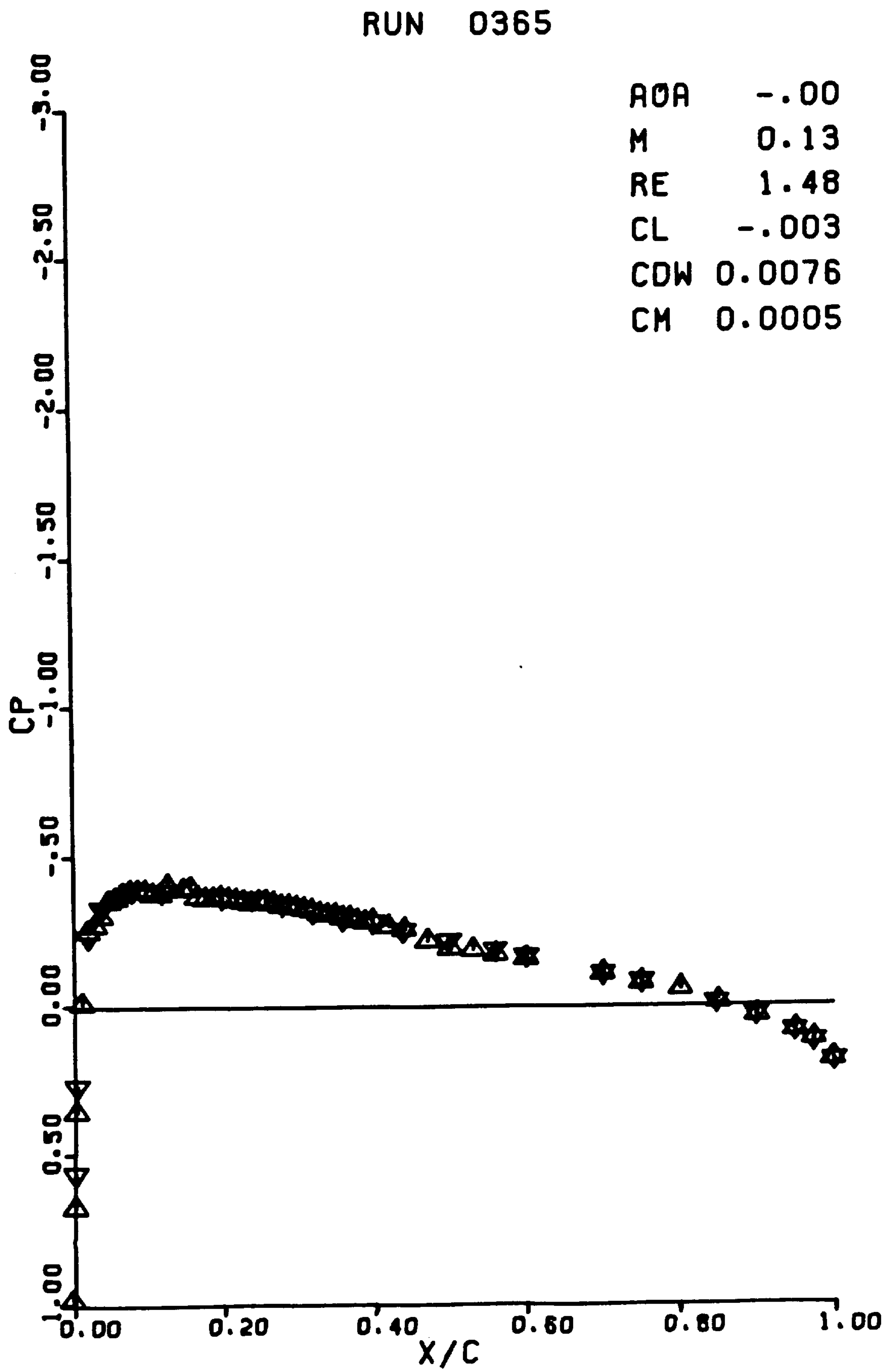
RUN 0365
AOA -.00
M 0.13
RE 1.48
CL -.003
CDW 0.0076
CM 0.0005
CP
-3.00
-2.50
-2.00
-1.50
-1.00
-.50
0.00
0.50
1.00
0.00
0.20
0.40
0.60
0.80
1.00
X/C

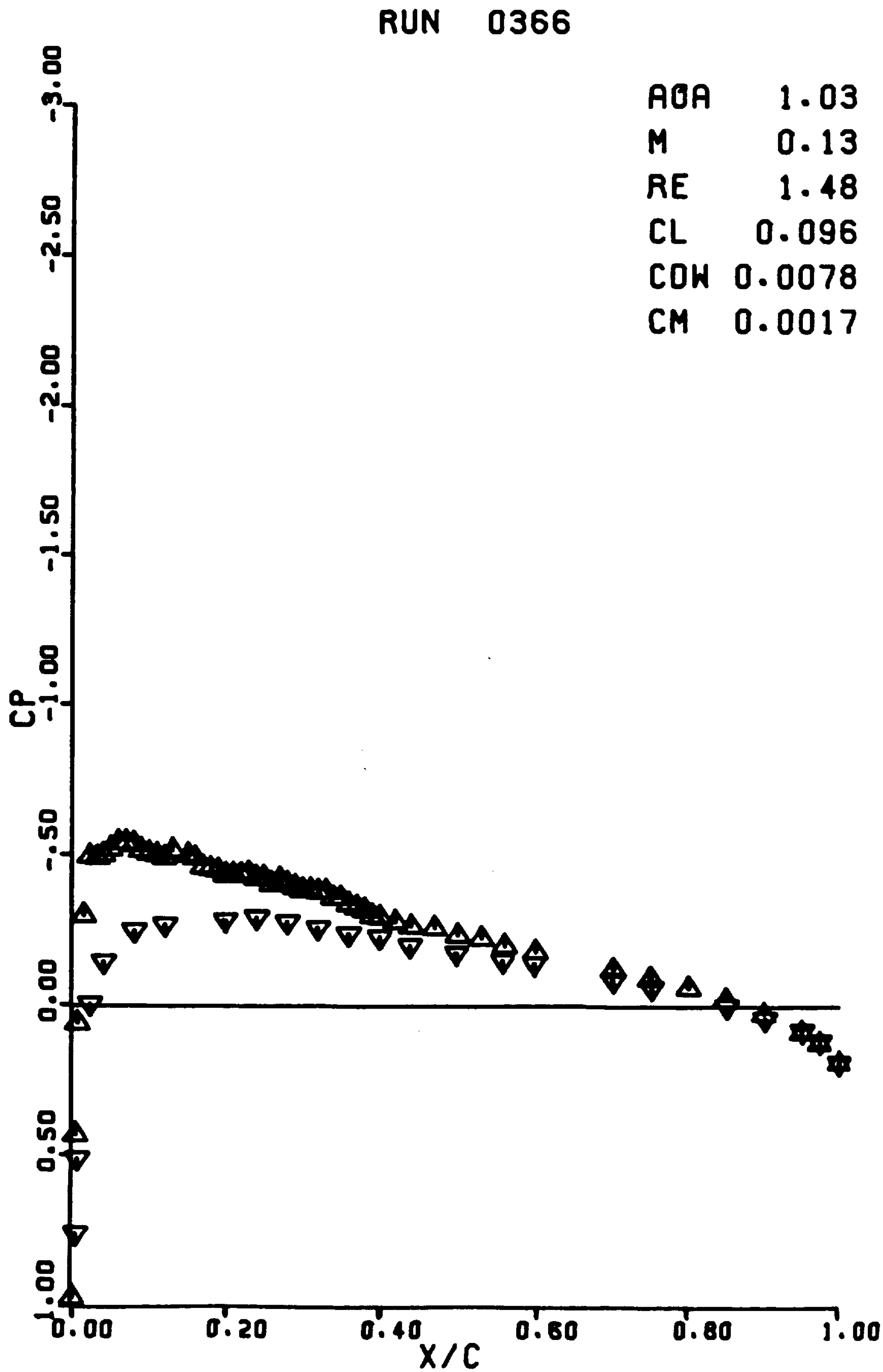
RUN 0366
AOA 1.03
M 0.13
RE 1.48
CL 0.096
CDW 0.0078
CM 0.0017
CP
-3.00
-2.50
-2.00
-1.50
-1.00
-.50
0.00
0.50
1.00
0.00
0.20
0.40
0.60
0.80
1.00
X/C

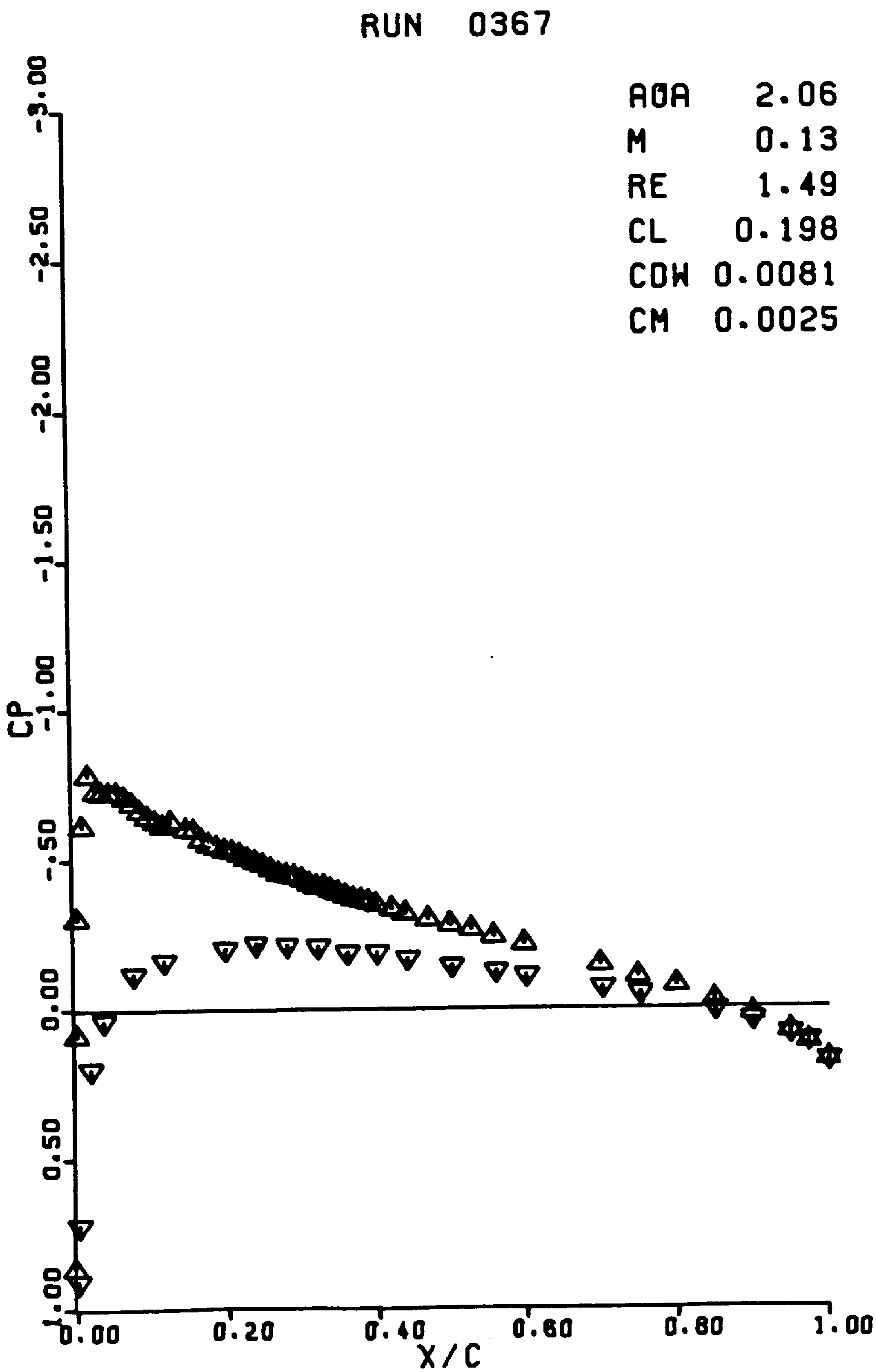
RUN 0367
AOA 2.06
M 0.13
RE 1.49
CL 0.198
CDW 0.0081
CM 0.0025
CP
-3.00
-2.50
-2.00
-1.50
-1.00
-.50
0.00
0.50
1.00
0.00
0.20
0.40
0.60
0.80
1.00
X/C

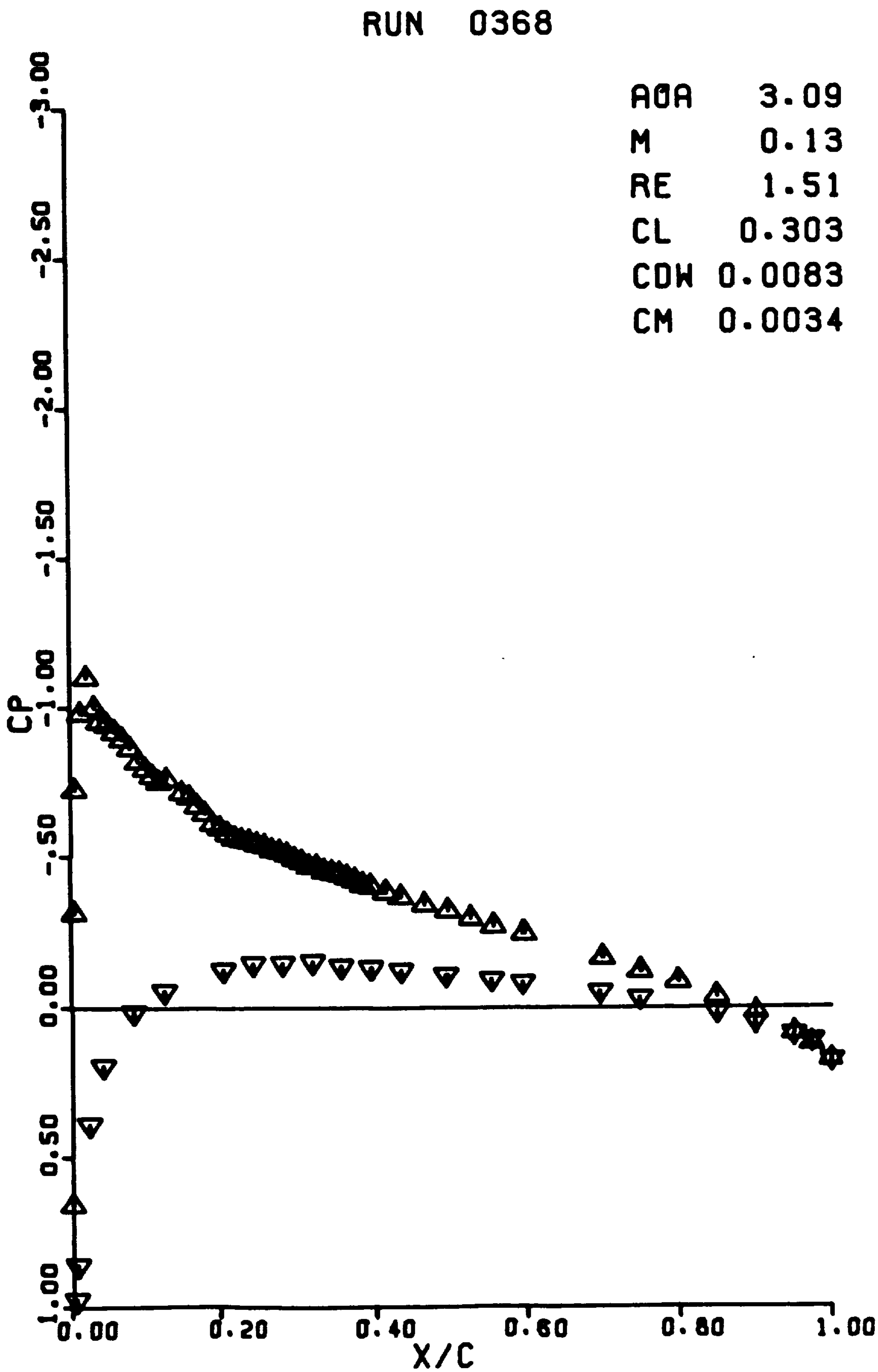
RUN 0368
AOA 3.09
M 0.13
RE 1.51
CL 0.303
CDW 0.0083
CM 0.0034
CP
-3.00
-2.50
-2.00
-1.50
-1.00
-.50
0.00
0.50
1.00
0.00
0.20
0.40
0.60
0.80
1.00
X/C

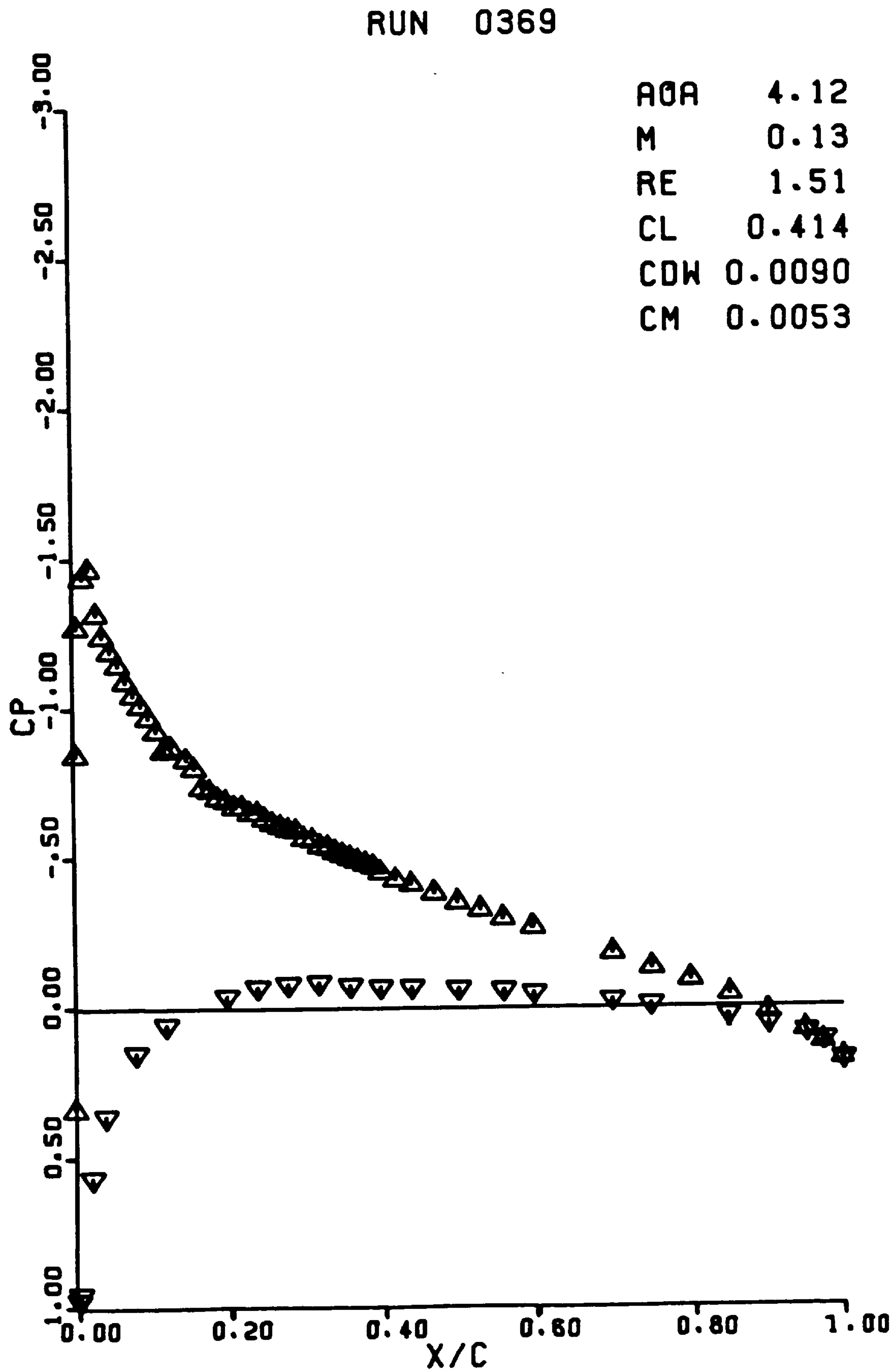

RUN 0369
AOA 4.12
M 0.13
RE 1.51
CL 0.414
CDW 0.0090
CM 0.0053
CP
-3.00
-2.50
-2.00
-1.50
-1.00
-.50
0.00
0.50
1.00
0.00
0.20
0.40
0.60
0.80
1.00
X/C

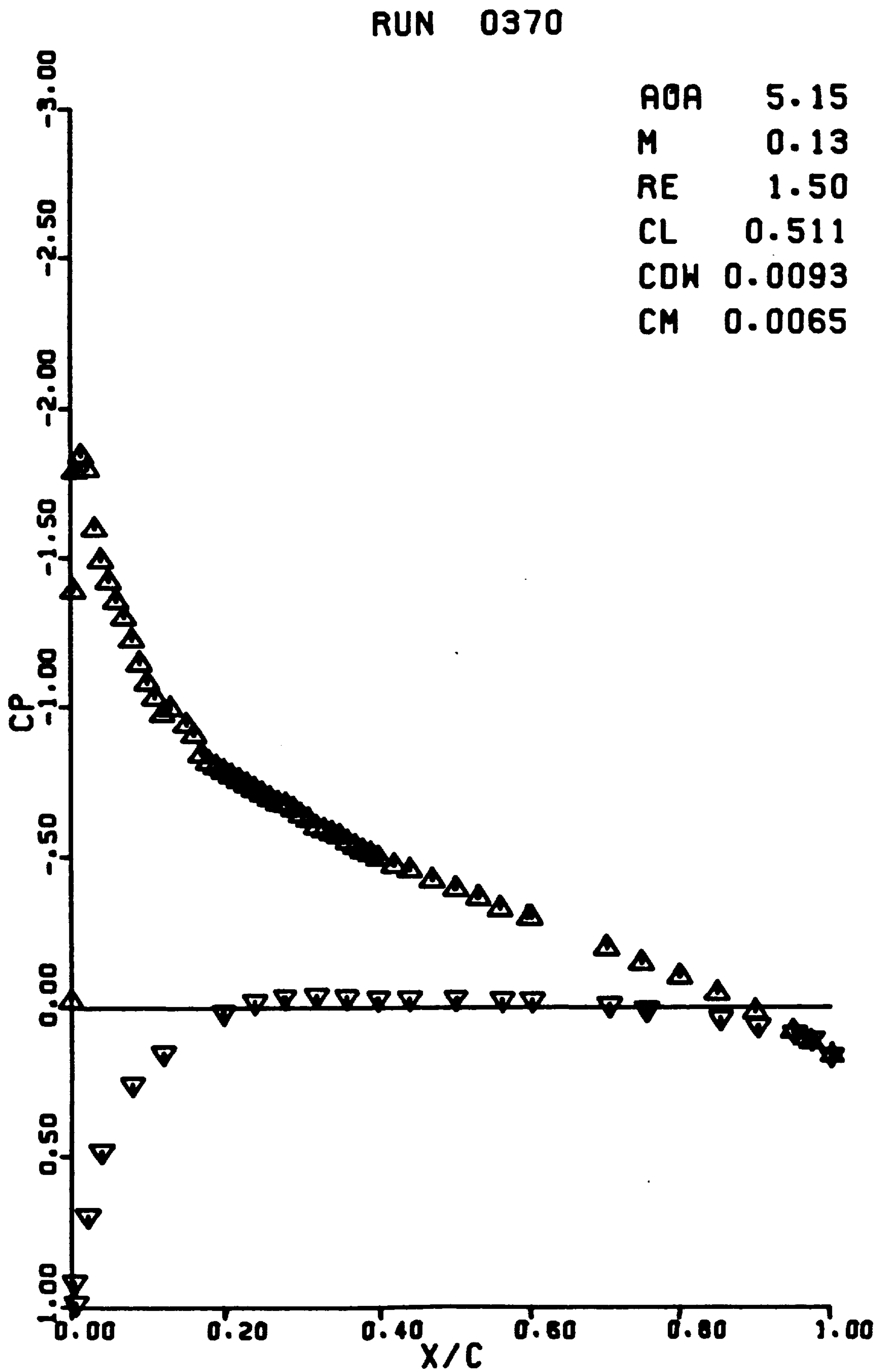
RUN 0370
AOA 5.15
M 0.13
RE 1.50
CL 0.511
CDW 0.0093
CM 0.0065
CP
-3.00
-2.50
-2.00
-1.50
-1.00
-.50
0.00
0.50
1.00
0.00
0.20
0.40
0.60
0.80
1.00
X/C

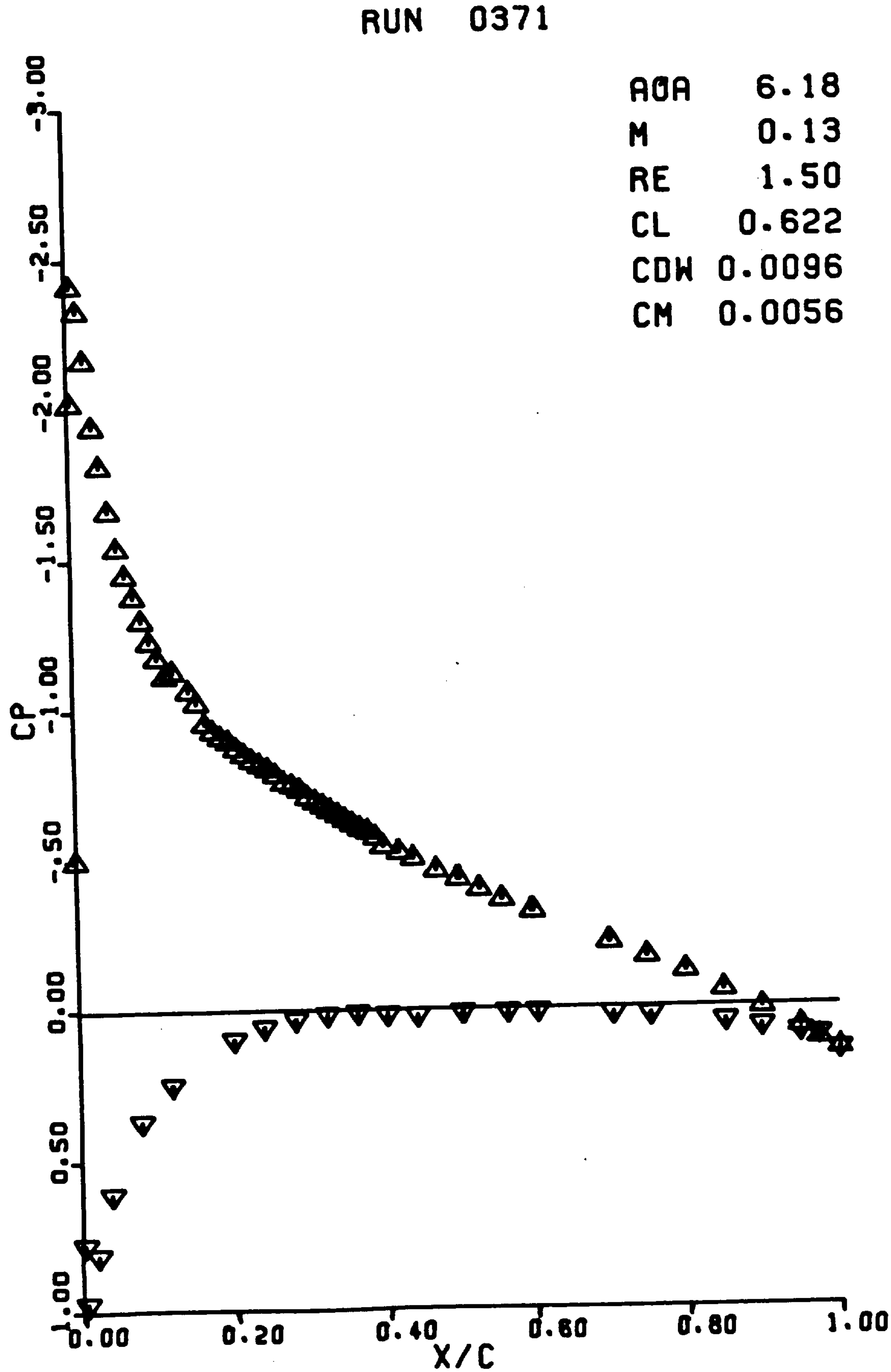
RUN 0371
AOA 6.18
M 0.13
RE 1.50
CL 0.622
CDW 0.0096
CM 0.0056
CP
-3.00
-2.50
-2.00
-1.50
-1.00
-.50
0.00
0.50
1.00
0.00
0.20
0.40
0.60
0.80
1.00
X/C

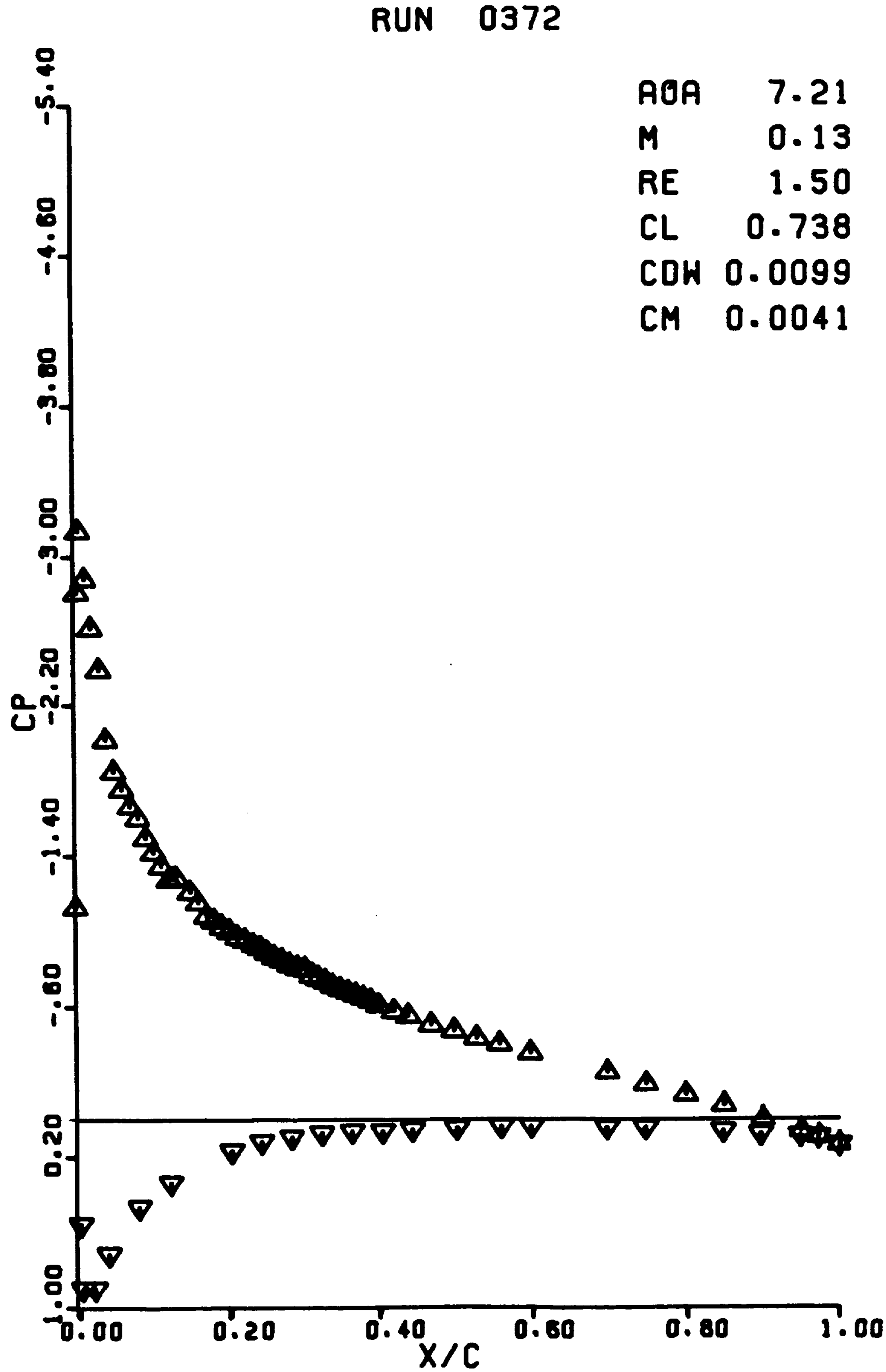

RUN 0372
AOA 7.21
M 0.13
RE 1.50
CL 0.738
CDW 0.0099
CM 0.0041
CP
-5.40
-4.60
-3.80
-3.00
-2.20
-1.40
-.60
0.20
1.00
0.00
0.20
0.40
0.60
0.80
1.00
X/C

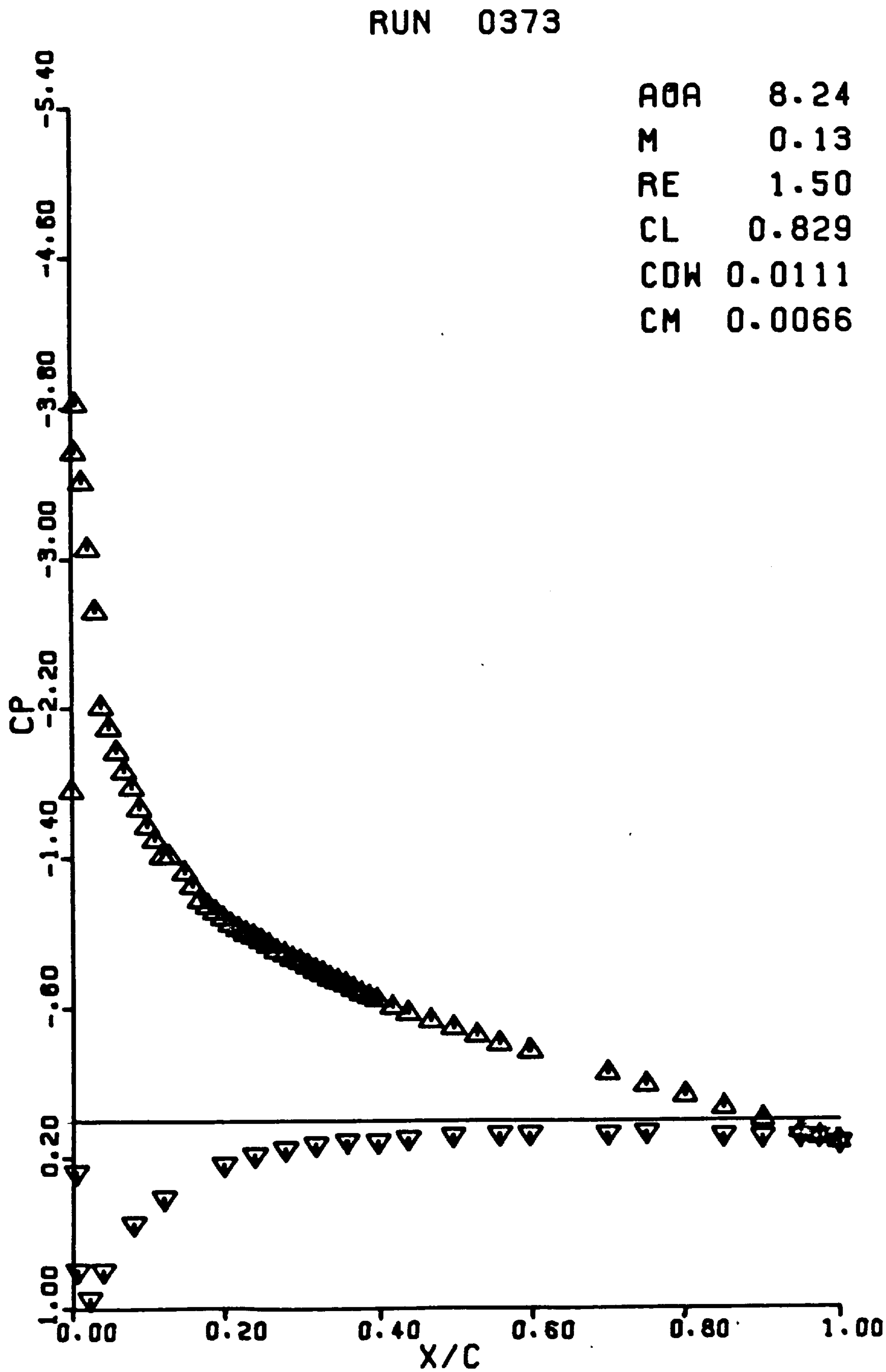
RUN 0373
AOA 8.24
M 0.13
RE 1.50
CL 0.829
CDW 0.0111
CM 0.0066
CP
-5.40
-4.60
-3.80
-3.00
-2.20
-1.40
-.60
0.20
1.00
0.00
0.20
0.40
0.60
0.80
1.00
X/C

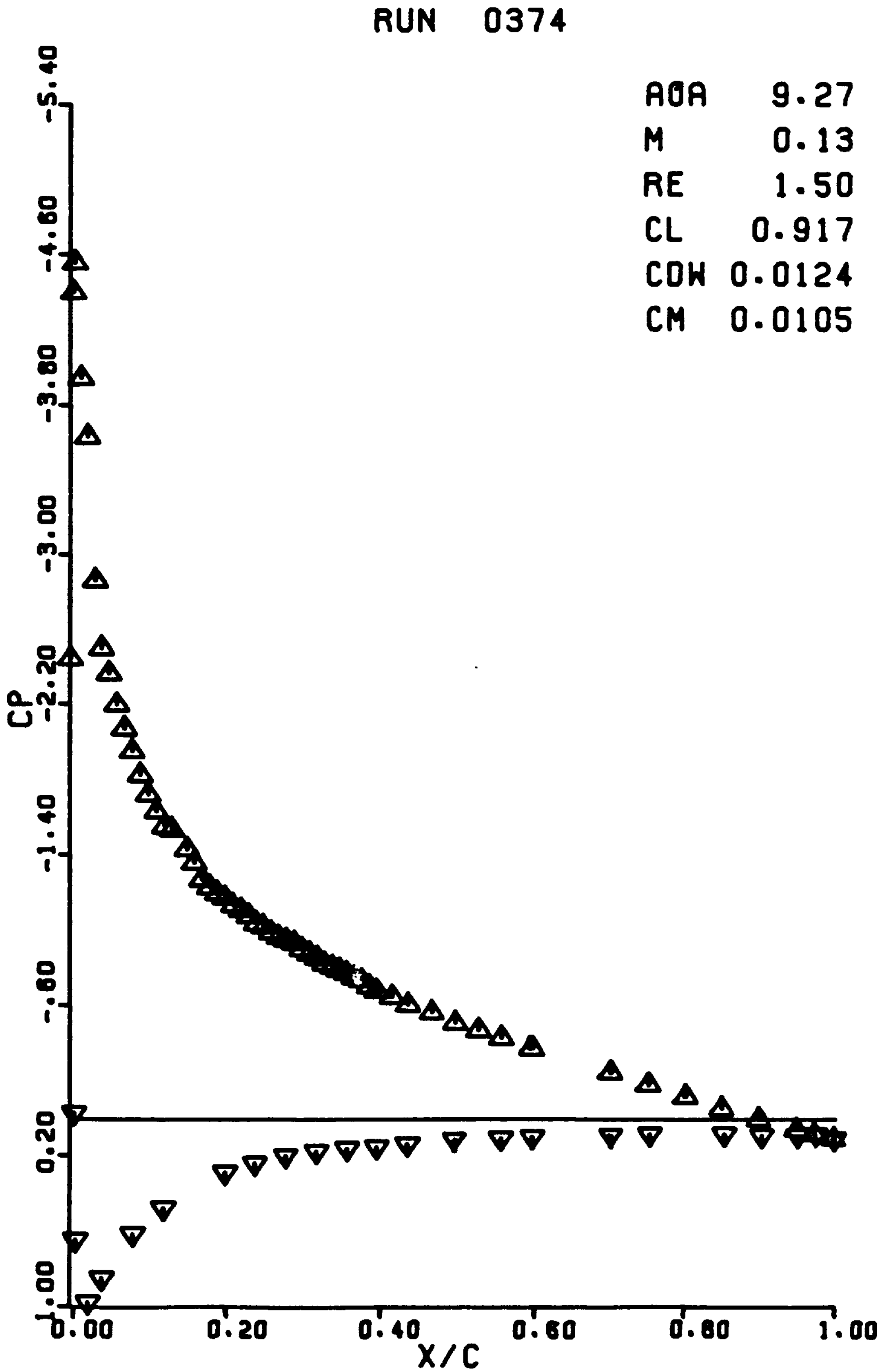
RUN 0374
AOA 9.27
M 0.13
RE 1.50
CL 0.917
CDW 0.0124
CM 0.0105
-5.40
-4.60
-3.80
-3.00
-2.20
-1.40
-.60
0.20
1.00
CP
0.00
0.20
0.40
0.60
0.80
1.00
X/C

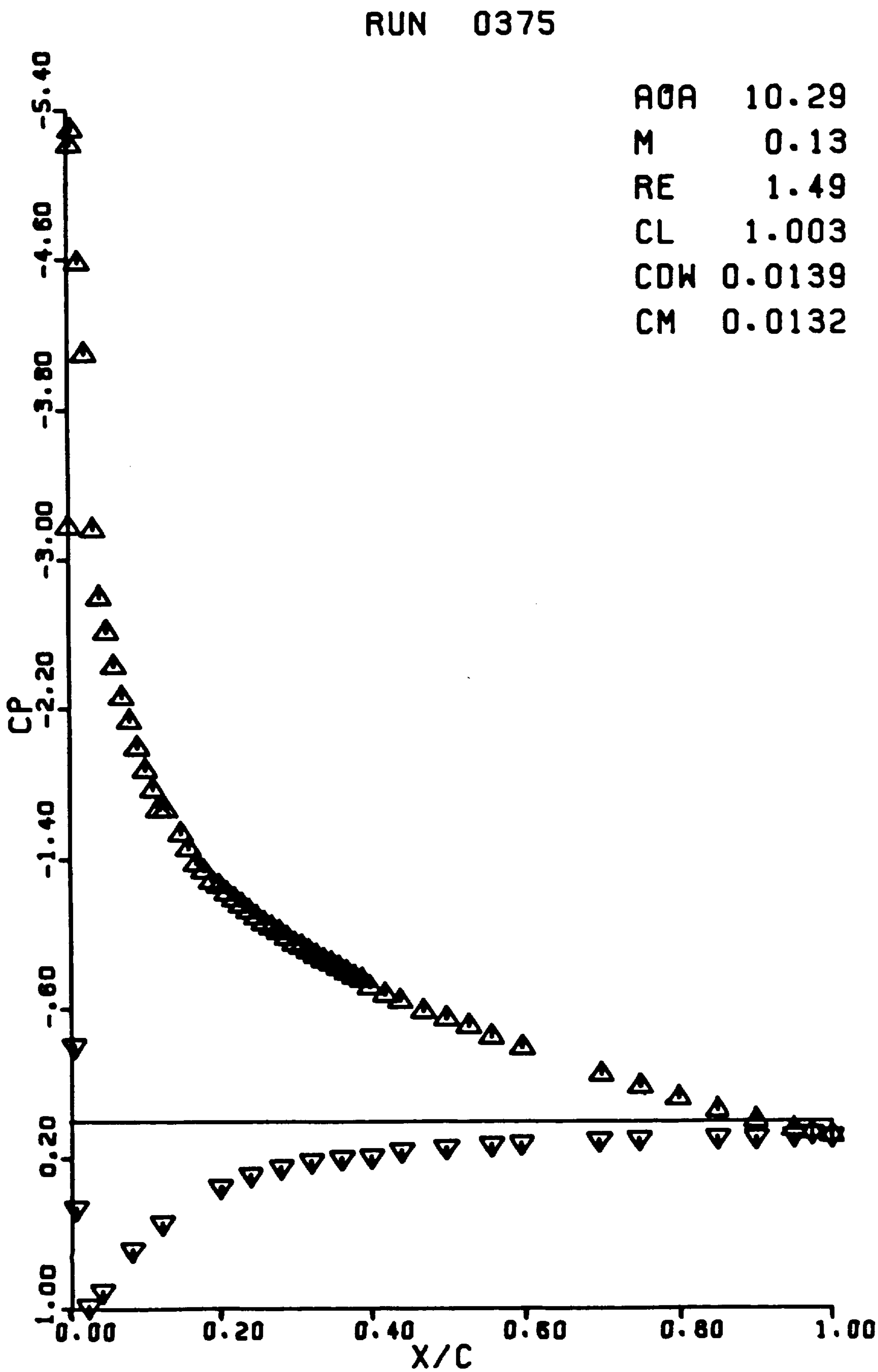
RUN 0375
AOA 10.29
M 0.13
RE 1.49
CL 1.003
CDW 0.0139
CM 0.0132
-5.40
-4.60
-3.80
-3.00
-2.20
CP
-1.40
-.60
0.20
1.00
0.00
0.20
0.40
0.60
0.80
1.00
X/C

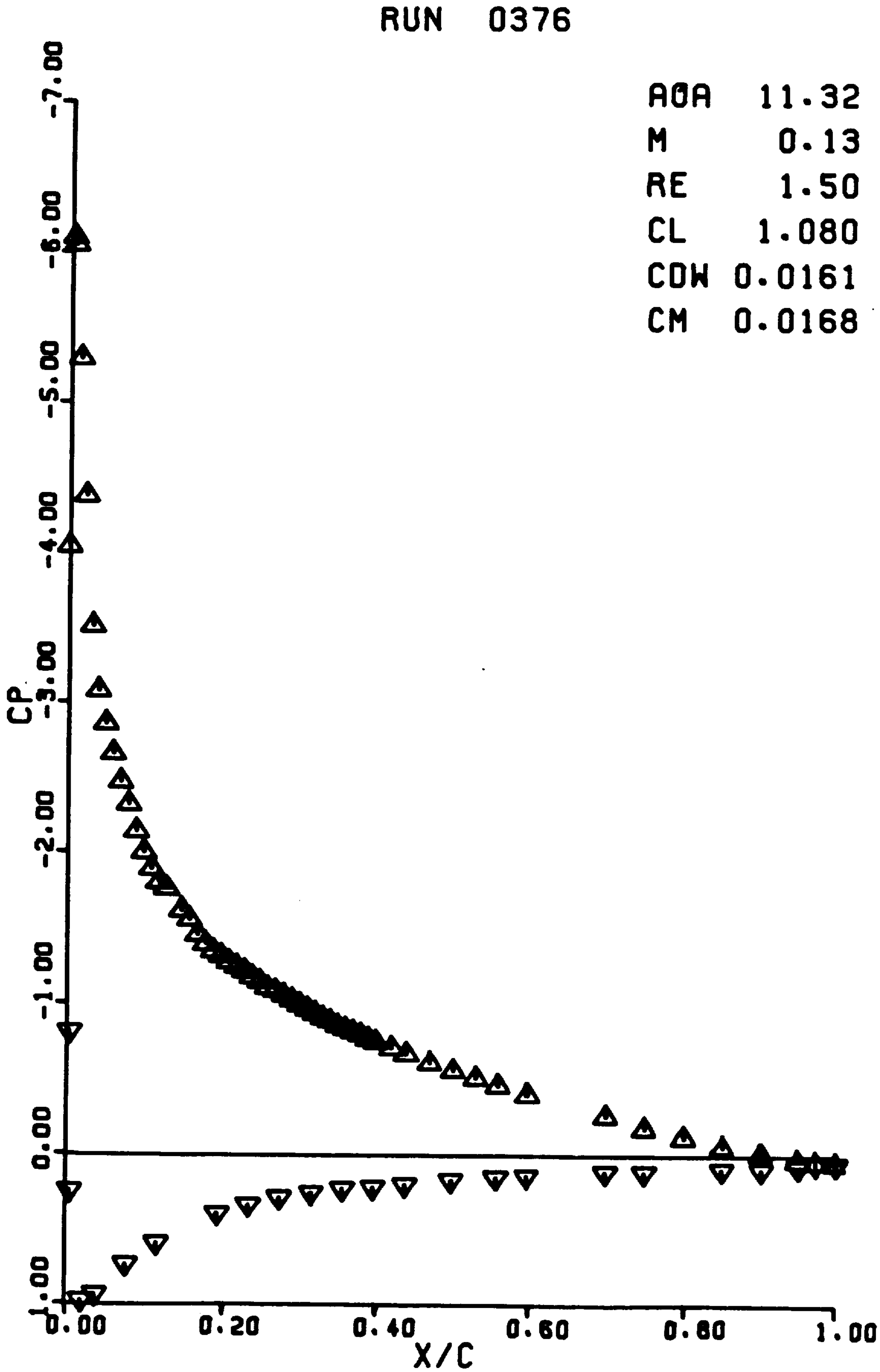
RUN 0376
AOA 11.32
M 0.13
RE 1.50
CL 1.080
CDW 0.0161
CM 0.0168
CP
-7.00
-6.00
-5.00
-4.00
-3.00
-2.00
-1.00
0.00
1.00
0.00
0.20
0.40
0.60
0.80
1.00
X/C

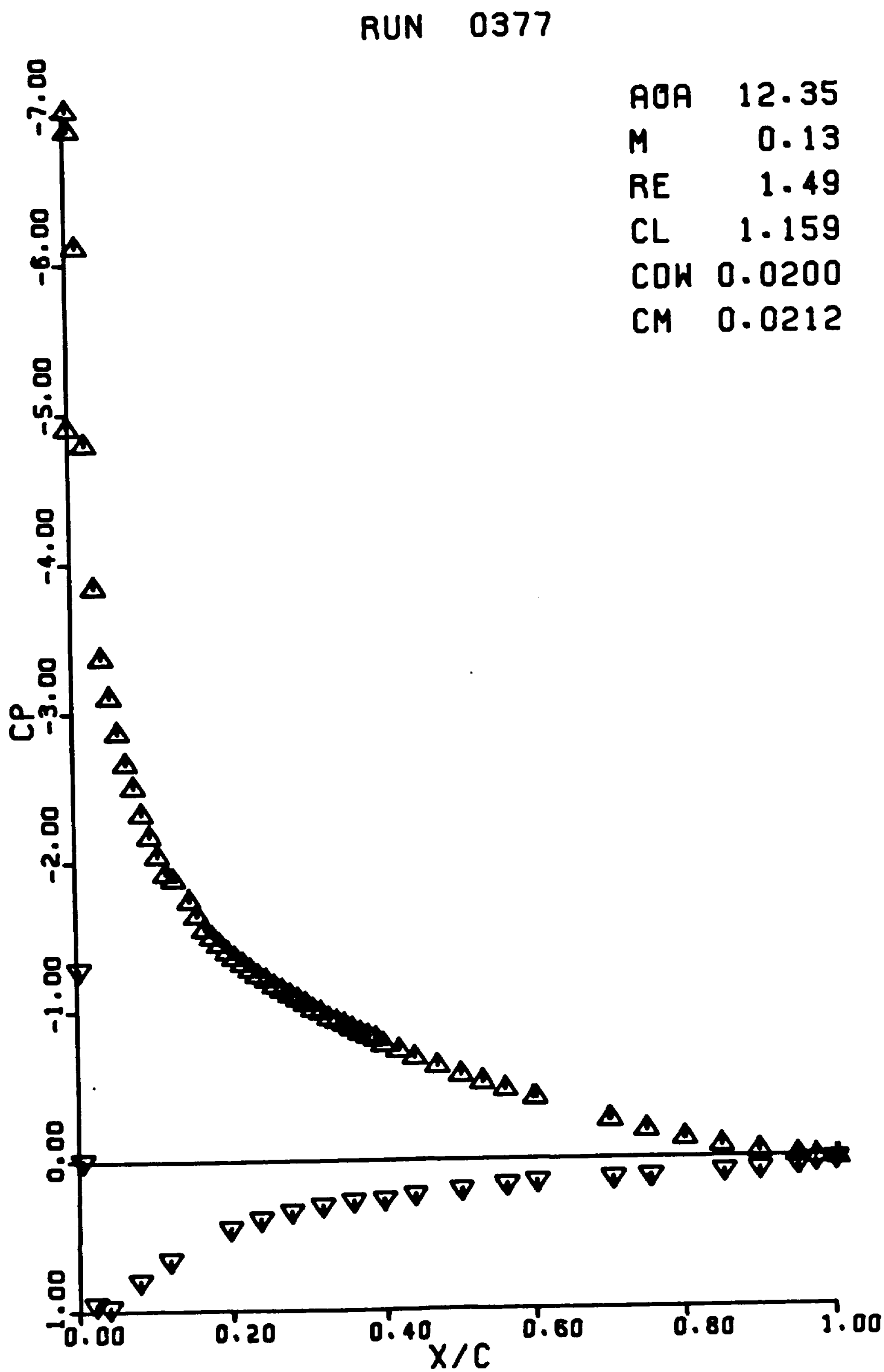

RUN 0377
AOA 12.35
M 0.13
RE 1.49
CL 1.159
CDW 0.0200
CM 0.0212
CP
-7.00
-6.00
-5.00
-4.00
-3.00
-2.00
-1.00
0.00
1.00
0.00
0.20
0.40
0.60
0.80
1.00
X/C

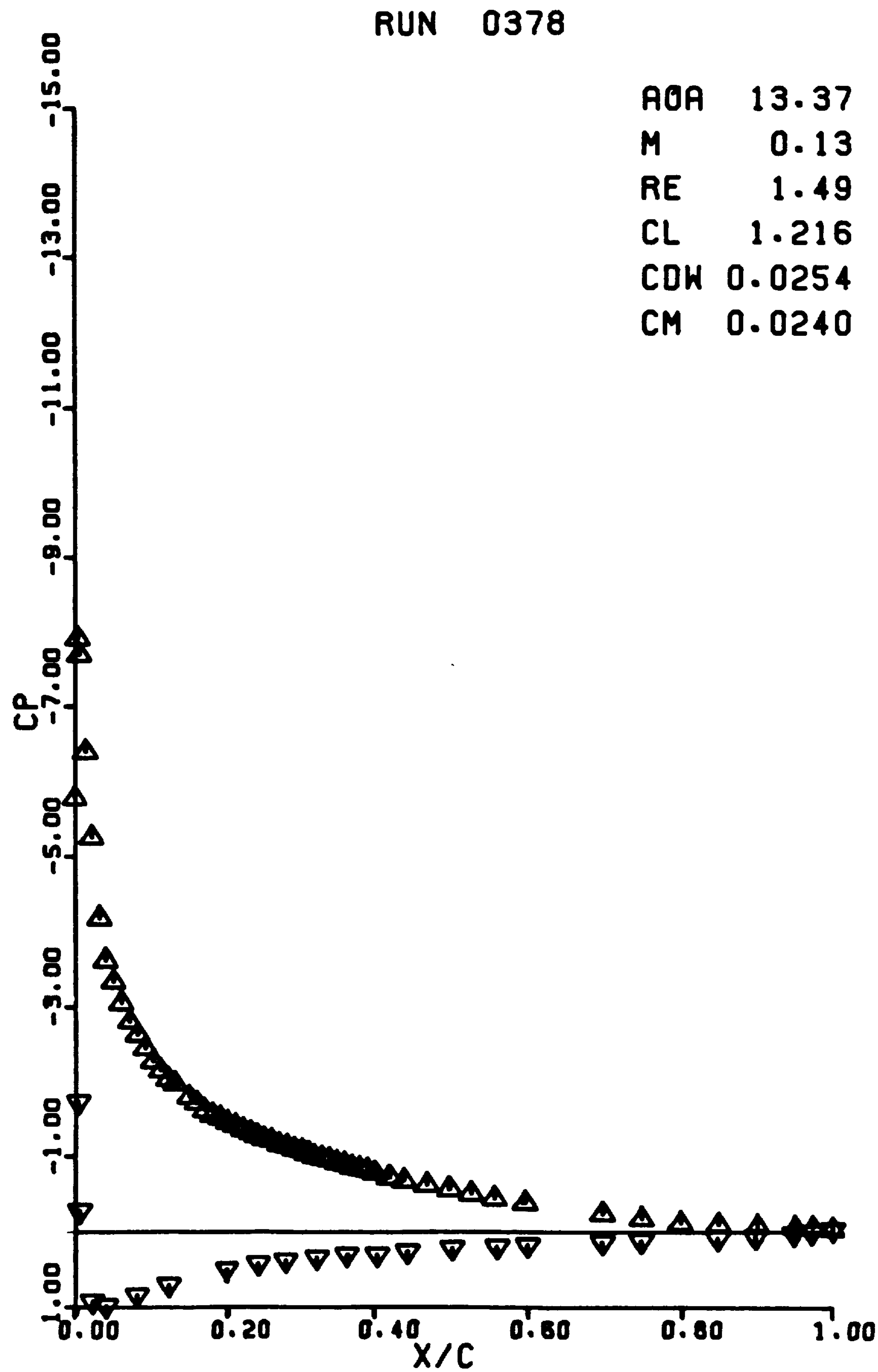

RUN 0378
AOA 13.37
M 0.13
RE 1.49
CL 1.216
CDW 0.0254
CM 0.0240
CP
-15.00
-13.00
-11.00
-9.00
-7.00
-5.00
-3.00
-1.00
1.00
0.00
0.20
0.40
0.60
0.80
1.00
X/C

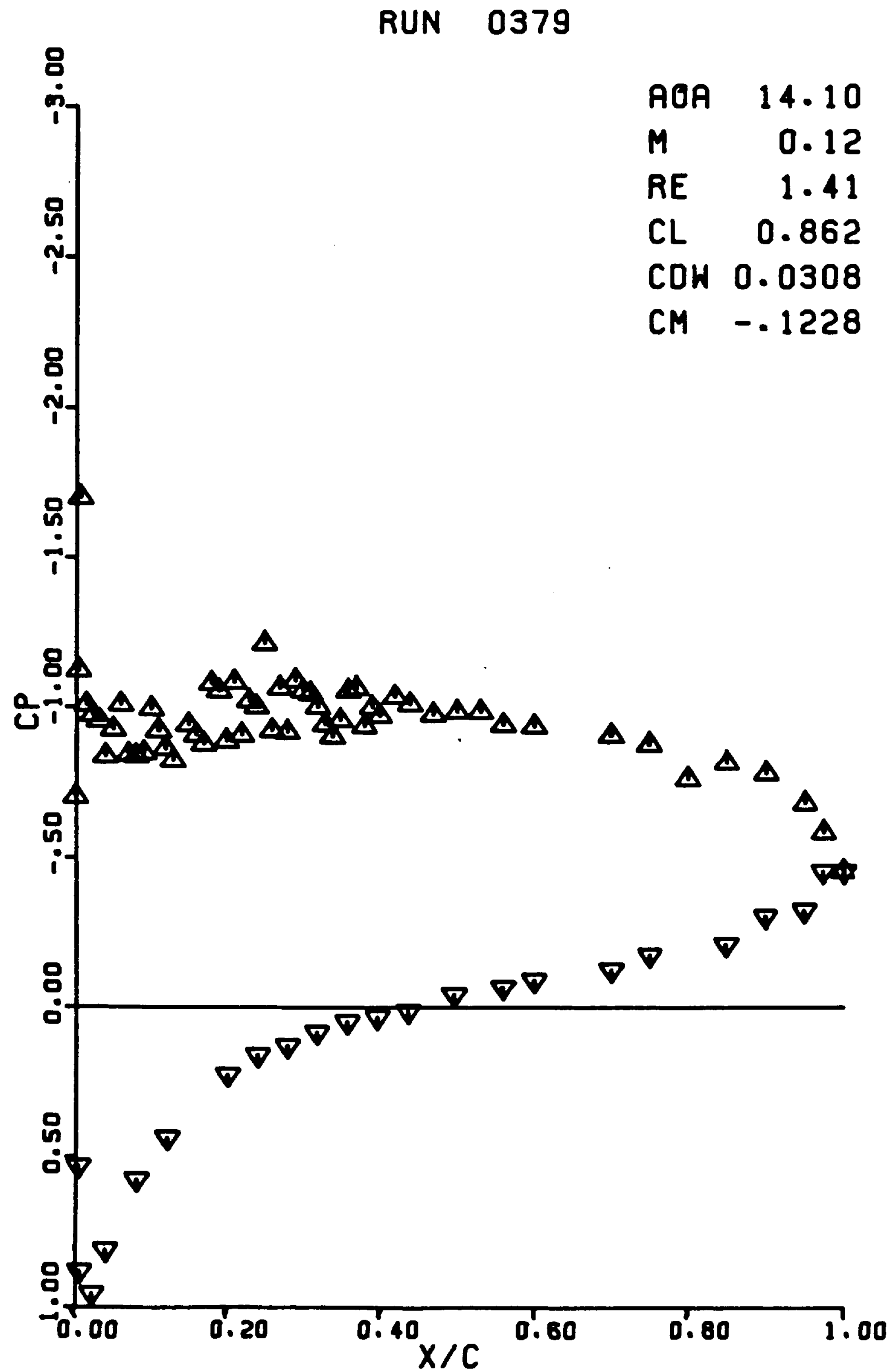
RUN 0379
AOA 14.10
M 0.12
RE 1.41
CL 0.862
CDW 0.0308
CM -.1228
CP
X/C
-3.00
-2.50
-2.00
-1.50
-1.00
-.50
0.00
0.50
1.00
0.00
0.20
0.40
0.60
0.80
1.00

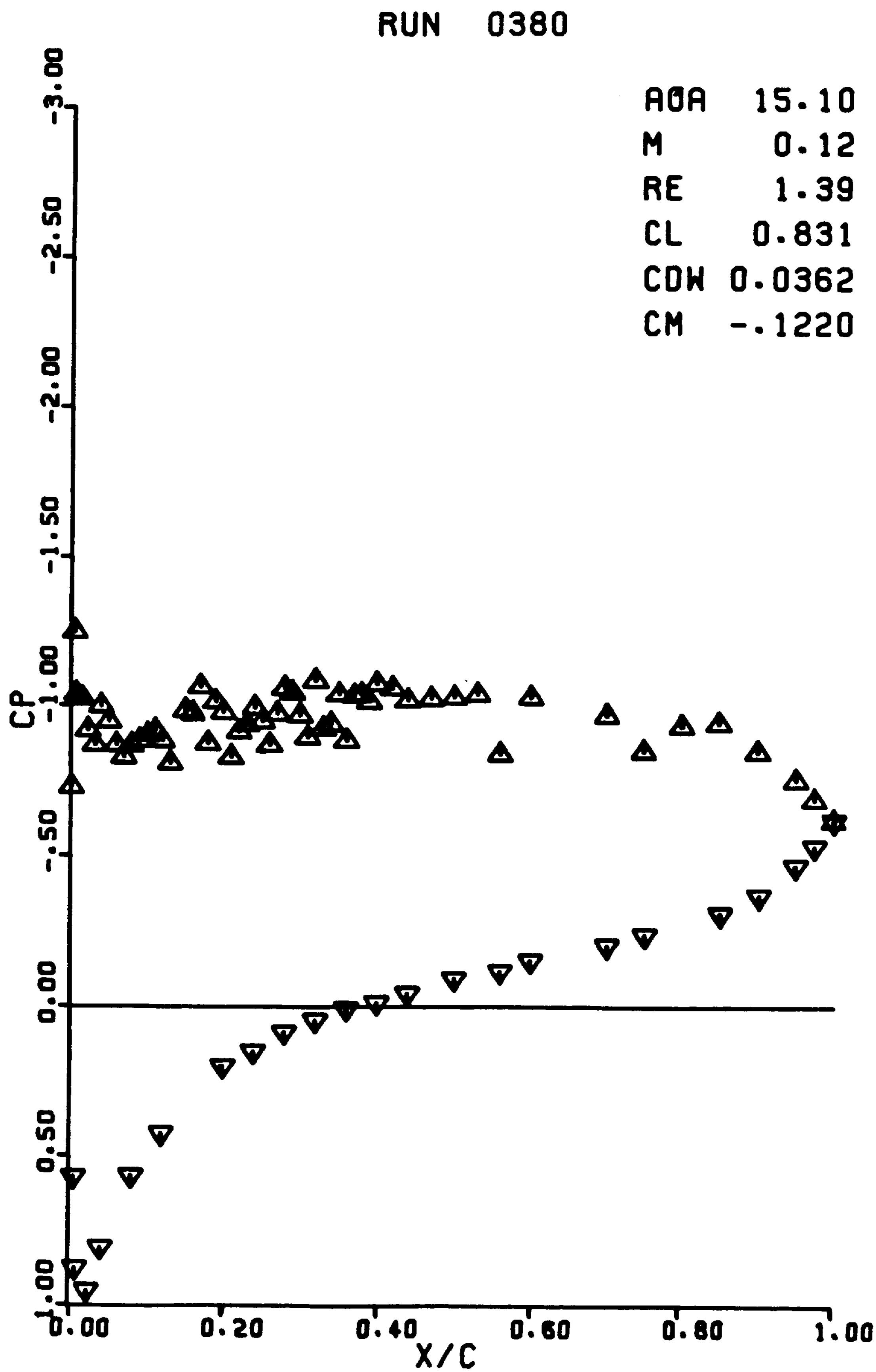

RUN 0380
AOA 15.10
M 0.12
RE 1.39
CL 0.831
CDW 0.0362
CM -.1220
CP
-3.00
-2.50
-2.00
-1.50
-1.00
-.50
0.00
0.50
1.00
0.00
0.20
0.40
0.60
0.80
1.00
X/C

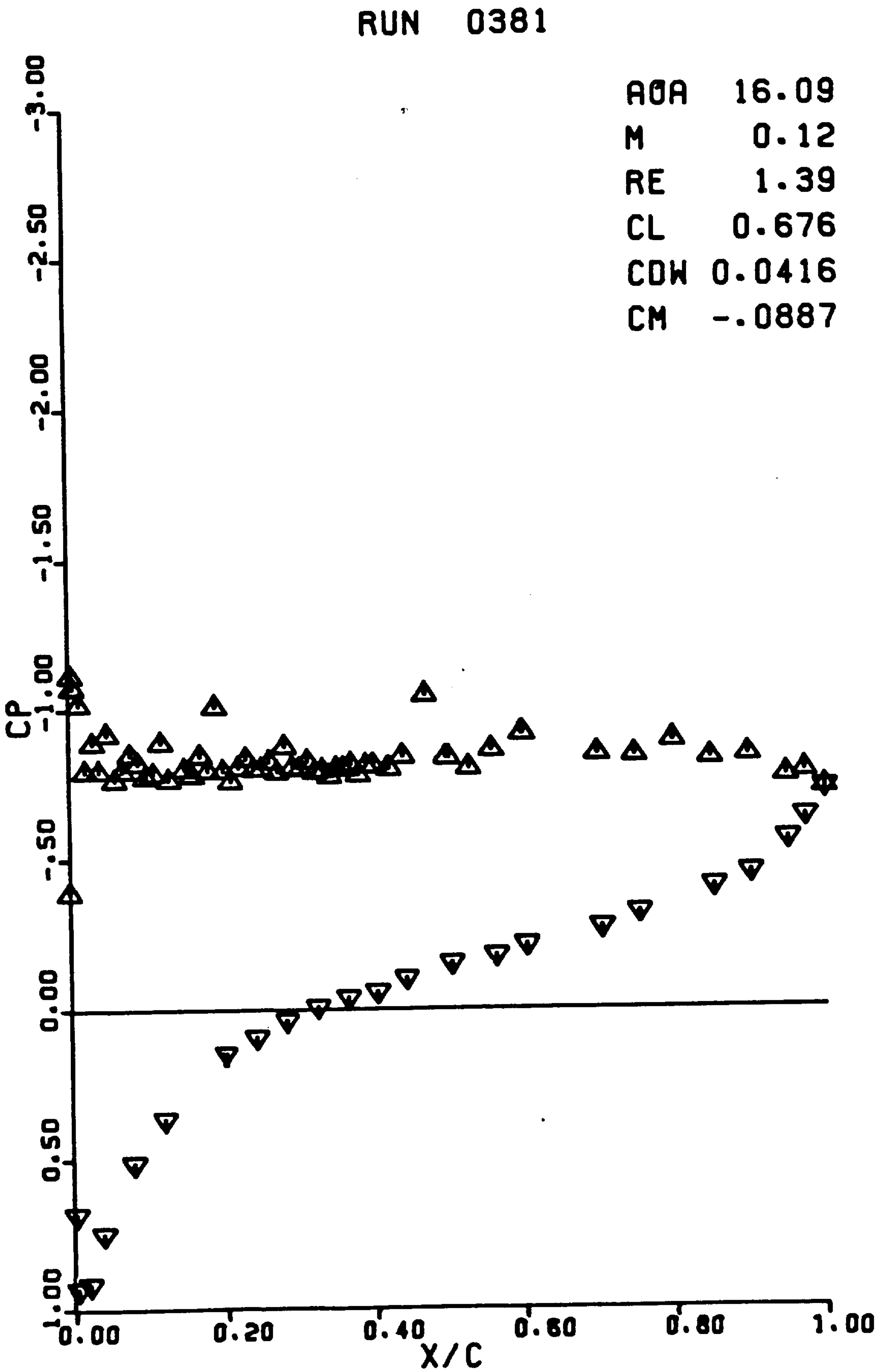
RUN 0381
AOA 16.09
M 0.12
RE 1.39
CL 0.676
CDW 0.0416
CM -.0887
CP
-3.00
-2.50
-2.00
-1.50
-1.00
-.50
0.00
0.50
1.00
0.00
0.20
0.40
0.60
0.80
1.00
X/C

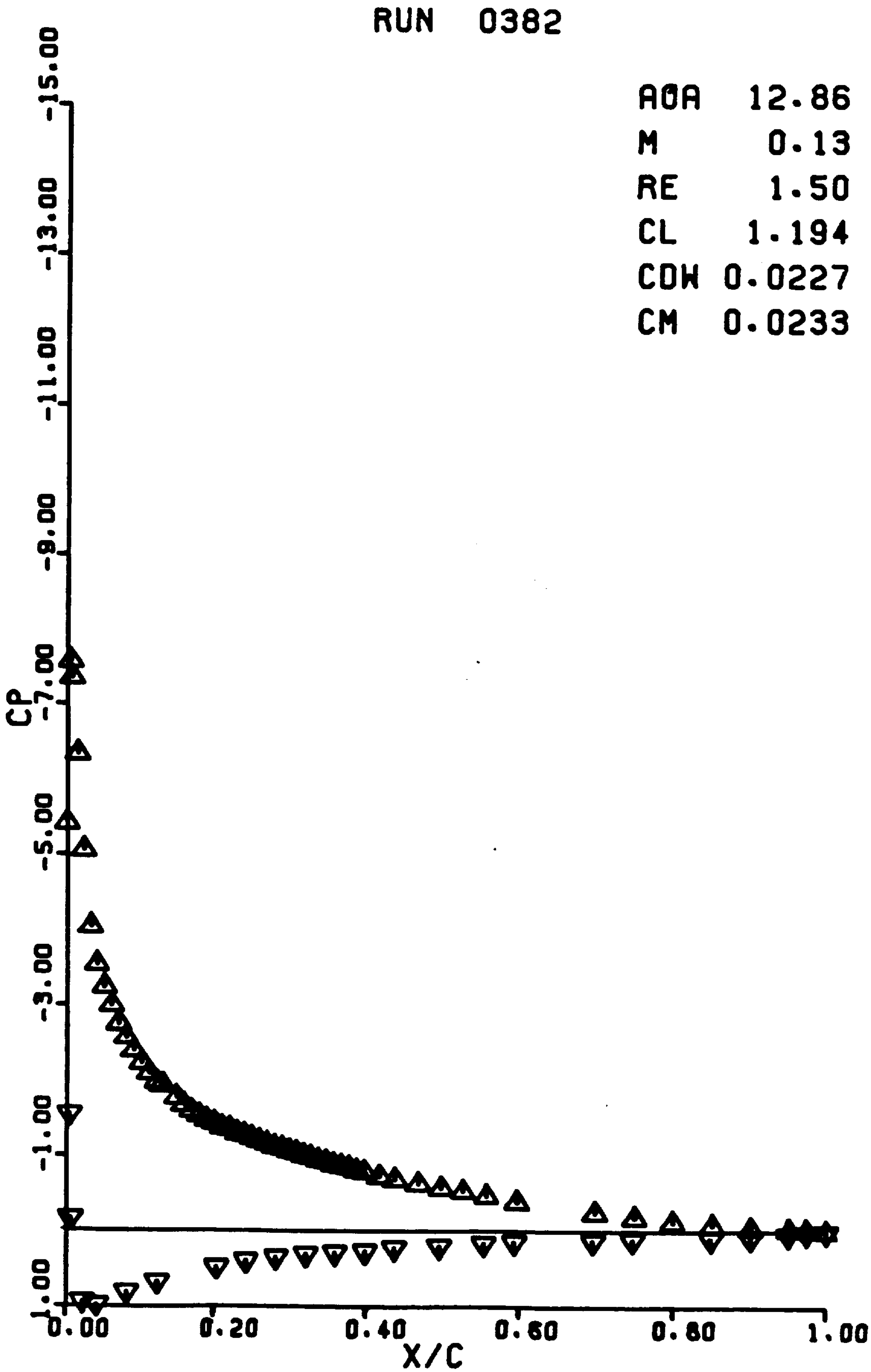
RUN 0382
AOA 12.86
M 0.13
RE 1.50
CL 1.194
CDW 0.0227
CM 0.0233
CP
-15.00
-13.00
-11.00
-9.00
-7.00
-5.00
-3.00
-1.00
1.00
0.00
0.20
0.40
0.60
0.80
1.00
X/C

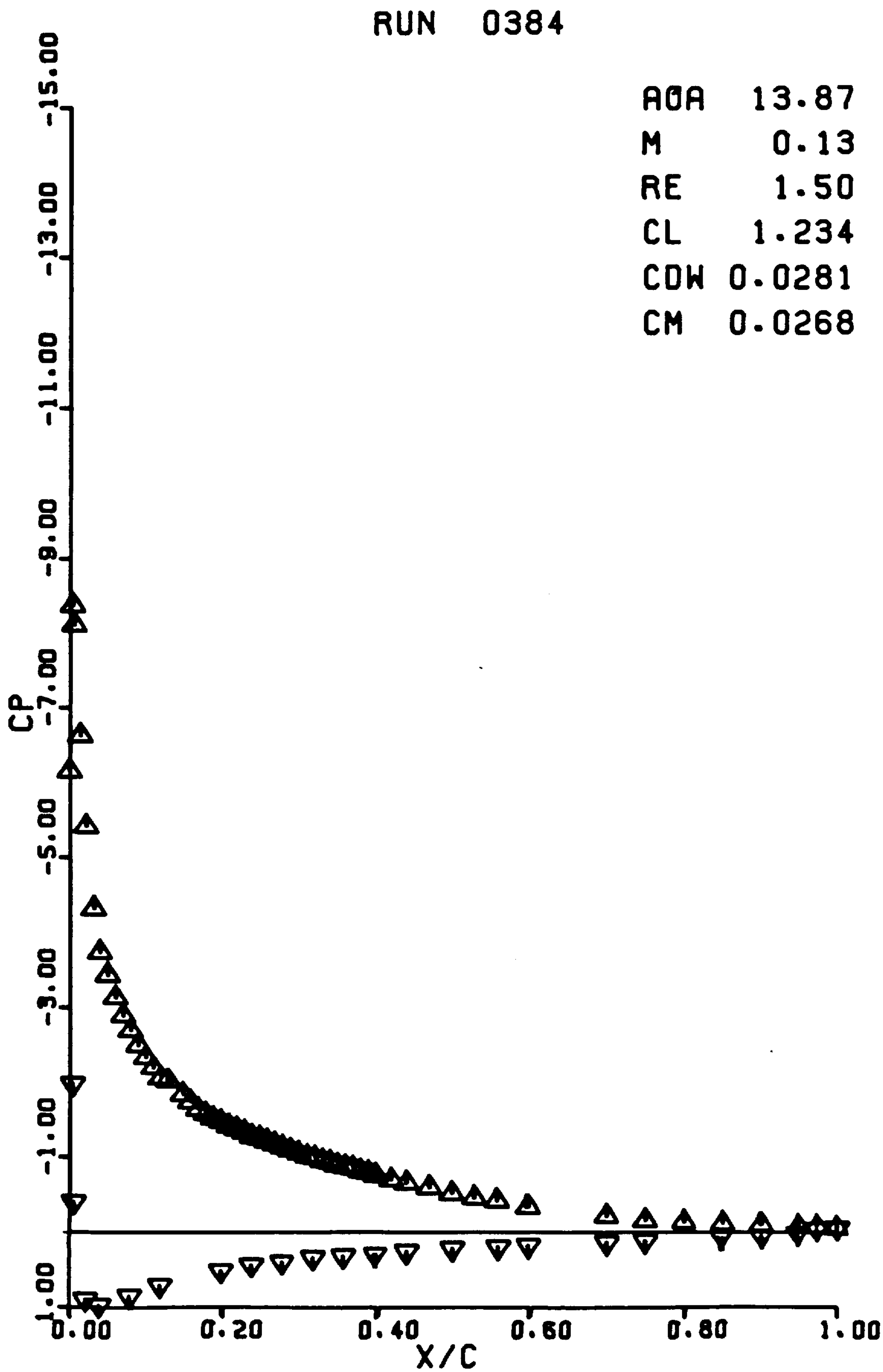
RUN 0384
AOA 13.87
M 0.13
RE 1.50
CL 1.234
CDW 0.0281
CM 0.0268
CP
-15.00
-13.00
-11.00
-9.00
-7.00
-5.00
-3.00
-1.00
1.00
0.00
0.20
0.40
0.60
0.80
1.00
X/C

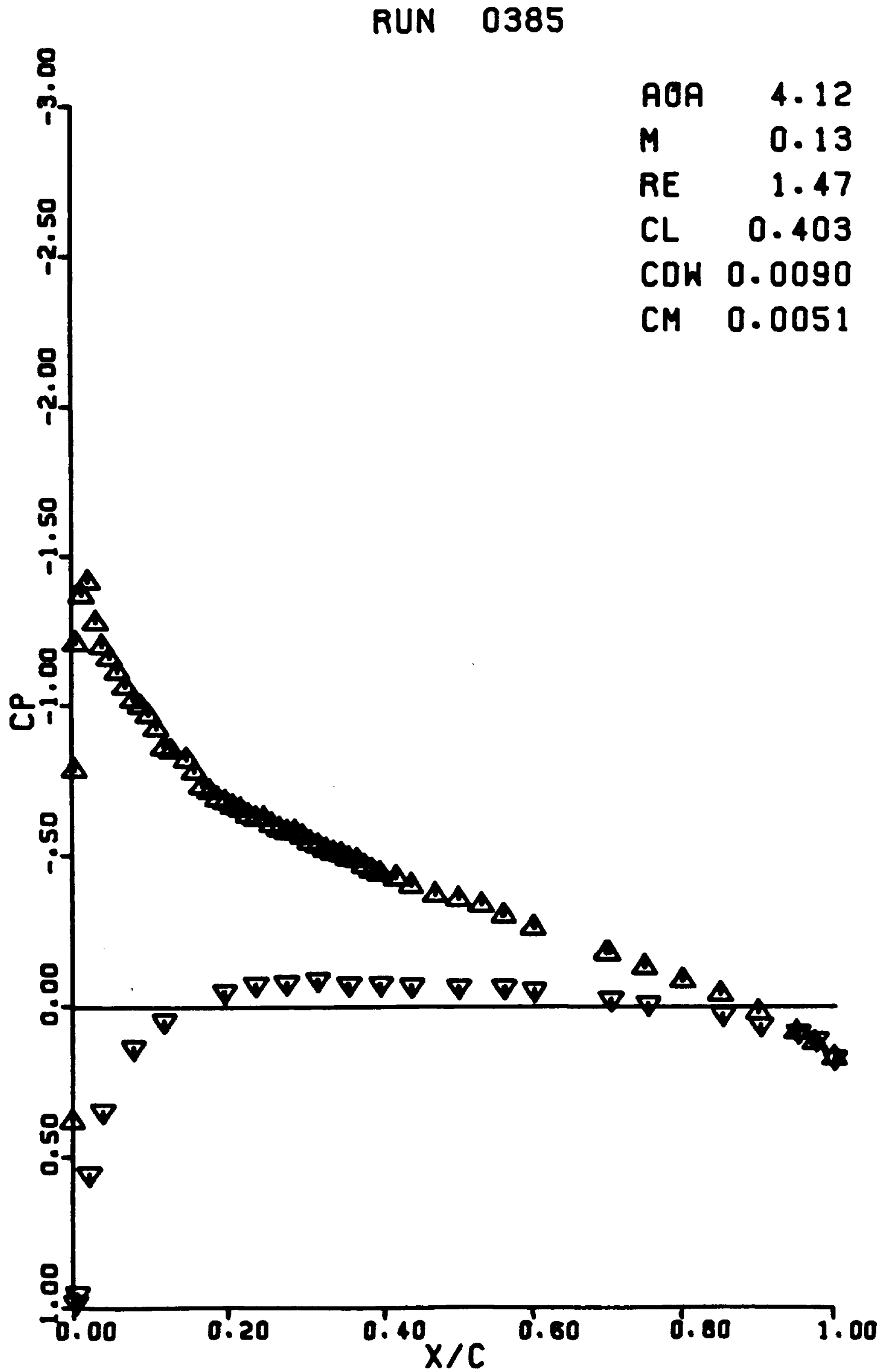

RUN 0385
AOA 4.12
M 0.13
RE 1.47
CL 0.403
CDW 0.0090
CM 0.0051
CP
-3.00
-2.50
-2.00
-1.50
-1.00
-.50
0.00
0.50
1.00
0.00
0.20
0.40
0.60
0.80
1.00
X/C

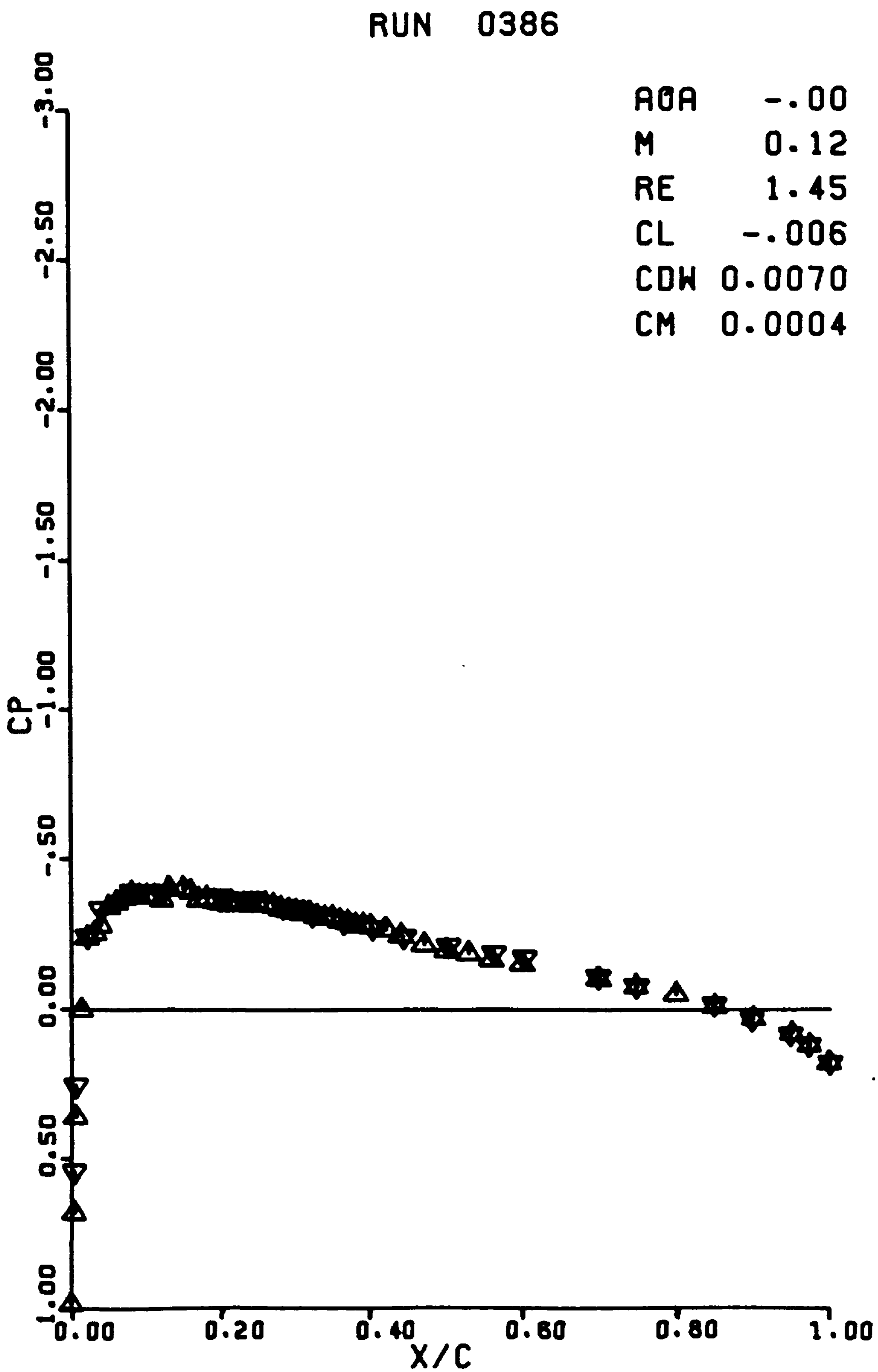
RUN 0386
AOA -.00
M 0.12
RE 1.45
CL -.006
CDW 0.0070
CM 0.0004
CP
-3.00
-2.50
-2.00
-1.50
-1.00
-.50
0.00
0.50
1.00
0.00
0.20
0.40
0.60
0.80
1.00
X/C

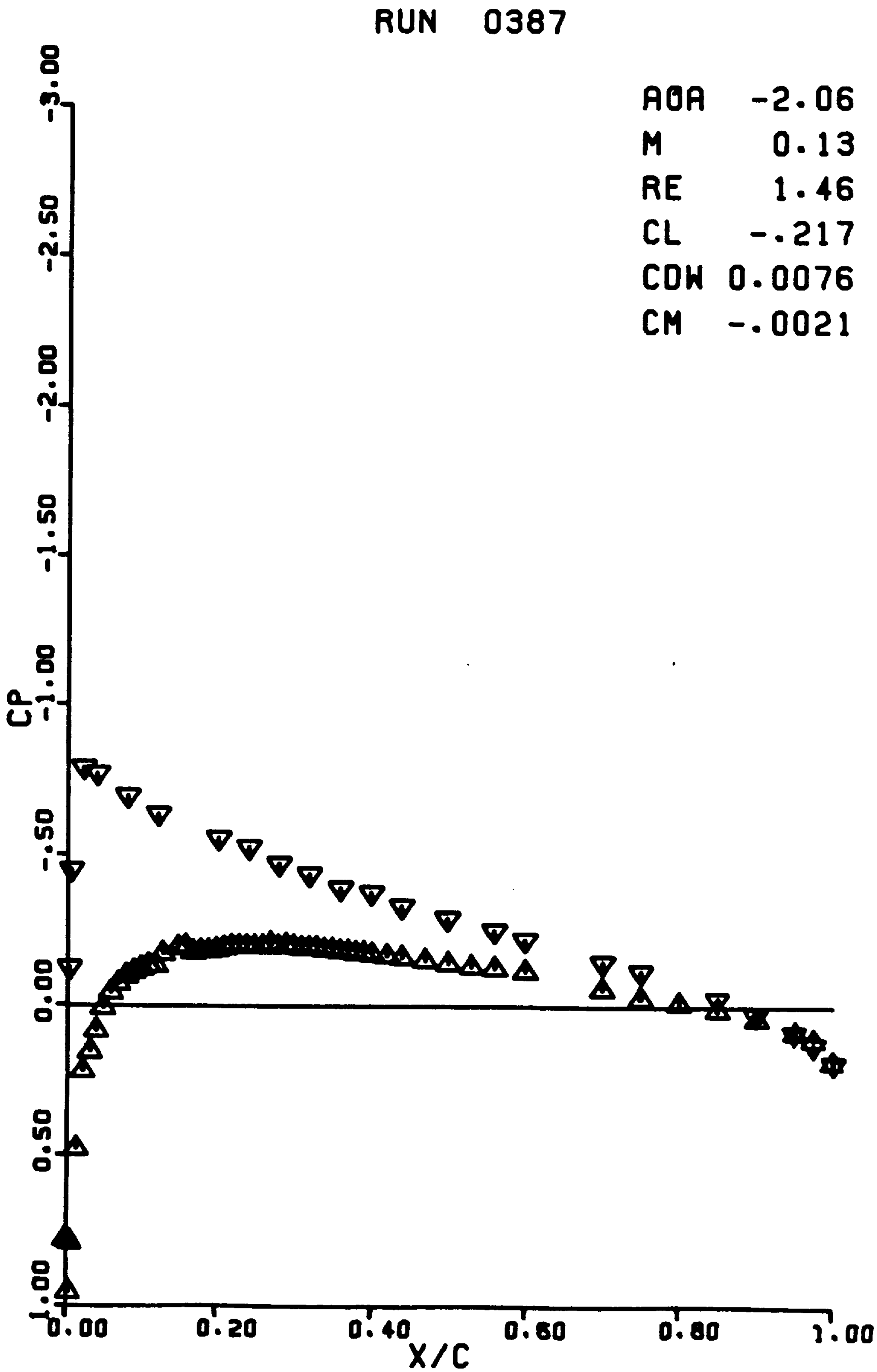
RUN 0387
AOA -2.06
M 0.13
RE 1.46
CL -.217
CDW 0.0076
CM -.0021
CP
-3.00
-2.50
-2.00
-1.50
-1.00
-.50
0.00
0.50
1.00
0.00
0.20
0.40
0.60
0.80
1.00
X/C

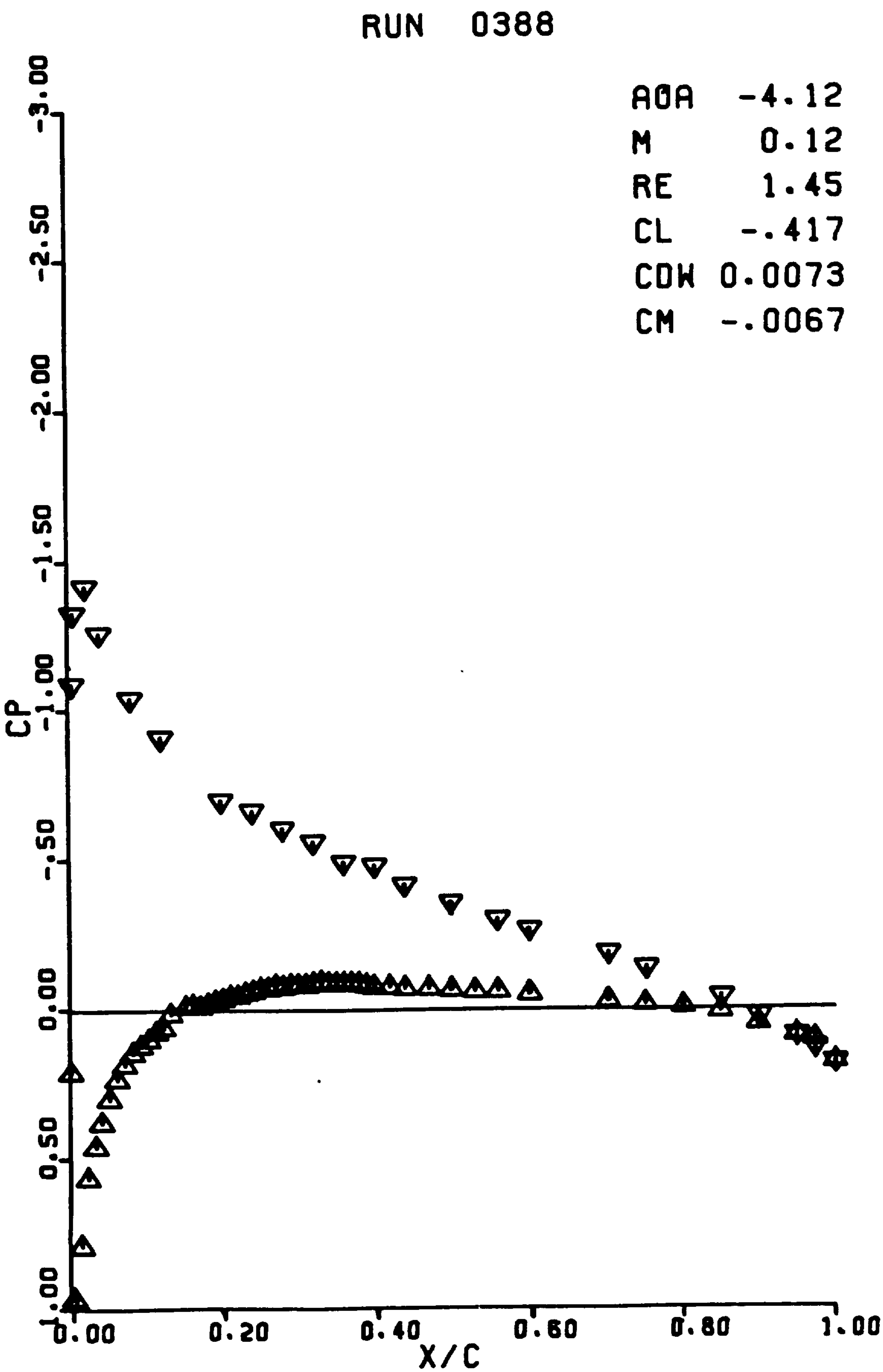
RUN 0388
AOA -4.12
M 0.12
RE 1.45
CL -.417
CDW 0.0073
CM -.0067
CP
-3.00
-2.50
-2.00
-1.50
-1.00
-.50
0.00
0.50
1.00
0.00
0.20
0.40
0.60
0.80
1.00
X/C

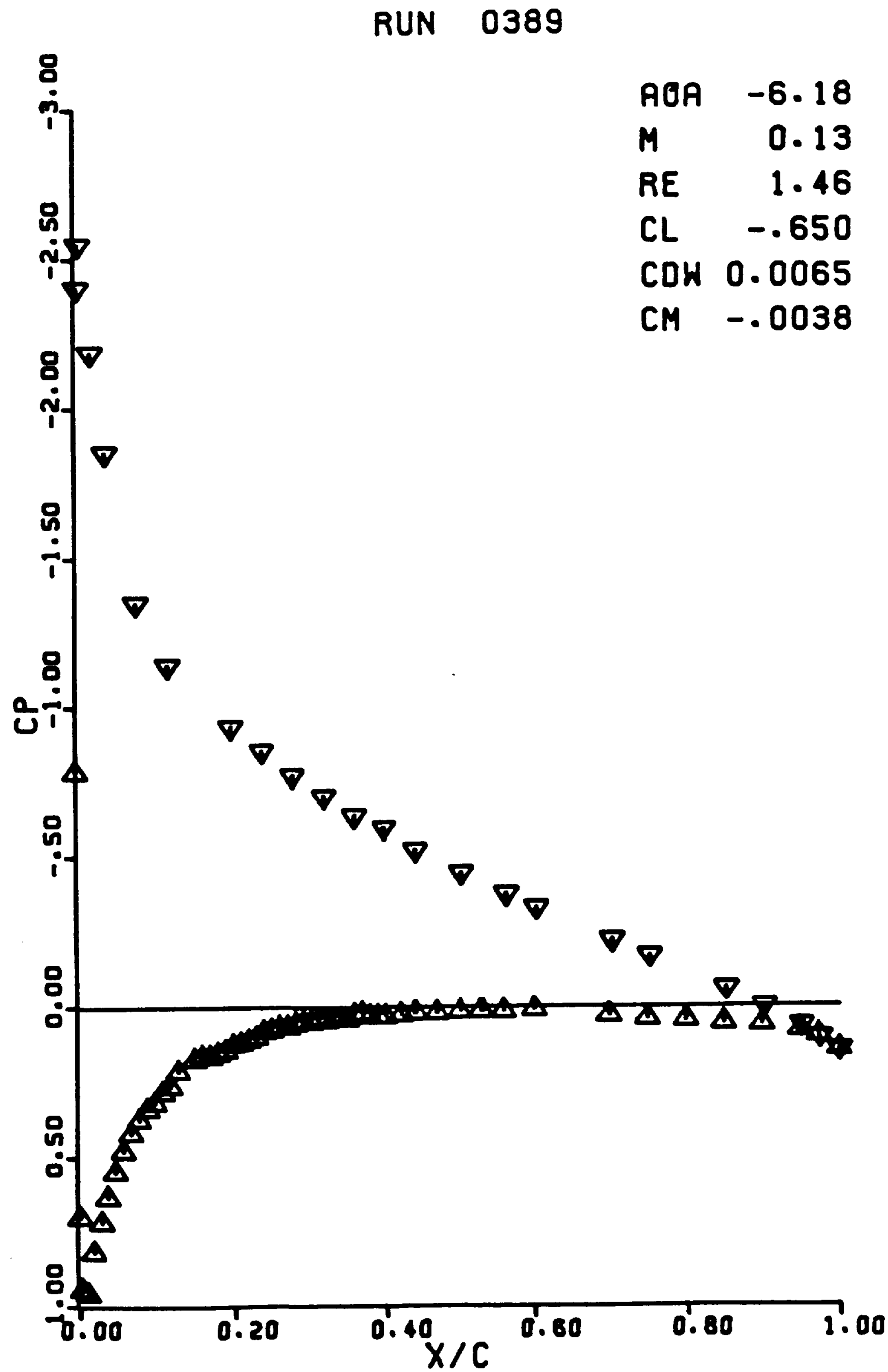
RUN 0389
AOA -6.18
M 0.13
RE 1.46
CL -.650
CDW 0.0065
CM -.0038
CP
-3.00
-2.50
-2.00
-1.50
-1.00
-.50
0.00
0.50
1.00
0.00
0.20
0.40
0.60
0.80
1.00
X/C

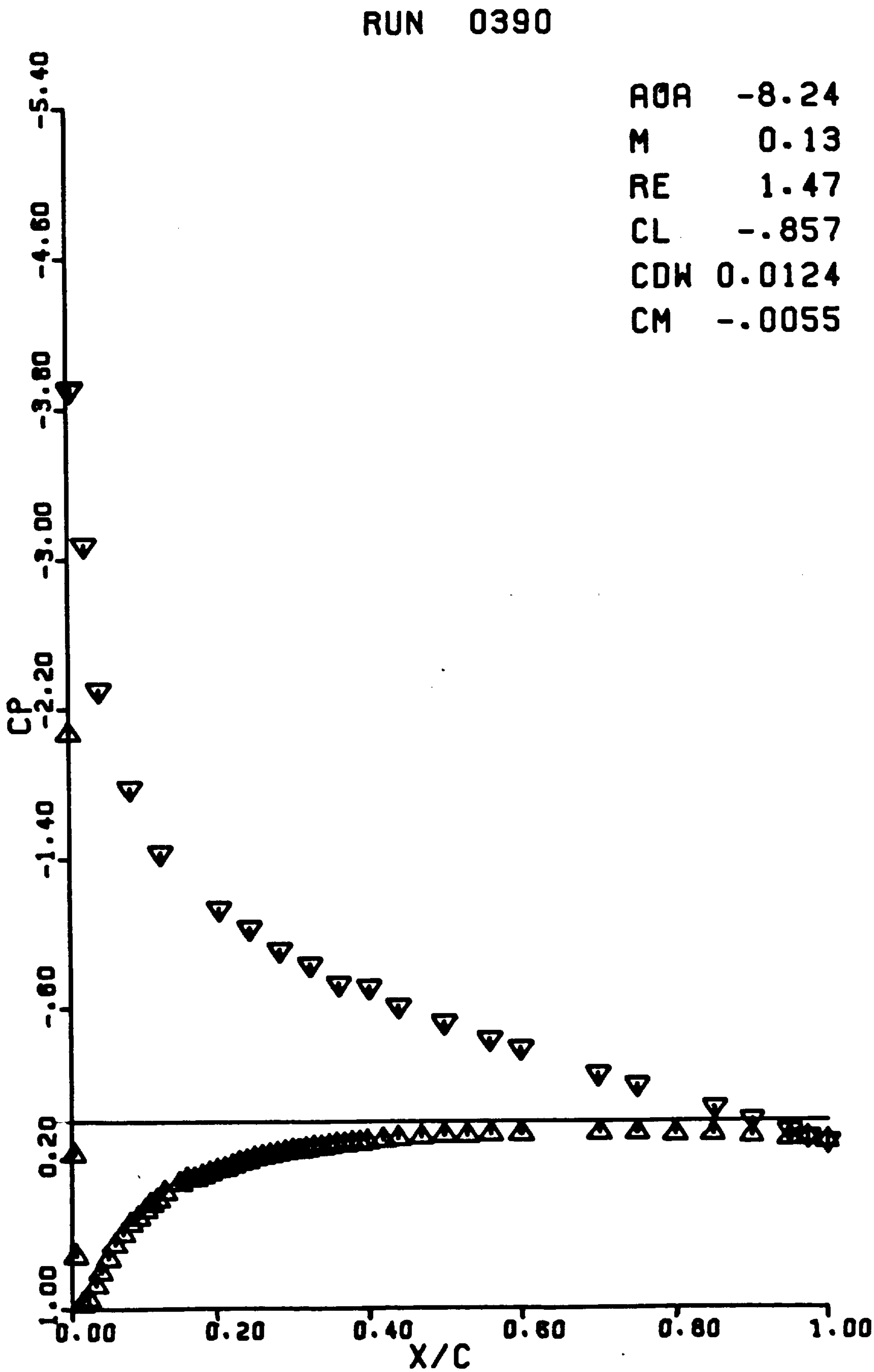
RUN 0390
AOA -8.24
M 0.13
RE 1.47
CL -.857
CDW 0.0124
CM -.0055
CP
-5.40
-4.60
-3.80
-3.00
-2.20
-1.40
-.60
0.20
1.00
0.00
0.20
0.40
0.60
0.80
1.00
X/C

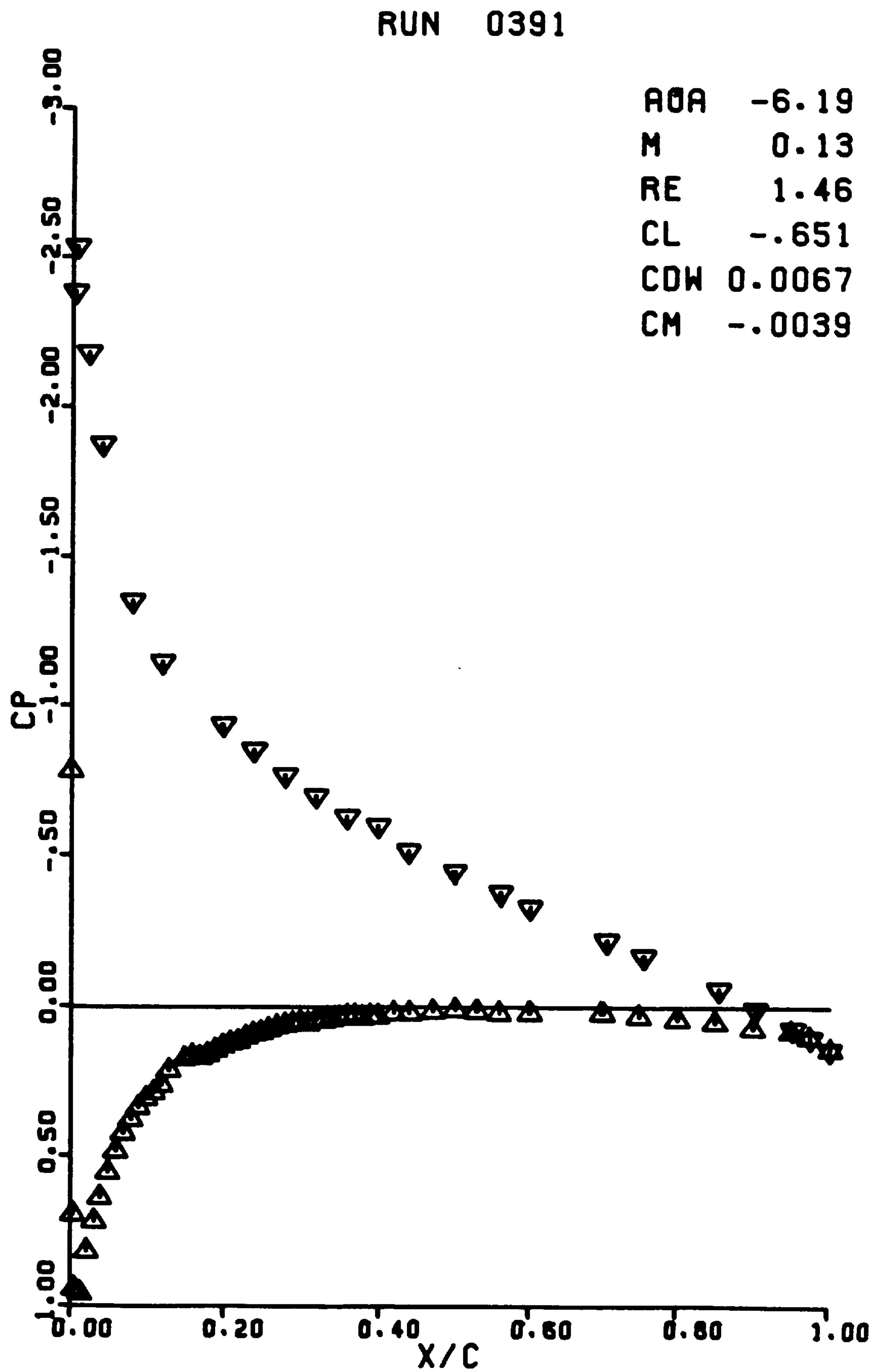
RUN 0391
AOA -6.19
M 0.13
RE 1.46
CL -.651
CDW 0.0067
CM -.0039
CP
-3.00
-2.50
-2.00
-1.50
-1.00
-.50
0.00
0.50
1.00
0.00
0.20
0.40
0.60
0.80
1.00
X/C

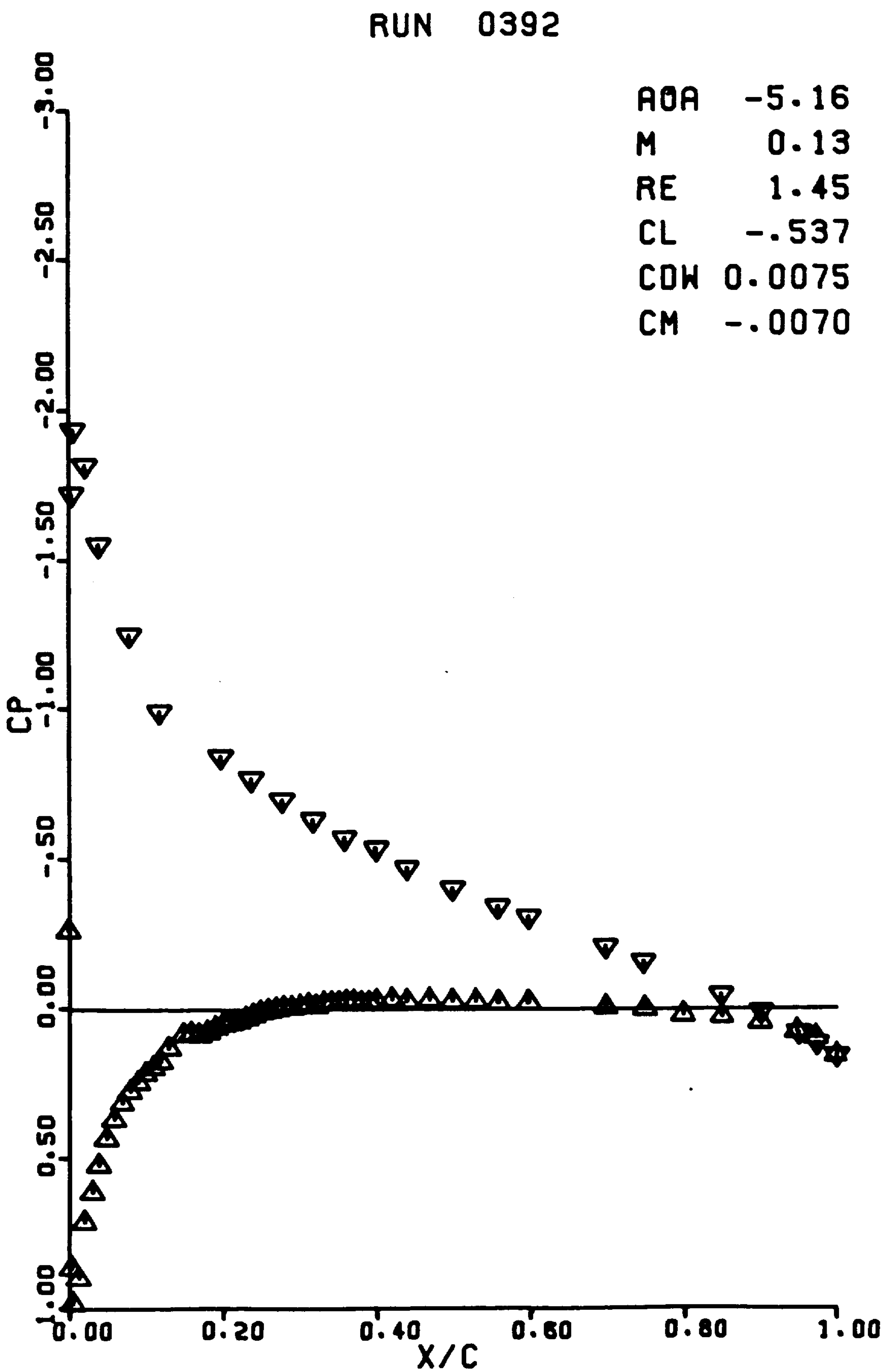
RUN 0392
AOA -5.16
M 0.13
RE 1.45
CL -.537
CDW 0.0075
CM -.0070
CP
-3.00
-2.50
-2.00
-1.50
-1.00
-.50
0.00
0.50
1.00
0.00
0.20
0.40
0.60
0.80
1.00
X/C

c.2

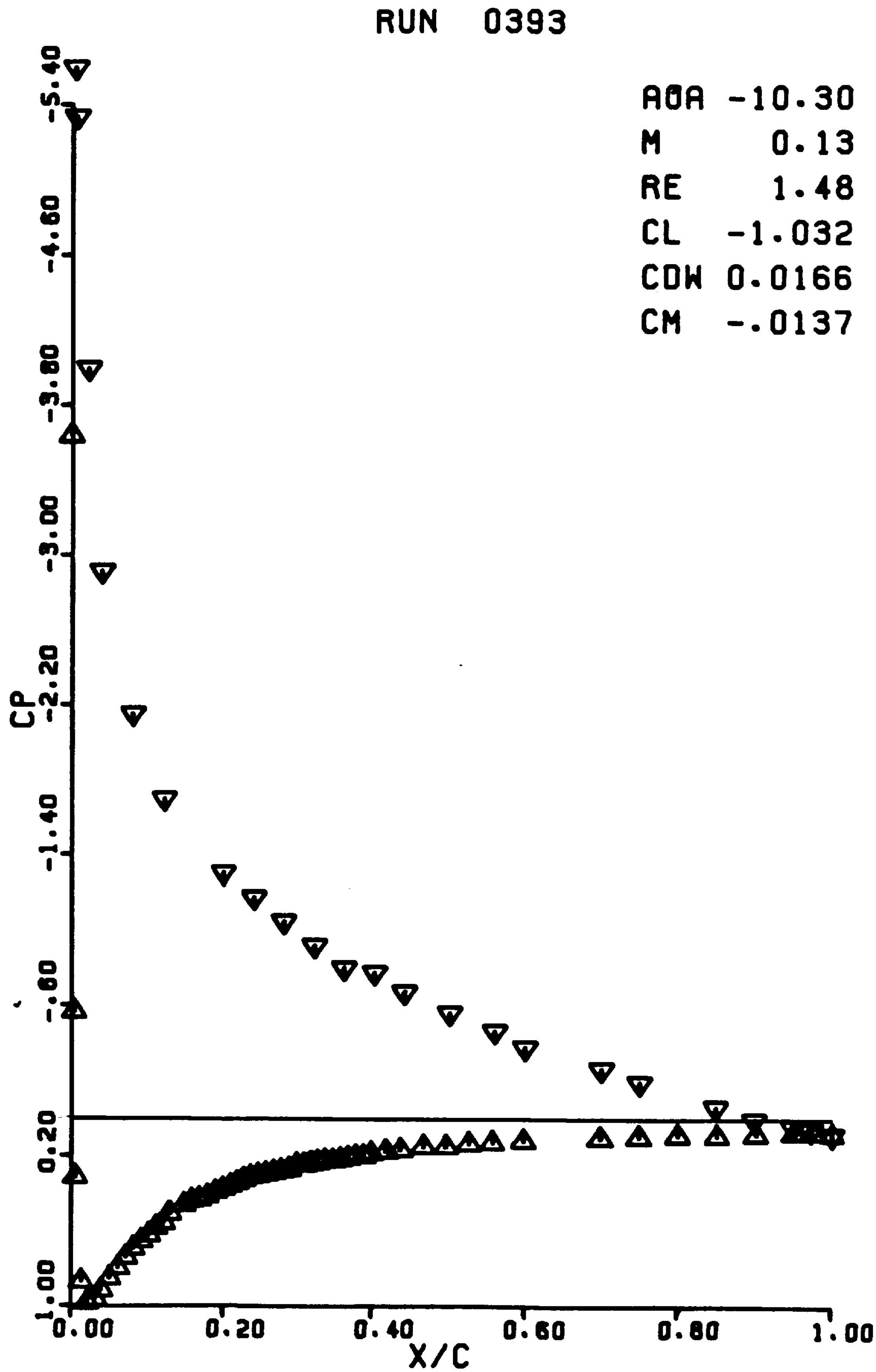
RUN 0393
AOA -10.30
M 0.13
RE 1.48
CL -1.032
CDW 0.0166
CM -.0137
CP
X/C
-5.40
-4.60
-3.80
-3.00
-2.20
-1.40
-.60
0.20
1.00
0.00
0.20
0.40
0.60
0.80
1.00

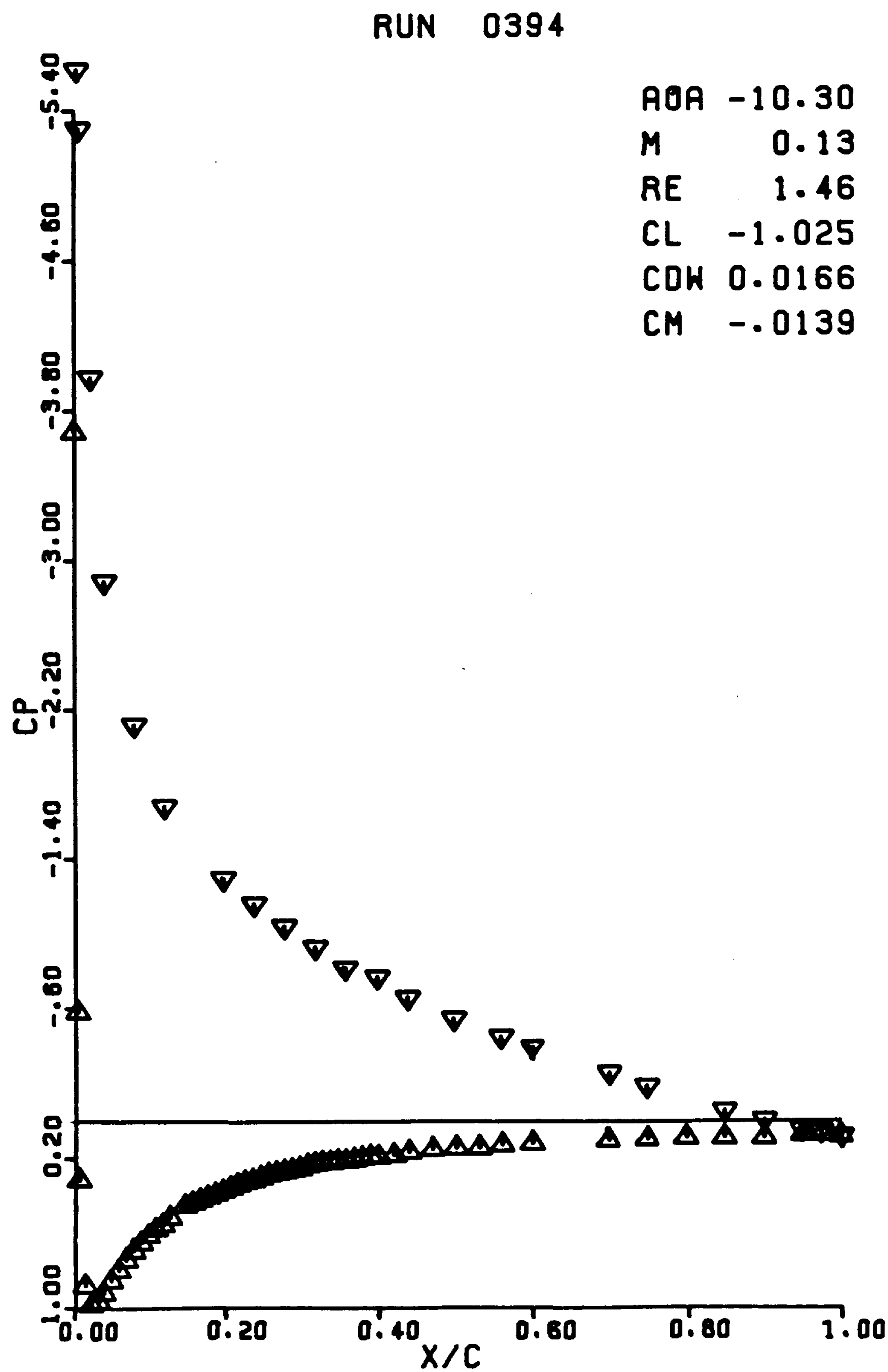
RUN 0394
AOA -10.30
M 0.13
RE 1.46
CL -1.025
CDW 0.0166
CM -.0139
CP
-5.40
-4.60
-3.80
-3.00
-2.20
-1.40
-.60
0.20
1.00
0.00
0.20
0.40
0.60
0.80
1.00
X/C

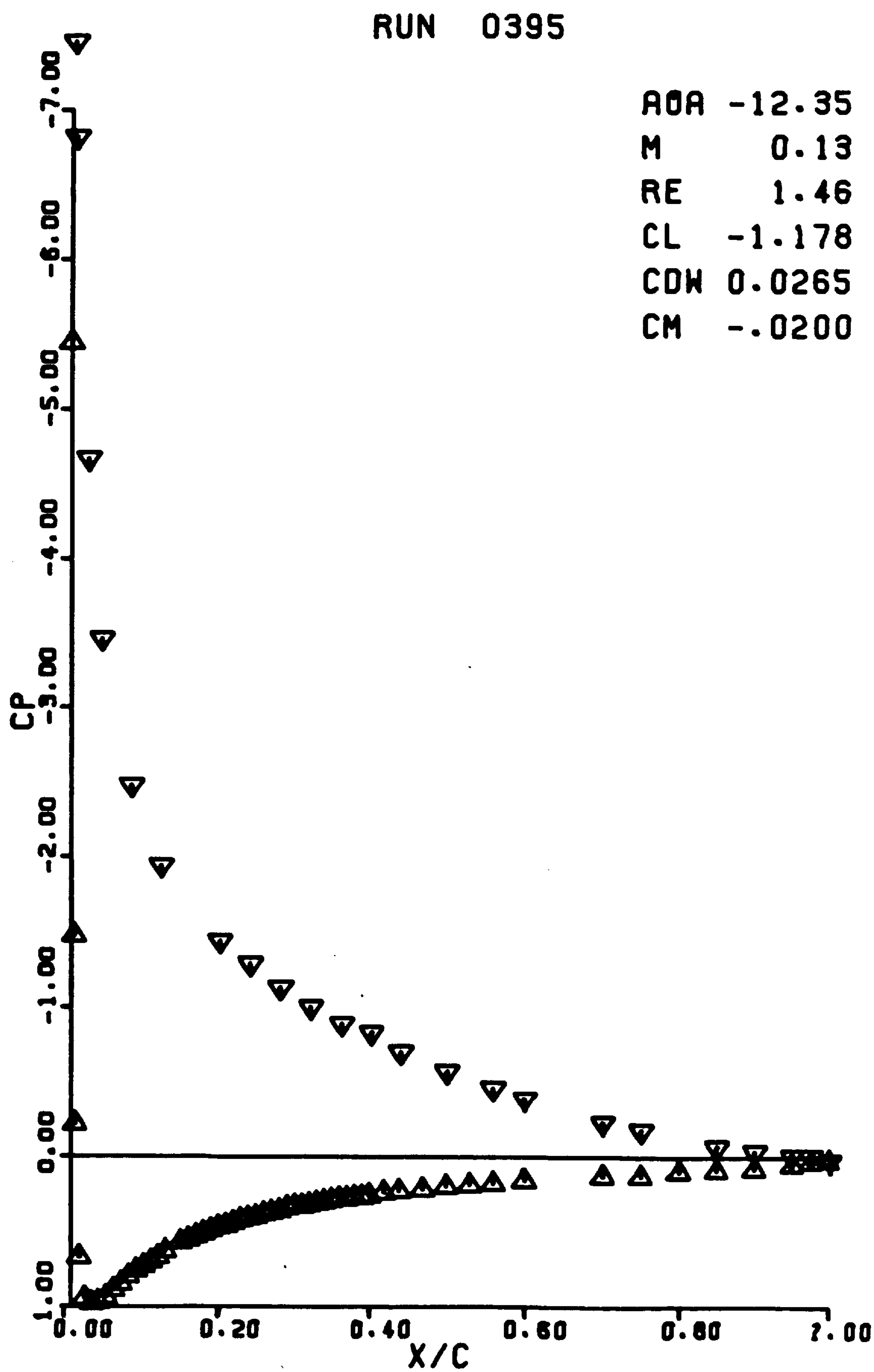
RUN 0395
AOA -12.35
M 0.13
RE 1.46
CL -1.178
CDW 0.0265
CM -.0200
CP
-7.00
-6.00
-5.00
-4.00
-3.00
-2.00
-1.00
0.00
1.00
0.00
0.20
0.40
0.60
0.80
1.00
X/C

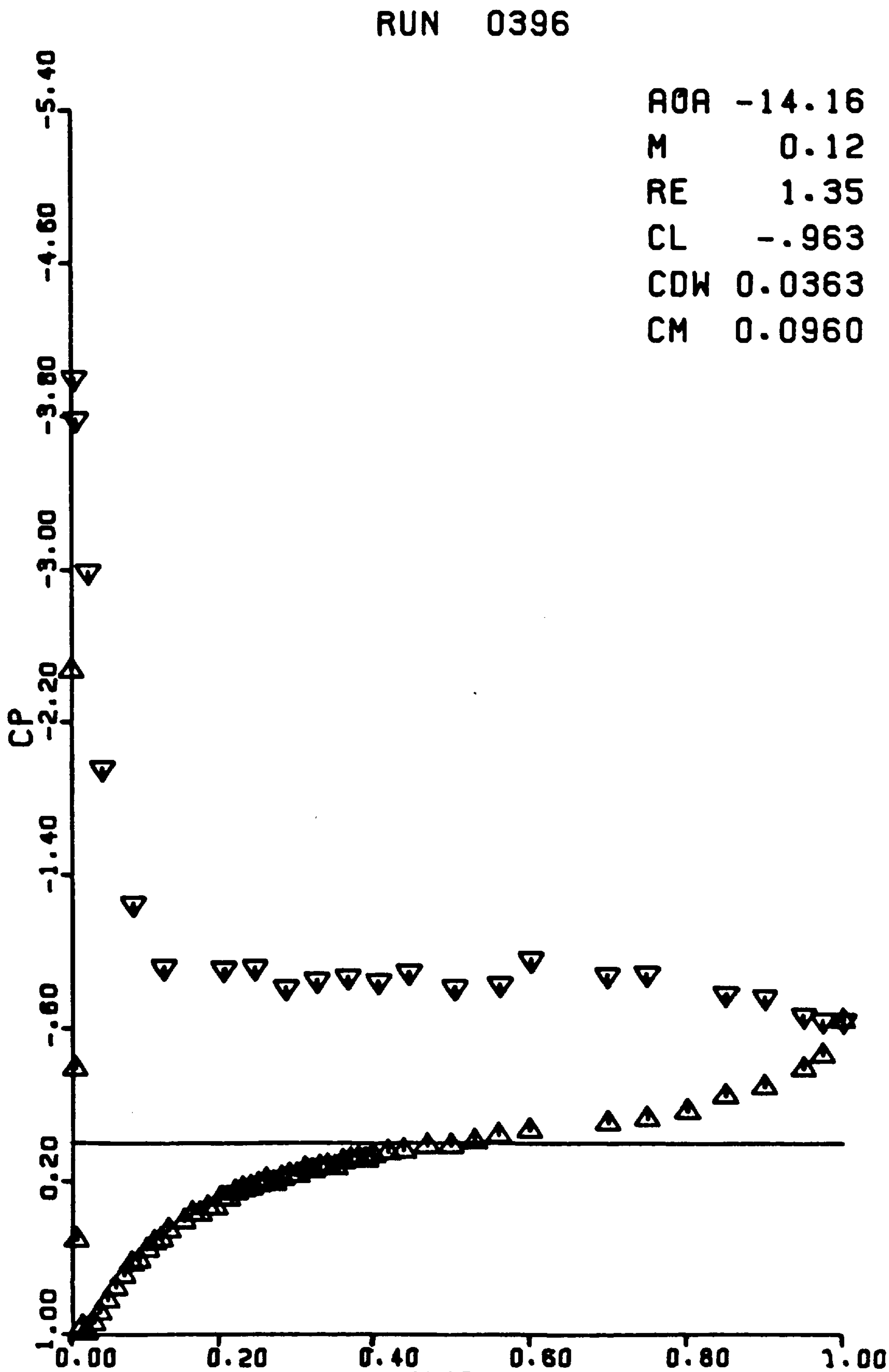
RUN 0396
AOA -14.16
M 0.12
RE 1.35
CL -.963
CDW 0.0363
CM 0.0960
CP
X/C
-5.40
-4.60
-3.80
-3.00
-2.20
-1.40
-.60
0.20
1.00
0.00
0.20
0.40
0.60
0.80
1.00

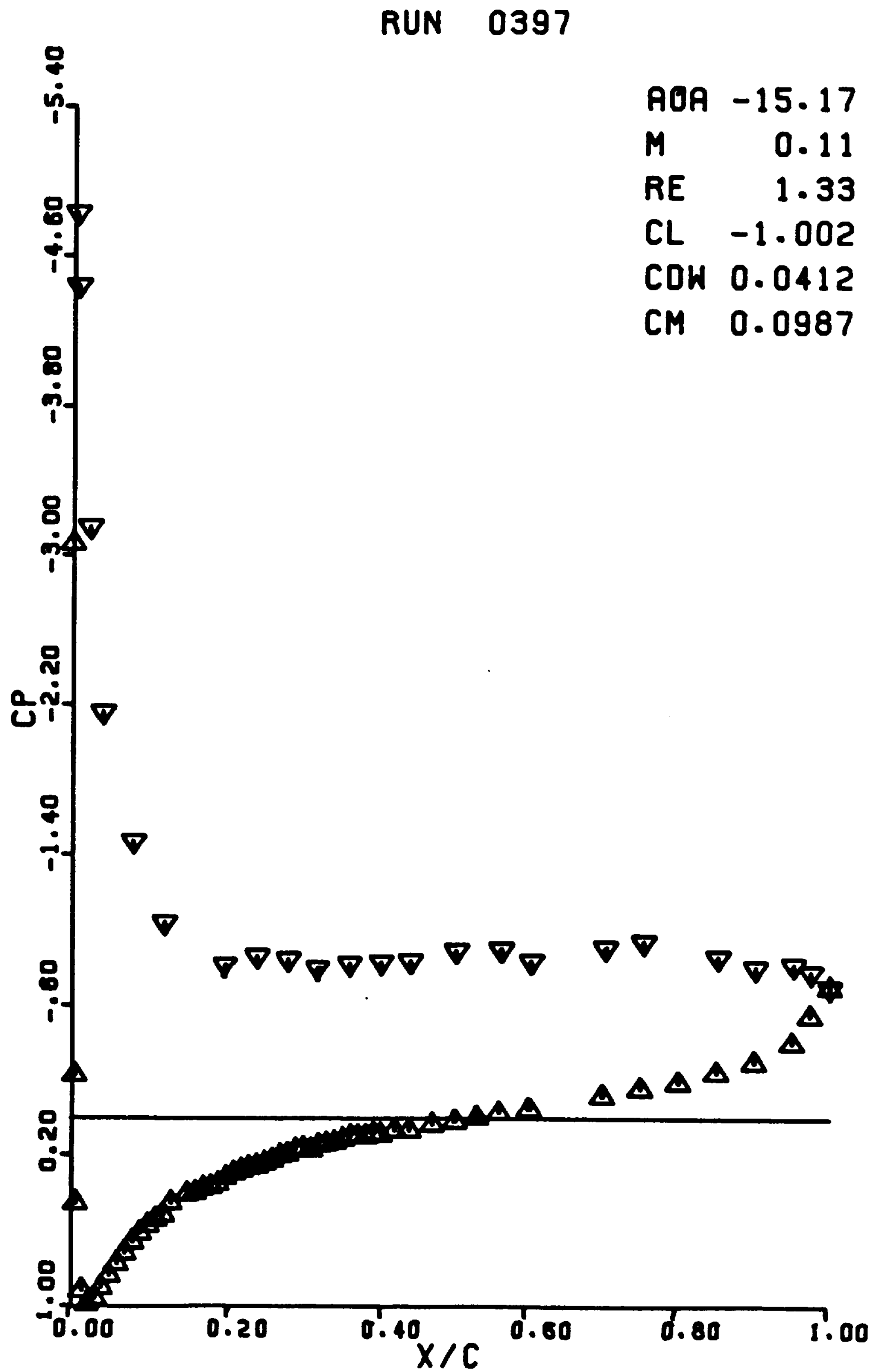

RUN 0397
AOA -15.17
M 0.11
RE 1.33
CL -1.002
CDW 0.0412
CM 0.0987
CP
-5.40
-4.60
-3.80
-3.00
-2.20
-1.40
-.60
0.20
1.00
0.00
0.20
0.40
0.60
0.80
1.00
X/C

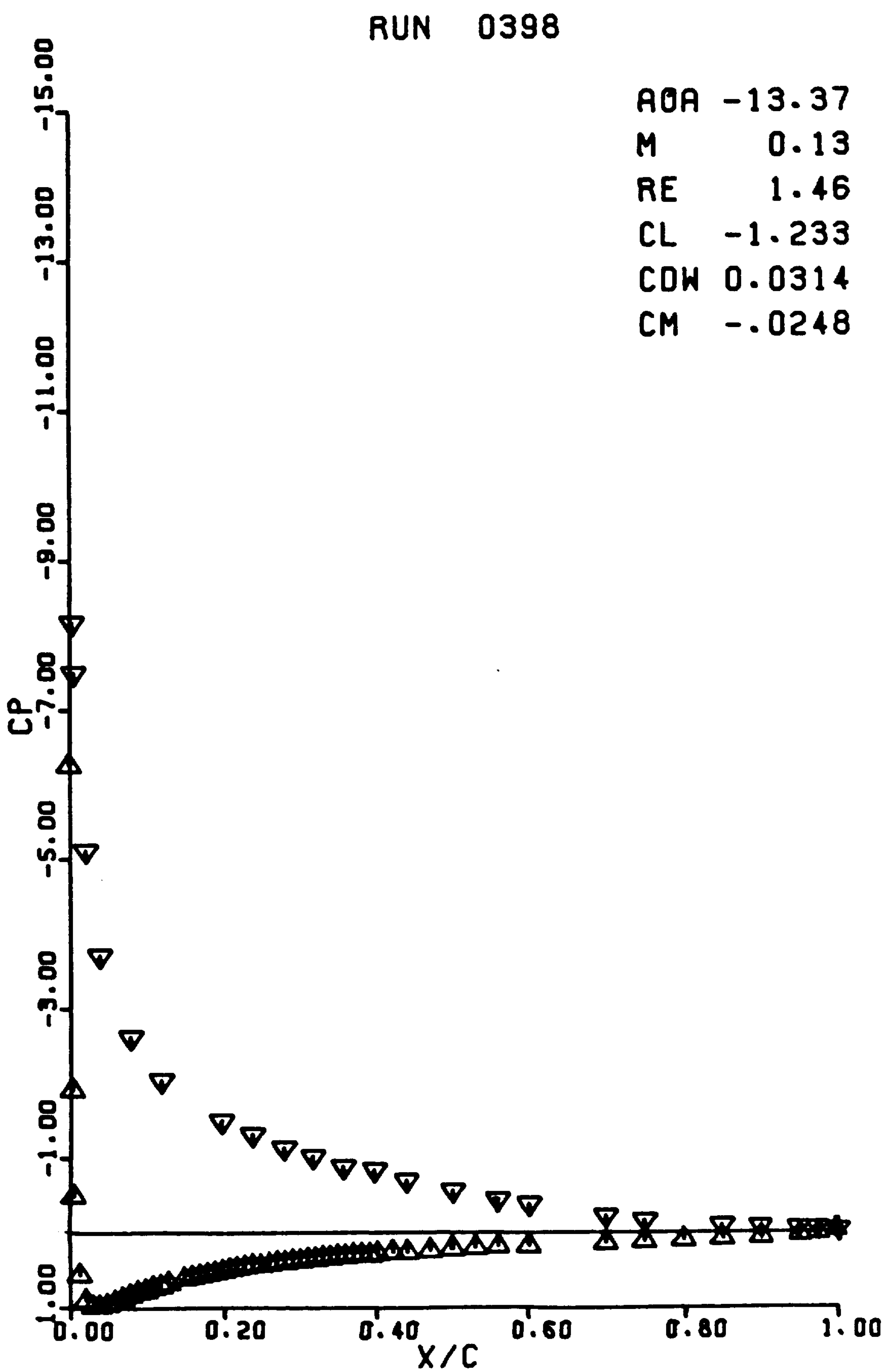
RUN 0398
AOA -13.37
M 0.13
RE 1.46
CL -1.233
CDW 0.0314
CM -.0248
CP
-15.00
-13.00
-11.00
-9.00
-7.00
-5.00
-3.00
-1.00
1.00
0.00
0.20
0.40
0.60
0.80
1.00
X/C

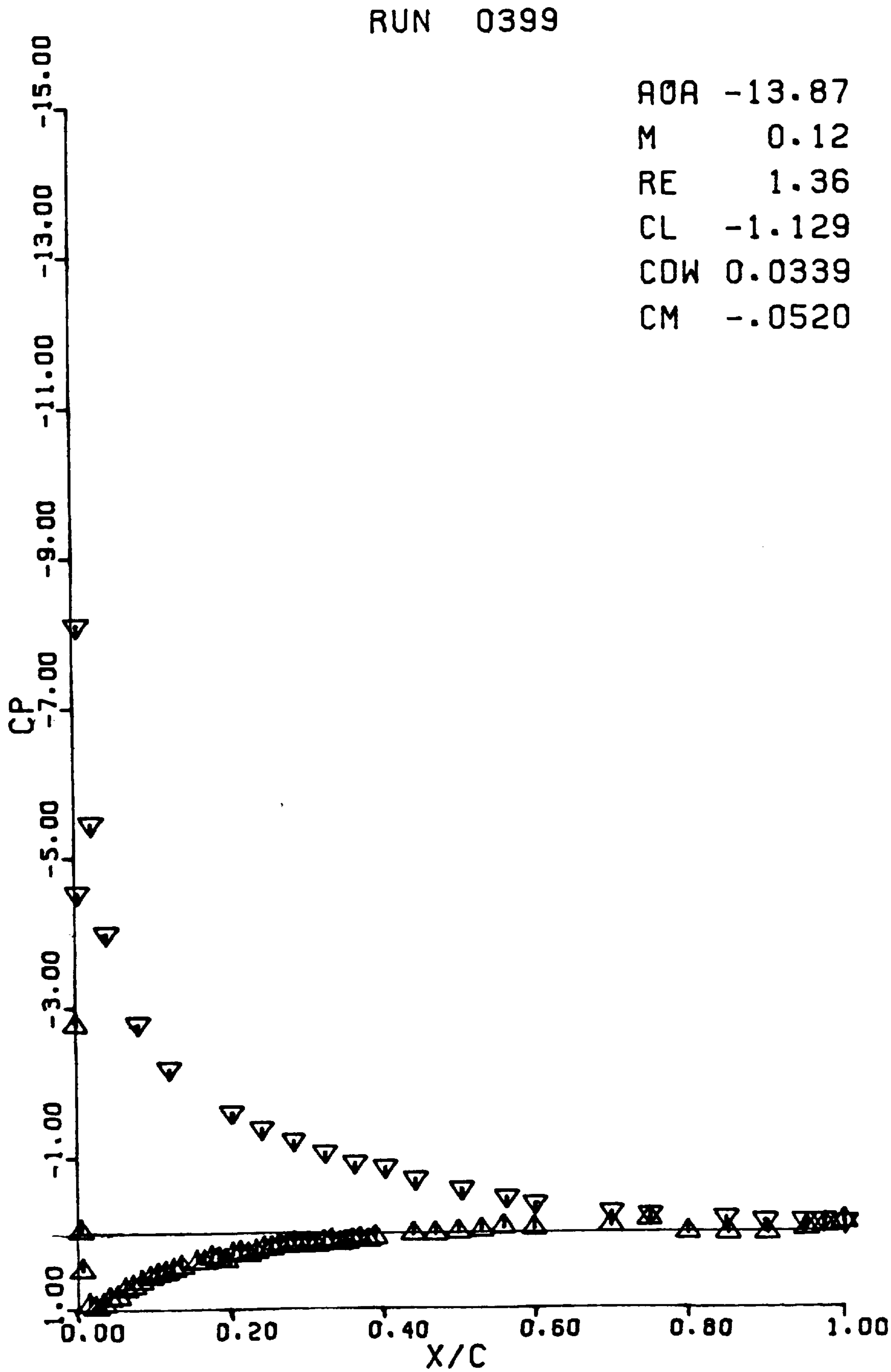

RUN 0399
AOA -13.87
M 0.12
RE 1.36
CL -1.129
CDW 0.0339
CM -.0520
CP
-15.00
-13.00
-11.00
-9.00
-7.00
-5.00
-3.00
-1.00
1.00
0.00
0.20
0.40
0.60
0.80
1.00
X/C

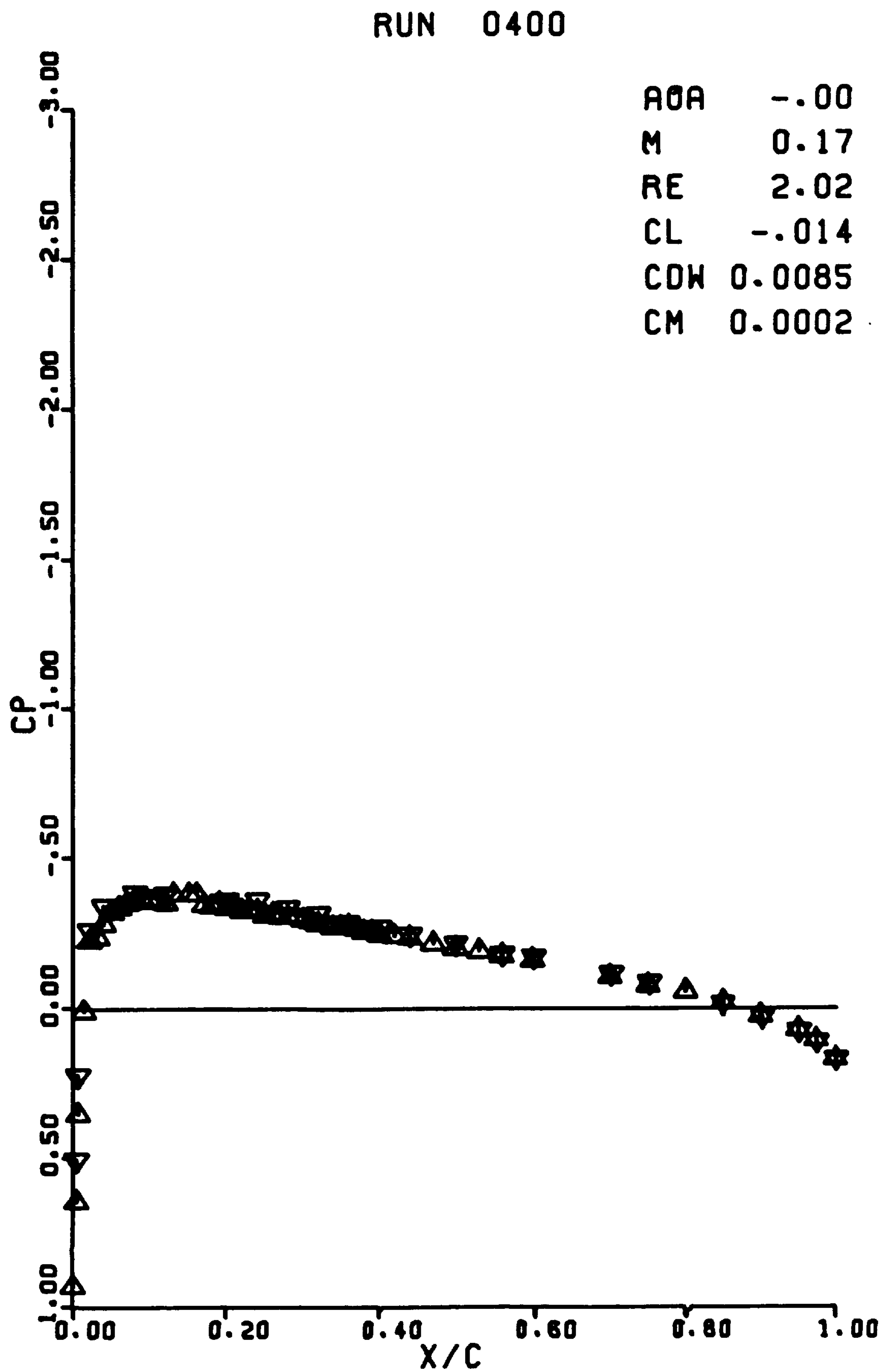
RUN 0400
AOA -.00
M 0.17
RE 2.02
CL -.014
CDW 0.0085
CM 0.0002
CP
-3.00
-2.50
-2.00
-1.50
-1.00
-.50
0.00
0.50
1.00
0.00
0.20
0.40
0.60
0.80
1.00
X/C

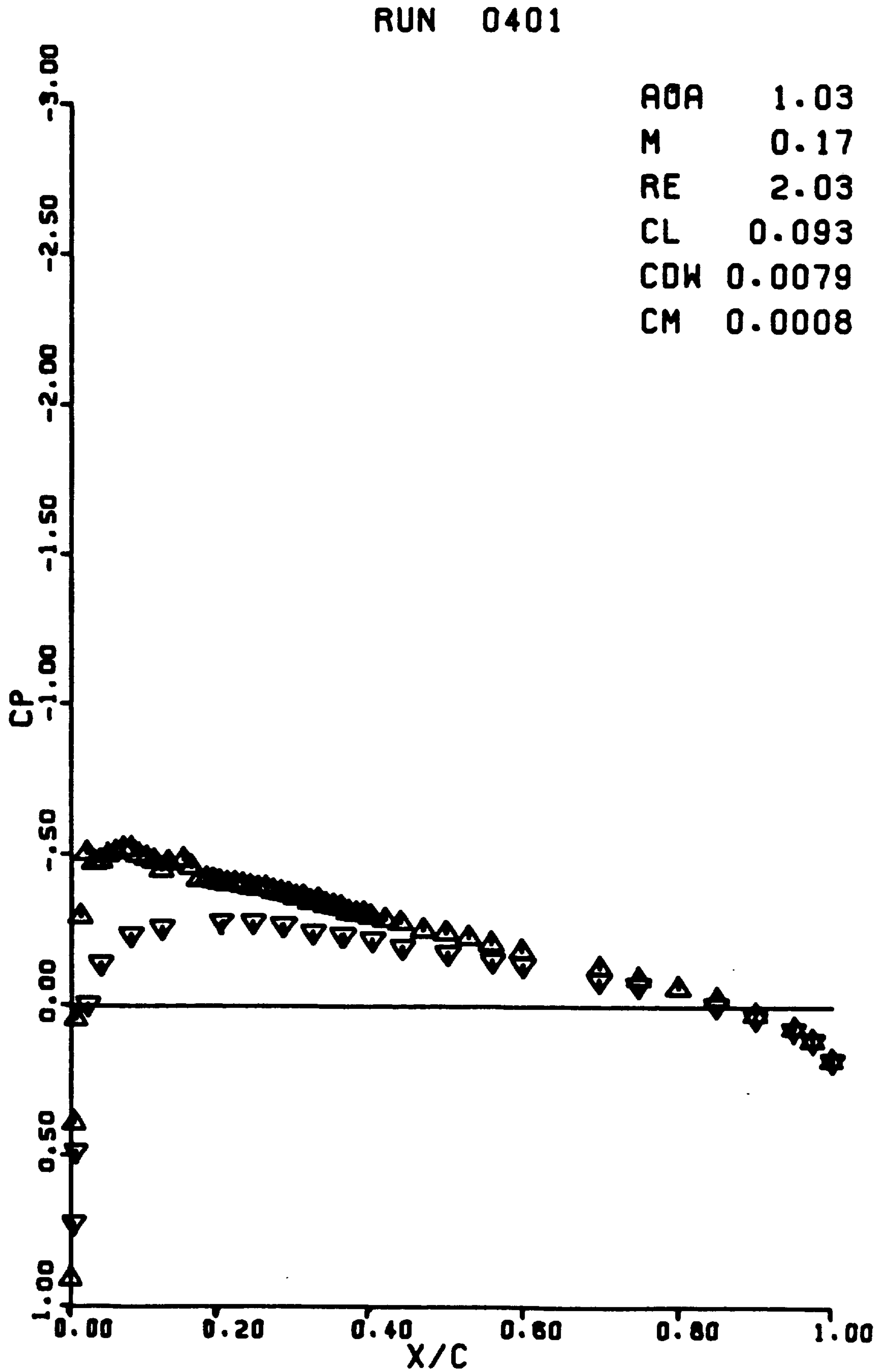
RUN 0401
AOA 1.03
M 0.17
RE 2.03
CL 0.093
CDW 0.0079
CM 0.0008
CP
-3.00
-2.50
-2.00
-1.50
-1.00
-.50
0.00
0.50
1.00
0.00
0.20
0.40
0.60
0.80
1.00
X/C

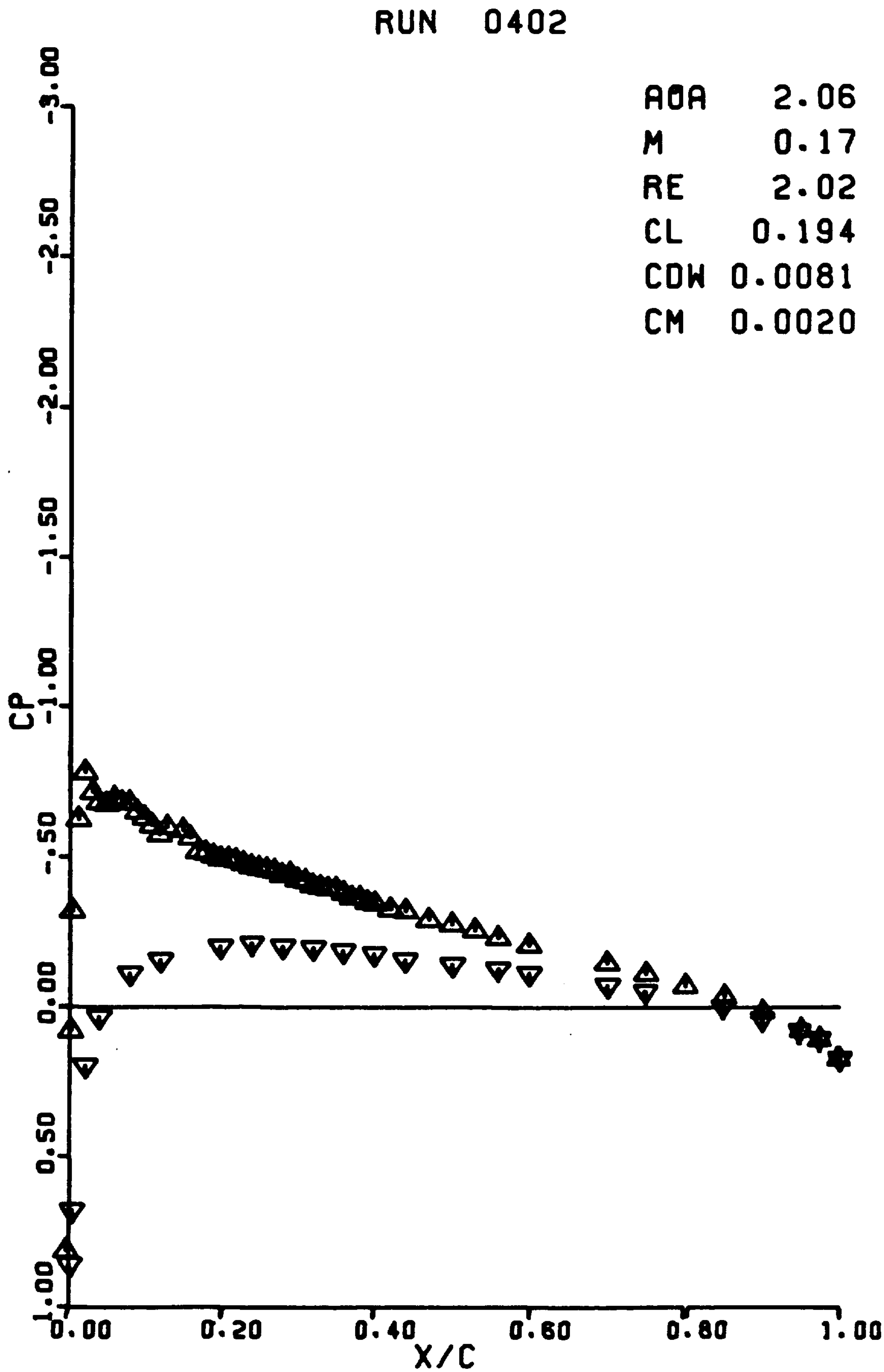
RUN 0402
AOA 2.06
M 0.17
RE 2.02
CL 0.194
CDW 0.0081
CM 0.0020
CP
-3.00
-2.50
-2.00
-1.50
-1.00
-.50
0.00
0.50
1.00
0.00
0.20
0.40
0.60
0.80
1.00
X/C

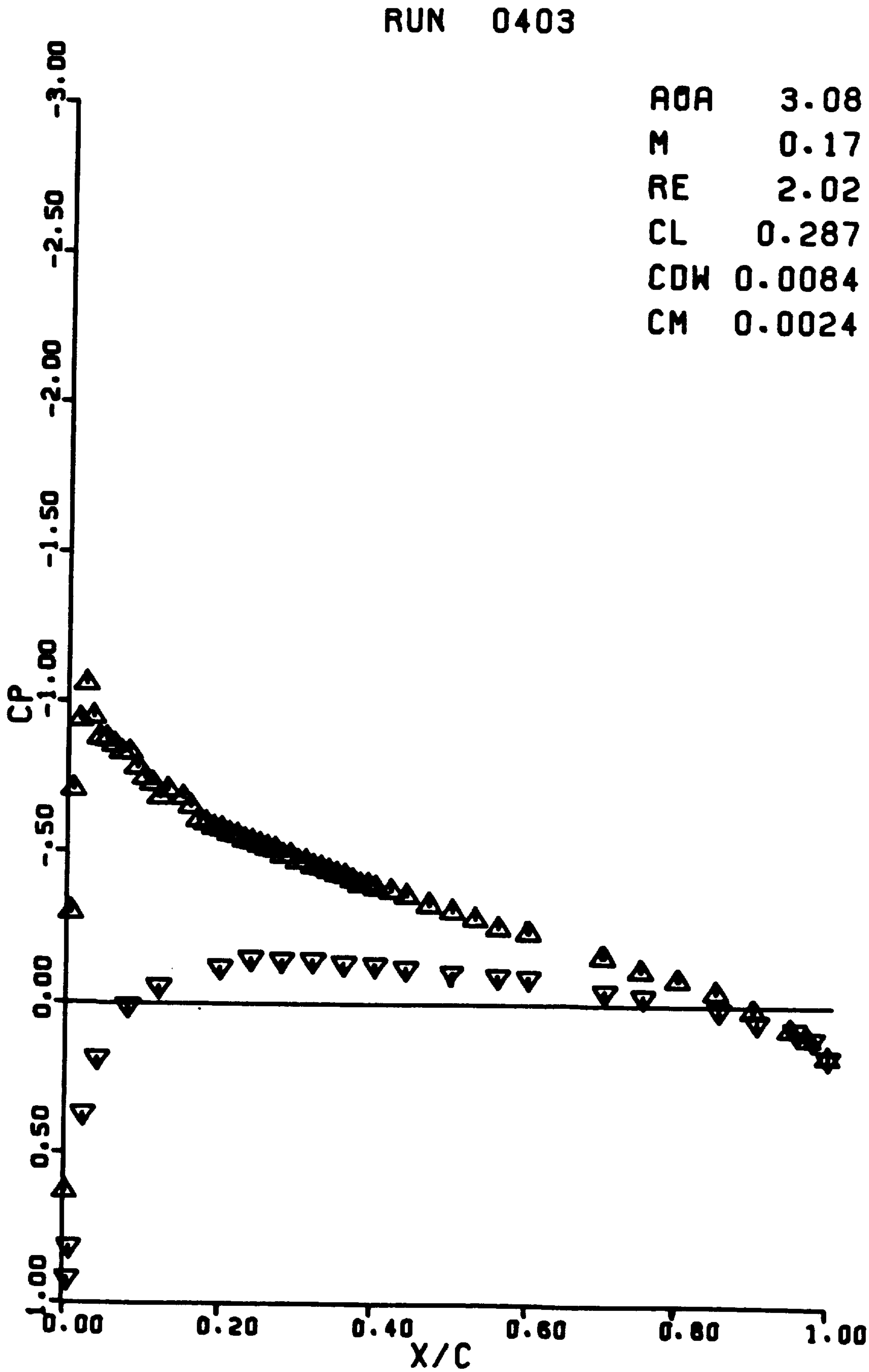

RUN 0403
AOA 3.08
M 0.17
RE 2.02
CL 0.287
CDW 0.0084
CM 0.0024
CP
-3.00
-2.50
-2.00
-1.50
-1.00
-.50
0.00
0.50
1.00
0.00
0.20
0.40
0.60
0.80
1.00
X/C

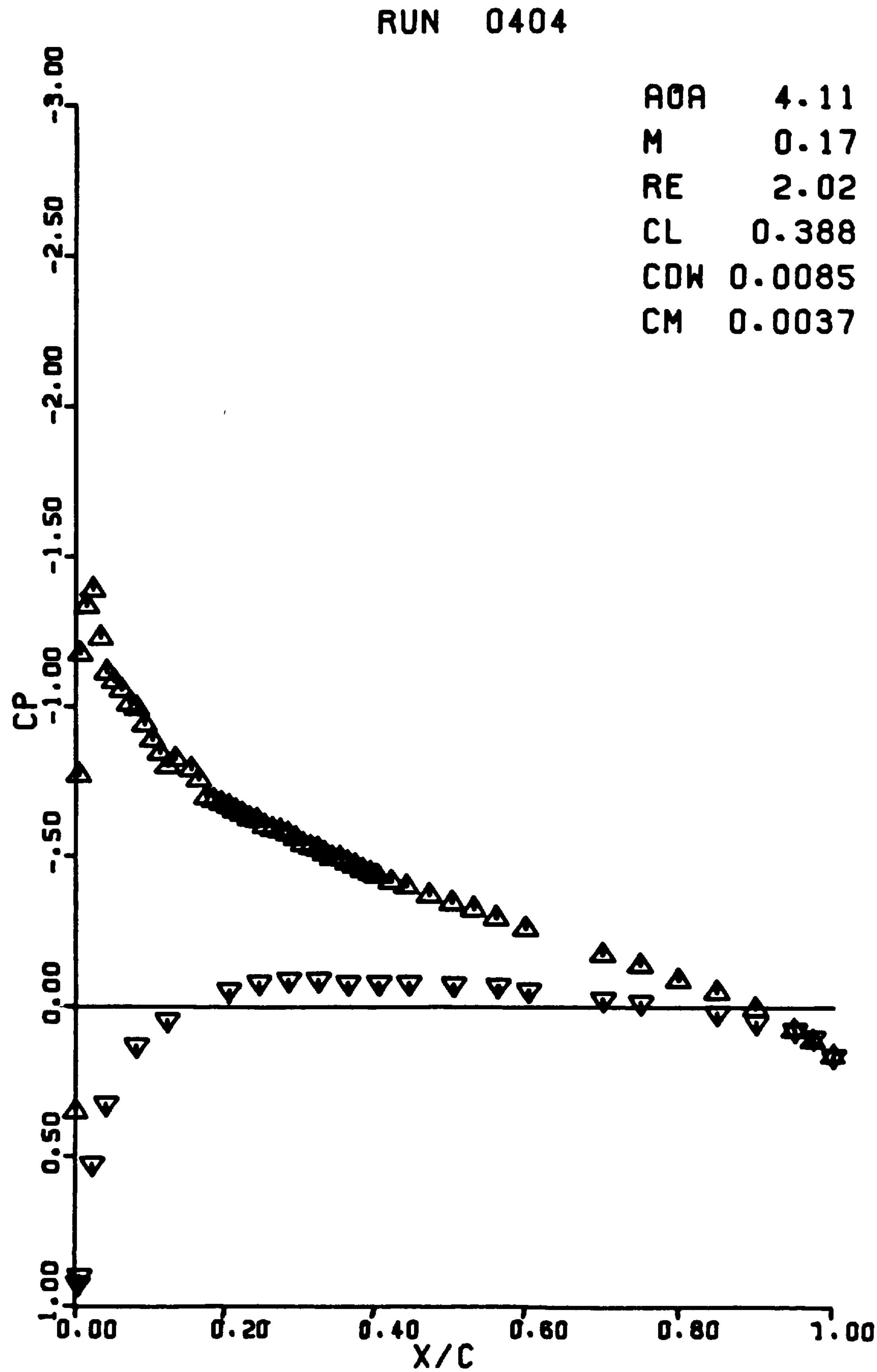
RUN 0404
AOA 4.11
M 0.17
RE 2.02
CL 0.388
CDW 0.0085
CM 0.0037
CP
-3.00
-2.50
-2.00
-1.50
-1.00
-.50
0.00
0.50
1.00
0.00
0.20
0.40
0.60
0.80
1.00
X/C

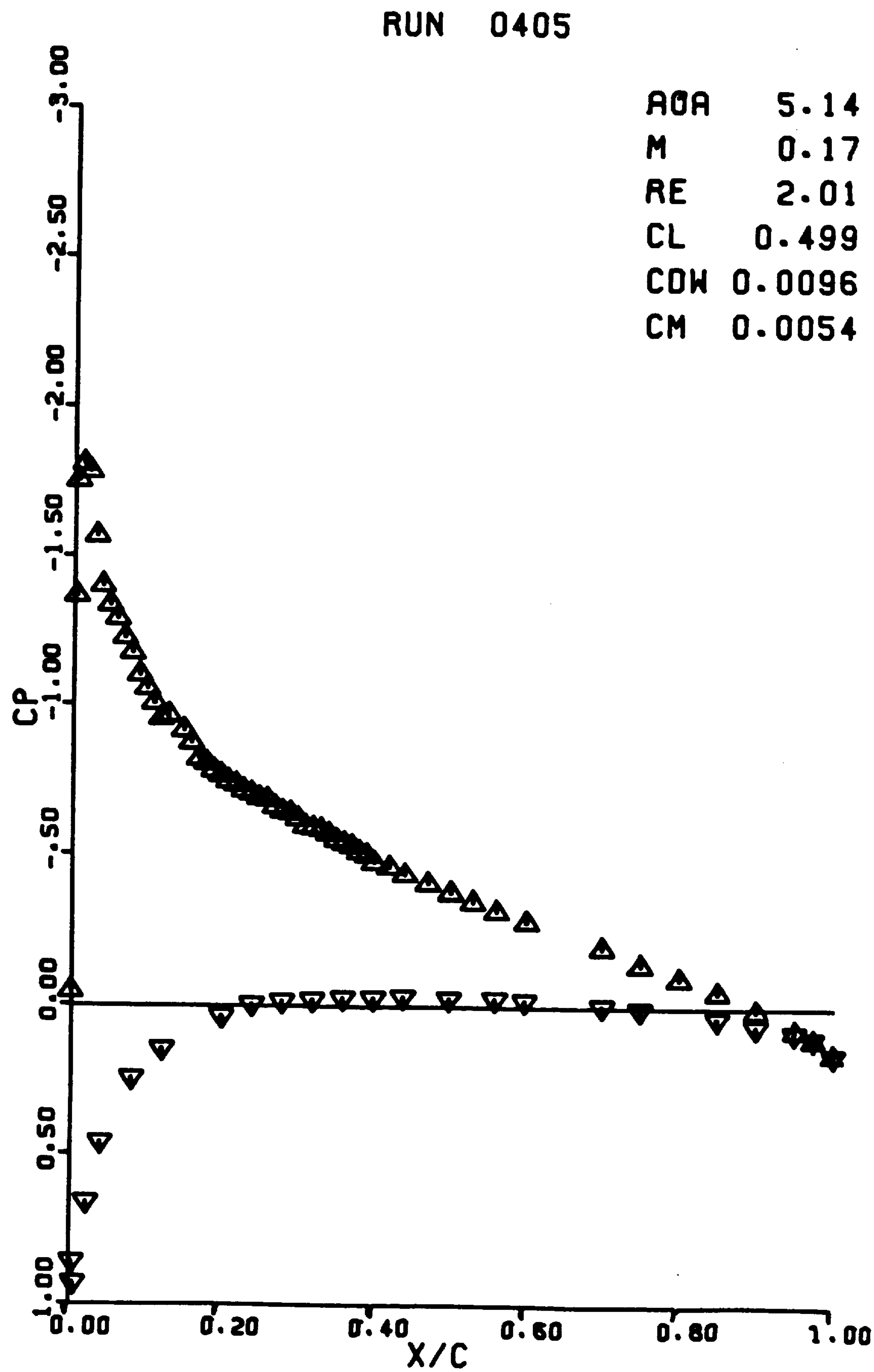
RUN 0405
AOA 5.14
M 0.17
RE 2.01
CL 0.499
CDW 0.0096
CM 0.0054
CP
-3.00
-2.50
-2.00
-1.50
-1.00
-.50
0.00
0.50
1.00
0.00
0.20
0.40
0.60
0.80
1.00
X/C

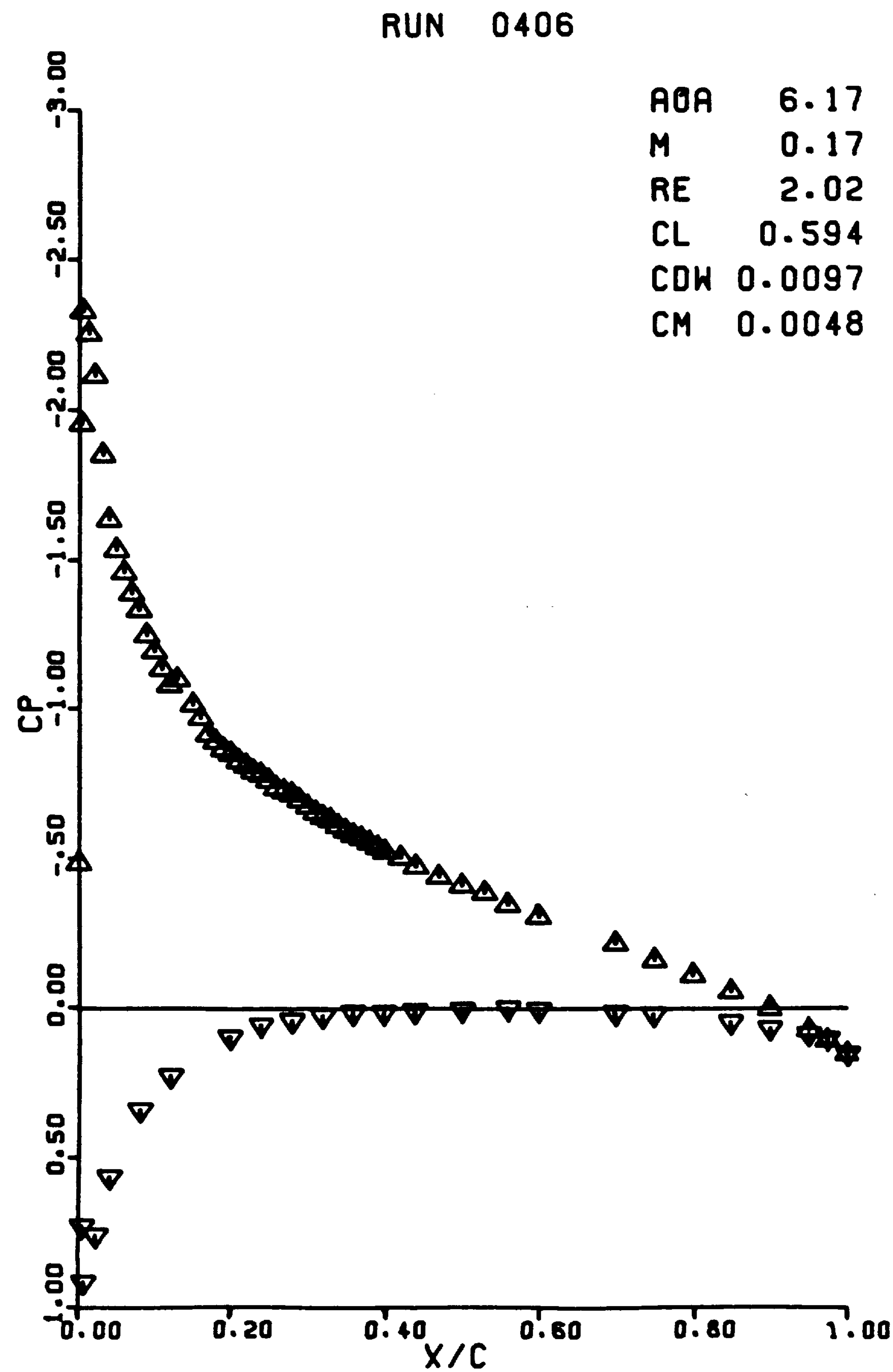
RUN 0406
AOA 6.17
M 0.17
RE 2.02
CL 0.594
CDW 0.0097
CM 0.0048
CP
-3.00
-2.50
-2.00
-1.50
-1.00
-.50
0.00
0.50
1.00
0.00
0.20
0.40
0.60
0.80
1.00
X/C

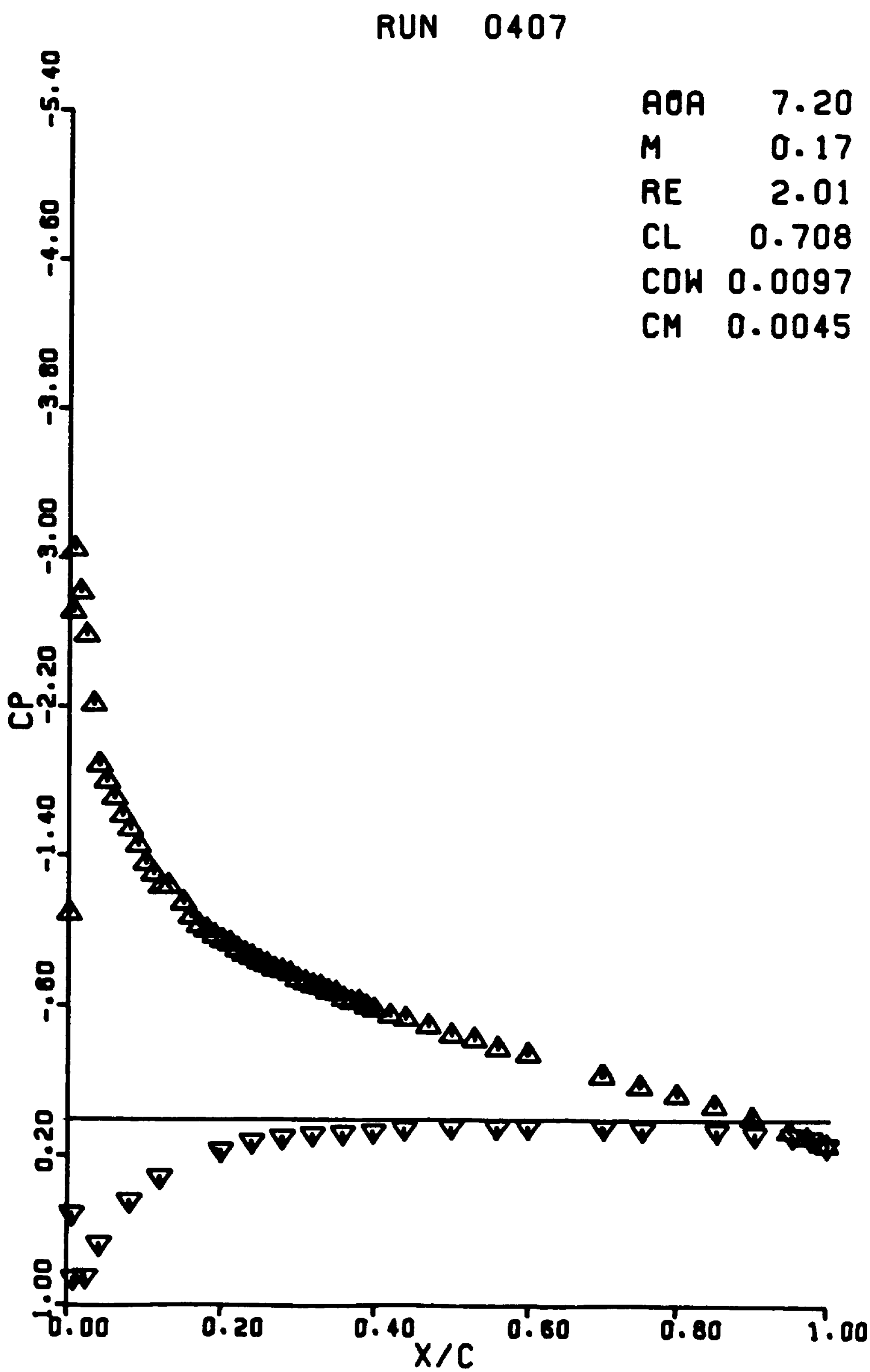
RUN 0407
AOA 7.20
M 0.17
RE 2.01
CL 0.708
CDW 0.0097
CM 0.0045
CP
-5.40
-4.60
-3.80
-3.00
-2.20
-1.40
-.60
0.20
1.00
0.00
0.20
0.40
0.60
0.80
1.00
X/C

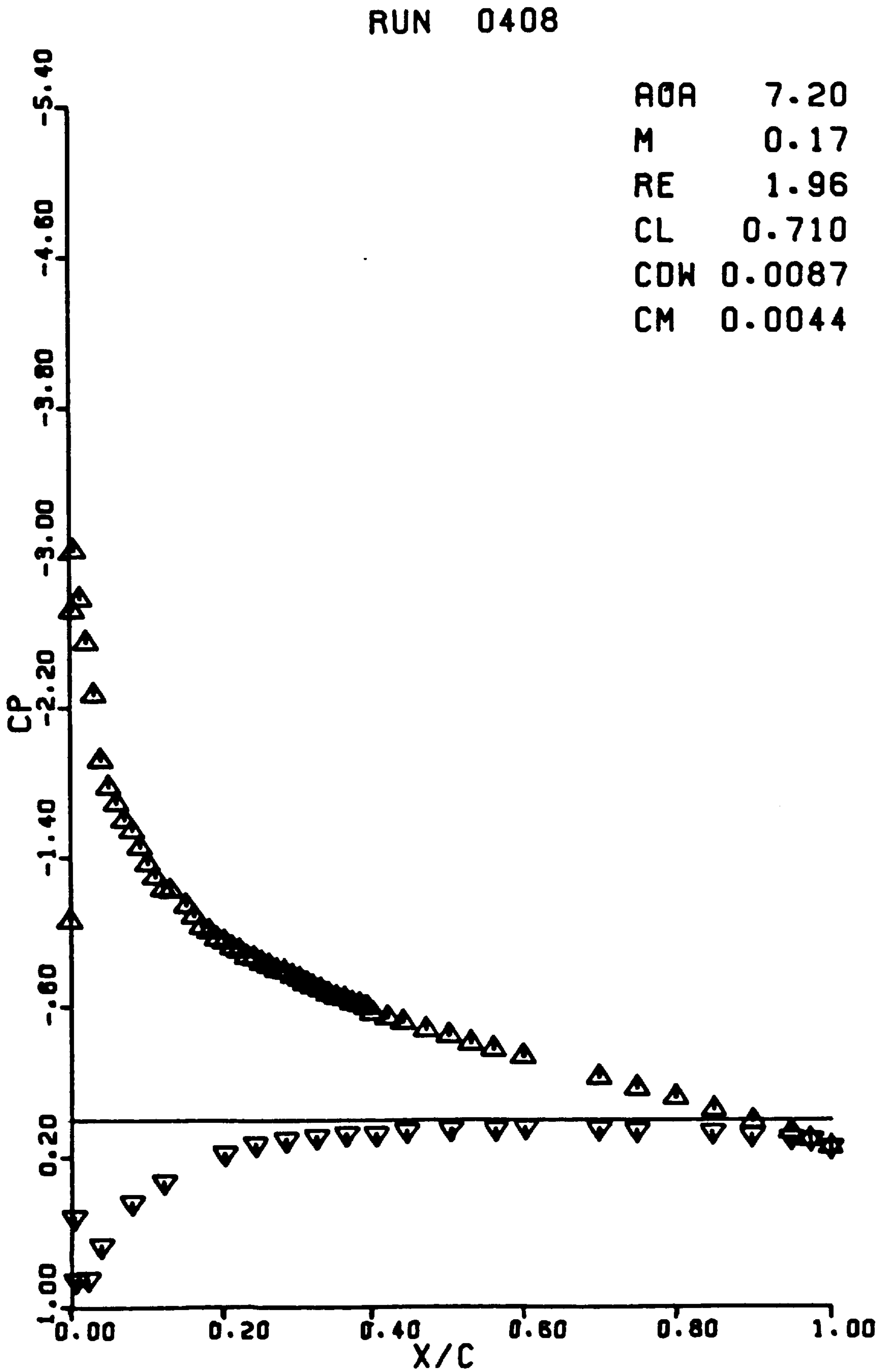
RUN 0408
AOA 7.20
M 0.17
RE 1.96
CL 0.710
CDW 0.0087
CM 0.0044
CP
-5.40
-4.60
-3.80
-3.00
-2.20
-1.40
-.60
0.20
1.00
0.00
0.20
0.40
0.60
0.80
1.00
X/C

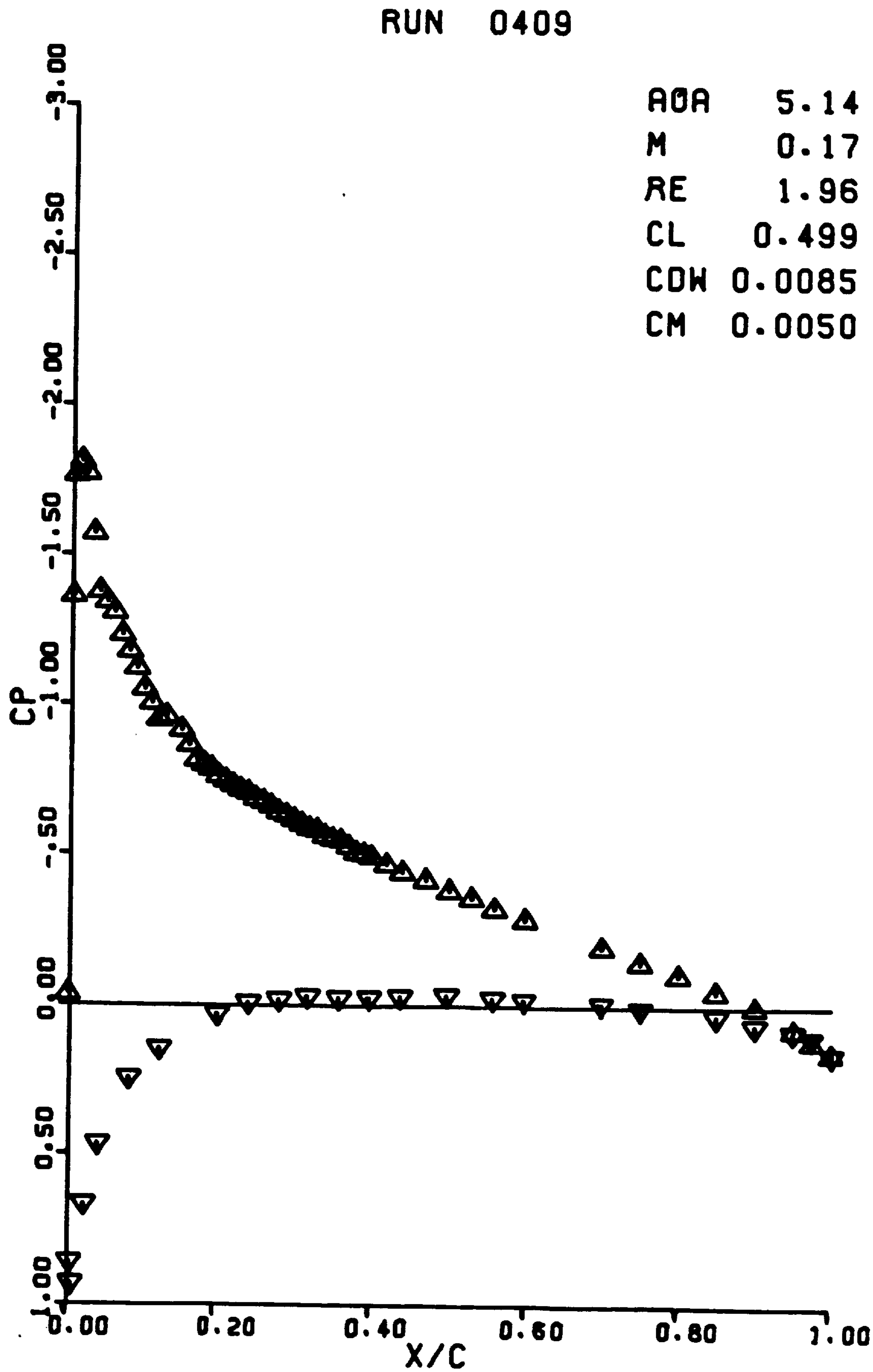

RUN 0409
AOA 5.14
M 0.17
RE 1.96
CL 0.499
CDW 0.0085
CM 0.0050
CP
-3.00
-2.50
-2.00
-1.50
-1.00
-.50
0.00
0.50
1.00
0.00
0.20
0.40
0.60
0.80
1.00
X/C

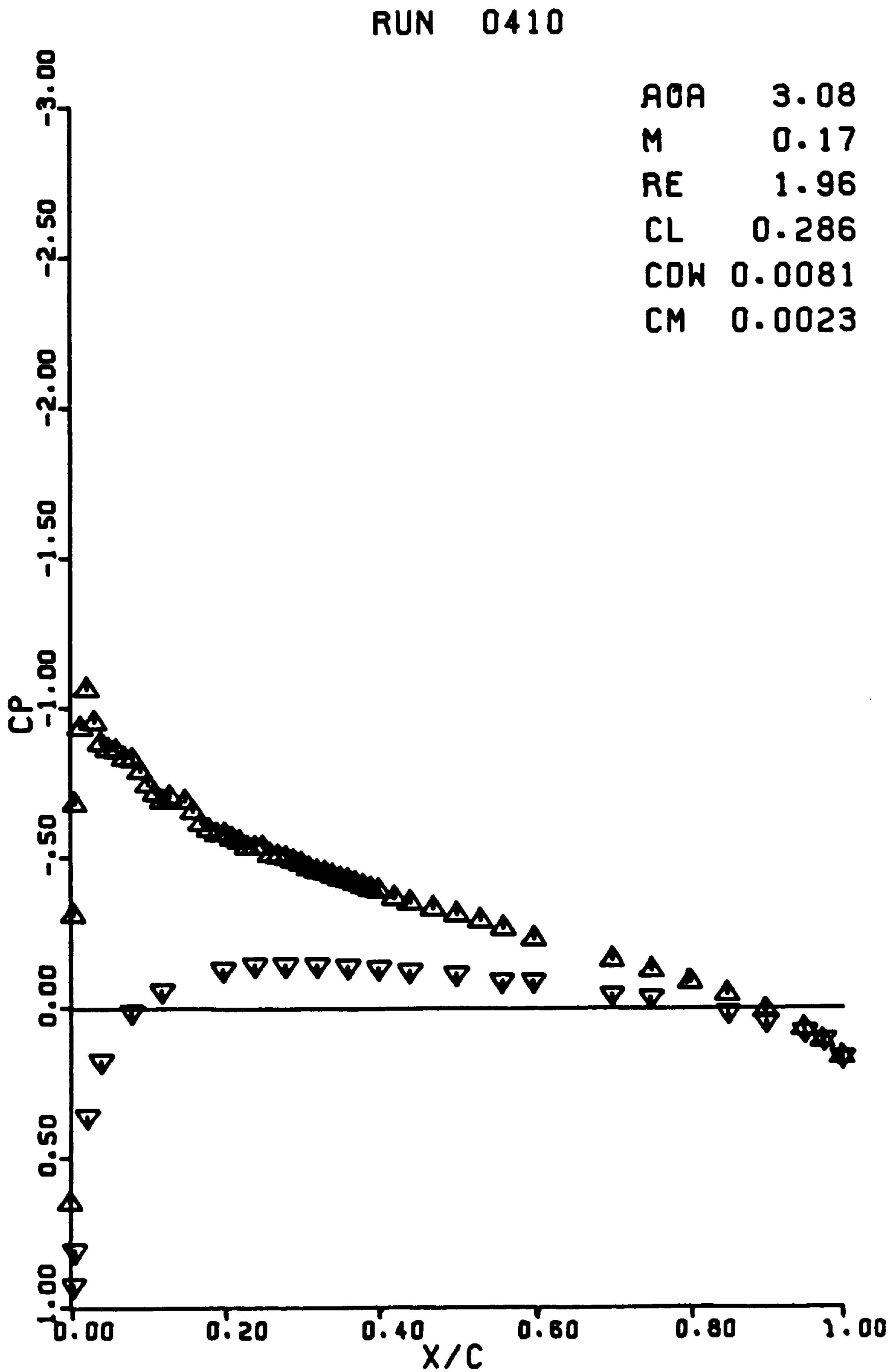
RUN 0410
AOA 3.08
M 0.17
RE 1.96
CL 0.286
CDW 0.0081
CM 0.0023
CP
-3.00
-2.50
-2.00
-1.50
-1.00
-.50
0.00
0.50
1.00
0.00
0.20
0.40
0.60
0.80
1.00
X/C

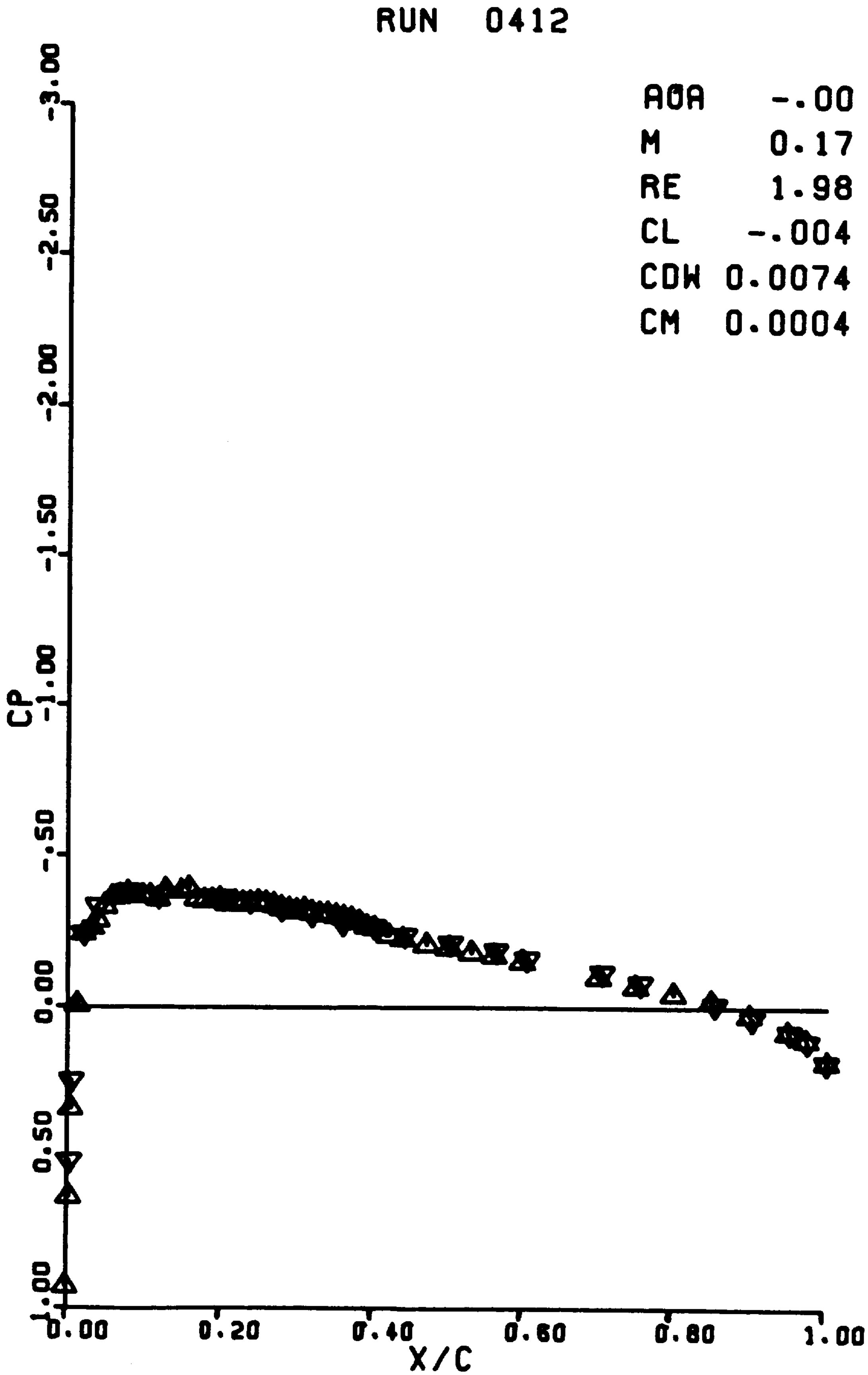
RUN 0412
AOA -.00
M 0.17
RE 1.98
CL -.004
CDW 0.0074
CM 0.0004
CP
-3.00
-2.50
-2.00
-1.50
-1.00
-.50
0.00
0.50
1.00
0.00
0.20
0.40
0.60
0.80
1.00
X/C

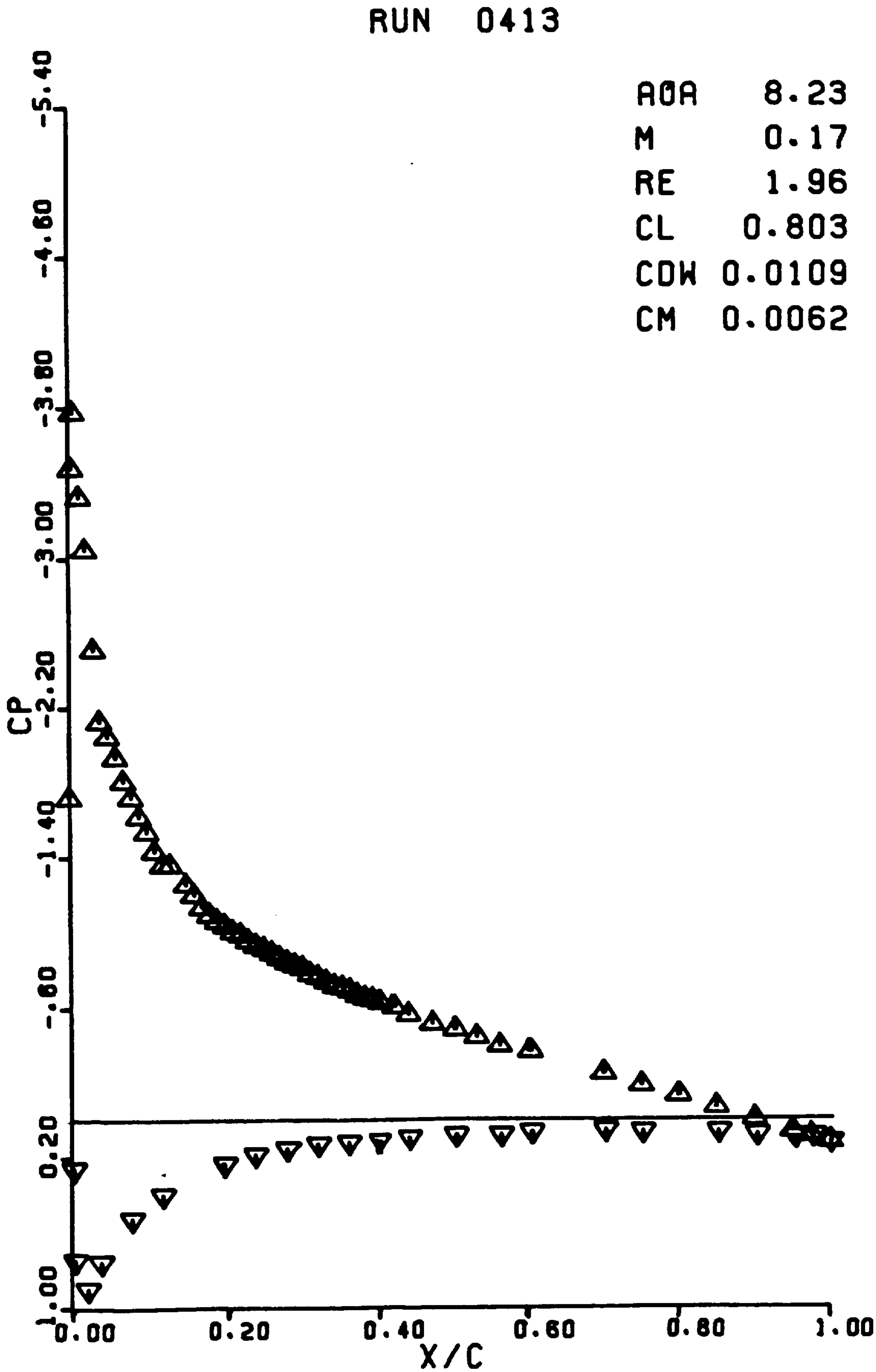

RUN 0413
AOA 8.23
M 0.17
RE 1.96
CL 0.803
CDW 0.0109
CM 0.0062
CP
-5.40
-4.60
-3.80
-3.00
-2.20
-1.40
-.60
0.20
1.00
0.00
0.20
0.40
0.60
0.80
1.00
X/C

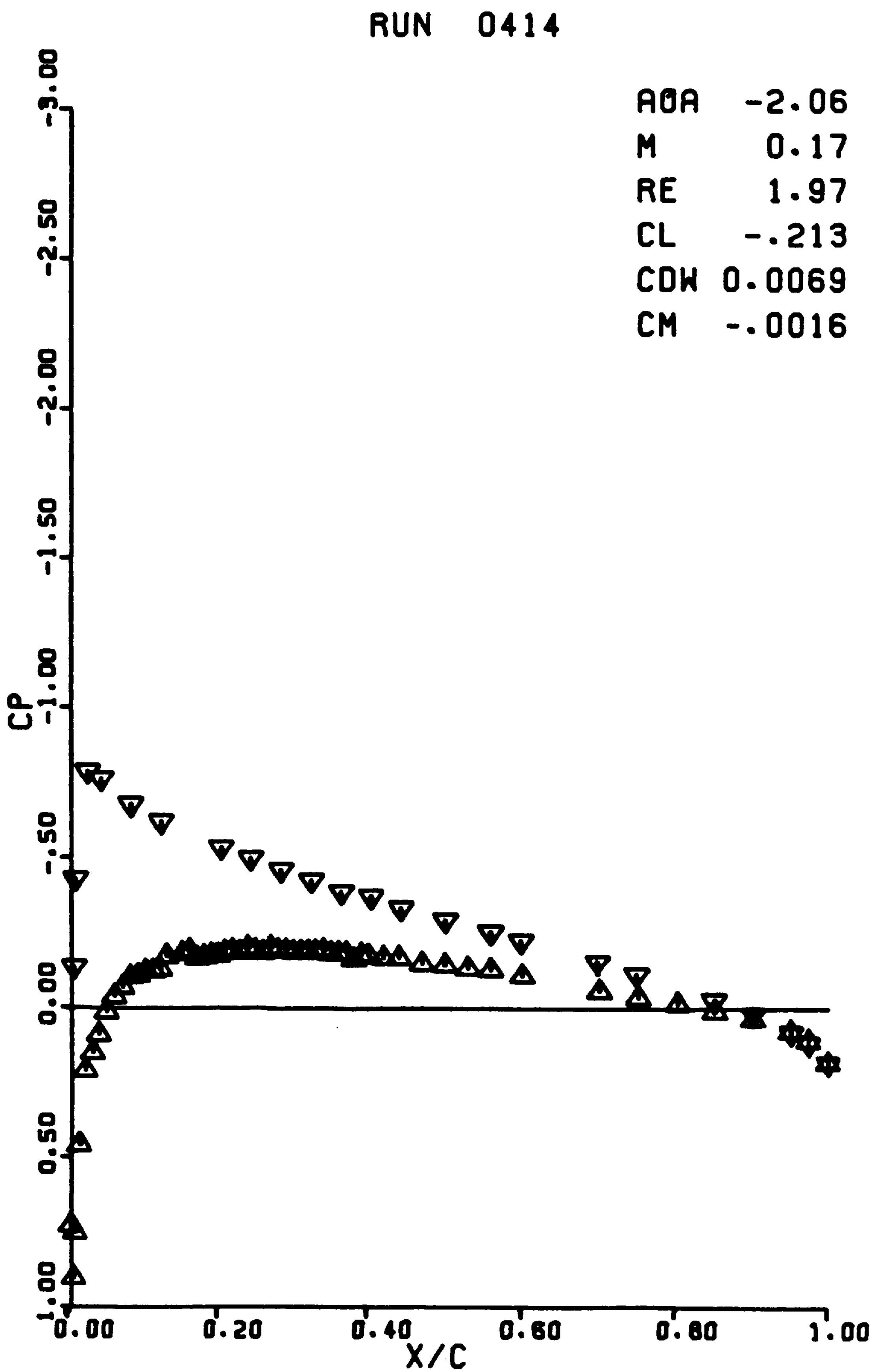
RUN 0414
AOA -2.06
M 0.17
RE 1.97
CL -.213
CDW 0.0069
CM -.0016
CP
-3.00
-2.50
-2.00
-1.50
-1.00
-.50
0.00
0.50
1.00
0.00
0.20
0.40
0.60
0.80
1.00
X/C

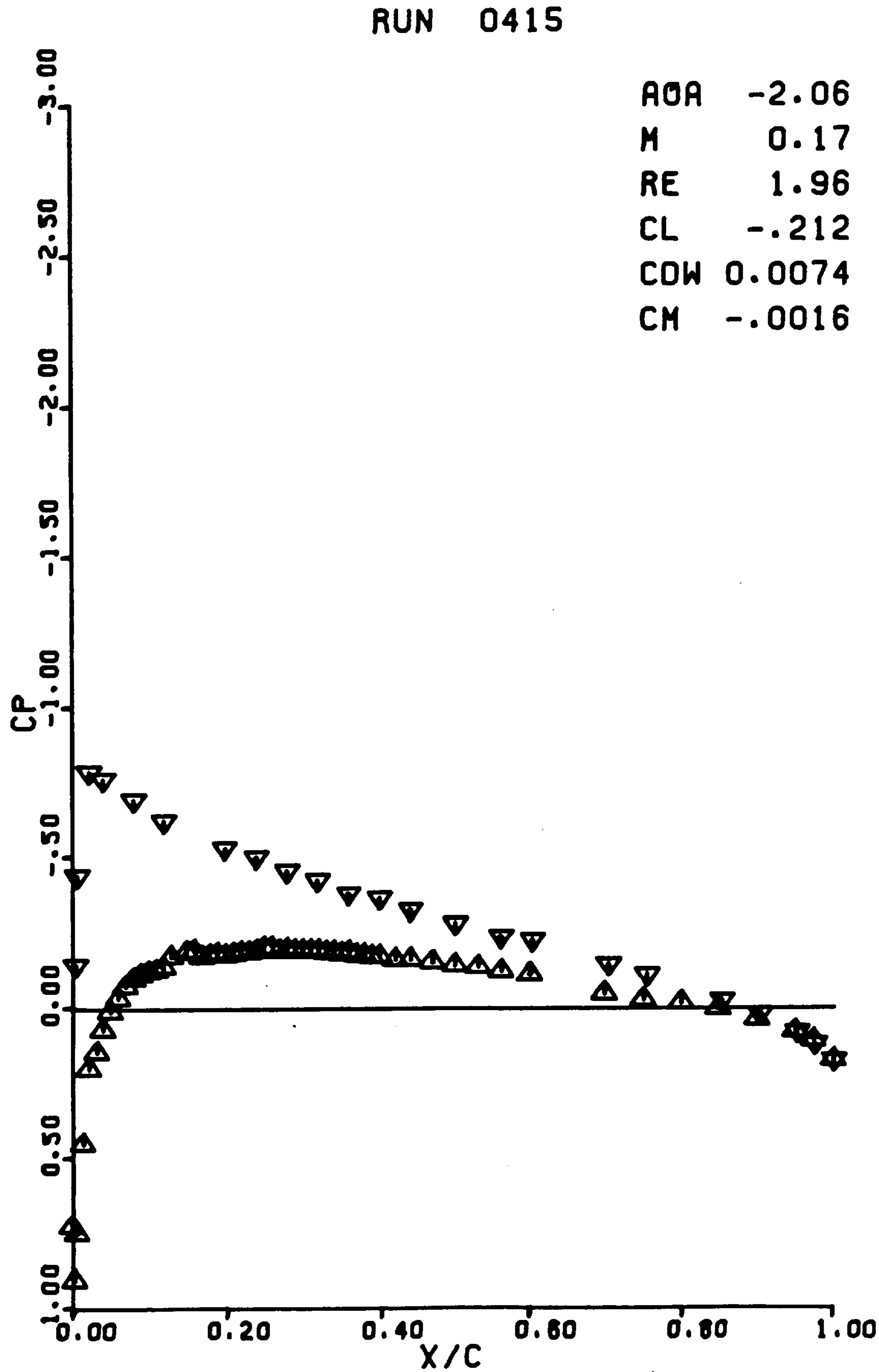
RUN 0415
AOA -2.06
M 0.17
RE 1.96
CL -.212
CDW 0.0074
CM -.0016
CP
-3.00
-2.50
-2.00
-1.50
-1.00
-.50
0.00
0.50
1.00
0.00
0.20
0.40
0.60
0.80
1.00
X/C

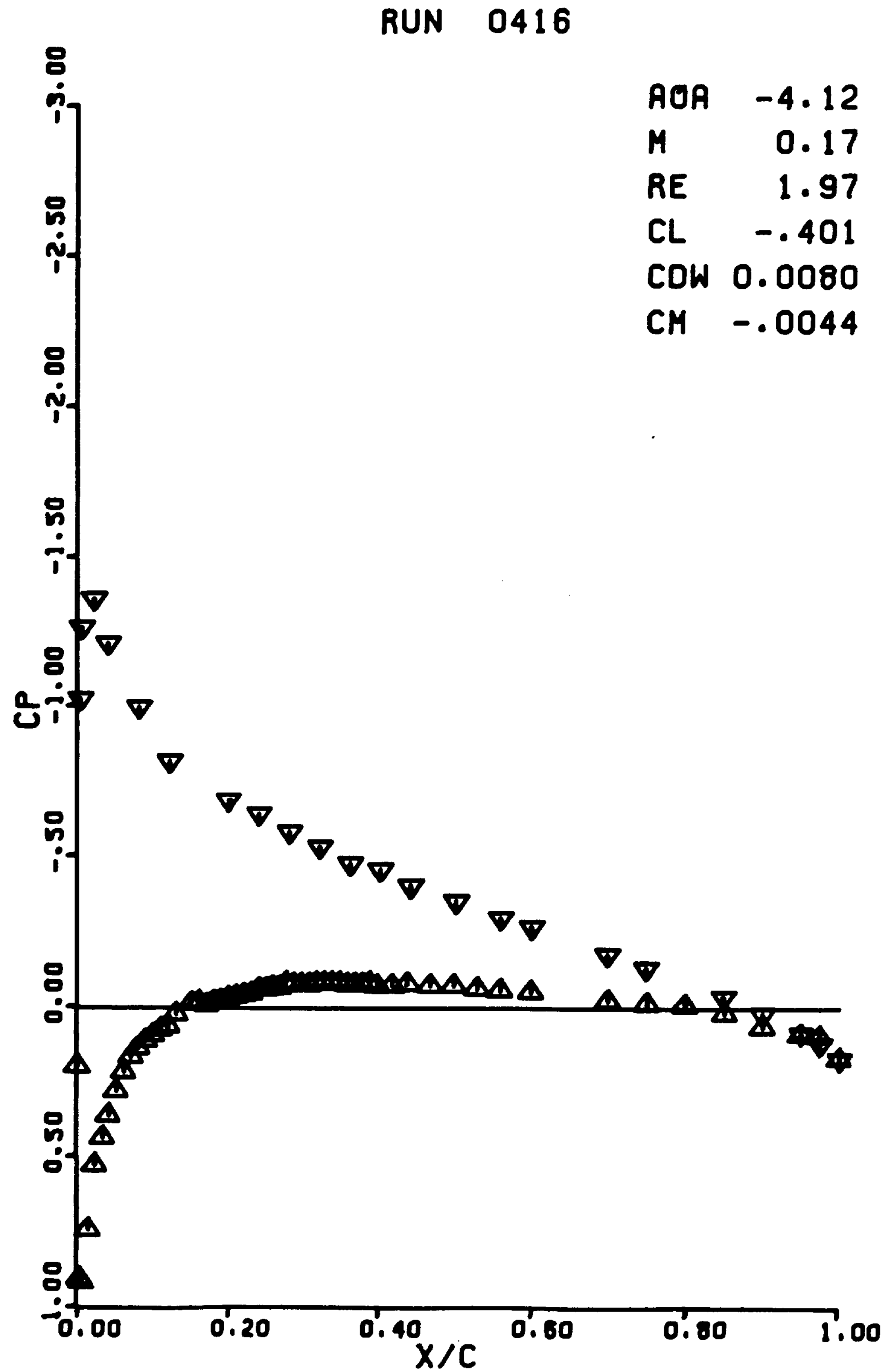
RUN 0416
AOA -4.12
M 0.17
RE 1.97
CL -.401
CDW 0.0080
CM -.0044
CP
X/C
-3.00
-2.50
-2.00
-1.50
-1.00
-.50
0.00
0.50
1.00
0.00
0.20
0.40
0.60
0.80
1.00

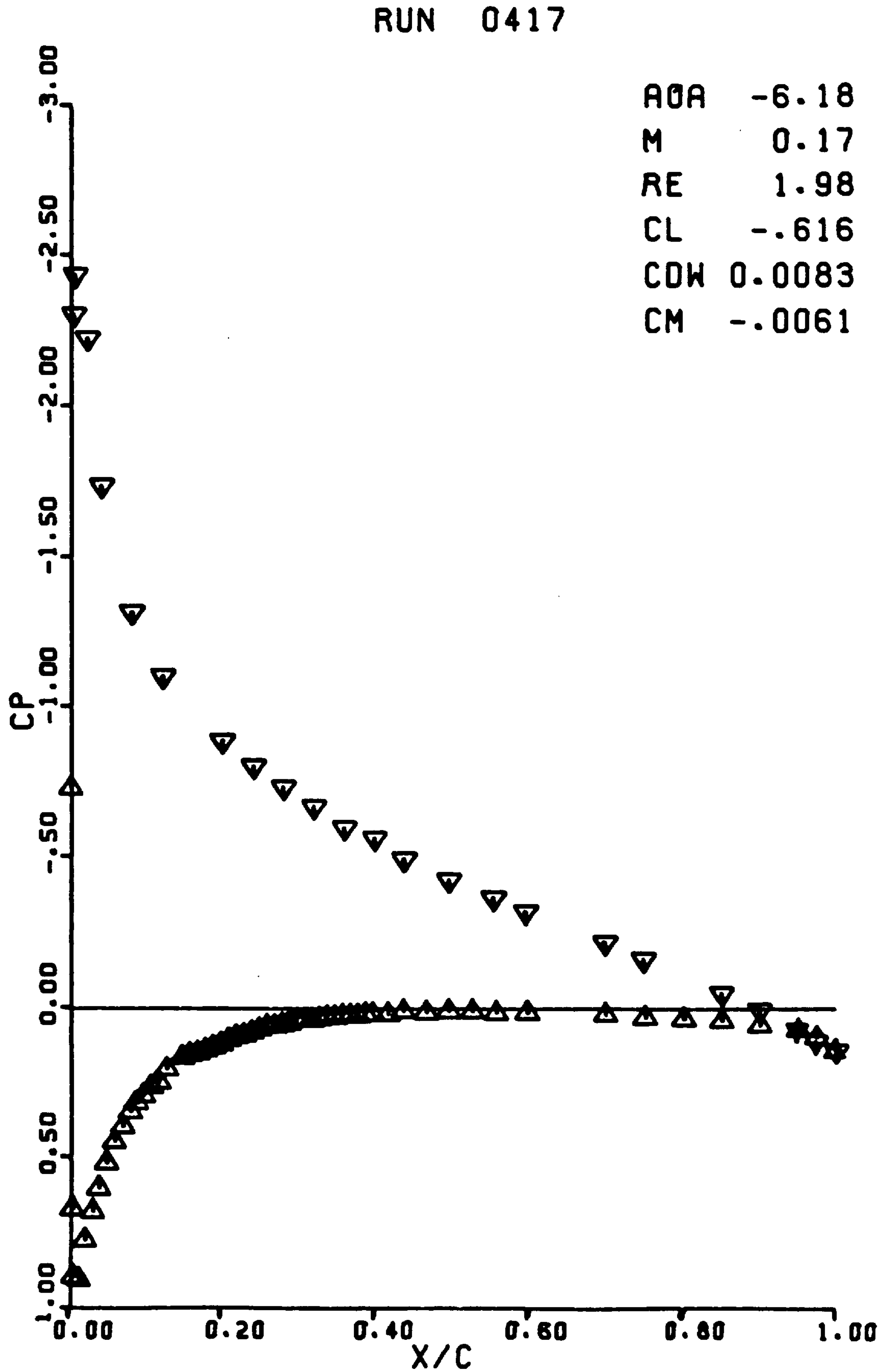
RUN 0417
AOA -6.18
M 0.17
RE 1.98
CL -.616
CDW 0.0083
CM -.0061
CP
-3.00
-2.50
-2.00
-1.50
-1.00
-.50
0.00
0.50
1.00
0.00
0.20
0.40
0.60
0.80
1.00
X/C

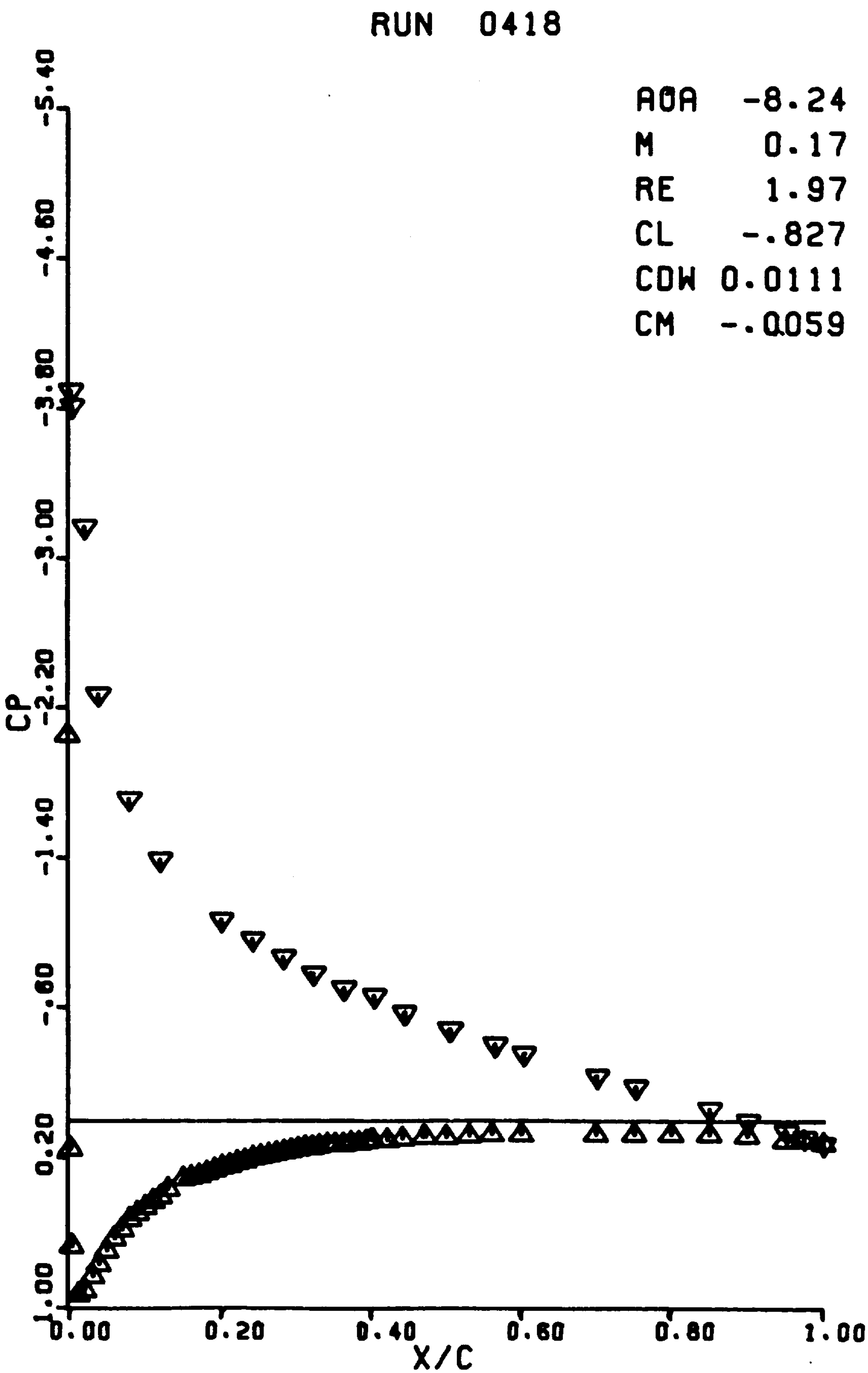

RUN 0418
AOA -8.24
M 0.17
RE 1.97
CL -.827
CDW 0.0111
CM -.0059
CP
-5.40
-4.60
-3.80
-3.00
-2.20
-1.40
-.60
0.20
1.00
0.00
0.20
0.40
0.60
0.80
1.00
X/C

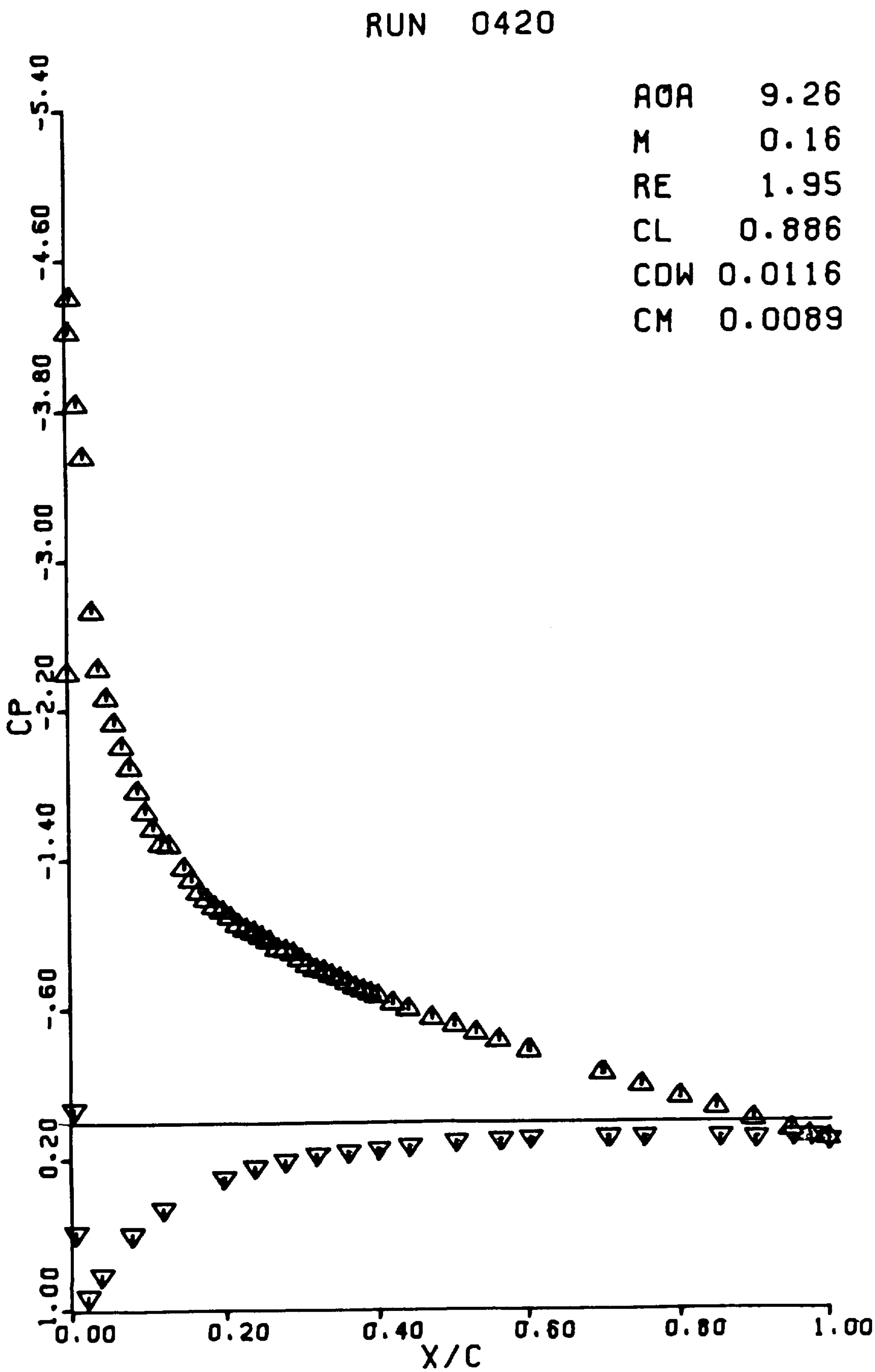
RUN 0420
AOA 9.26
M 0.16
RE 1.95
CL 0.886
CDW 0.0116
CM 0.0089
CP
-5.40
-4.60
-3.80
-3.00
-2.20
-1.40
-.60
0.20
1.00
X/C
0.00
0.20
0.40
0.60
0.80
1.00

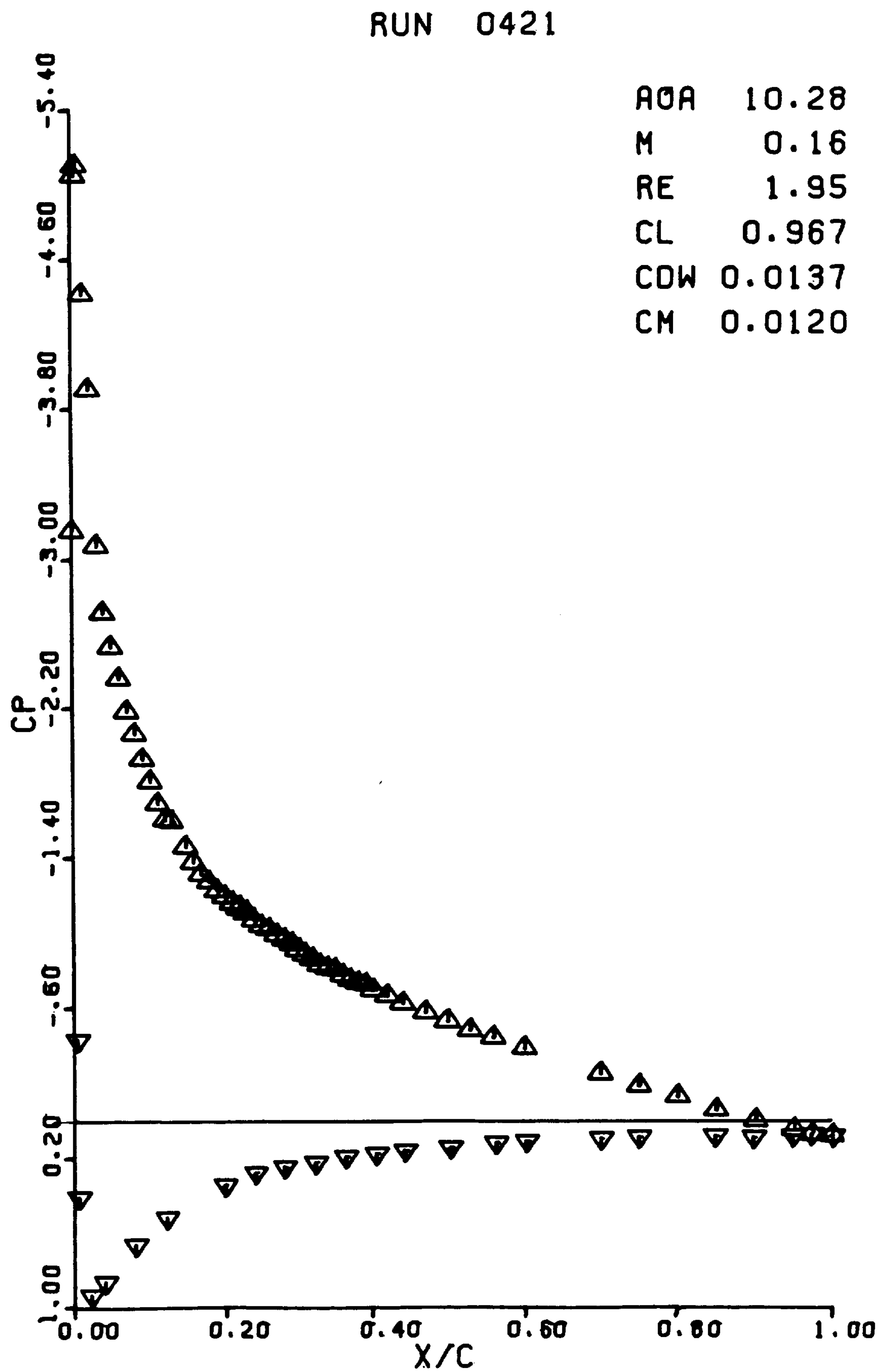
RUN 0421
AOA 10.28
M 0.16
RE 1.95
CL 0.967
CDW 0.0137
CM 0.0120
CP
-5.40
-4.60
-3.80
-3.00
-2.20
-1.40
-.60
0.20
1.00
X/C
0.00
0.20
0.40
0.60
0.80
1.00

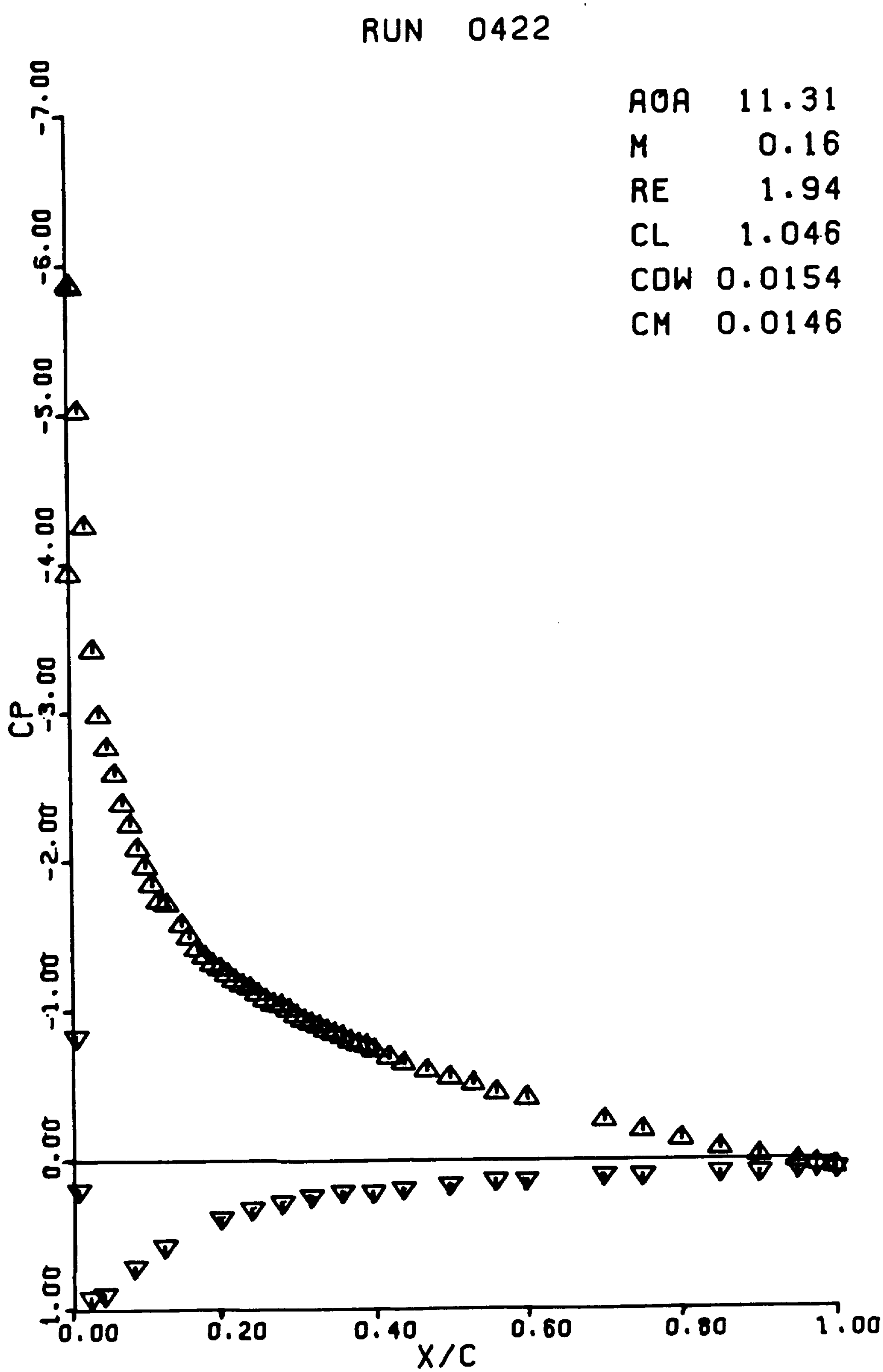
RUN 0422
AOA 11.31
M 0.16
RE 1.94
CL 1.046
CDW 0.0154
CM 0.0146
CP
-7.00
-6.00
-5.00
-4.00
-3.00
-2.00
-1.00
0.00
1.00
0.00
0.20
0.40
0.60
0.80
1.00
X/C

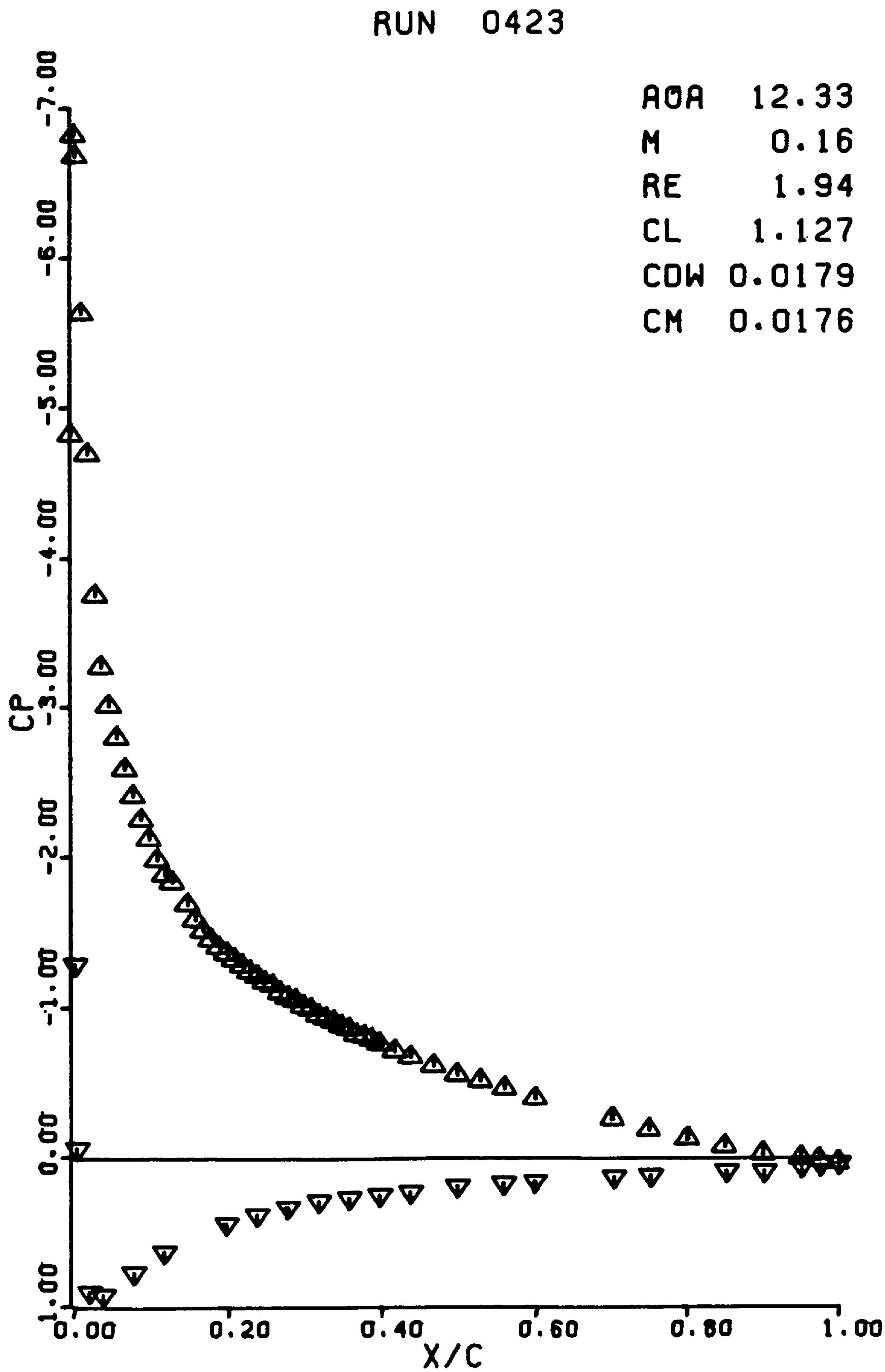

RUN 0423
AOA 12.33
M 0.16
RE 1.94
CL 1.127
CDW 0.0179
CM 0.0176
CP
-7.00
-6.00
-5.00
-4.00
-3.00
-2.00
-1.00
0.00
1.00
X/C
0.00
0.20
0.40
0.60
0.80
1.00

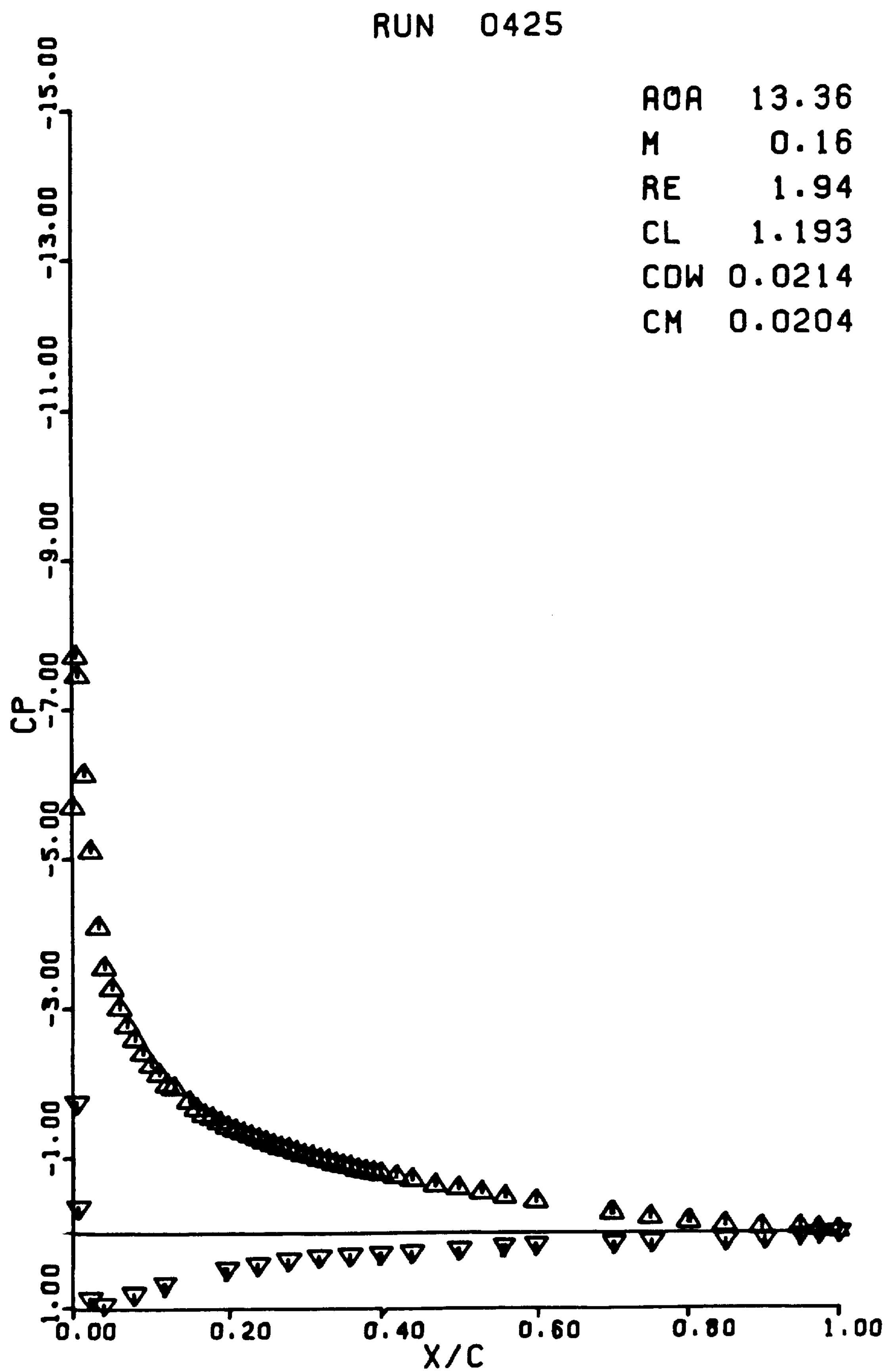
RUN 0425
AOA 13.36
M 0.16
RE 1.94
CL 1.193
CDW 0.0214
CM 0.0204
CP
-15.00
-13.00
-11.00
-9.00
-7.00
-5.00
-3.00
-1.00
1.00
0.00
0.20
0.40
0.60
0.80
1.00
X/C

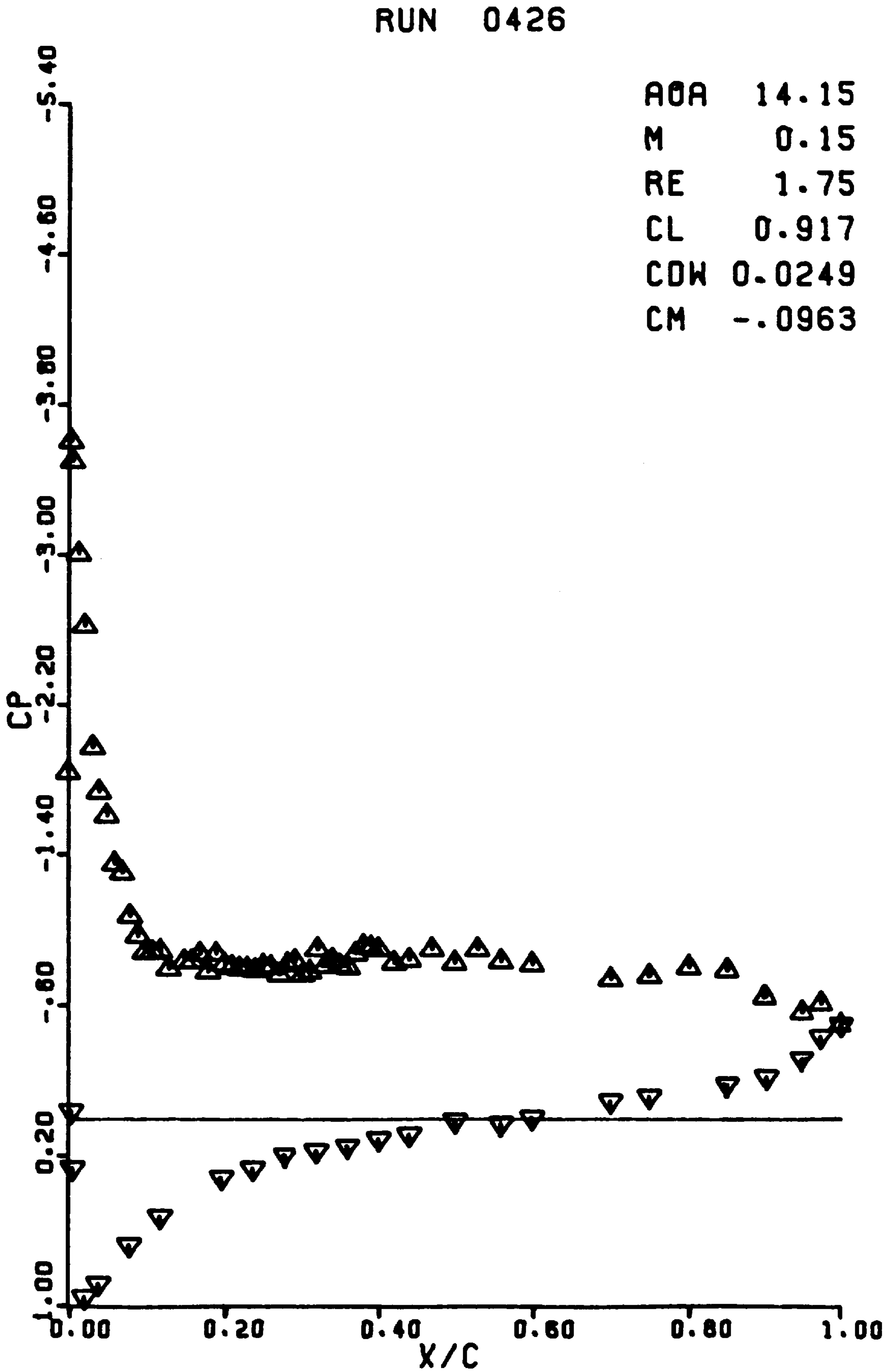
RUN 0426
AOA 14.15
M 0.15
RE 1.75
CL 0.917
CDW 0.0249
CM -.0963
CP
-5.40
-4.60
-3.80
-3.00
-2.20
-1.40
-.60
0.20
1.00
0.00
0.20
0.40
0.60
0.80
1.00
X/C

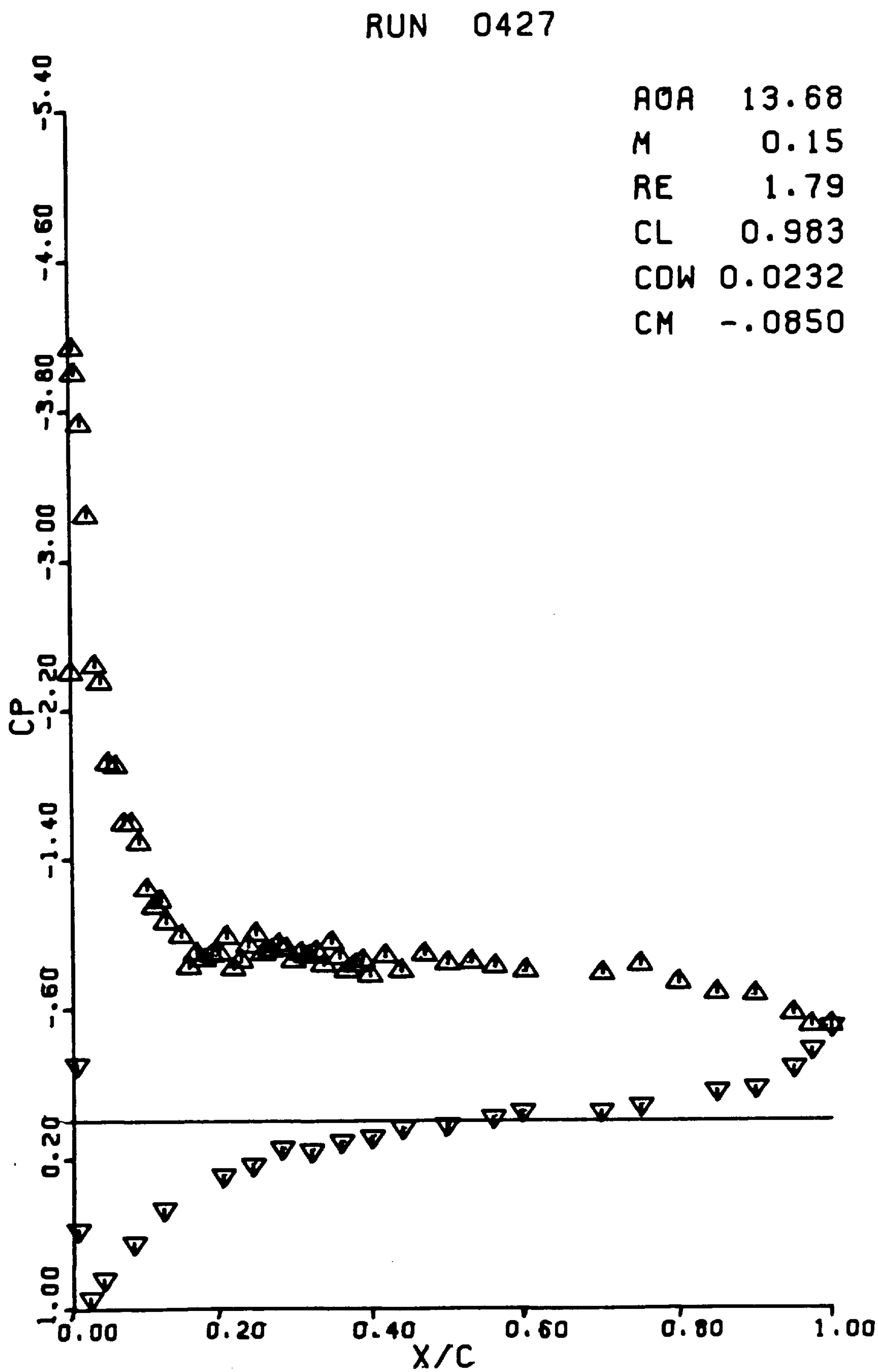

RUN 0427
AOA 13.68
M 0.15
RE 1.79
CL 0.983
CDW 0.0232
CM -.0850
CP
-5.40
-4.60
-3.80
-3.00
-2.20
-1.40
-.60
0.20
1.00
0.00
0.20
0.40
0.60
0.80
1.00
X/C

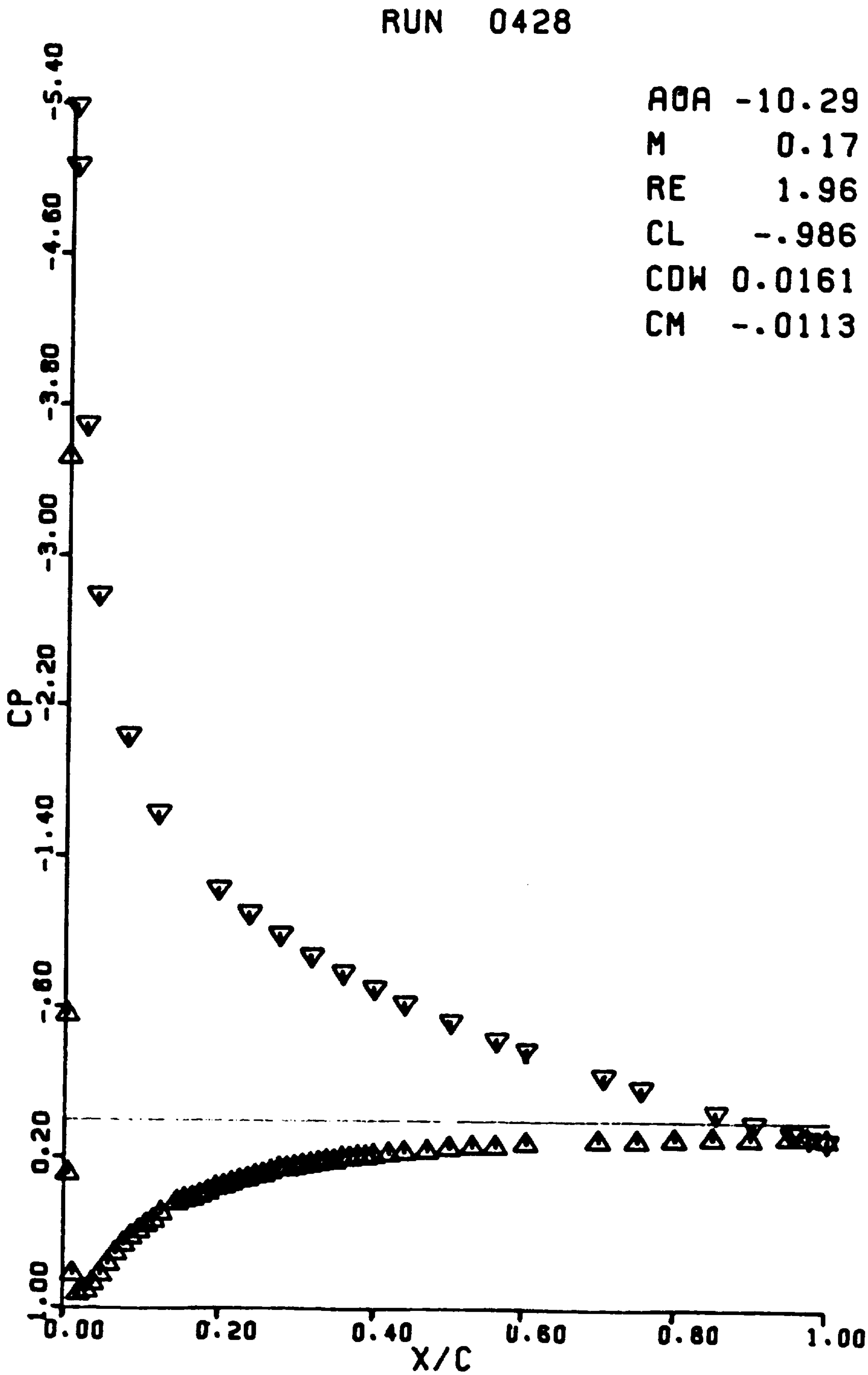
RUN 0428
AOA -10.29
M 0.17
RE 1.96
CL -.986
CDW 0.0161
CM -.0113
CP
-5.40
-4.60
-3.80
-3.00
-2.20
-1.40
-.60
0.20
1.00
X/C
0.00
0.20
0.40
0.60
0.80
1.00

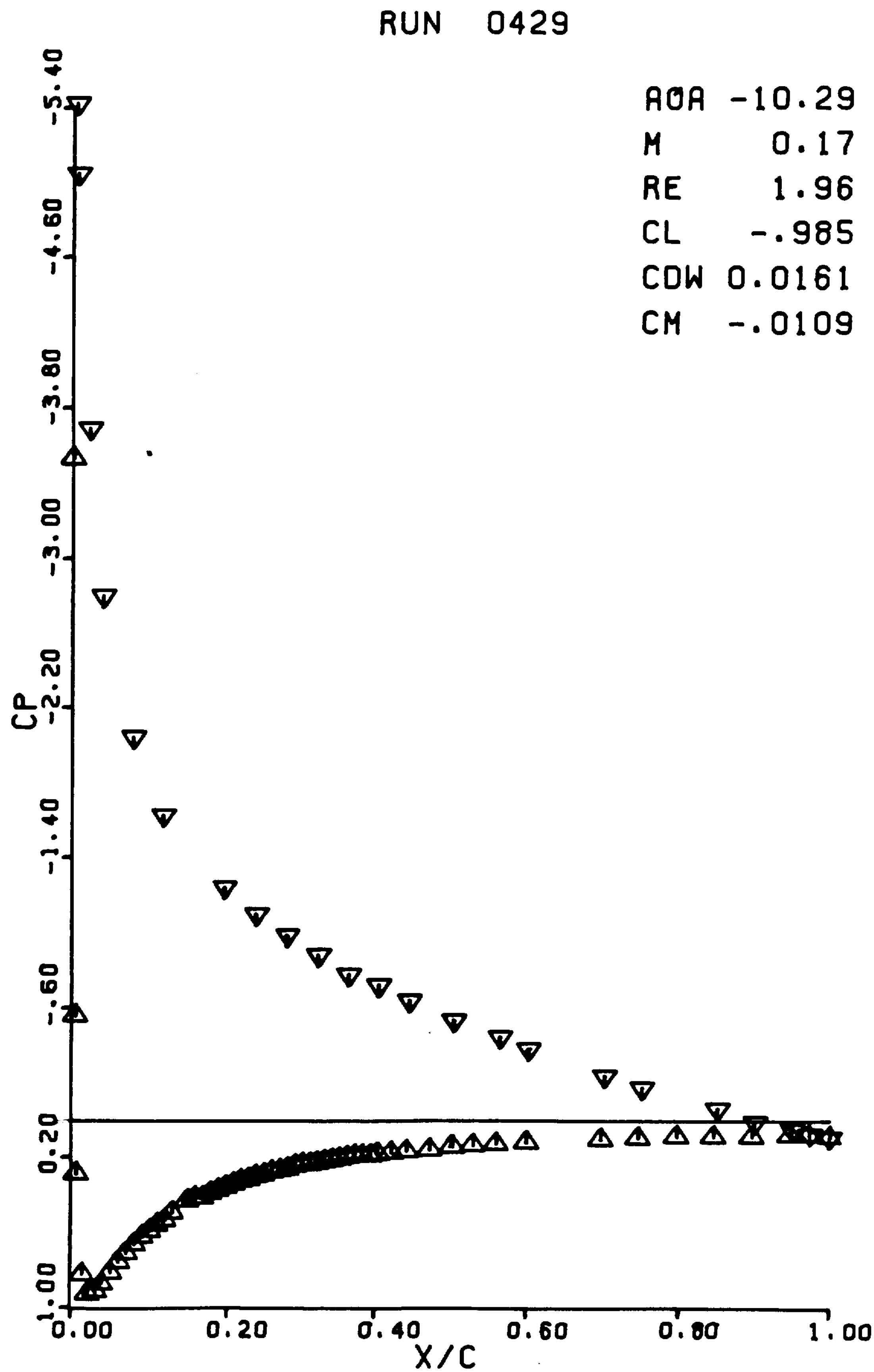
RUN 0429
AOA -10.29
M 0.17
RE 1.96
CL -.985
CDW 0.0161
CM -.0109
CP
-5.40
-4.60
-3.80
-3.00
-2.20
-1.40
-.60
0.20
1.00
X/C
0.00
0.20
0.40
0.60
0.80
1.00

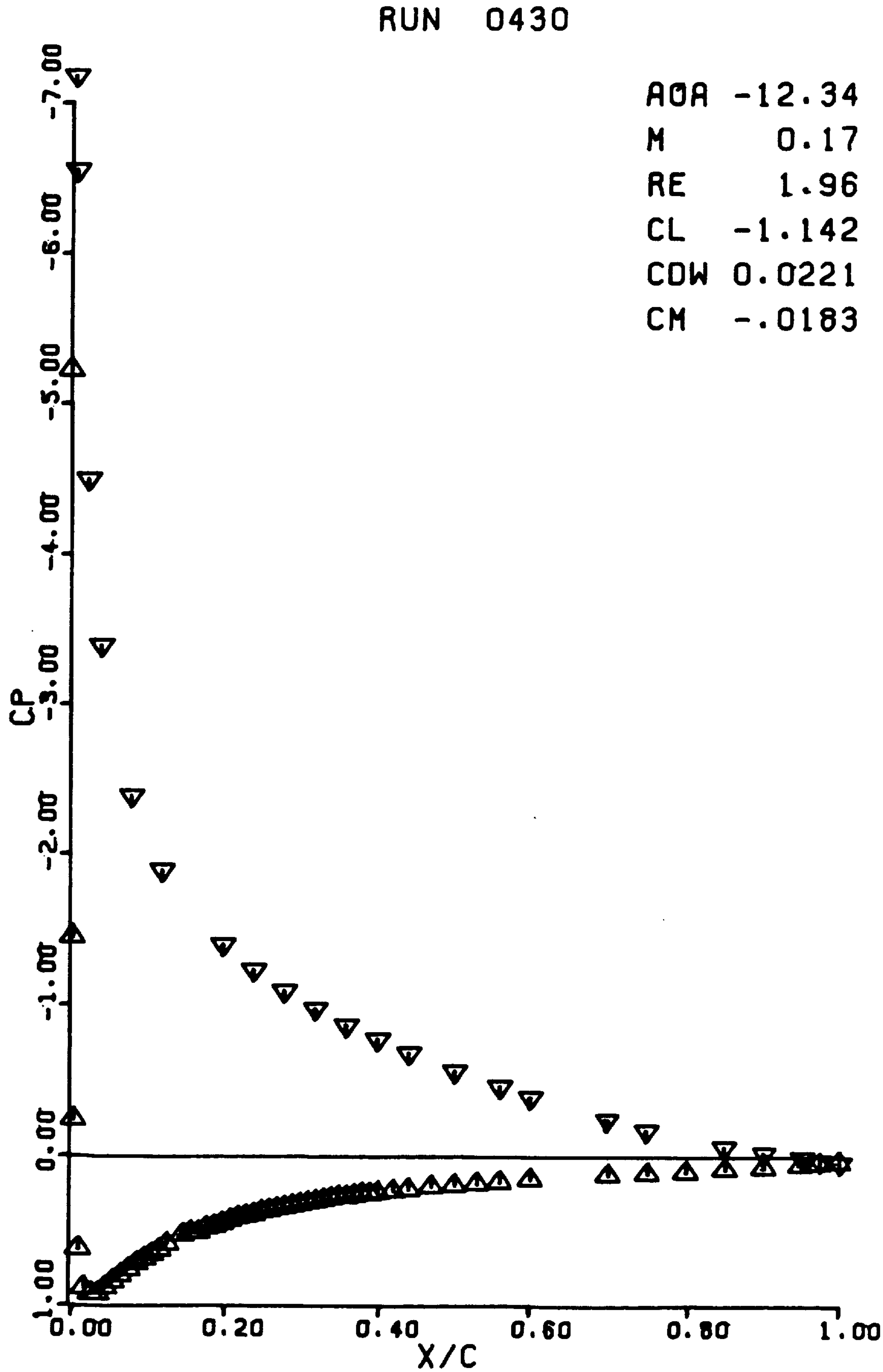

RUN 0430
AOA -12.34
M 0.17
RE 1.96
CL -1.142
CDW 0.0221
CM -.0183
CP
-7.00
-6.00
-5.00
-4.00
-3.00
-2.00
-1.00
0.00
1.00
0.00
0.20
0.40
0.60
0.80
1.00
X/C

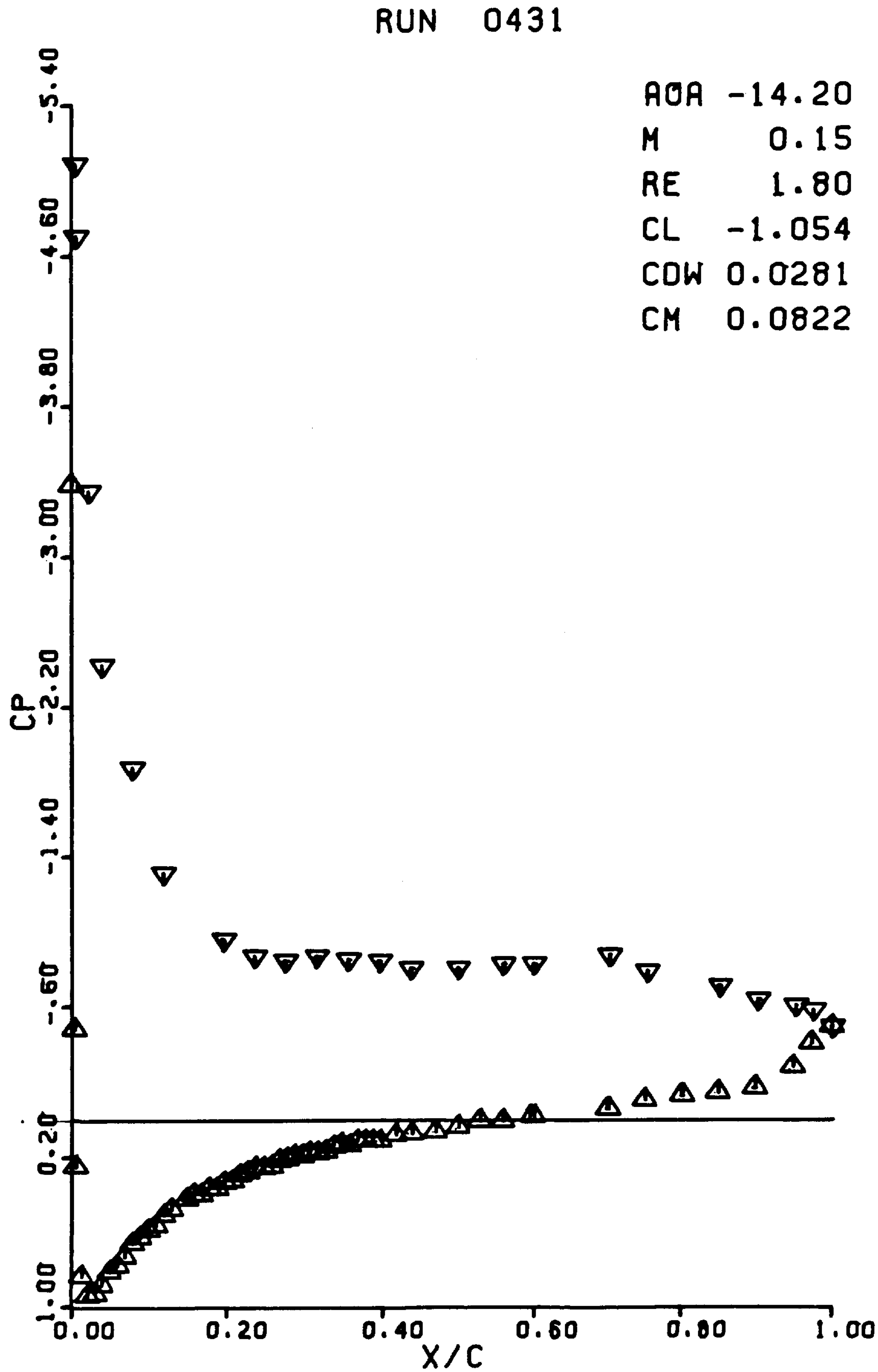
RUN 0431
AOA -14.20
M 0.15
RE 1.80
CL -1.054
CDW 0.0281
CM 0.0822
CP
X/C
-5.40
-4.60
-3.80
-3.00
-2.20
-1.40
-.60
0.20
1.00
0.00
0.20
0.40
0.60
0.80
1.00

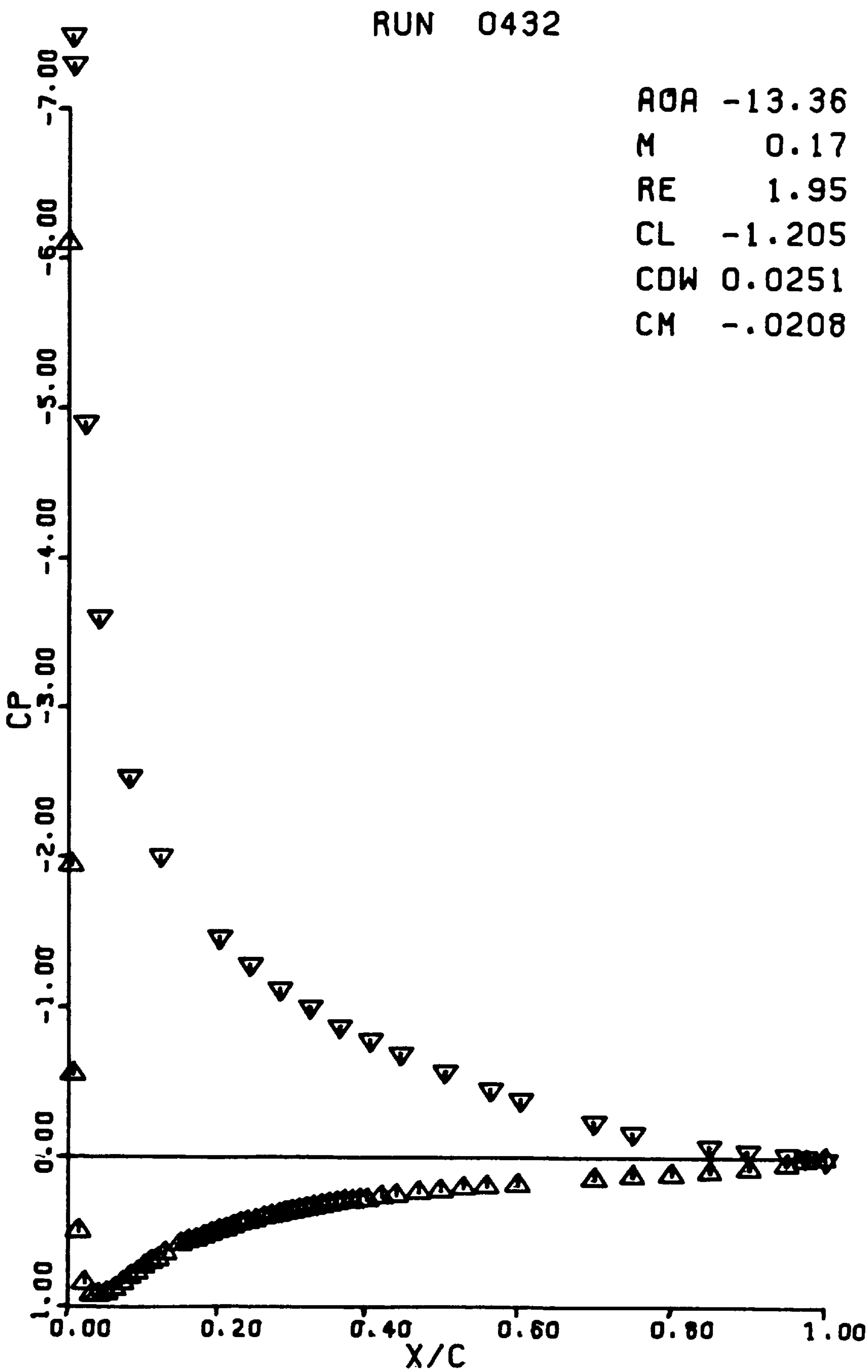

RUN 0432
AOA -13.36
M 0.17
RE 1.95
CL -1.205
CDW 0.0251
CM -.0208
CP
-7.00
-6.00
-5.00
-4.00
-3.00
-2.00
-1.00
0.00
1.00
0.00
0.20
0.40
0.60
0.80
1.00
X/C

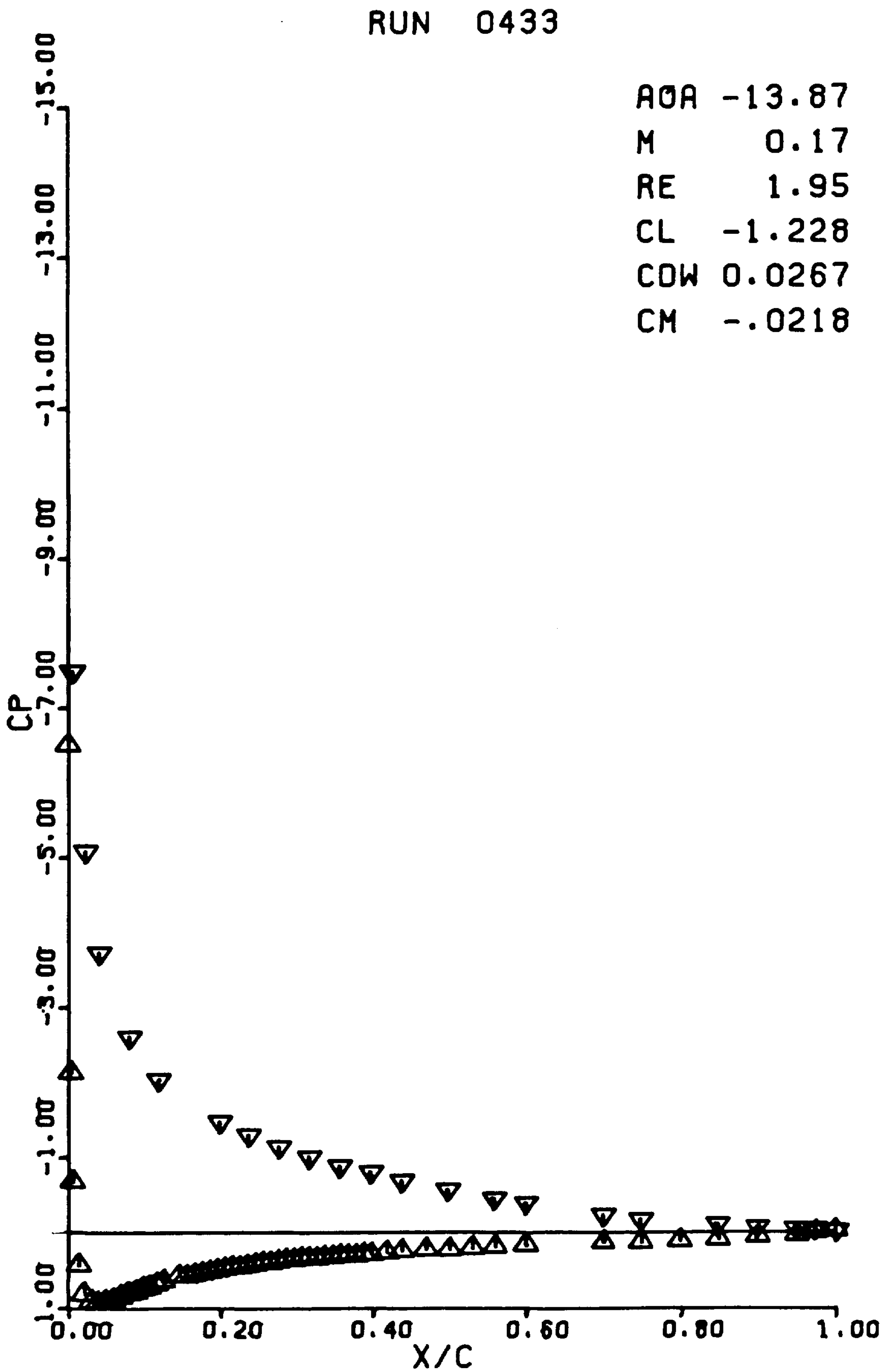

RUN 0433
AOA -13.87
M 0.17
RE 1.95
CL -1.228
CDW 0.0267
CM -.0218
CP
-15.00
-13.00
-11.00
-9.00
-7.00
-5.00
-3.00
-1.00
1.00
0.00
0.20
0.40
0.60
0.80
1.00
X/C

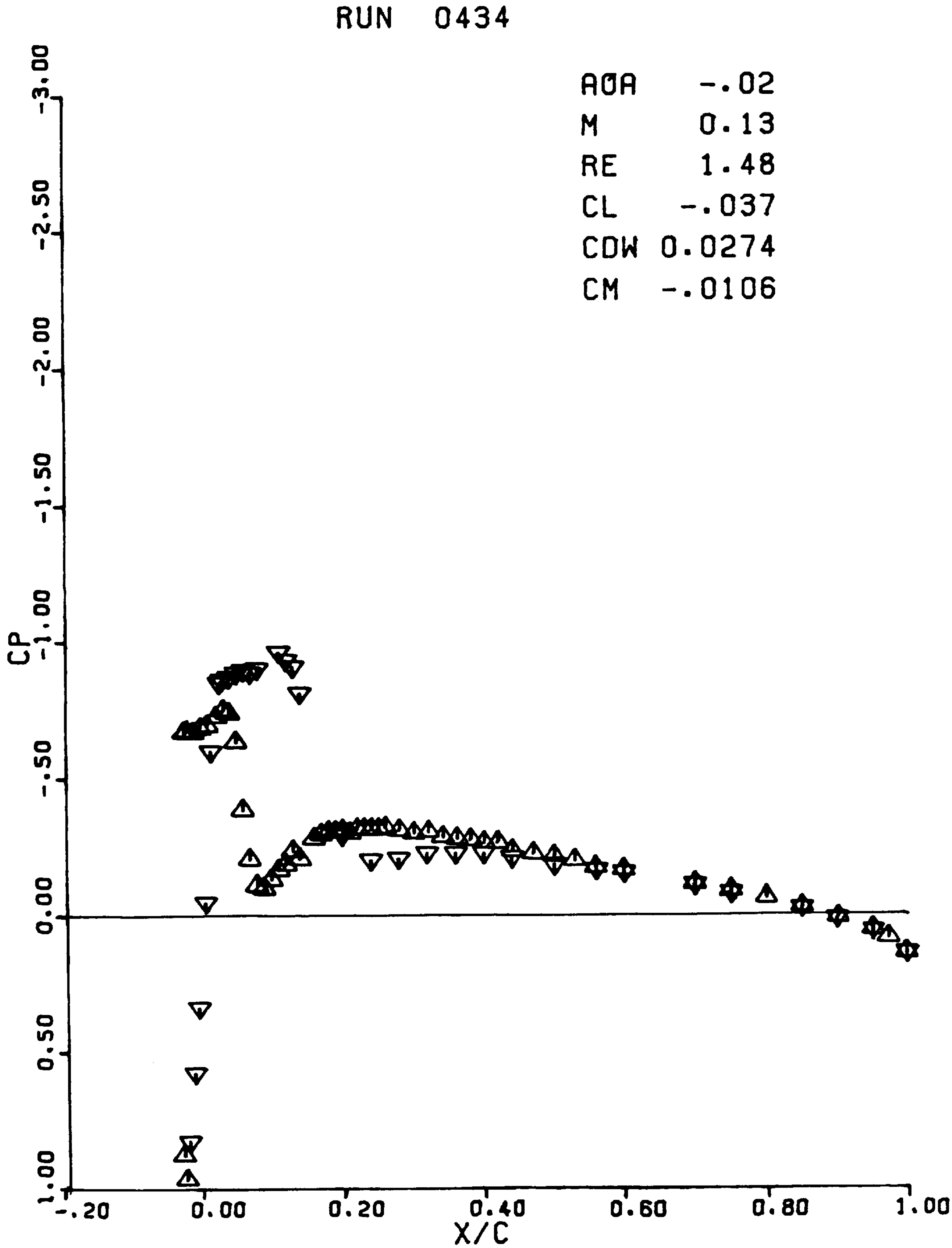

RUN 0434
AOA -.02
M 0.13
RE 1.48
CL -.037
CDW 0.0274
CM -.0106
CP
-3.00
-2.50
-2.00
-1.50
-1.00
-.50
0.00
0.50
1.00
-.20
0.00
0.20
0.40
0.60
0.80
1.00
X/C

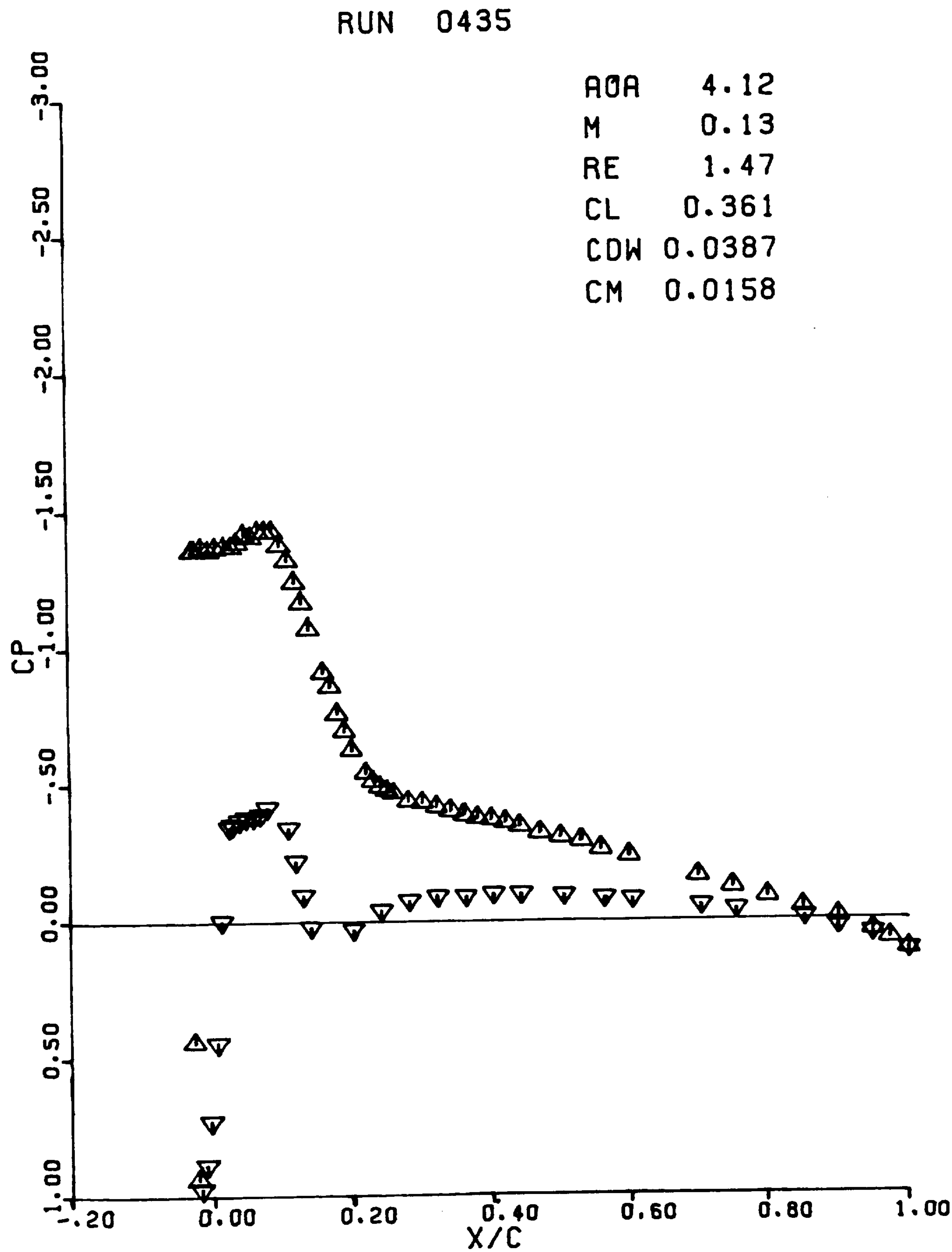

RUN 0435
AOA 4.12
M 0.13
RE 1.47
CL 0.361
CDW 0.0387
CM 0.0158
CP
-3.00
-2.50
-2.00
-1.50
-1.00
-.50
0.00
0.50
1.00
-.20
0.00
0.20
0.40
0.60
0.80
1.00
X/C

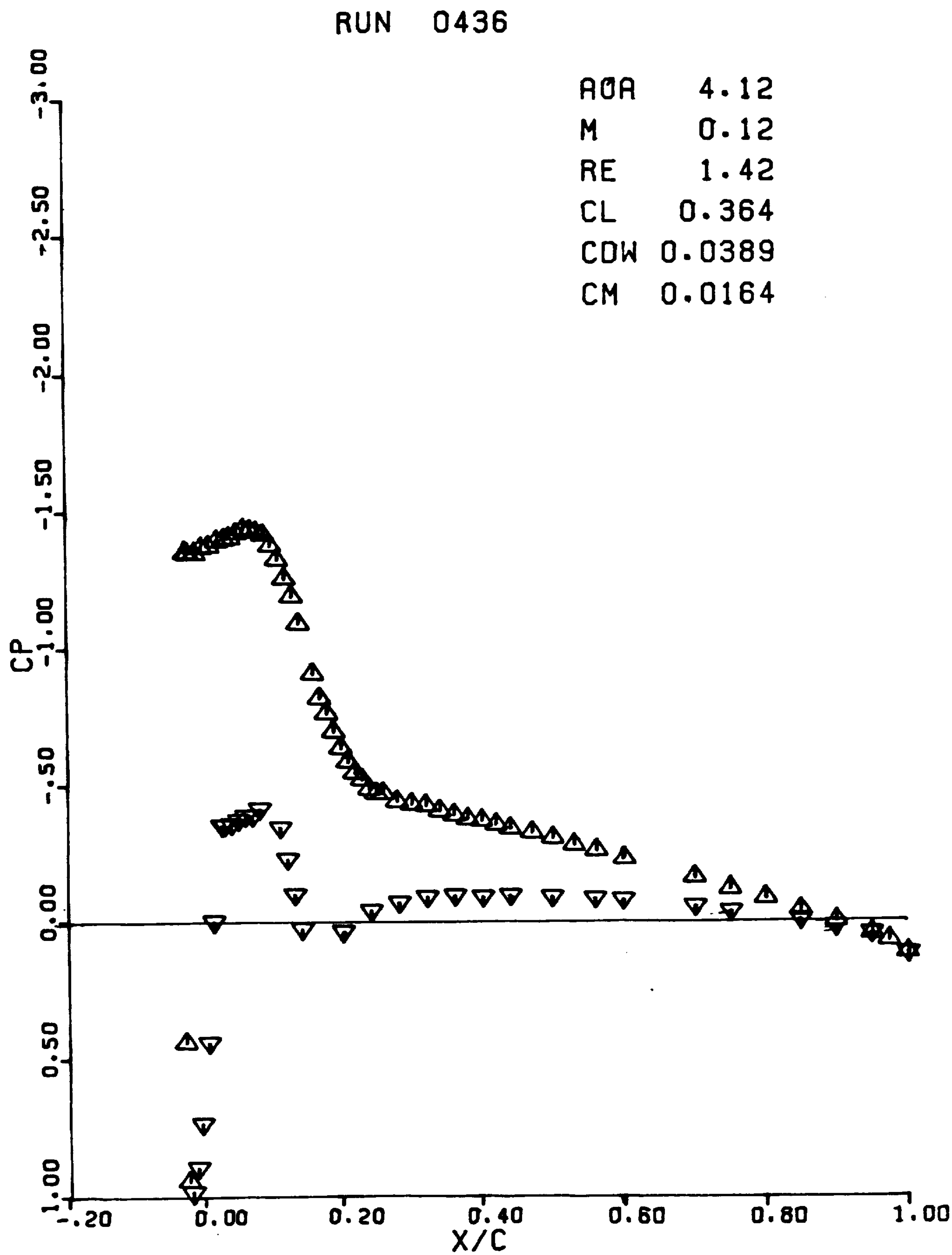
RUN 0436
AOA 4.12
M 0.12
RE 1.42
CL 0.364
CDW 0.0389
CM 0.0164
CP
-3.00
-2.50
-2.00
-1.50
-1.00
-.50
0.00
0.50
1.00
-.20
0.00
0.20
0.40
0.60
0.80
1.00
X/C

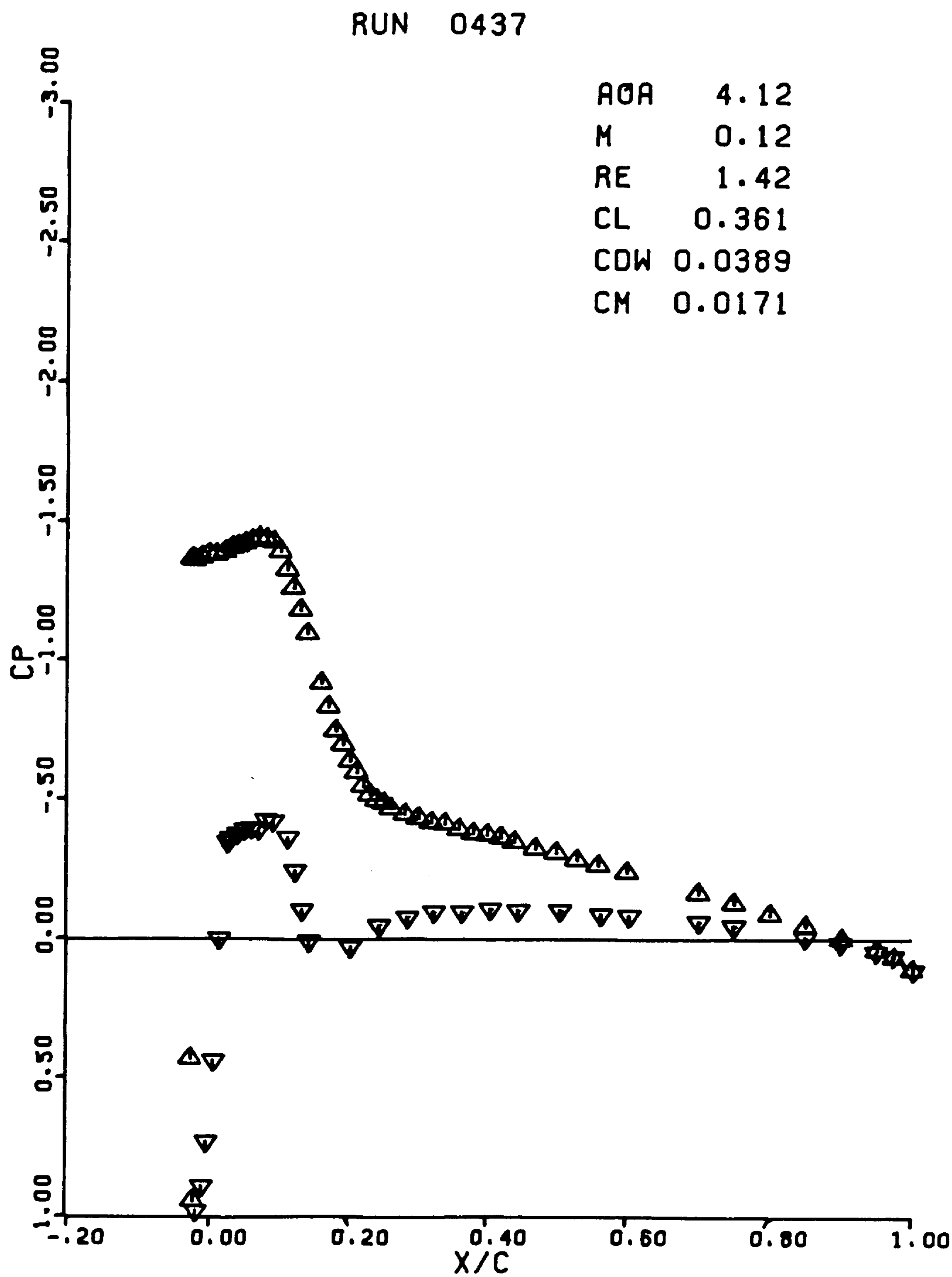

RUN 0437
AOA 4.12
M 0.12
RE 1.42
CL 0.361
CDW 0.0389
CM 0.0171
CP
-3.00
-2.50
-2.00
-1.50
-1.00
-.50
0.00
0.50
1.00
-.20
0.00
0.20
0.40
0.60
0.80
1.00
X/C

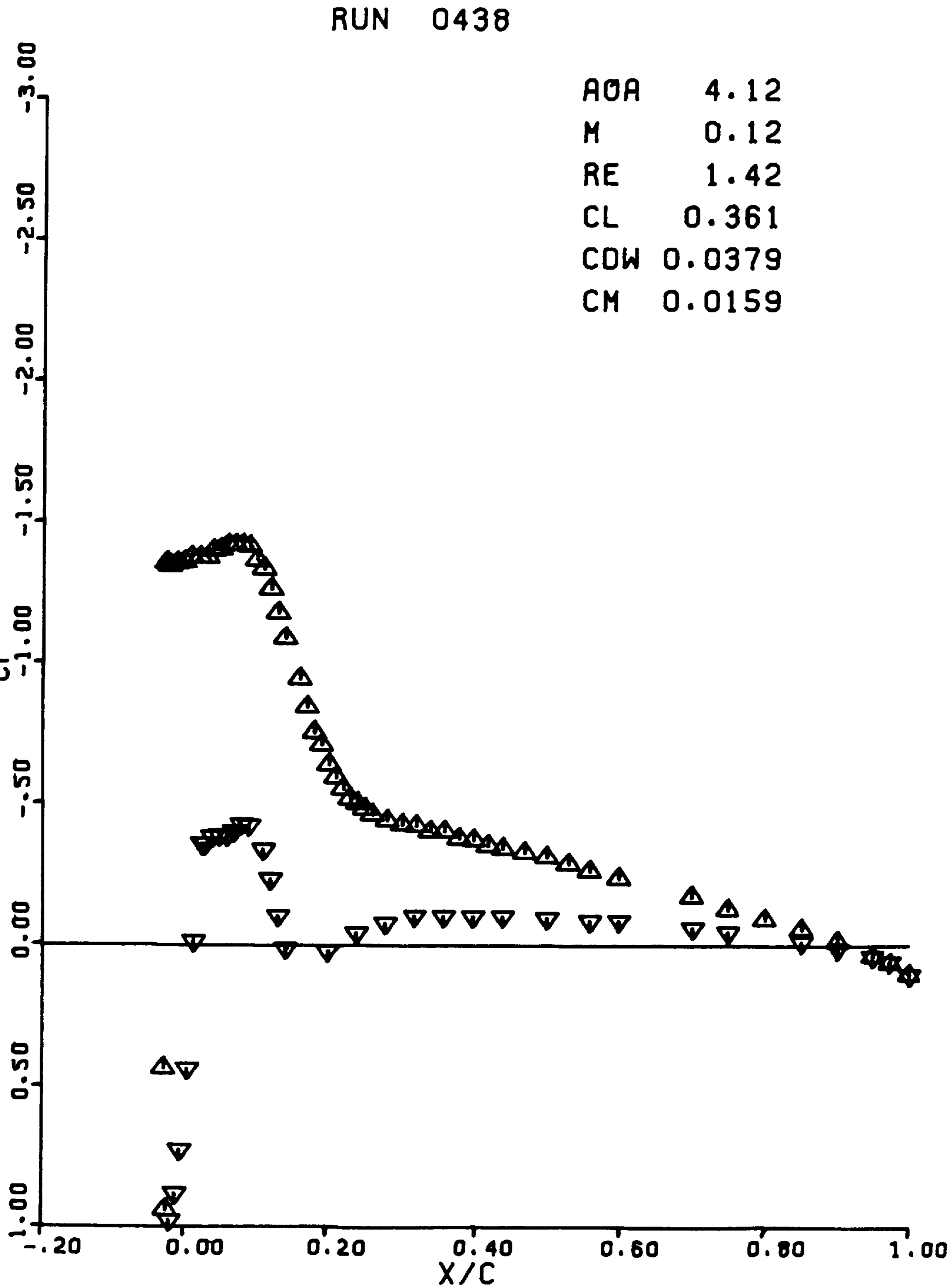
RUN 0438
AOA 4.12
M 0.12
RE 1.42
CL 0.361
CDW 0.0379
CM 0.0159
-3.00
-2.50
-2.00
-1.50
-1.00
CP
-.50
0.00
0.50
1.00
-.20
0.00
0.20
0.40
0.60
0.80
1.00
X/C

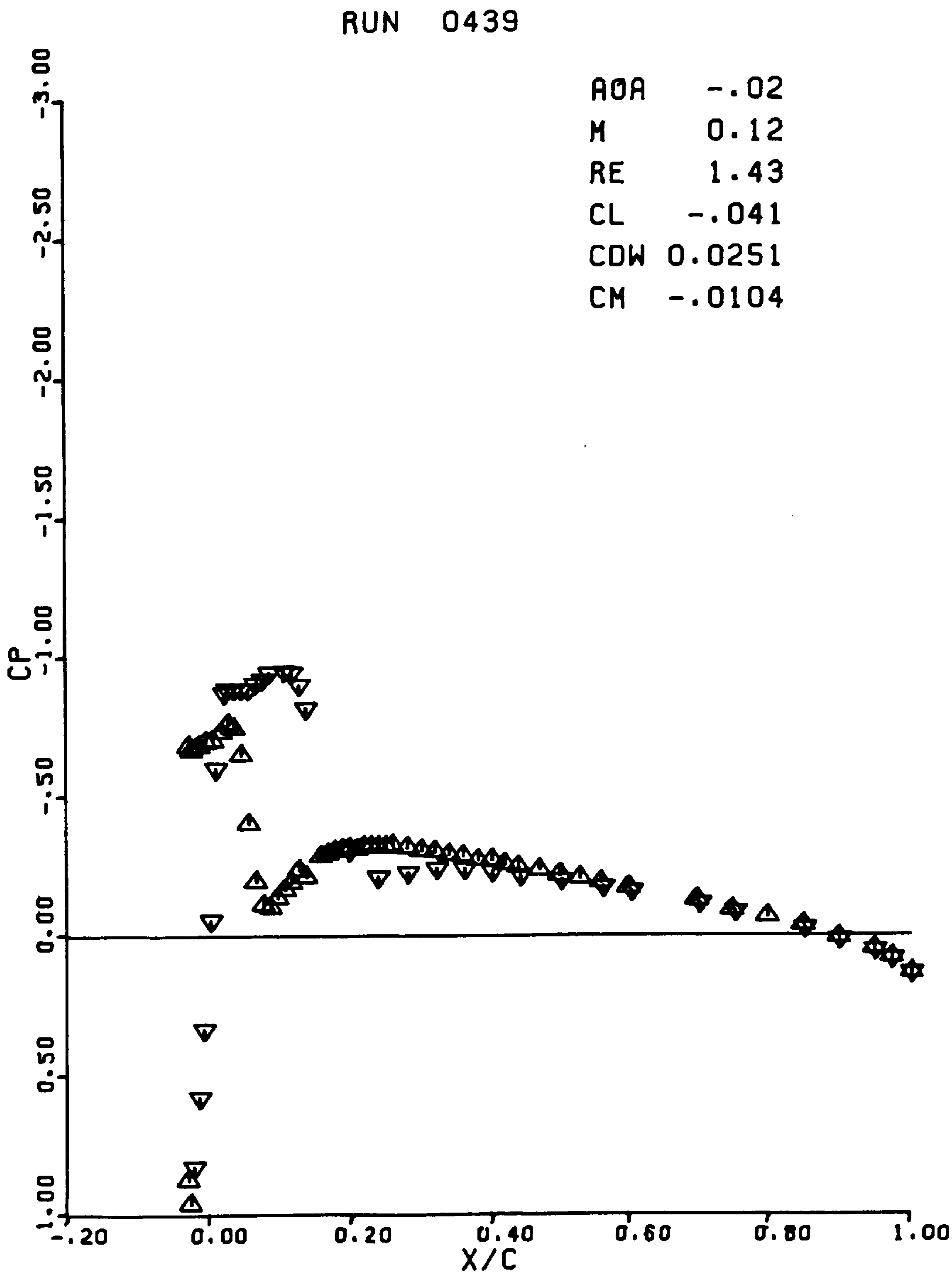
RUN 0439
AOA -.02
M 0.12
RE 1.43
CL -.041
CDW 0.0251
CM -.0104
CP
-3.00
-2.50
-2.00
-1.50
-1.00
-.50
0.00
0.50
1.00
X/C
-.20
0.00
0.20
0.40
0.60
0.80
1.00

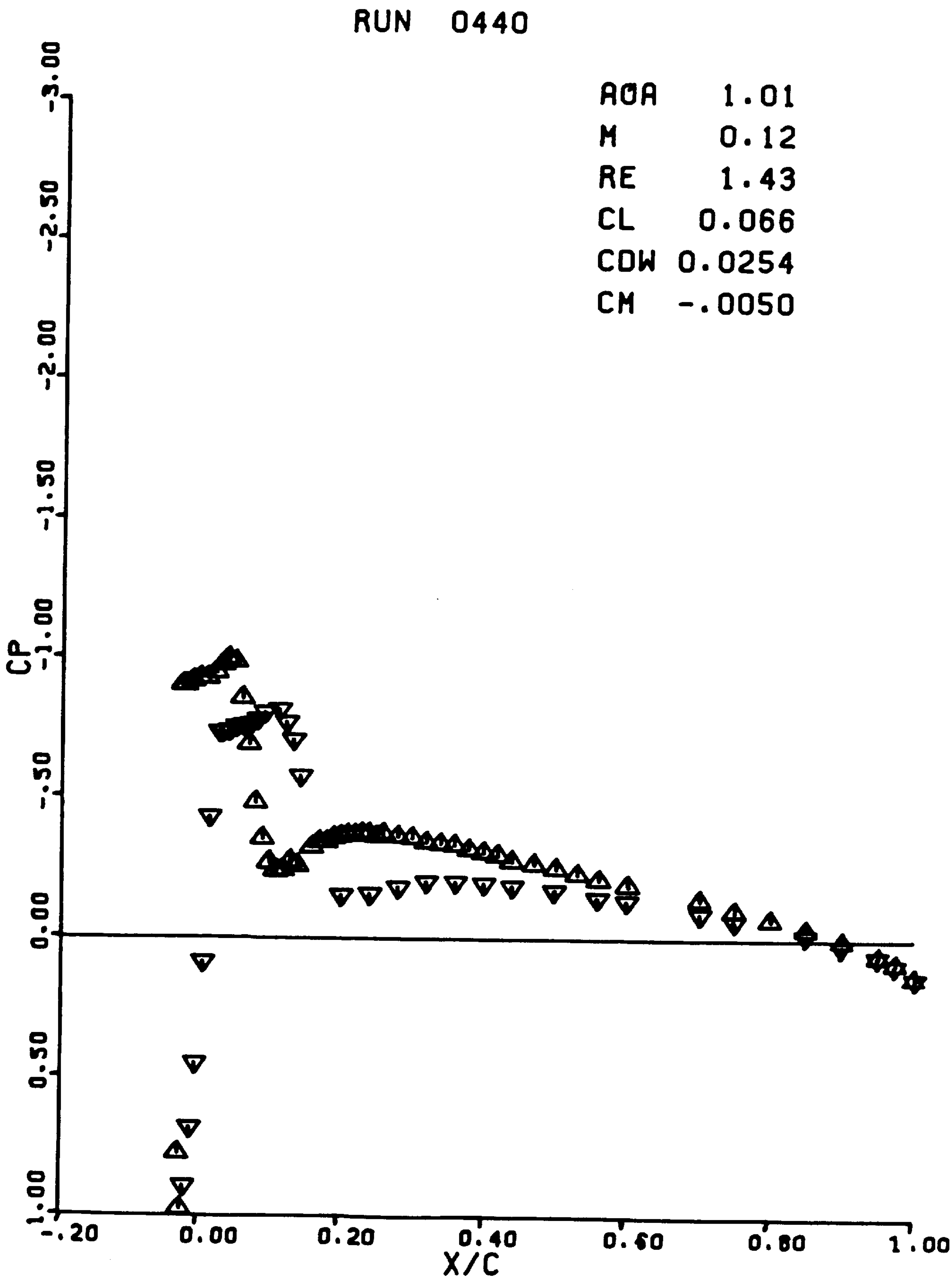
RUN 0440
AOA 1.01
M 0.12
RE 1.43
CL 0.066
CDW 0.0254
CM -.0050
CP
-3.00
-2.50
-2.00
-1.50
-1.00
-.50
0.00
0.50
1.00
-.20
0.00
0.20
0.40
0.60
0.80
1.00
X/C

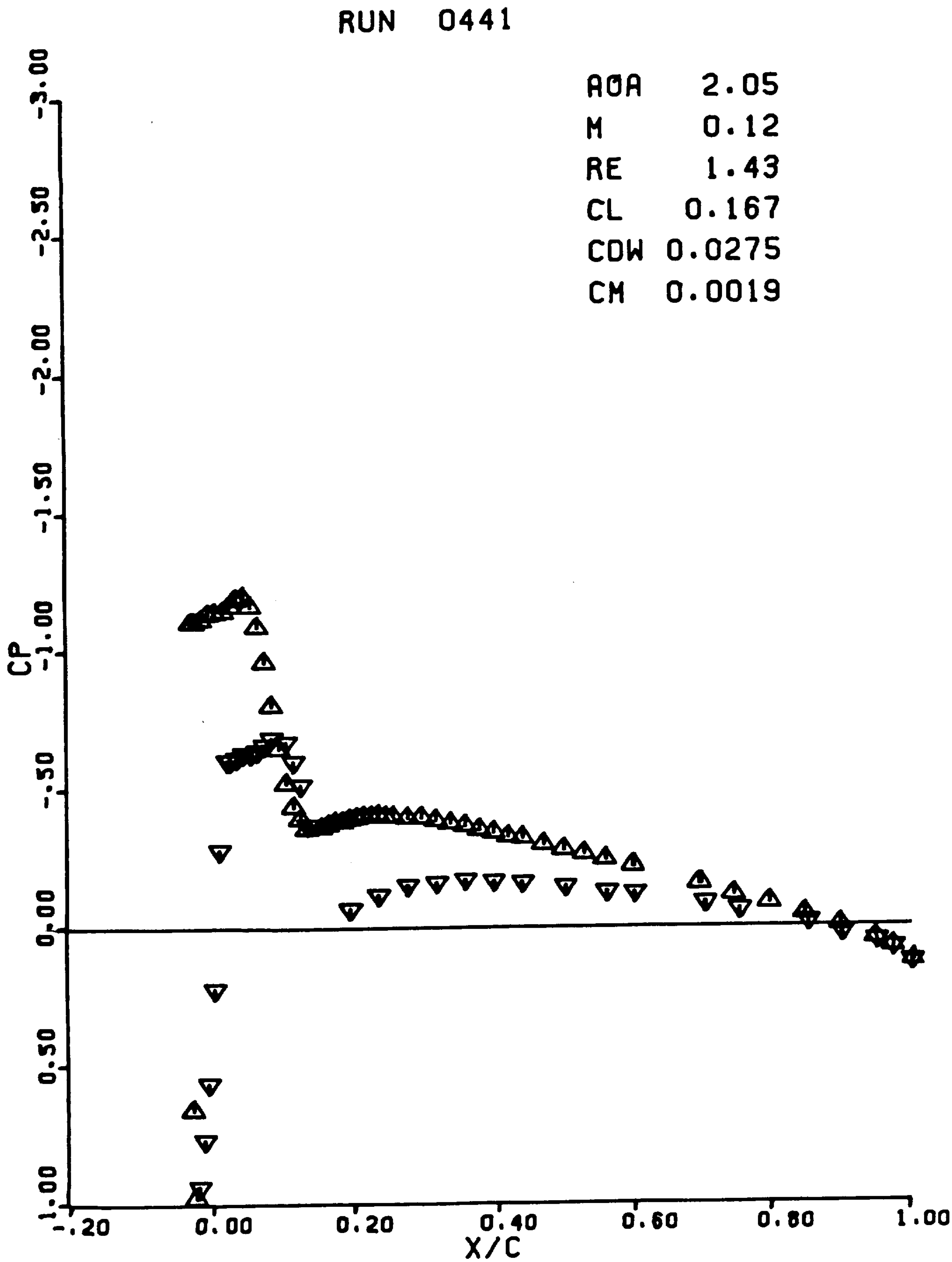
RUN 0441
AOA 2.05
M 0.12
RE 1.43
CL 0.167
CDW 0.0275
CM 0.0019
CP
-3.00
-2.50
-2.00
-1.50
-1.00
-.50
0.00
0.50
1.00
-.20
0.00
0.20
0.40
0.60
0.80
1.00
X/C

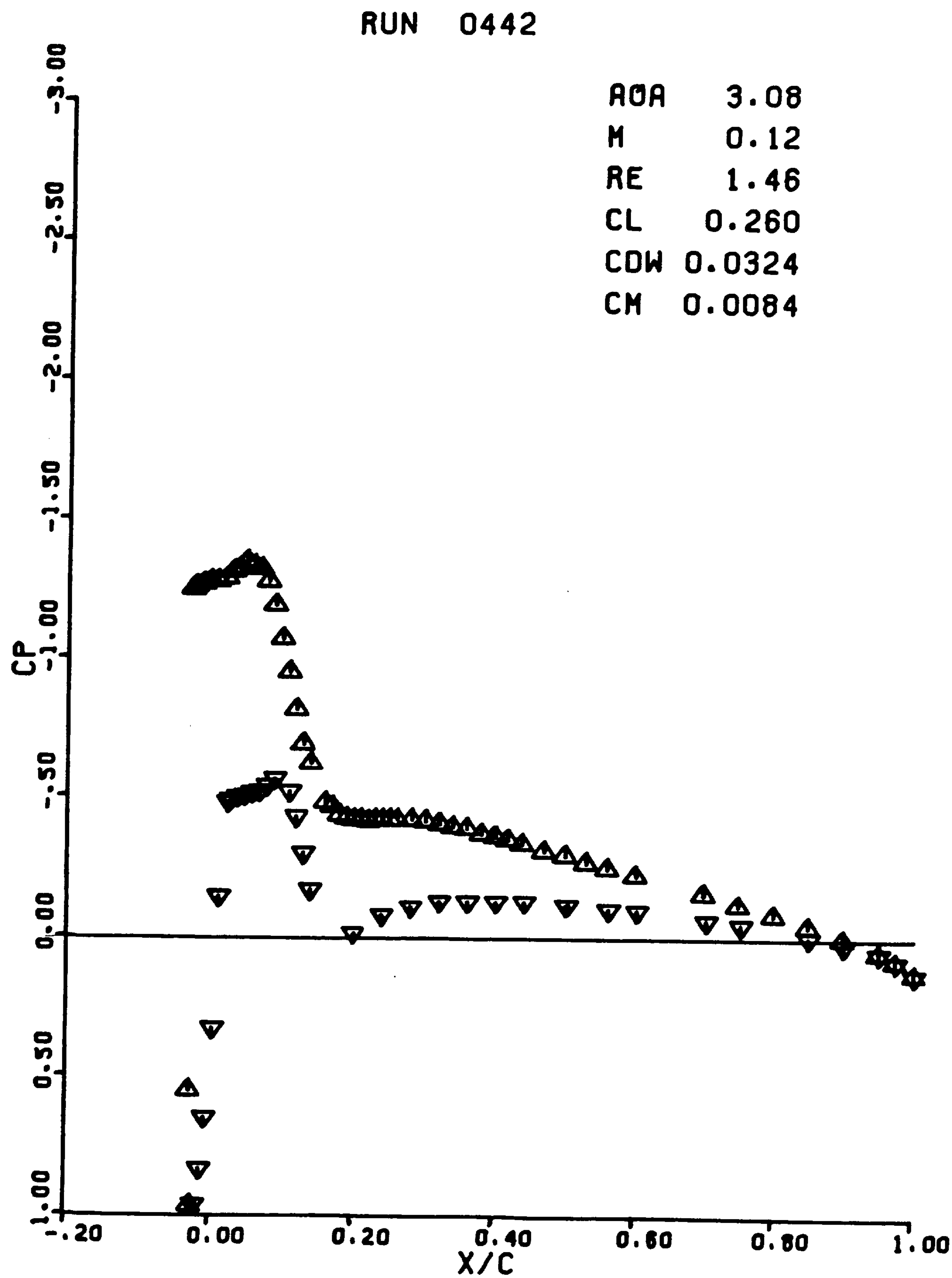
RUN 0442
AOA 3.08
M 0.12
RE 1.46
CL 0.260
CDW 0.0324
CM 0.0084
CP
-3.00
-2.50
-2.00
-1.50
-1.00
-.50
0.00
0.50
1.00
-.20
0.00
0.20
0.40
0.60
0.80
1.00
X/C

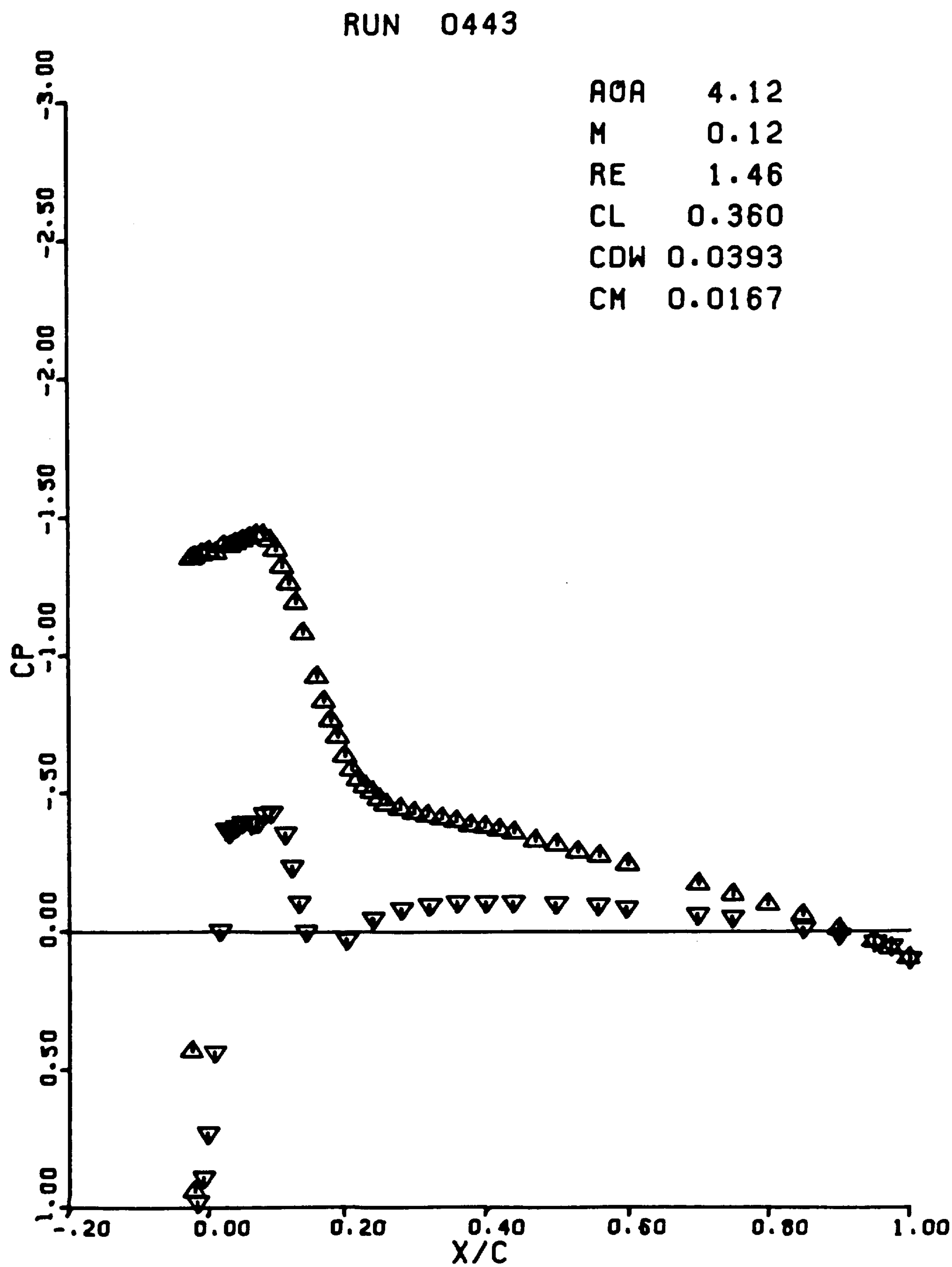

RUN 0443
AOA 4.12
M 0.12
RE 1.46
CL 0.360
CDW 0.0393
CM 0.0167
CP
-3.00
-2.50
-2.00
-1.50
-1.00
-.50
0.00
0.50
1.00
-.20
0.00
0.20
0.40
0.60
0.80
1.00
X/C

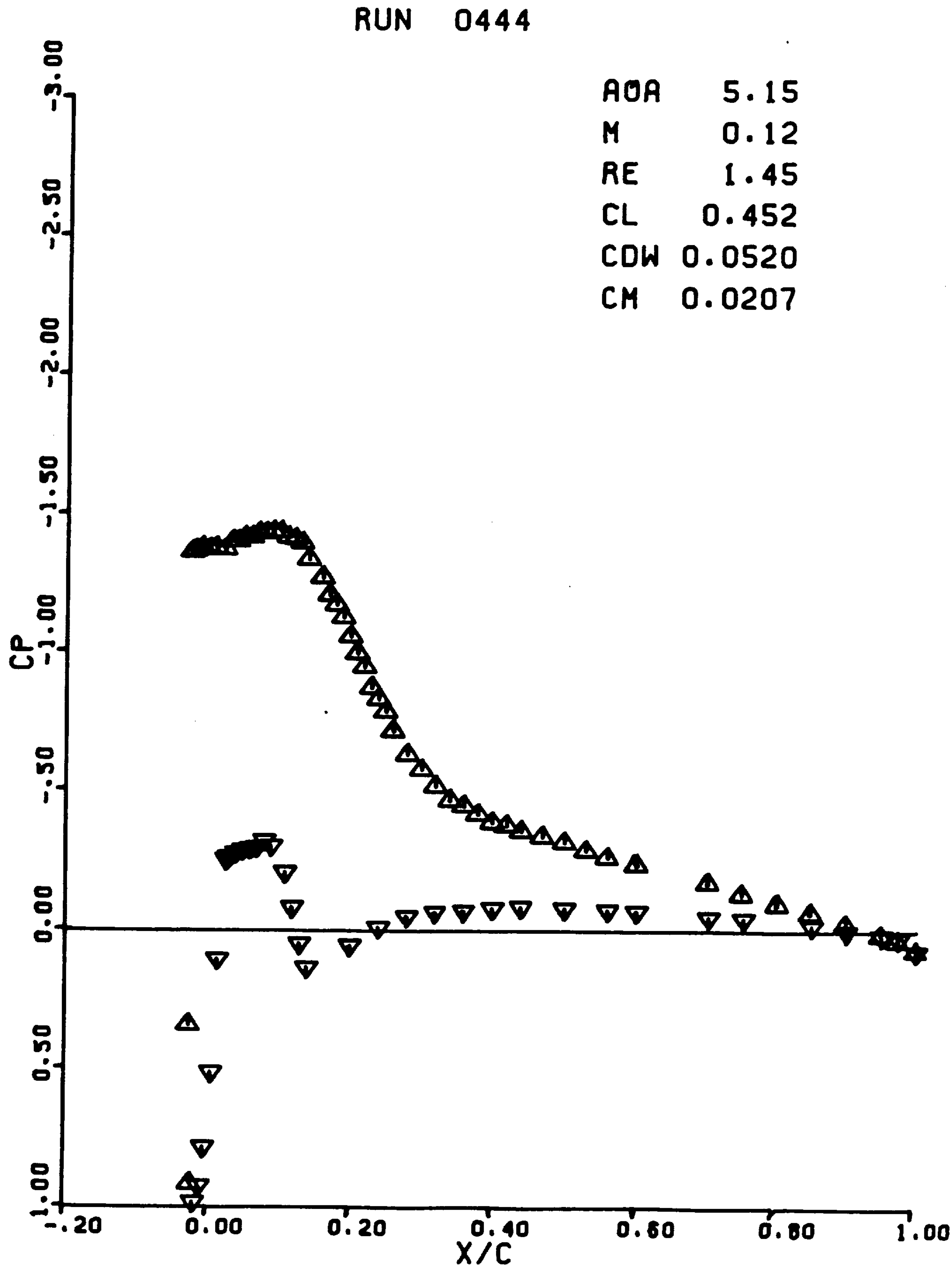

RUN 0444
AOA 5.15
M 0.12
RE 1.45
CL 0.452
CDW 0.0520
CM 0.0207
CP
-3.00
-2.50
-2.00
-1.50
-1.00
-.50
0.00
0.50
1.00
-.20
0.00
0.20
0.40
0.60
0.80
1.00
X/C

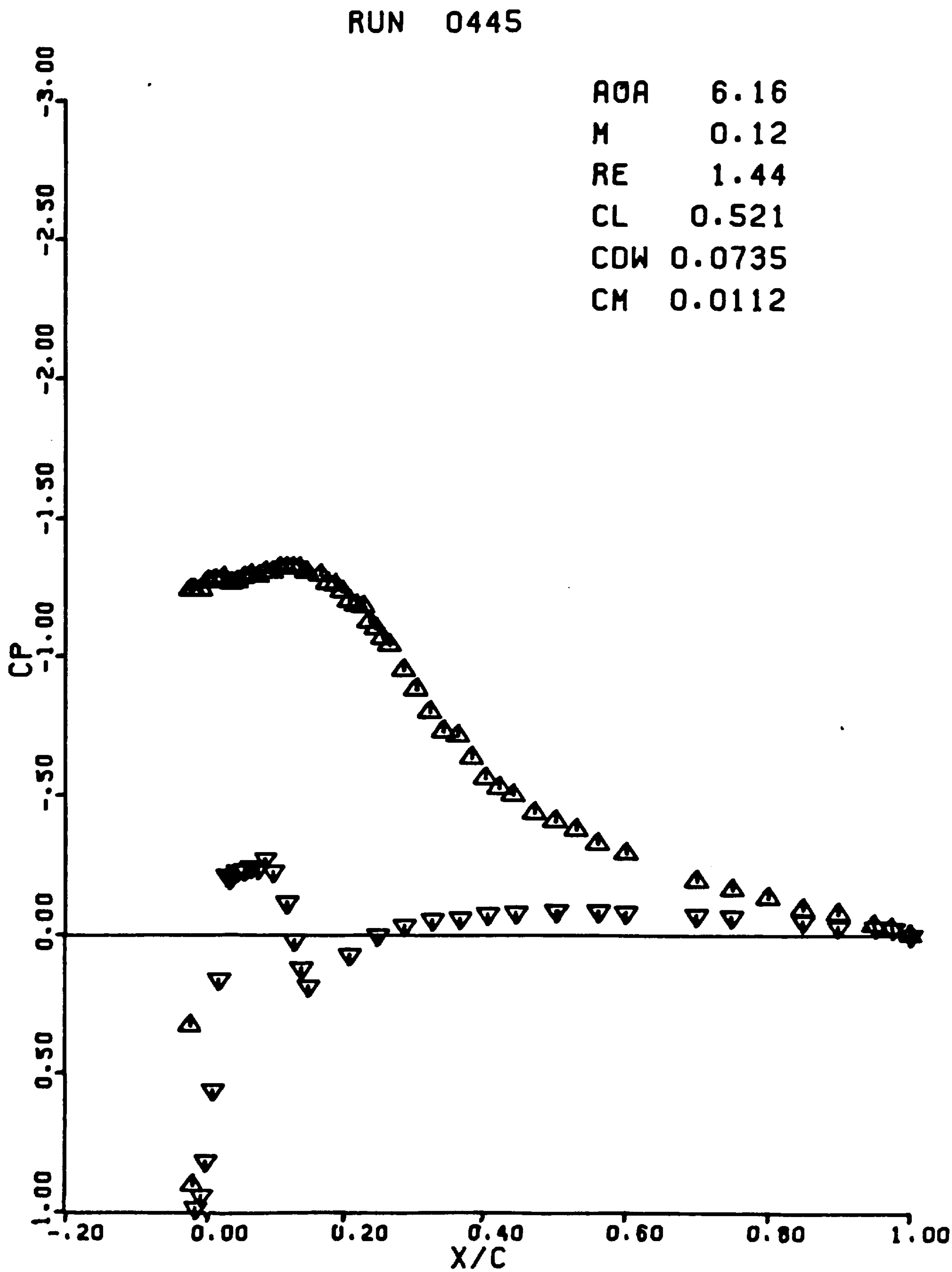
RUN 0445
AOA 6.16
M 0.12
RE 1.44
CL 0.521
CDW 0.0735
CM 0.0112
CP
-3.00
-2.50
-2.00
-1.50
-1.00
-.50
0.00
0.50
1.00
-.20
0.00
0.20
0.40
0.60
0.80
1.00
X/C

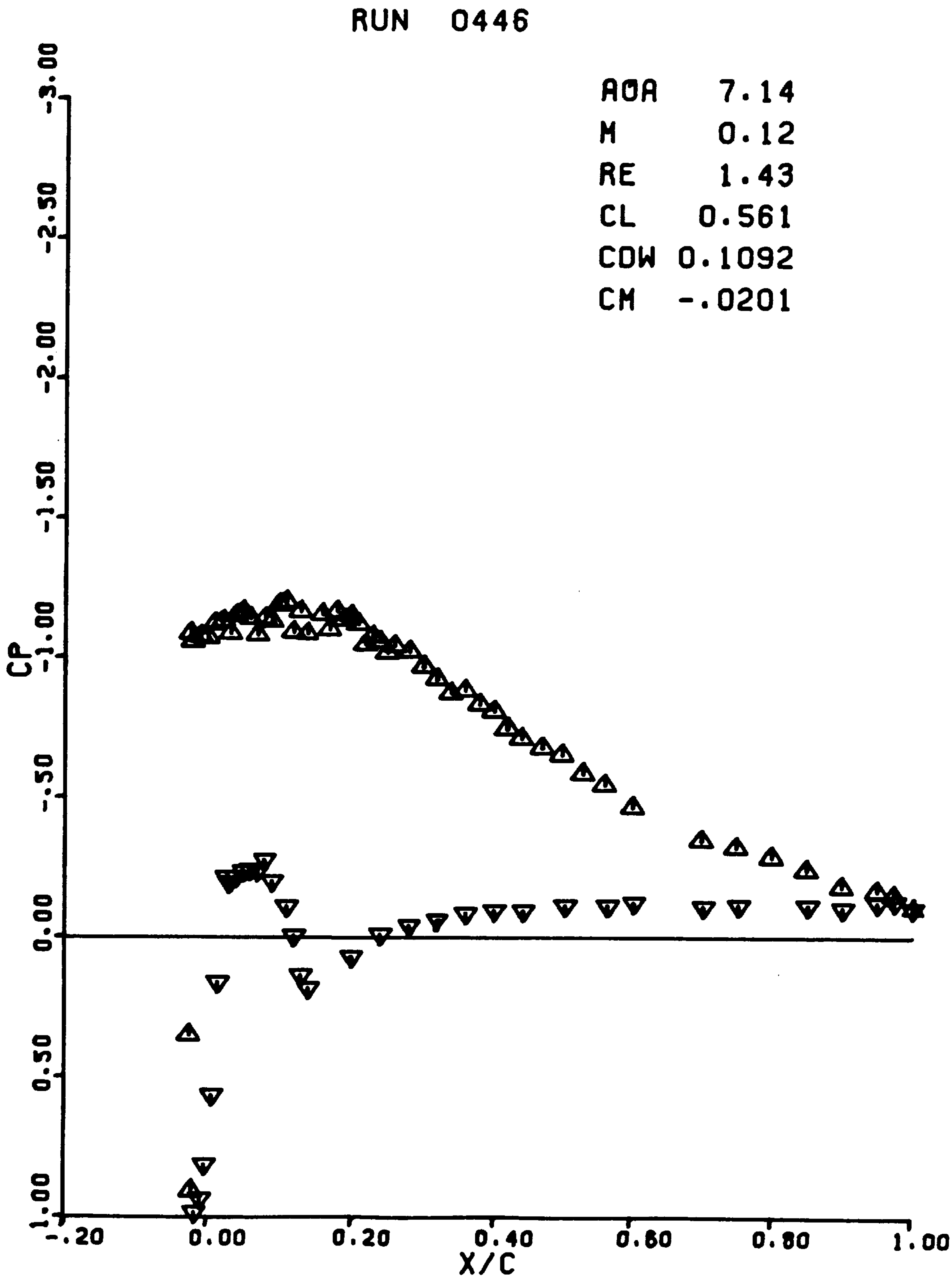
RUN 0446
AOA 7.14
M 0.12
RE 1.43
CL 0.561
CDW 0.1092
CM -.0201
CP
-3.00
-2.50
-2.00
-1.50
-1.00
-.50
0.00
0.50
1.00
-.20
0.00
0.20
0.40
0.60
0.80
1.00
X/C

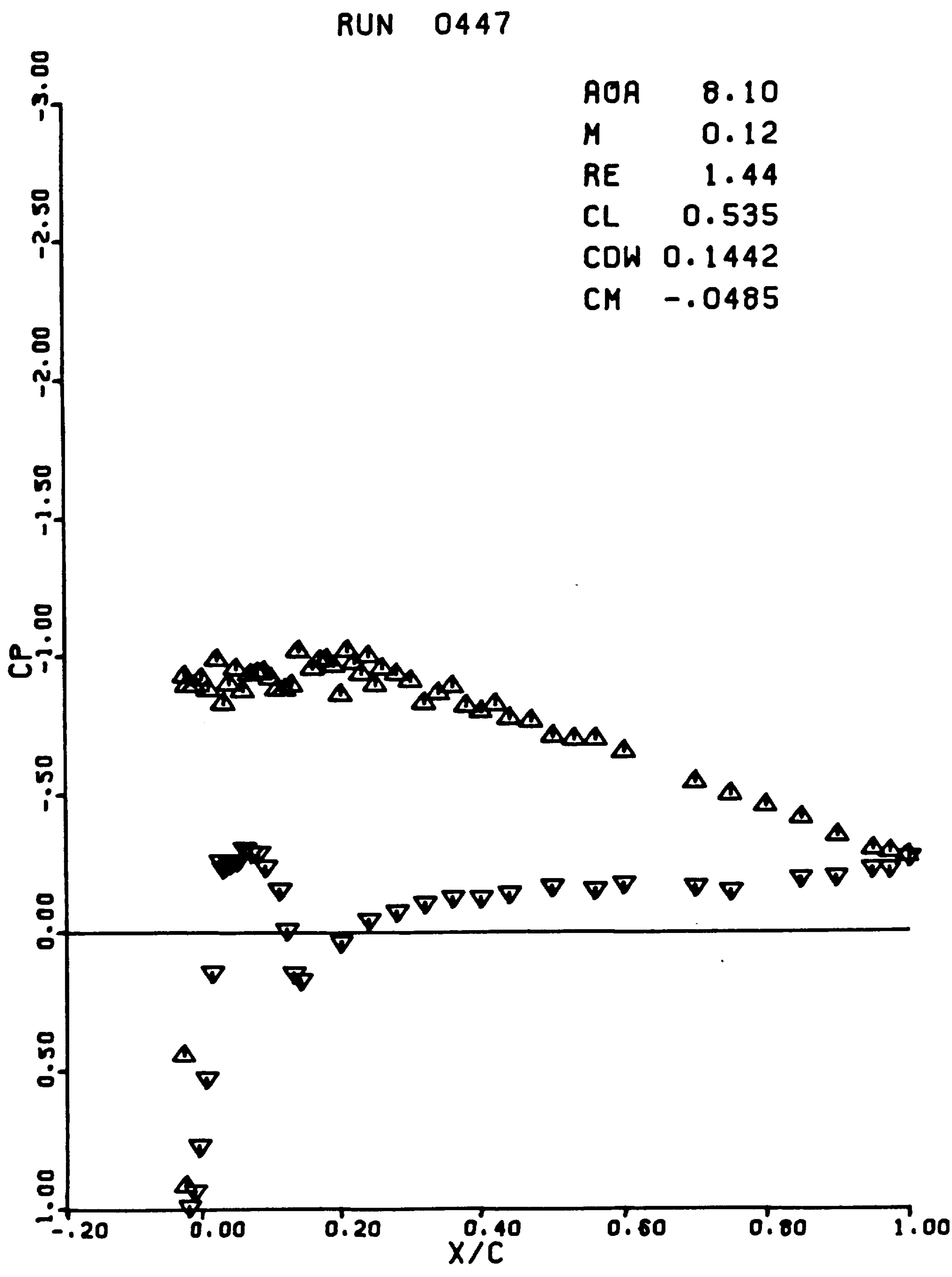
RUN 0447
AOA 8.10
M 0.12
RE 1.44
CL 0.535
CDW 0.1442
CM -.0485
CP
-3.00
-2.50
-2.00
-1.50
-1.00
-.50
0.00
0.50
1.00
-.20
0.00
0.20
0.40
0.60
0.80
1.00
X/C

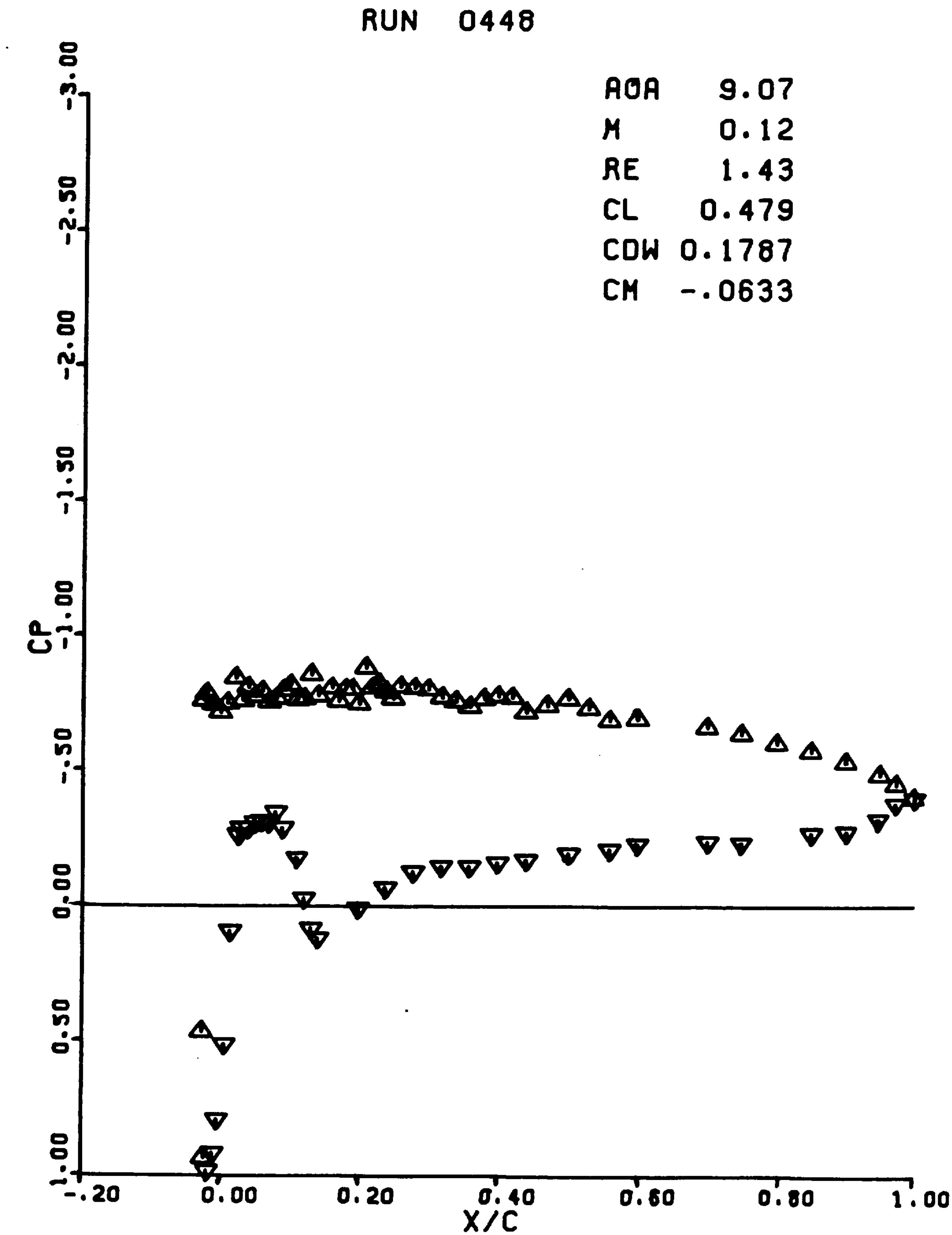
RUN 0448
AOA 9.07
M 0.12
RE 1.43
CL 0.479
CDW 0.1787
CM -.0633
CP
-3.00
-2.50
-2.00
-1.50
-1.00
-.50
0.00
0.50
1.00
-.20
0.00
0.20
0.40
0.60
0.80
1.00
X/C

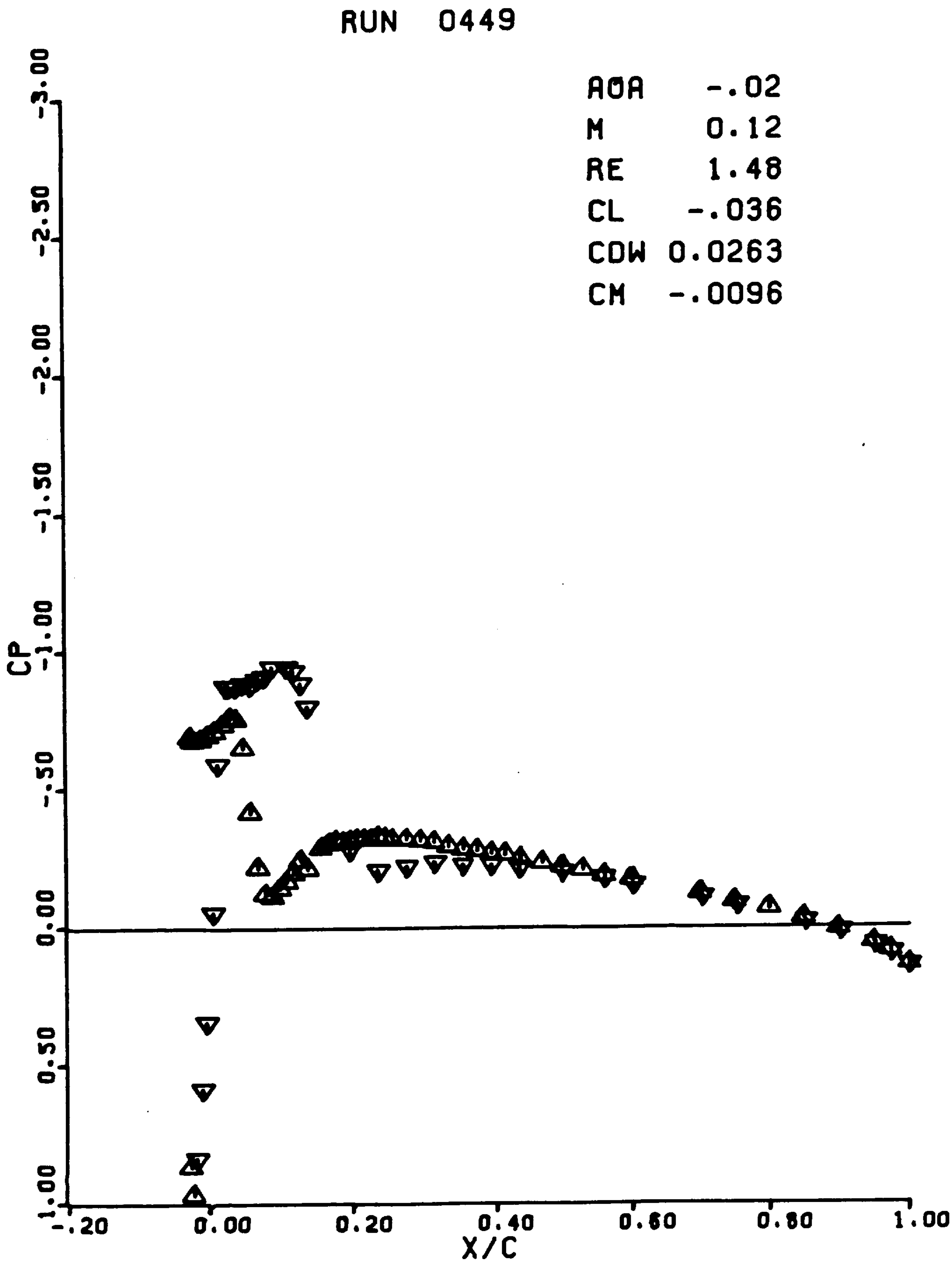

RUN 0449
AOA -.02
M 0.12
RE 1.48
CL -.036
CDW 0.0263
CM -.0096
CP
-3.00
-2.50
-2.00
-1.50
-1.00
-.50
0.00
0.50
1.00
-.20
0.00
0.20
0.40
0.60
0.80
1.00
X/C

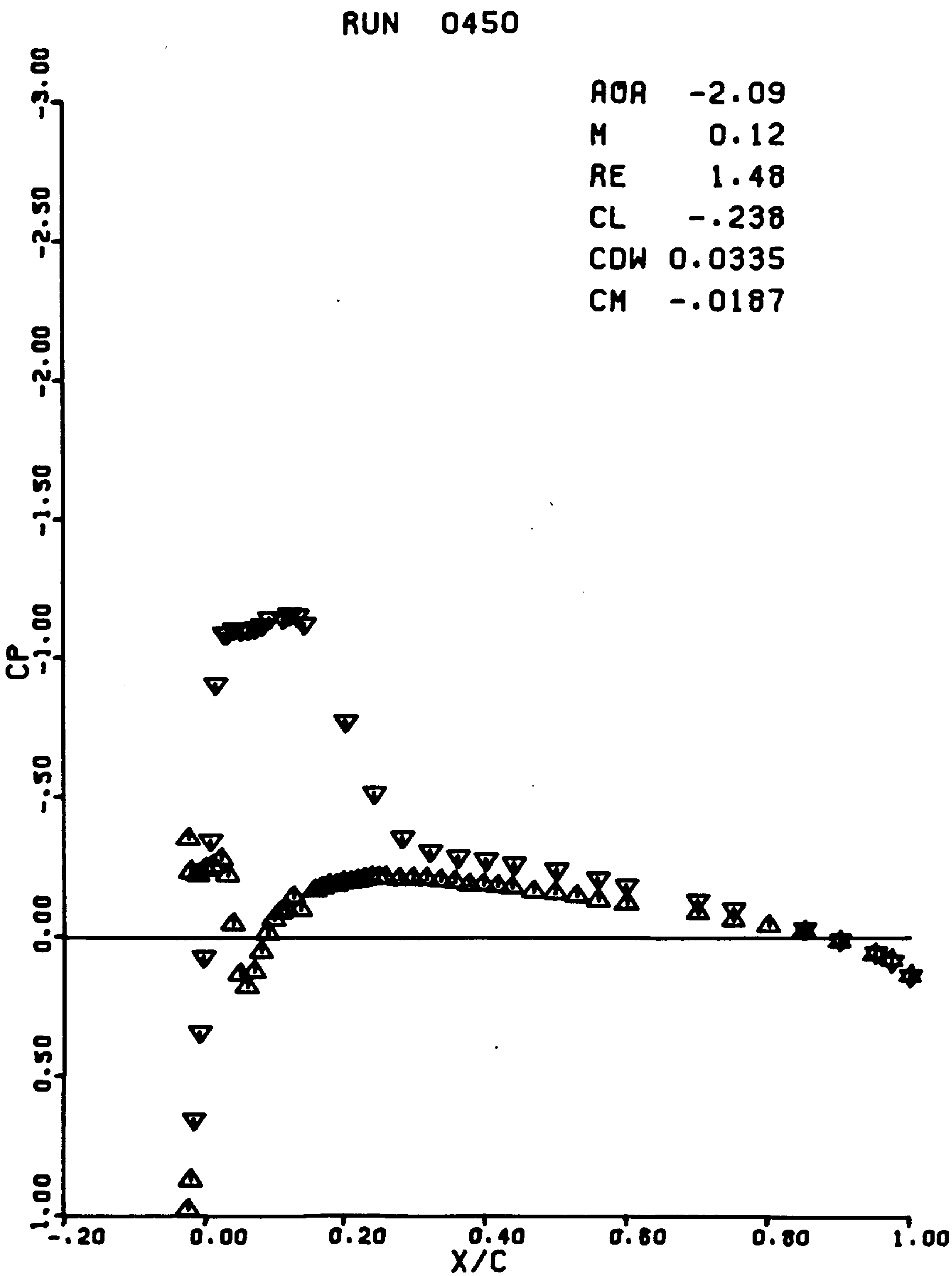
RUN 0450
AOA -2.09
M 0.12
RE 1.48
CL -.238
CDW 0.0335
CM -.0187
CP
-3.00
-2.50
-2.00
-1.50
-1.00
-.50
0.00
0.50
1.00
-.20
0.00
0.20
0.40
0.60
0.80
1.00
X/C

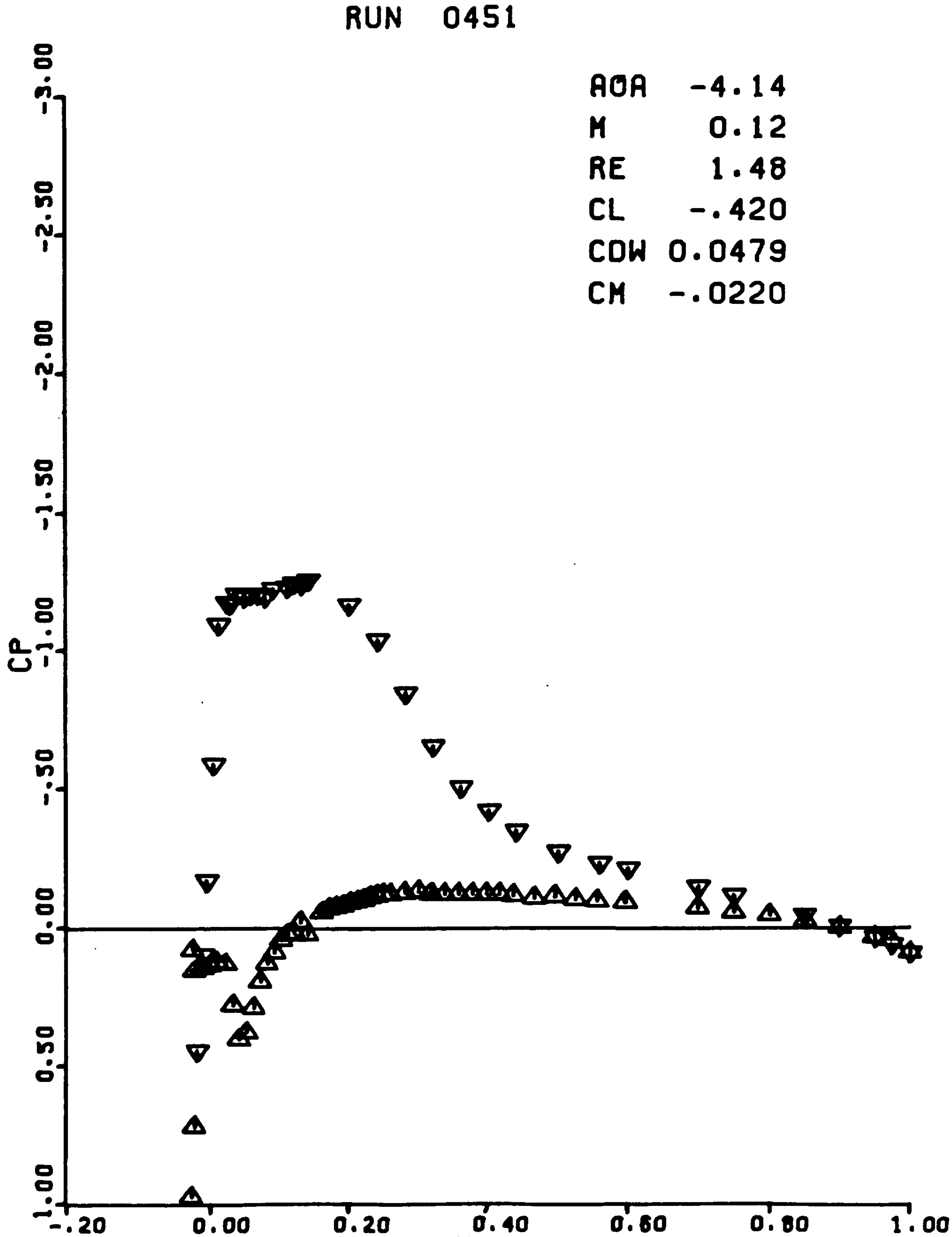
RUN 0451
AOA -4.14
M 0.12
RE 1.48
CL -.420
CDW 0.0479
CM -.0220
CP
-3.00
-2.50
-2.00
-1.50
-1.00
-.50
0.00
0.50
1.00
-.20
0.00
0.20
0.40
0.60
0.80
1.00
X/C

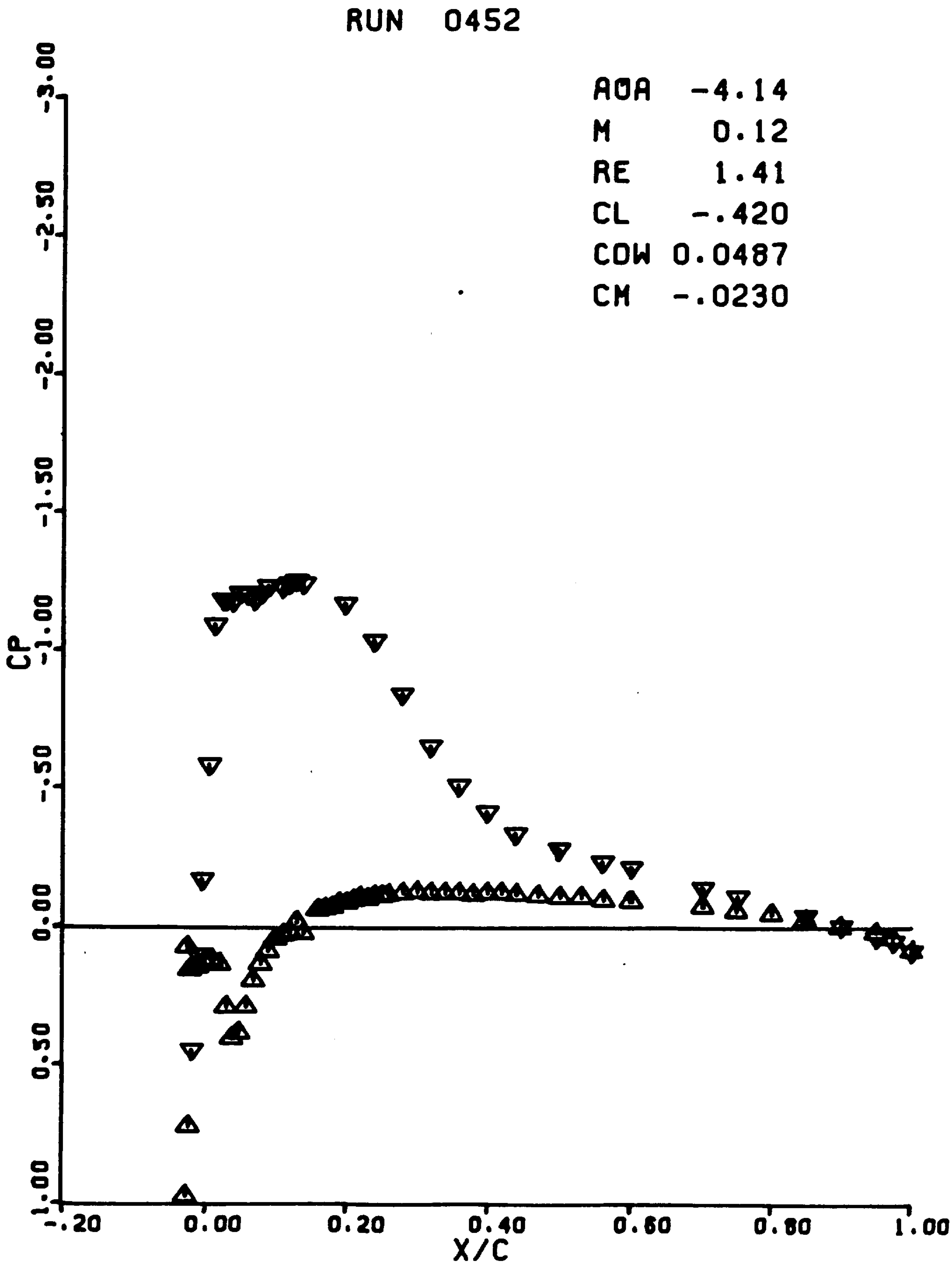
RUN 0452
AOA -4.14
M 0.12
RE 1.41
CL -.420
CDW 0.0487
CM -.0230
CP
-3.00
-2.50
-2.00
-1.50
-1.00
-.50
0.00
0.50
1.00
-.20
0.00
0.20
0.40
0.60
0.80
1.00
X/C

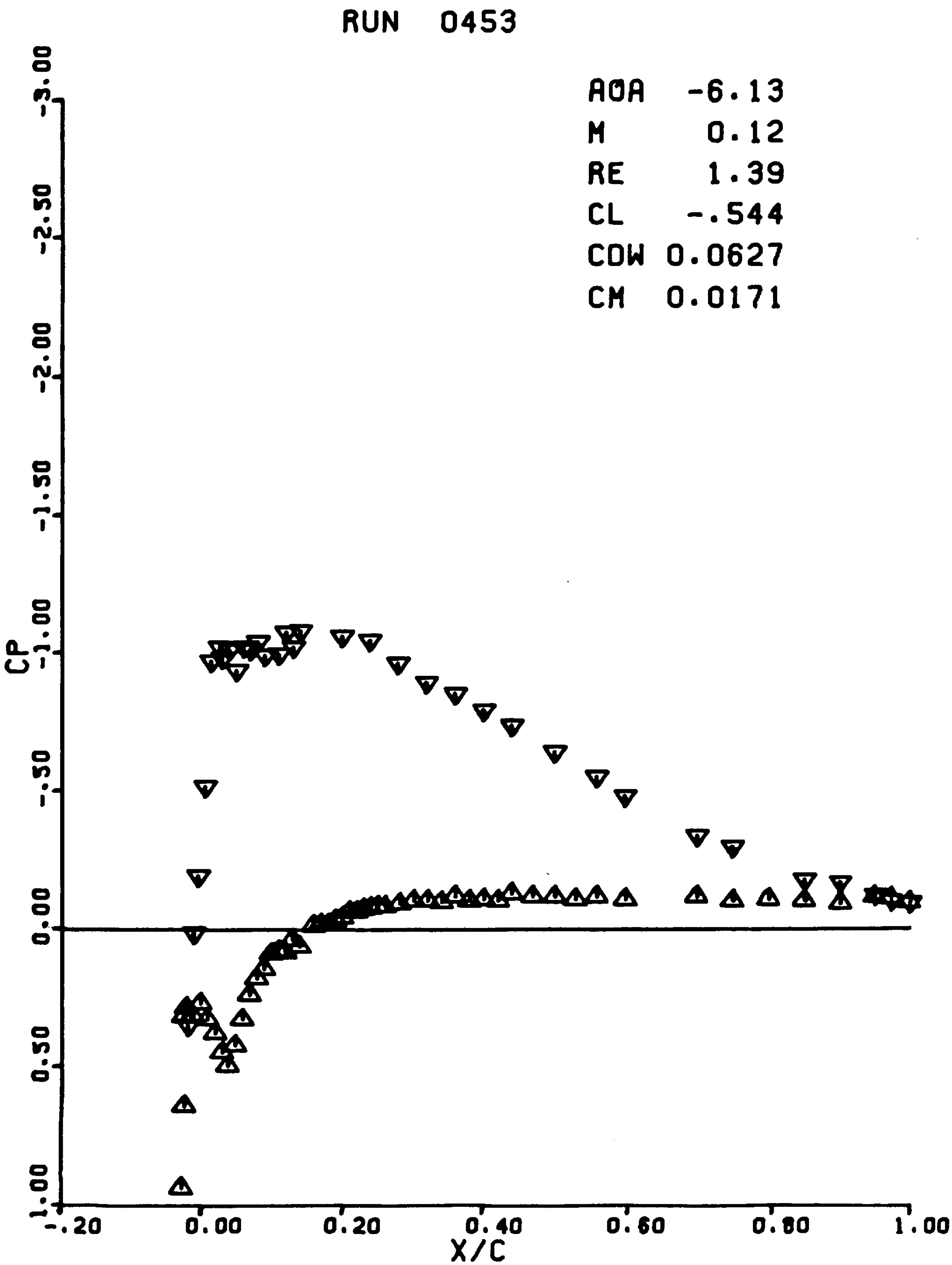
RUN 0453
AOA -6.13
M 0.12
RE 1.39
CL -.544
CDW 0.0627
CM 0.0171
CP
-3.00
-2.50
-2.00
-1.50
-1.00
-.50
0.00
0.50
1.00
-.20
0.00
0.20
0.40
0.60
0.80
1.00
X/C

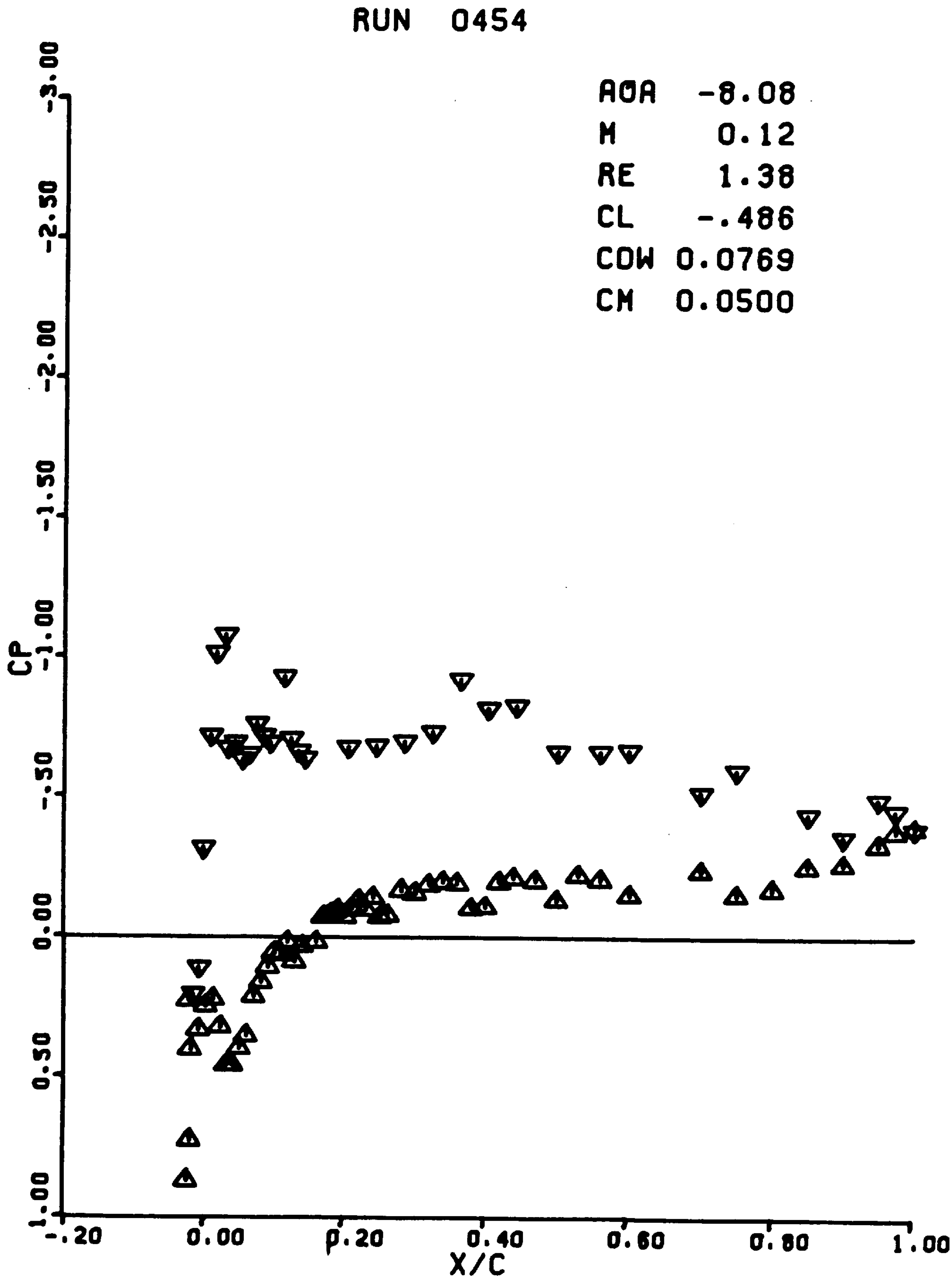

RUN 0454
AOA -8.08
M 0.12
RE 1.38
CL -.486
CDW 0.0769
CM 0.0500
CP
X/C
-3.00
-2.50
-2.00
-1.50
-1.00
-.50
0.00
0.50
1.00
-.20
0.00
0.20
0.40
0.60
0.80
1.00

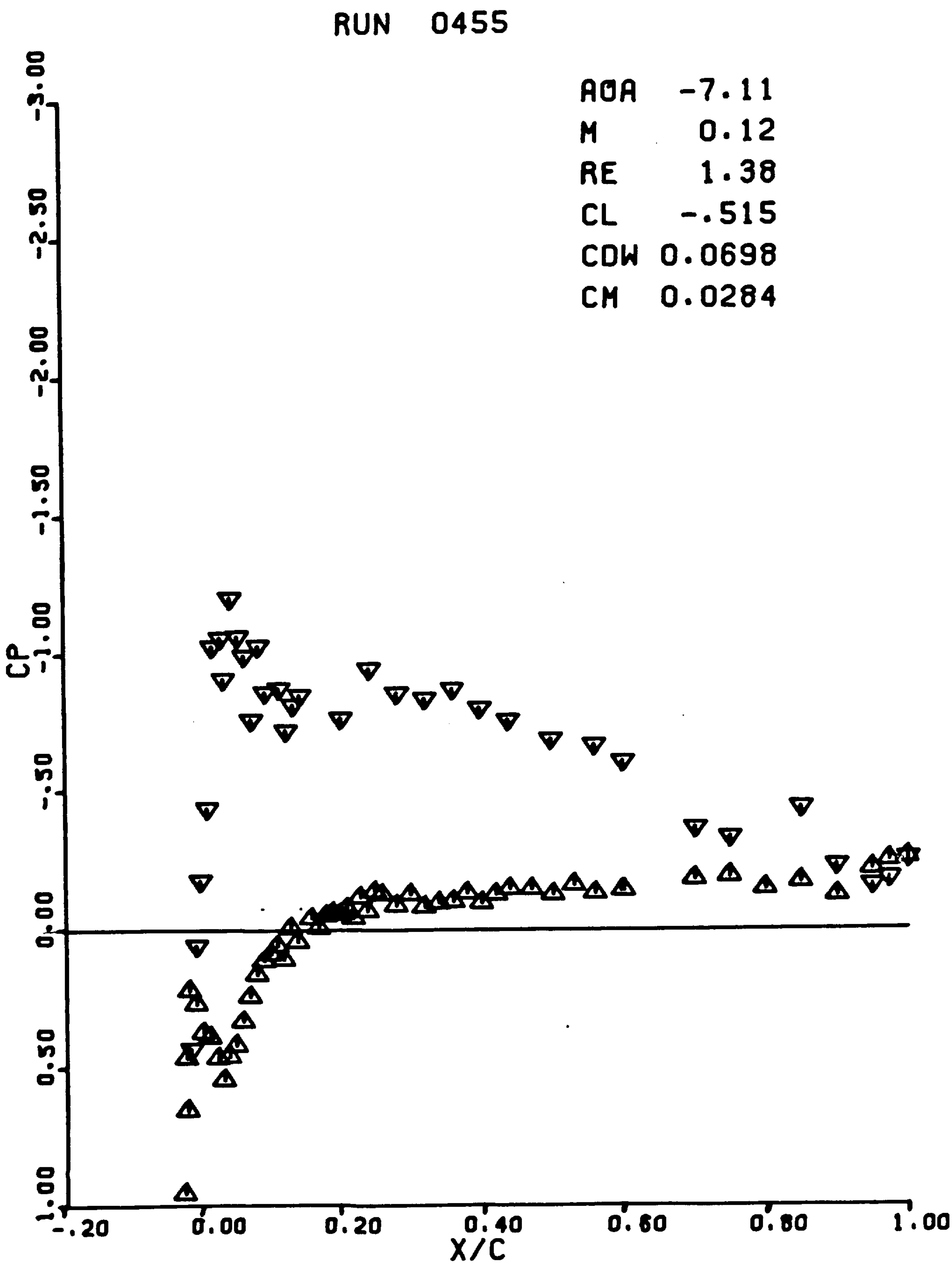
RUN 0455
AOA -7.11
M 0.12
RE 1.38
CL -.515
CDW 0.0698
CM 0.0284
CP
-3.00
-2.50
-2.00
-1.50
-1.00
-.50
0.00
0.50
1.00
-.20
0.00
0.20
0.40
0.60
0.80
1.00
X/C

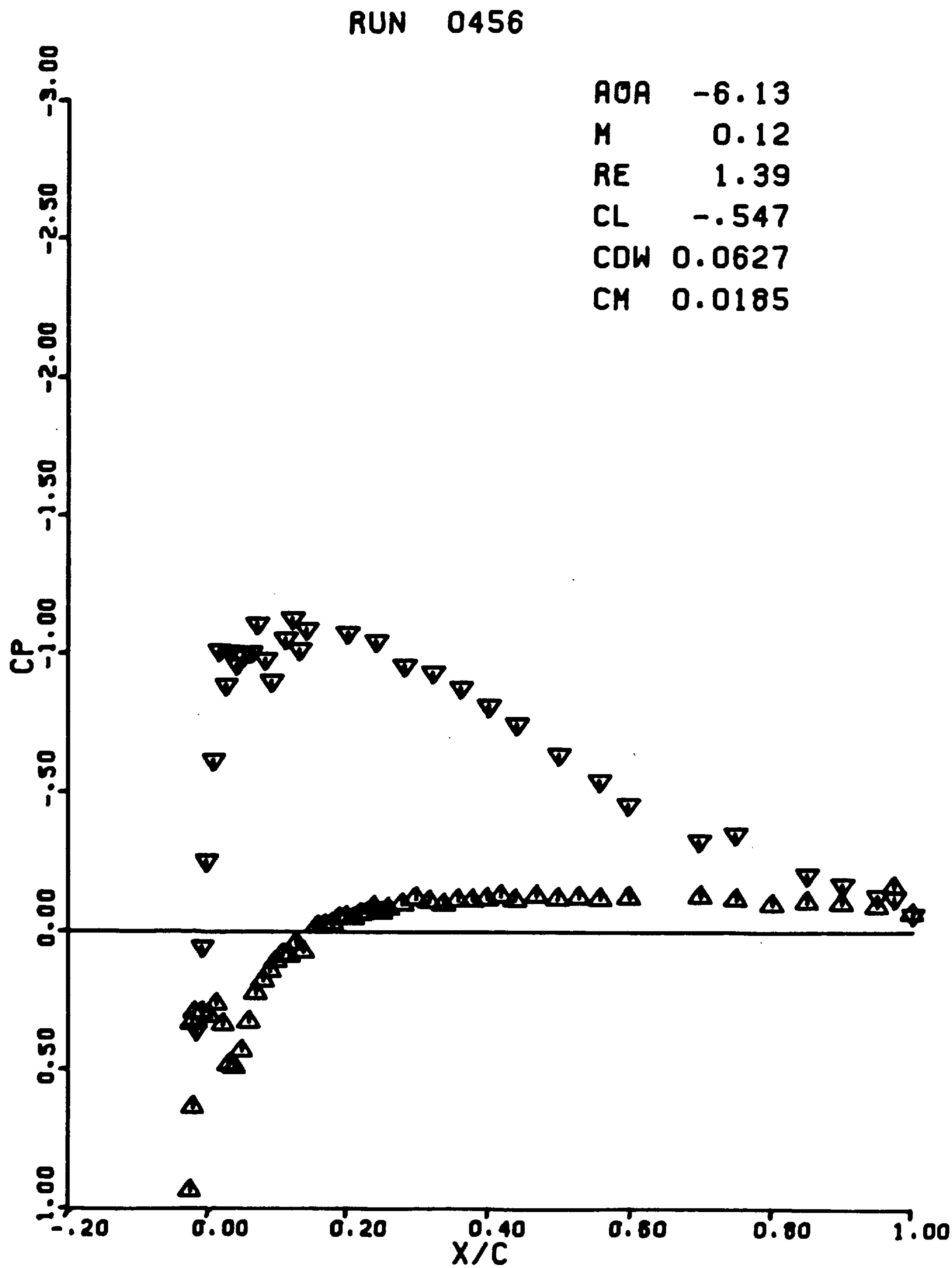
RUN 0456
AOA -6.13
M 0.12
RE 1.39
CL -.547
CDW 0.0627
CM 0.0185
CP
X/C
-3.00
-2.50
-2.00
-1.50
-1.00
-.50
0.00
0.50
1.00
-.20
0.00
0.20
0.40
0.60
0.80
1.00

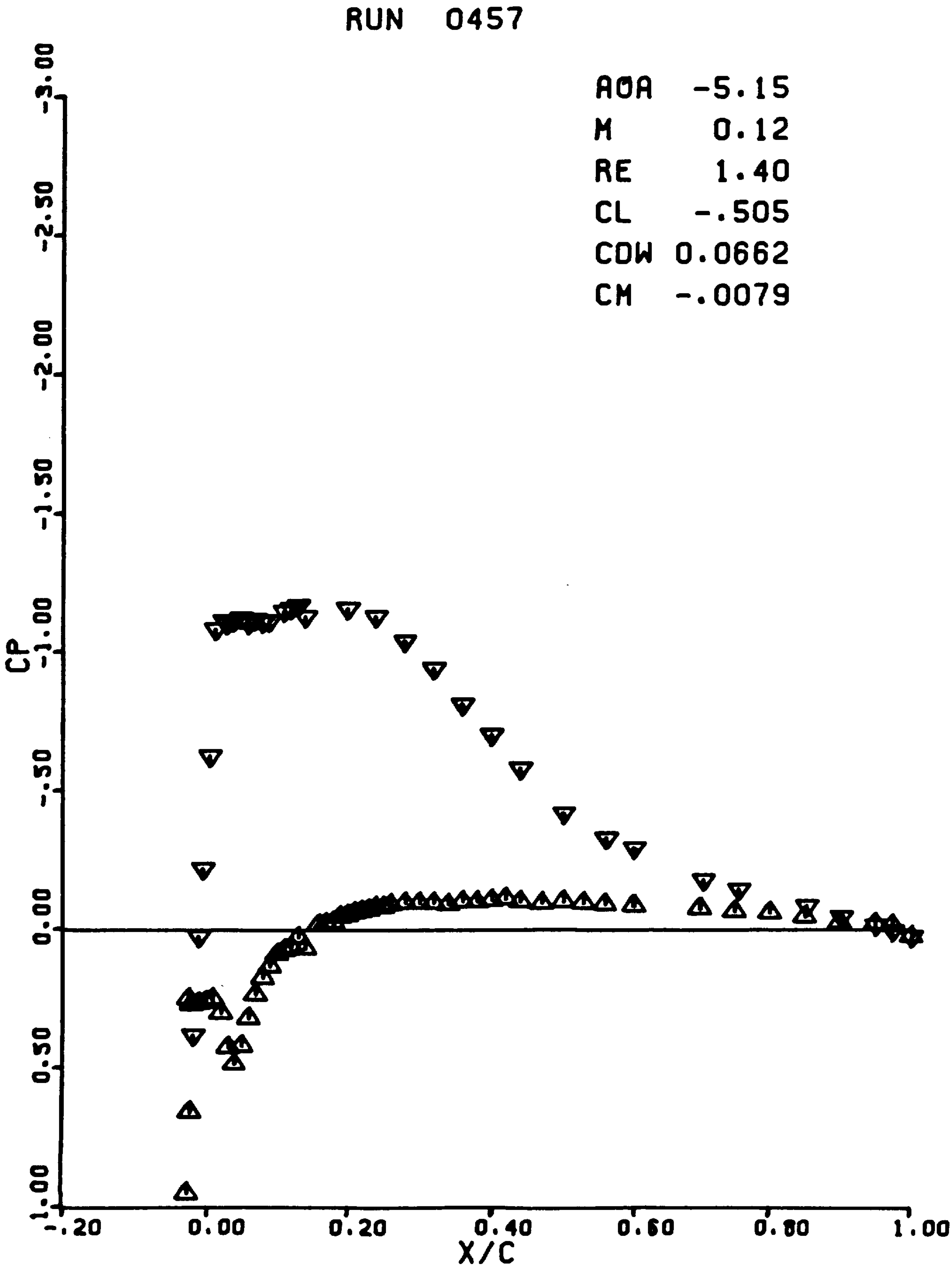
RUN 0457
AOA -5.15
M 0.12
RE 1.40
CL -.505
CDW 0.0662
CM -.0079
CP
-3.00
-2.50
-2.00
-1.50
-1.00
-.50
0.00
0.50
1.00
-.20
0.00
0.20
0.40
0.60
0.80
1.00
X/C

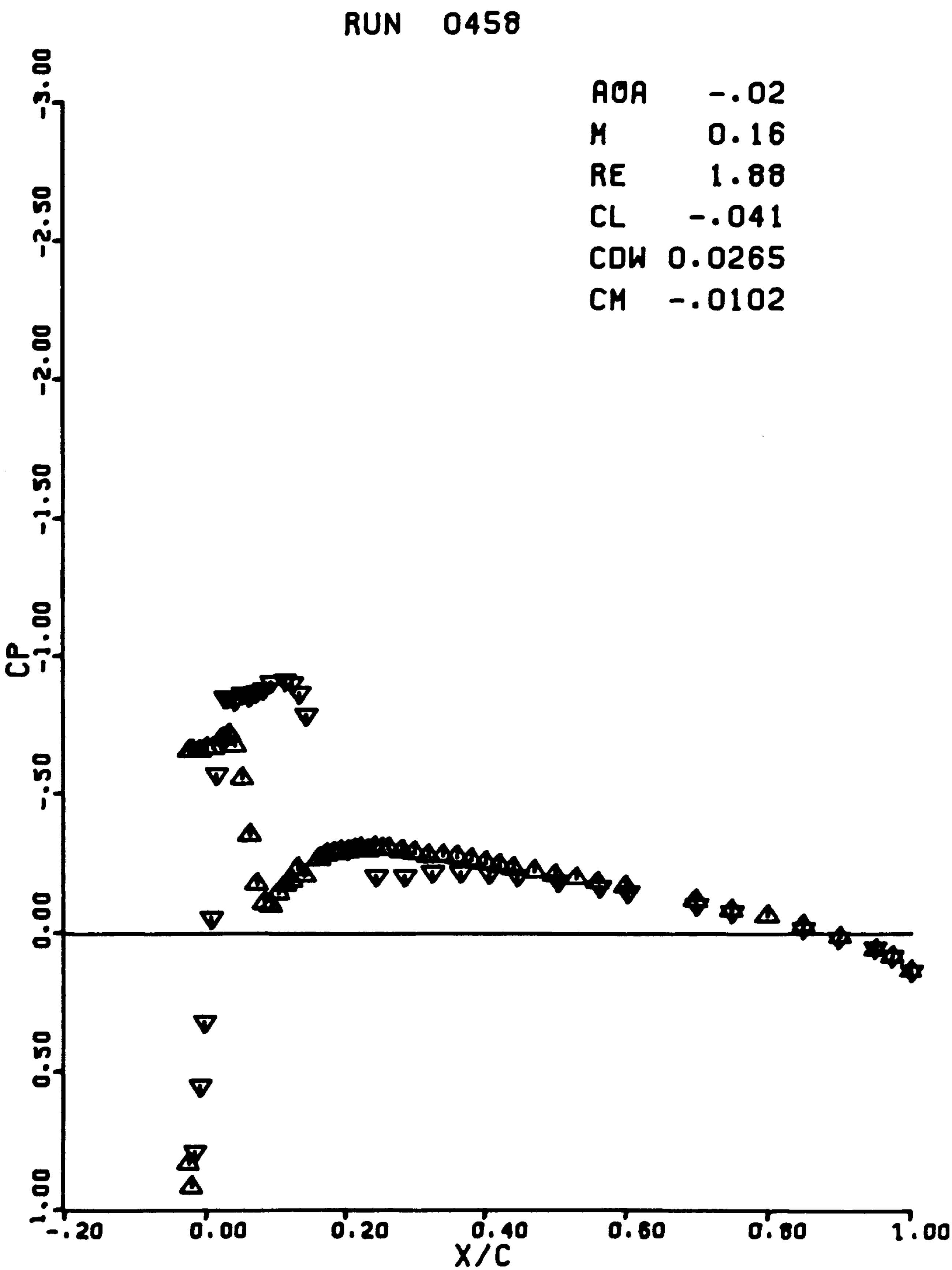
RUN 0458
AOA -.02
M 0.16
RE 1.88
CL -.041
CDW 0.0265
CM -.0102
CP
-3.00
-2.50
-2.00
-1.50
-1.00
-.50
0.00
0.50
1.00
-.20
0.00
0.20
0.40
0.60
0.80
1.00
X/C

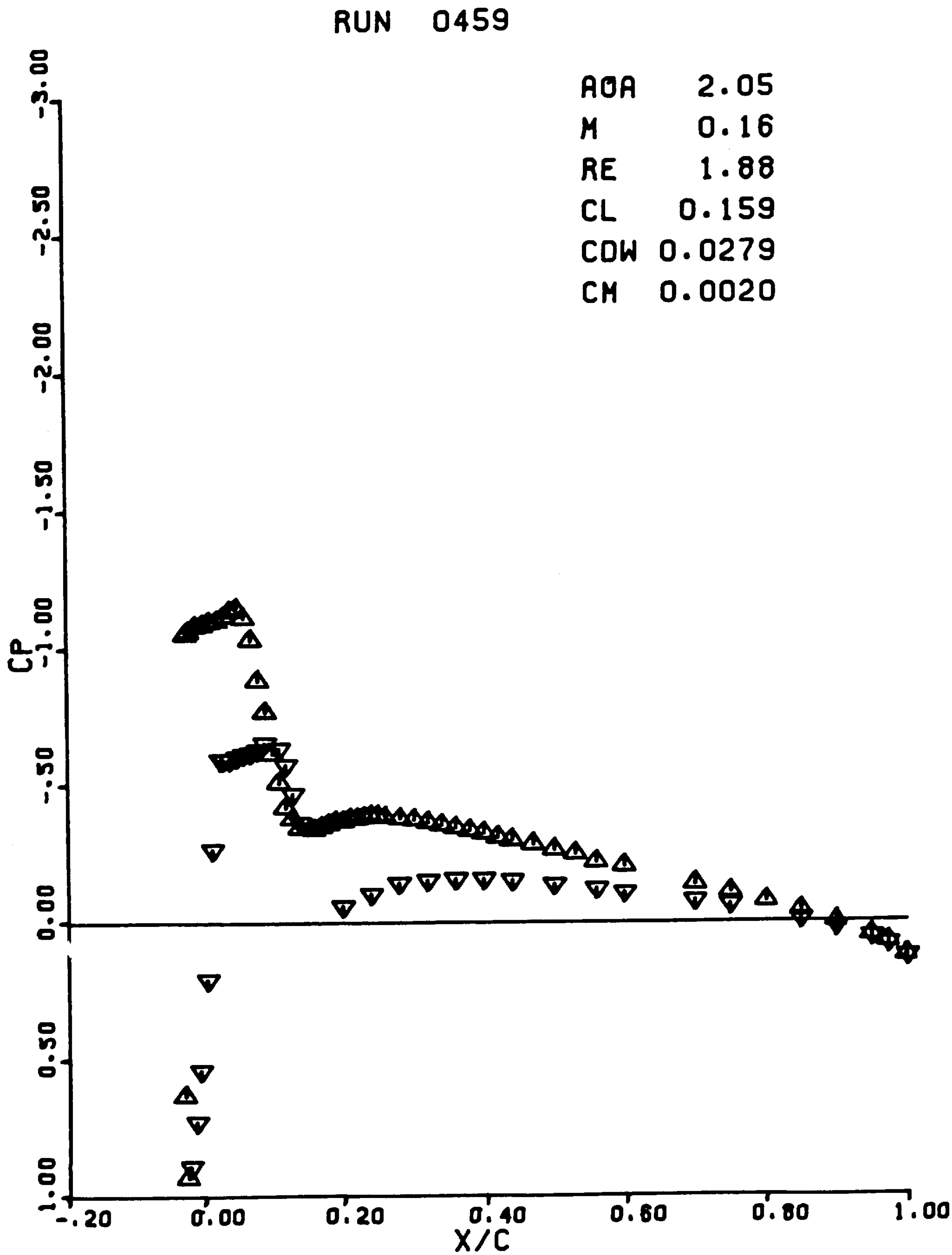
RUN 0459
AOA 2.05
M 0.16
RE 1.88
CL 0.159
CDW 0.0279
CM 0.0020
CP
-3.00
-2.50
-2.00
-1.50
-1.00
-.50
0.00
0.50
1.00
-.20
0.00
0.20
0.40
0.60
0.80
1.00
X/C

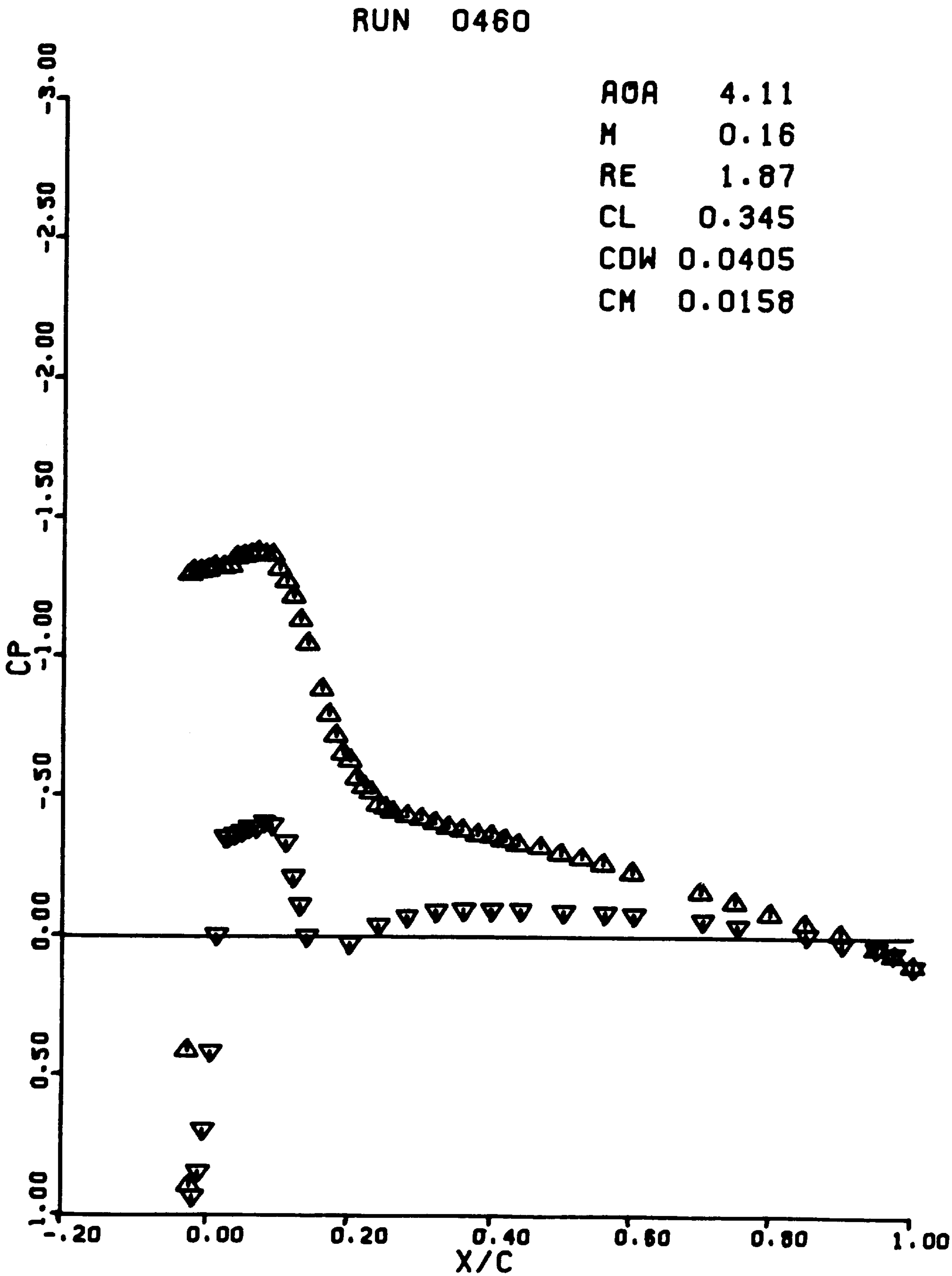
RUN 0460
AOA 4.11
M 0.16
RE 1.87
CL 0.345
CDW 0.0405
CM 0.0158
CP
-3.00
-2.50
-2.00
-1.50
-1.00
-.50
0.00
0.50
1.00
X/C
-.20
0.00
0.20
0.40
0.60
0.80
1.00

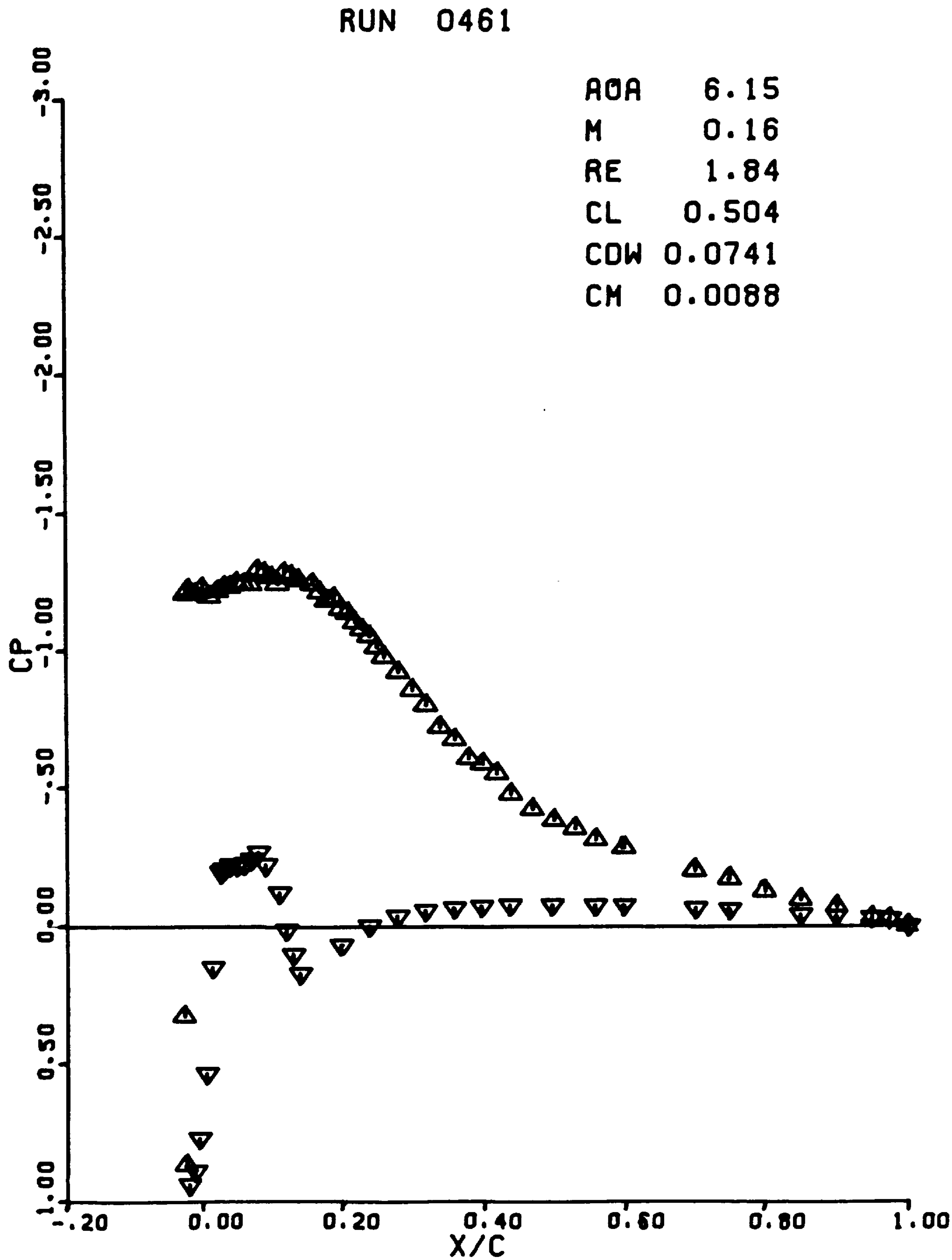

RUN 0461
AOA 6.15
M 0.16
RE 1.84
CL 0.504
CDW 0.0741
CM 0.0088
CP
-3.00
-2.50
-2.00
-1.50
-1.00
-.50
0.00
0.50
1.00
X/C
-.20
0.00
0.20
0.40
0.60
0.80
1.00

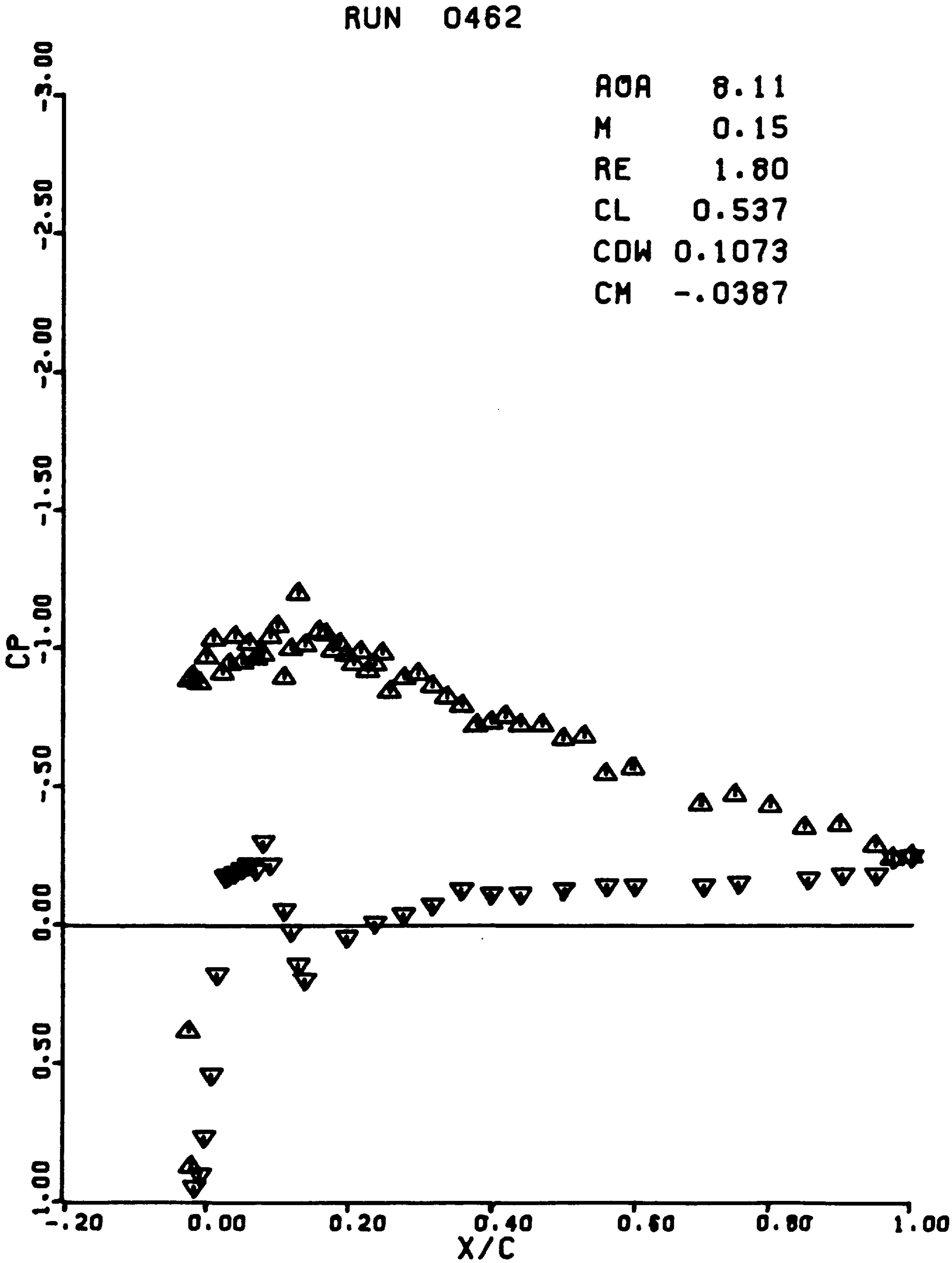
RUN 0462
AOA 8.11
M 0.15
RE 1.80
CL 0.537
CDW 0.1073
CM -.0387
CP
-3.00
-2.50
-2.00
-1.50
-1.00
-.50
0.00
0.50
1.00
X/C
-.20
0.00
0.20
0.40
0.60
0.80
1.00

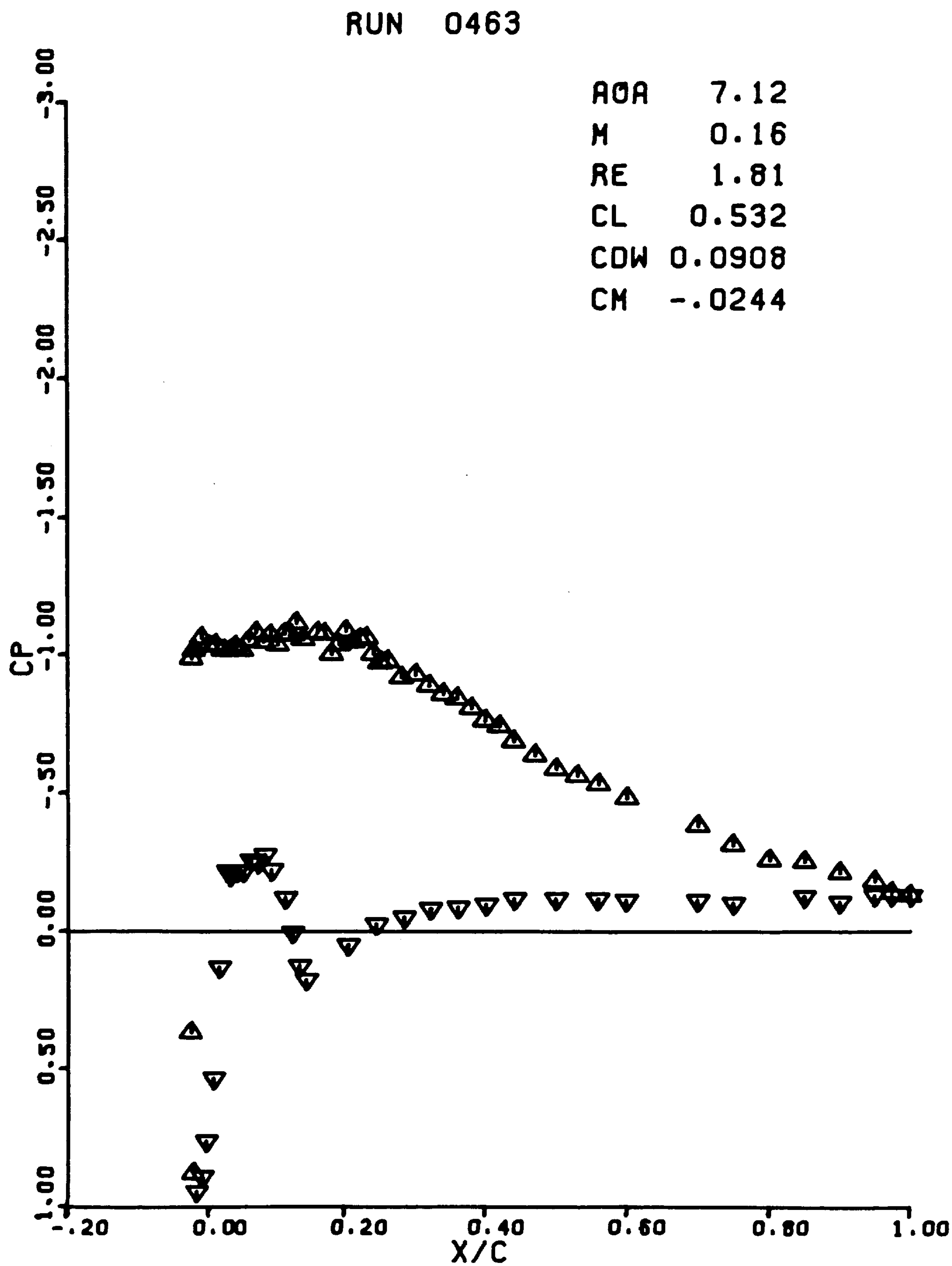
RUN 0463
AOA 7.12
M 0.16
RE 1.81
CL 0.532
CDW 0.0908
CM -.0244
CP
-3.00
-2.50
-2.00
-1.50
-1.00
-.50
0.00
0.50
1.00
-.20
0.00
0.20
0.40
0.60
0.80
1.00
X/C

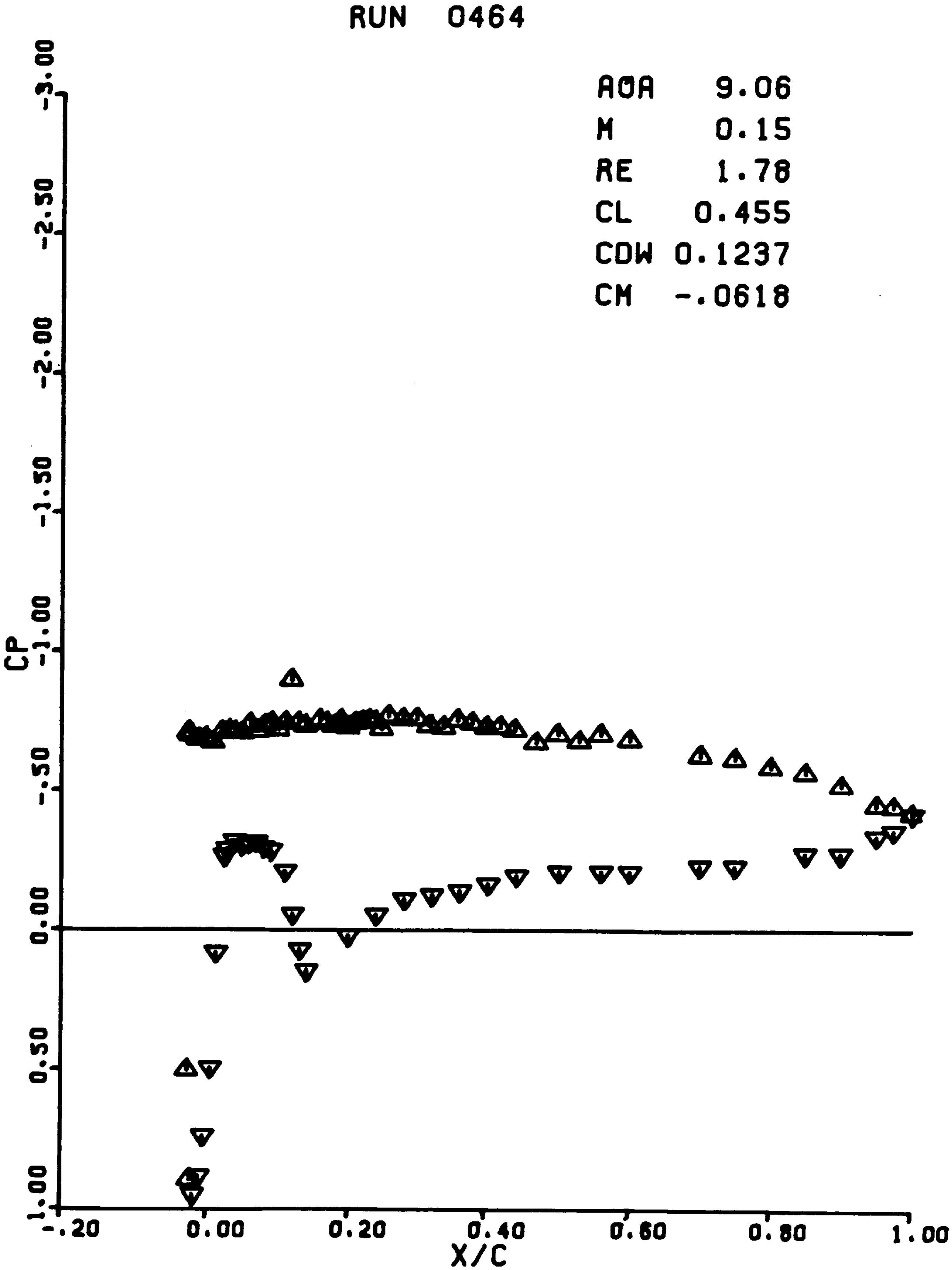
RUN 0464
AOA 9.06
M 0.15
RE 1.78
CL 0.455
CDW 0.1237
CM -.0618
CP
-3.00
-2.50
-2.00
-1.50
-1.00
-.50
0.00
0.50
1.00
X/C
-.20
0.00
0.20
0.40
0.60
0.80
1.00

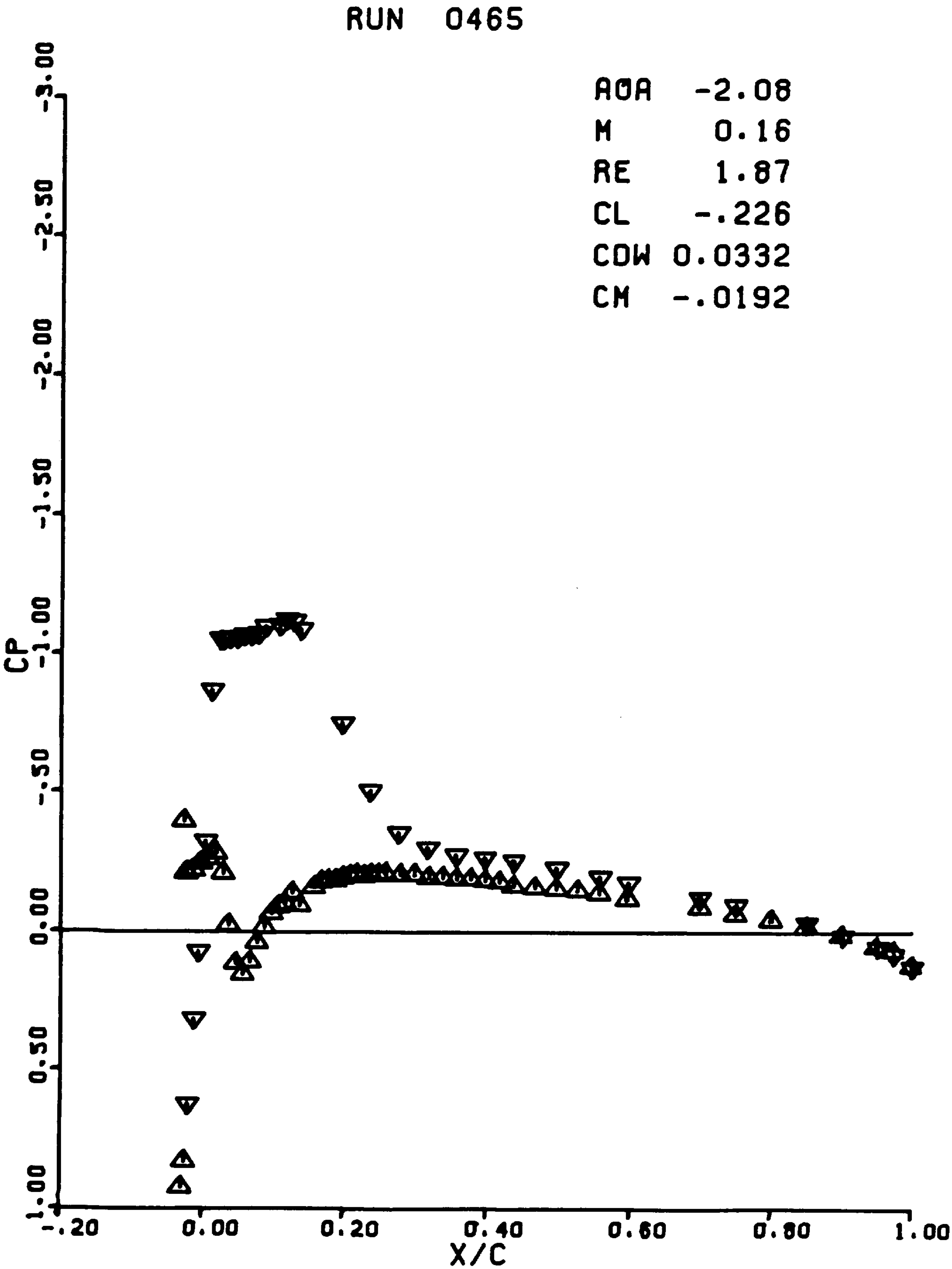
RUN 0465
AOA -2.08
M 0.16
RE 1.87
CL -.226
CDW 0.0332
CM -.0192
CP
-3.00
-2.50
-2.00
-1.50
-1.00
-.50
0.00
0.50
1.00
X/C
-.20
0.00
0.20
0.40
0.60
0.80
1.00

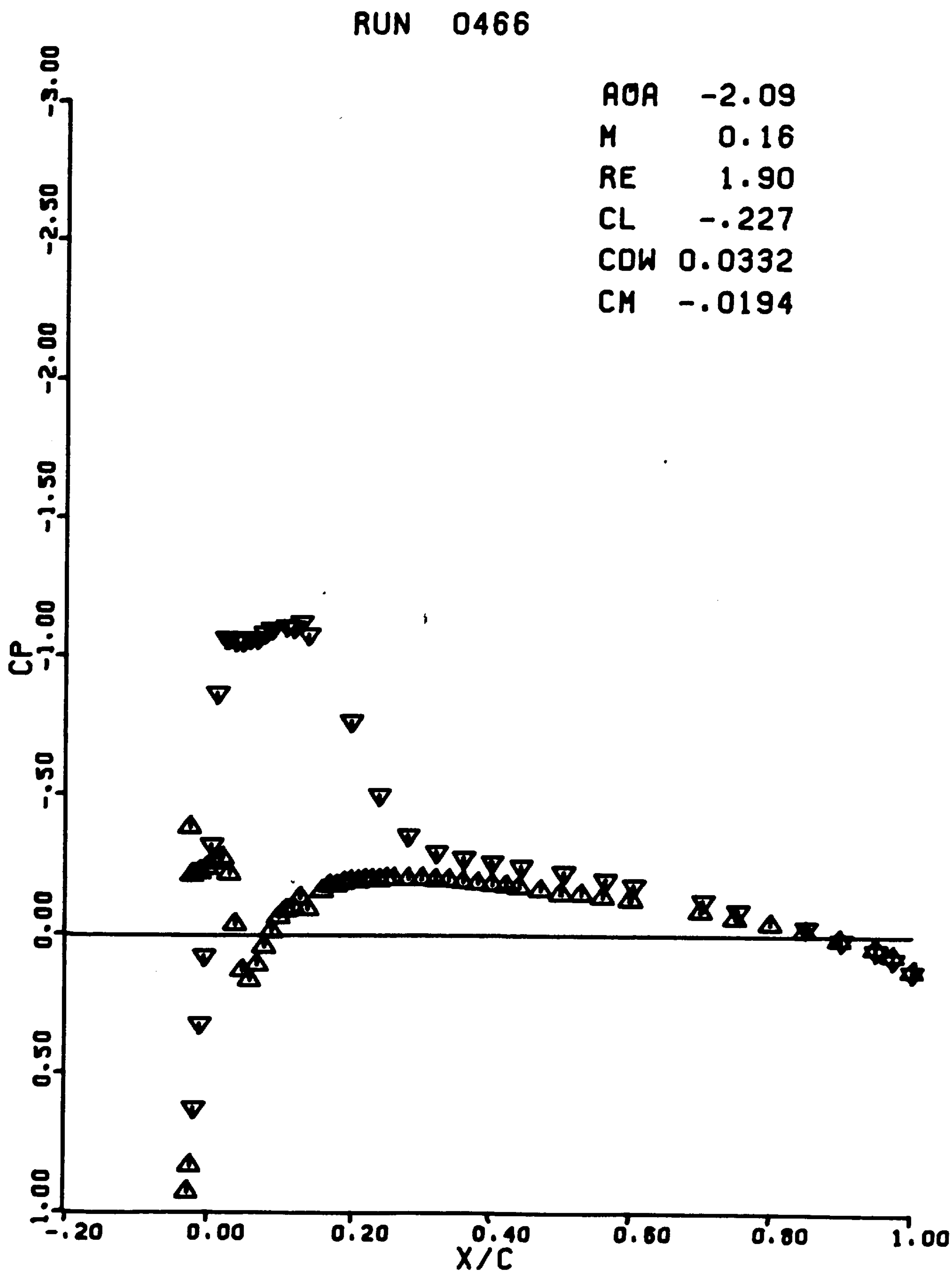

RUN 0466
AOA -2.09
M 0.16
RE 1.90
CL -.227
CDW 0.0332
CM -.0194
CP
-3.00
-2.50
-2.00
-1.50
-1.00
-.50
0.00
0.50
1.00
-.20
0.00
0.20
0.40
0.60
0.80
1.00
X/C

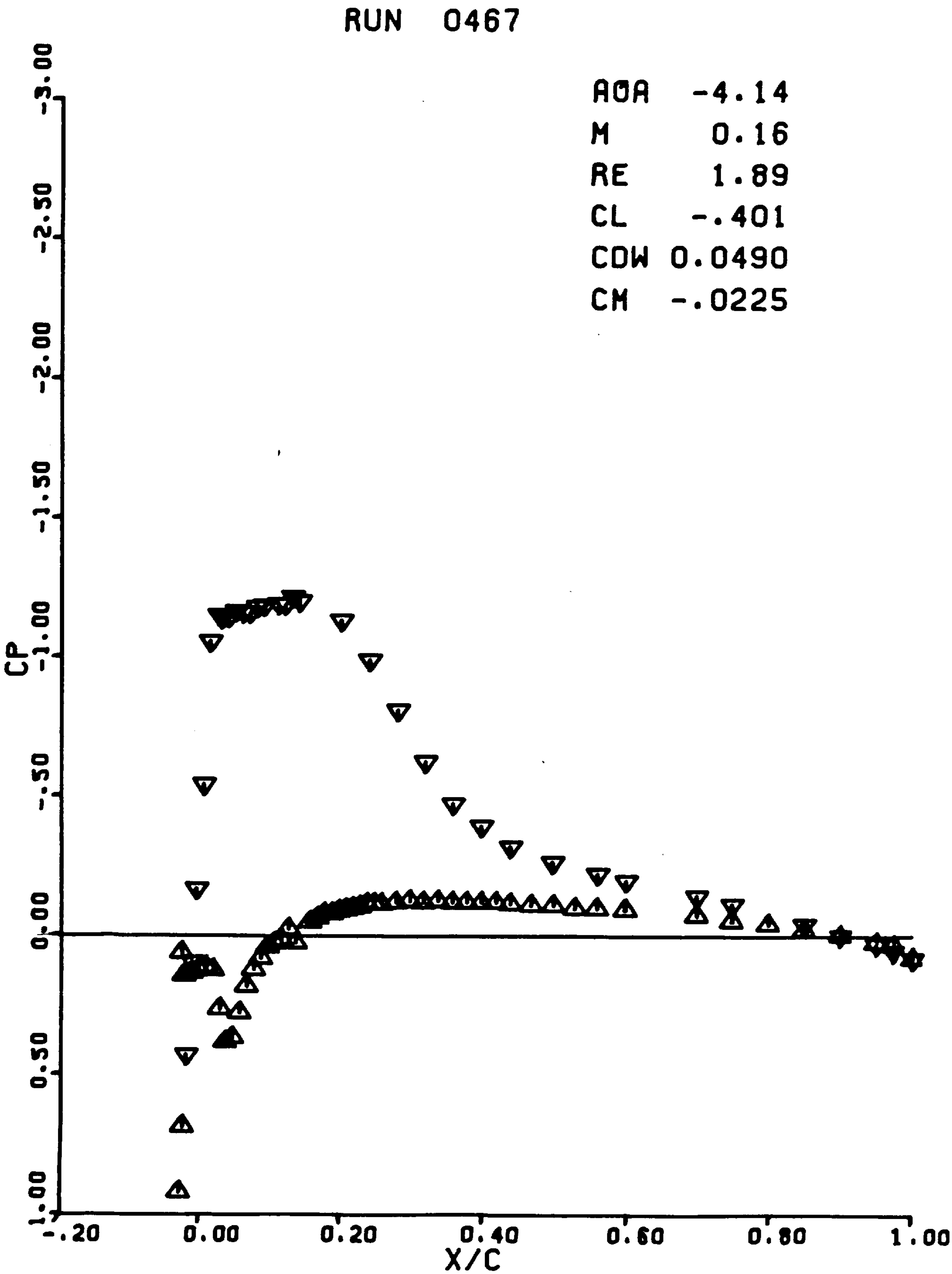
RUN 0467
AOA -4.14
M 0.16
RE 1.89
CL -.401
CDW 0.0490
CM -.0225
CP
-3.00
-2.50
-2.00
-1.50
-1.00
-.50
0.00
0.50
1.00
X/C
-.20
0.00
0.20
0.40
0.60
0.80
1.00

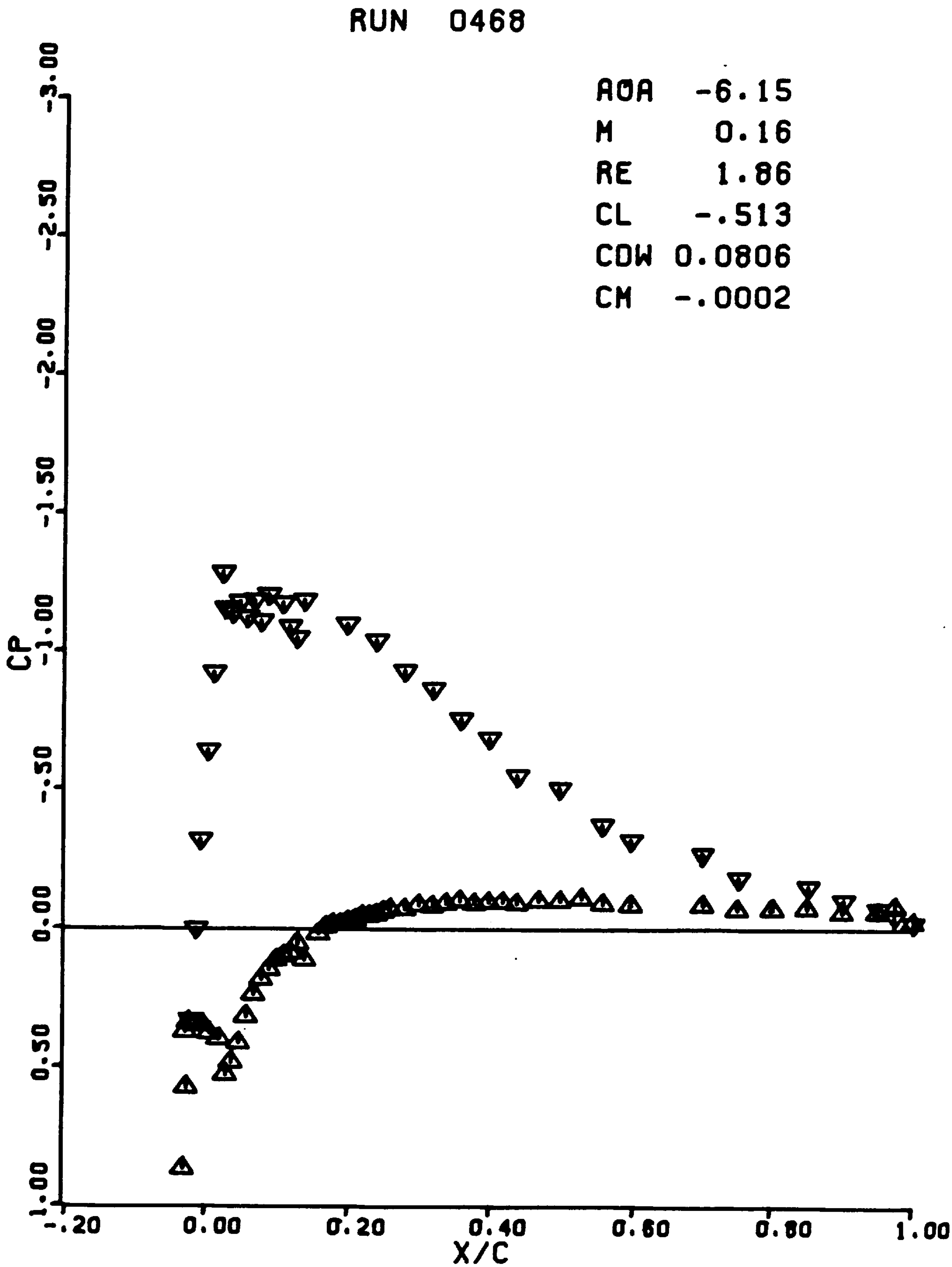

RUN 0468
AOA -6.15
M 0.16
RE 1.86
CL -.513
CDW 0.0806
CM -.0002
CP
-3.00
-2.50
-2.00
-1.50
-1.00
-.50
0.00
0.50
1.00
-.20
0.00
0.20
0.40
0.60
0.80
1.00
X/C

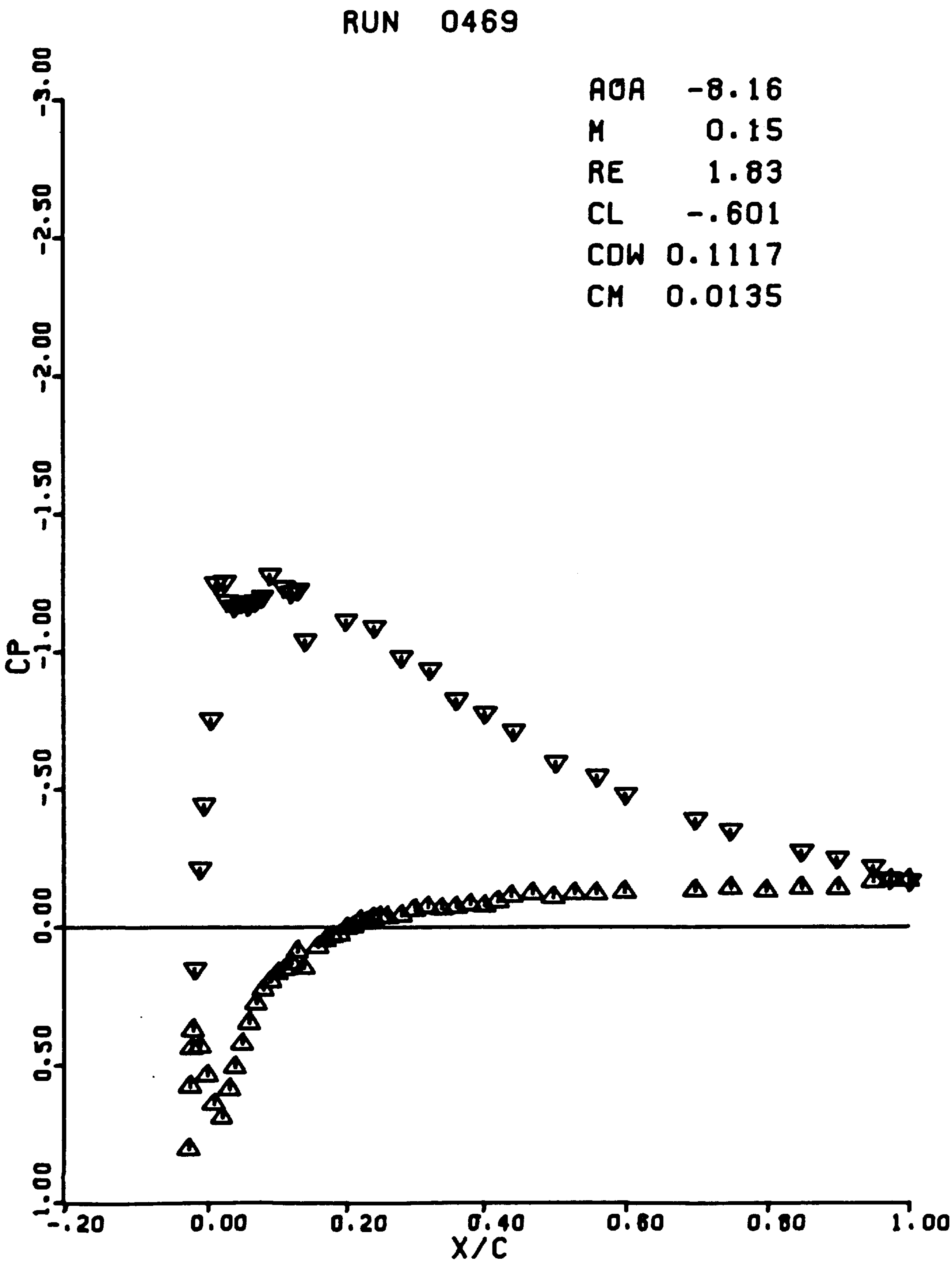
RUN 0469
AOA -8.16
M 0.15
RE 1.83
CL -.601
CDW 0.1117
CM 0.0135
CP
-3.00
-2.50
-2.00
-1.50
-1.00
-.50
0.00
0.50
1.00
-.20
0.00
0.20
0.40
0.60
0.80
1.00
X/C

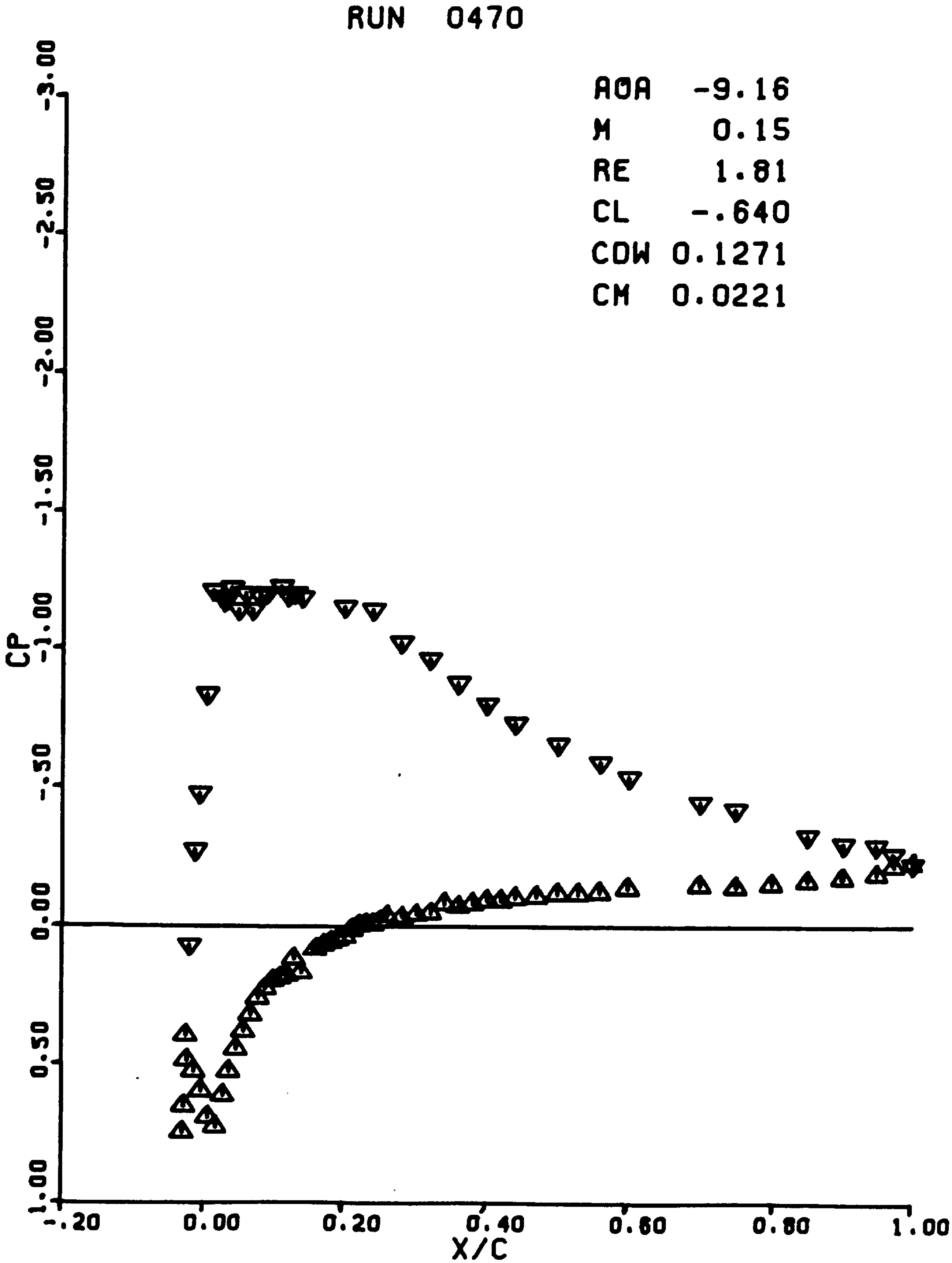
RUN 0470
AOA -9.16
M 0.15
RE 1.81
CL -.640
CDW 0.1271
CM 0.0221
CP
X/C
-3.00
-2.50
-2.00
-1.50
-1.00
-.50
0.00
0.50
1.00
-.20
0.00
0.20
0.40
0.60
0.80
1.00

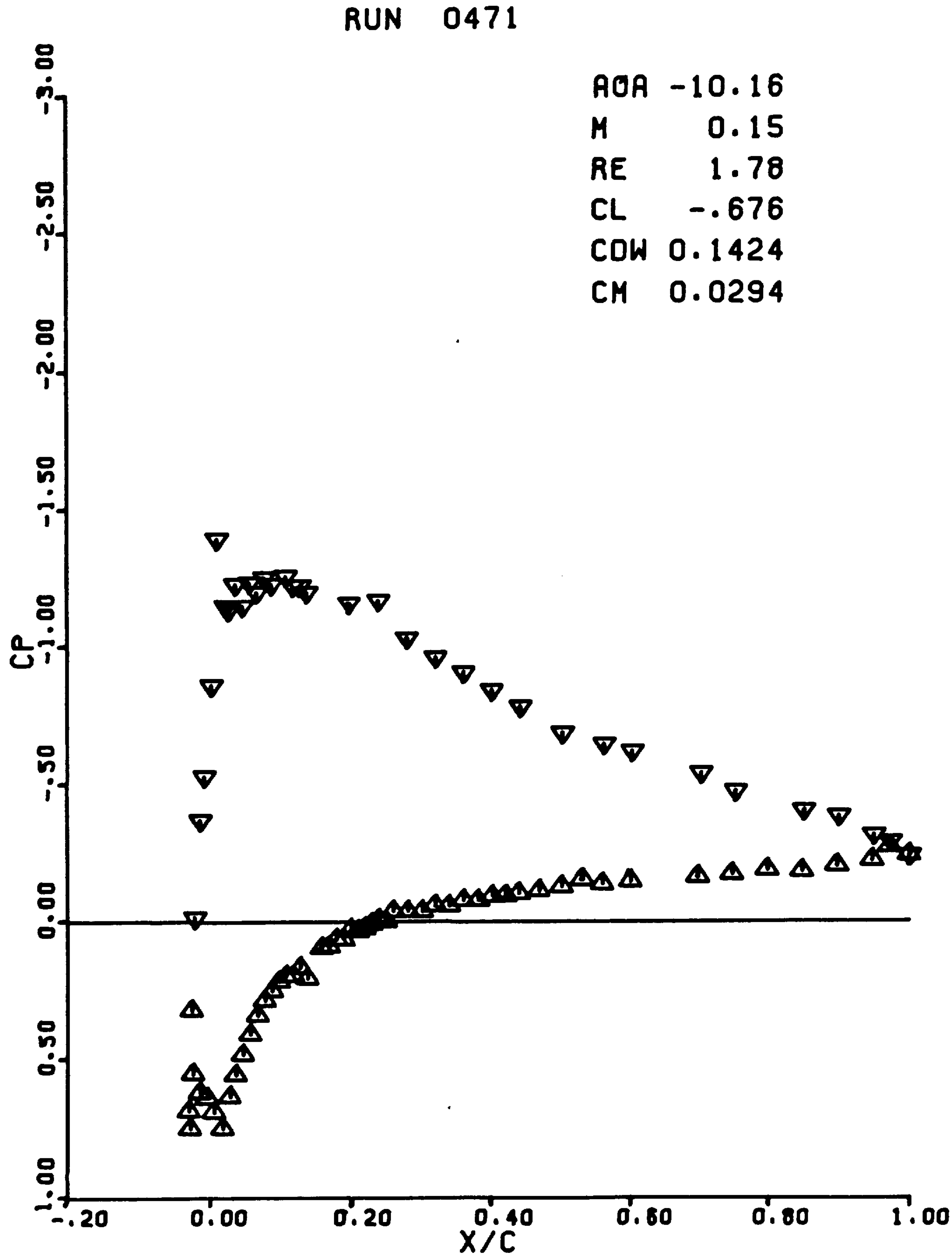

RUN 0471
AOA -10.16
M 0.15
RE 1.78
CL -.676
CDW 0.1424
CM 0.0294
CP
X/C
-3.00
-2.50
-2.00
-1.50
-1.00
-.50
0.00
0.50
1.00
-.20
0.00
0.20
0.40
0.60
0.80
1.00

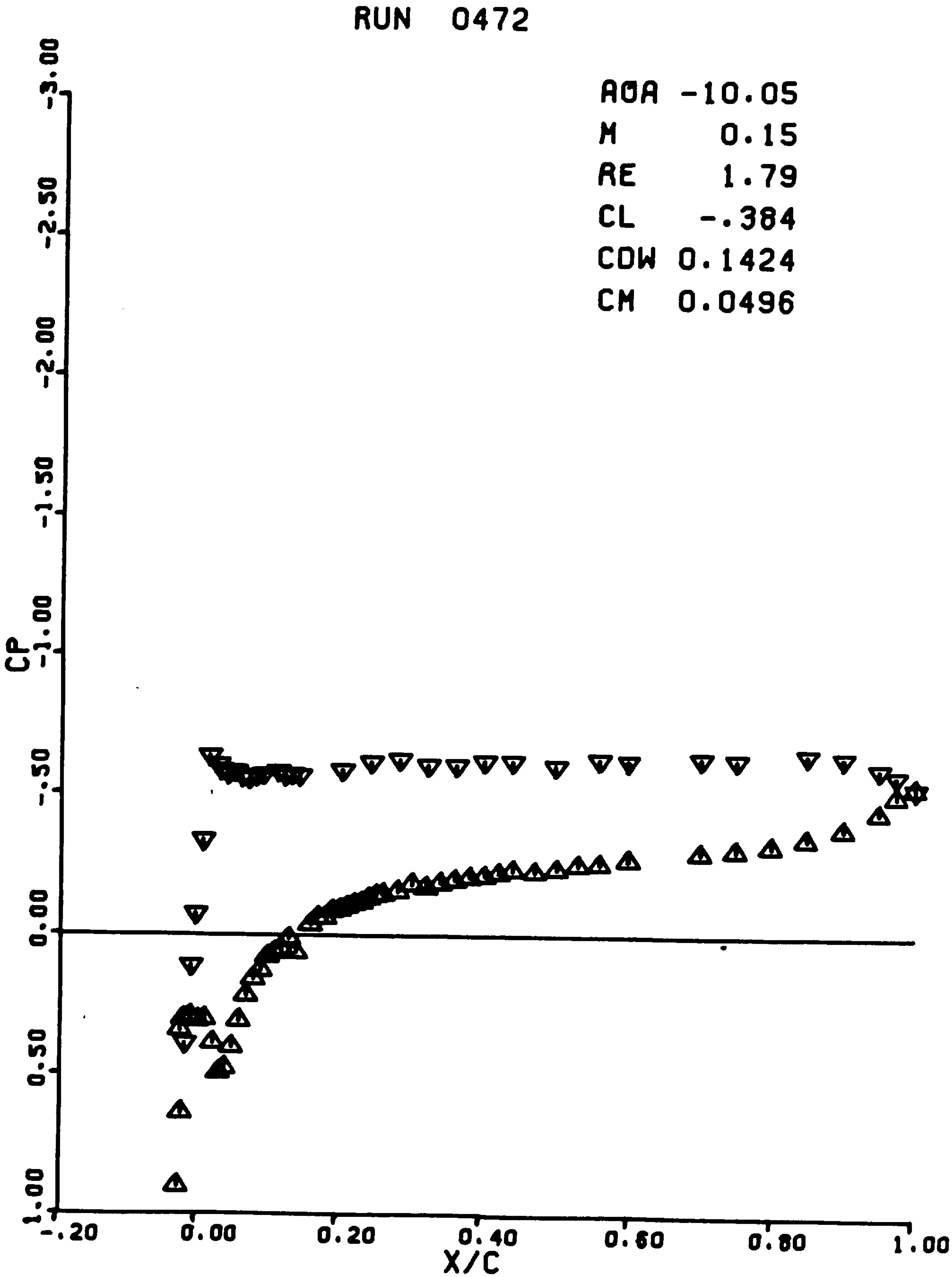

RUN 0472
AOA -10.05
M 0.15
RE 1.79
CL -.384
CDW 0.1424
CM 0.0496
CP
X/C
-3.00
-2.50
-2.00
-1.50
-1.00
-.50
0.00
0.50
1.00
-.20
0.00
0.20
0.40
0.60
0.80
1.00

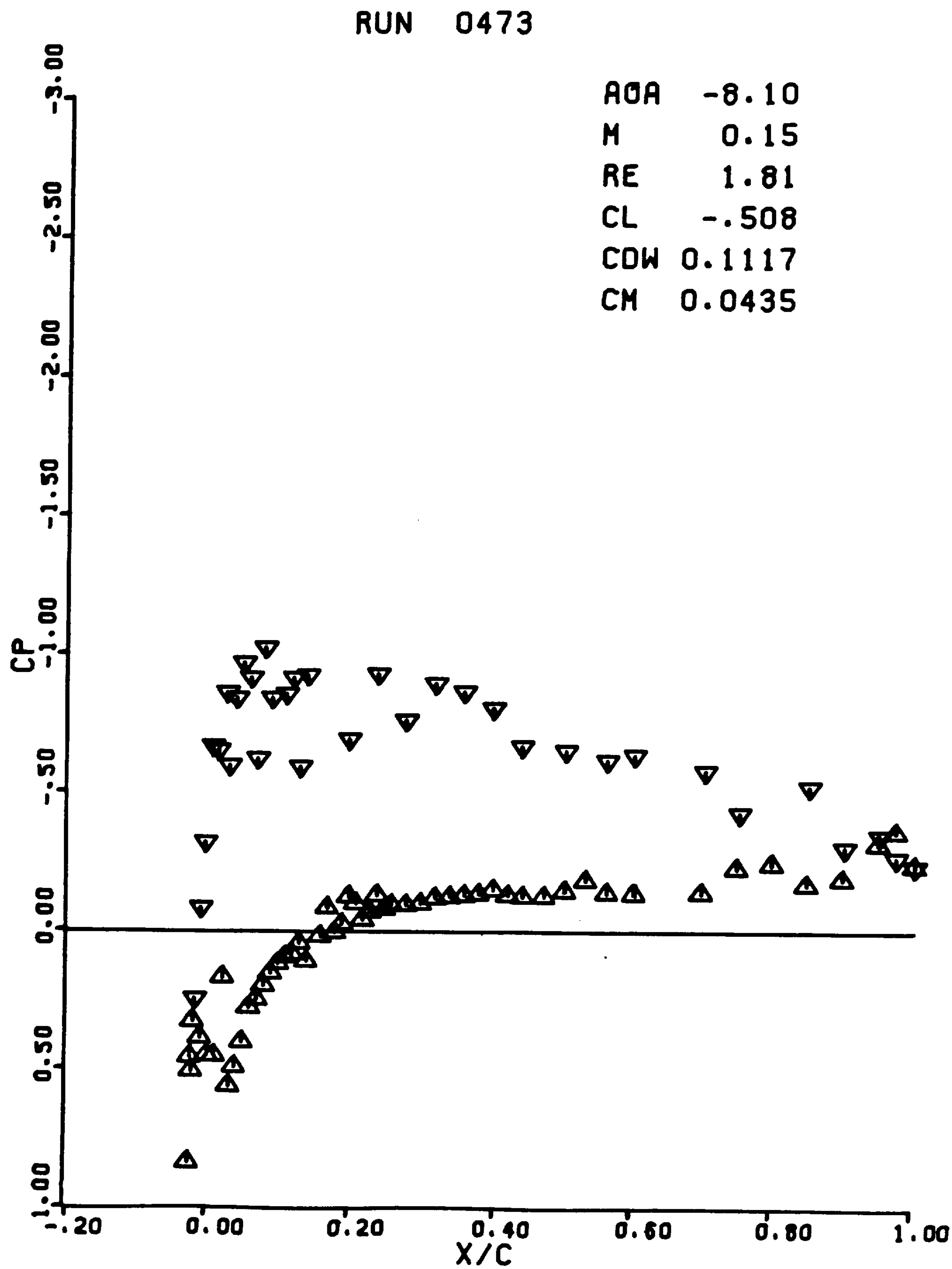
RUN 0473
AOA -8.10
M 0.15
RE 1.81
CL -.508
CDW 0.1117
CM 0.0435
CP
-3.00
-2.50
-2.00
-1.50
-1.00
-.50
0.00
0.50
1.00
-.20
0.00
0.20
0.40
0.60
0.80
1.00
X/C

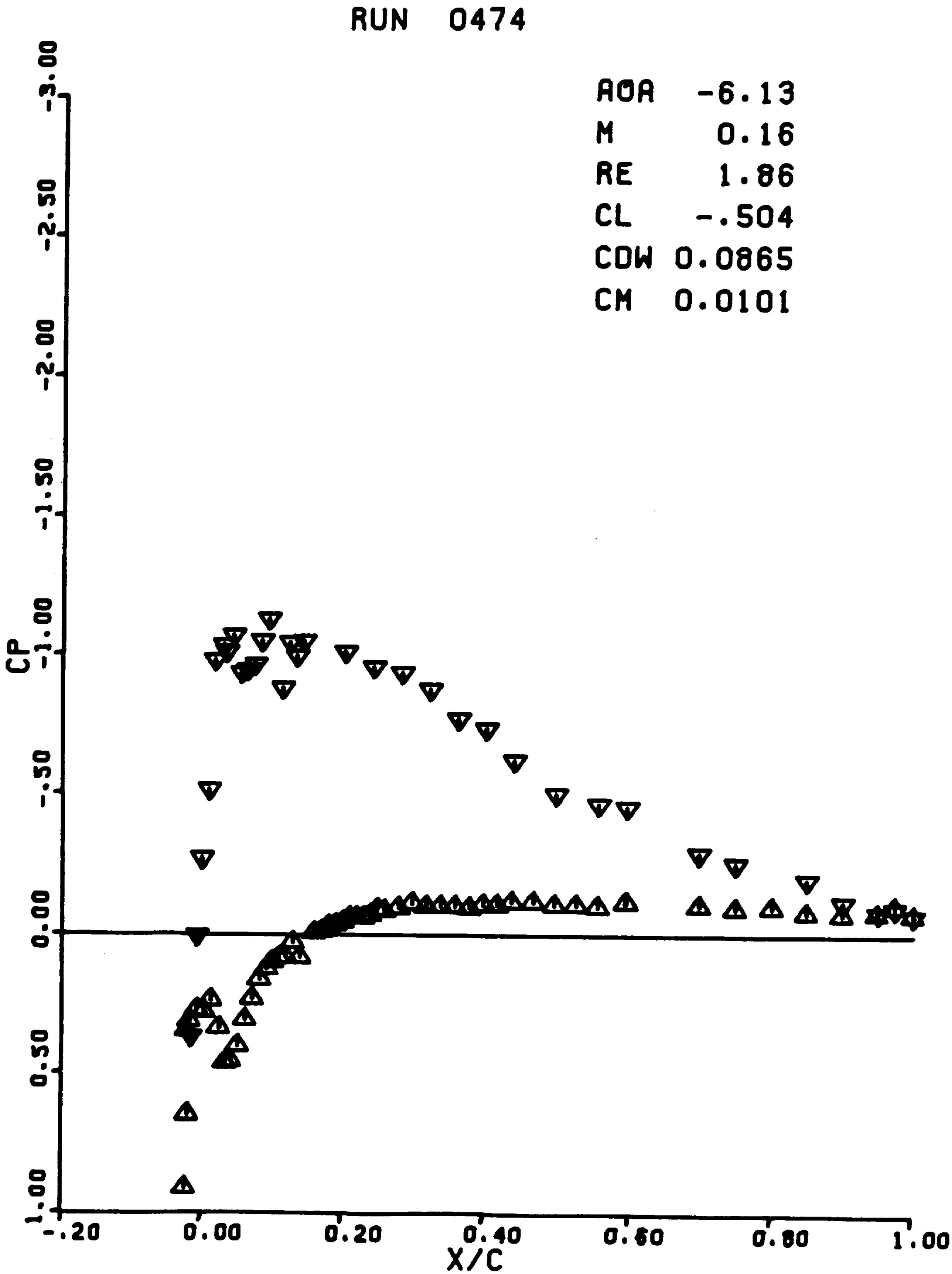
RUN 0474
AOA -6.13
M 0.16
RE 1.86
CL -.504
CDW 0.0865
CM 0.0101
CP
-3.00
-2.50
-2.00
-1.50
-1.00
-.50
0.00
0.50
1.00
-.20
0.00
0.20
0.40
0.60
0.80
1.00
X/C

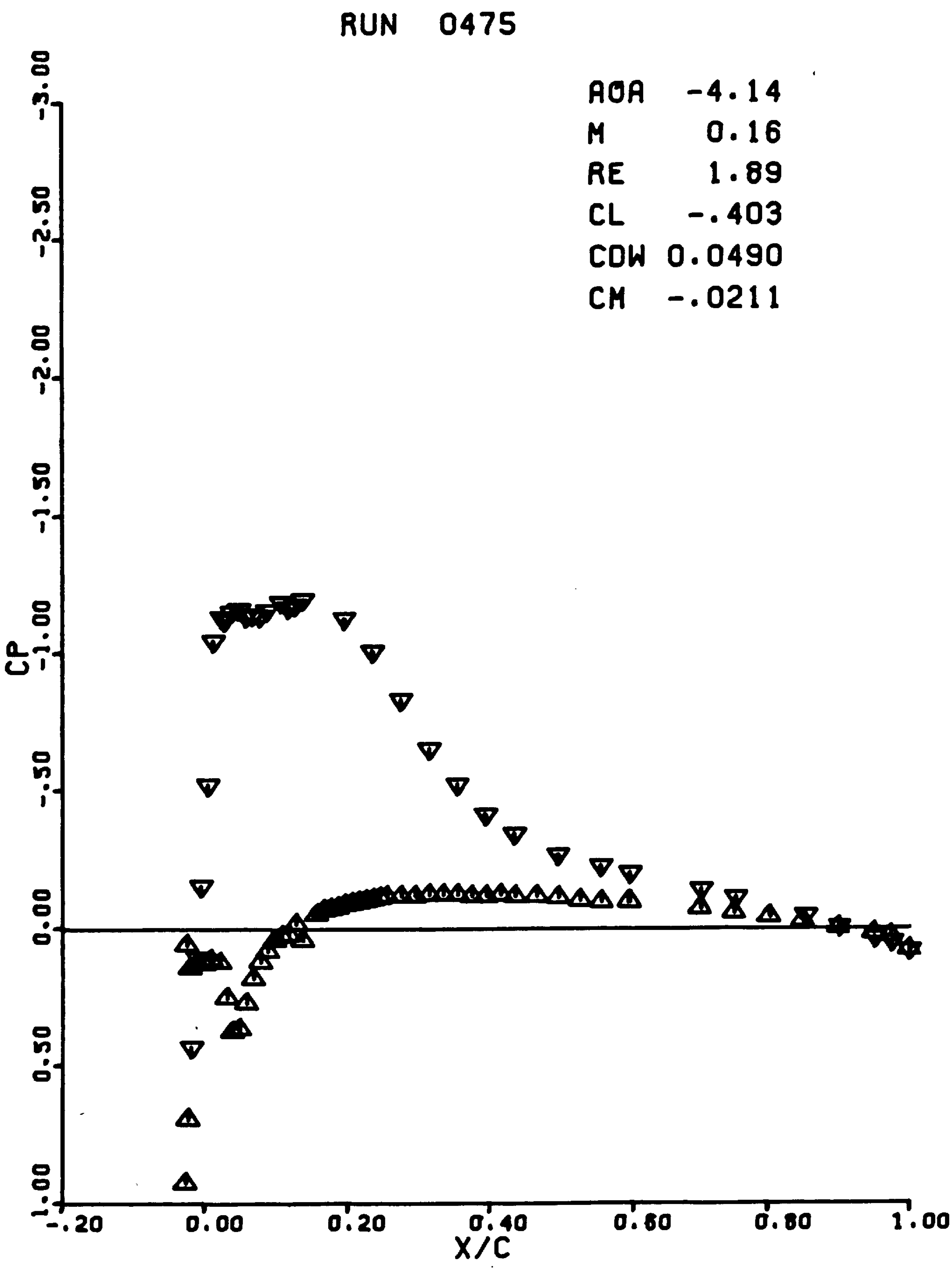
RUN 0475
AOA -4.14
M 0.16
RE 1.89
CL -.403
CDW 0.0490
CM -.0211
CP
-3.00
-2.50
-2.00
-1.50
-1.00
-.50
0.00
0.50
1.00
-.20
0.00
0.20
0.40
0.60
0.80
1.00
X/C

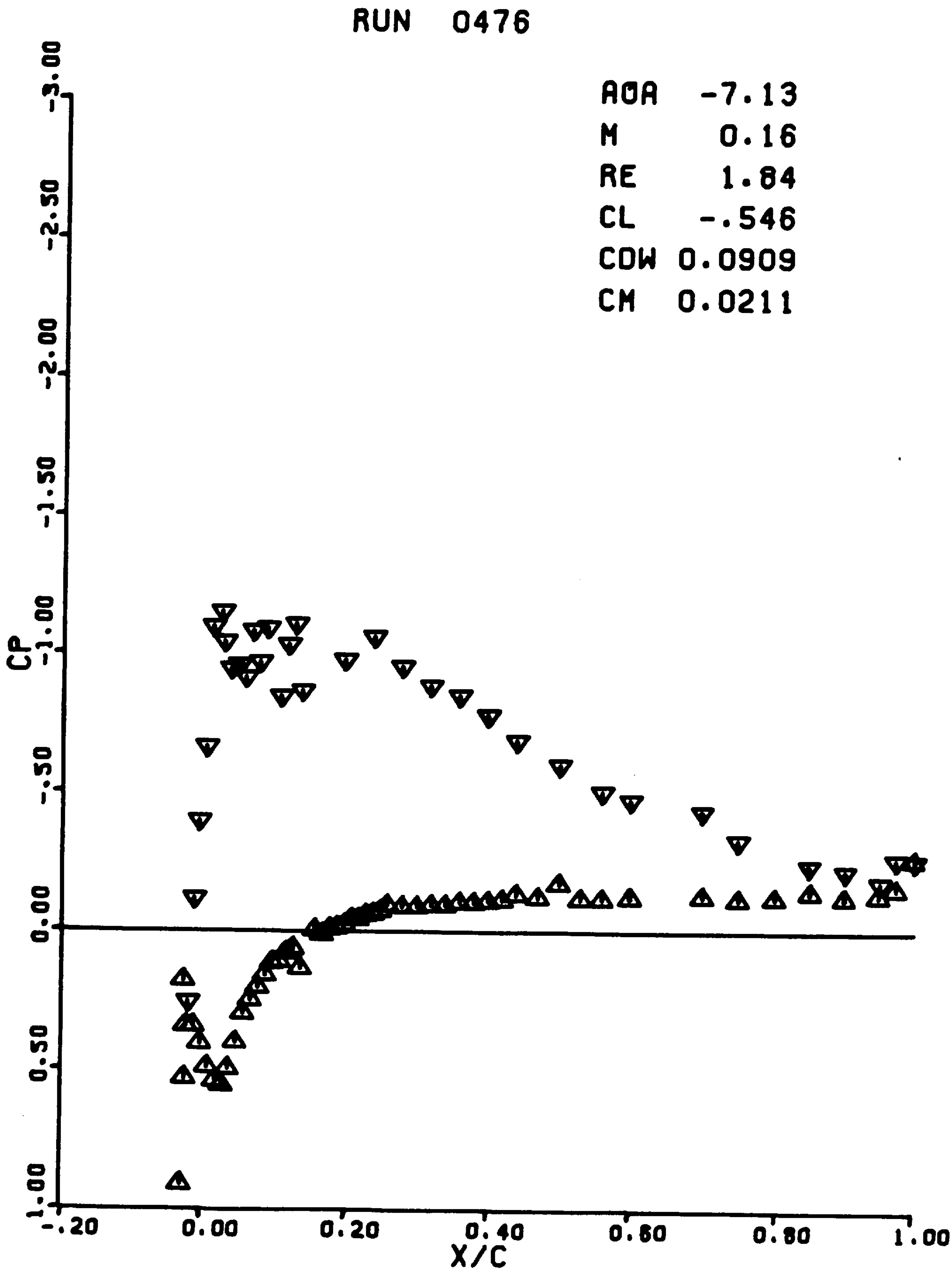

RUN 0476
AOA -7.13
M 0.16
RE 1.84
CL -.546
CDW 0.0909
CM 0.0211
CP
-3.00
-2.50
-2.00
-1.50
-1.00
-.50
0.00
0.50
1.00
-.20
0.00
0.20
0.40
0.60
0.80
1.00
X/C

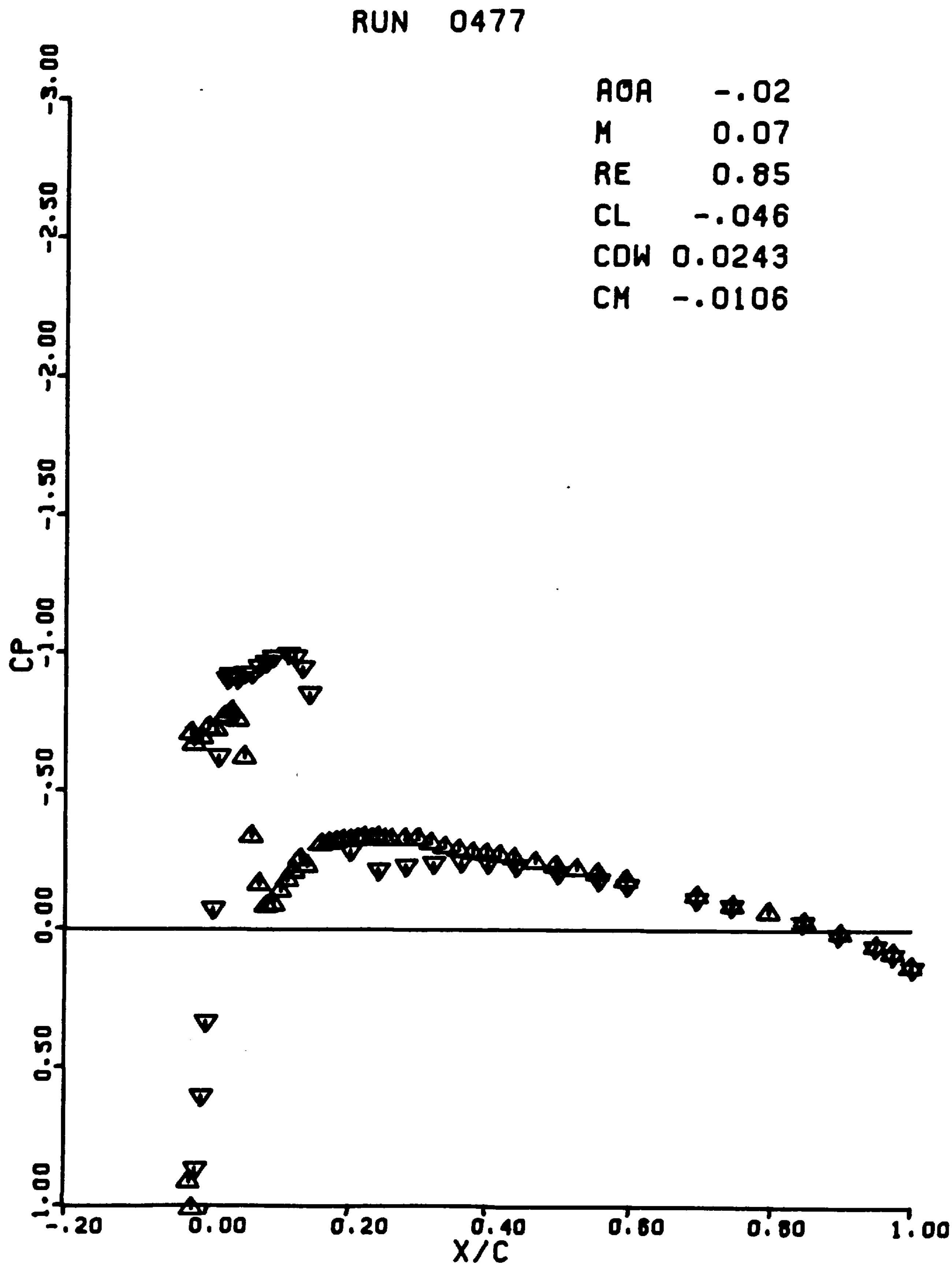
RUN 0477
AOA -.02
M 0.07
RE 0.85
CL -.046
CDW 0.0243
CM -.0106
CP
-3.00
-2.50
-2.00
-1.50
-1.00
-.50
0.00
0.50
1.00
-.20
0.00
0.20
0.40
0.60
0.80
1.00
X/C

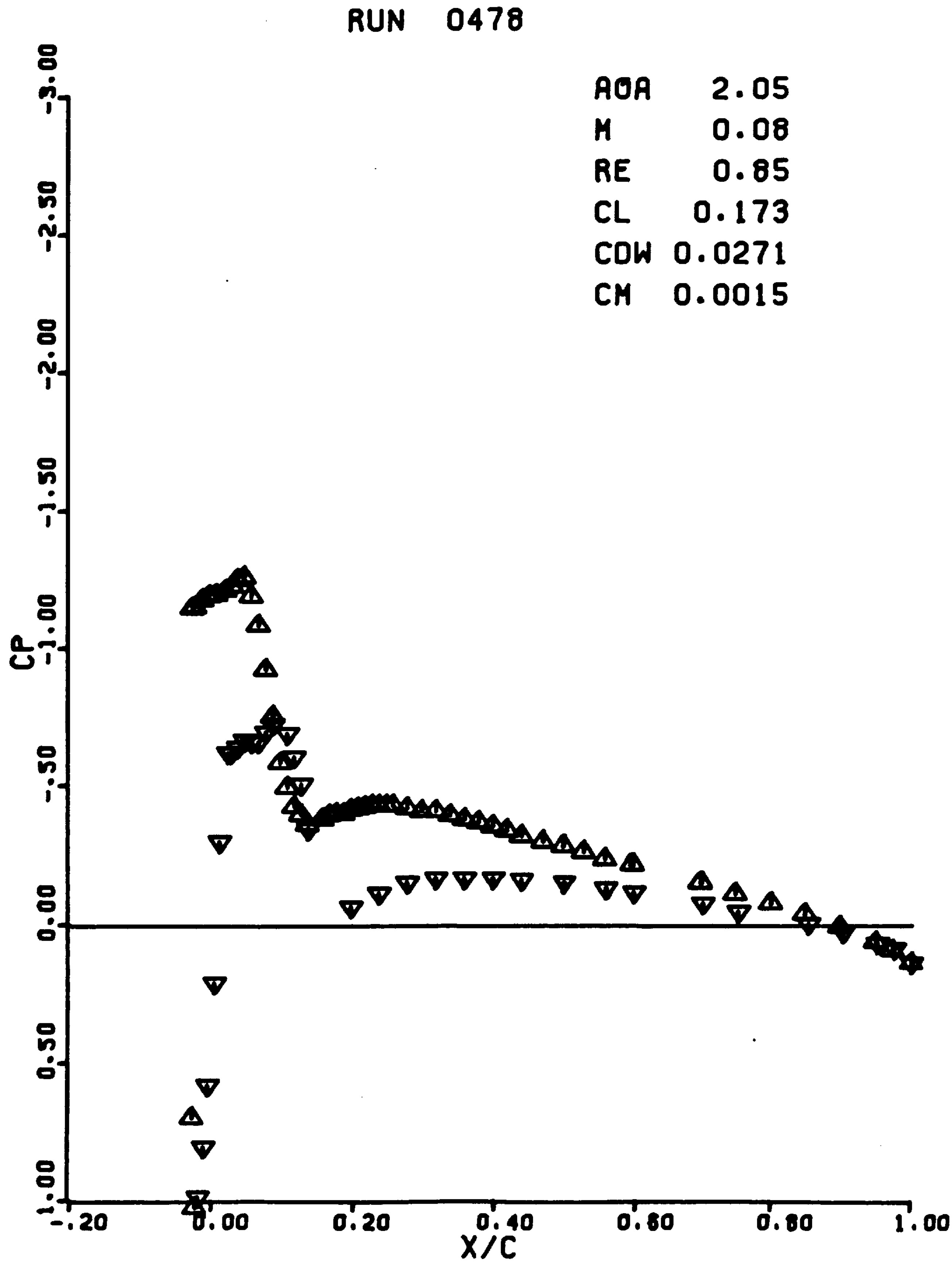
RUN 0478
AOA 2.05
M 0.08
RE 0.85
CL 0.173
CDW 0.0271
CM 0.0015
CP
-3.00
-2.50
-2.00
-1.50
-1.00
-.50
0.00
0.50
1.00
-.20
0.00
0.20
0.40
0.60
0.80
1.00
X/C

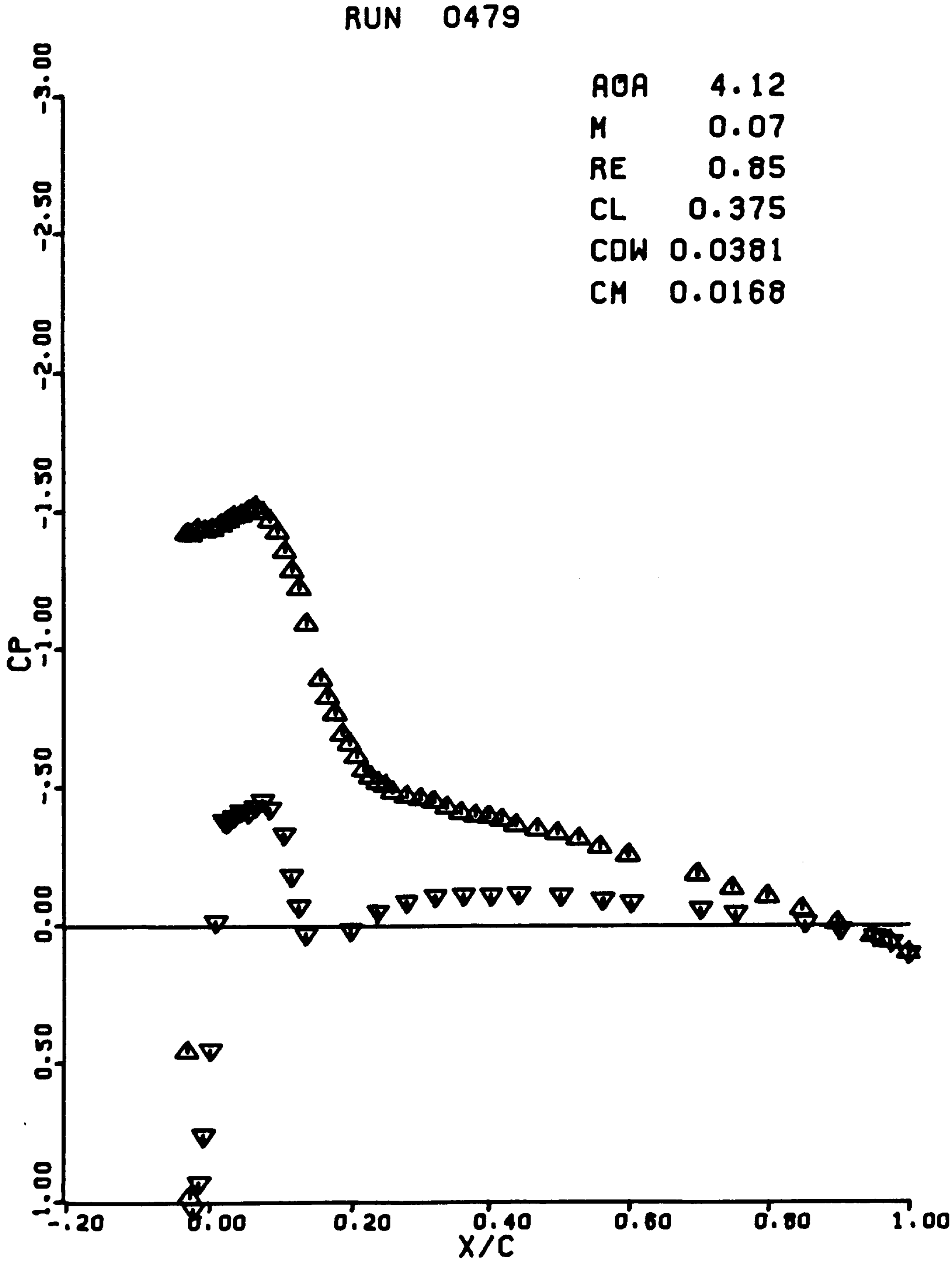
RUN 0479
AOA 4.12
M 0.07
RE 0.85
CL 0.375
CDW 0.0381
CM 0.0168
CP
-3.00
-2.50
-2.00
-1.50
-1.00
-.50
0.00
0.50
1.00
-.20
0.00
0.20
0.40
0.60
0.80
1.00
X/C

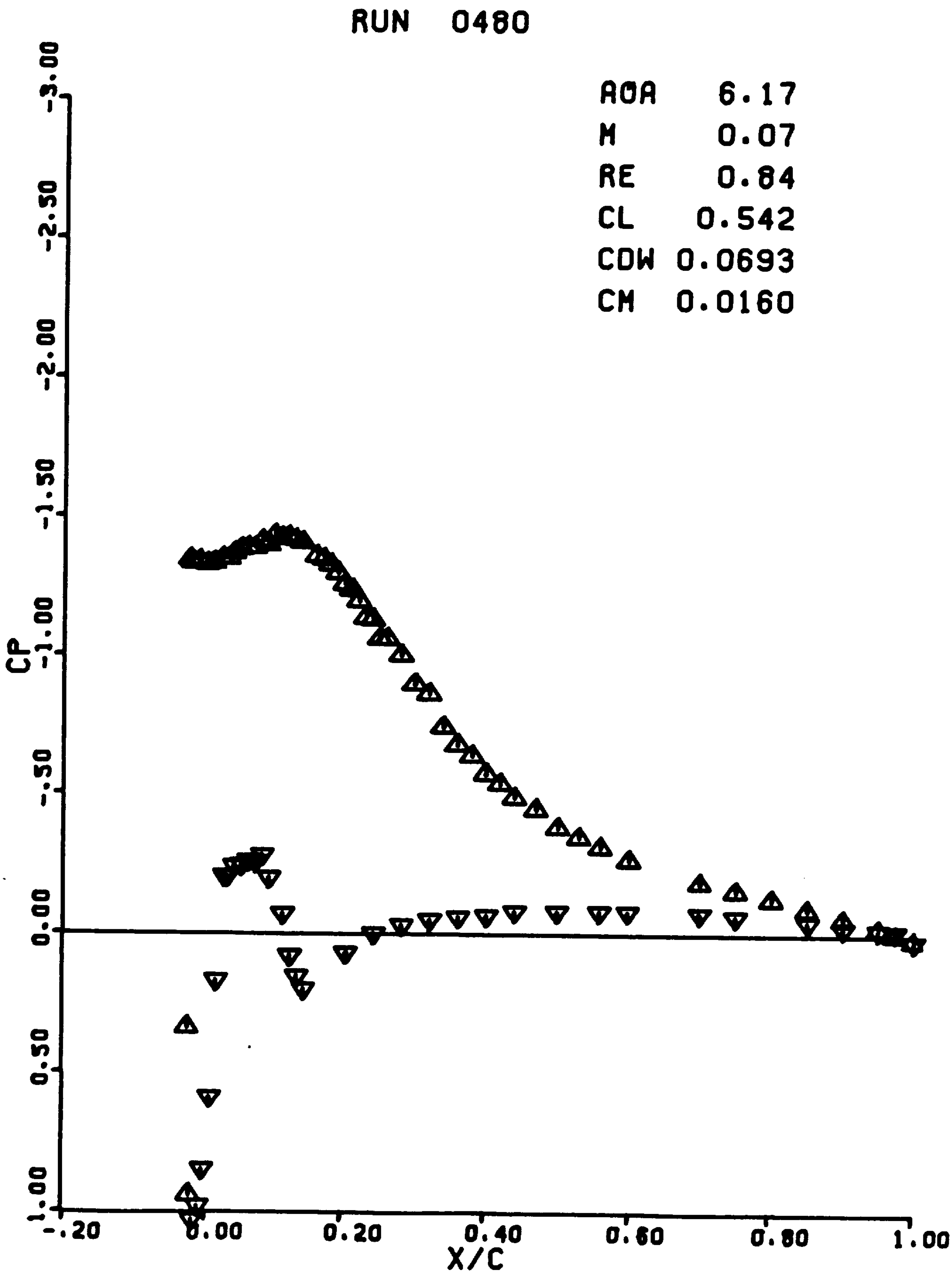

RUN 0480
AOA 6.17
M 0.07
RE 0.84
CL 0.542
CDW 0.0693
CM 0.0160
CP
-3.00
-2.50
-2.00
-1.50
-1.00
-.50
0.00
0.50
1.00
-.20
0.00
0.20
0.40
0.60
0.80
1.00
X/C

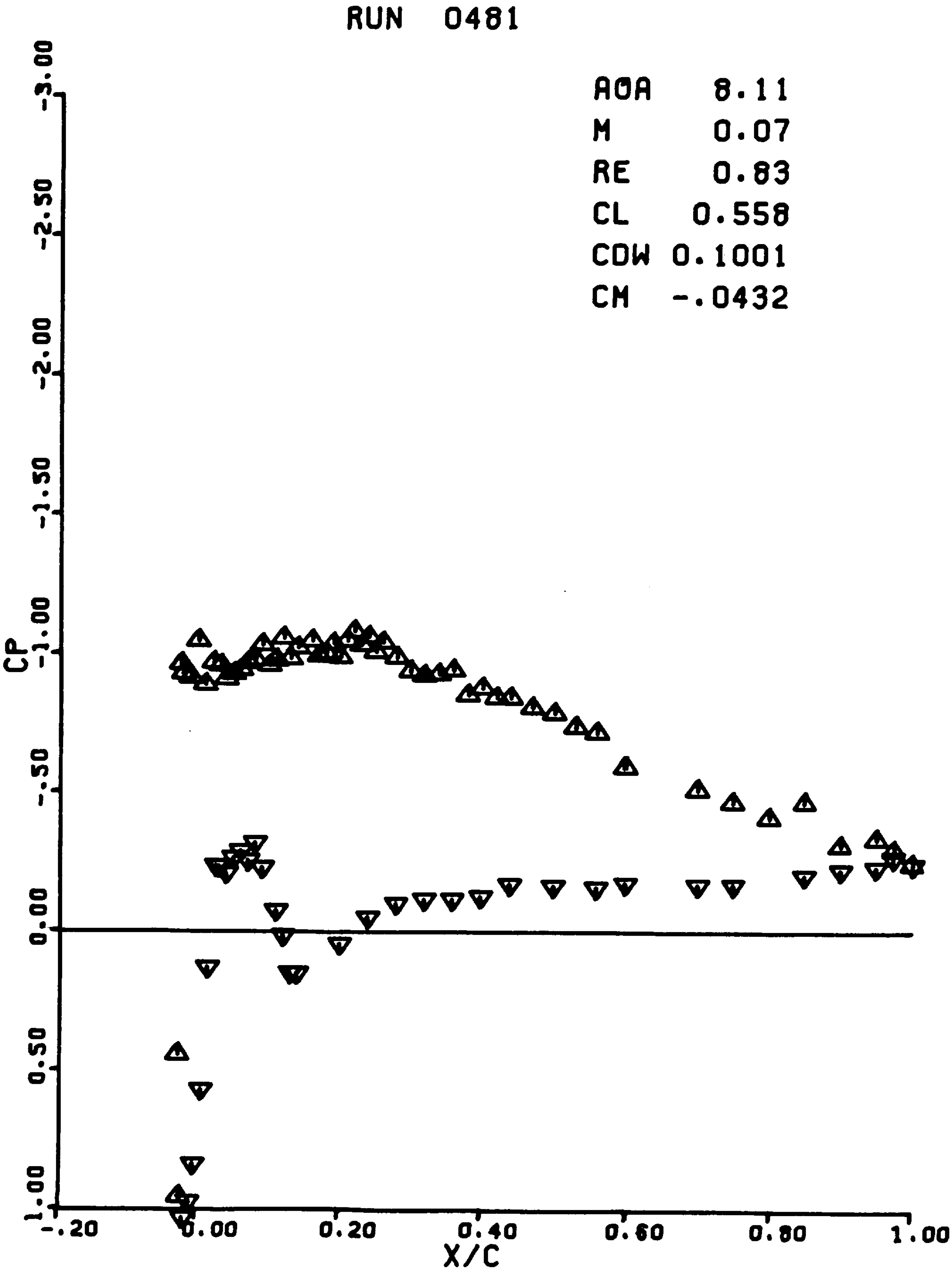
RUN 0481
AOA 8.11
M 0.07
RE 0.83
CL 0.558
CDW 0.1001
CM -.0432
CP
-3.00
-2.50
-2.00
-1.50
-1.00
-.50
0.00
0.50
1.00
X/C
-.20
0.00
0.20
0.40
0.60
0.80
1.00

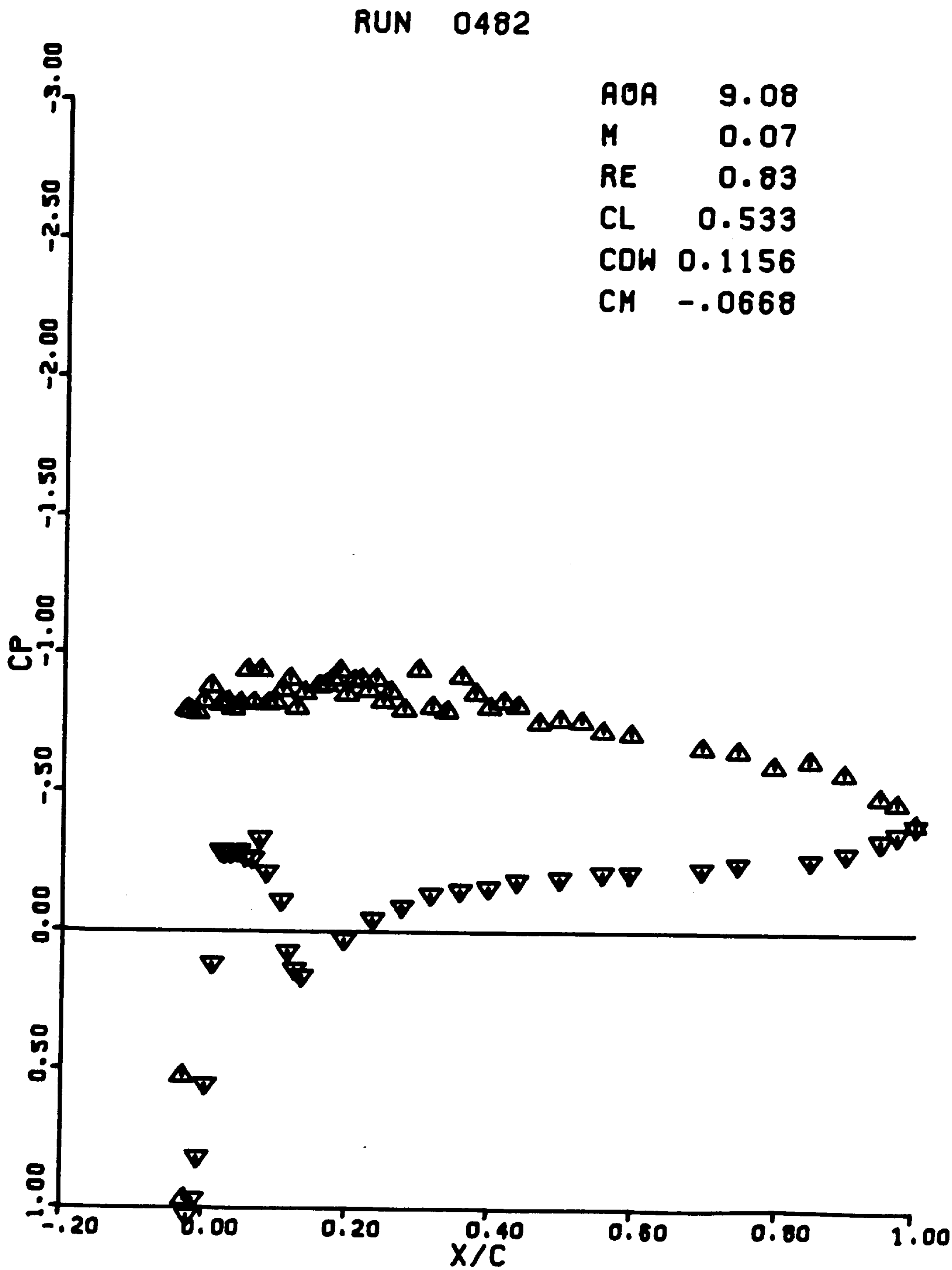

RUN 0482
AOA 9.08
M 0.07
RE 0.83
CL 0.533
CDW 0.1156
CM -.0668
CP
-3.00
-2.50
-2.00
-1.50
-1.00
-.50
0.00
0.50
1.00
-.20
0.00
0.20
0.40
0.60
0.80
1.00
X/C

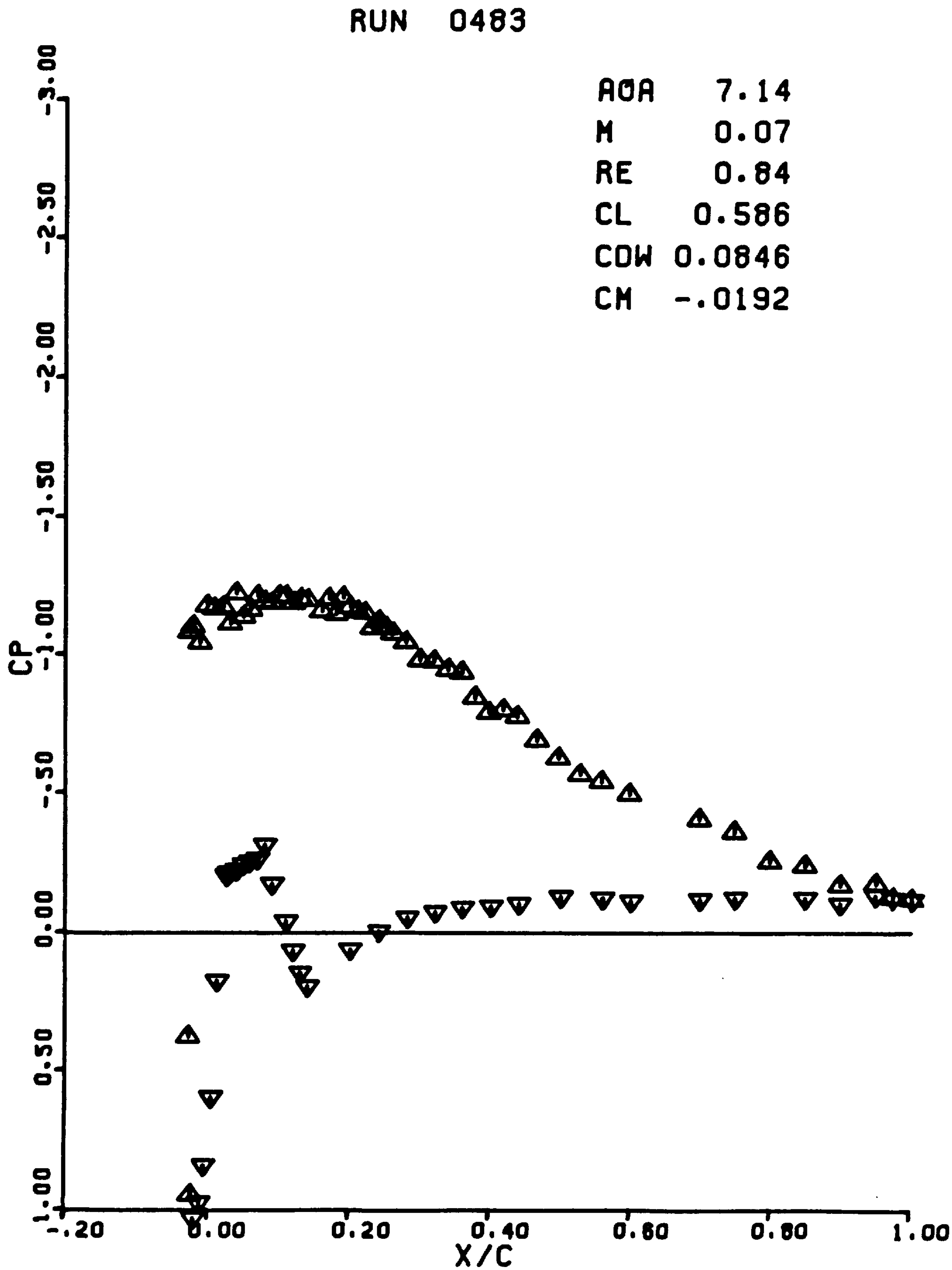
RUN 0483
AOA 7.14
M 0.07
RE 0.84
CL 0.586
CDW 0.0846
CM -.0192
CP
-3.00
-2.50
-2.00
-1.50
-1.00
-.50
0.00
0.50
1.00
-.20
0.00
0.20
0.40
0.60
0.80
1.00
X/C

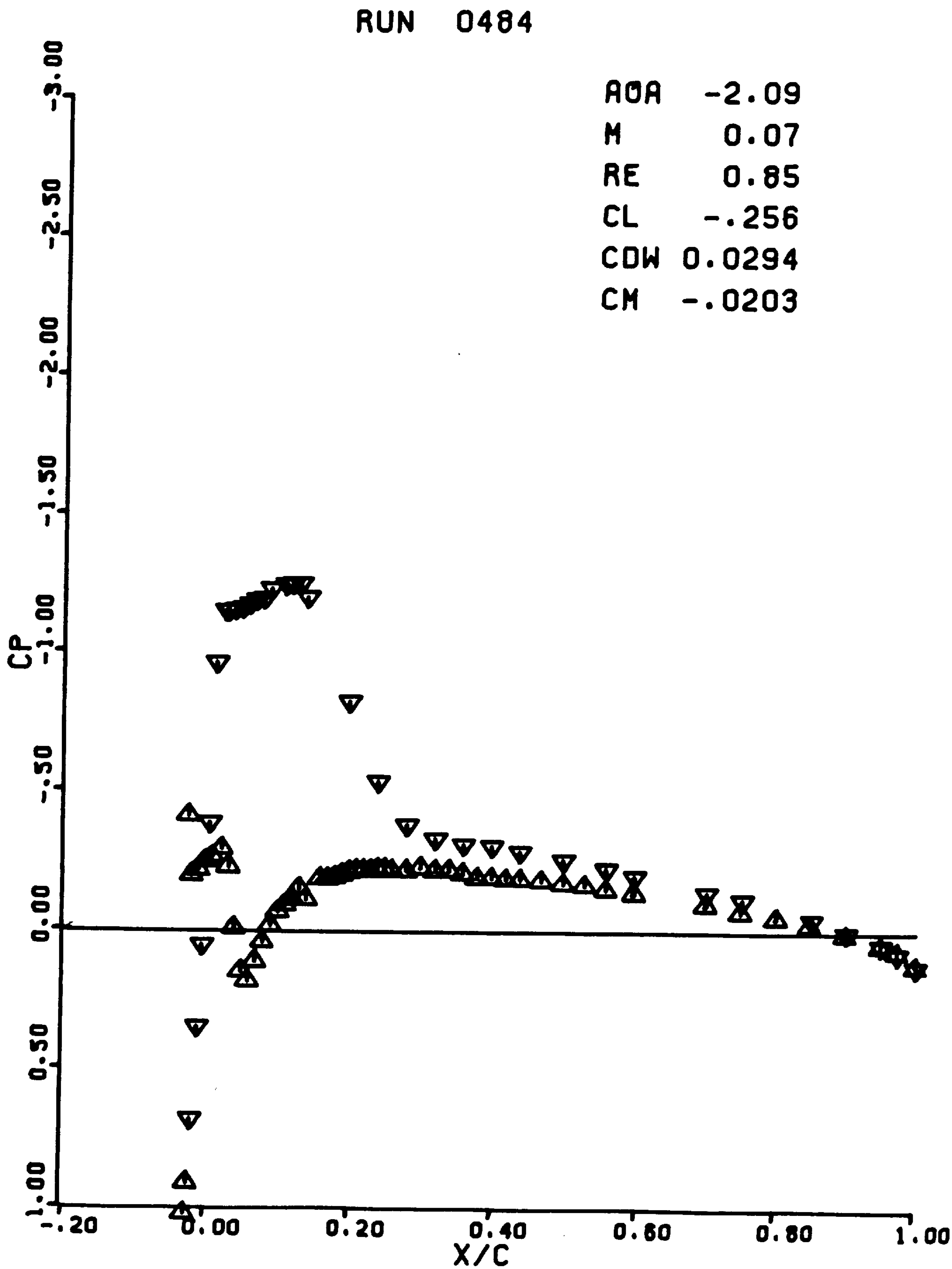
RUN 0484
AOA -2.09
M 0.07
RE 0.85
CL -.256
CDW 0.0294
CM -.0203
CP
-3.00
-2.50
-2.00
-1.50
-1.00
-.50
0.00
0.50
1.00
-.20
0.00
0.20
0.40
0.60
0.80
1.00
X/C

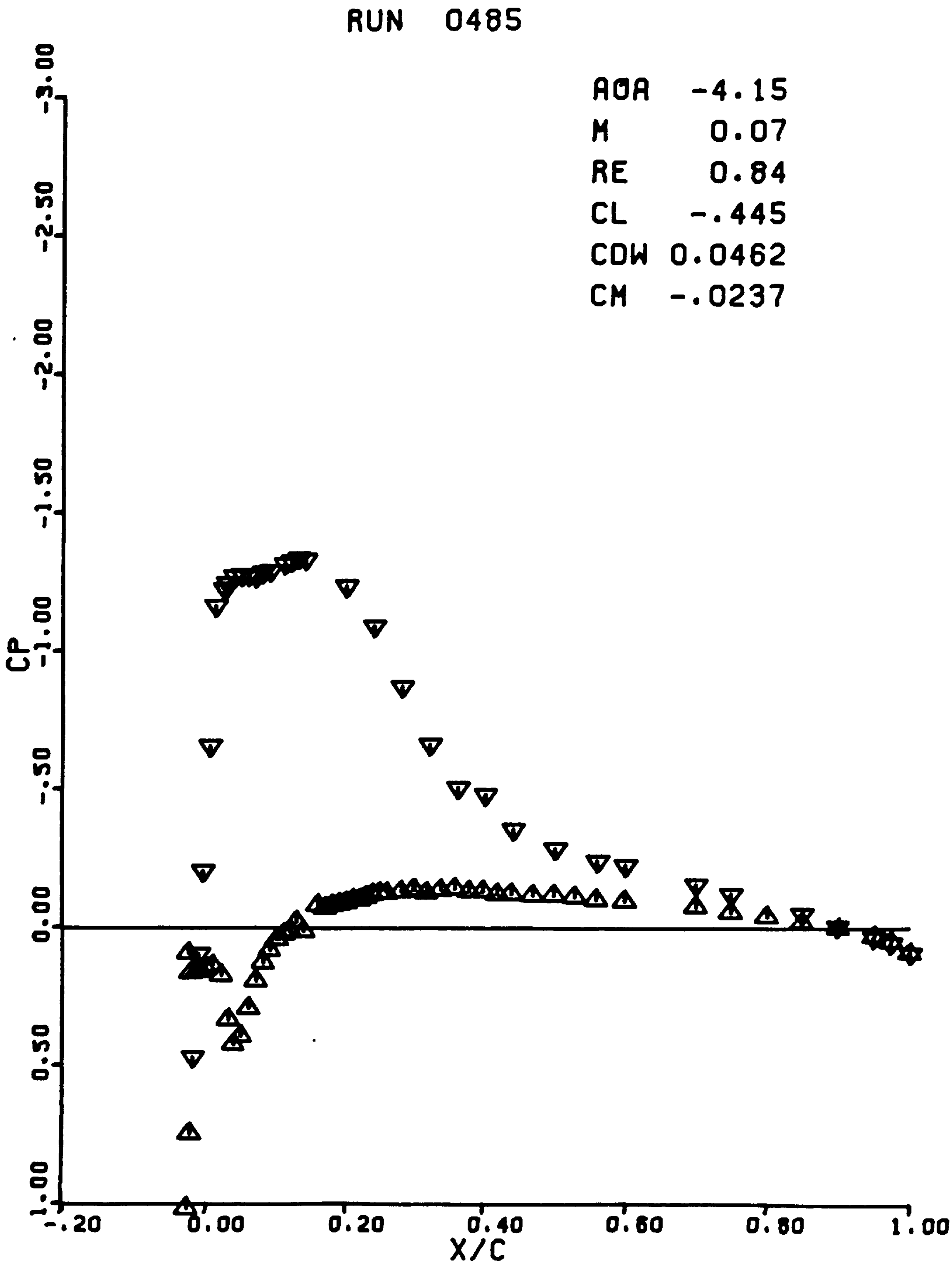

RUN 0485
AOA -4.15
M 0.07
RE 0.84
CL -.445
CDW 0.0462
CM -.0237
CP
-3.00
-2.50
-2.00
-1.50
-1.00
-.50
0.00
0.50
1.00
-.20
0.00
0.20
0.40
0.60
0.80
1.00
X/C

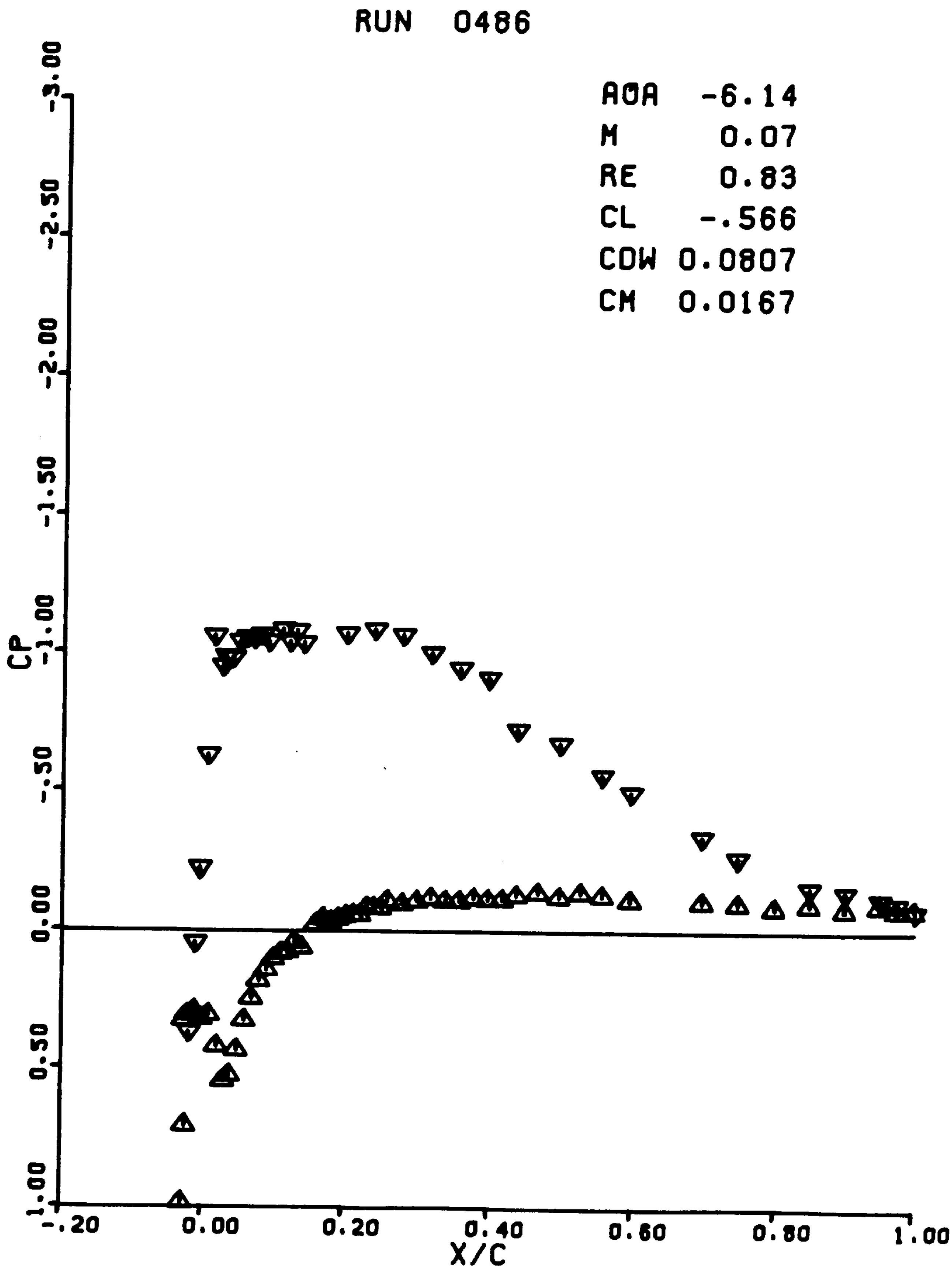
RUN 0486
AOA -6.14
M 0.07
RE 0.83
CL -.566
CDW 0.0807
CM 0.0167
CP
-3.00
-2.50
-2.00
-1.50
-1.00
-.50
0.00
0.50
1.00
-.20
0.00
0.20
0.40
0.60
0.80
1.00
X/C

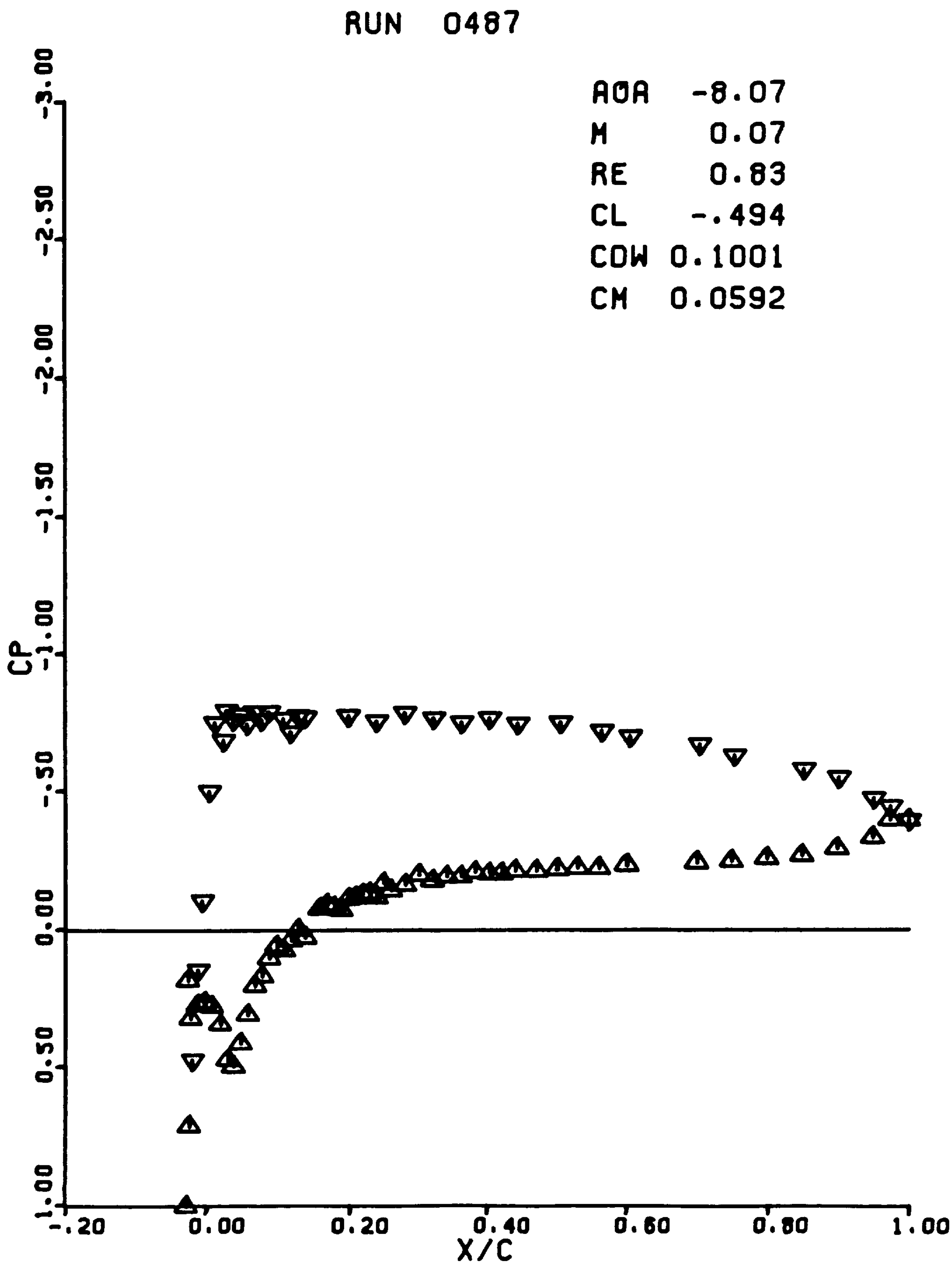
RUN 0487
AOA -8.07
M 0.07
RE 0.83
CL -.494
CDW 0.1001
CM 0.0592
CP
X/C
-3.00
-2.50
-2.00
-1.50
-1.00
-.50
0.00
0.50
1.00
-.20
0.00
0.20
0.40
0.60
0.80
1.00

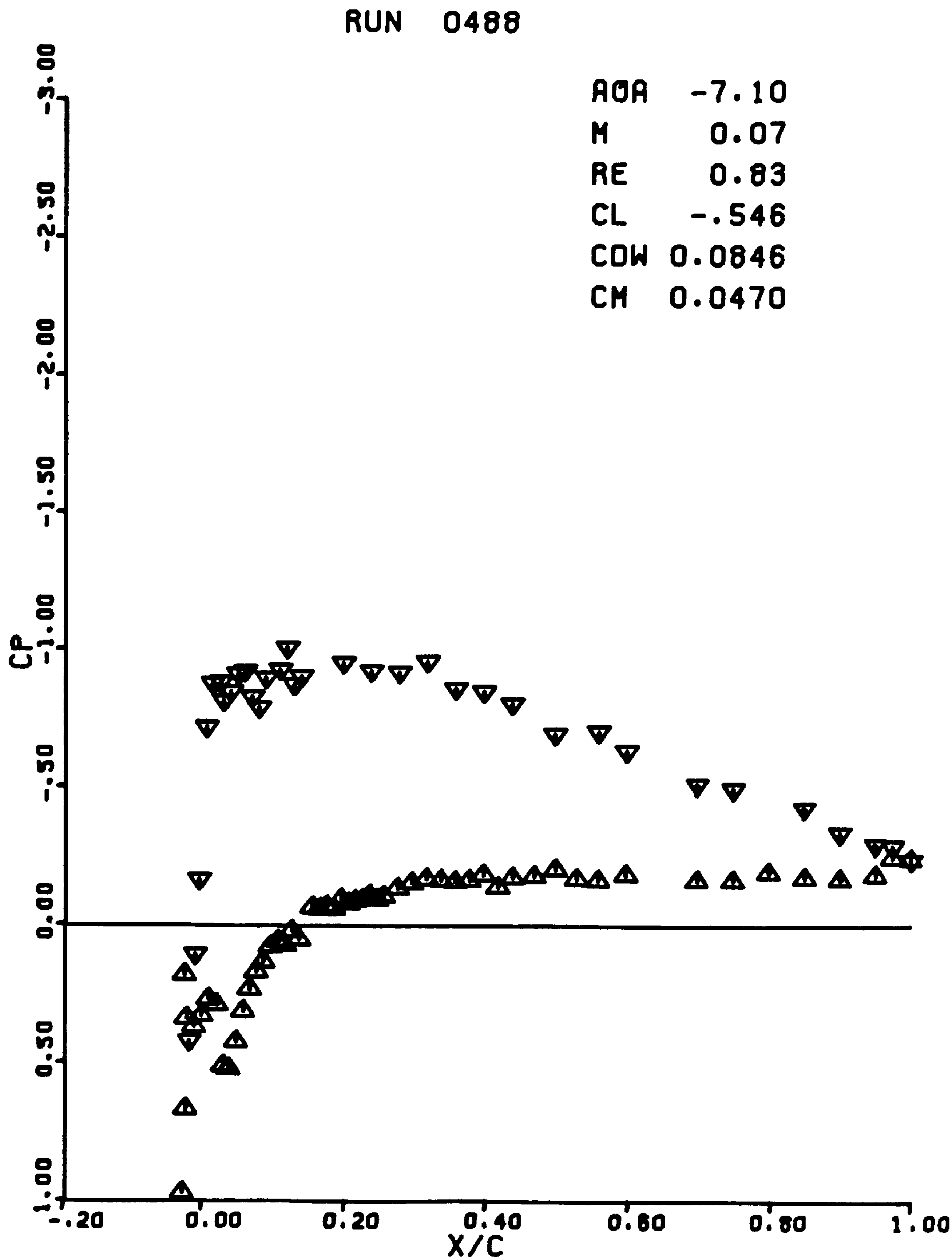
RUN 0488
AOA -7.10
M 0.07
RE 0.83
CL -.546
CDW 0.0846
CM 0.0470
CP
-3.00
-2.50
-2.00
-1.50
-1.00
-.50
0.00
0.50
1.00
-.20
0.00
0.20
0.40
0.60
0.80
1.00
X/C

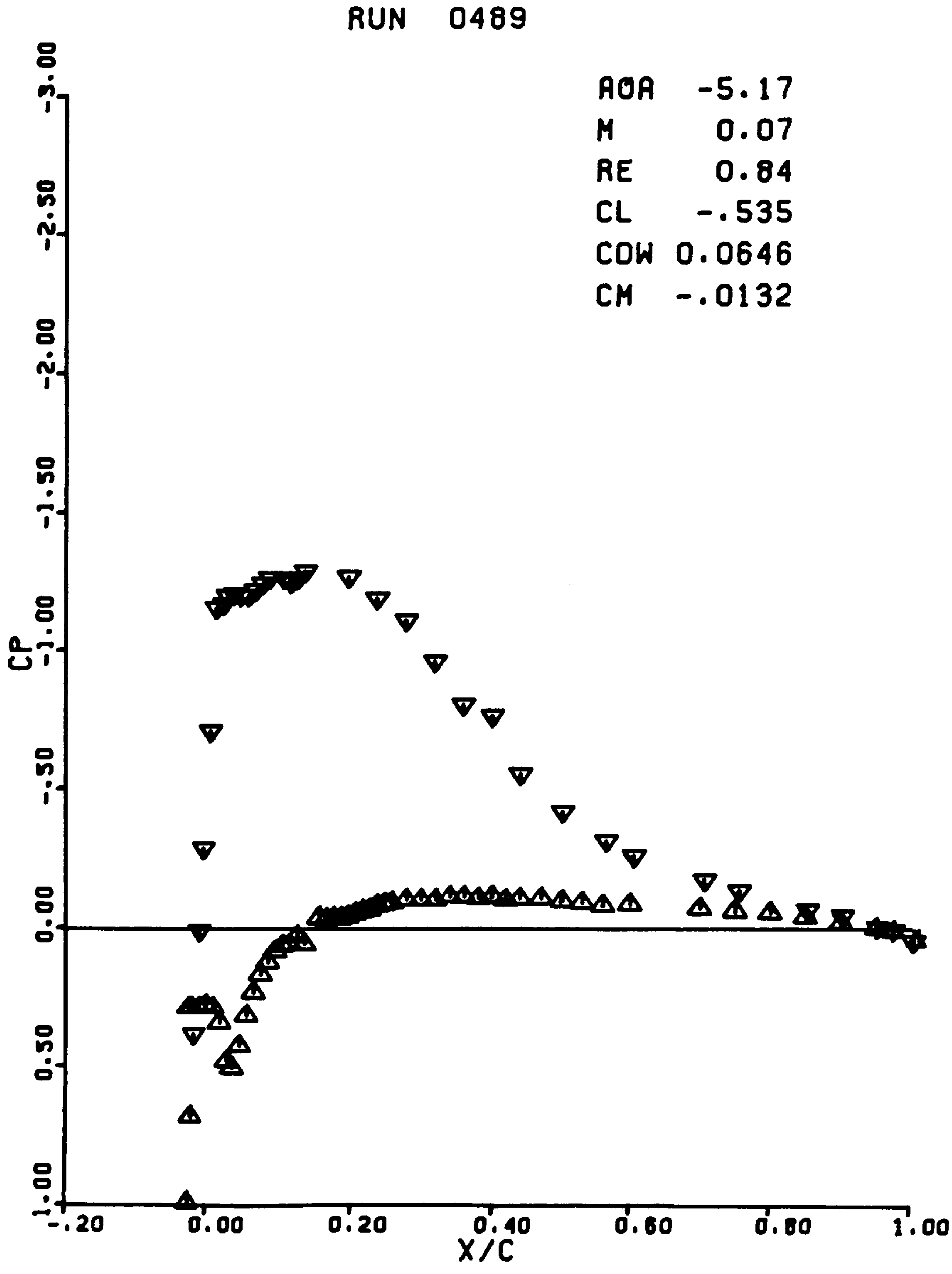

RUN 0489
AOA -5.17
M 0.07
RE 0.84
CL -.535
CDW 0.0646
CM -.0132
CP
-3.00
-2.50
-2.00
-1.50
-1.00
-.50
0.00
0.50
1.00
X/C
-.20
0.00
0.20
0.40
0.60
0.80
1.00

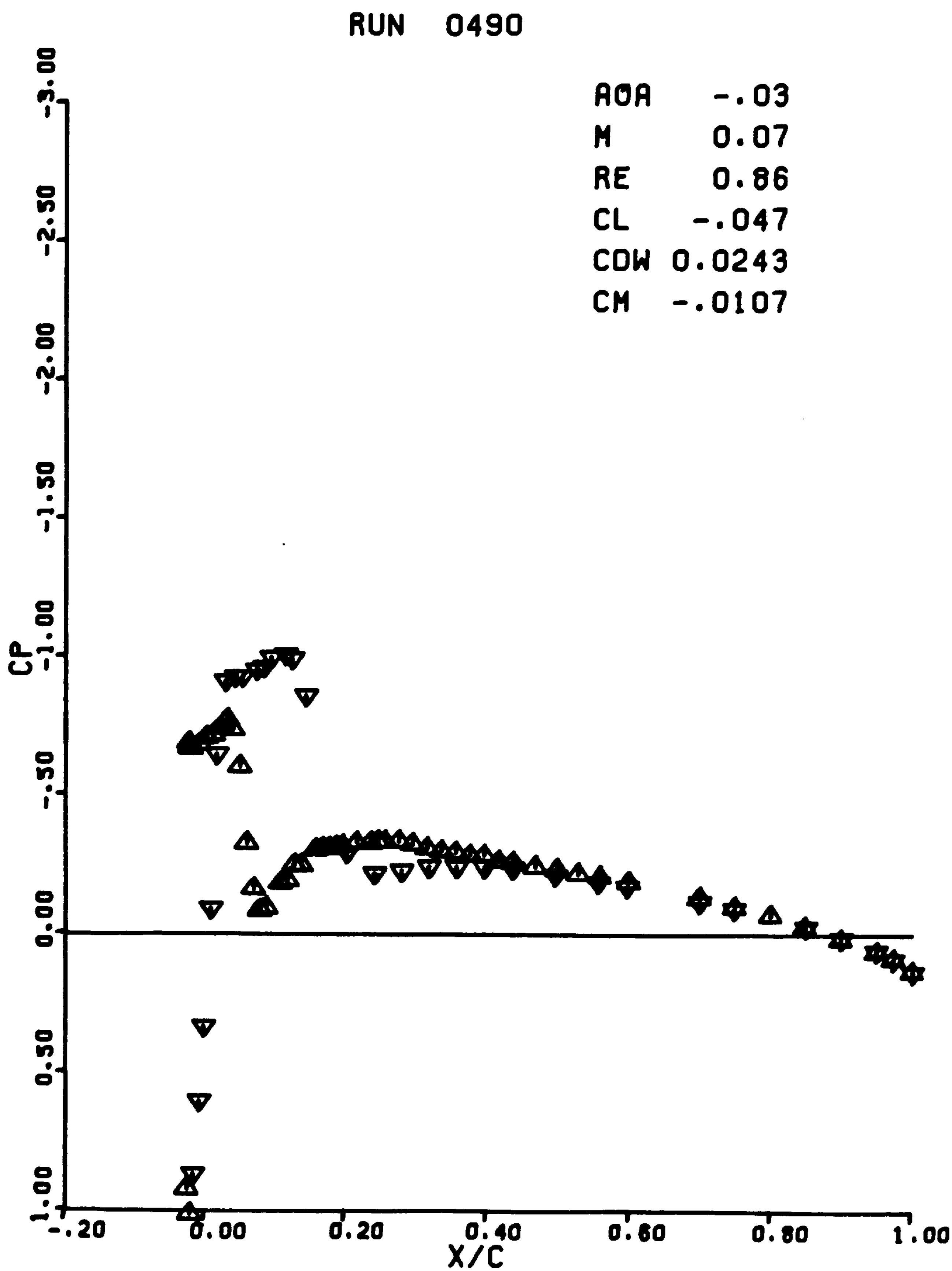
RUN 0490
AOA -.03
M 0.07
RE 0.86
CL -.047
CDW 0.0243
CM -.0107
CP
-3.00
-2.50
-2.00
-1.50
-1.00
-.50
0.00
0.50
1.00
-.20
0.00
0.20
0.40
0.60
0.80
1.00
X/C

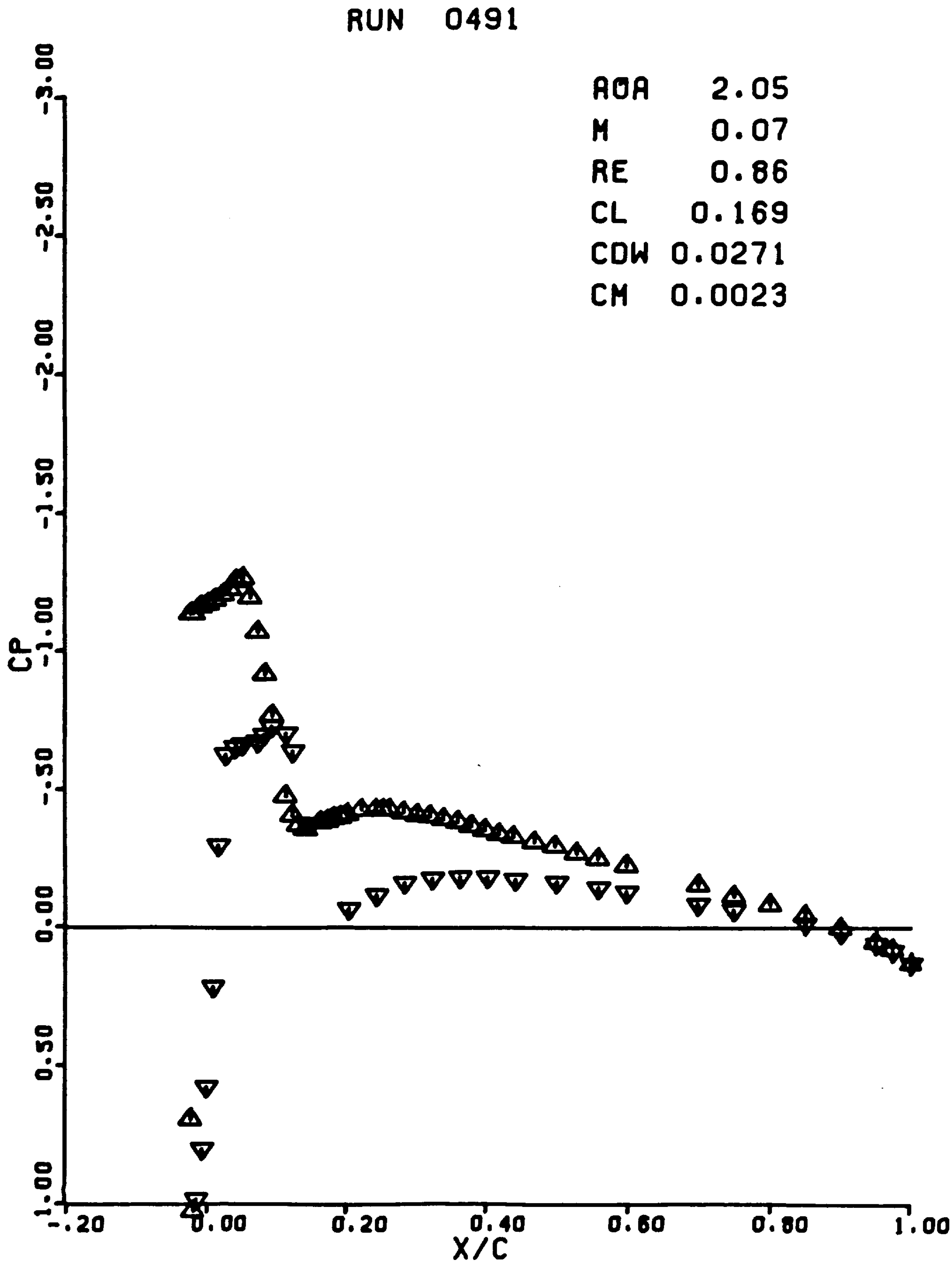
RUN 0491
AOA 2.05
M 0.07
RE 0.86
CL 0.169
CDW 0.0271
CM 0.0023
CP
X/C
-3.00
-2.50
-2.00
-1.50
-1.00
-.50
0.00
0.50
1.00
-.20
0.00
0.20
0.40
0.60
0.80
1.00

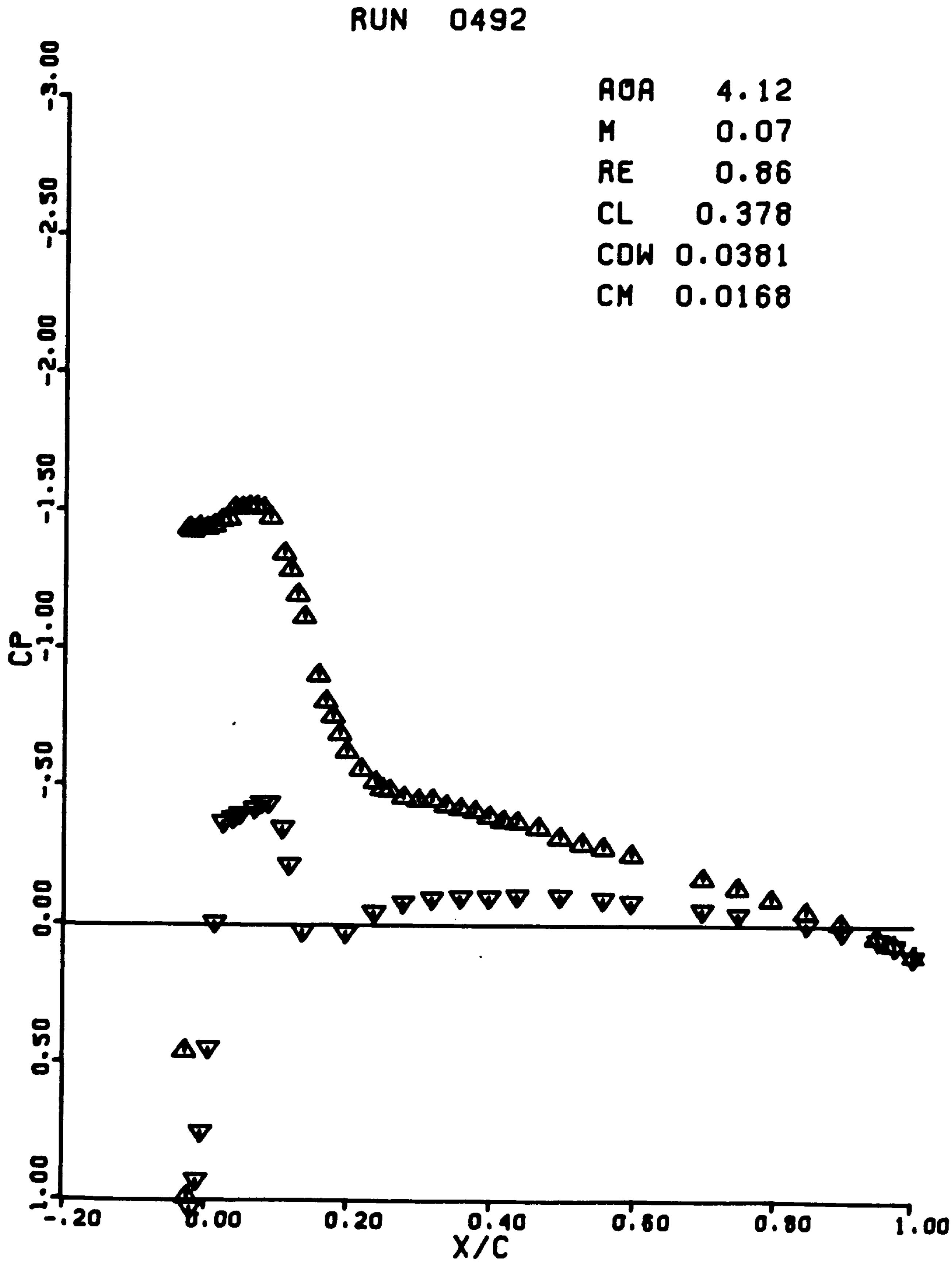
RUN 0492
AOA 4.12
M 0.07
RE 0.86
CL 0.378
CDW 0.0381
CM 0.0168
CP
-3.00
-2.50
-2.00
-1.50
-1.00
-.50
0.00
0.50
1.00
X/C
-.20
0.00
0.20
0.40
0.60
0.80
1.00

C-3

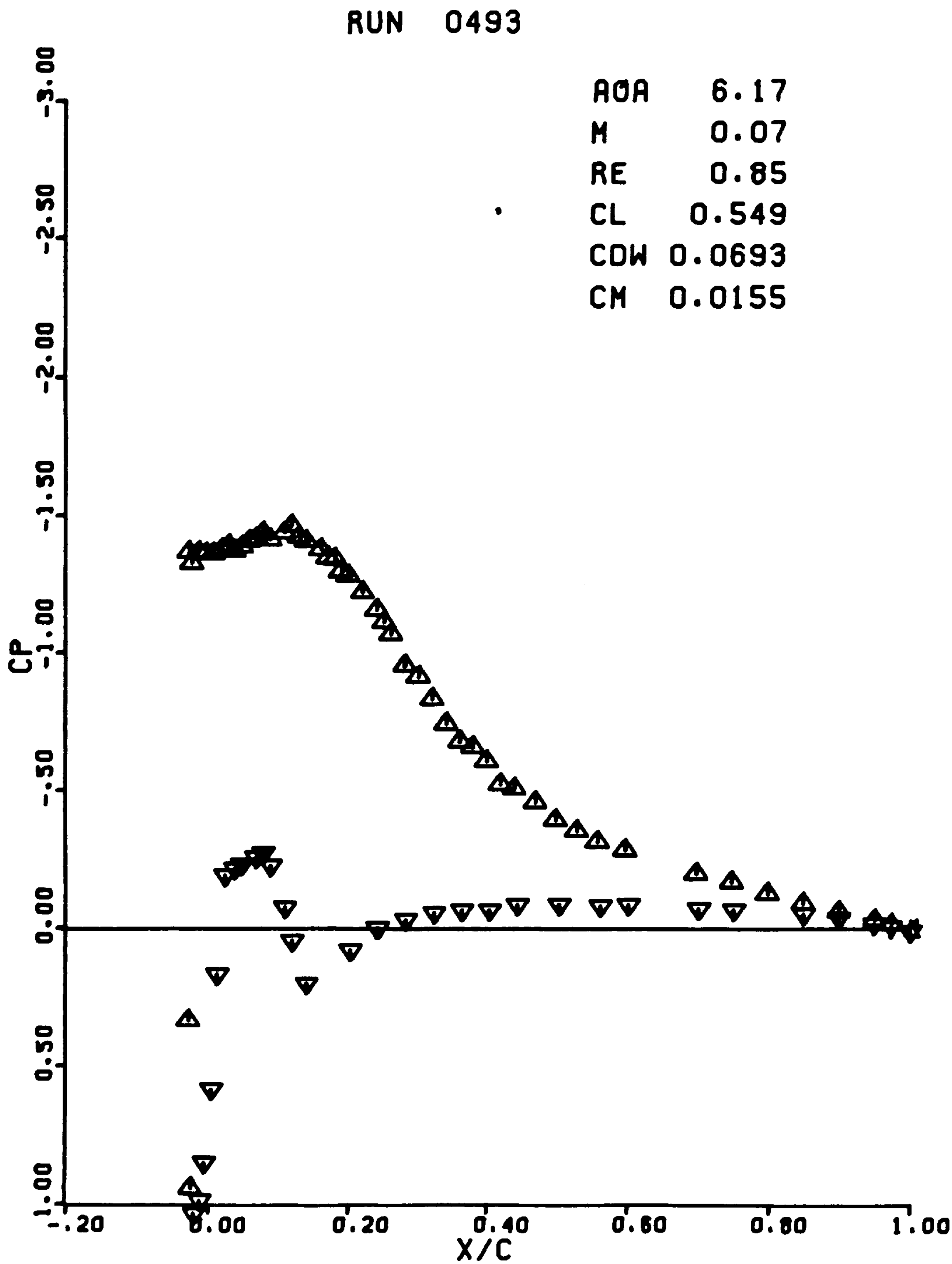
RUN 0493
AOA 6.17
M 0.07
RE 0.85
CL 0.549
CDW 0.0693
CM 0.0155
CP
-3.00
-2.50
-2.00
-1.50
-1.00
-.50
0.00
0.50
1.00
-.20
0.00
0.20
0.40
0.60
0.80
1.00
X/C

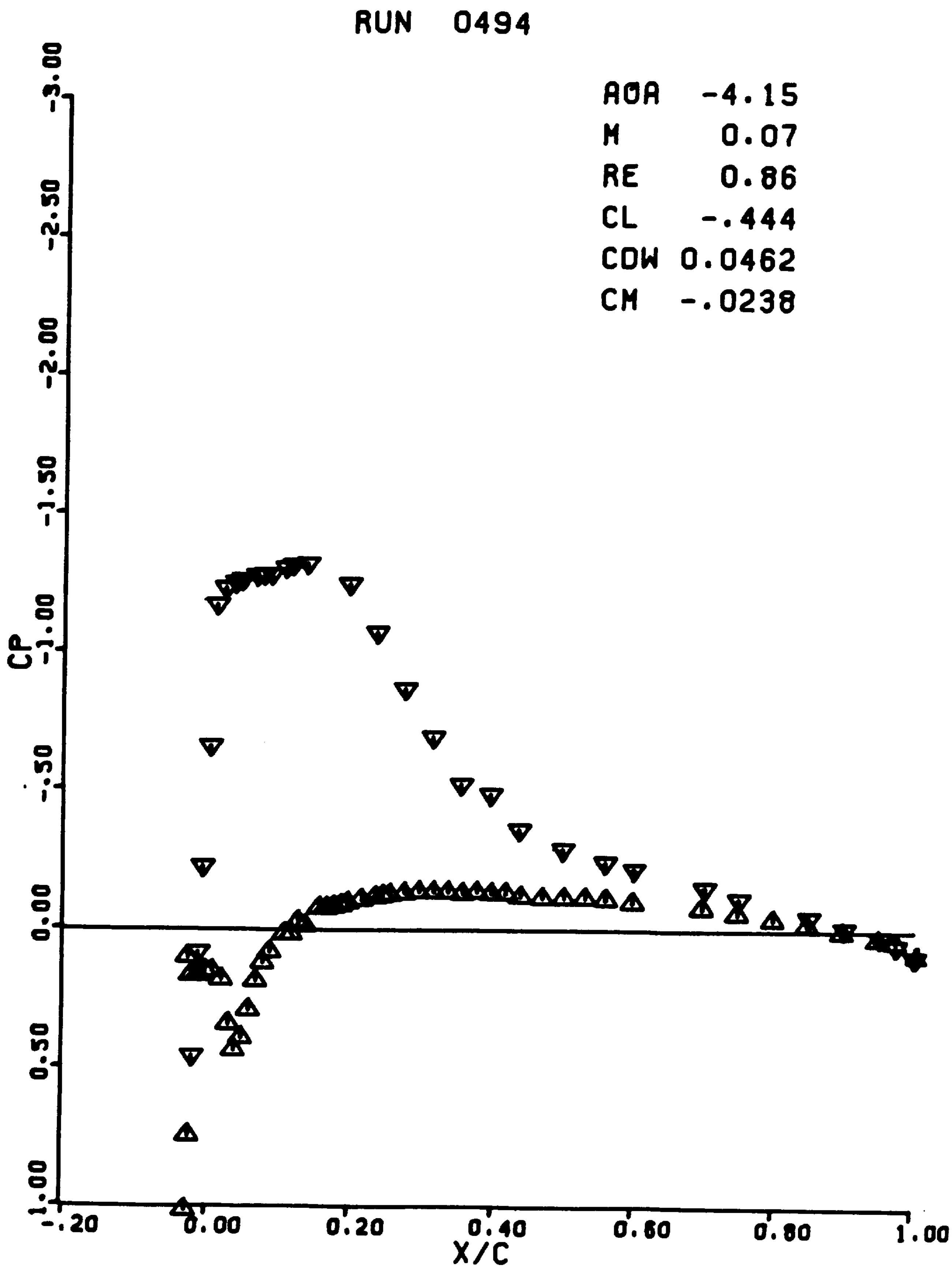

RUN 0494
AOA -4.15
M 0.07
RE 0.86
CL -.444
CDW 0.0462
CM -.0238
CP
-3.00
-2.50
-2.00
-1.50
-1.00
-.50
0.00
0.50
1.00
-.20
0.00
0.20
0.40
0.60
0.80
1.00
X/C

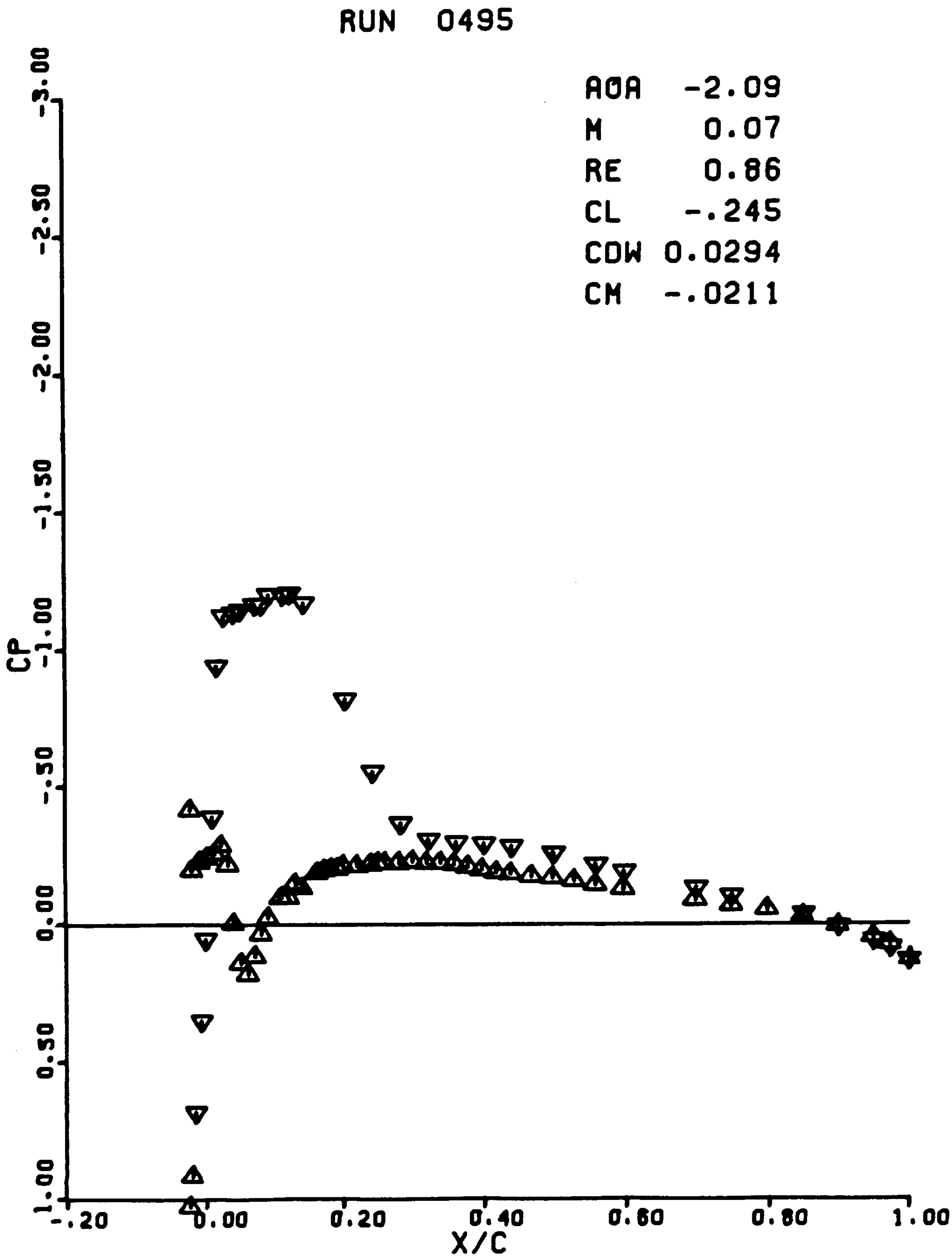
RUN 0495
AOA -2.09
M 0.07
RE 0.86
CL -.245
CDW 0.0294
CM -.0211
CP
-3.00
-2.50
-2.00
-1.50
-1.00
-.50
0.00
0.50
1.00
-.20
0.00
0.20
0.40
0.60
0.80
1.00
X/C

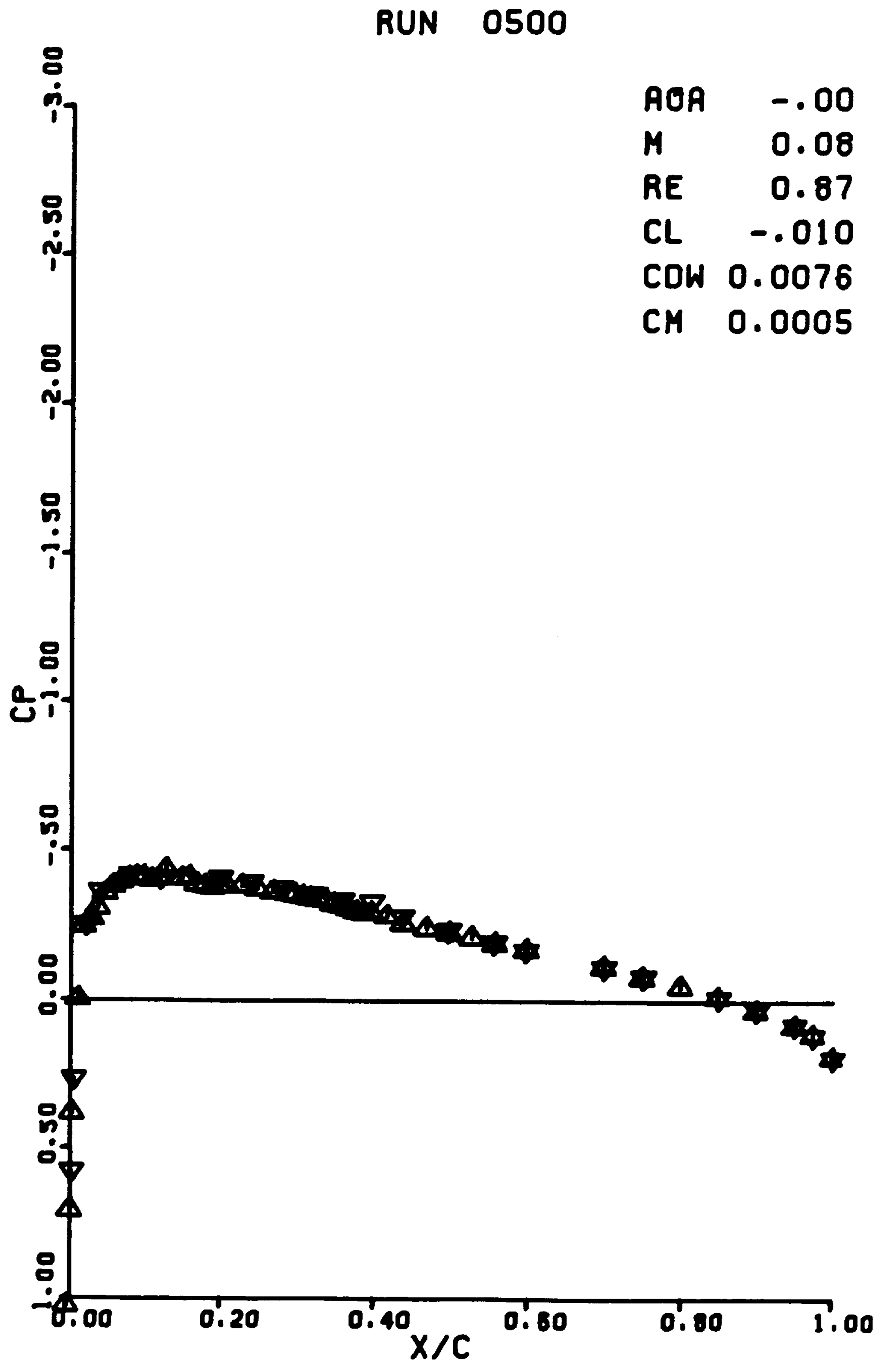
RUN 0500
AOA -.00
M 0.08
RE 0.87
CL -.010
CDW 0.0076
CM 0.0005
CP
-3.00
-2.50
-2.00
-1.50
-1.00
-.50
0.00
0.50
1.00
0.00
0.20
0.40
0.60
0.80
1.00
X/C

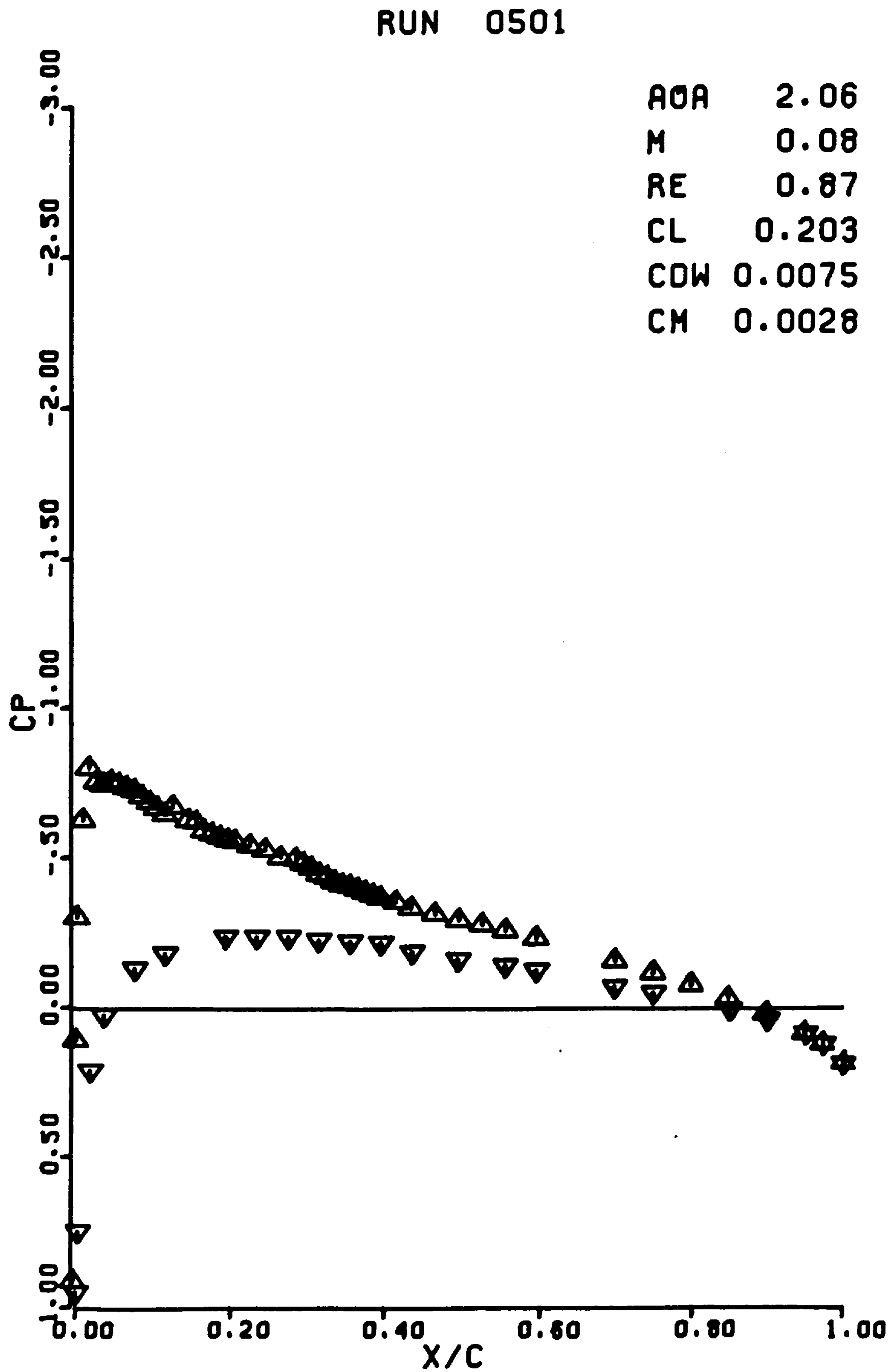

RUN 0501
AOA 2.06
M 0.08
RE 0.87
CL 0.203
CDW 0.0075
CM 0.0028
CP
-3.00
-2.50
-2.00
-1.50
-1.00
-.50
0.00
0.50
1.00
0.00
0.20
0.40
0.60
0.80
1.00
X/C

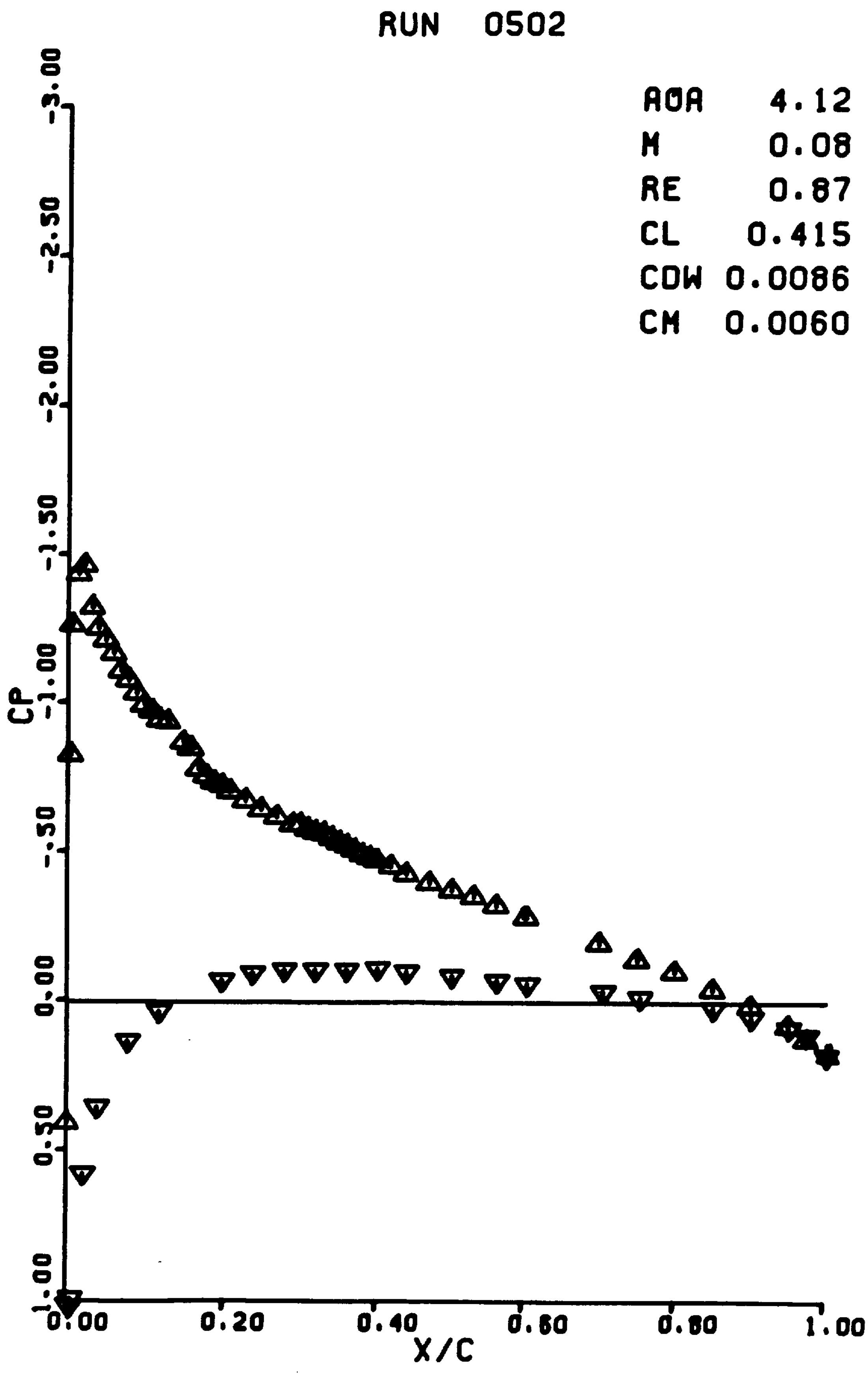

RUN 0502
AOA 4.12
M 0.08
RE 0.87
CL 0.415
CDW 0.0086
CM 0.0060
CP
-3.00
-2.50
-2.00
-1.50
-1.00
-.50
0.00
0.50
1.00
0.00
0.20
0.40
0.60
0.80
1.00
X/C

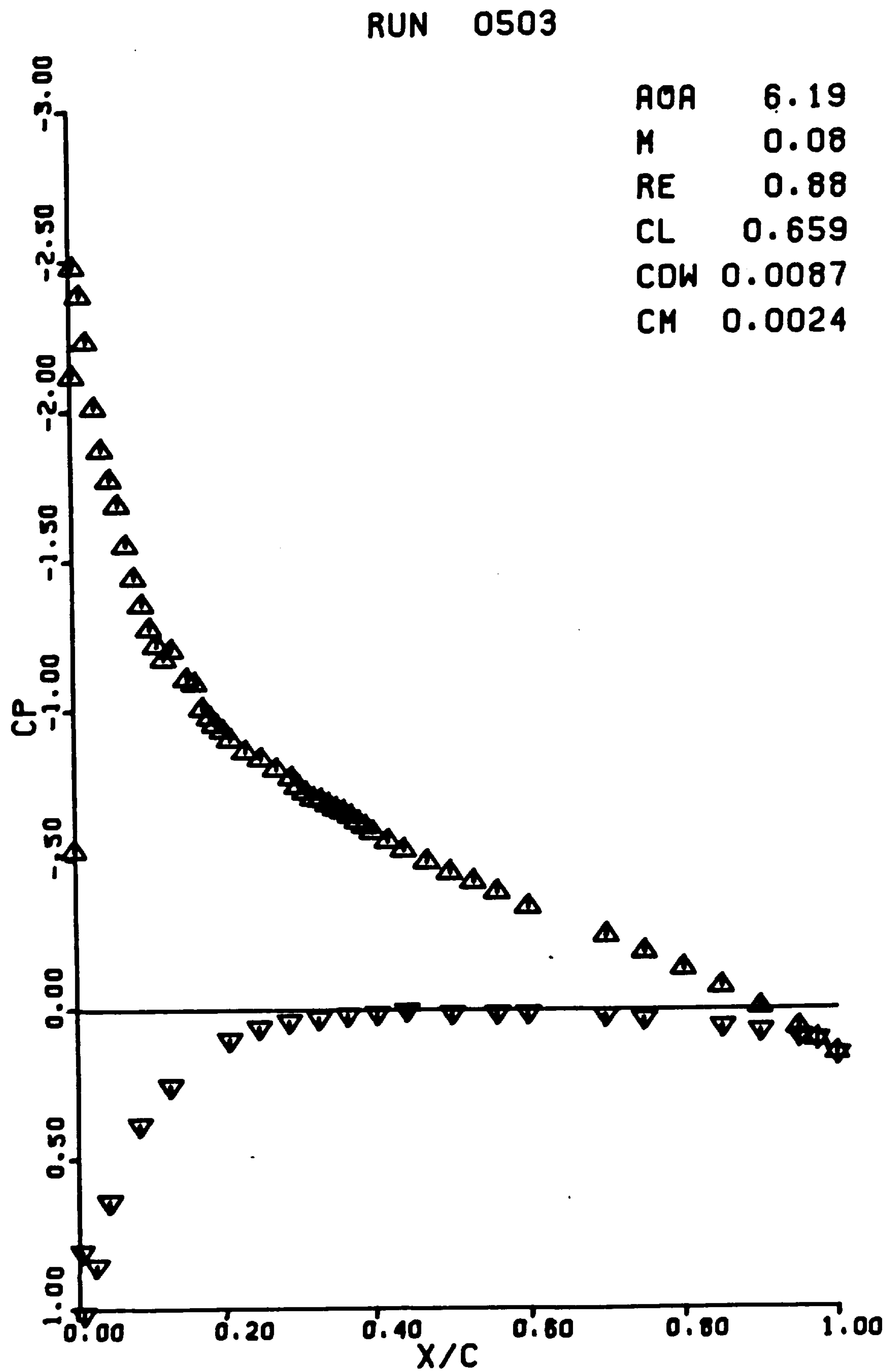
RUN 0503
AOA 6.19
M 0.08
RE 0.88
CL 0.659
CDW 0.0087
CM 0.0024
CP
-3.00
-2.50
-2.00
-1.50
-1.00
-.50
0.00
0.50
1.00
0.00
0.20
0.40
0.60
0.80
1.00
X/C

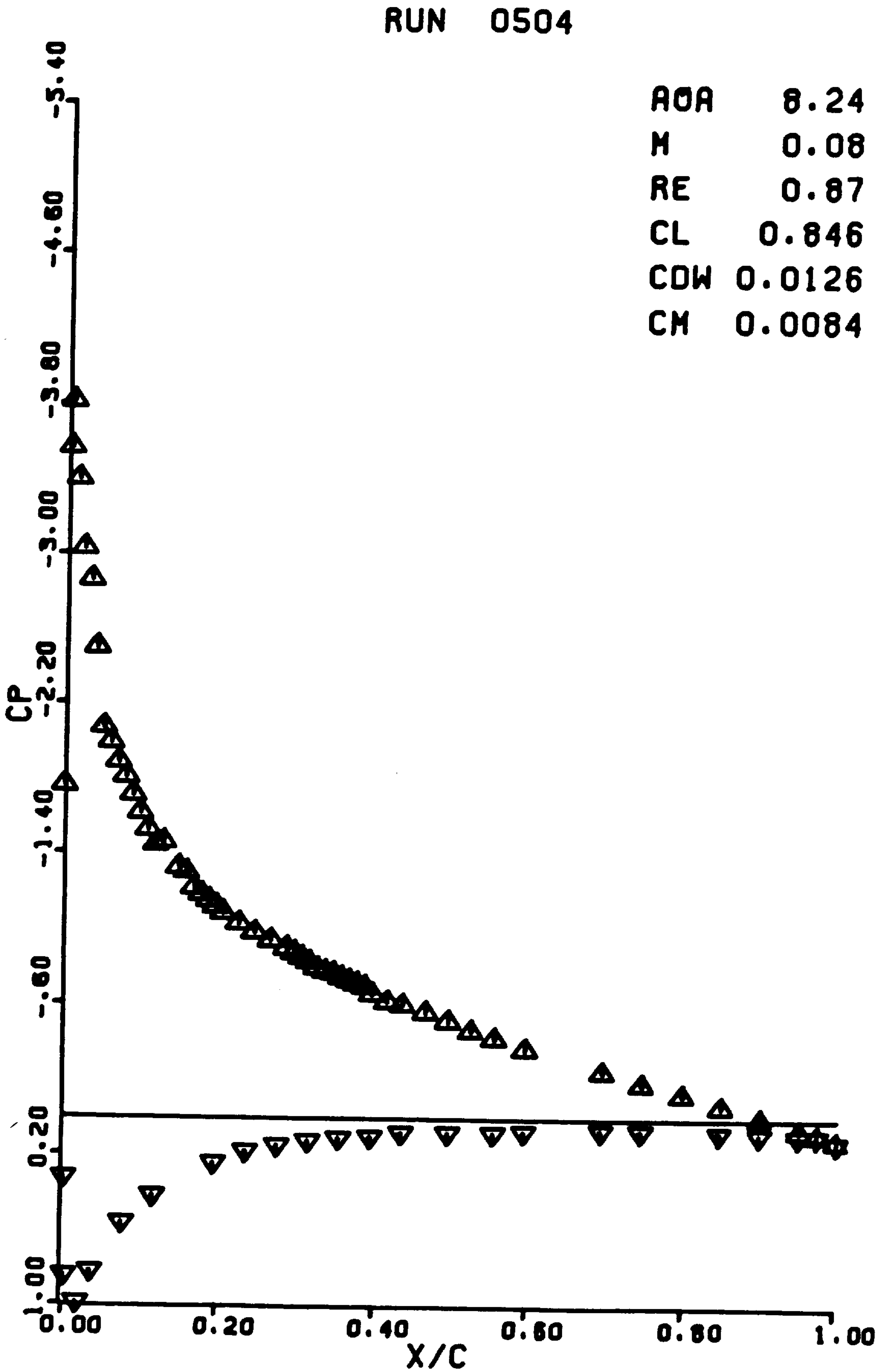
RUN 0504
AOA 8.24
M 0.08
RE 0.87
CL 0.846
CDW 0.0126
CM 0.0084
CP
-5.40
-4.60
-3.80
-3.00
-2.20
-1.40
-.60
0.20
1.00
0.00
0.20
0.40
0.60
0.80
1.00
X/C

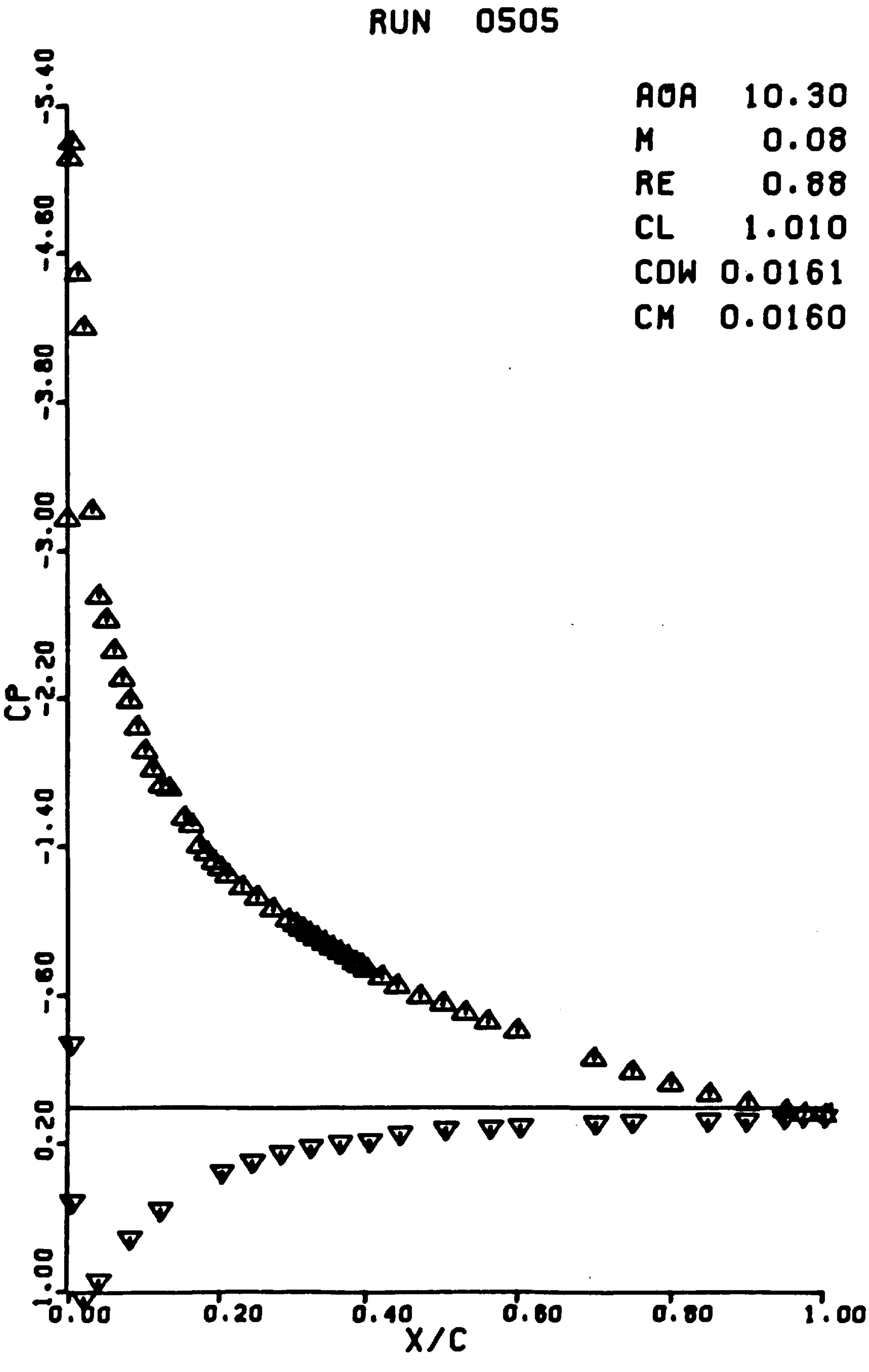
RUN 0505
AOA 10.30
M 0.08
RE 0.88
CL 1.010
CDW 0.0161
CM 0.0160
CP
-5.40
-4.60
-3.80
-3.00
-2.20
-1.40
-.60
0.20
1.00
0.00
0.20
0.40
0.60
0.80
1.00
X/C

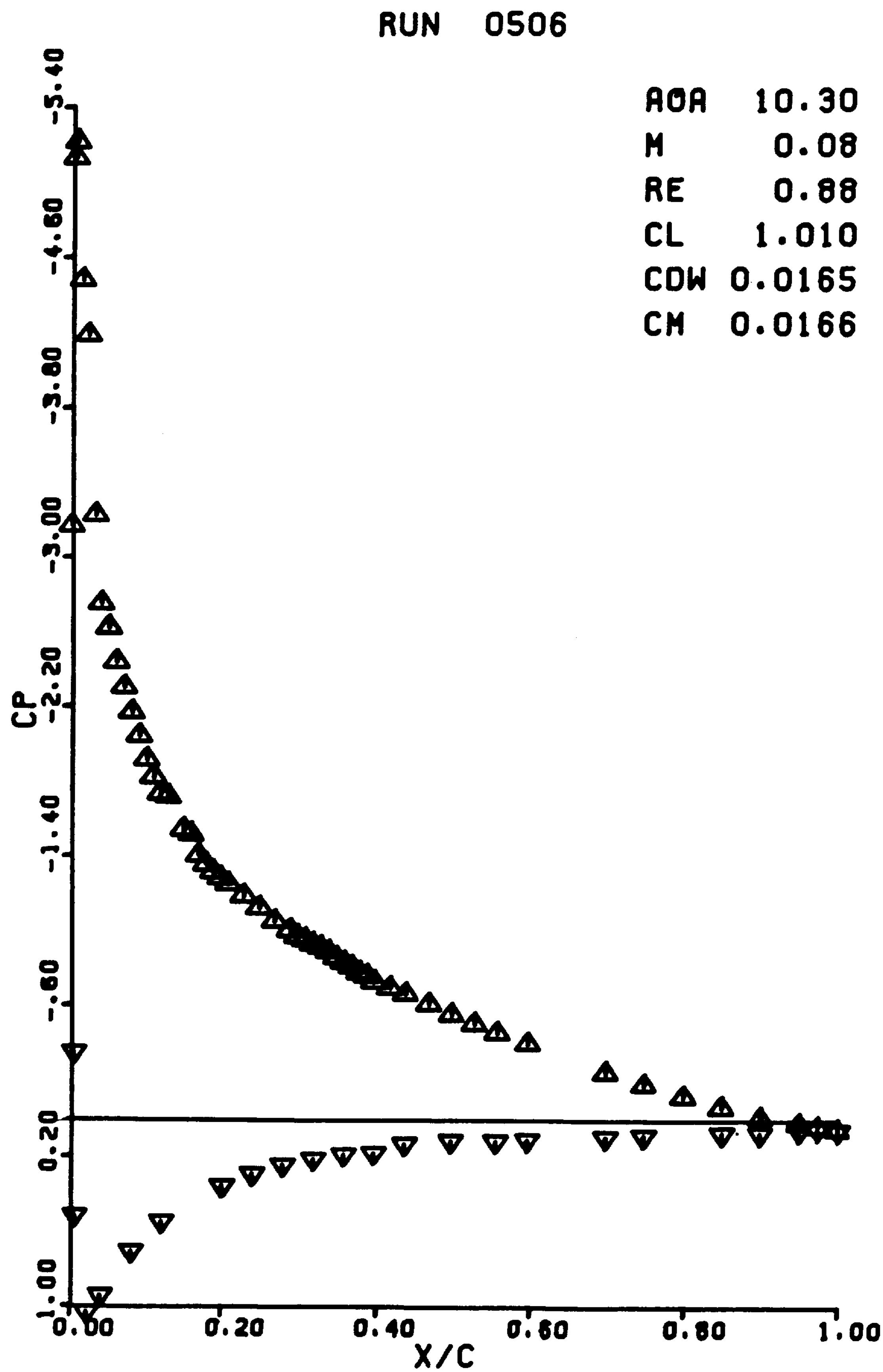
RUN 0506
AOA 10.30
M 0.08
RE 0.88
CL 1.010
CDW 0.0165
CM 0.0166
CP
-5.40
-4.60
-3.80
-3.00
-2.20
-1.40
-.60
0.20
1.00
X/C
0.00
0.20
0.40
0.60
0.80
1.00

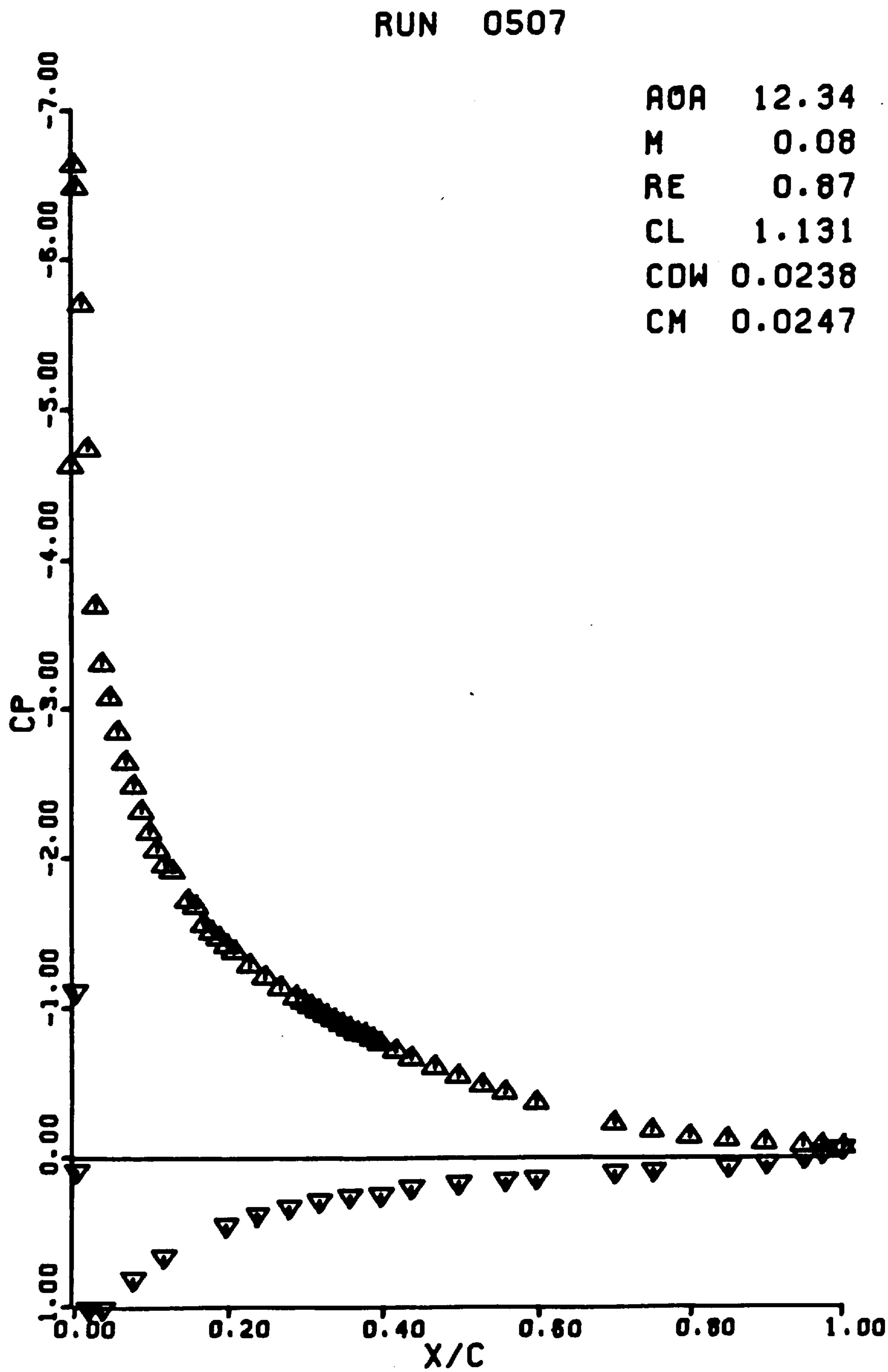

RUN 0507
AOA 12.34
M 0.08
RE 0.87
CL 1.131
CDW 0.0238
CM 0.0247
CP
-7.00
-6.00
-5.00
-4.00
-3.00
-2.00
-1.00
0.00
1.00
0.00
0.20
0.40
0.60
0.80
1.00
X/C

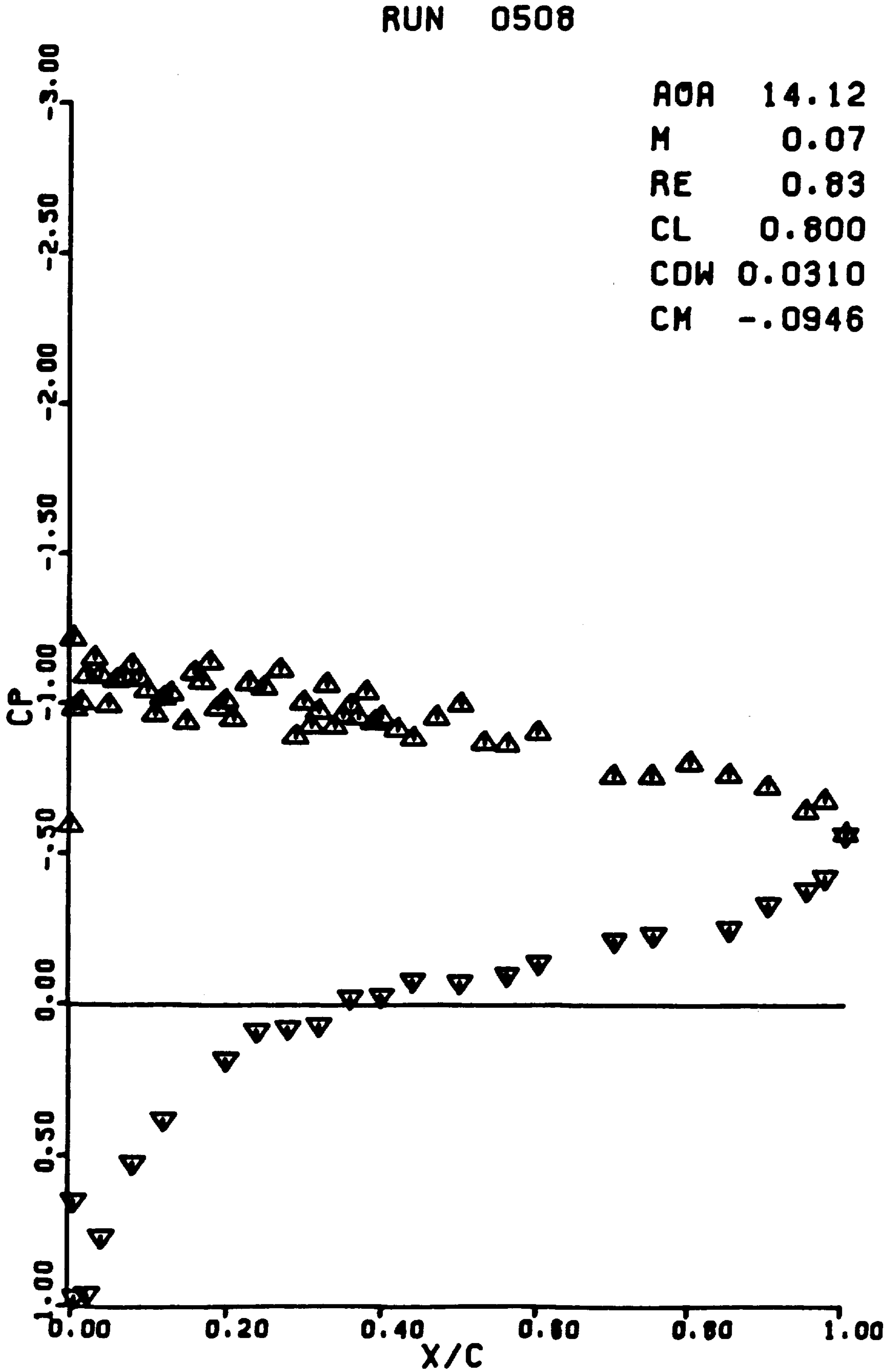
RUN 0508
AOA 14.12
M 0.07
RE 0.83
CL 0.800
CDW 0.0310
CM -.0946
CP
-3.00
-2.50
-2.00
-1.50
-1.00
-.50
0.00
0.50
1.00
0.00
0.20
0.40
0.60
0.80
1.00
X/C

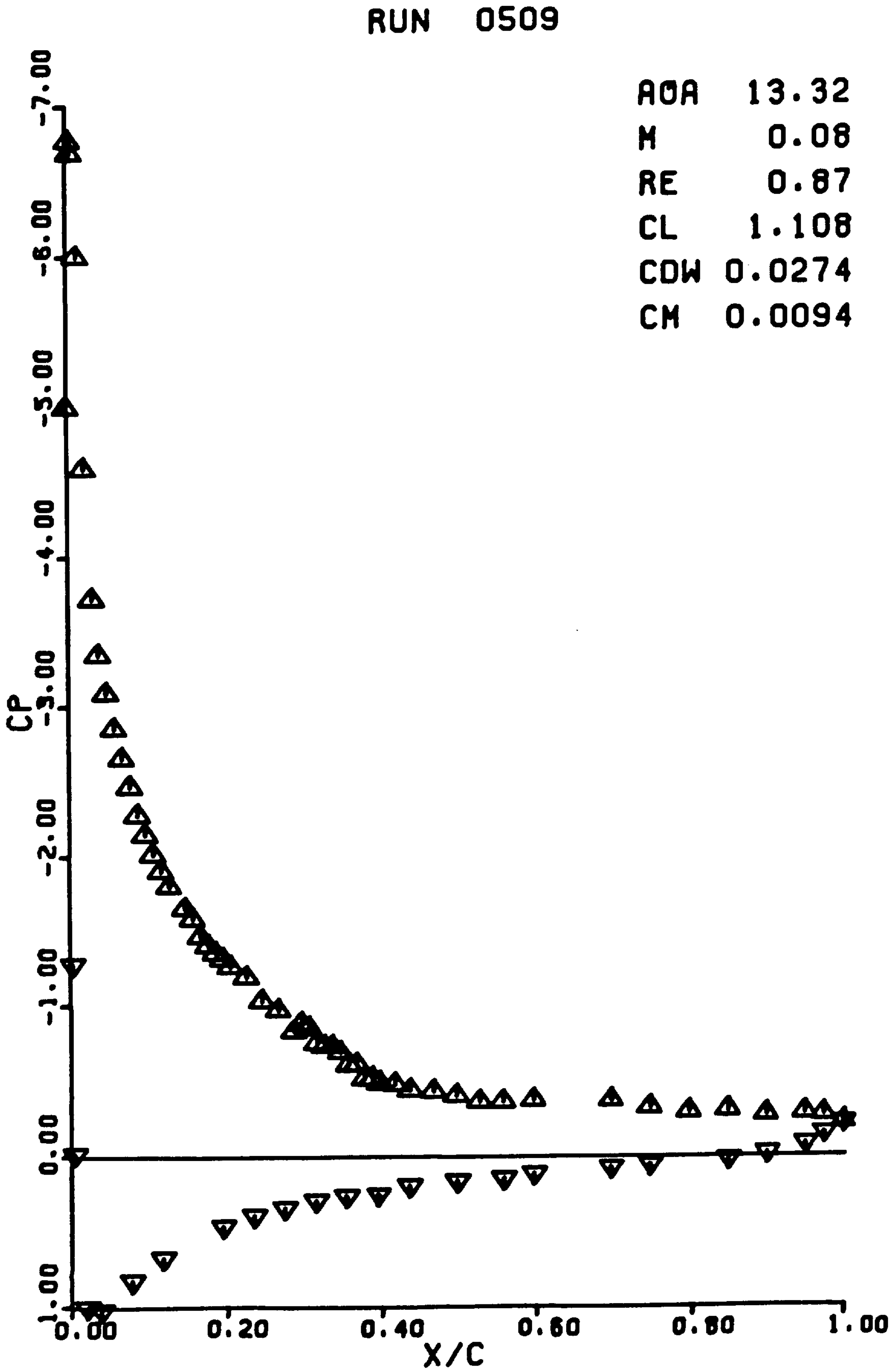

RUN 0509
AOA 13.32
M 0.08
RE 0.87
CL 1.108
CDW 0.0274
CM 0.0094
CP
-7.00
-6.00
-5.00
-4.00
-3.00
-2.00
-1.00
0.00
1.00
0.00
0.20
0.40
0.60
0.80
1.00
X/C

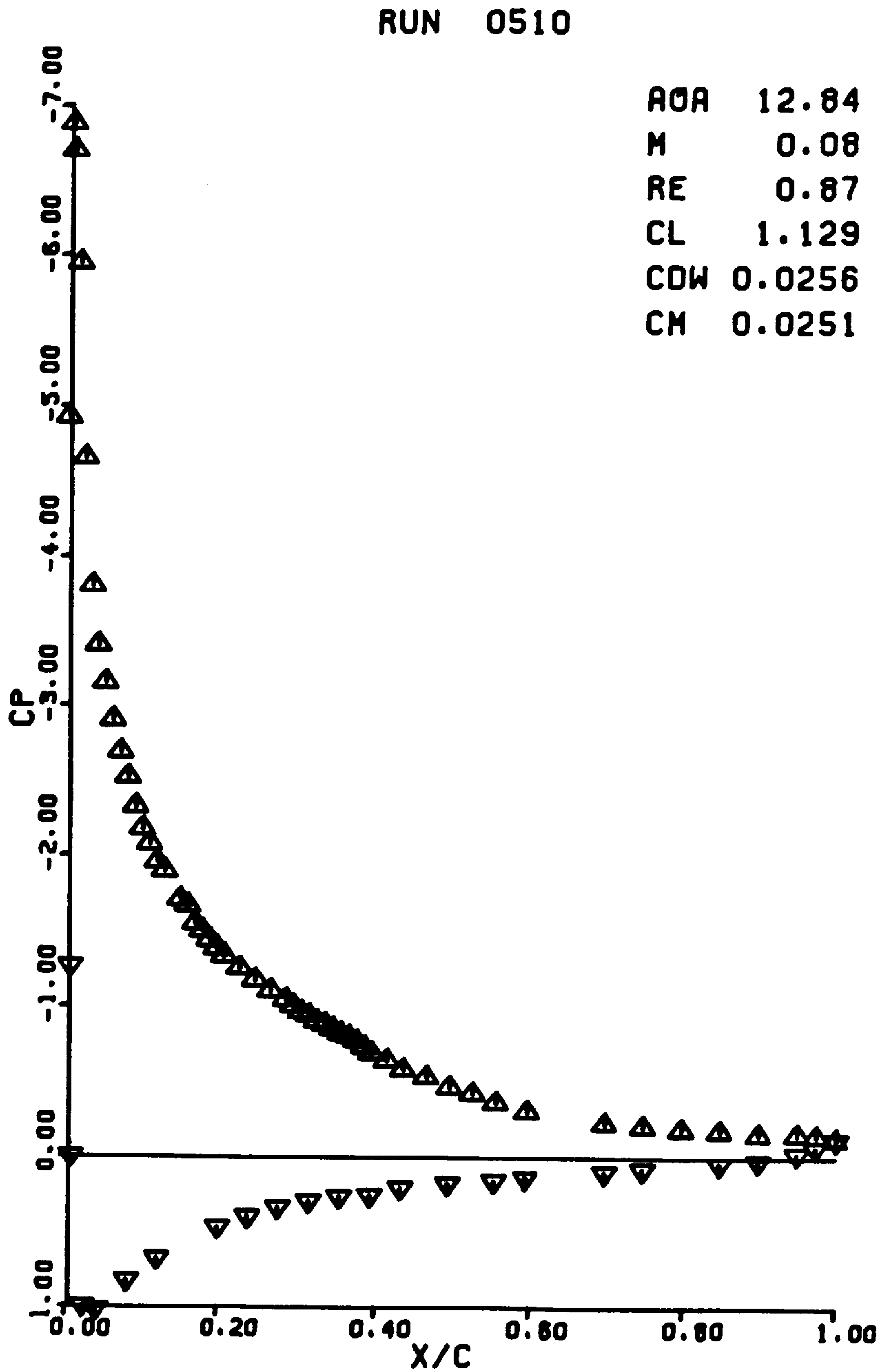
RUN 0510
AOA 12.84
M 0.08
RE 0.87
CL 1.129
CDW 0.0256
CM 0.0251
CP
-7.00
-6.00
-5.00
-4.00
-3.00
-2.00
-1.00
0.00
1.00
0.00
0.20
0.40
0.60
0.80
1.00
X/C

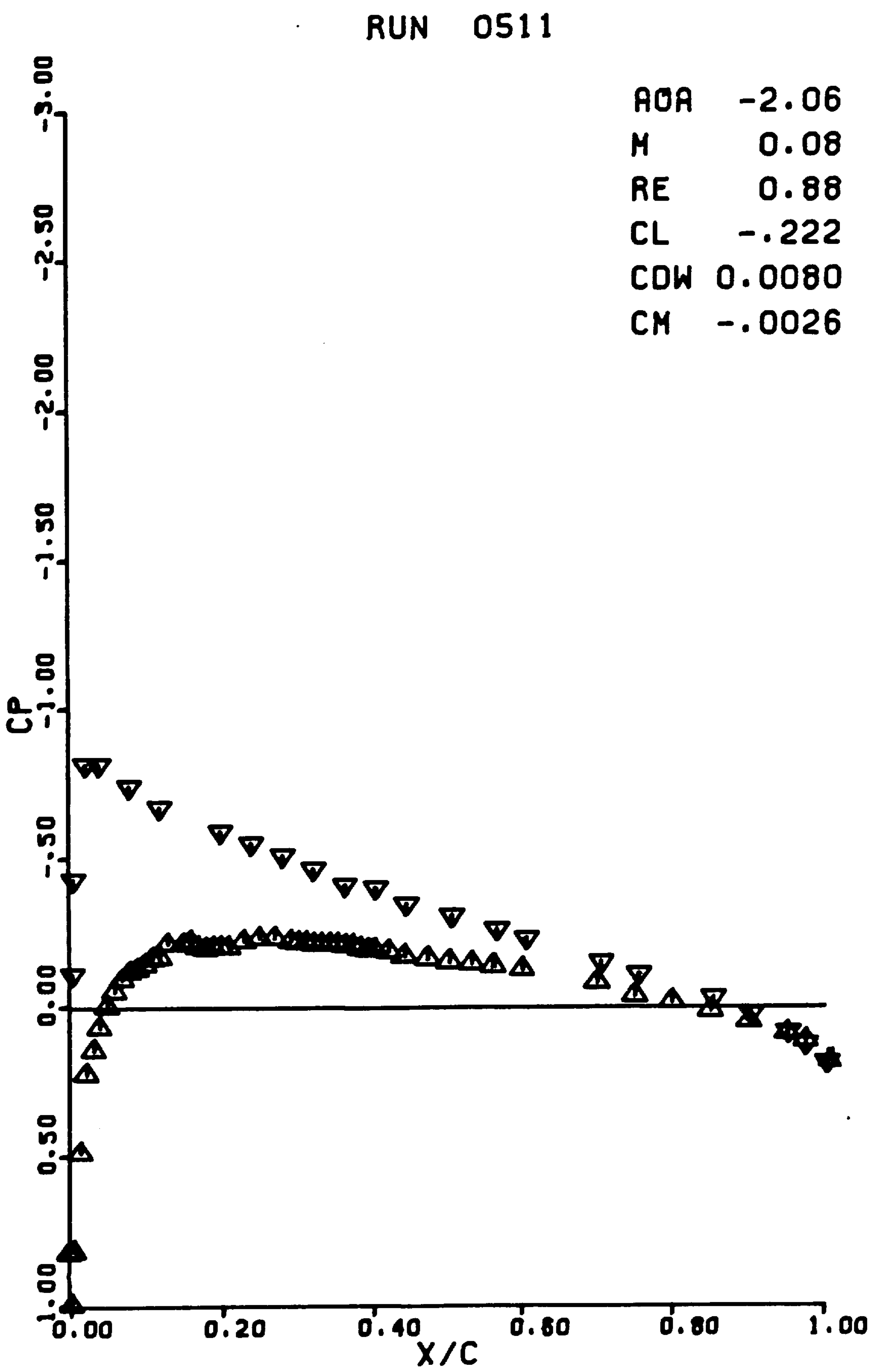
RUN 0511
AOA -2.06
M 0.08
RE 0.88
CL -.222
CDW 0.0080
CM -.0026
CP
X/C
-3.00
-2.50
-2.00
-1.50
-1.00
-.50
0.00
0.50
1.00
0.00
0.20
0.40
0.60
0.80
1.00

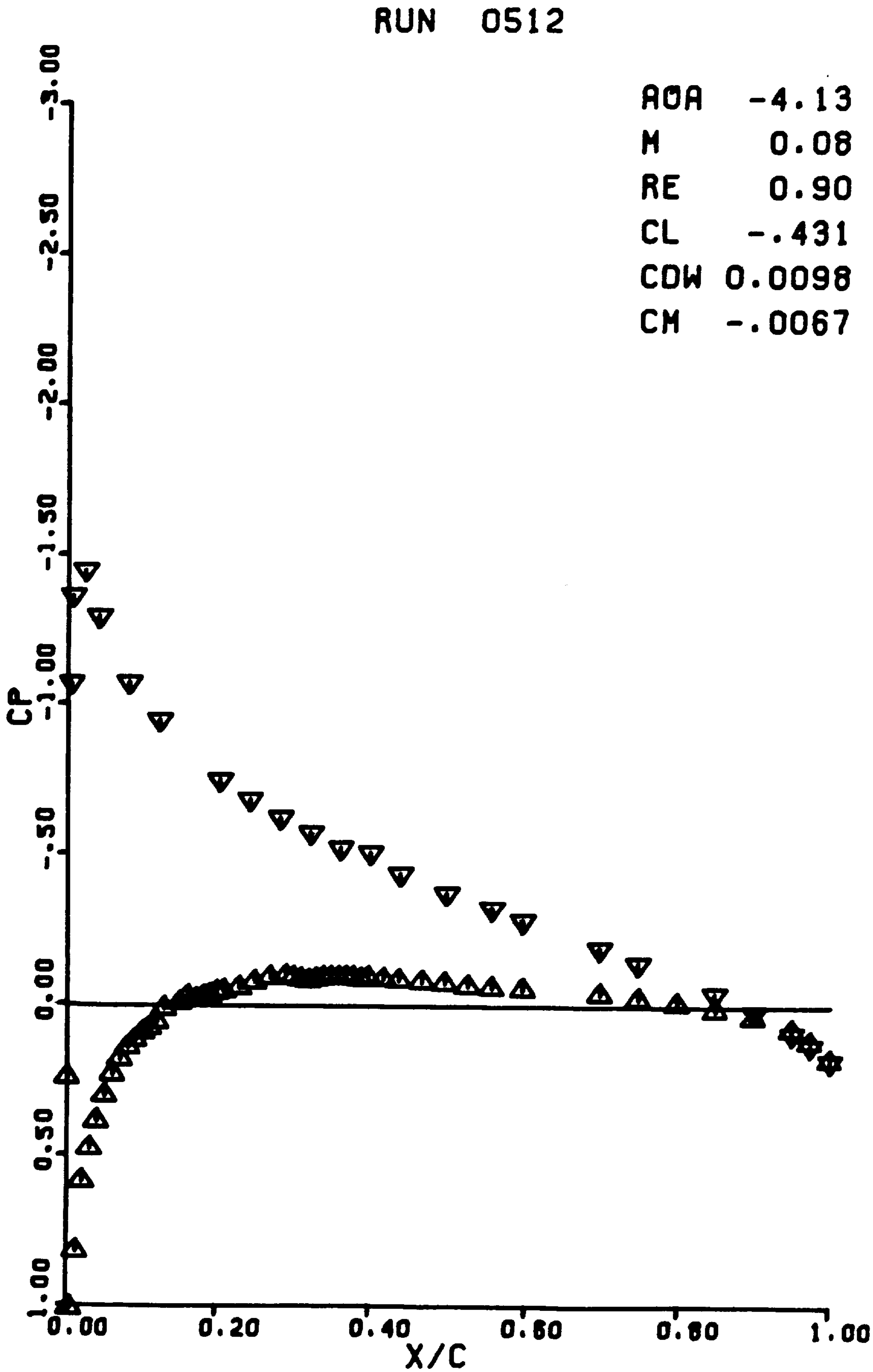

RUN 0512
AOA -4.13
M 0.08
RE 0.90
CL -.431
CDW 0.0098
CM -.0067
CP
-3.00
-2.50
-2.00
-1.50
-1.00
-.50
0.00
0.50
1.00
0.00
0.20
0.40
0.60
0.80
1.00
X/C

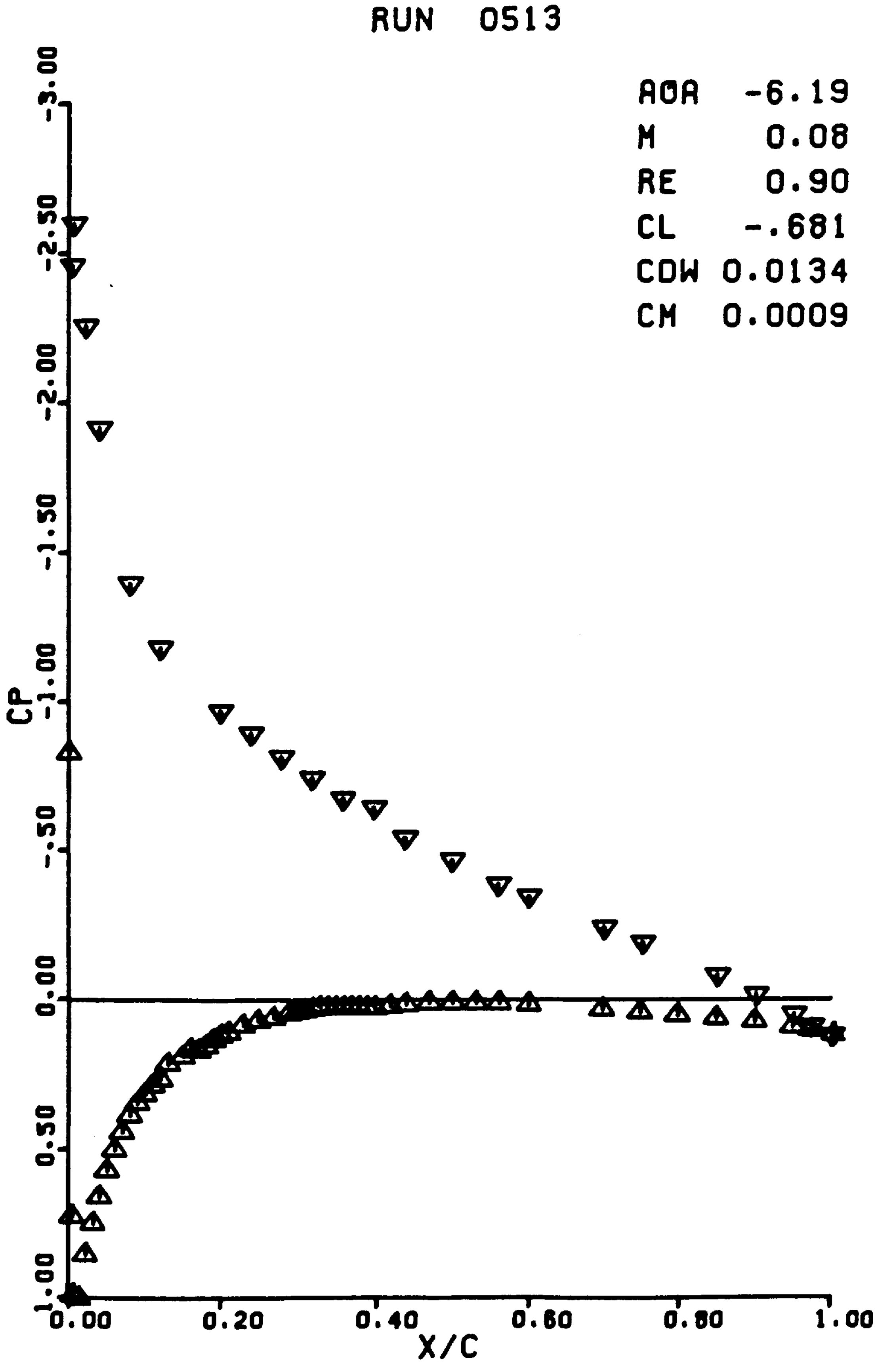
RUN 0513
AOA -6.19
M 0.08
RE 0.90
CL -.681
CDW 0.0134
CM 0.0009
CP
-3.00
-2.50
-2.00
-1.50
-1.00
-.50
0.00
0.50
1.00
0.00
0.20
0.40
0.60
0.80
1.00
X/C

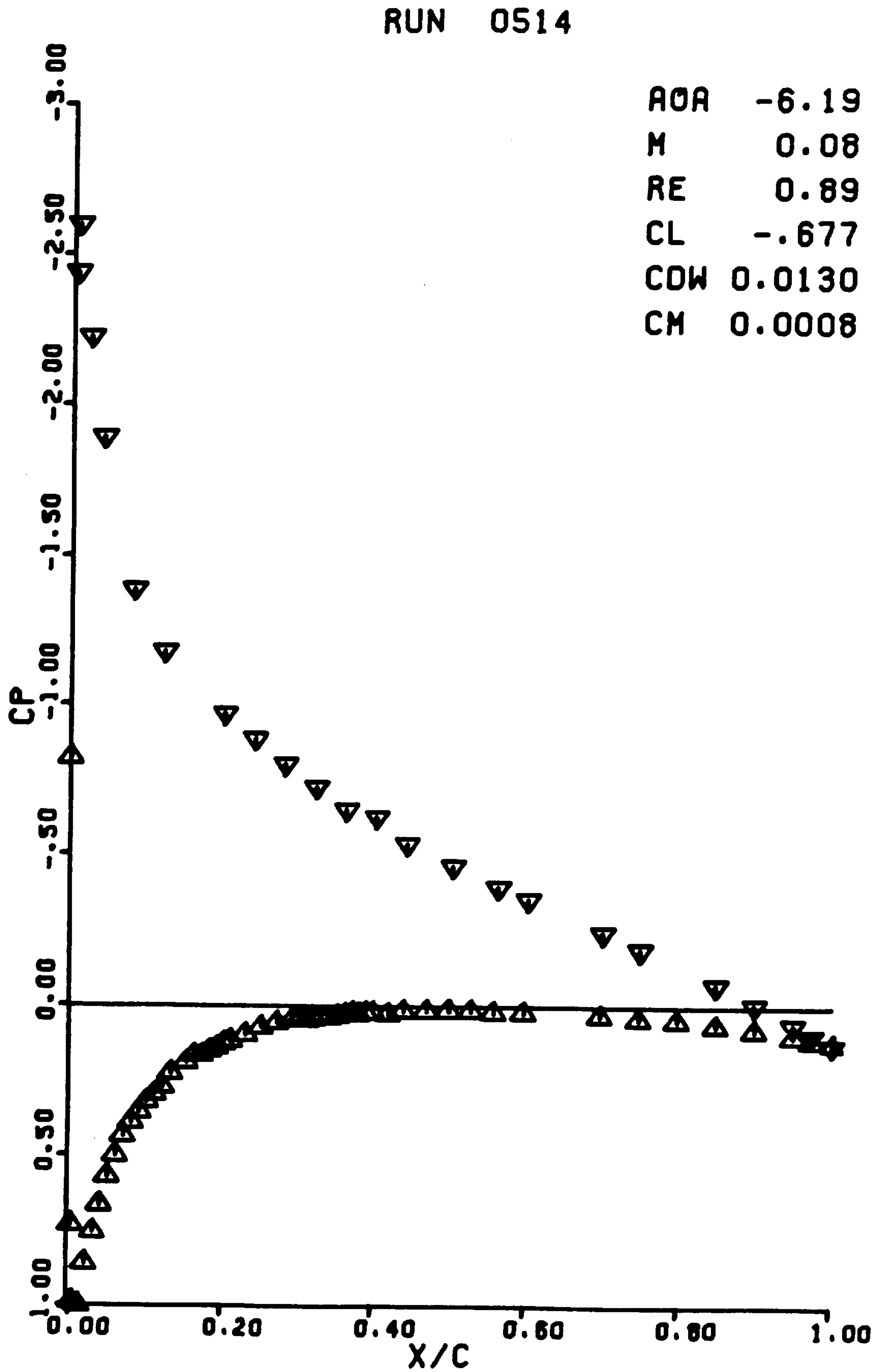
RUN 0514
AOA -6.19
M 0.08
RE 0.89
CL -.677
CDW 0.0130
CM 0.0008
CP
-3.00
-2.50
-2.00
-1.50
-1.00
-.50
0.00
0.50
1.00
X/C
0.00
0.20
0.40
0.60
0.80
1.00

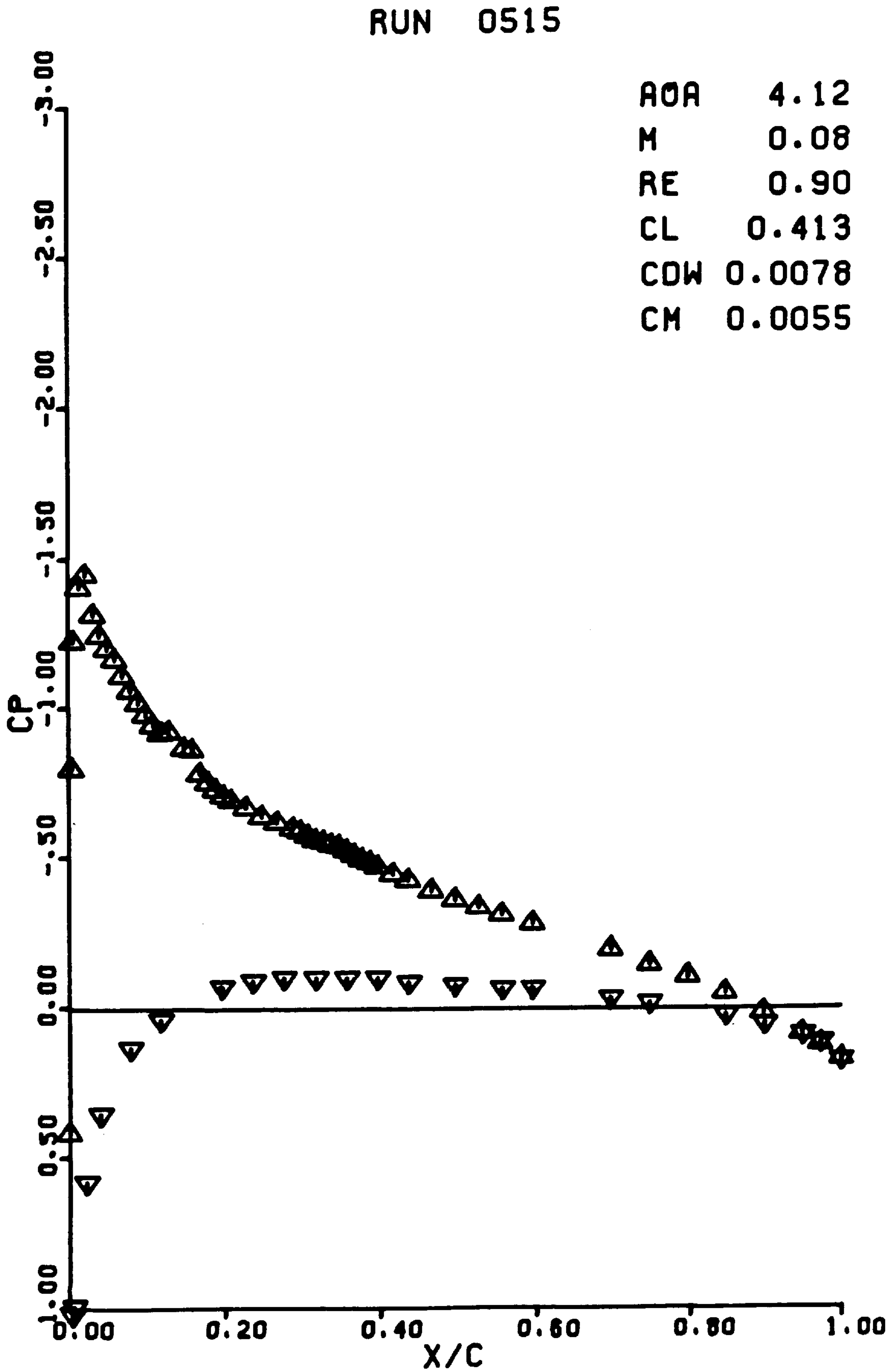

RUN 0515
AOA 4.12
M 0.08
RE 0.90
CL 0.413
CDW 0.0078
CM 0.0055
CP
-3.00
-2.50
-2.00
-1.50
-1.00
-.50
0.00
0.50
1.00
0.00
0.20
0.40
0.60
0.80
1.00
X/C

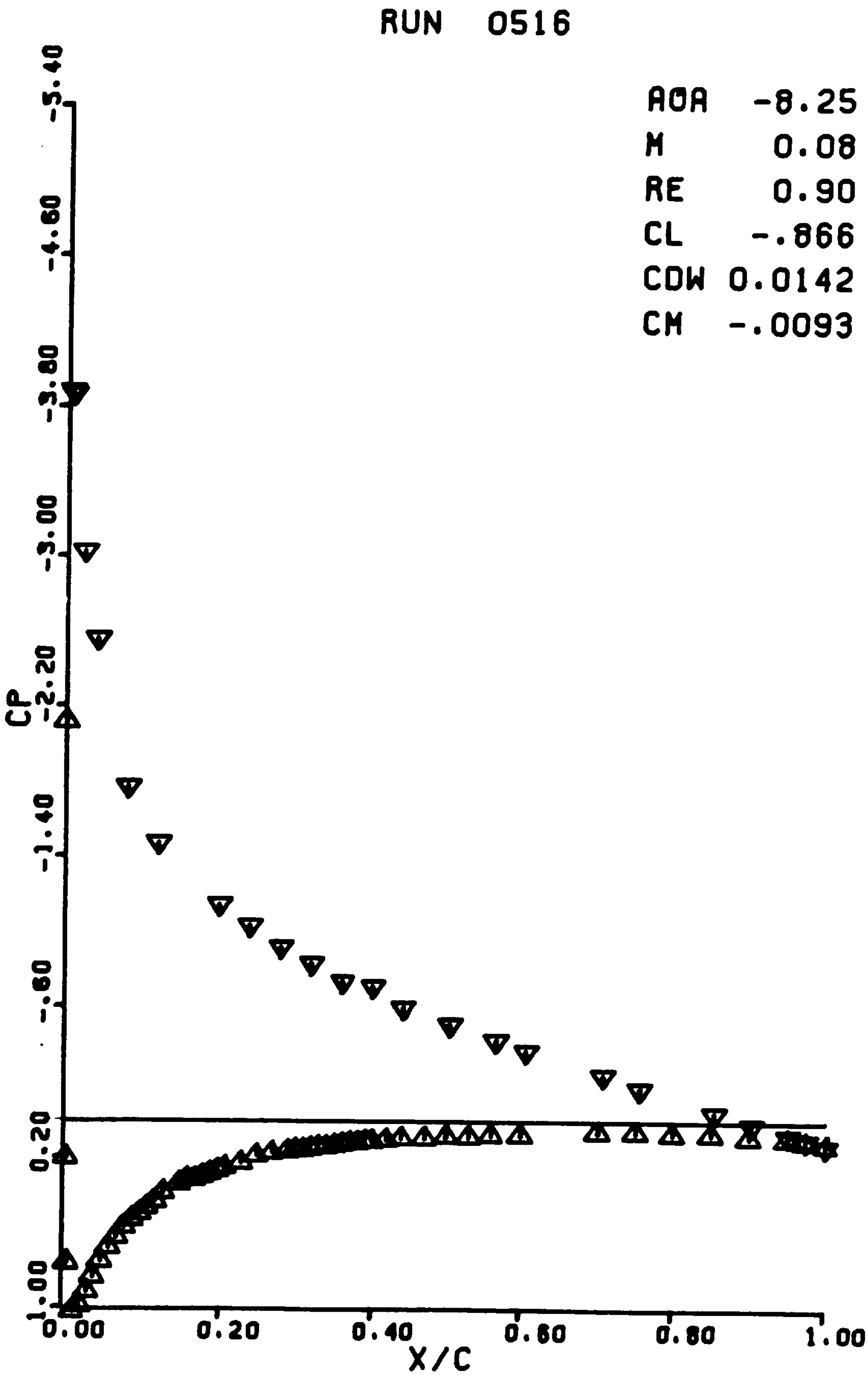
RUN 0516
AOA -8.25
M 0.08
RE 0.90
CL -.866
CDW 0.0142
CM -.0093
CP
-5.40
-4.60
-3.80
-3.00
-2.20
-1.40
-.60
0.20
1.00
0.00
0.20
0.40
0.60
0.80
1.00
X/C

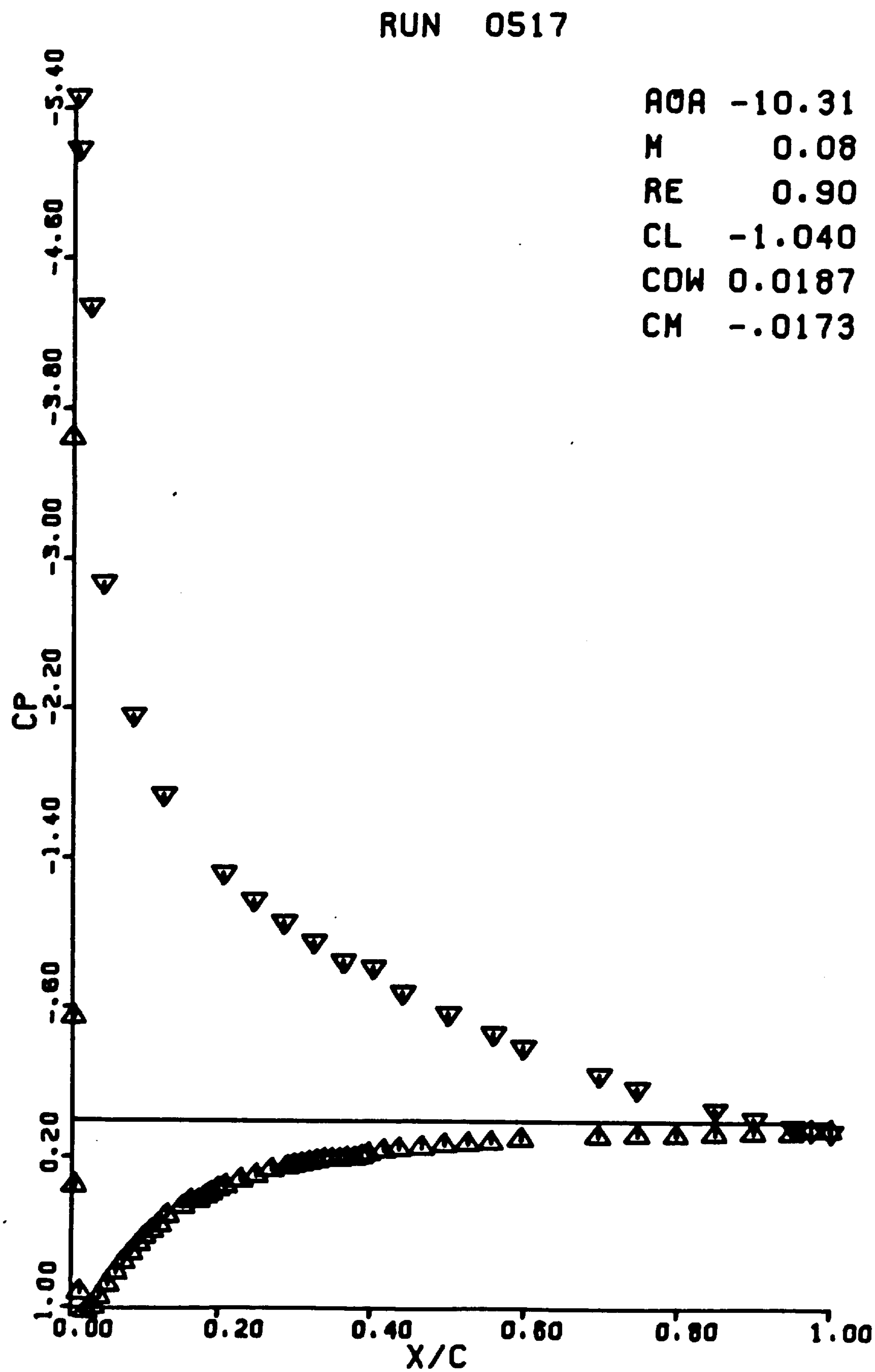
RUN 0517
AOA -10.31
M 0.08
RE 0.90
CL -1.040
CDW 0.0187
CM -.0173
CP
-5.40
-4.60
-3.80
-3.00
-2.20
-1.40
-.60
0.20
1.00
0.00
0.20
0.40
0.60
0.80
1.00
X/C

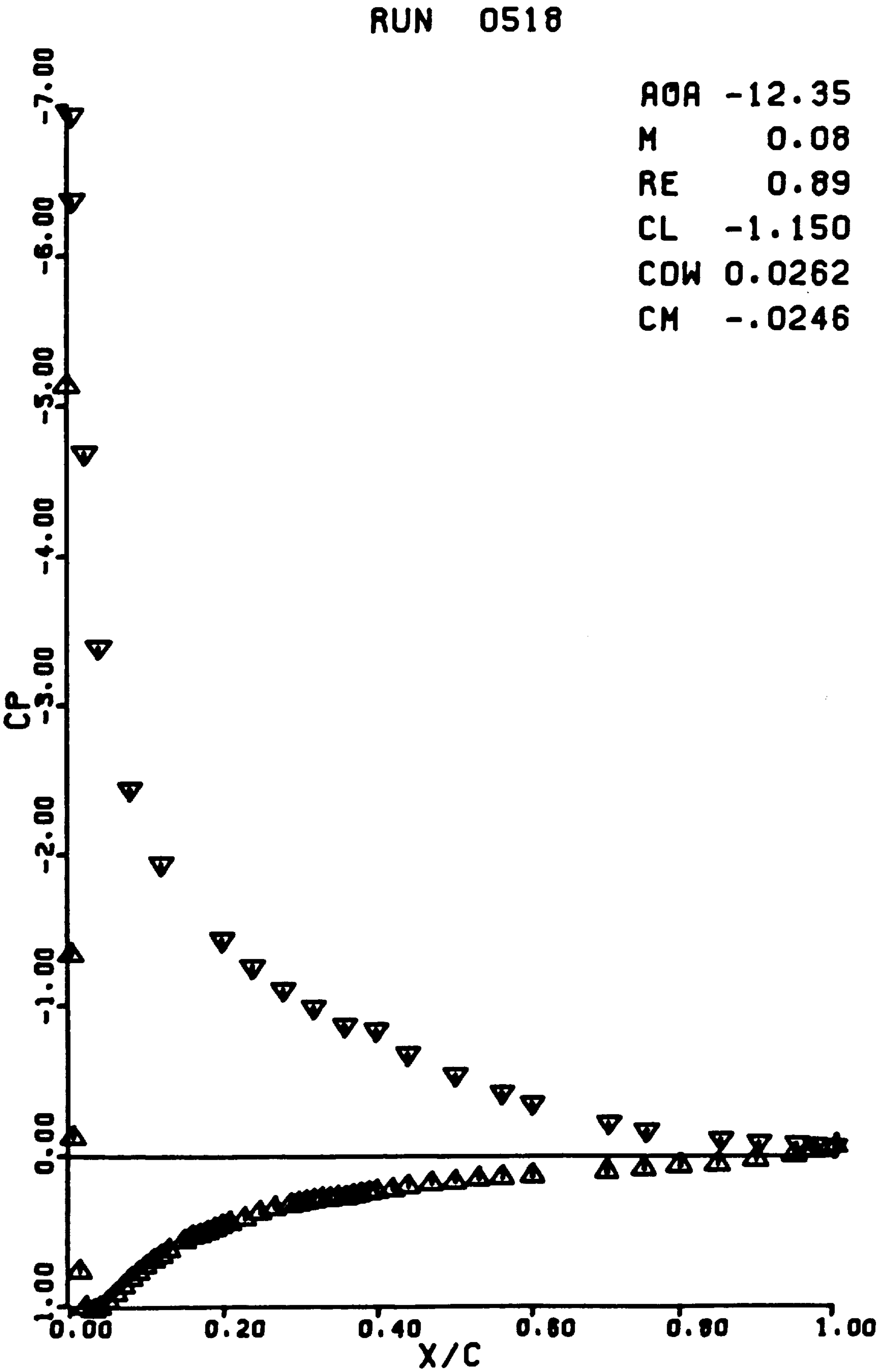
RUN 0518
AOA -12.35
M 0.08
RE 0.89
CL -1.150
CDW 0.0262
CM -.0246
CP
-7.00
-6.00
-5.00
-4.00
-3.00
-2.00
-1.00
0.00
1.00
0.00
0.20
0.40
0.60
0.80
1.00
X/C

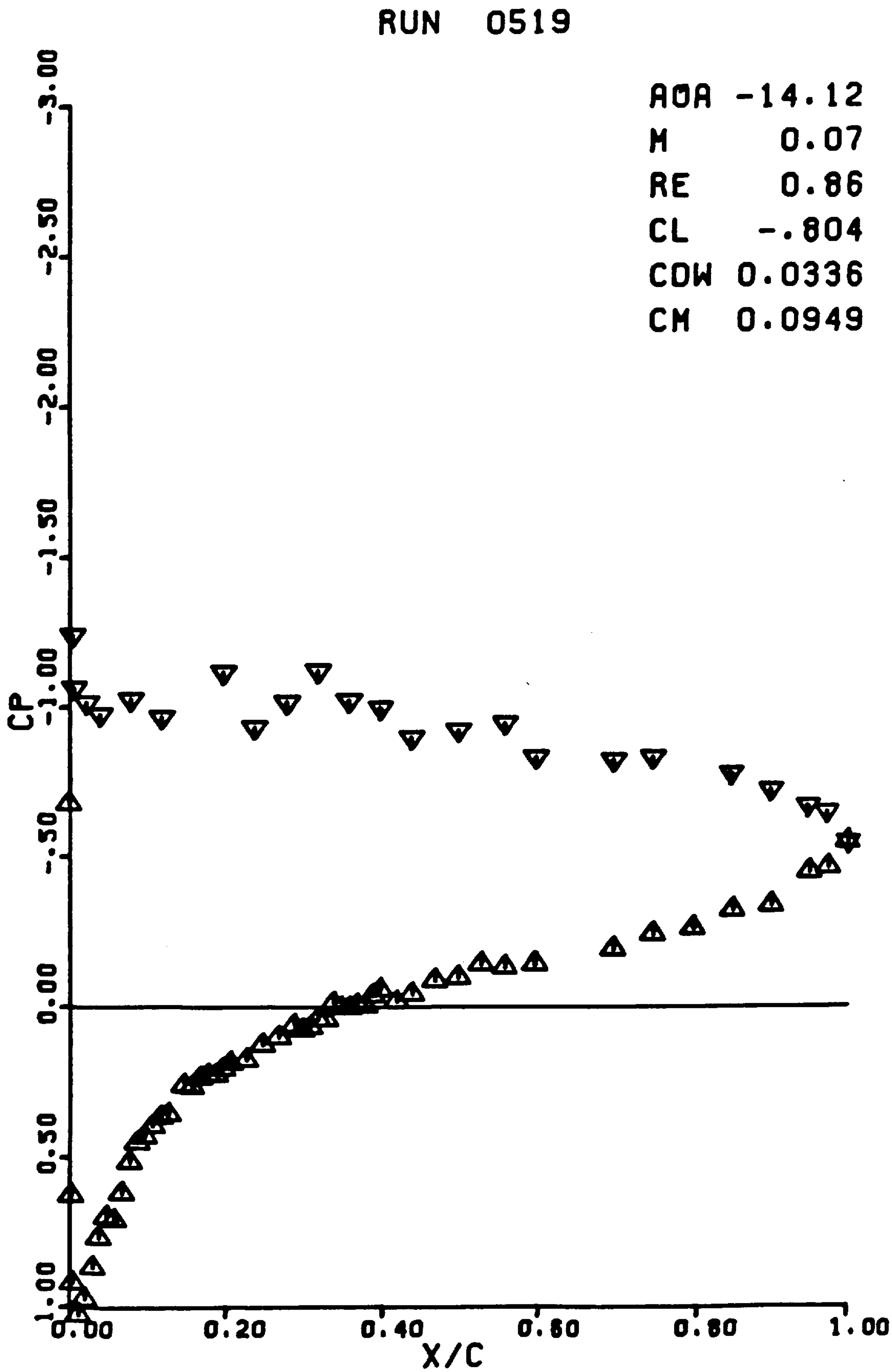
RUN 0519
AOA -14.12
M 0.07
RE 0.86
CL -.804
CDW 0.0336
CM 0.0949
CP
-3.00
-2.50
-2.00
-1.50
-1.00
-.50
0.00
0.50
1.00
0.00
0.20
0.40
0.60
0.80
1.00
X/C

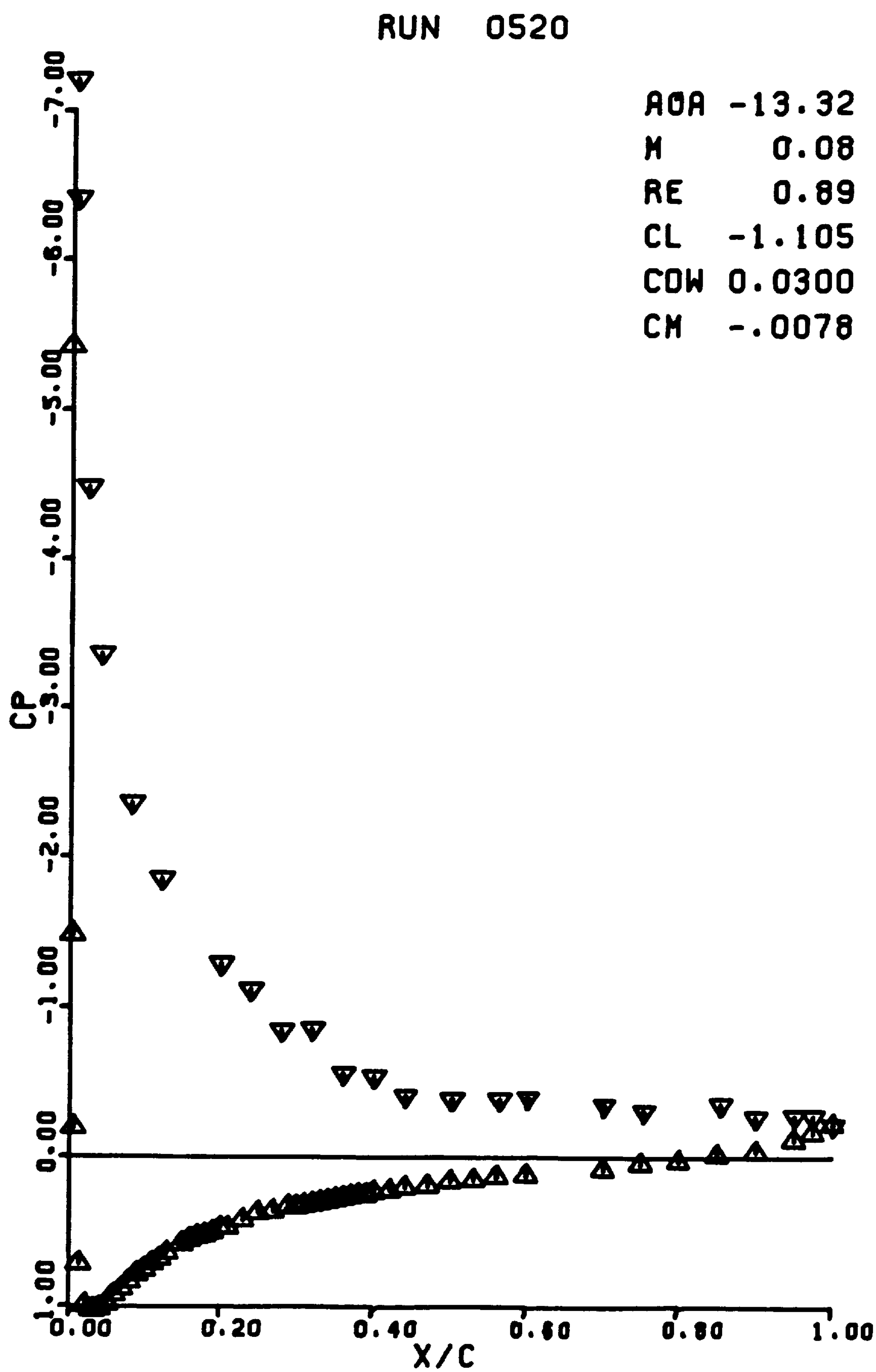
RUN 0520
AOA -13.32
M 0.08
RE 0.89
CL -1.105
CDW 0.0300
CM -.0078
CP
-7.00
-6.00
-5.00
-4.00
-3.00
-2.00
-1.00
0.00
1.00
0.00
0.20
0.40
0.60
0.80
1.00
X/C

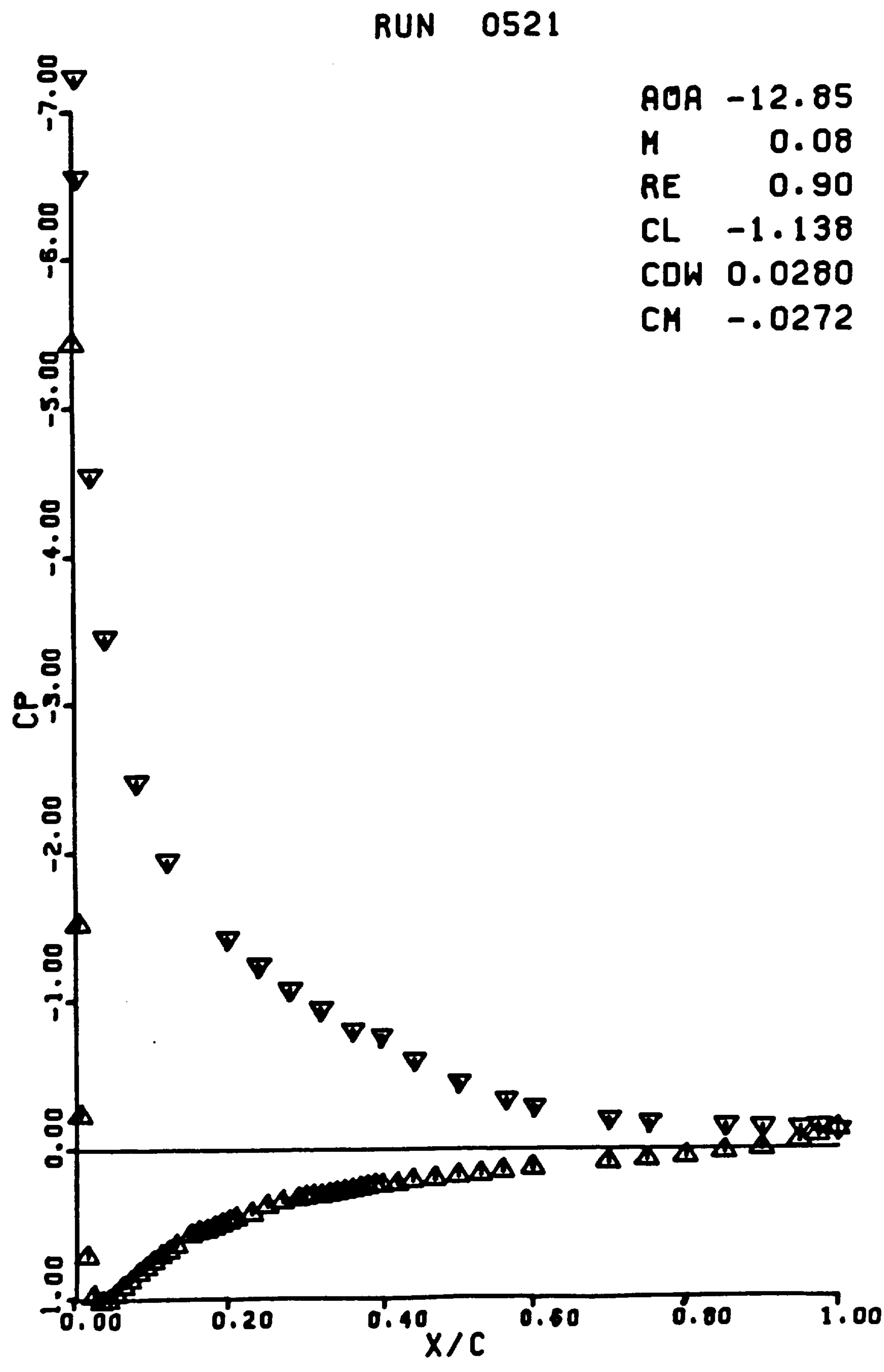
RUN 0521
AOA -12.85
M 0.08
RE 0.90
CL -1.138
CDW 0.0280
CM -.0272
CP
-7.00
-6.00
-5.00
-4.00
-3.00
-2.00
-1.00
0.00
1.00
0.00
0.20
0.40
0.60
0.80
1.00
X/C

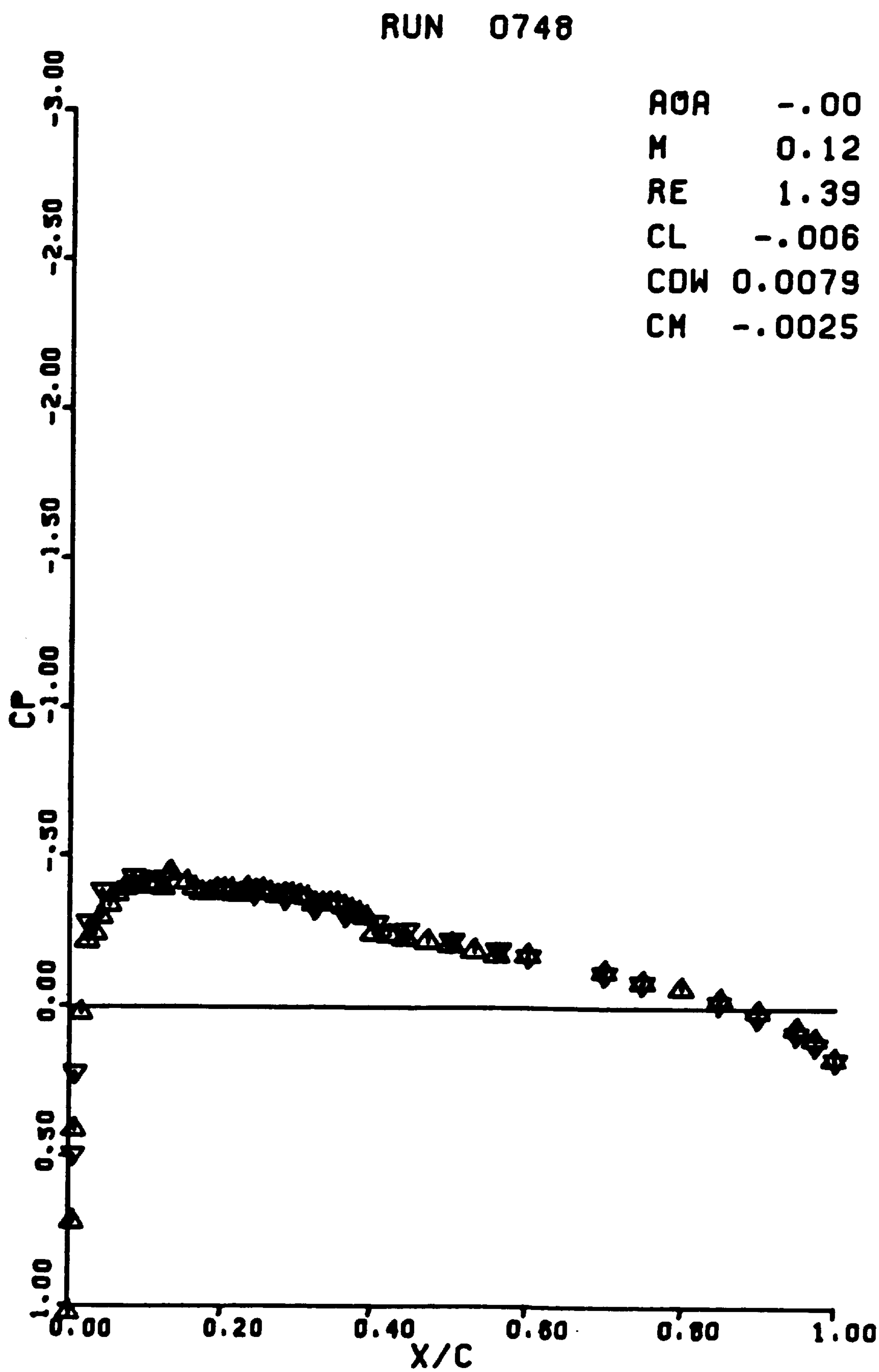
RUN 0748
AOA -.00
M 0.12
RE 1.39
CL -.006
CDW 0.0079
CM -.0025
CP
-3.00
-2.50
-2.00
-1.50
-1.00
-.50
0.00
0.50
1.00
0.00
0.20
0.40
0.60
0.80
1.00
X/C

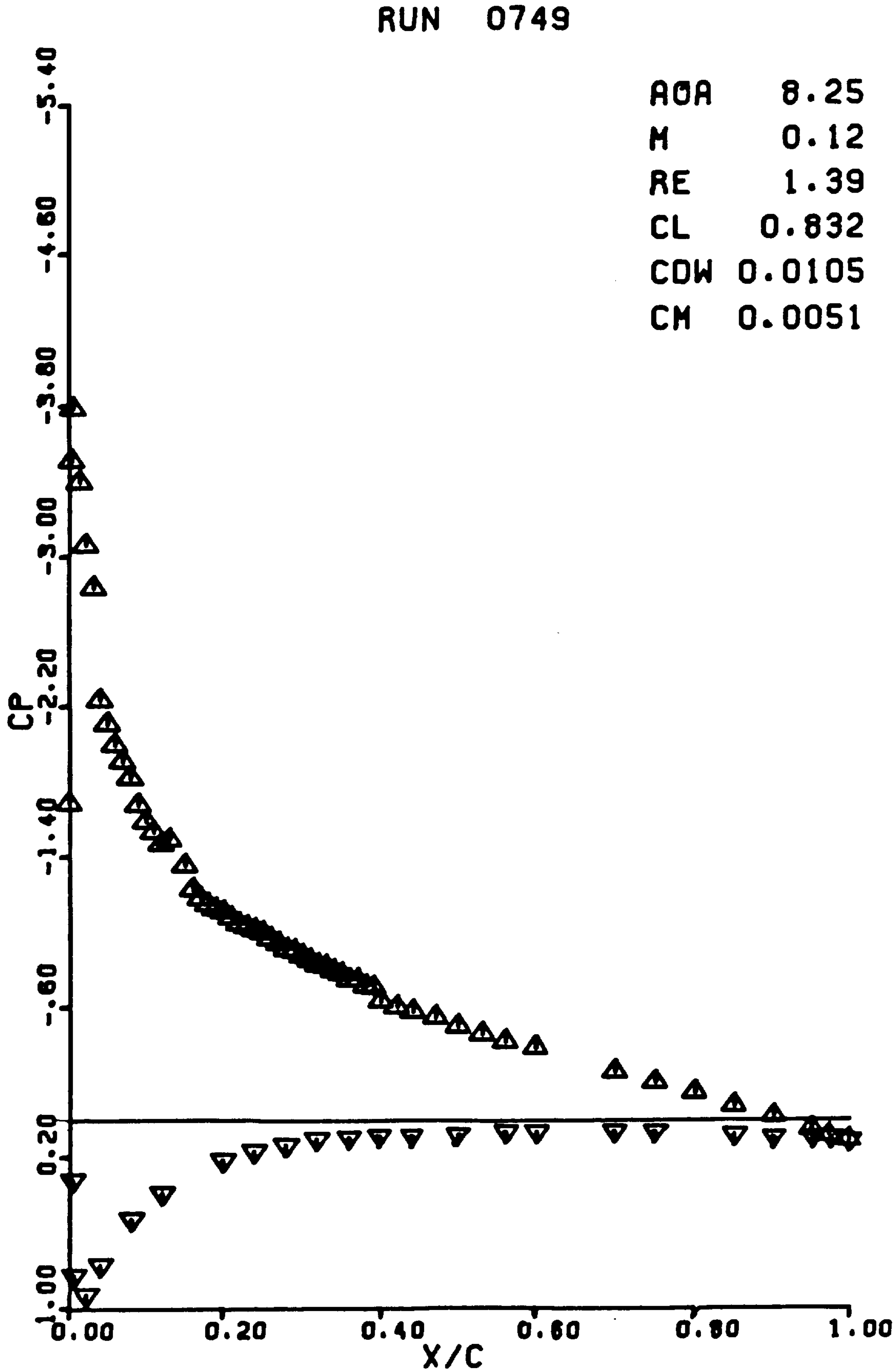
RUN 0749
AOA 8.25
M 0.12
RE 1.39
CL 0.832
CDW 0.0105
CM 0.0051
CP
-5.40
-4.60
-3.80
-3.00
-2.20
-1.40
-.60
0.20
1.00
X/C
0.00
0.20
0.40
0.60
0.80
1.00

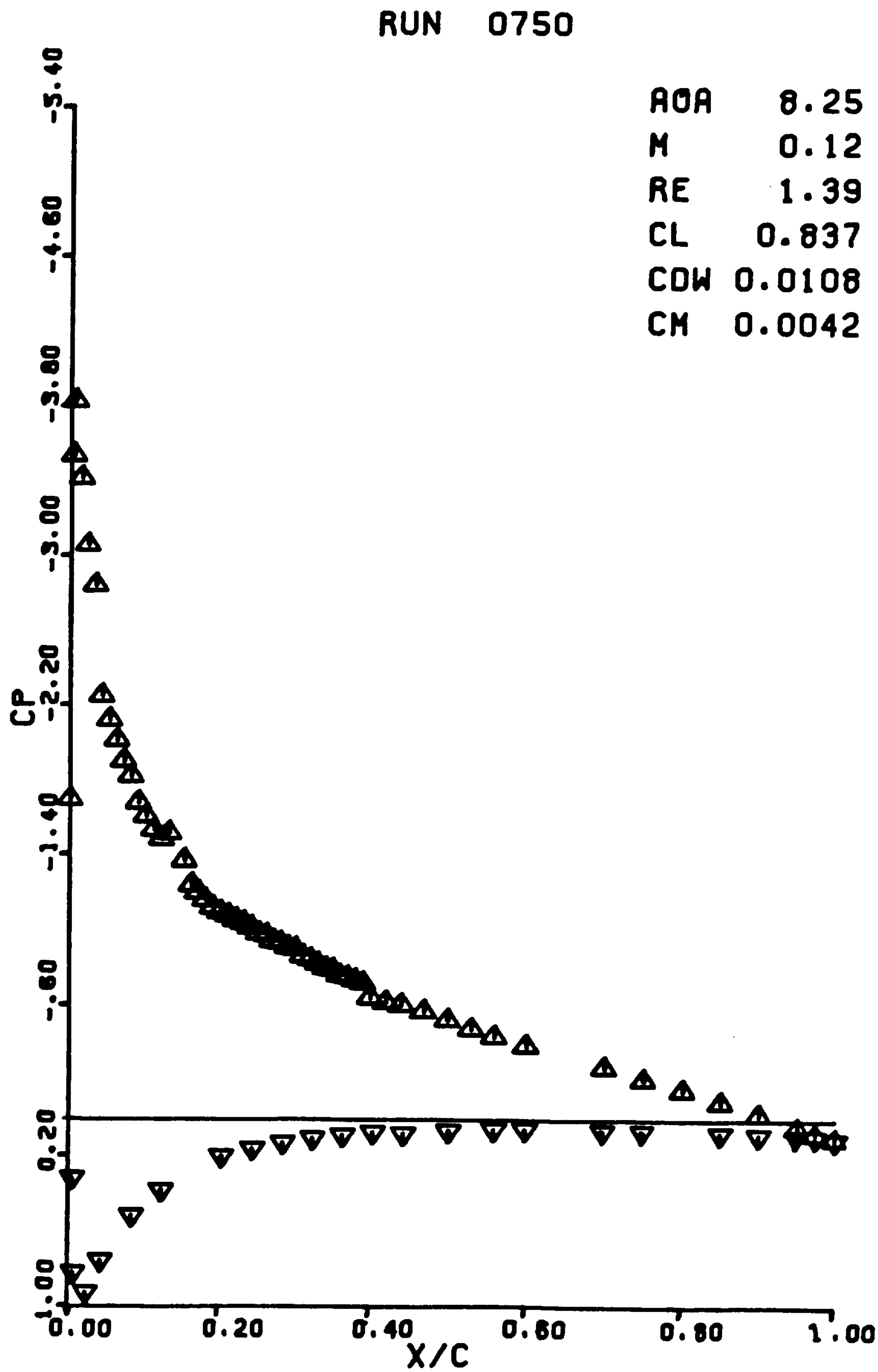
RUN 0750
AOA 8.25
M 0.12
RE 1.39
CL 0.837
CDW 0.0108
CM 0.0042
CP
-5.40
-4.60
-3.80
-3.00
-2.20
-1.40
-.60
0.20
1.00
0.00
0.20
0.40
0.60
0.80
1.00
X/C

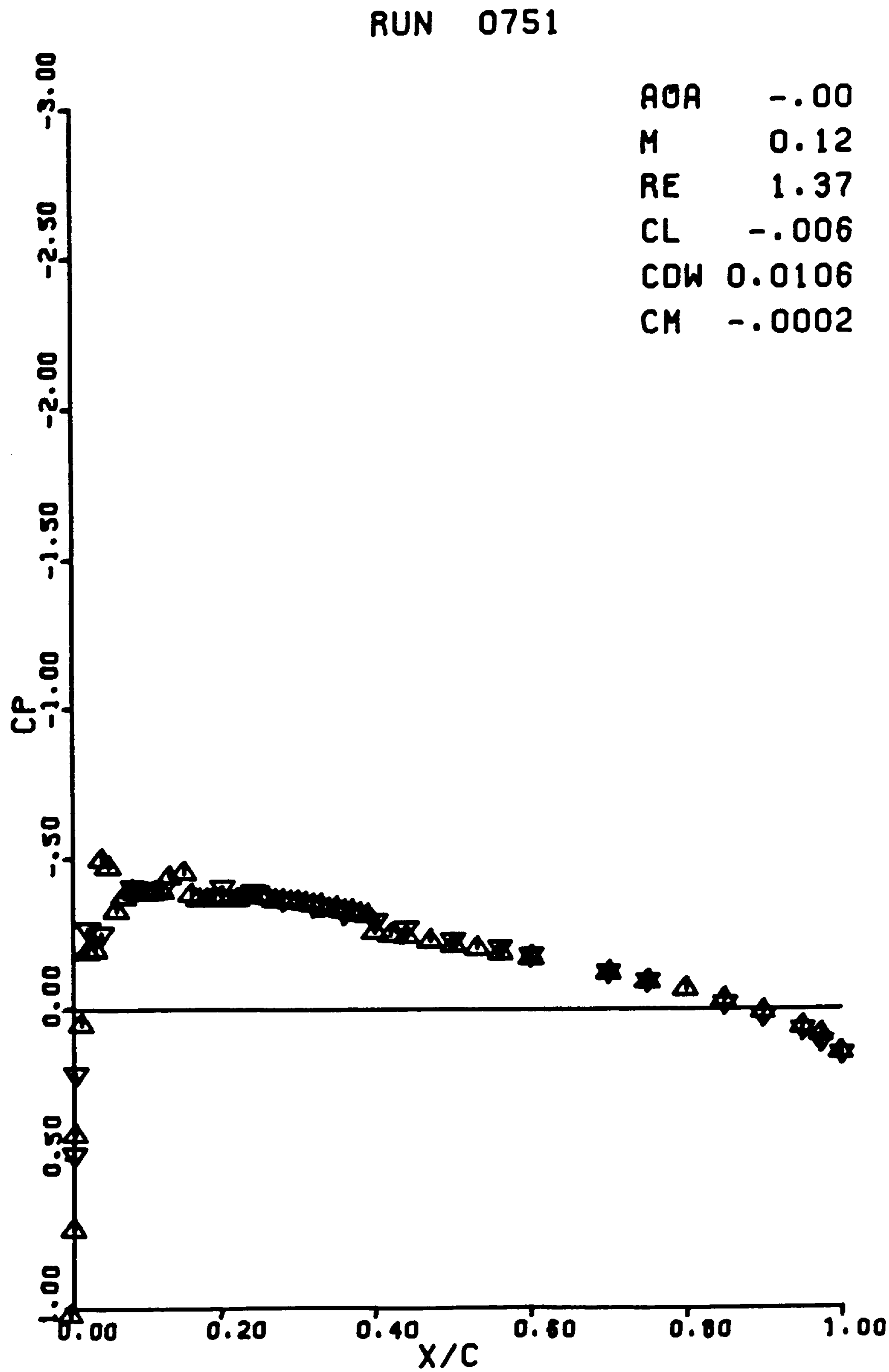
RUN 0751
AOA -.00
M 0.12
RE 1.37
CL -.006
CDW 0.0106
CM -.0002
CP
-3.00
-2.50
-2.00
-1.50
-1.00
-.50
0.00
0.50
1.00
X/C
0.00
0.20
0.40
0.60
0.80
1.00

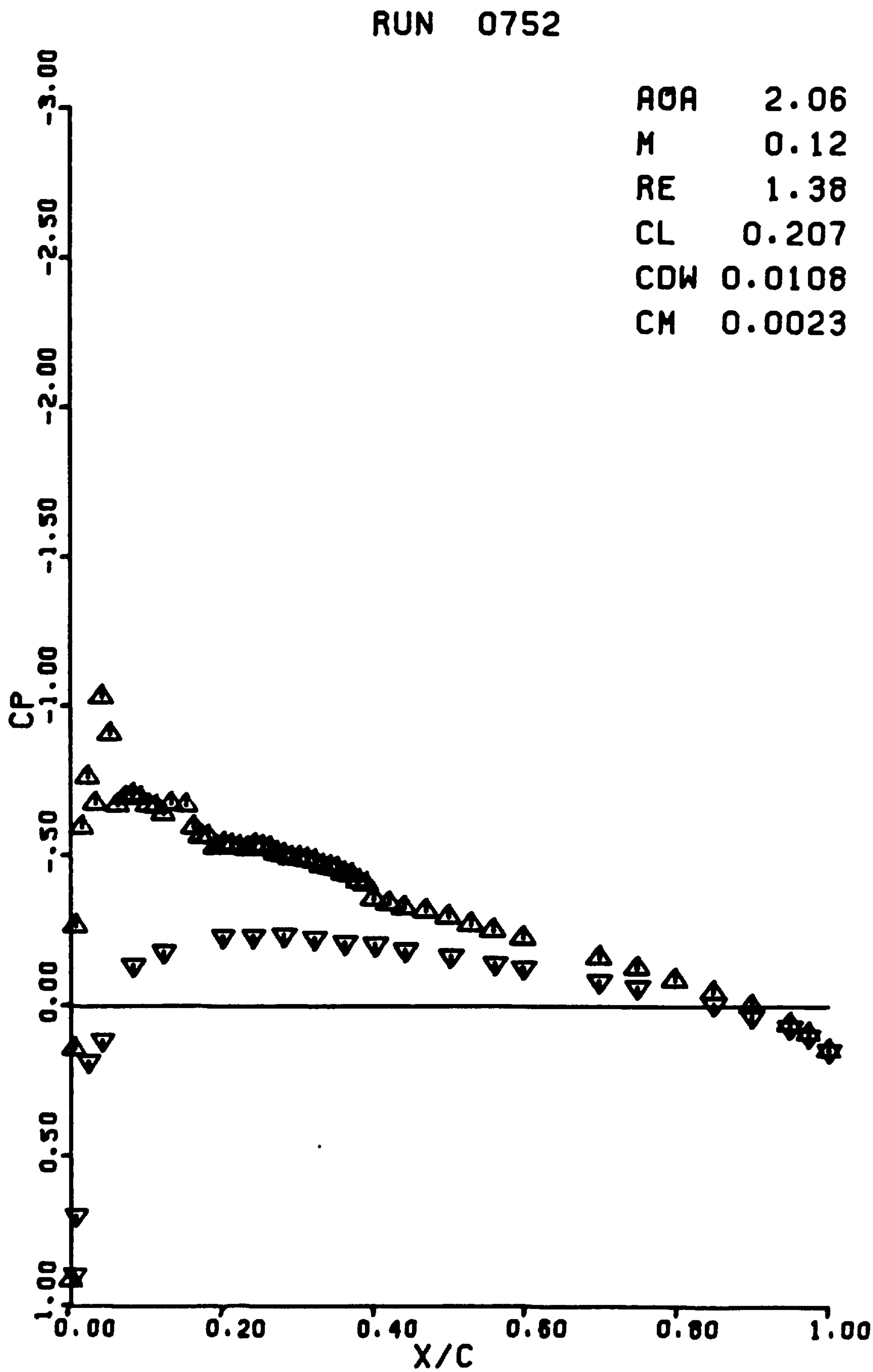
RUN 0752
AOA 2.06
M 0.12
RE 1.38
CL 0.207
CDW 0.0108
CM 0.0023
CP
-3.00
-2.50
-2.00
-1.50
-1.00
-.50
0.00
0.50
1.00
0.00
0.20
0.40
0.60
0.80
1.00
X/C

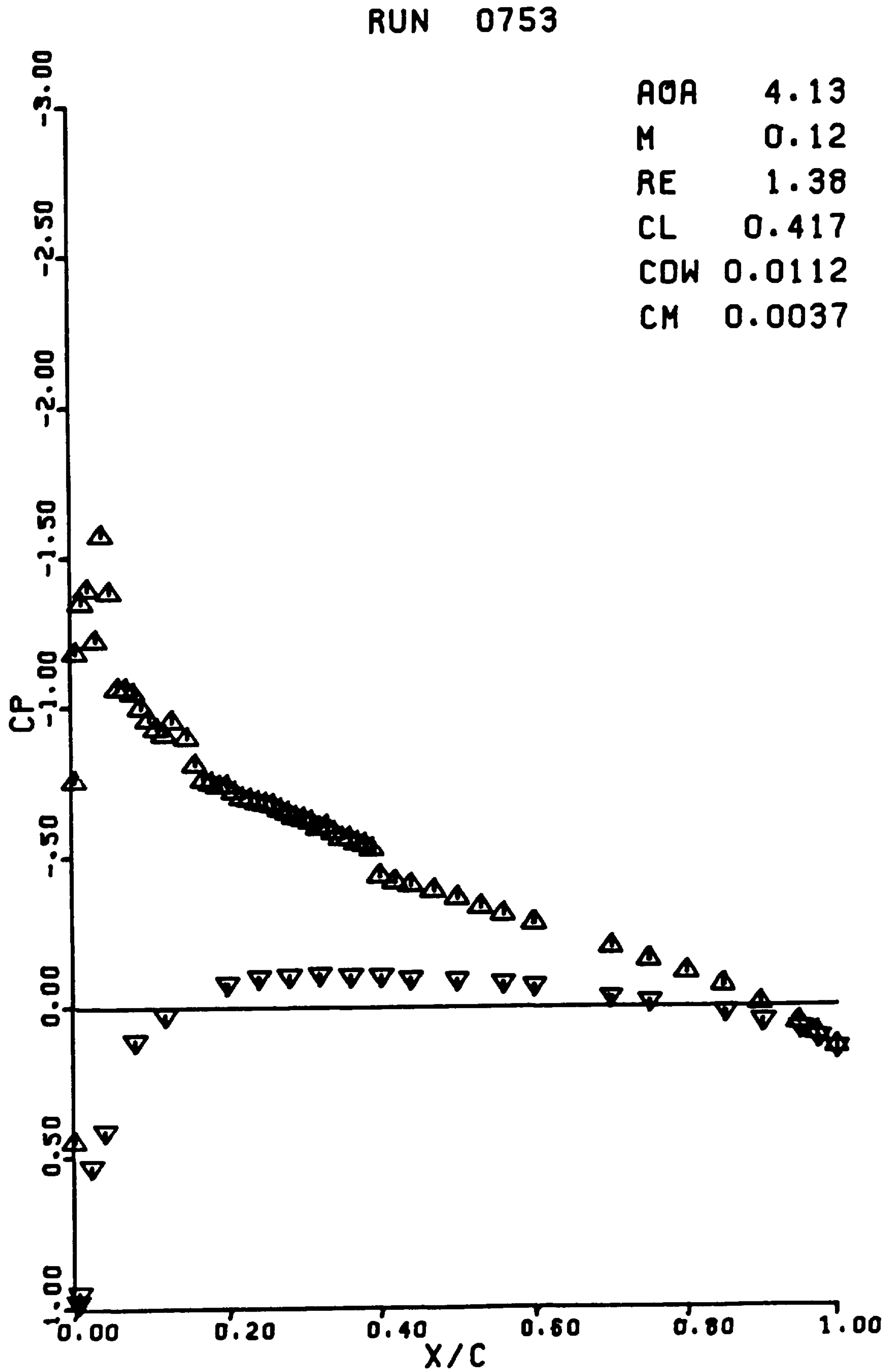
RUN 0753
AOA 4.13
M 0.12
RE 1.38
CL 0.417
CDW 0.0112
CM 0.0037
CP
-3.00
-2.50
-2.00
-1.50
-1.00
-.50
0.00
0.50
1.00
0.00
0.20
0.40
0.60
0.80
1.00
X/C

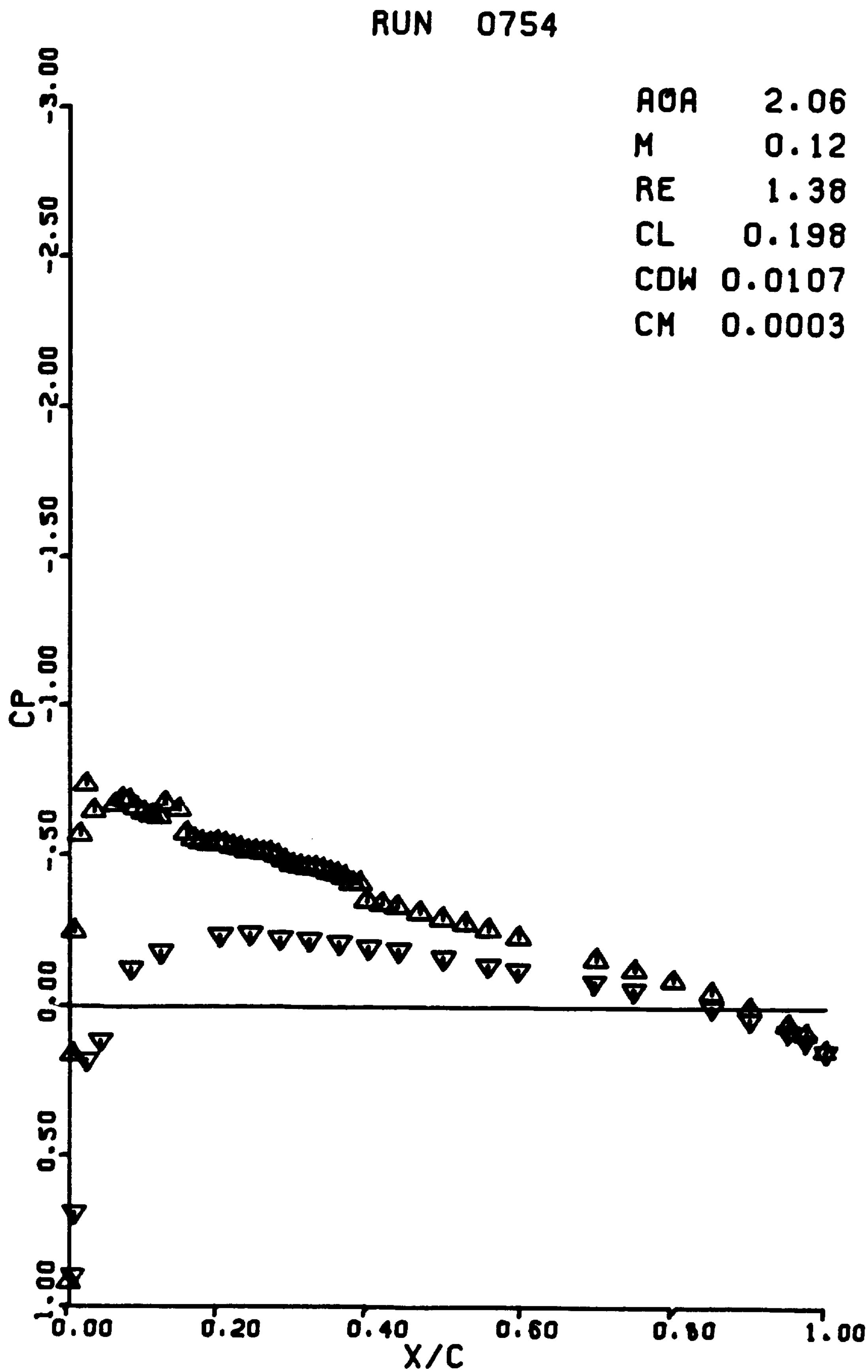

RUN 0754
AOA 2.06
M 0.12
RE 1.38
CL 0.198
CDW 0.0107
CM 0.0003
CP
-3.00
-2.50
-2.00
-1.50
-1.00
-.50
0.00
0.50
1.00
0.00
0.20
0.40
0.60
0.80
1.00
X/C

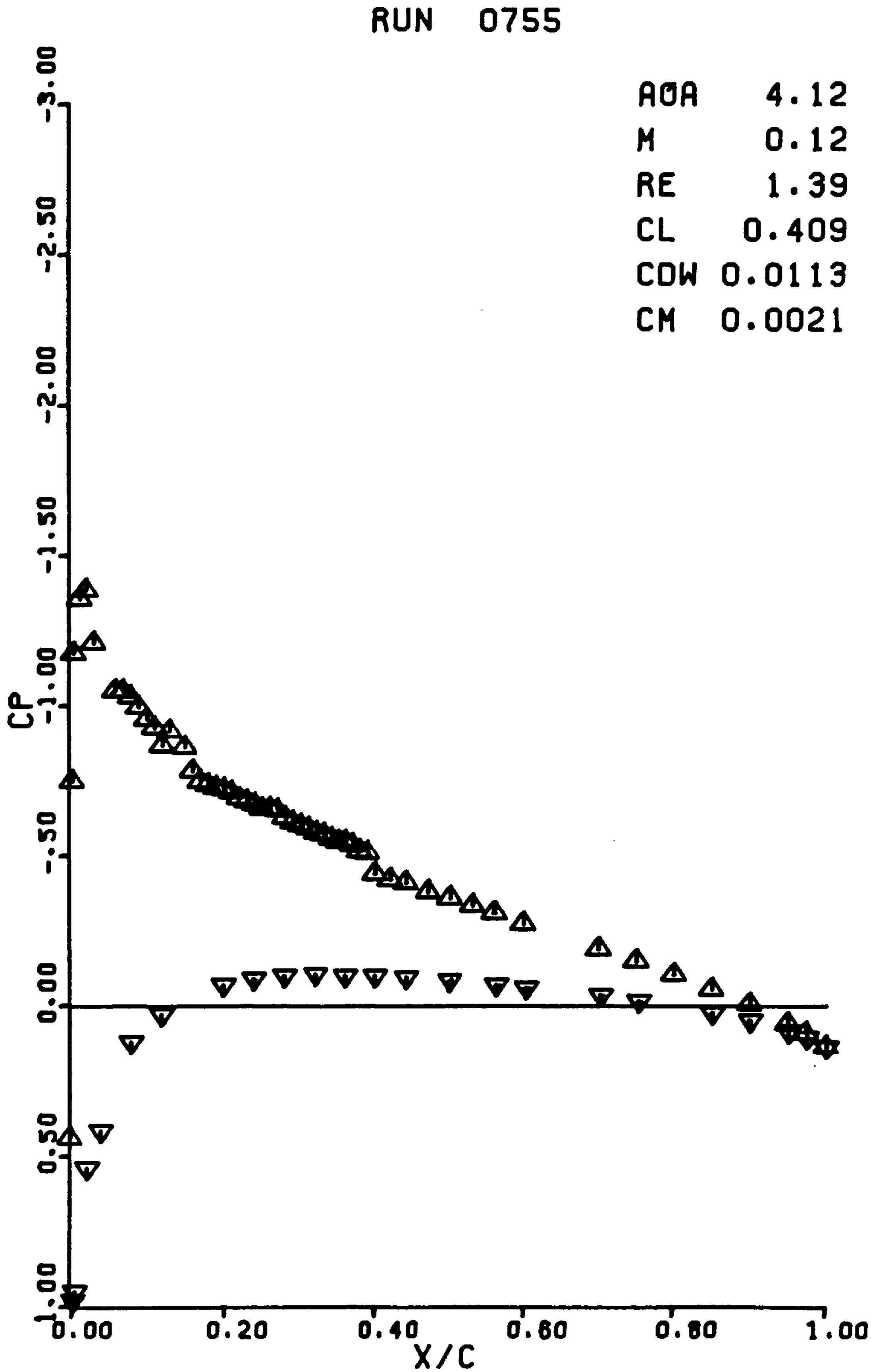
RUN 0755
AOA 4.12
M 0.12
RE 1.39
CL 0.409
CDW 0.0113
CM 0.0021
CP
-3.00
-2.50
-2.00
-1.50
-1.00
-.50
0.00
0.50
1.00
0.00
0.20
0.40
0.60
0.80
1.00
X/C

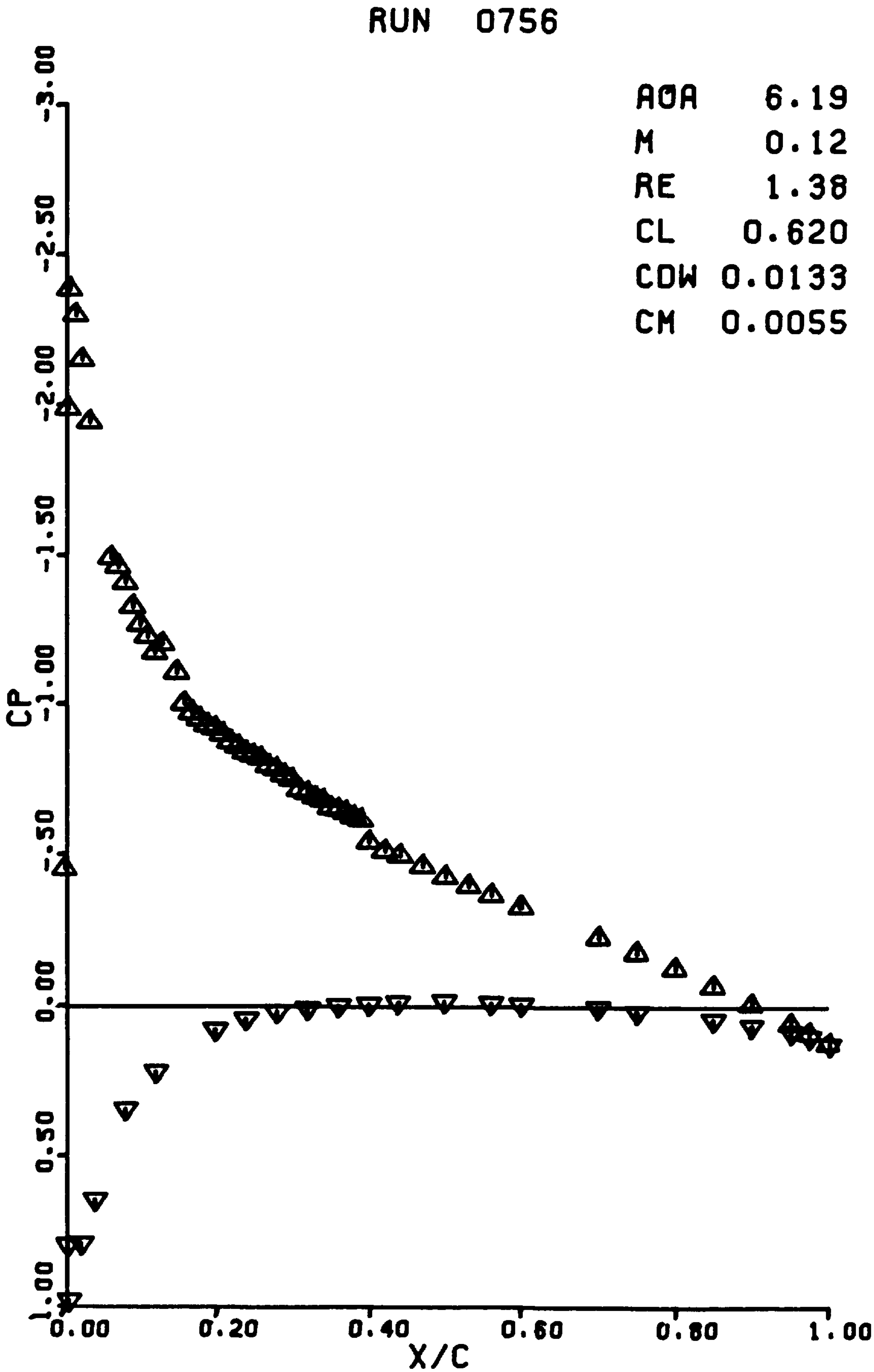
RUN 0756
AOA 6.19
M 0.12
RE 1.38
CL 0.620
CDW 0.0133
CM 0.0055
CP
X/C
-3.00
-2.50
-2.00
-1.50
-1.00
-.50
0.00
0.50
1.00
0.00
0.20
0.40
0.60
0.80
1.00

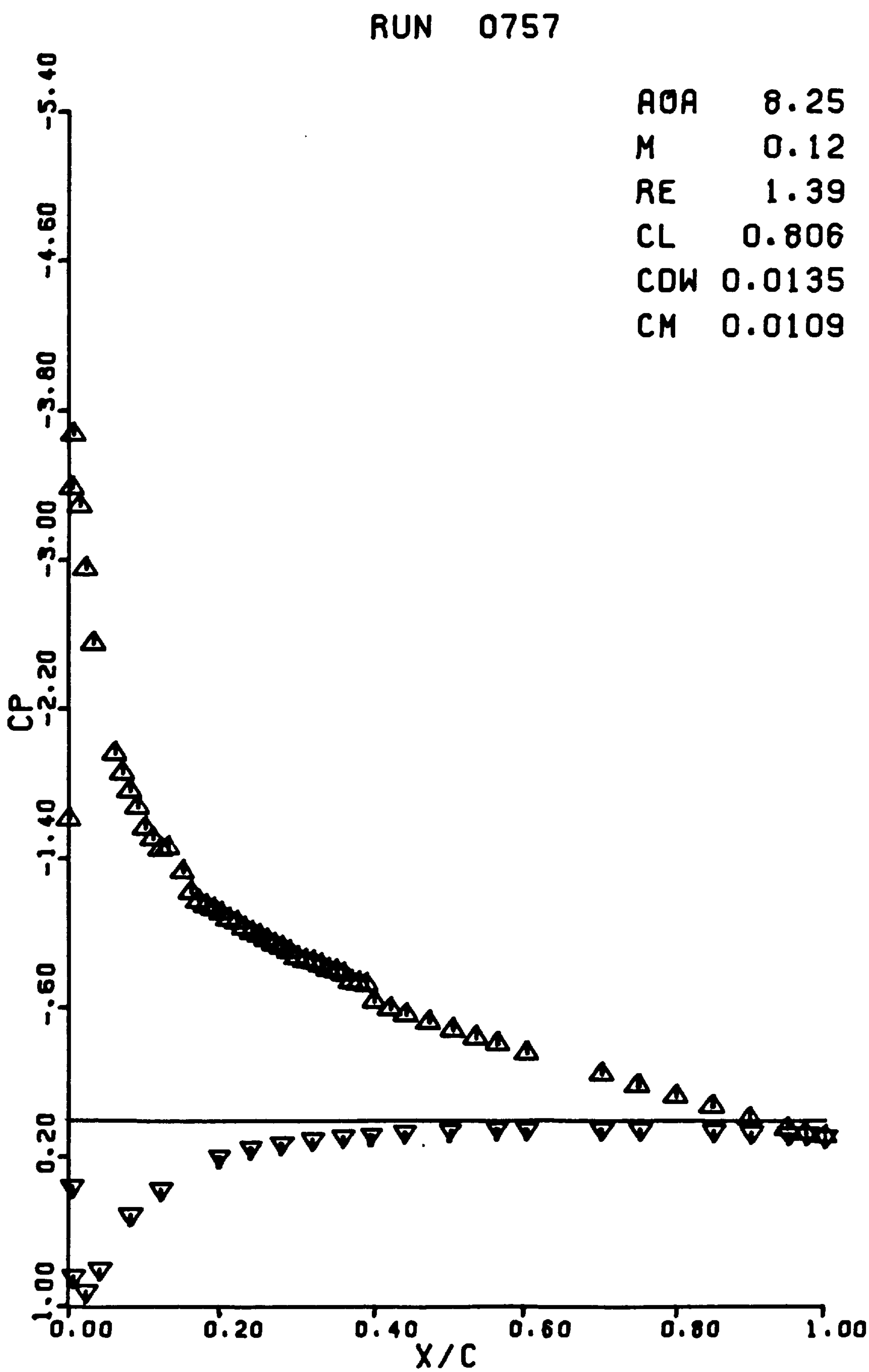

RUN 0757
AOA 8.25
M 0.12
RE 1.39
CL 0.806
CDW 0.0135
CM 0.0109
CP
-5.40
-4.60
-3.80
-3.00
-2.20
-1.40
-.60
0.20
1.00
0.00
0.20
0.40
0.60
0.80
1.00
X/C

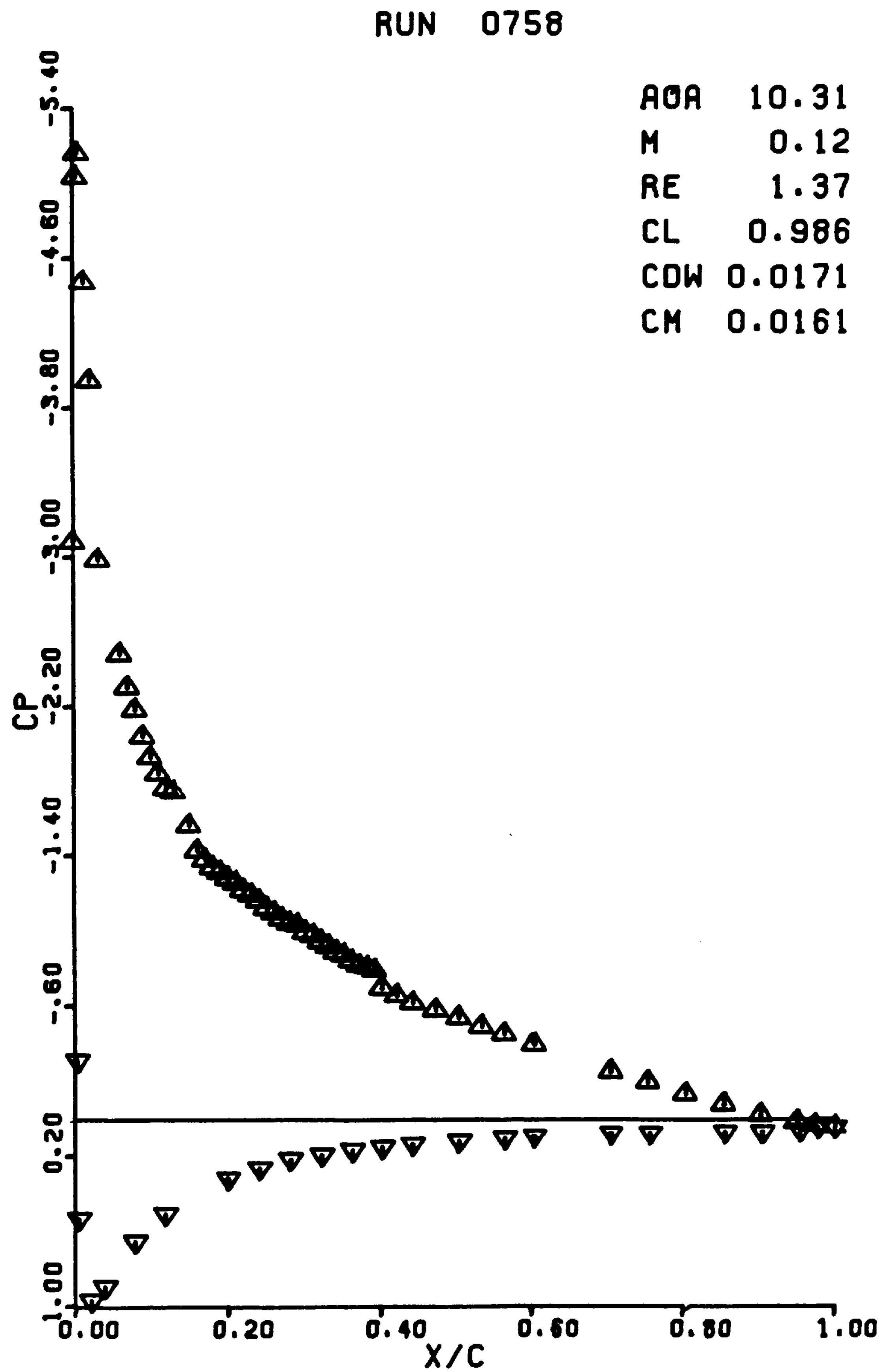
RUN 0758
AOA 10.31
M 0.12
RE 1.37
CL 0.986
CDW 0.0171
CM 0.0161
CP
-5.40
-4.60
-3.80
-3.00
-2.20
-1.40
-.60
0.20
1.00
0.00
0.20
0.40
0.60
0.80
1.00
X/C

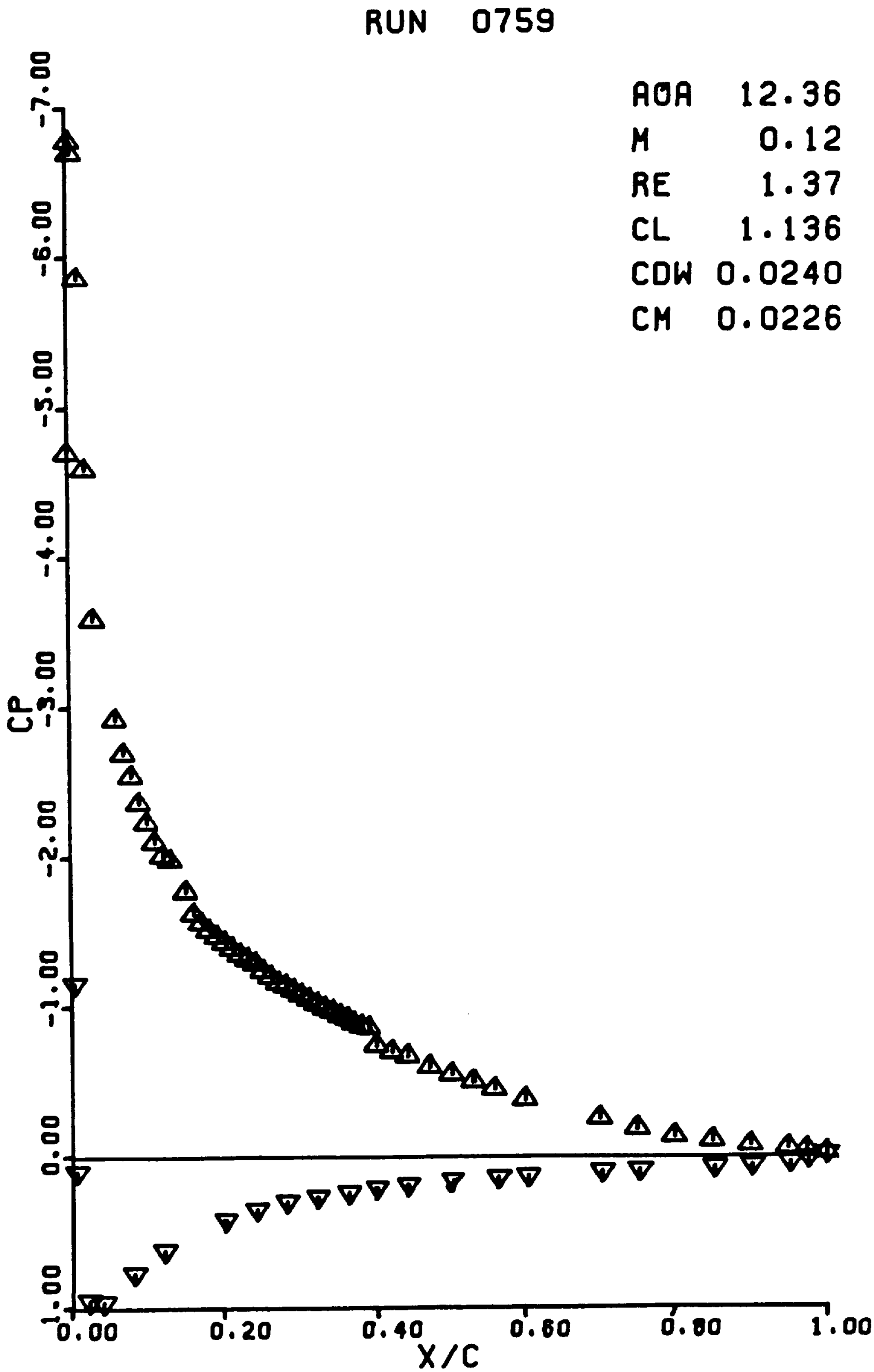

RUN 0759
AOA 12.36
M 0.12
RE 1.37
CL 1.136
CDW 0.0240
CM 0.0226
CP
-7.00
-6.00
-5.00
-4.00
-3.00
-2.00
-1.00
0.00
1.00
0.00
0.20
0.40
0.60
0.80
1.00
X/C

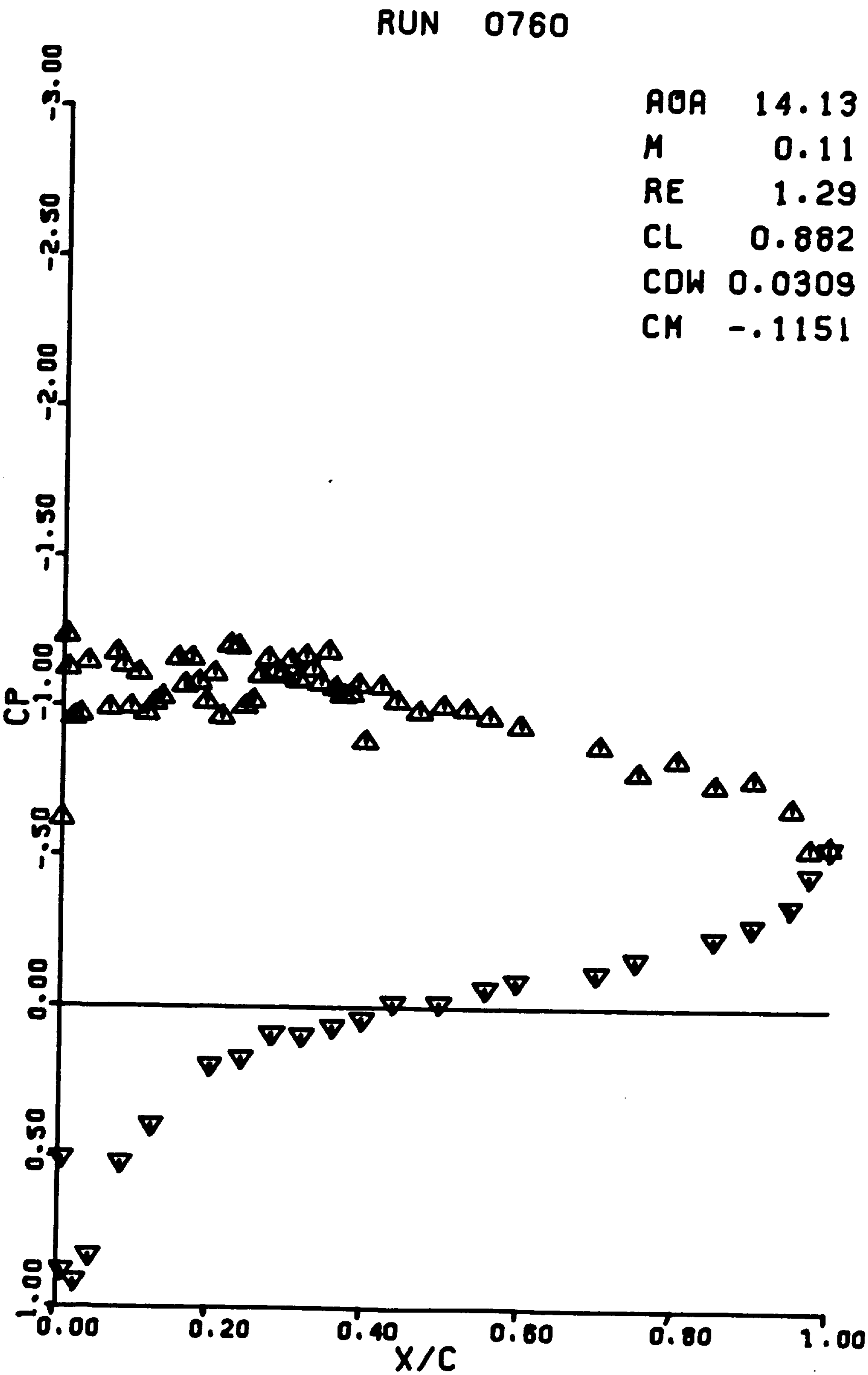

RUN 0760
AOA 14.13
M 0.11
RE 1.29
CL 0.882
CDW 0.0309
CM -.1151
CP
-3.00
-2.50
-2.00
-1.50
-1.00
-.50
0.00
0.50
1.00
0.00
0.20
0.40
0.60
0.80
1.00
X/C

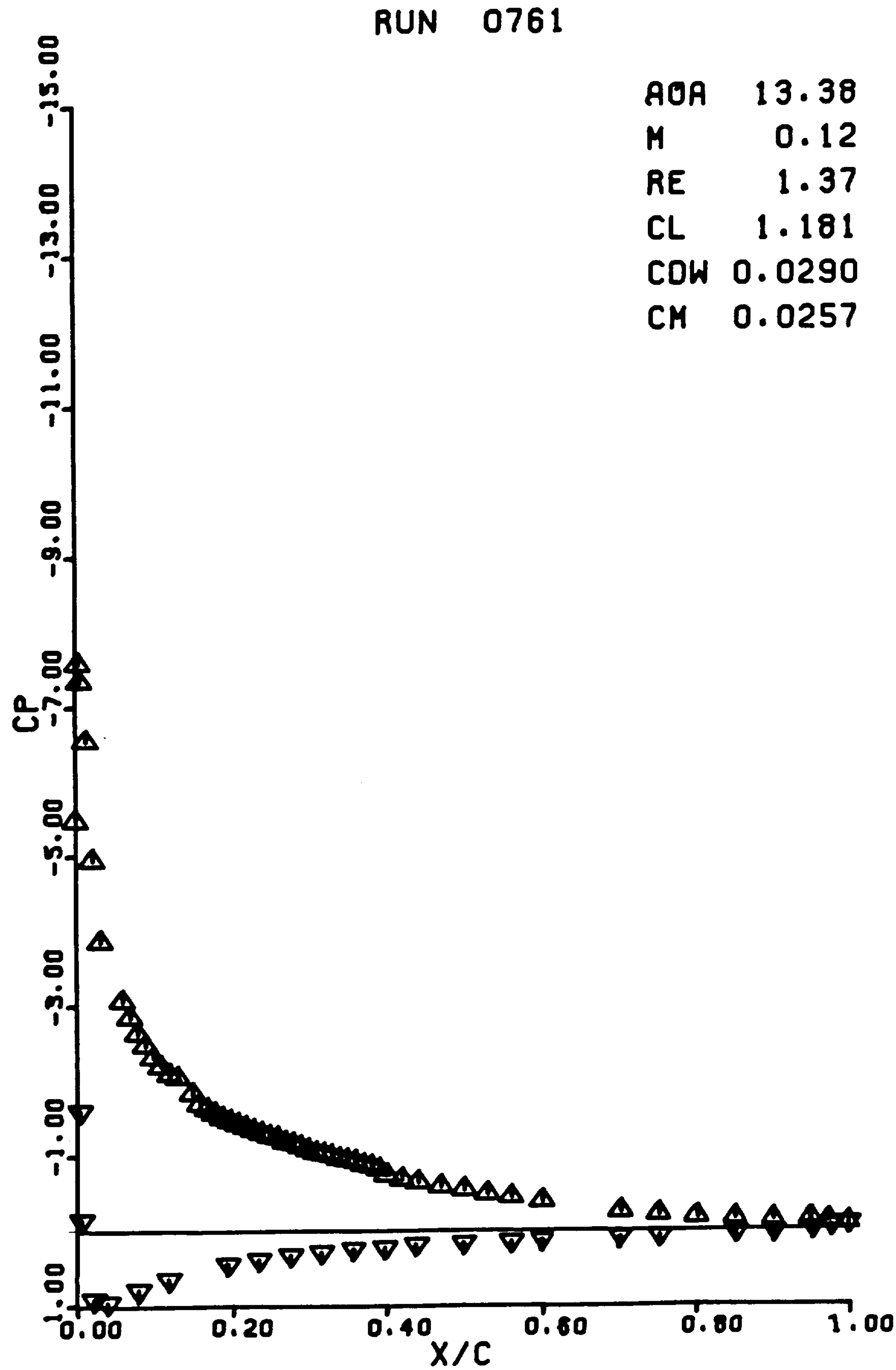
RUN 0761
AOA 13.38
M 0.12
RE 1.37
CL 1.181
CDW 0.0290
CM 0.0257
CP
-15.00
-13.00
-11.00
-9.00
-7.00
-5.00
-3.00
-1.00
1.00
0.00
0.20
0.40
0.60
0.80
1.00
X/C

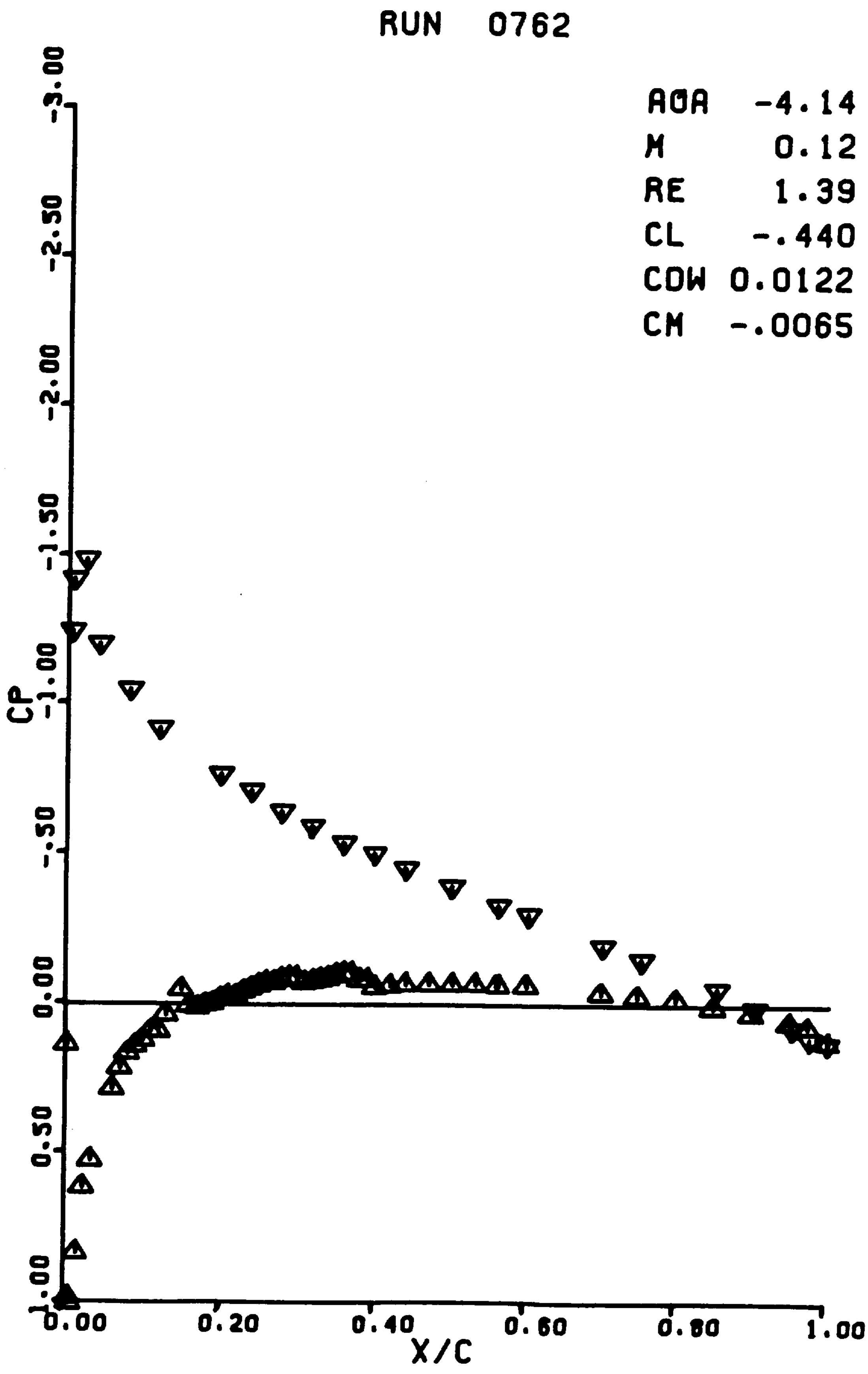

RUN 0762
AOA -4.14
M 0.12
RE 1.39
CL -.440
CDW 0.0122
CM -.0065
CP
-3.00
-2.50
-2.00
-1.50
-1.00
-.50
0.00
0.50
1.00
0.00
0.20
0.40
0.60
0.80
1.00
X/C

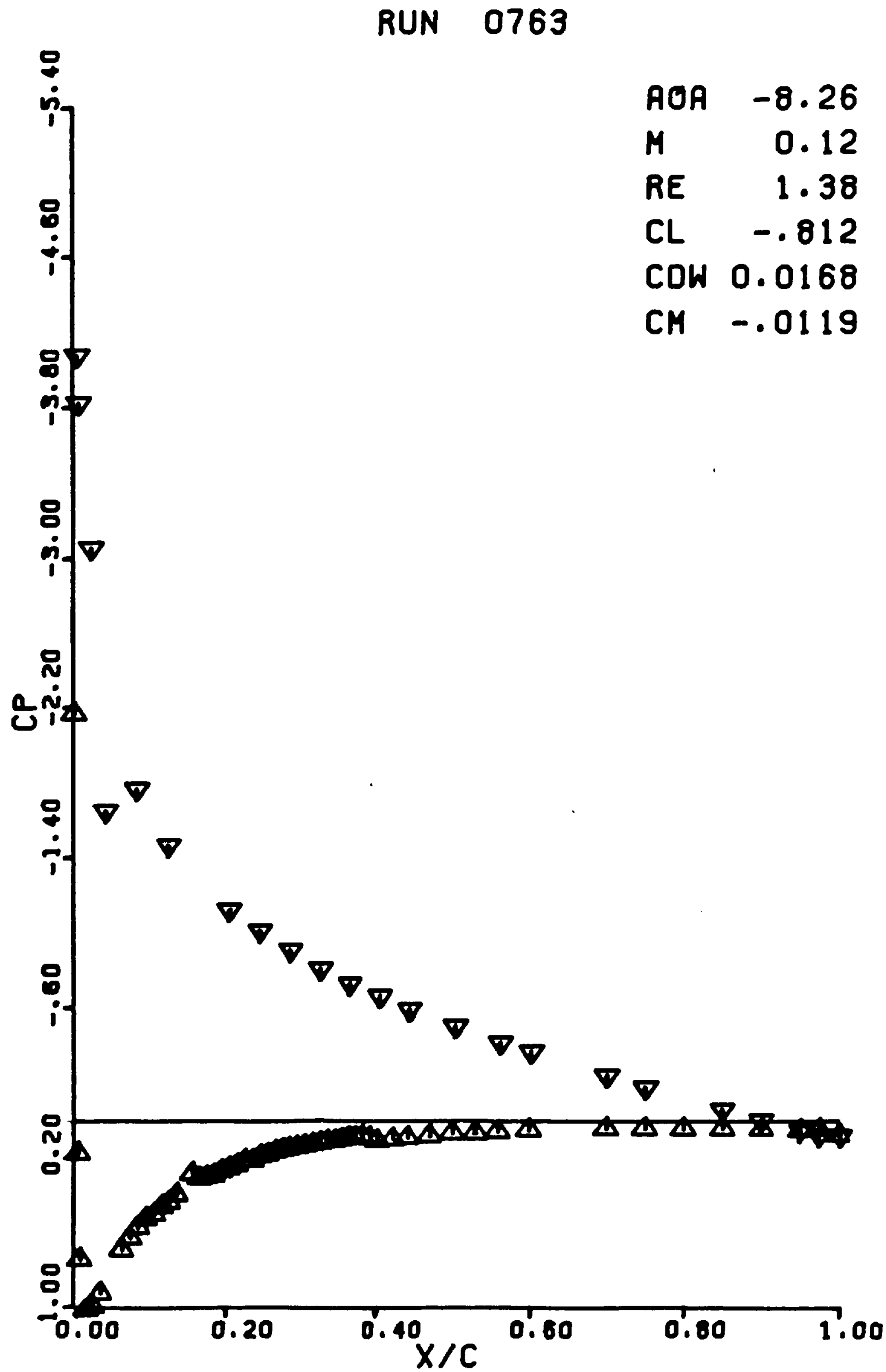
RUN 0763
AOA -8.26
M 0.12
RE 1.38
CL -.812
CDW 0.0168
CM -.0119
CP
X/C
-5.40
-4.60
-3.80
-3.00
-2.20
-1.40
-.60
0.20
1.00
0.00
0.20
0.40
0.60
0.80
1.00

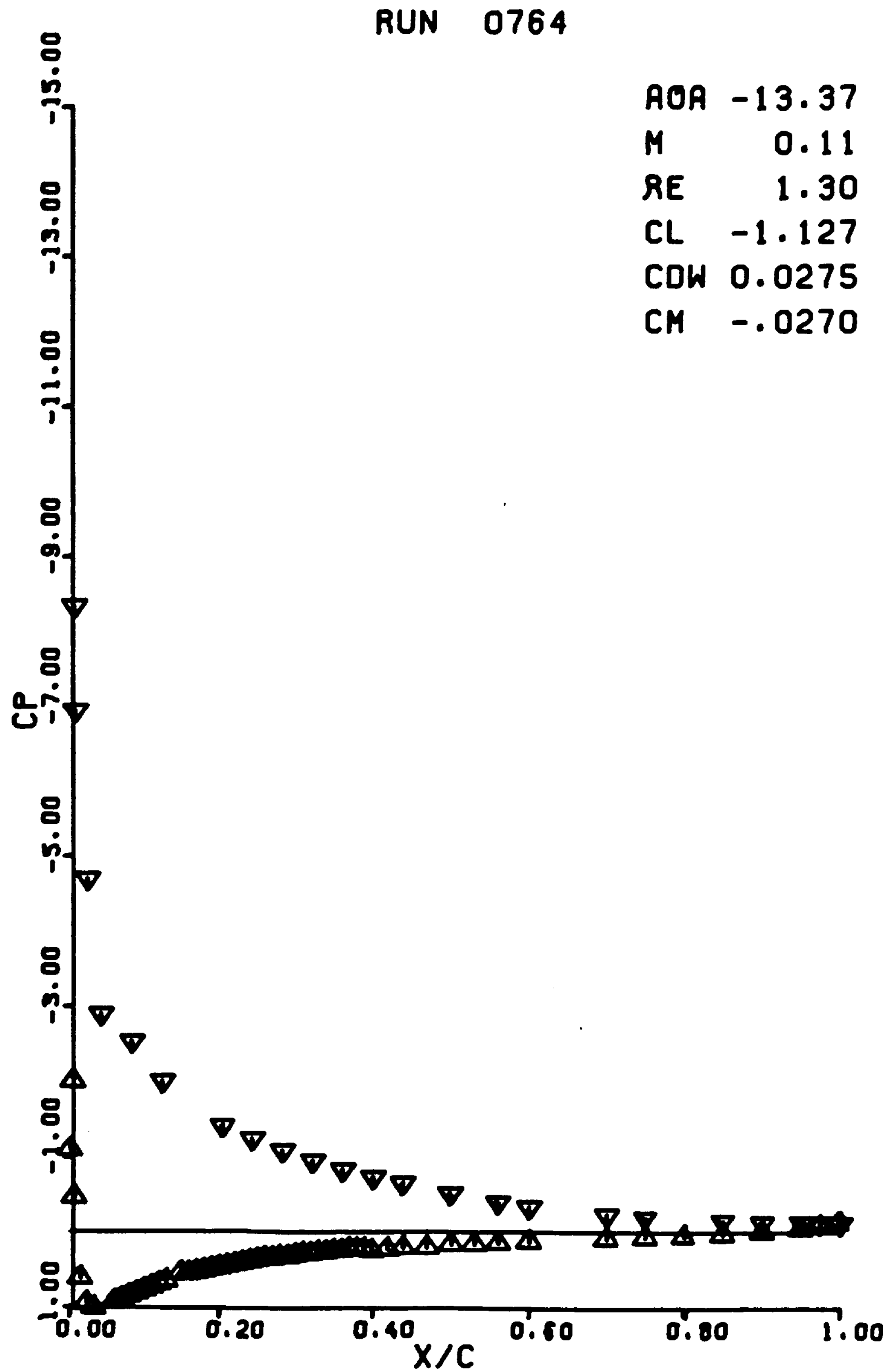
RUN 0764
AOA -13.37
M 0.11
RE 1.30
CL -1.127
CDW 0.0275
CM -.0270
CP
-15.00
-13.00
-11.00
-9.00
-7.00
-5.00
-3.00
-1.00
1.00
0.00
0.20
0.40
0.60
0.80
1.00
X/C

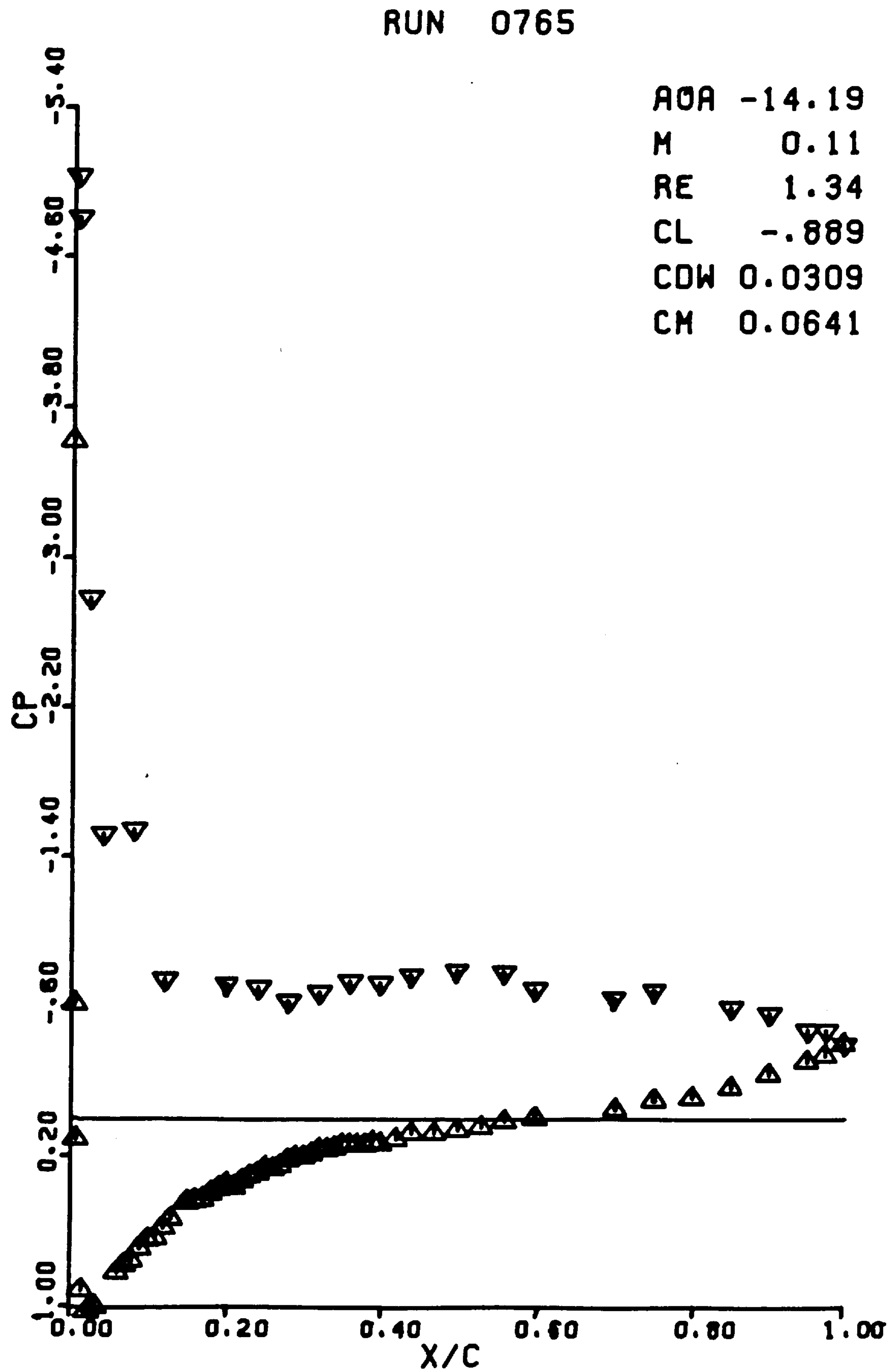

RUN 0765
AOA -14.19
M 0.11
RE 1.34
CL -.889
CDW 0.0309
CM 0.0641
CP
X/C

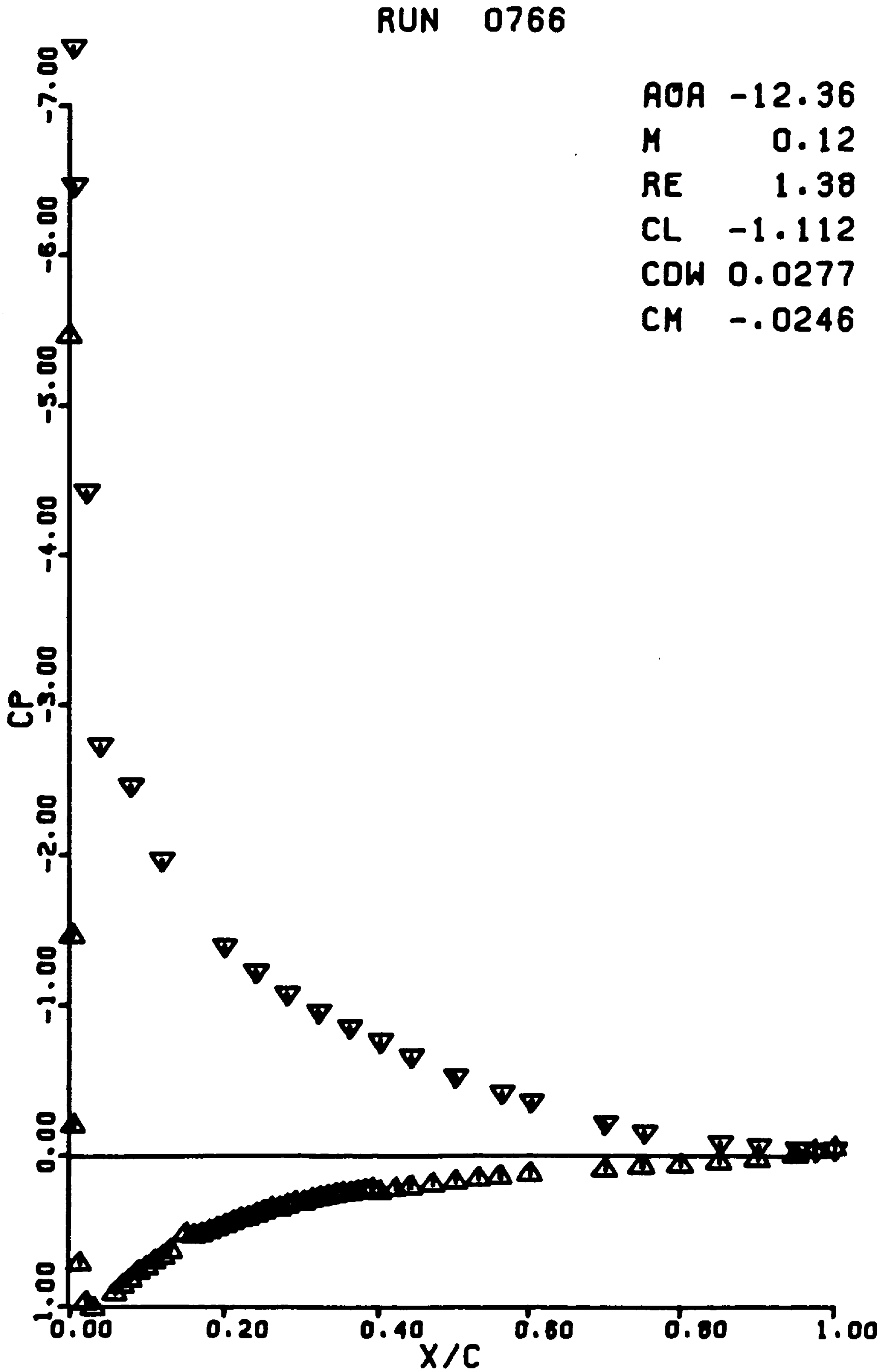
RUN 0766
AOA -12.36
M 0.12
RE 1.38
CL -1.112
CDW 0.0277
CM -.0246
CP
-7.00
-6.00
-5.00
-4.00
-3.00
-2.00
-1.00
0.00
1.00
0.00
0.20
0.40
0.60
0.80
1.00
X/C

APPENDIX C

WAKE SURVEYS

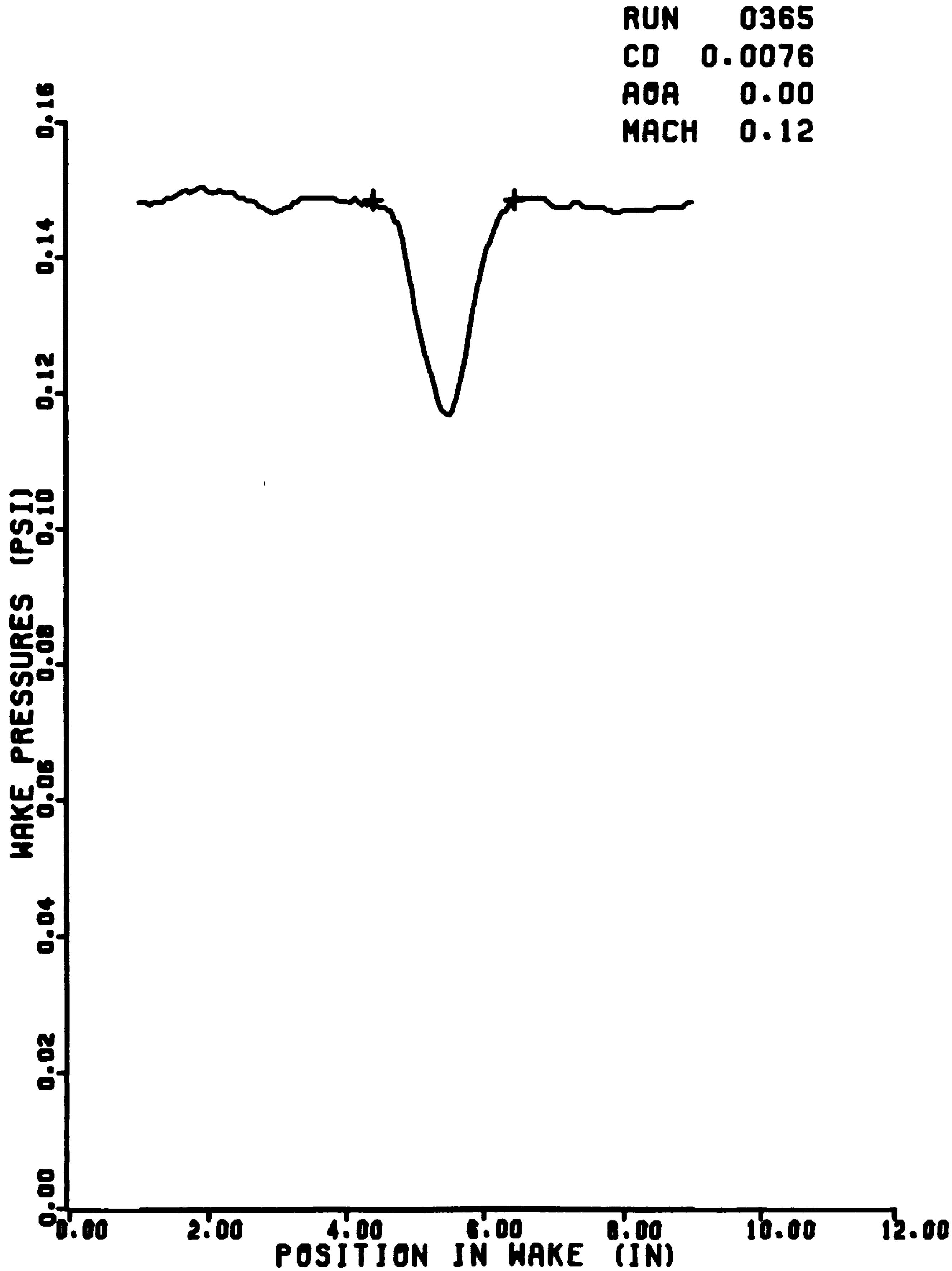
RUN 0365
CD 0.0076
AOA 0.00
MACH 0.12
WAKE PRESSURES (PSI)
0.00
0.02
0.04
0.06
0.08
0.10
0.12
0.14
0.16
0.00
2.00
4.00
6.00
8.00
10.00
12.00
POSITION IN WAKE (IN)

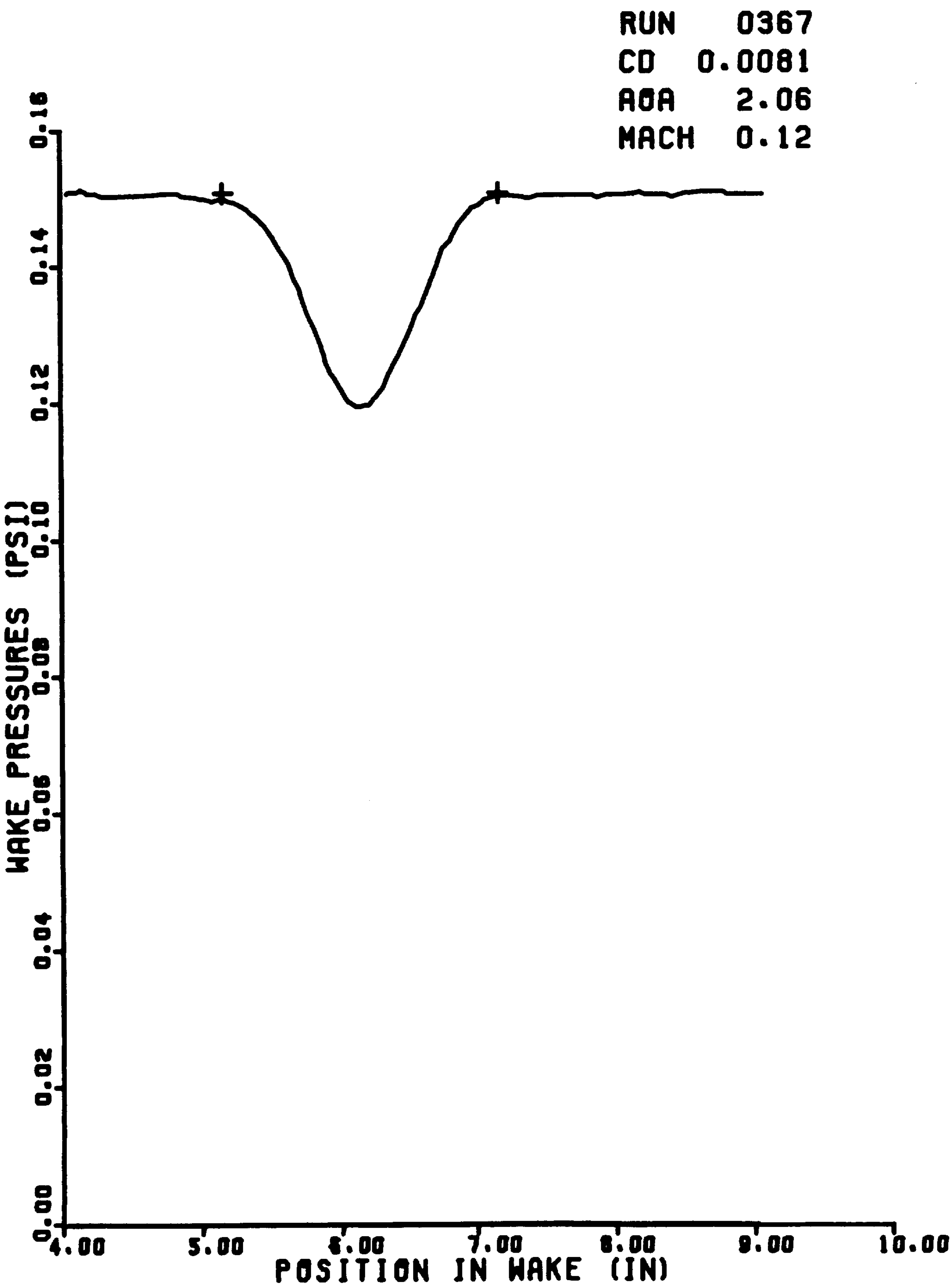

RUN 0367
CD 0.0081
AOA 2.06
MACH 0.12
WAKE PRESSURES (PSI)
0.00
0.02
0.04
0.06
0.08
0.10
0.12
0.14
0.16
4.00
5.00
6.00
7.00
8.00
9.00
10.00
POSITION IN WAKE (IN)

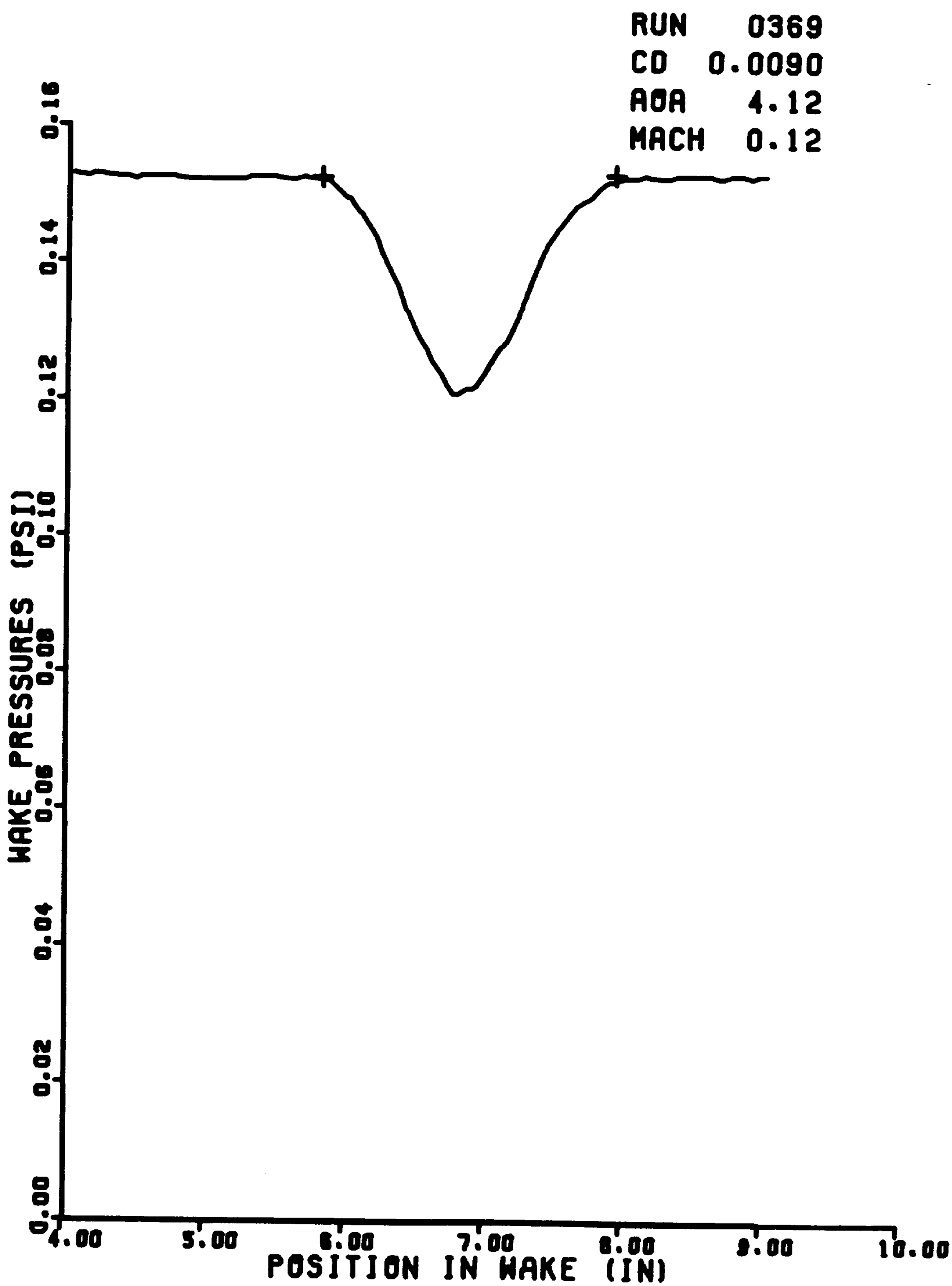
RUN 0369
CD 0.0090
AOA 4.12
MACH 0.12
WAKE PRESSURES (PSI)
0.00
0.02
0.04
0.06
0.08
0.10
0.12
0.14
0.16
4.00
5.00
6.00
7.00
8.00
9.00
10.00
POSITION IN WAKE (IN)

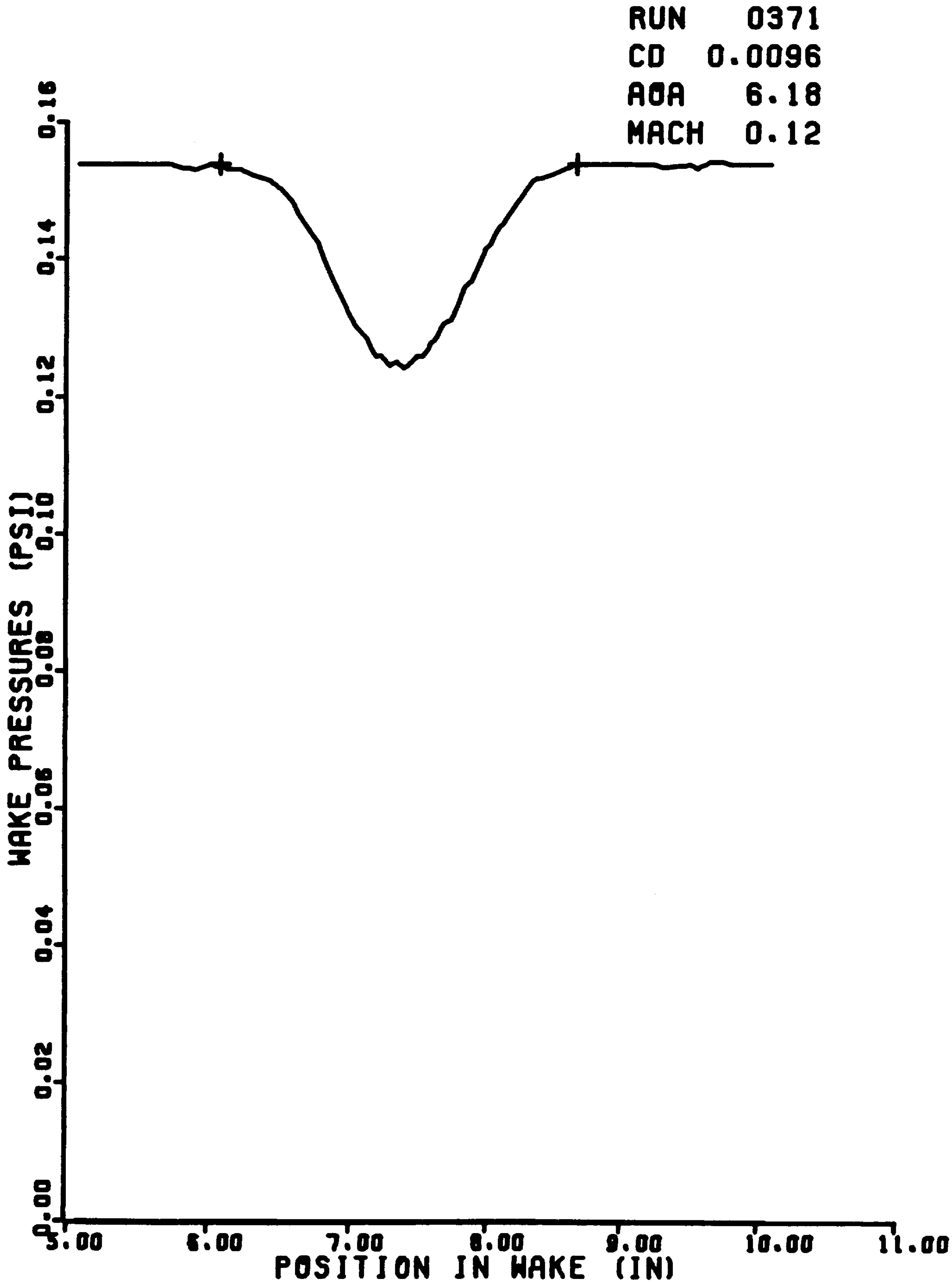
RUN 0371
CD 0.0096
AOA 6.18
MACH 0.12
WAKE PRESSURES (PSI)
0.00
0.02
0.04
0.06
0.08
0.10
0.12
0.14
0.16
5.00
6.00
7.00
8.00
9.00
10.00
11.00
POSITION IN WAKE (IN)

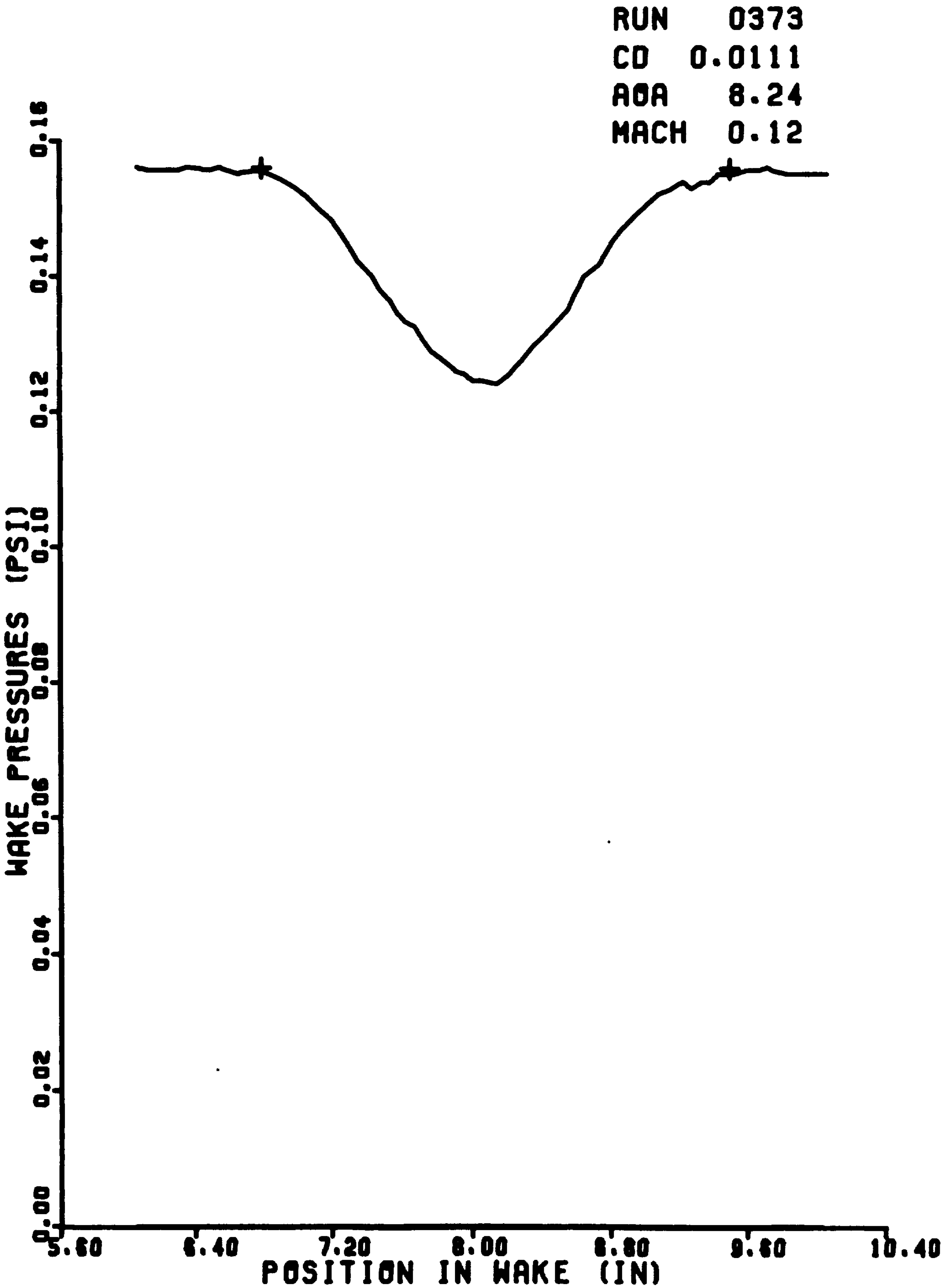
RUN 0373
CD 0.0111
AOA 8.24
MACH 0.12
WAKE PRESSURES (PSI)
0.00
0.02
0.04
0.06
0.08
0.10
0.12
0.14
0.16
5.60
6.40
7.20
8.00
8.80
9.60
10.40
POSITION IN WAKE (IN)

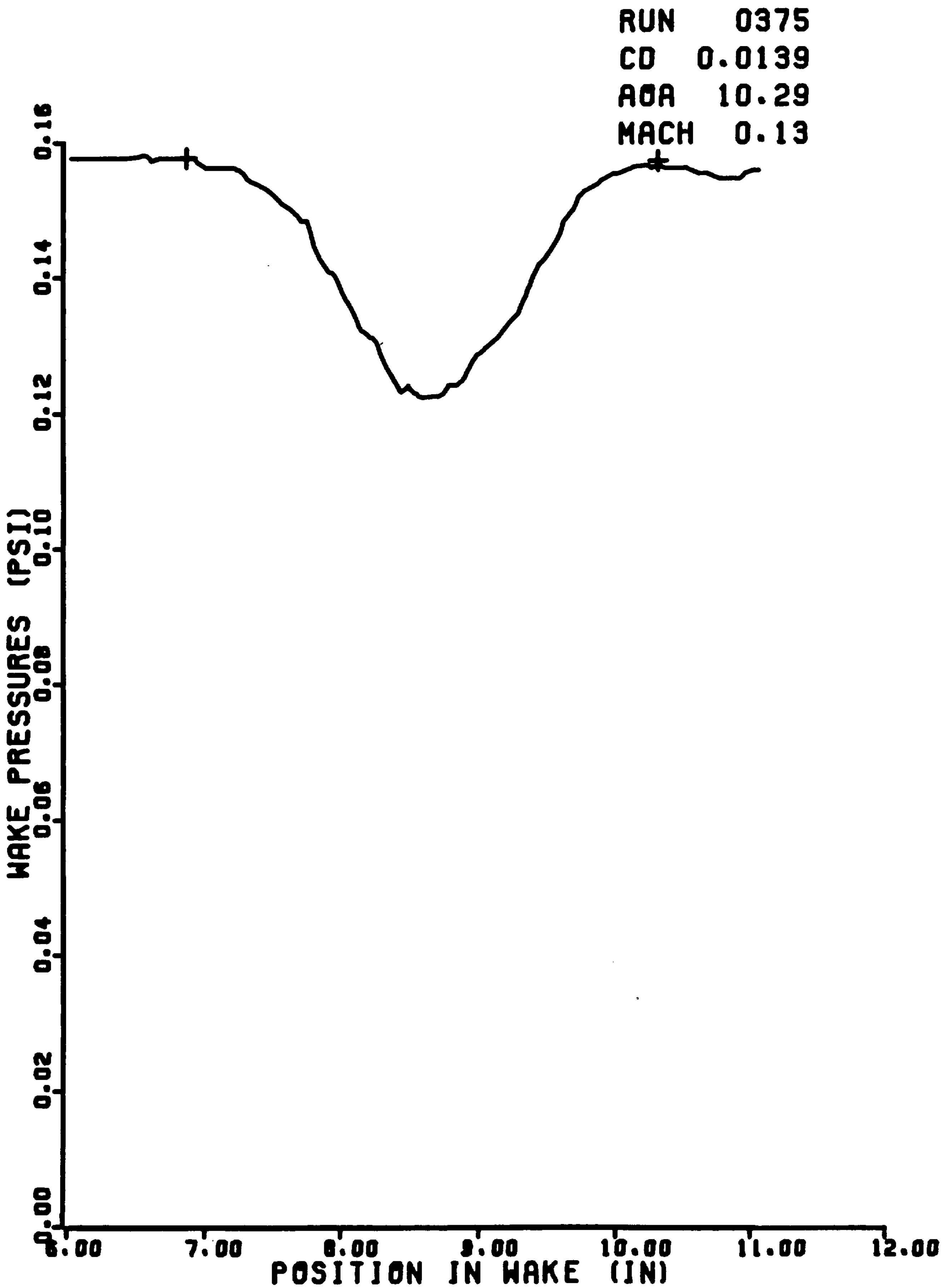
RUN 0375
CD 0.0139
AOA 10.29
MACH 0.13
WAKE PRESSURES (PSI)
0.00
0.02
0.04
0.06
0.08
0.10
0.12
0.14
0.16
6.00
7.00
8.00
9.00
10.00
11.00
12.00
POSITION IN WAKE (IN)

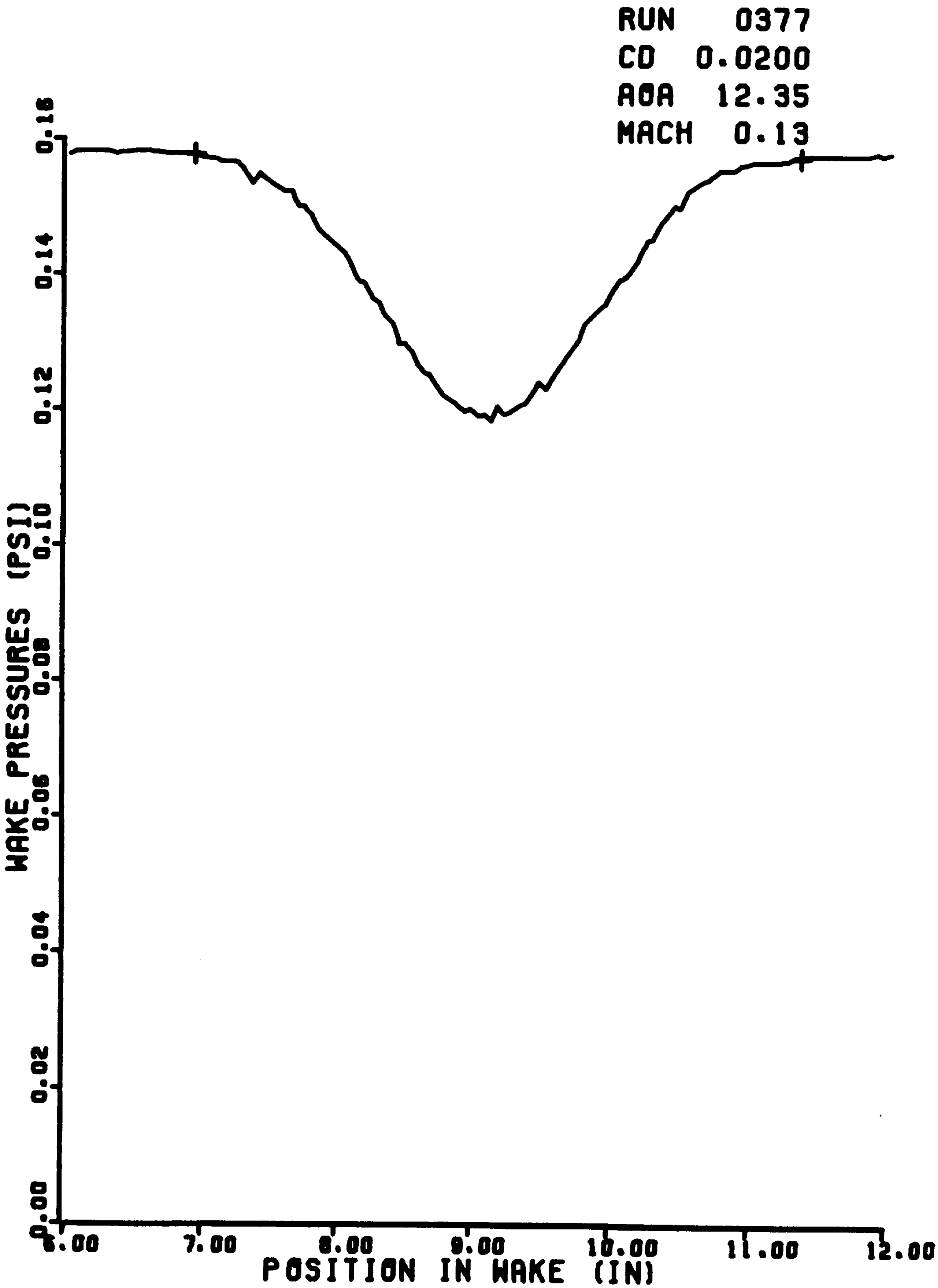

RUN 0377
CD 0.0200
AOA 12.35
MACH 0.13
WAKE PRESSURES (PSI)
0.00
0.02
0.04
0.06
0.08
0.10
0.12
0.14
0.16
6.00
7.00
8.00
9.00
10.00
11.00
12.00
POSITION IN WAKE (IN)

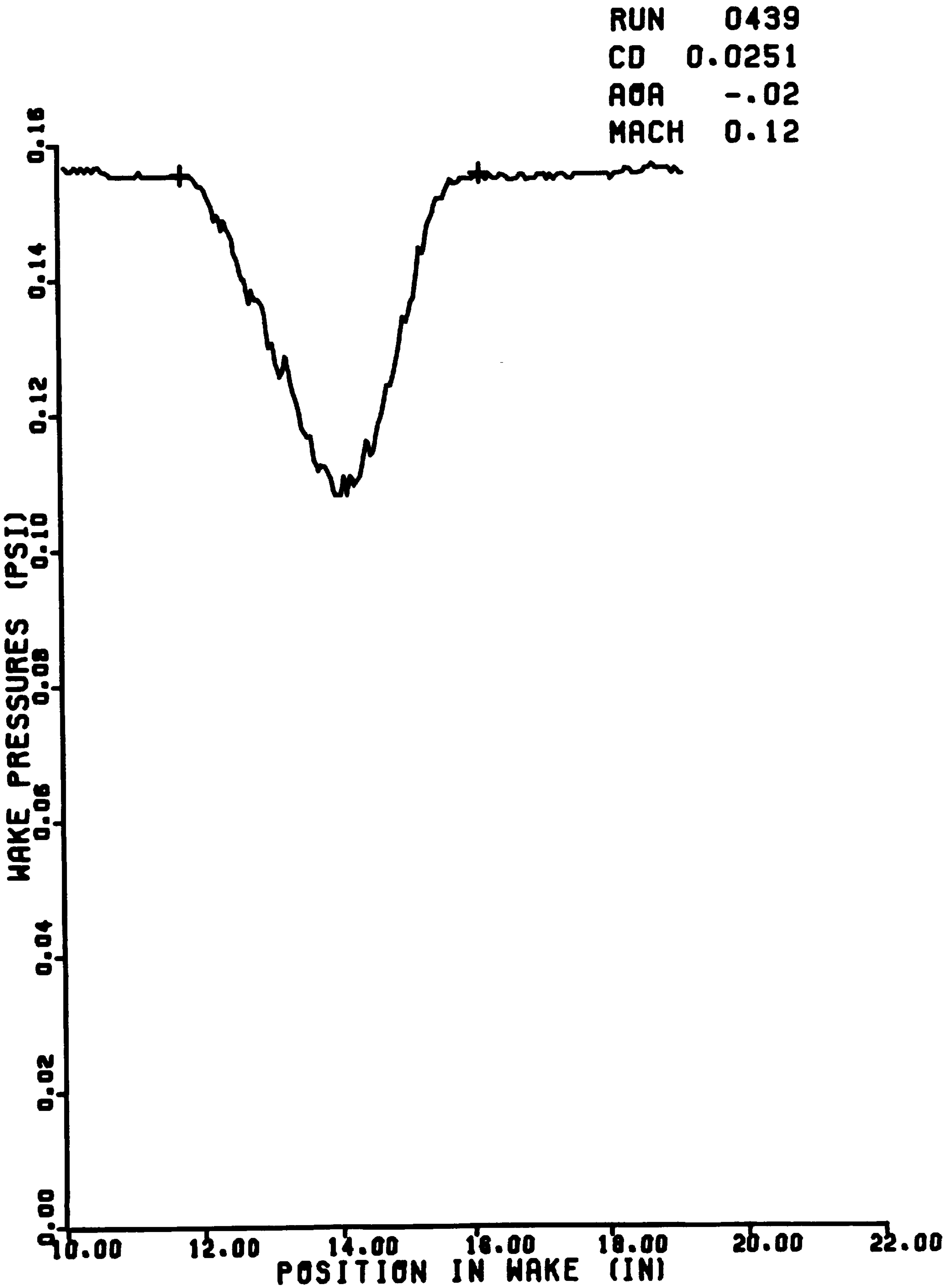
RUN 0439
CD 0.0251
AOA -.02
MACH 0.12
WAKE PRESSURES (PSI)
0.00
0.02
0.04
0.06
0.08
0.10
0.12
0.14
0.16
10.00
12.00
14.00
16.00
18.00
20.00
22.00
POSITION IN WAKE (IN)

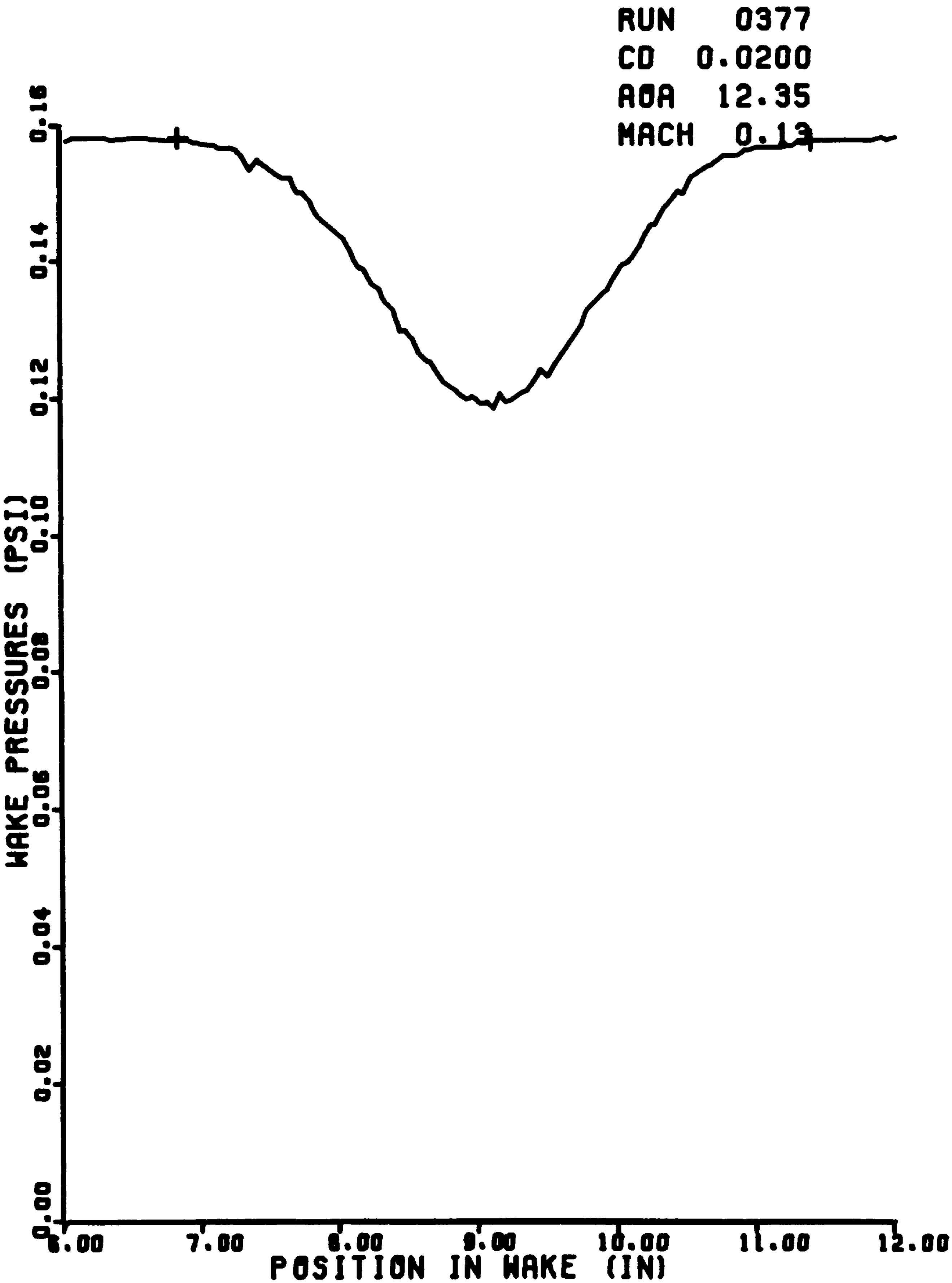
RUN 0377
CD 0.0200
AOA 12.35
MACH 0.13
WAKE PRESSURES (PSI)
0.00
0.02
0.04
0.06
0.08
0.10
0.12
0.14
0.16
6.00
7.00
8.00
9.00
10.00
11.00
12.00
POSITION IN WAKE (IN)

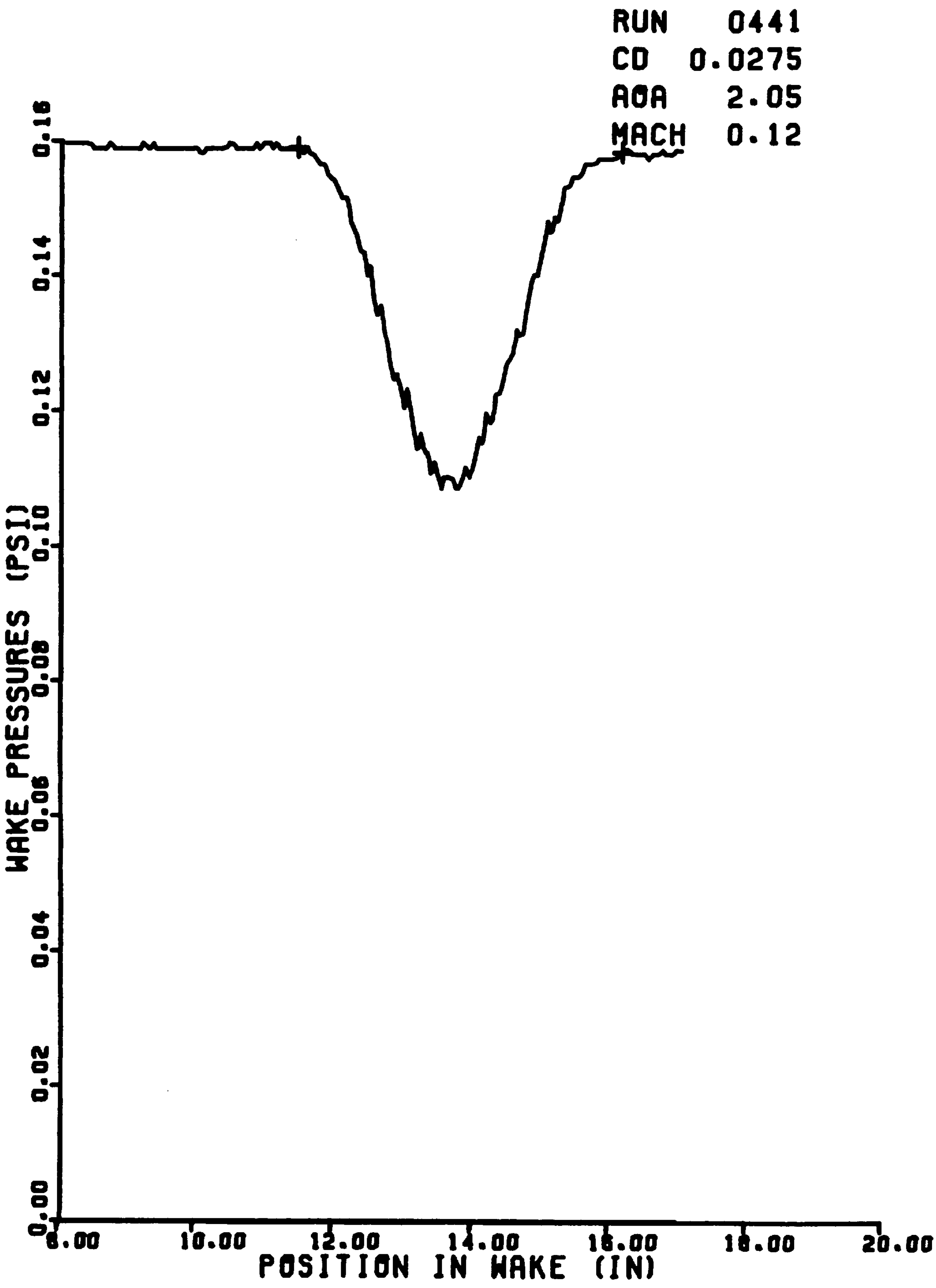
RUN 0441
CD 0.0275
AOA 2.05
MACH 0.12
WAKE PRESSURES (PSI)
0.16
0.14
0.12
0.10
0.08
0.06
0.04
0.02
0.00
8.00
10.00
12.00
14.00
16.00
18.00
20.00
POSITION IN WAKE (IN)

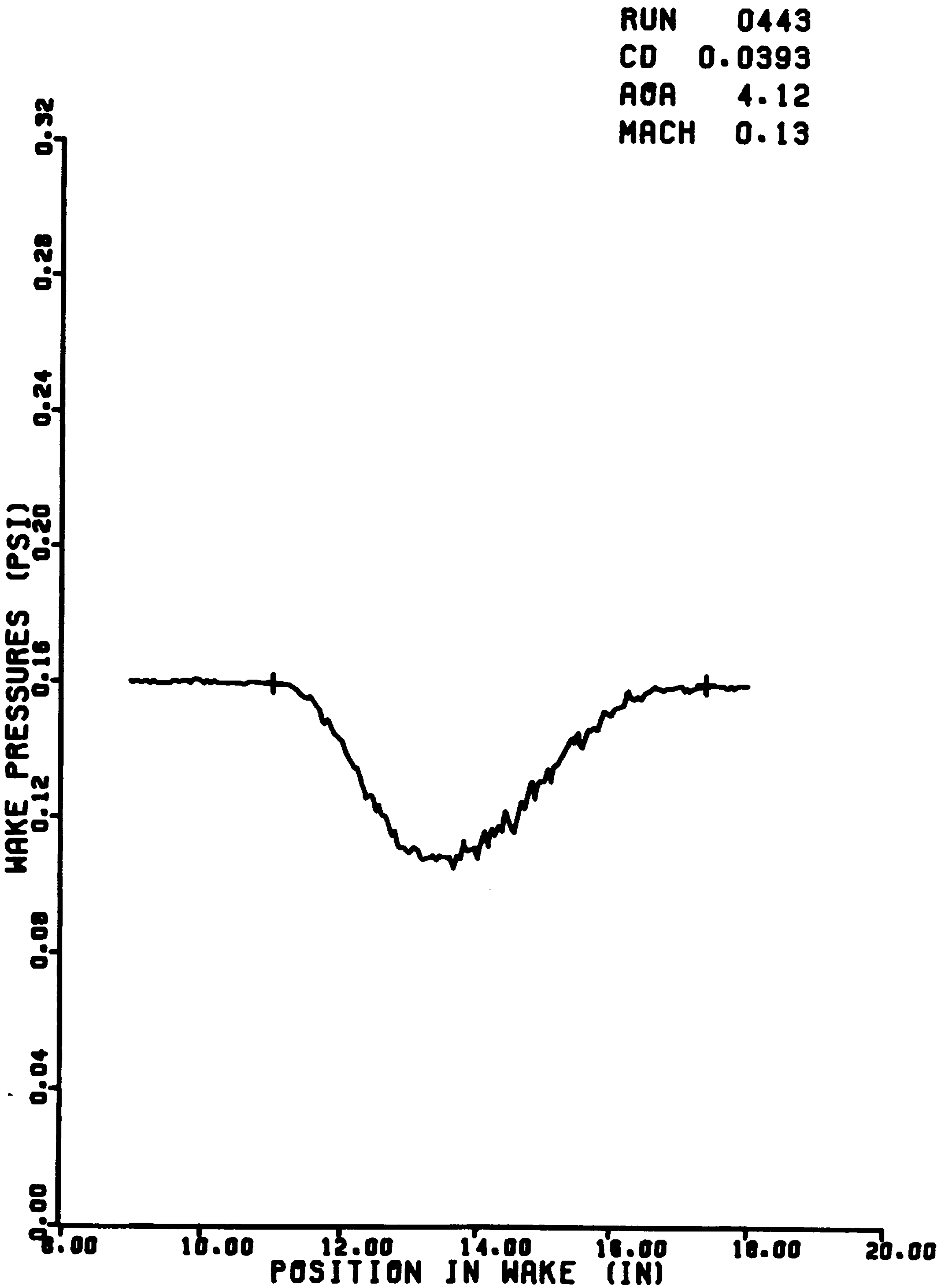
RUN 0443
CD 0.0393
AOA 4.12
MACH 0.13
WAKE PRESSURES (PSI)
0.00
0.04
0.08
0.12
0.16
0.20
0.24
0.28
0.32
8.00
10.00
12.00
14.00
16.00
18.00
20.00
POSITION IN WAKE (IN)

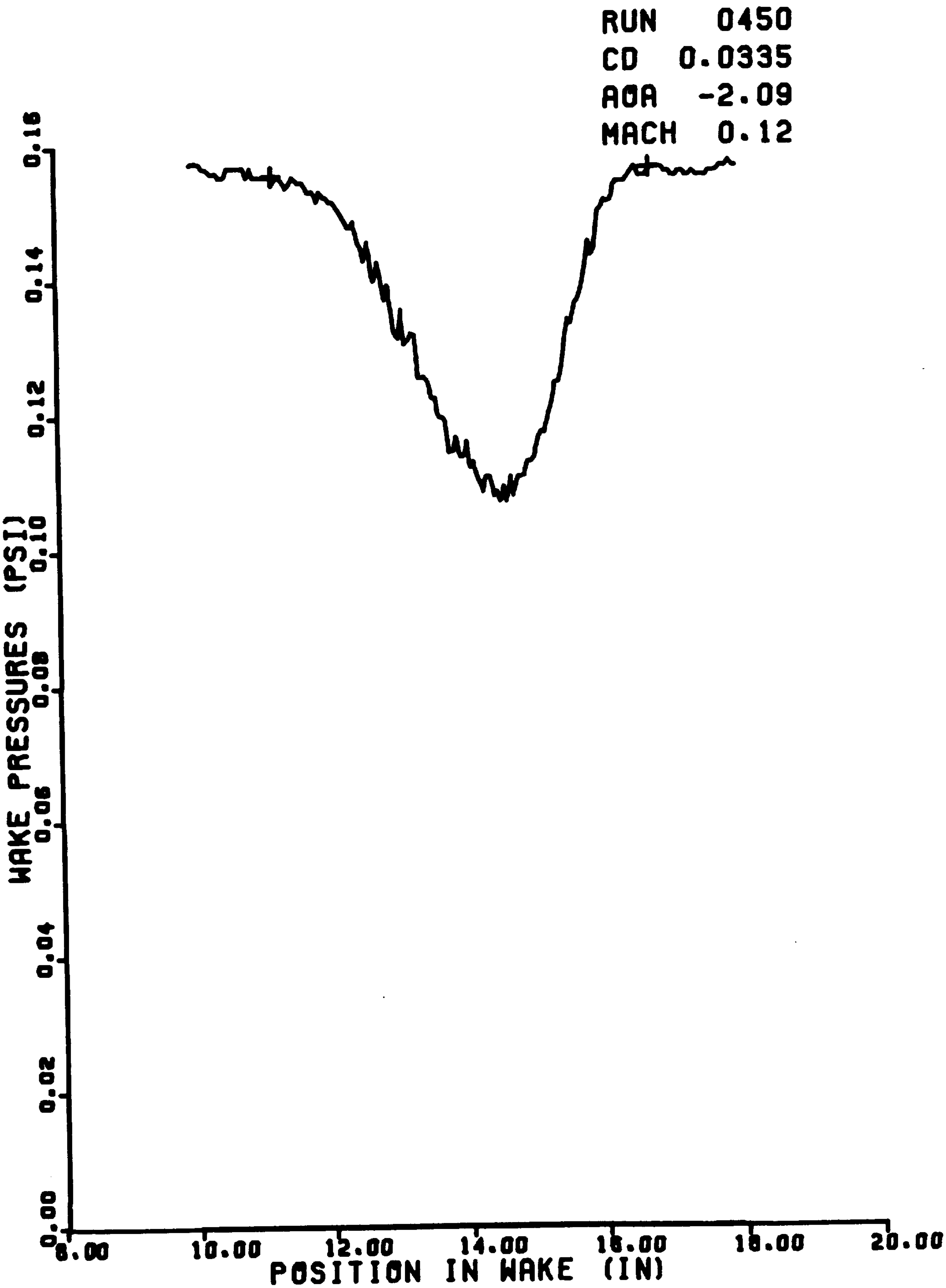
RUN 0450
CD 0.0335
AOA -2.09
MACH 0.12
WAKE PRESSURES (PSI)
0.00
0.02
0.04
0.06
0.08
0.10
0.12
0.14
0.16
8.00
10.00
12.00
14.00
16.00
18.00
20.00
POSITION IN WAKE (IN)

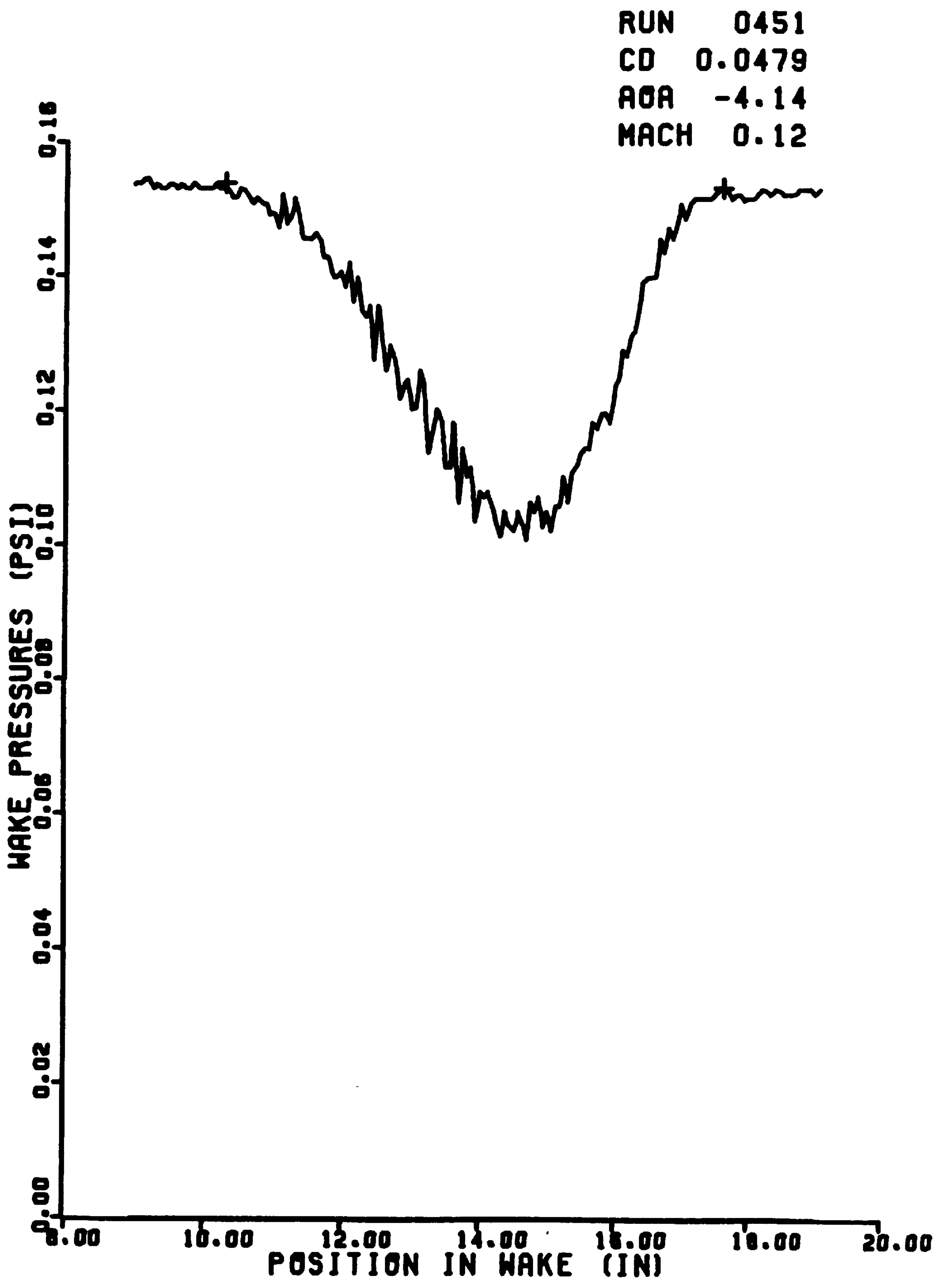
RUN 0451
CD 0.0479
AOA -4.14
MACH 0.12
WAKE PRESSURES (PSI)
0.00
0.02
0.04
0.06
0.08
0.10
0.12
0.14
0.16
8.00
10.00
12.00
14.00
16.00
18.00
20.00
POSITION IN WAKE (IN)

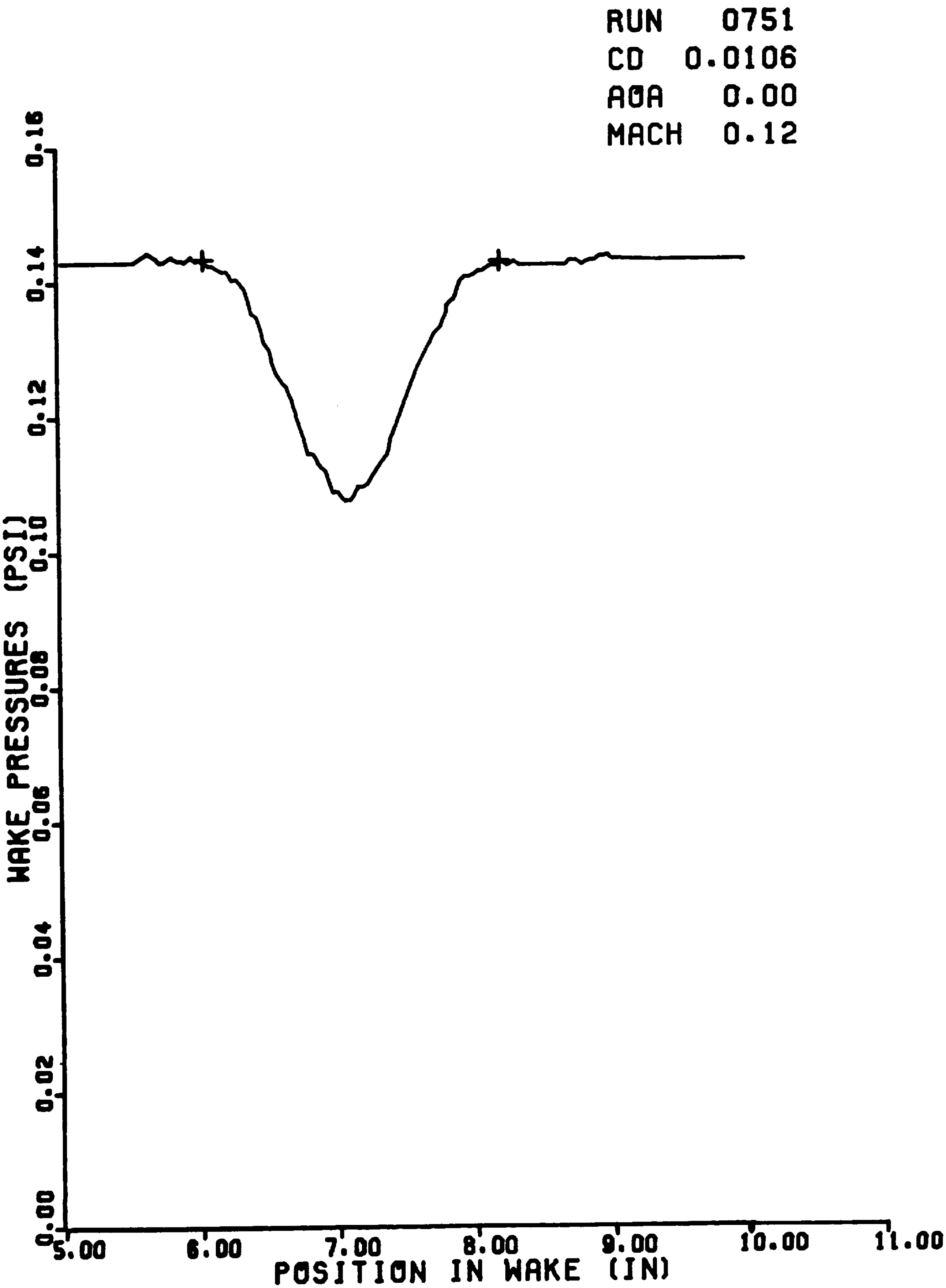
RUN 0751
CD 0.0106
AOA 0.00
MACH 0.12
WAKE PRESSURES (PSI)
0.00
0.02
0.04
0.06
0.08
0.10
0.12
0.14
0.16
5.00
6.00
7.00
8.00
9.00
10.00
11.00
POSITION IN WAKE (IN)

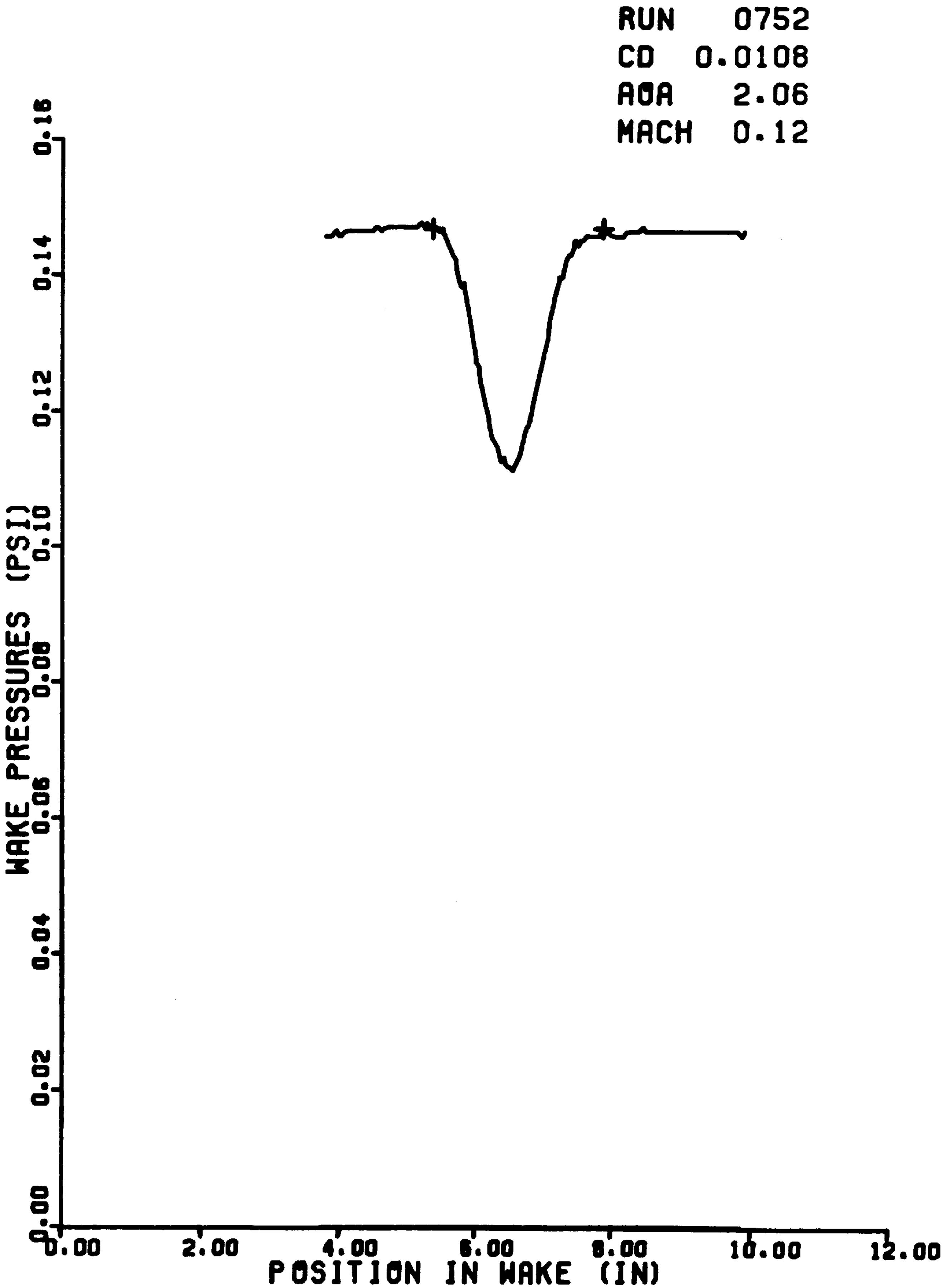
RUN 0752
CD 0.0108
AOA 2.06
MACH 0.12
WAKE PRESSURES (PSI)
0.00
0.02
0.04
0.06
0.08
0.10
0.12
0.14
0.16
0.00
2.00
4.00
6.00
8.00
10.00
12.00
POSITION IN WAKE (IN)

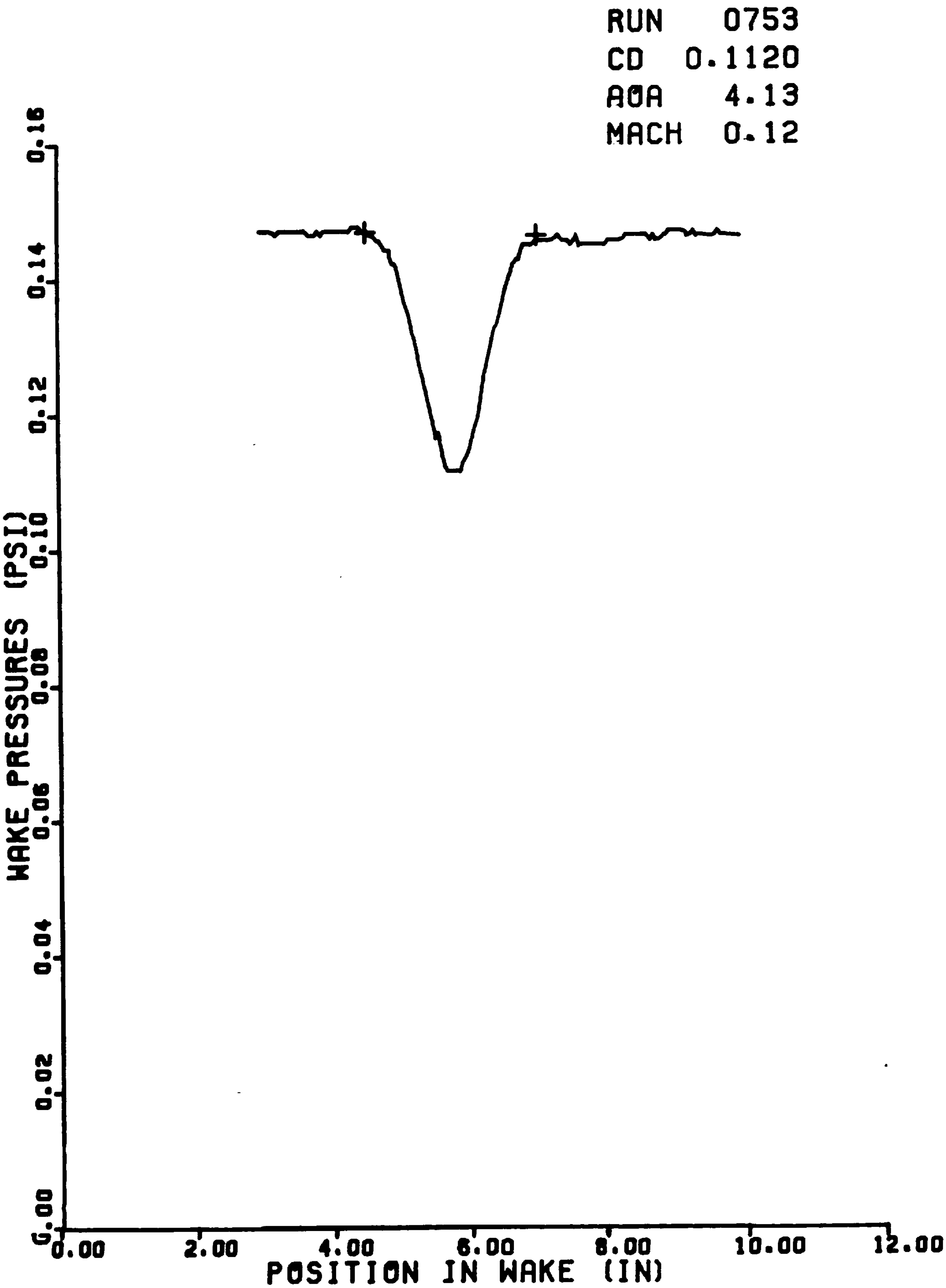
RUN 0753
CD 0.1120
AOA 4.13
MACH 0.12
WAKE PRESSURES (PSI)
0.00
0.02
0.04
0.06
0.08
0.10
0.12
0.14
0.16
0.00
2.00
4.00
6.00
8.00
10.00
12.00
POSITION IN WAKE (IN)

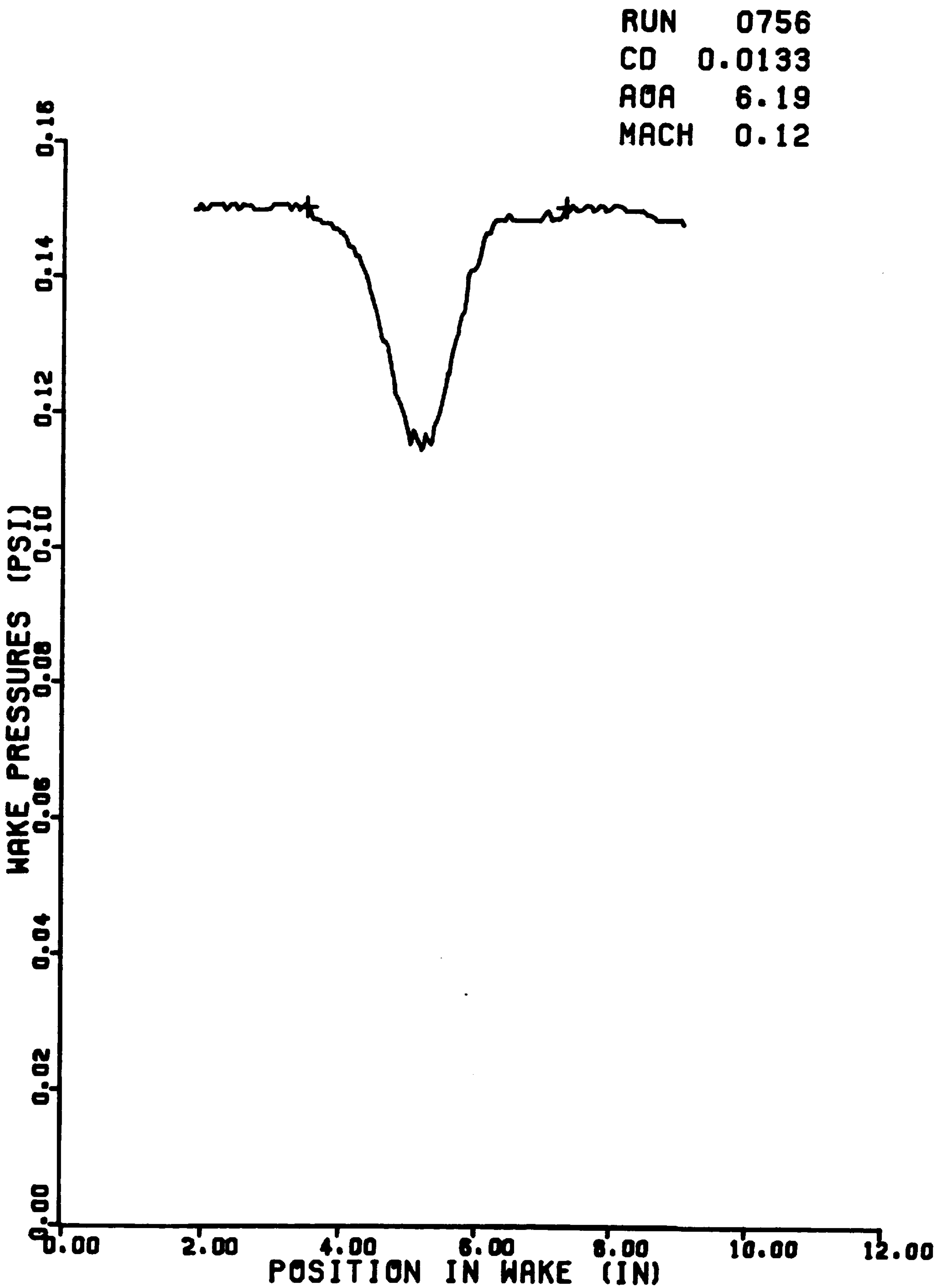
RUN 0756
CD 0.0133
AOA 6.19
MACH 0.12
WAKE PRESSURES (PSI)
0.00
0.02
0.04
0.06
0.08
0.10
0.12
0.14
0.16
0.00
2.00
4.00
6.00
8.00
10.00
12.00
POSITION IN WAKE (IN)

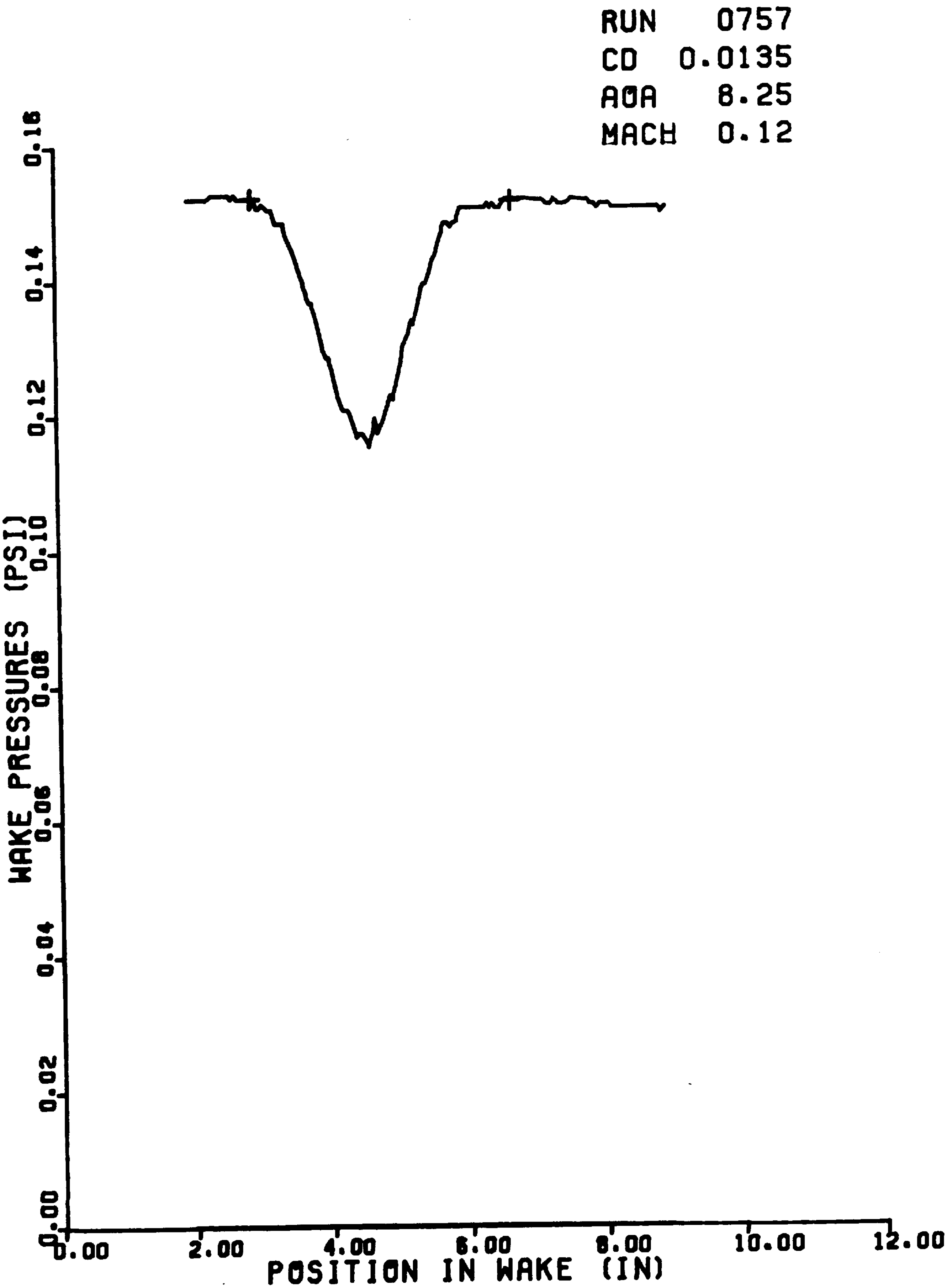
RUN 0757
CD 0.0135
AOA 8.25
MACH 0.12
WAKE PRESSURES (PSI)
0.00
0.02
0.04
0.06
0.08
0.10
0.12
0.14
0.16
0.00
2.00
4.00
6.00
8.00
10.00
12.00
POSITION IN WAKE (IN)

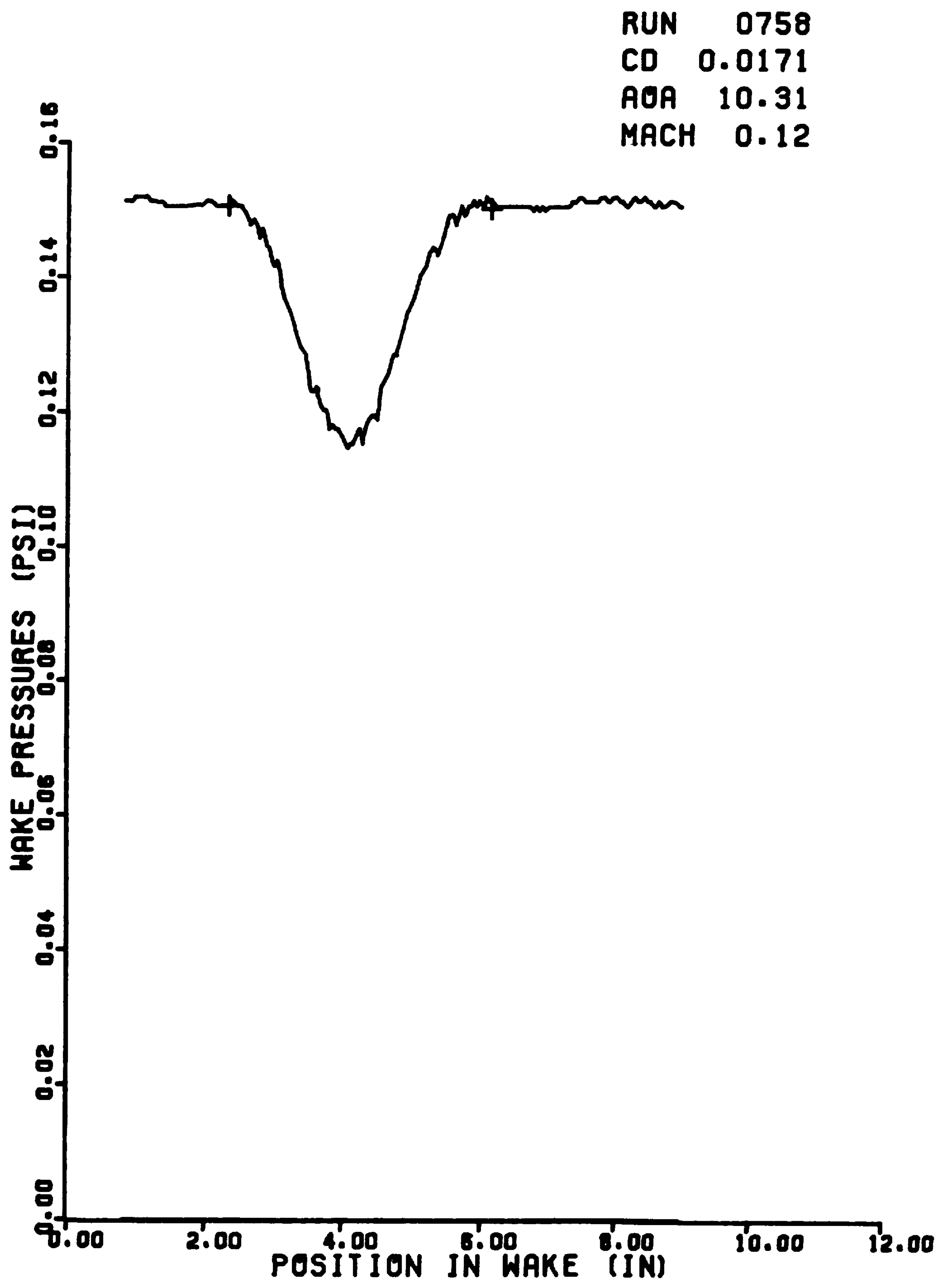
RUN 0758
CD 0.0171
AOA 10.31
MACH 0.12
WAKE PRESSURES (PSI)
0.00
0.02
0.04
0.06
0.08
0.10
0.12
0.14
0.16
0.00
2.00
4.00
6.00
8.00
10.00
12.00
POSITION IN WAKE (IN)

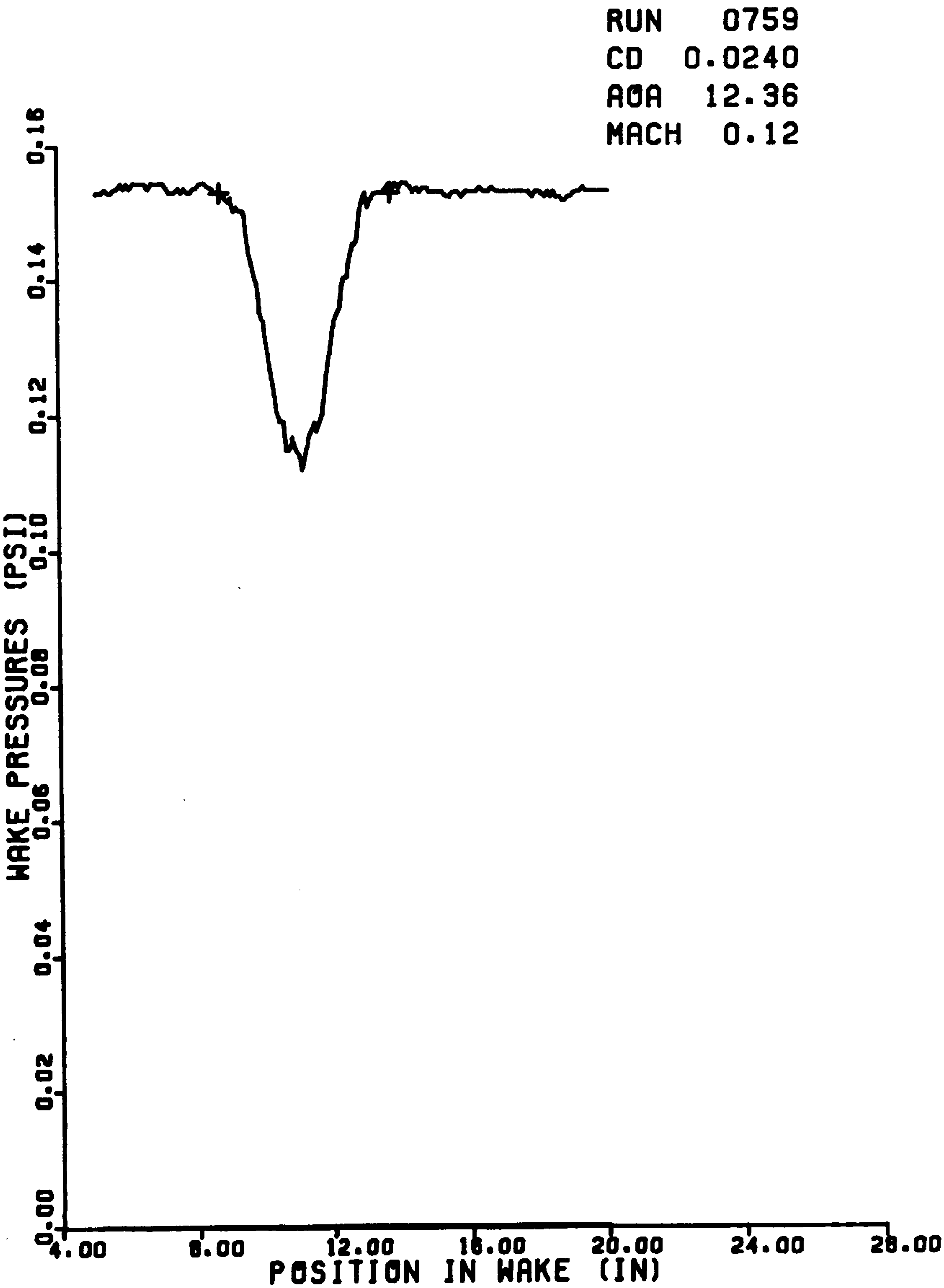
RUN 0759
CD 0.0240
AOA 12.36
MACH 0.12
WAKE PRESSURES (PSI)
0.00
0.02
0.04
0.06
0.08
0.10
0.12
0.14
0.16
4.00
8.00
12.00
16.00
20.00
24.00
28.00
POSITION IN WAKE (IN)

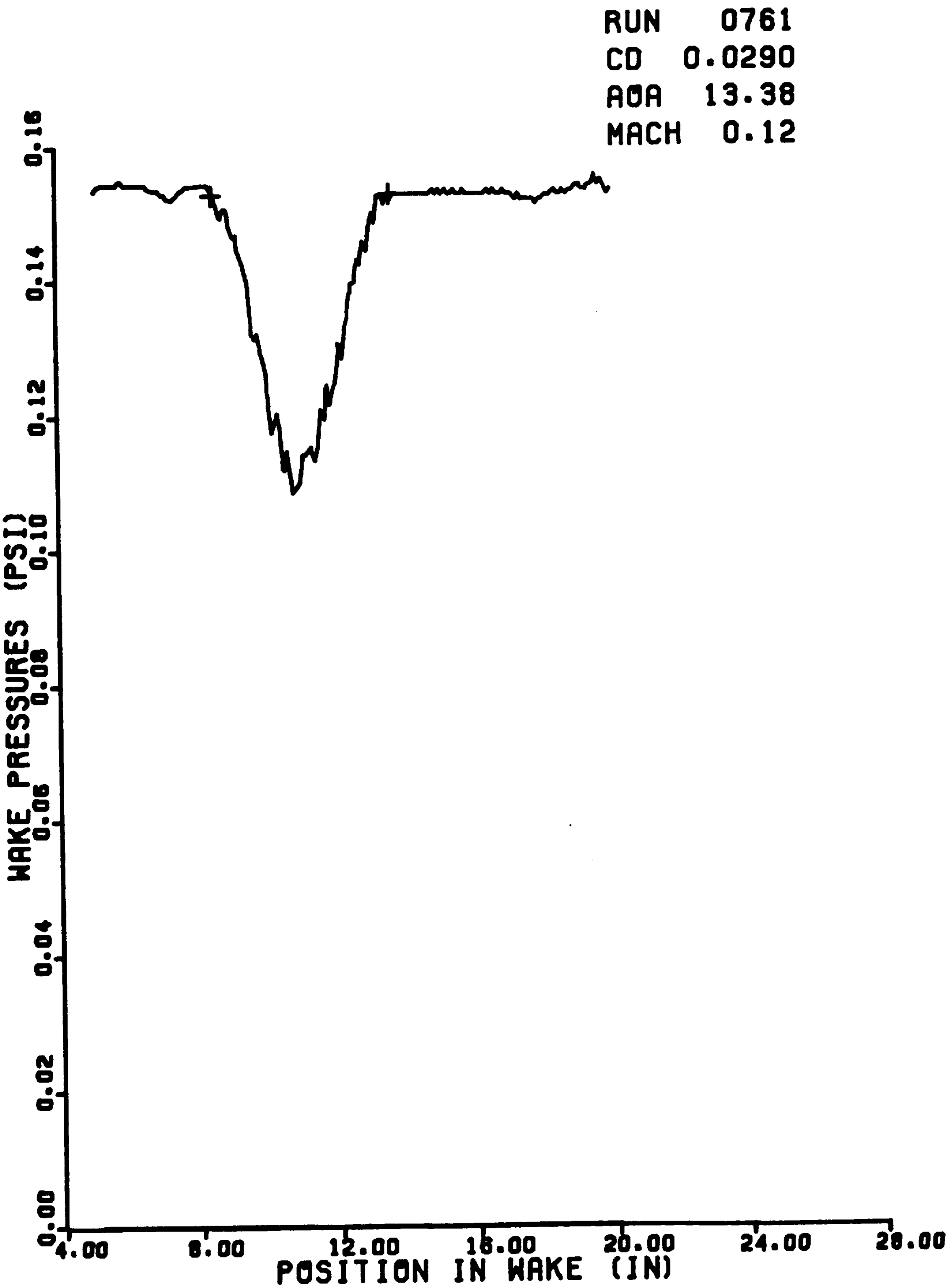
RUN 0761
CD 0.0290
AOA 13.38
MACH 0.12
WAKE PRESSURES (PSI)
0.00
0.02
0.04
0.06
0.08
0.10
0.12
0.14
0.16
4.00
8.00
12.00
16.00
20.00
24.00
28.00
POSITION IN WAKE (IN)

APPENDIX D

VELOCITY PROFILES

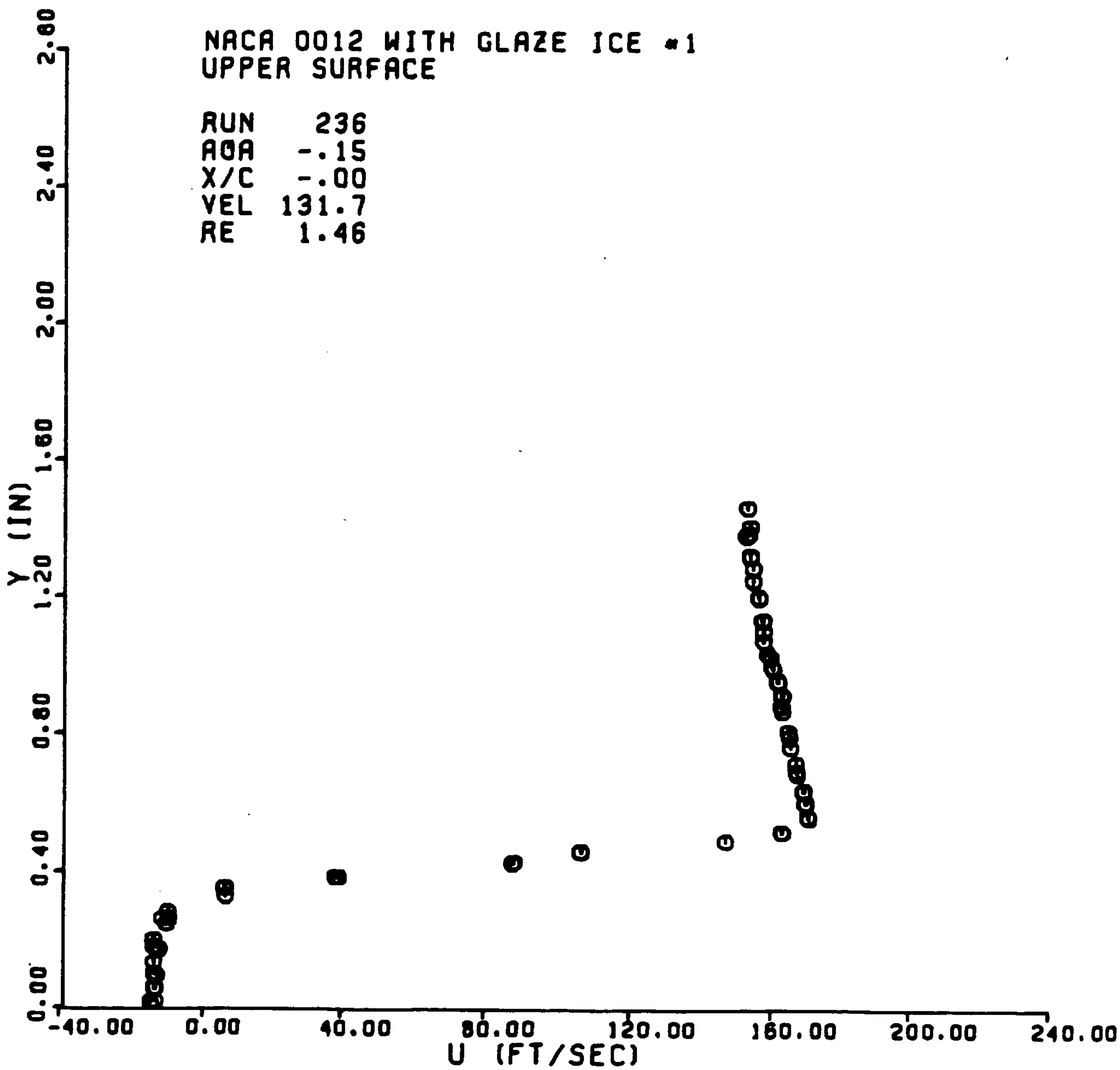

NACA 0012 WITH GLAZE ICE #1
UPPER SURFACE
RUN 236
AOA -.15
X/C -.00
VEL 131.7
RE 1.46
Y (IN)
0.00
0.40
0.80
1.20
1.60
2.00
2.40
2.80
-40.00
0.00
40.00
80.00
120.00
160.00
200.00
240.00
U (FT/SEC)

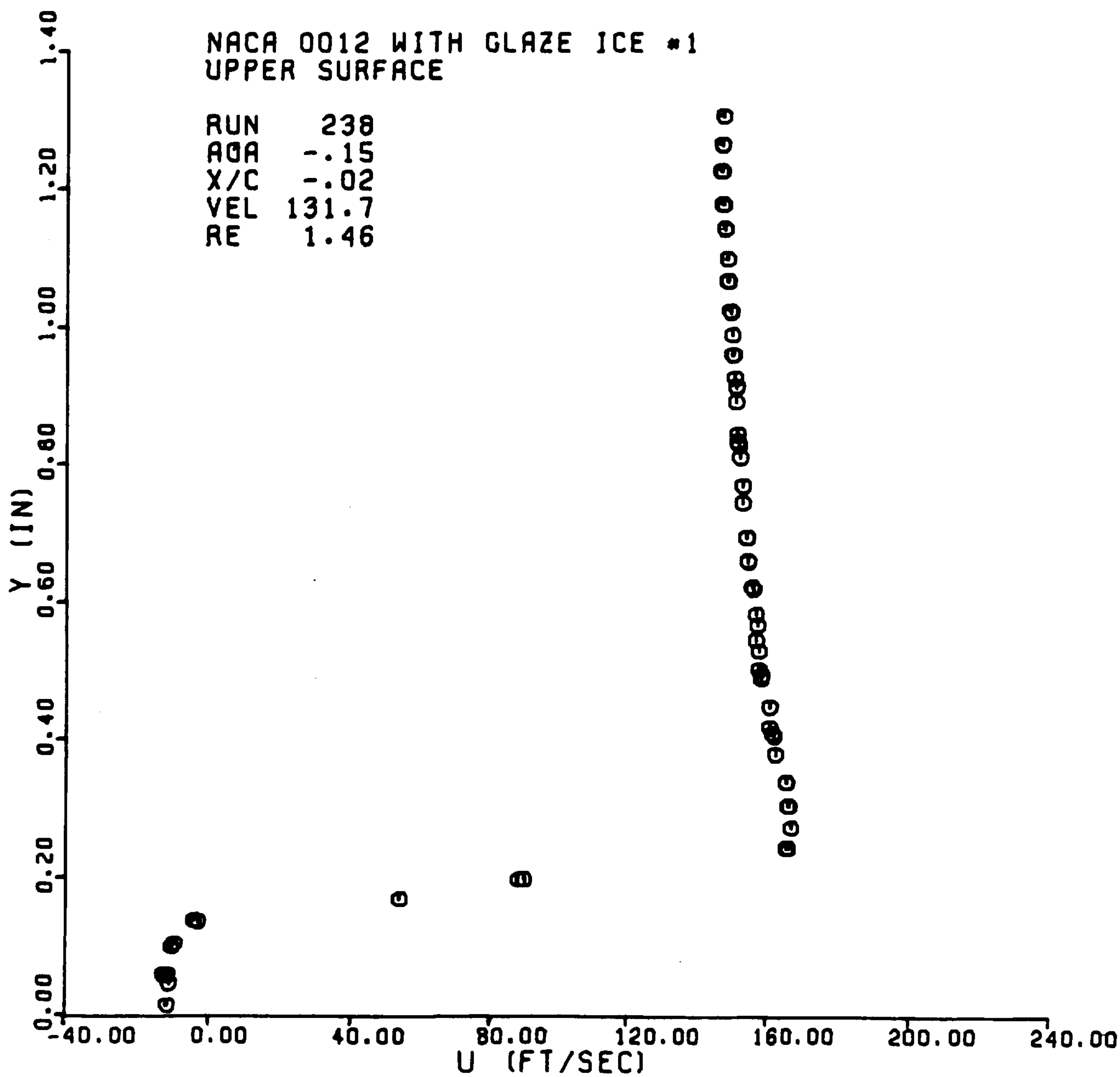

NACA 0012 WITH GLAZE ICE #1
UPPER SURFACE
RUN 238
AOA -.15
X/C -.02
VEL 131.7
RE 1.46
Y (IN)
0.00
0.20
0.40
0.60
0.80
1.00
1.20
1.40
-40.00
0.00
40.00
80.00
120.00
160.00
200.00
240.00
U (FT/SEC)

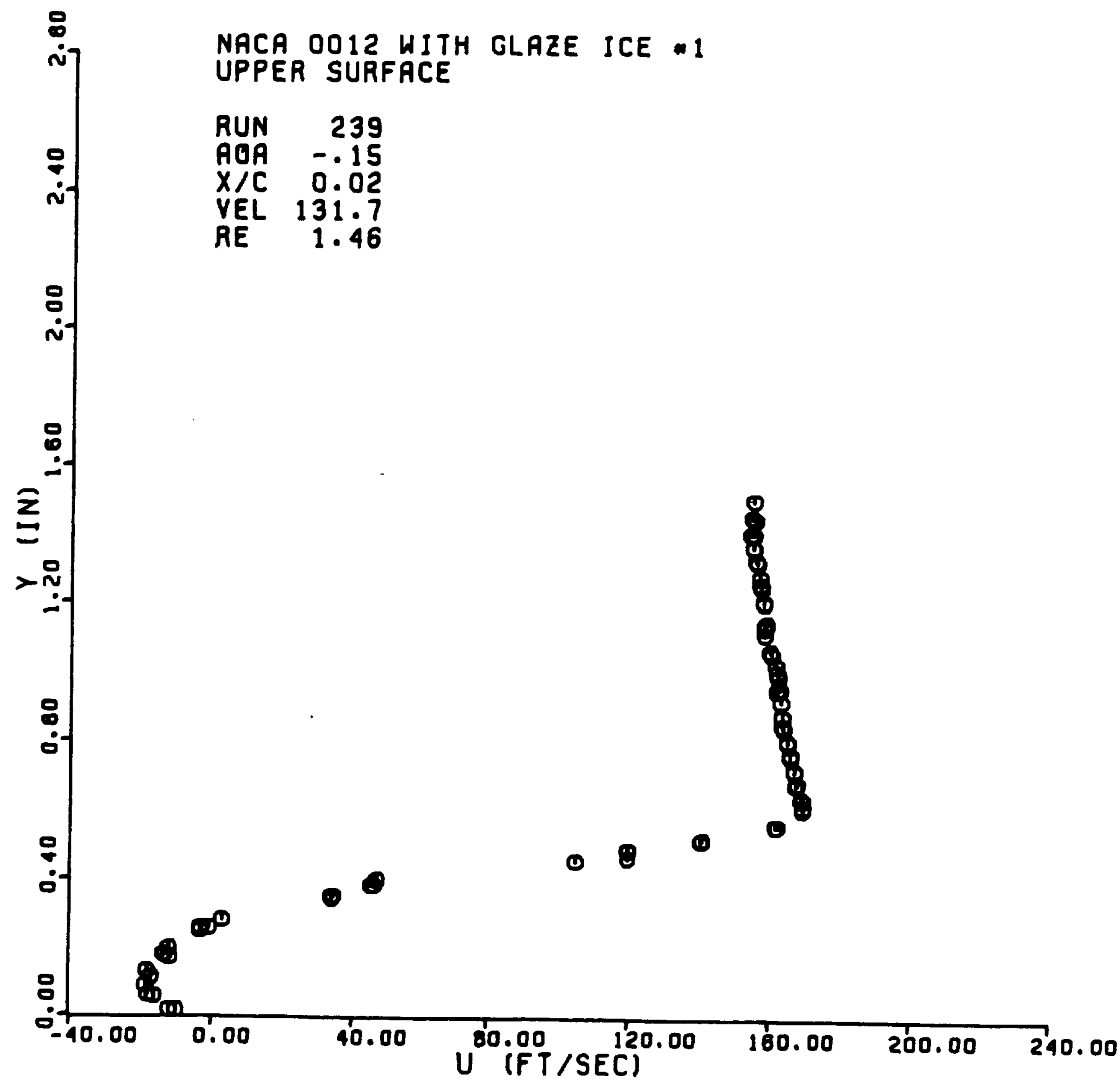
NACA 0012 WITH GLAZE ICE #1
UPPER SURFACE
RUN 239
AOA -.15
X/C 0.02
VEL 131.7
RE 1.46
Y (IN)
U (FT/SEC)
0.00
0.40
0.80
1.20
1.60
2.00
2.40
2.80
-40.00
0.00
40.00
80.00
120.00
160.00
200.00
240.00

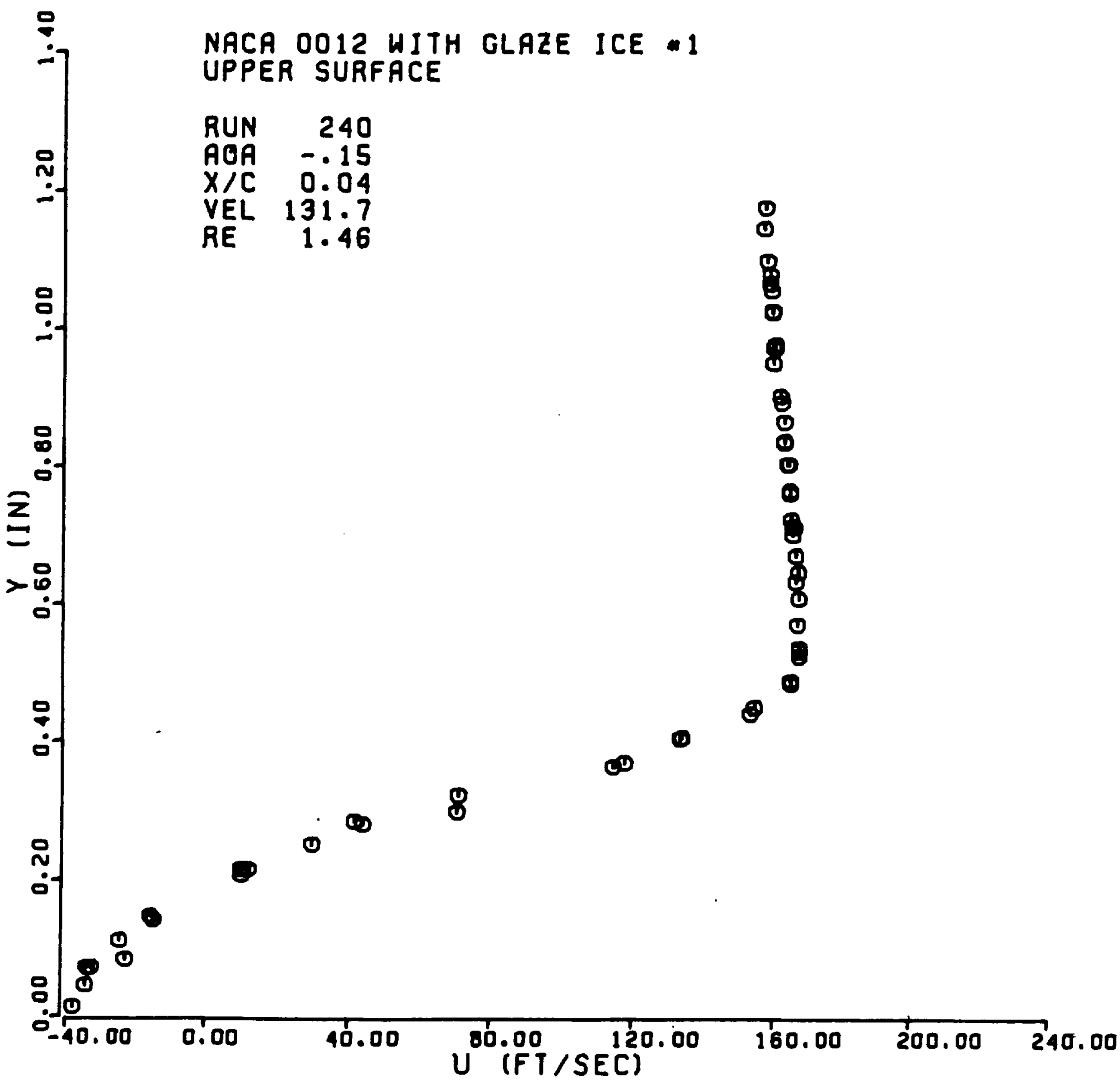
NACA 0012 WITH GLAZE ICE #1
UPPER SURFACE
RUN 240
AOA -.15
X/C 0.04
VEL 131.7
RE 1.46
Y (IN)
0.00
0.20
0.40
0.60
0.80
1.00
1.20
1.40
-40.00
0.00
40.00
80.00
120.00
160.00
200.00
240.00
U (FT/SEC)

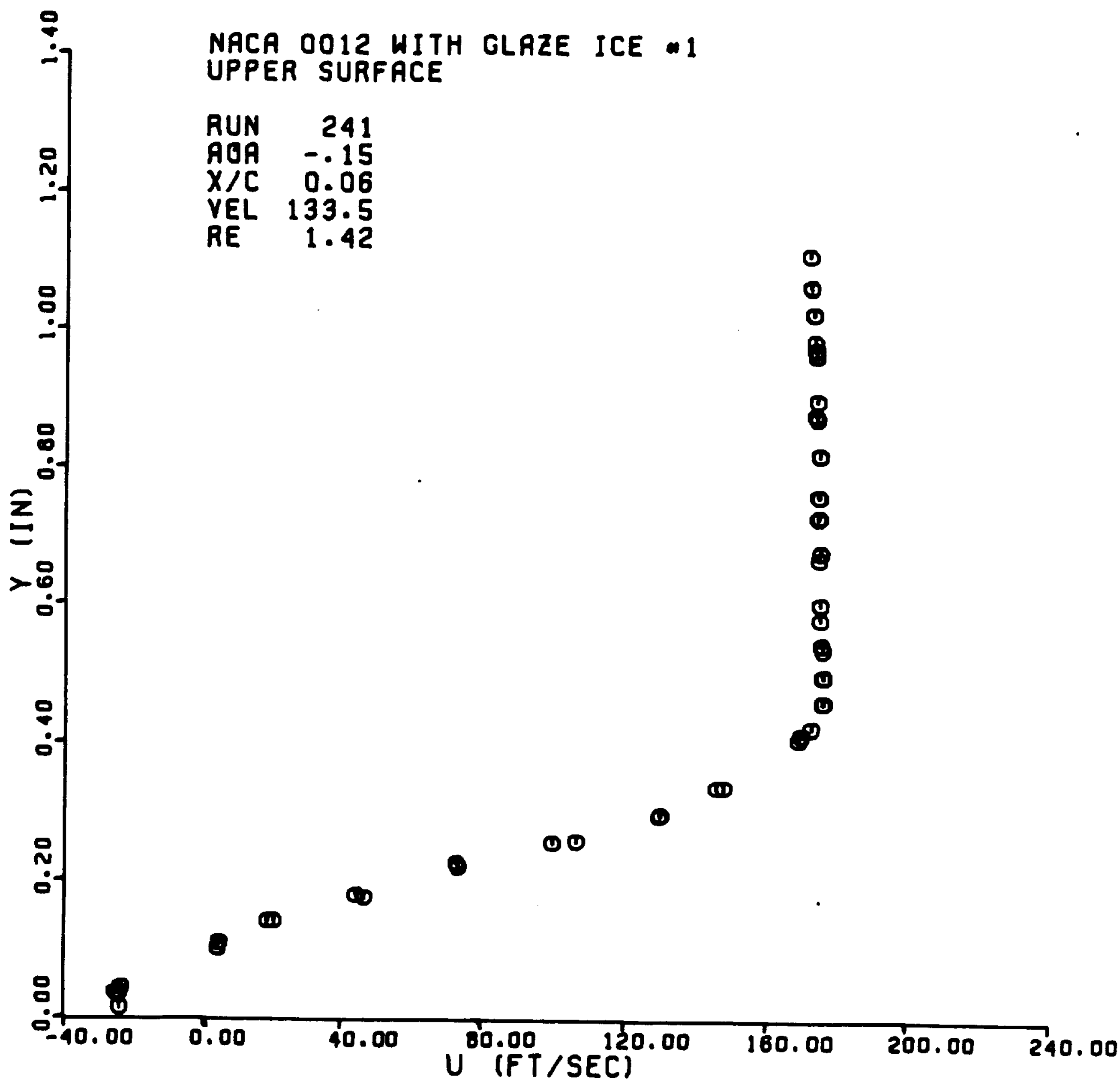
NACA 0012 WITH GLAZE ICE #1
UPPER SURFACE
RUN 241
AOA -.15
X/C 0.06
VEL 133.5
RE 1.42
Y (IN)
U (FT/SEC)
0.00
0.20
0.40
0.60
0.80
1.00
1.20
1.40
-40.00
0.00
40.00
80.00
120.00
160.00
200.00
240.00

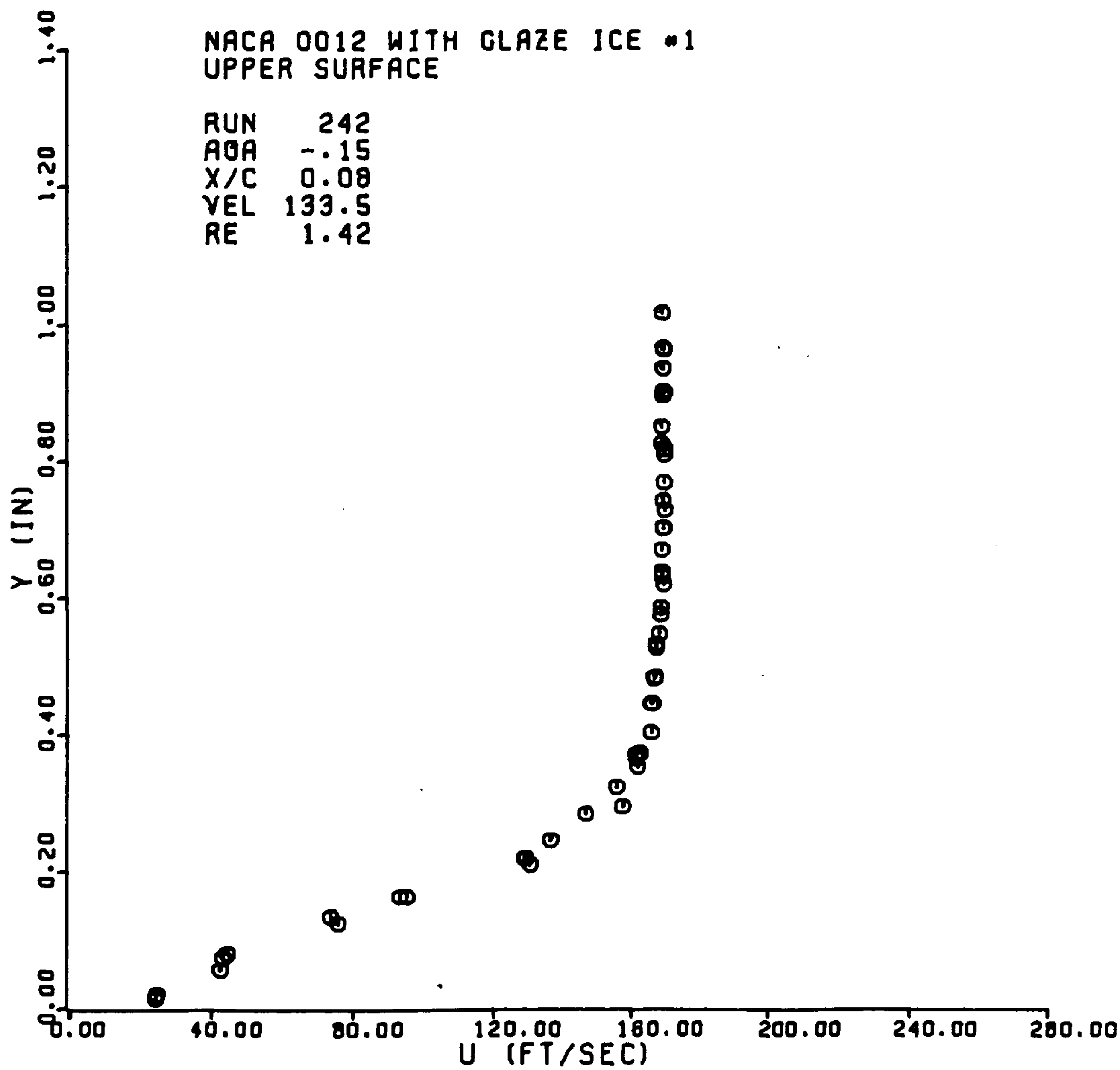
NACA 0012 WITH GLAZE ICE #1
UPPER SURFACE
RUN 242
AOA -.15
X/C 0.08
VEL 133.5
RE 1.42
Y (IN)
U (FT/SEC)
0.00
0.20
0.40
0.60
0.80
1.00
1.20
1.40
40.00
80.00
120.00
160.00
200.00
240.00
280.00

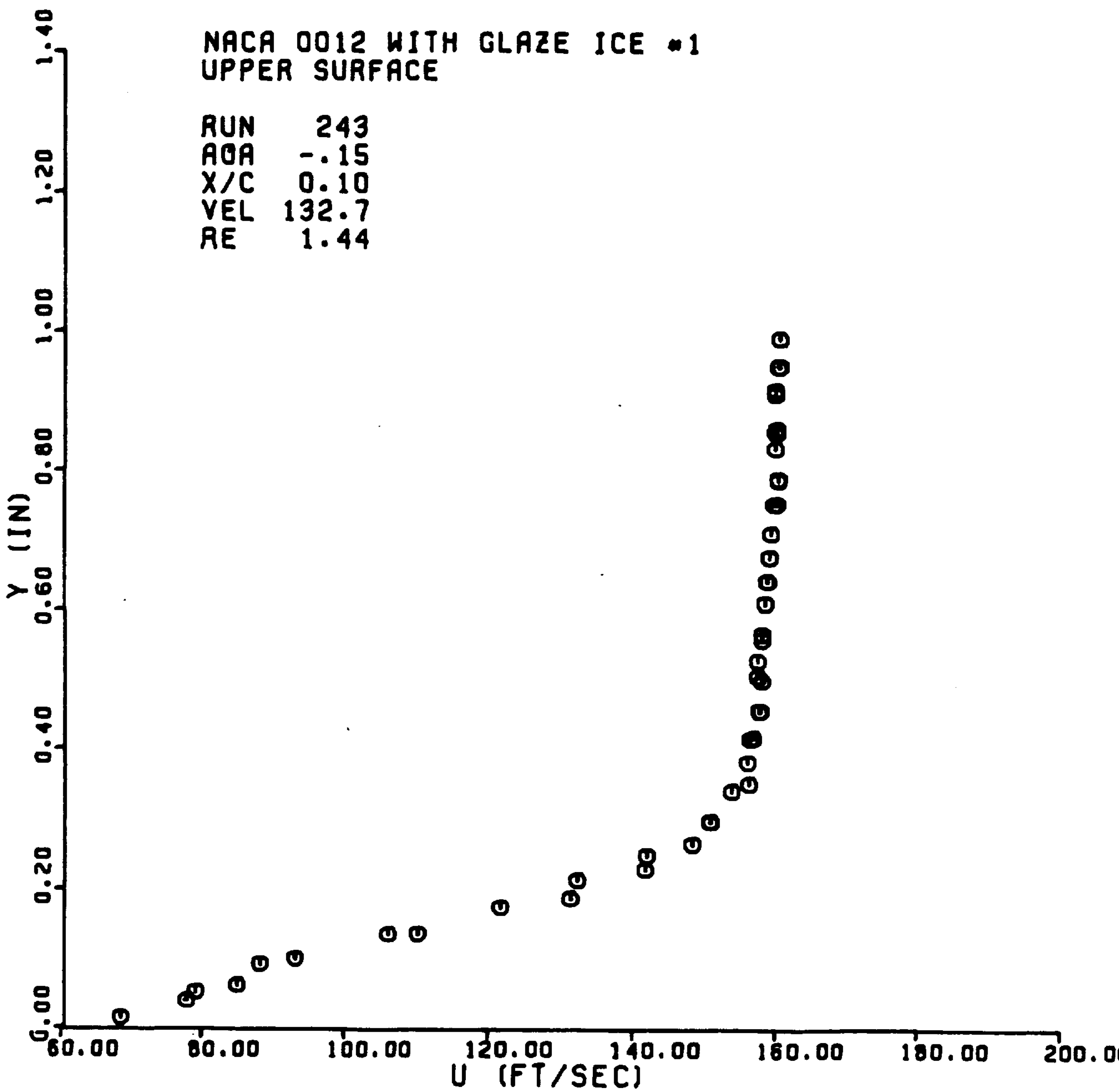
NACA 0012 WITH GLAZE ICE #1
UPPER SURFACE
RUN 243
AOA -.15
X/C 0.10
VEL 132.7
RE 1.44
Y (IN)
U (FT/SEC)
0.00
0.20
0.40
0.60
0.80
1.00
1.20
1.40
60.00
80.00
100.00
120.00
140.00
160.00
180.00
200.00

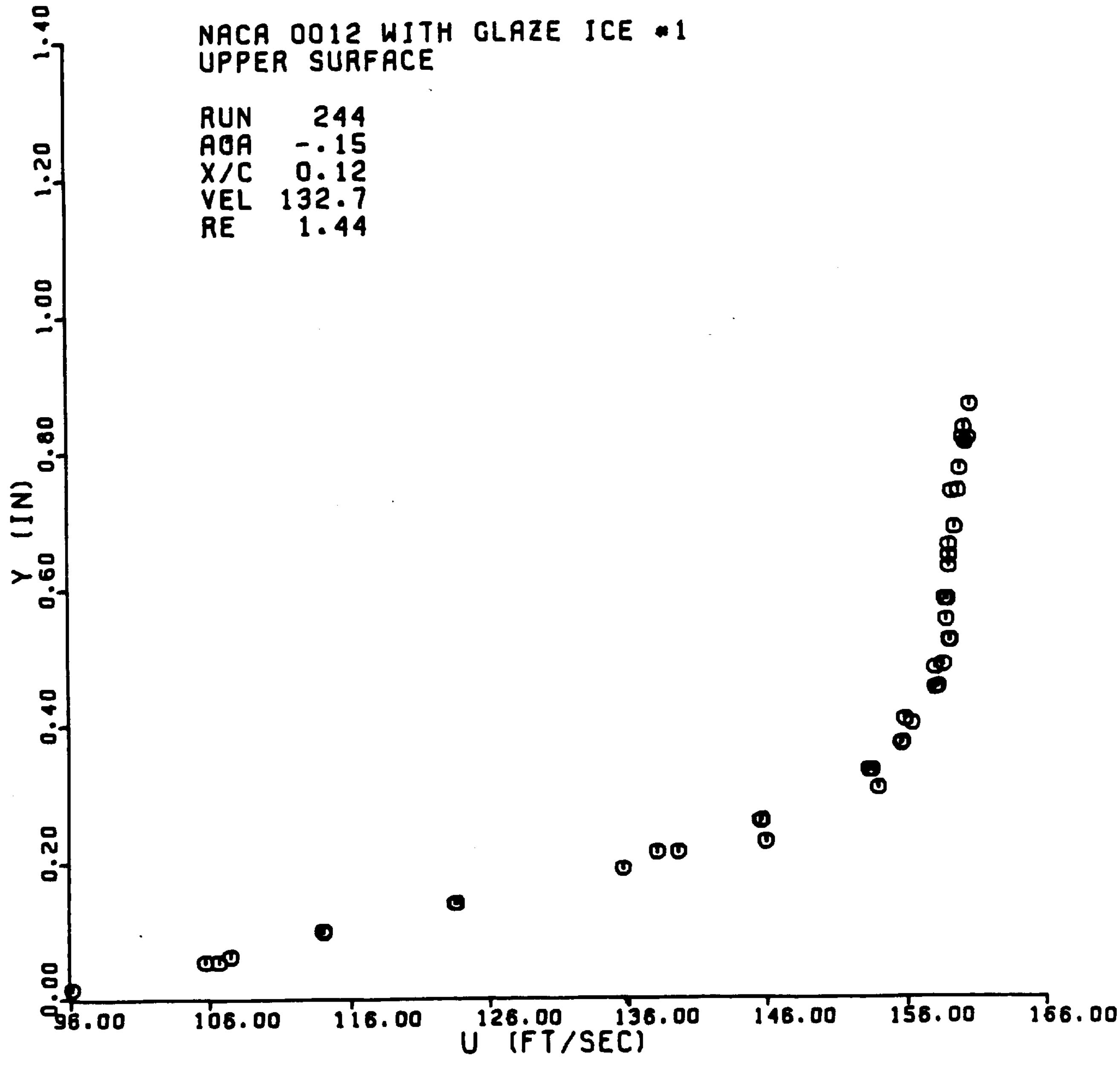
NACA 0012 WITH GLAZE ICE #1
UPPER SURFACE
RUN 244
AOA -.15
X/C 0.12
VEL 132.7
RE 1.44
Y (IN)
U (FT/SEC)
0.00
0.20
0.40
0.60
0.80
1.00
1.20
1.40
96.00
106.00
116.00
126.00
136.00
146.00
156.00
166.00

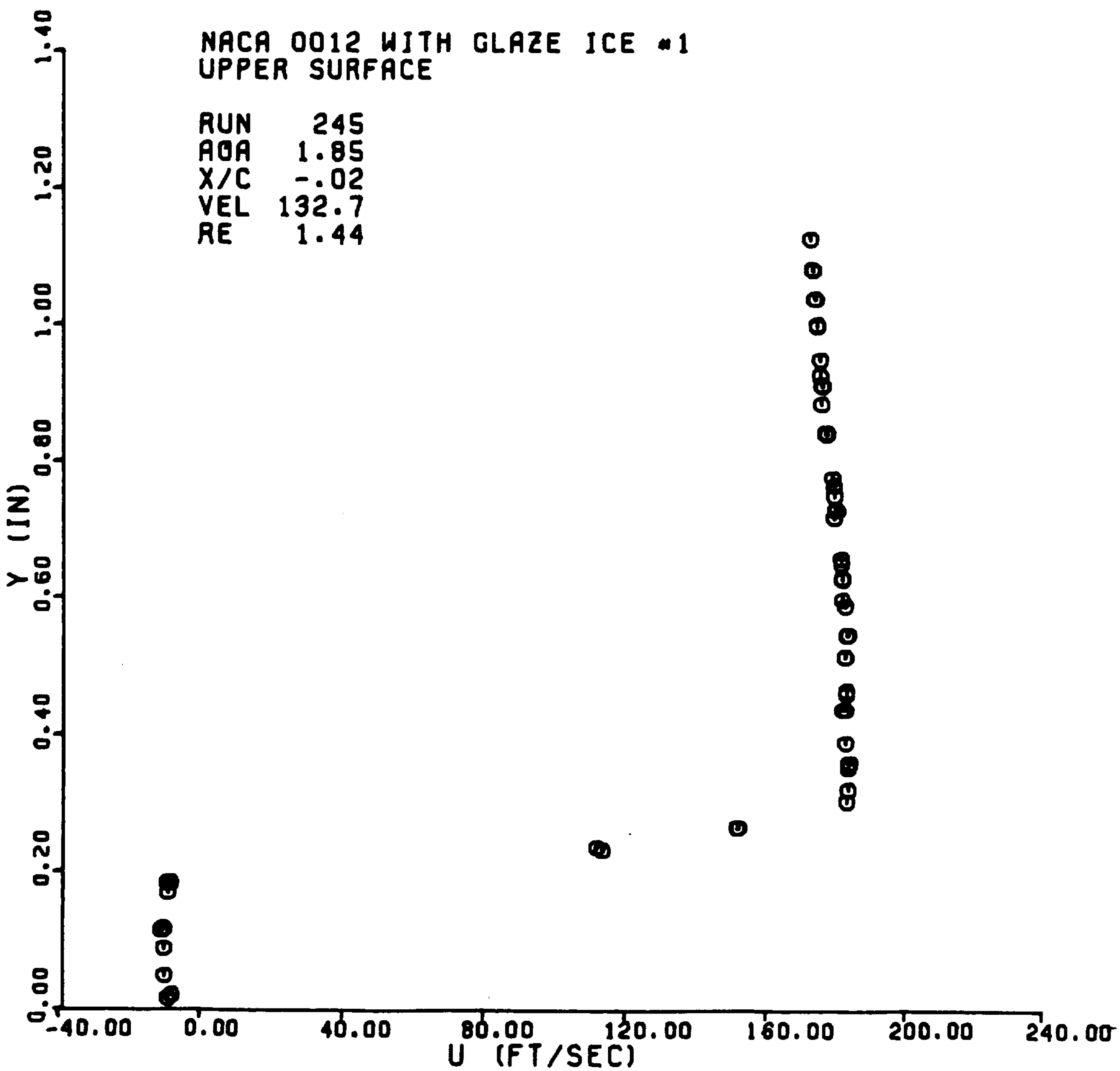
NACA 0012 WITH GLAZE ICE #1
UPPER SURFACE
RUN 245
AOA 1.85
X/C -.02
VEL 132.7
RE 1.44
Y (IN)
0.00
0.20
0.40
0.60
0.80
1.00
1.20
1.40
-40.00
0.00
40.00
80.00
120.00
160.00
200.00
240.00
U (FT/SEC)

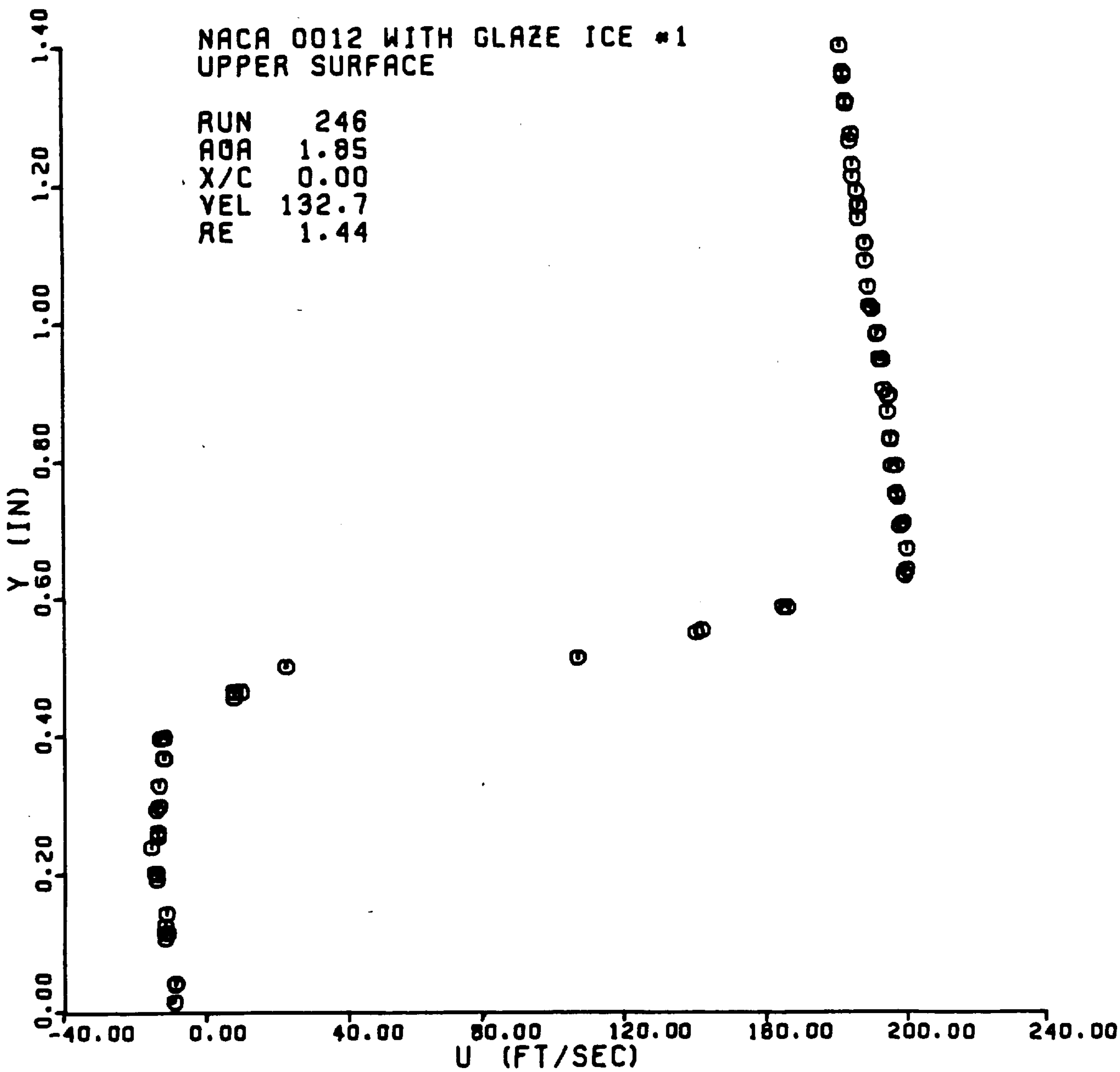
NACA 0012 WITH GLAZE ICE #1
UPPER SURFACE
RUN 246
AOA 1.85
X/C 0.00
VEL 132.7
RE 1.44
Y (IN)
0.00
0.20
0.40
0.60
0.80
1.00
1.20
1.40
-40.00
0.00
40.00
80.00
120.00
160.00
200.00
240.00
U (FT/SEC)

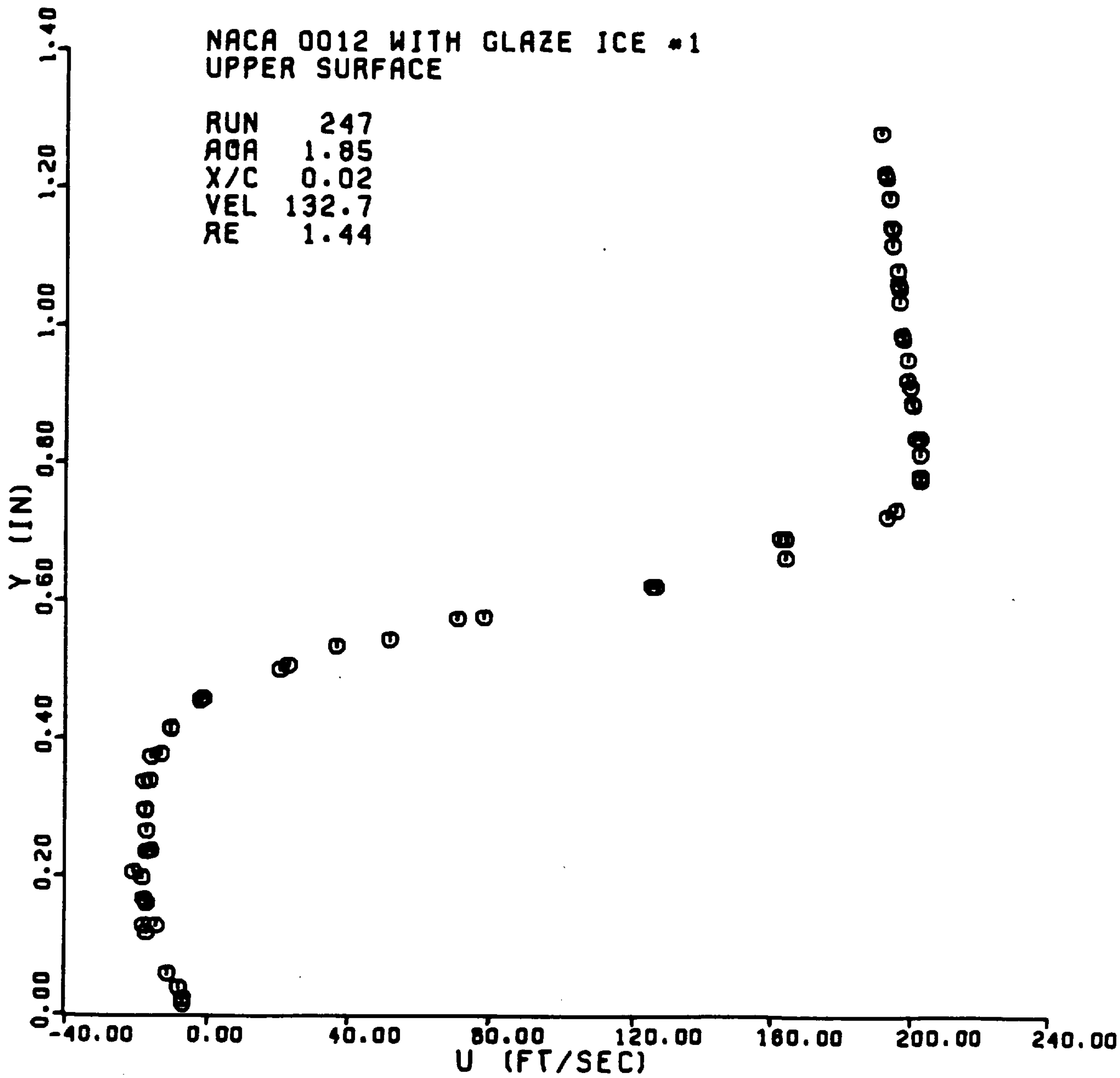
NACA 0012 WITH GLAZE ICE #1
UPPER SURFACE
RUN 247
AOA 1.85
X/C 0.02
VEL 132.7
RE 1.44
Y (IN)
0.00
0.20
0.40
0.60
0.80
1.00
1.20
1.40
-40.00
0.00
40.00
80.00
120.00
160.00
200.00
240.00
U (FT/SEC)

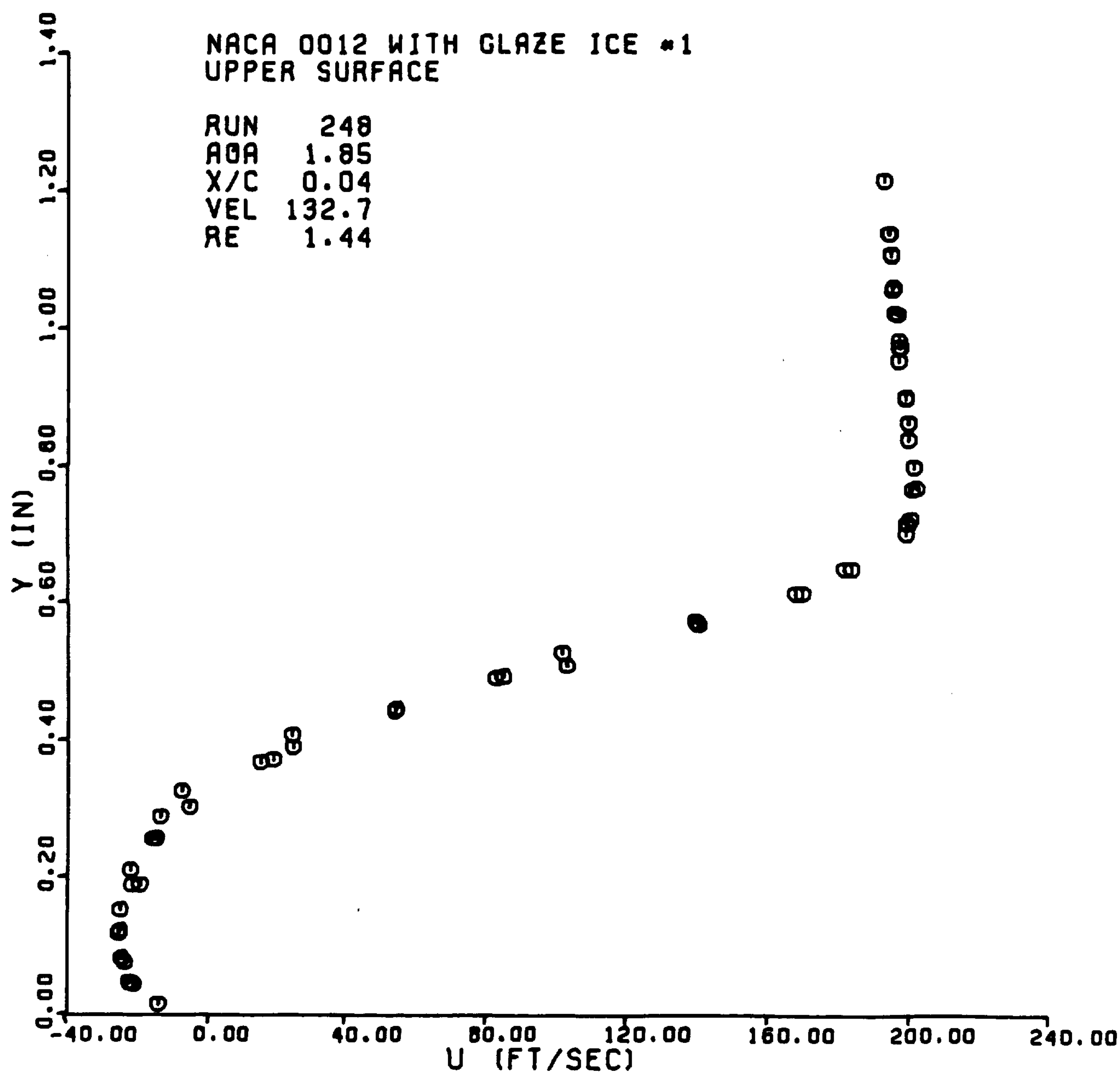
NACA 0012 WITH GLAZE ICE #1
UPPER SURFACE
RUN 248
AOA 1.85
X/C 0.04
VEL 132.7
RE 1.44
Y (IN)
0.00
0.20
0.40
0.60
0.80
1.00
1.20
1.40
U (FT/SEC)
-40.00
0.00
40.00
80.00
120.00
160.00
200.00
240.00

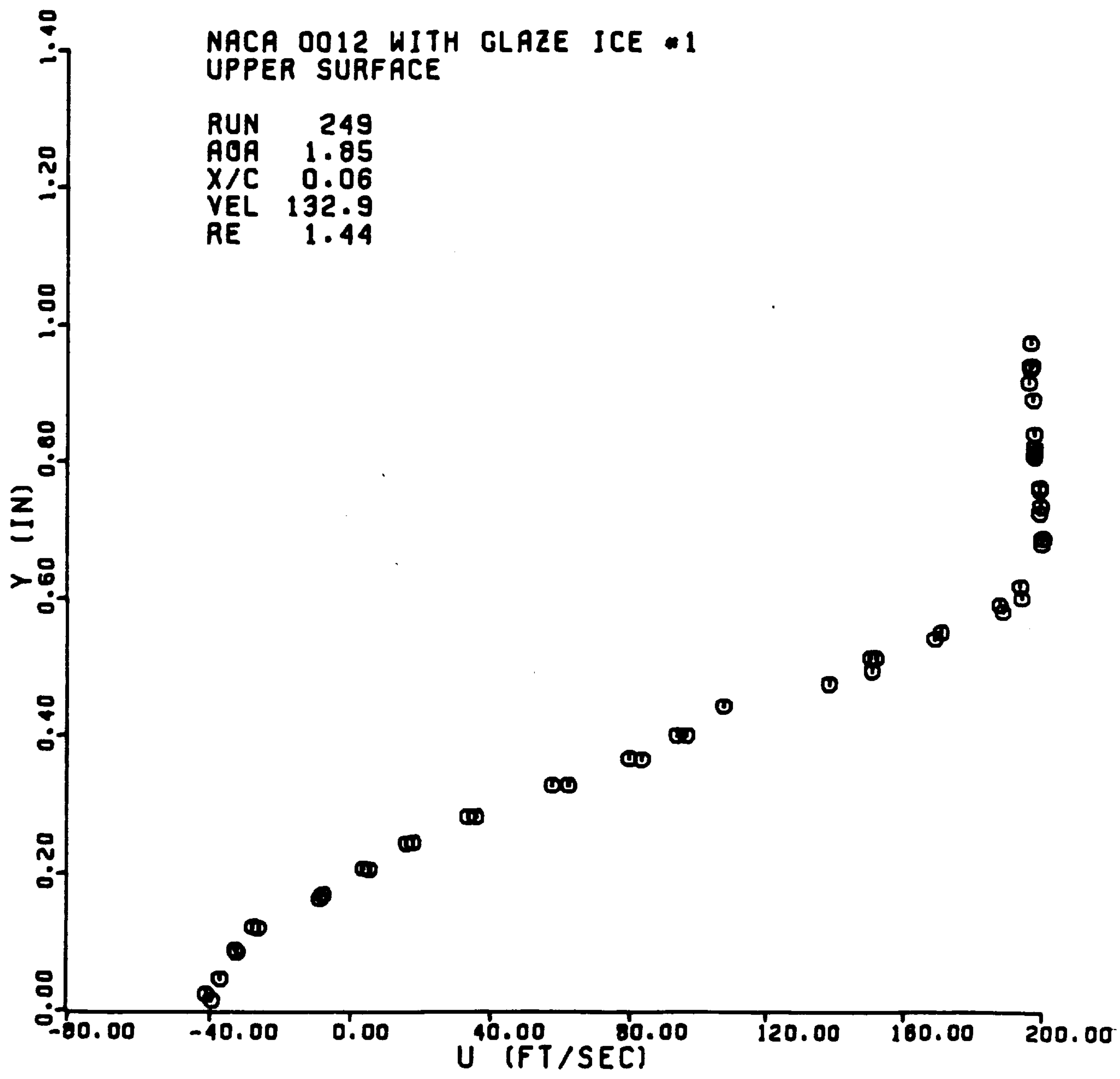
NACA 0012 WITH GLAZE ICE #1
UPPER SURFACE
RUN 249
AOA 1.85
X/C 0.06
VEL 132.9
RE 1.44
Y (IN)
U (FT/SEC)
0.00
0.20
0.40
0.60
0.80
1.00
1.20
1.40
-80.00
-40.00
0.00
40.00
80.00
120.00
160.00
200.00

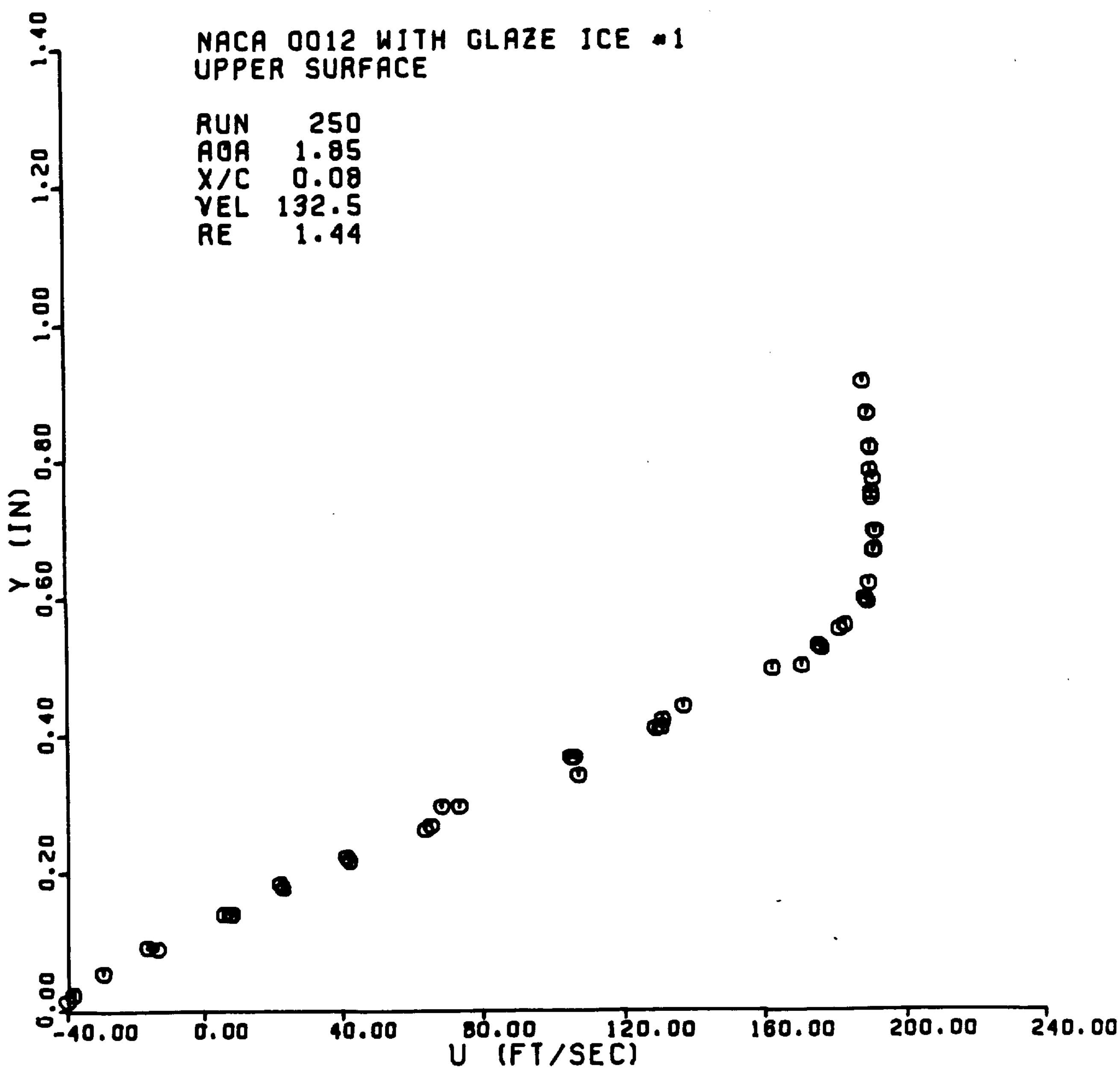
NACA 0012 WITH GLAZE ICE #1
UPPER SURFACE
RUN 250
AOA 1.85
X/C 0.08
VEL 132.5
RE 1.44
Y (IN)
0.00
0.20
0.40
0.60
0.80
1.00
1.20
1.40
-40.00
0.00
40.00
80.00
120.00
160.00
200.00
240.00
U (FT/SEC)

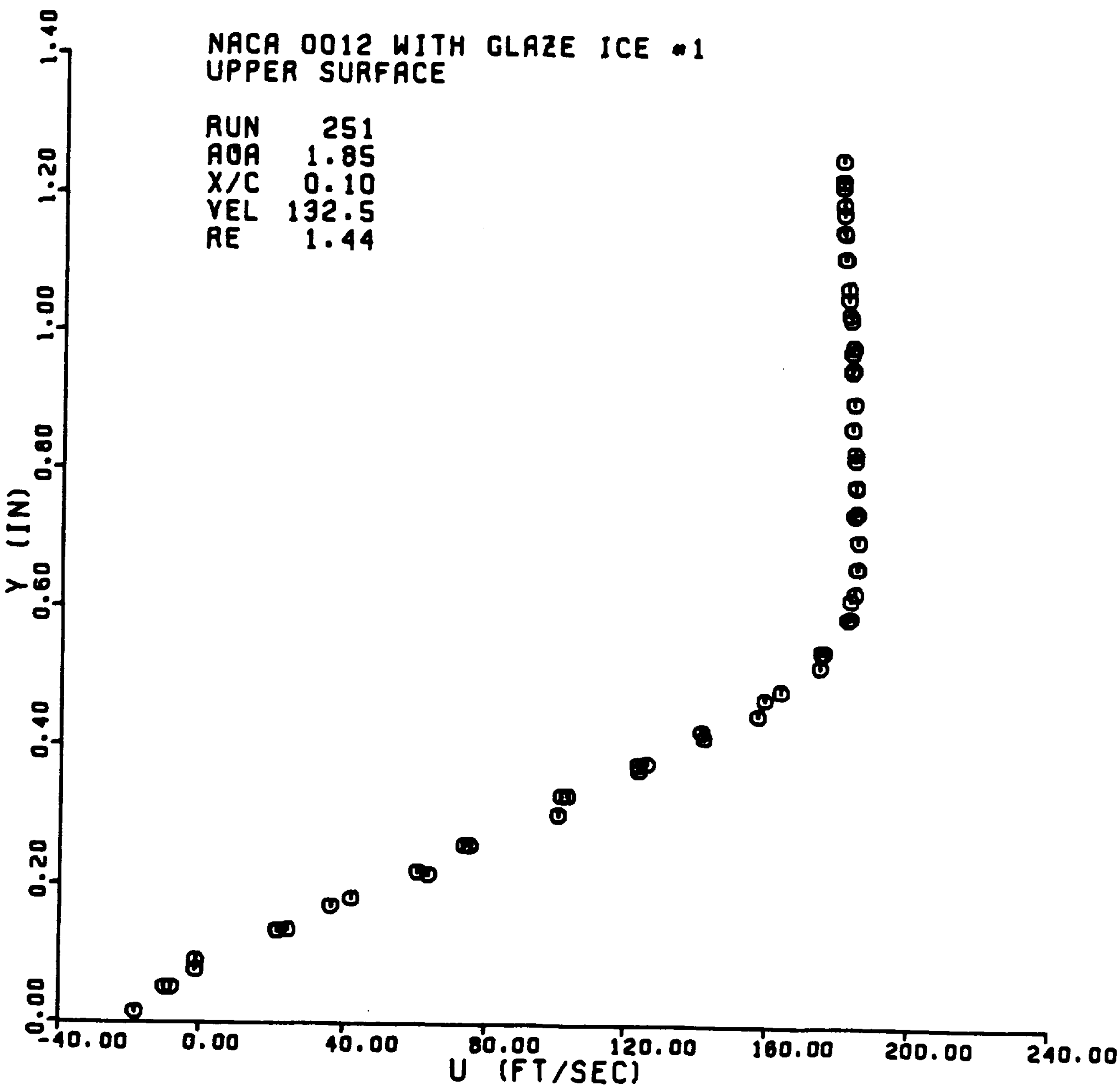

NACA 0012 WITH GLAZE ICE #1
UPPER SURFACE
RUN 251
AOA 1.85
X/C 0.10
VEL 132.5
RE 1.44
Y (IN)
0.00
0.20
0.40
0.60
0.80
1.00
1.20
1.40
-40.00
0.00
40.00
80.00
120.00
160.00
200.00
240.00
U (FT/SEC)

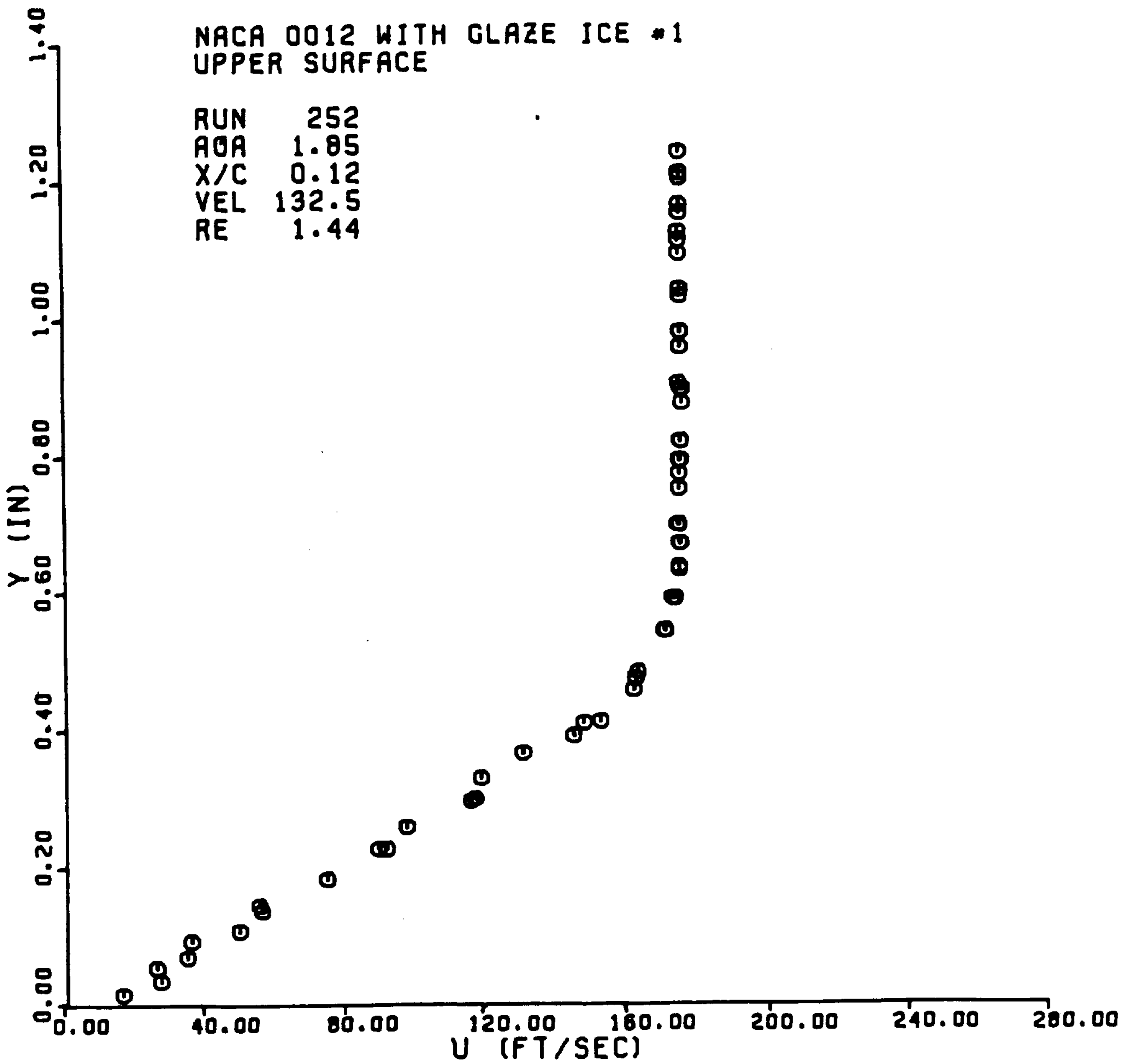
NACA 0012 WITH GLAZE ICE #1
UPPER SURFACE
RUN 252
AOA 1.85
X/C 0.12
VEL 132.5
RE 1.44
Y (IN)
0.00
0.20
0.40
0.60
0.80
1.00
1.20
1.40
0.00
40.00
80.00
120.00
160.00
200.00
240.00
280.00
U (FT/SEC)

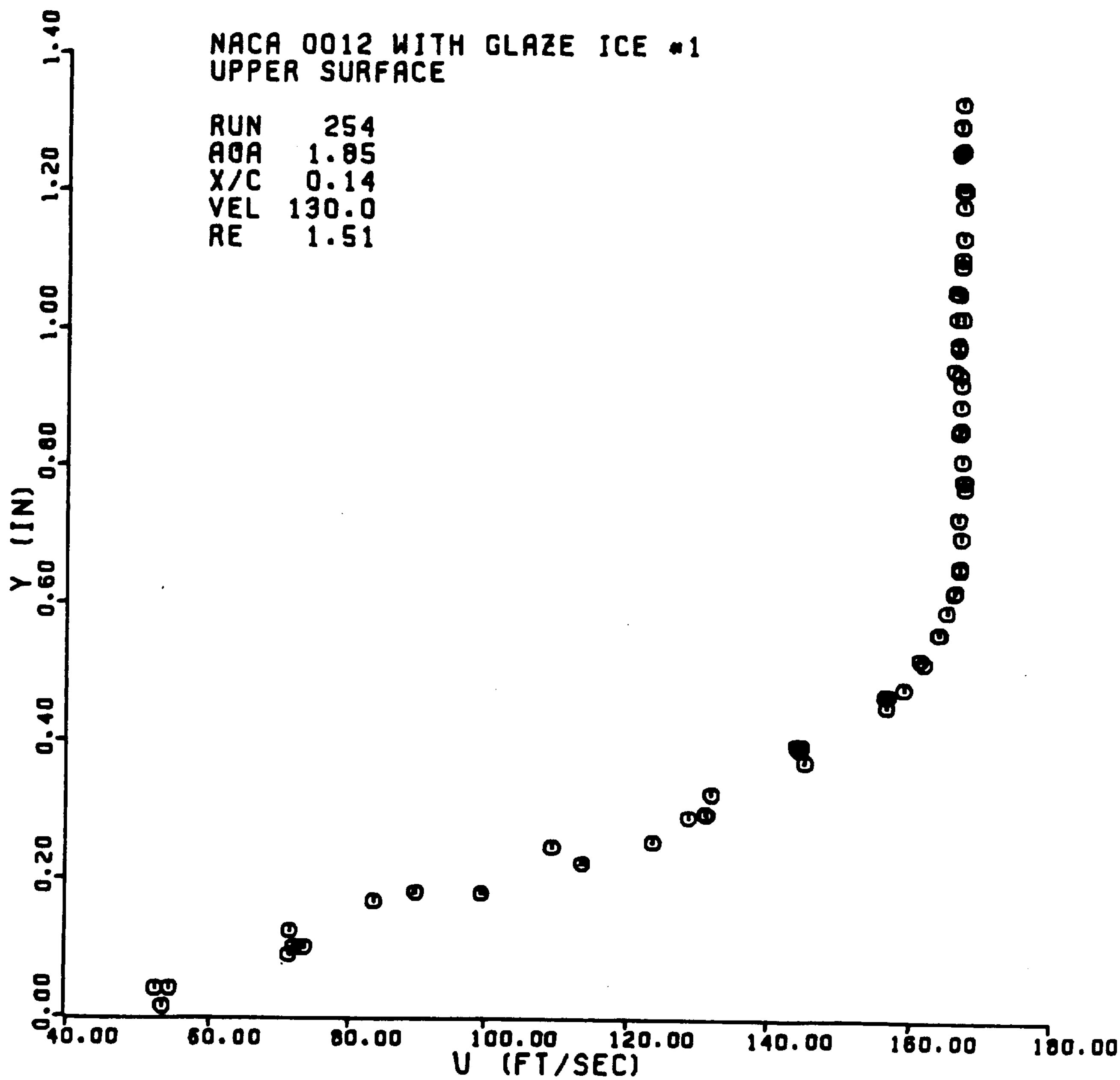
NACA 0012 WITH GLAZE ICE #1
UPPER SURFACE
RUN 254
AOA 1.85
X/C 0.14
VEL 130.0
RE 1.51
Y (IN)
U (FT/SEC)
0.00
0.20
0.40
0.60
0.80
1.00
1.20
1.40
40.00
60.00
80.00
100.00
120.00
140.00
160.00
180.00

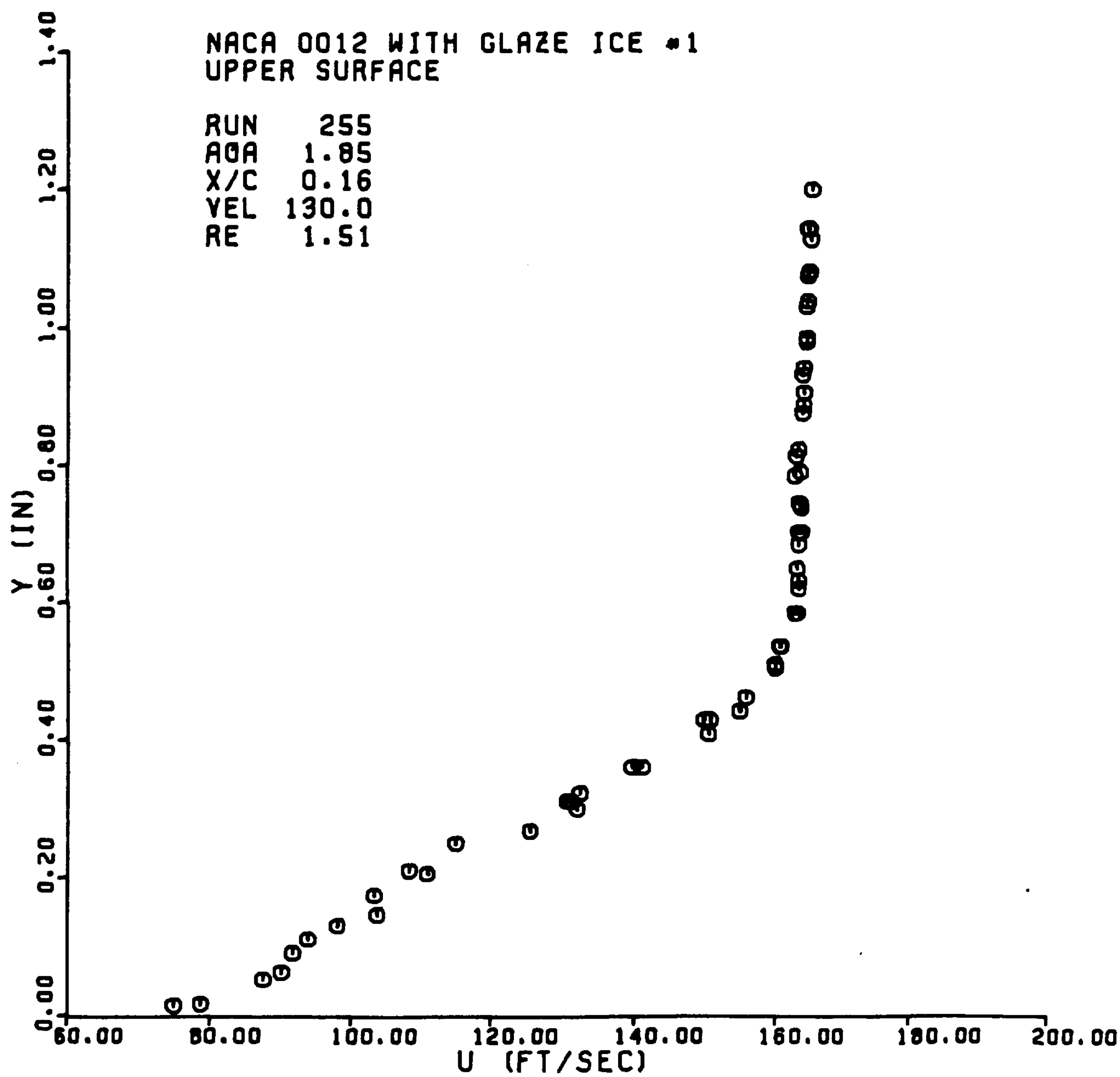
NACA 0012 WITH GLAZE ICE #1
UPPER SURFACE
RUN 255
AOA 1.85
X/C 0.16
VEL 130.0
RE 1.51
Y (IN)
0.00
0.20
0.40
0.60
0.80
1.00
1.20
1.40
60.00
80.00
100.00
120.00
140.00
160.00
180.00
200.00
U (FT/SEC)

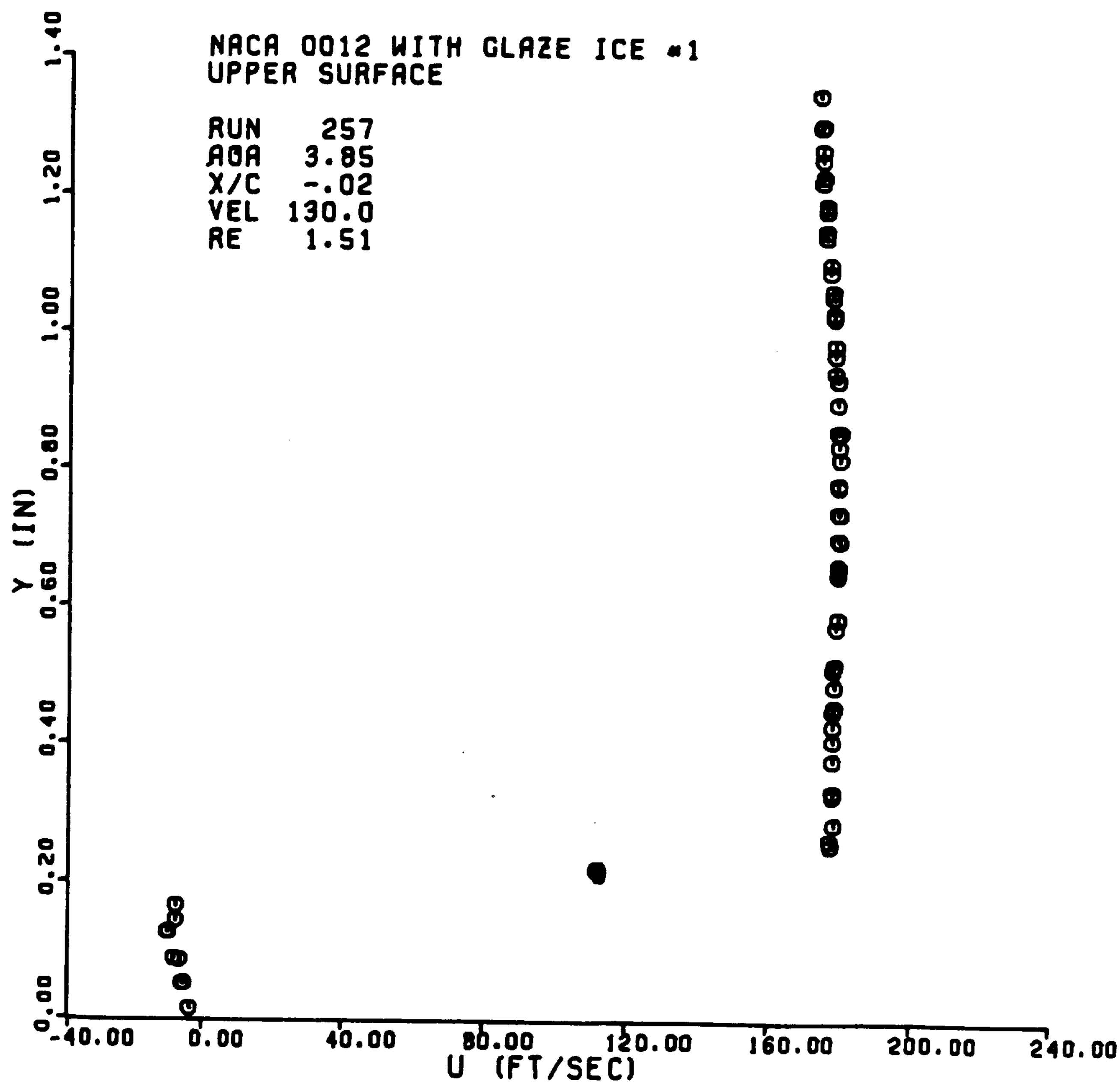
NACA 0012 WITH GLAZE ICE #1
UPPER SURFACE
RUN 257
AOA 3.85
X/C -.02
VEL 130.0
RE 1.51
Y (IN)
0.00
0.20
0.40
0.60
0.80
1.00
1.20
1.40
-40.00
0.00
40.00
80.00
120.00
160.00
200.00
240.00
U (FT/SEC)

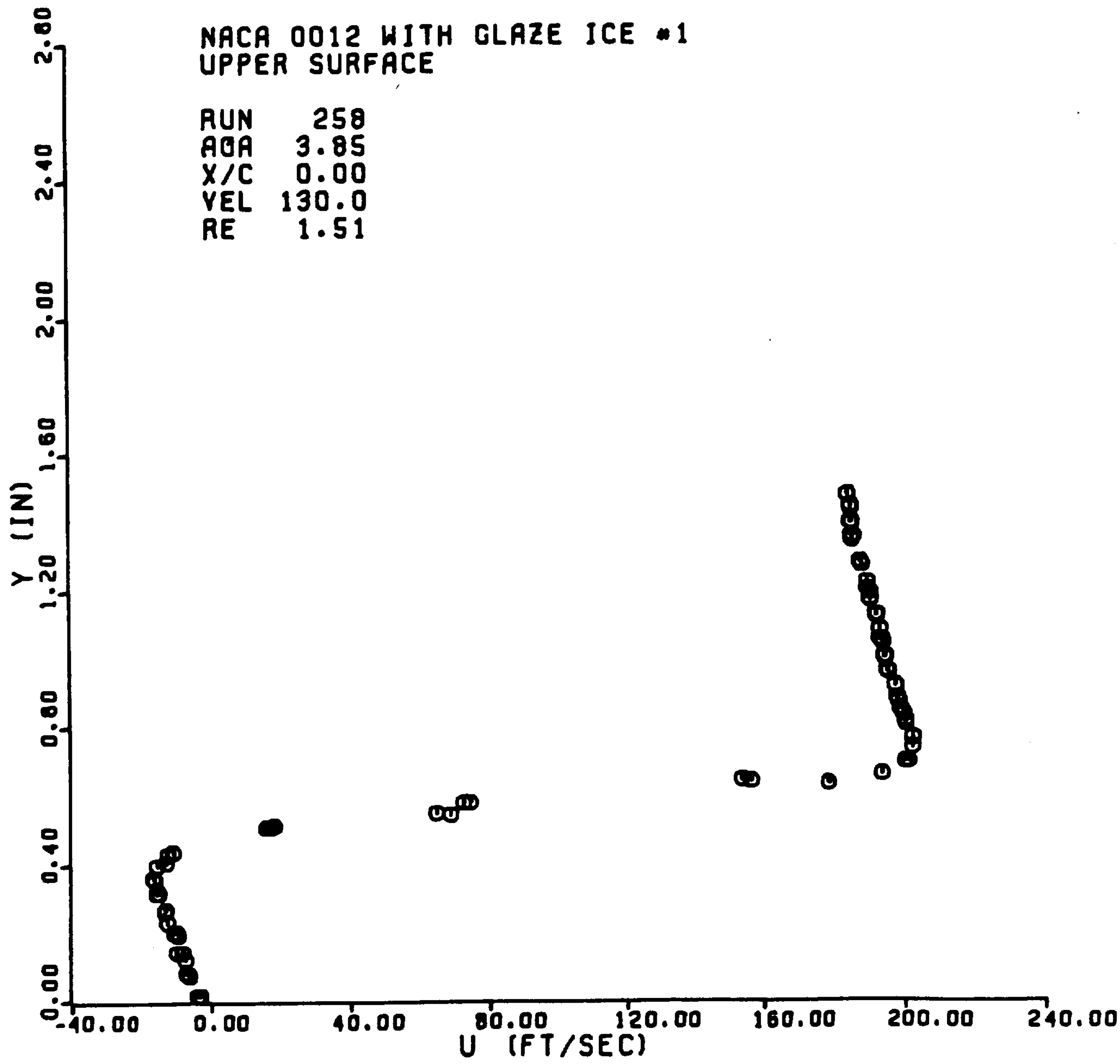

NACA 0012 WITH GLAZE ICE #1
UPPER SURFACE
RUN 258
AOA 3.85
X/C 0.00
VEL 130.0
RE 1.51
Y (IN)
U (FT/SEC)
0.00
0.40
0.80
1.20
1.60
2.00
2.40
2.80
-40.00
0.00
40.00
80.00
120.00
160.00
200.00
240.00

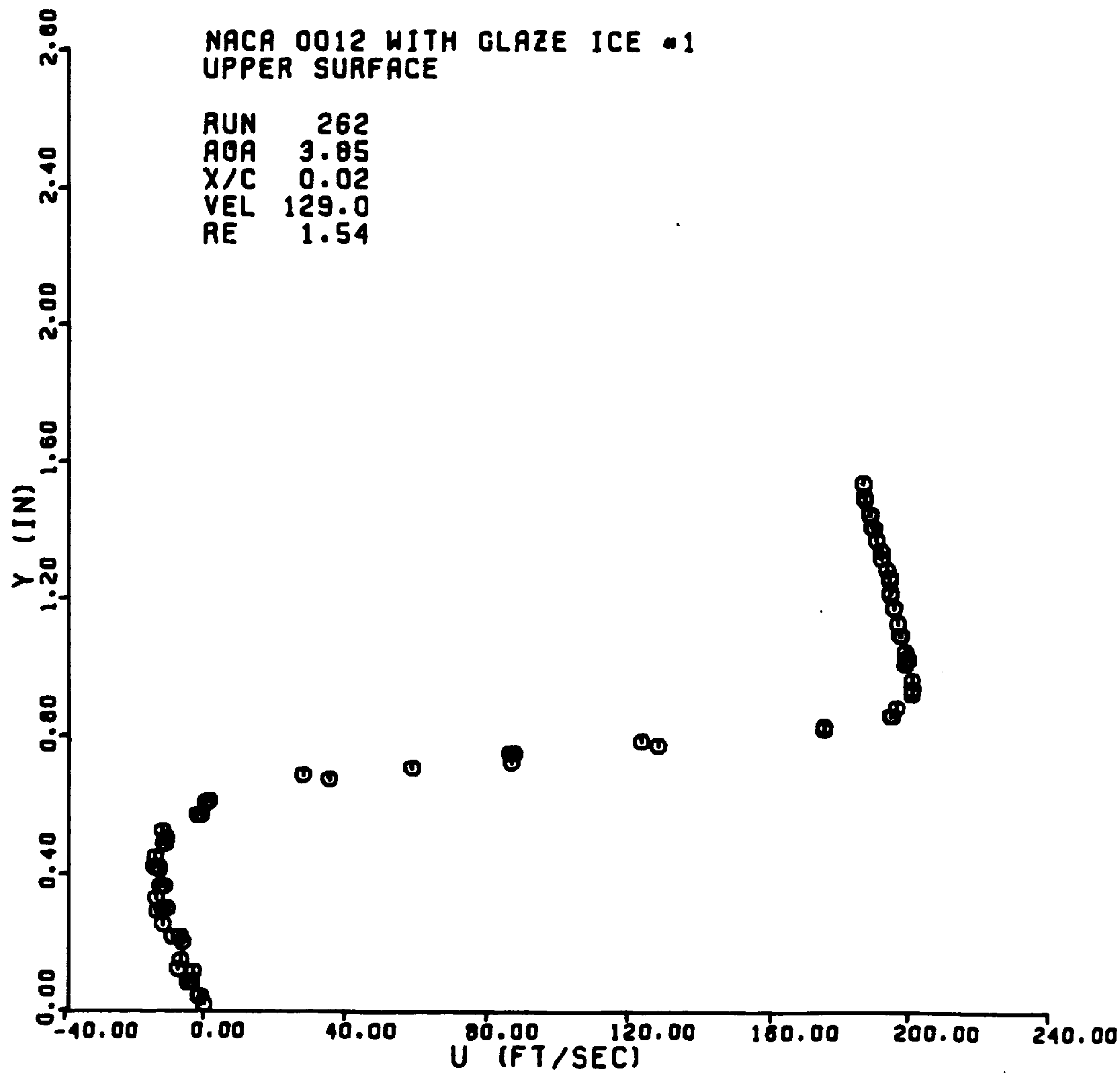
NACA 0012 WITH GLAZE ICE #1
UPPER SURFACE
RUN 262
AOA 3.85
X/C 0.02
VEL 129.0
RE 1.54
Y (IN)
U (FT/SEC)
0.00
0.40
0.80
1.20
1.60
2.00
2.40
2.80
-40.00
0.00
40.00
80.00
120.00
160.00
200.00
240.00

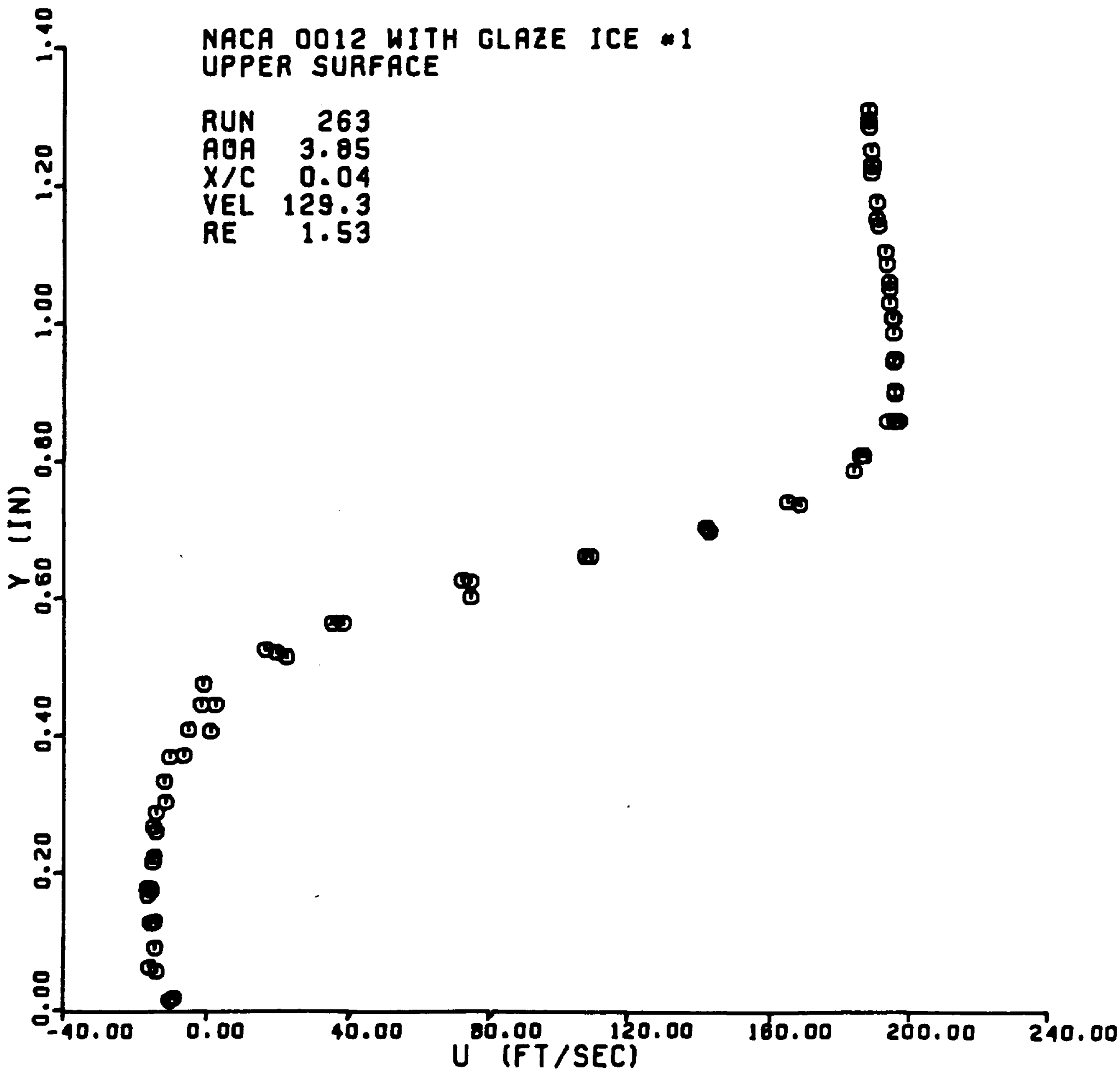

NACA 0012 WITH GLAZE ICE #1
UPPER SURFACE
RUN 263
AOA 3.85
X/C 0.04
VEL 129.3
RE 1.53
Y (IN)
0.00
0.20
0.40
0.60
0.80
1.00
1.20
1.40
-40.00
0.00
40.00
80.00
120.00
160.00
200.00
240.00
U (FT/SEC)

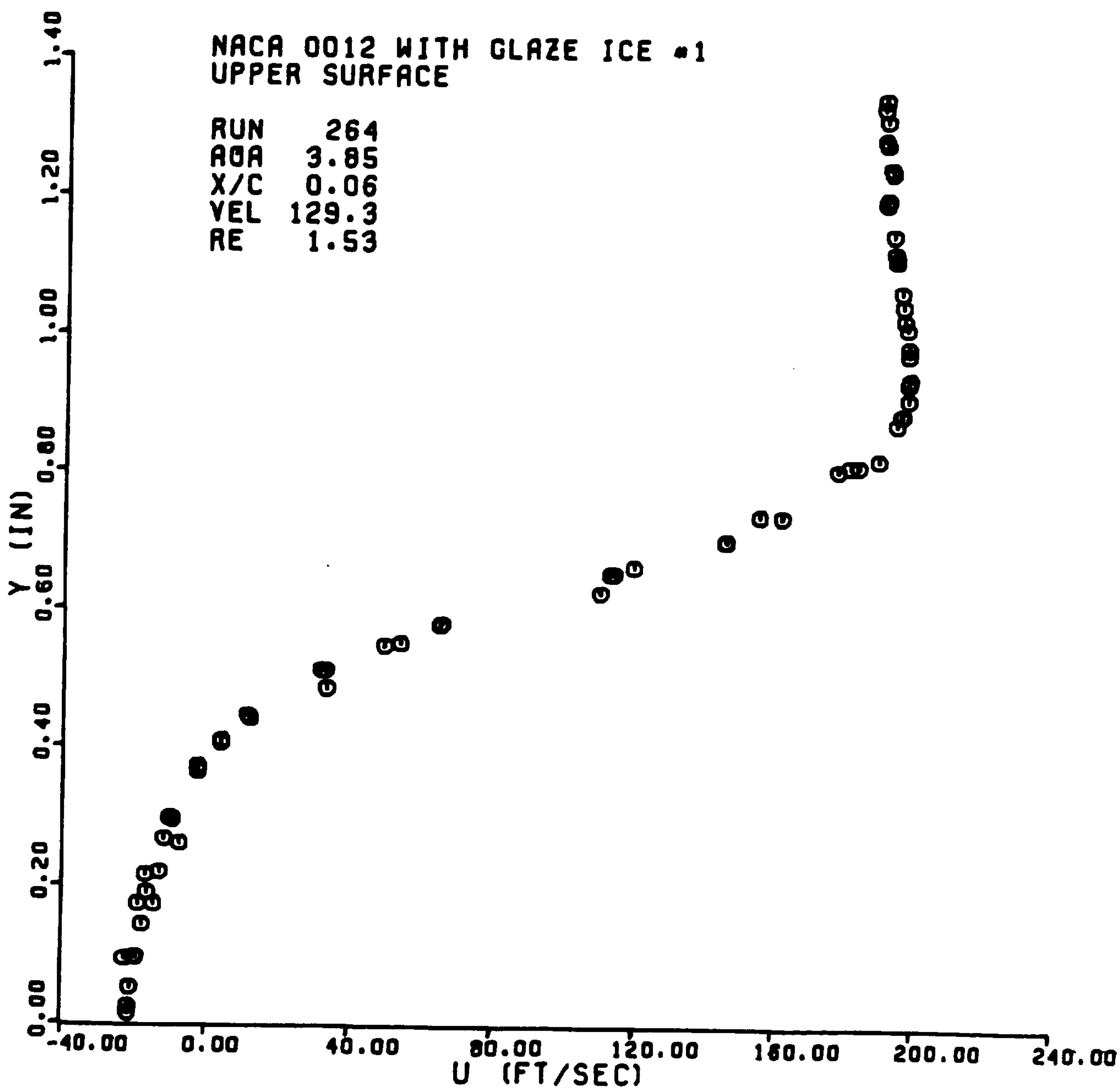
NACA 0012 WITH GLAZE ICE #1
UPPER SURFACE
RUN 264
AOA 3.85
X/C 0.06
VEL 129.3
RE 1.53
Y (IN)
0.00
0.20
0.40
0.60
0.80
1.00
1.20
1.40
-40.00
0.00
40.00
80.00
120.00
160.00
200.00
240.00
U (FT/SEC)

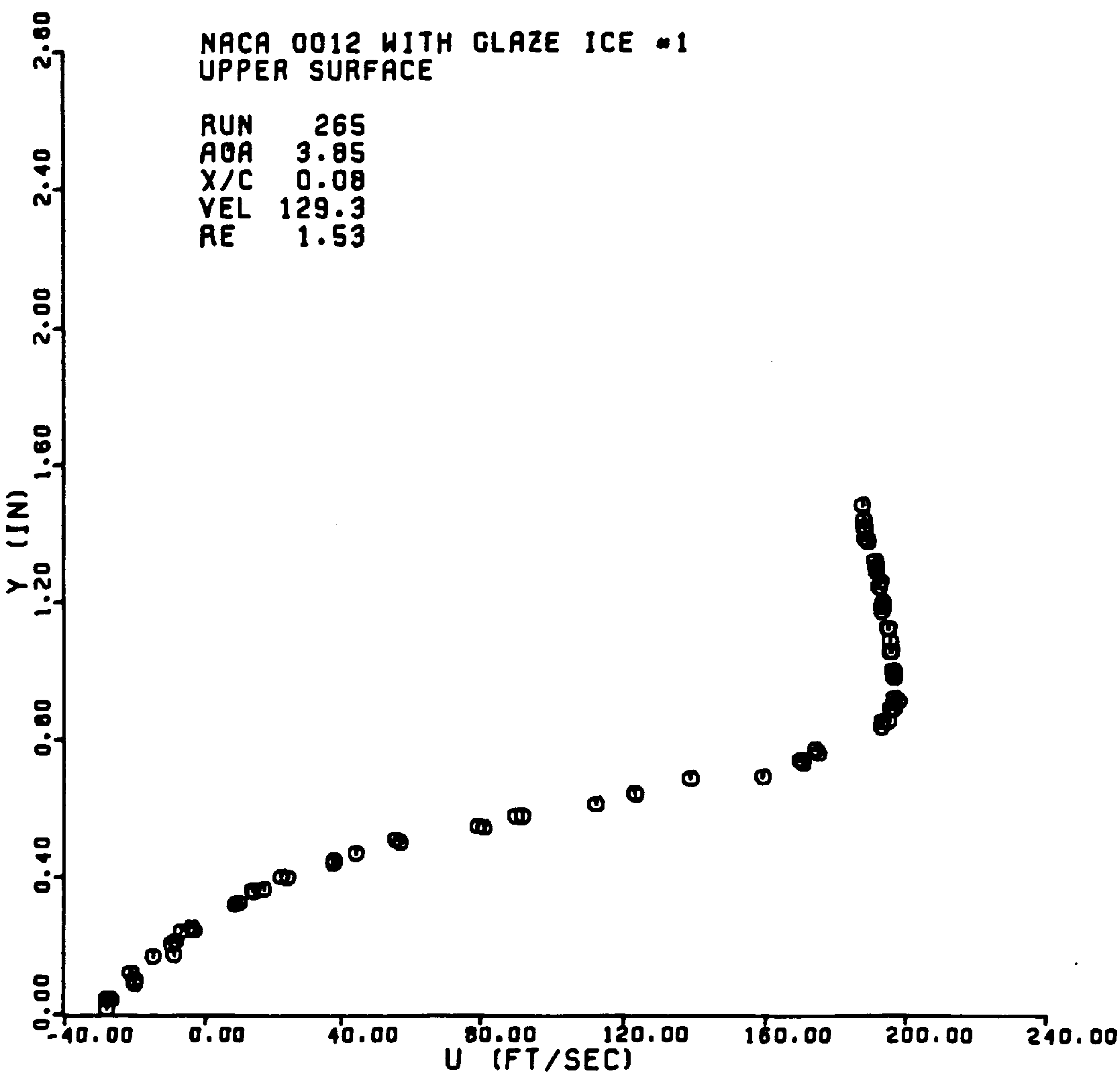

NACA 0012 WITH GLAZE ICE #1
UPPER SURFACE
RUN 265
AOA 3.85
X/C 0.08
VEL 129.3
RE 1.53
Y (IN)
0.00
0.40
0.80
1.20
1.60
2.00
2.40
2.80
-40.00
0.00
40.00
80.00
120.00
160.00
200.00
240.00
U (FT/SEC)

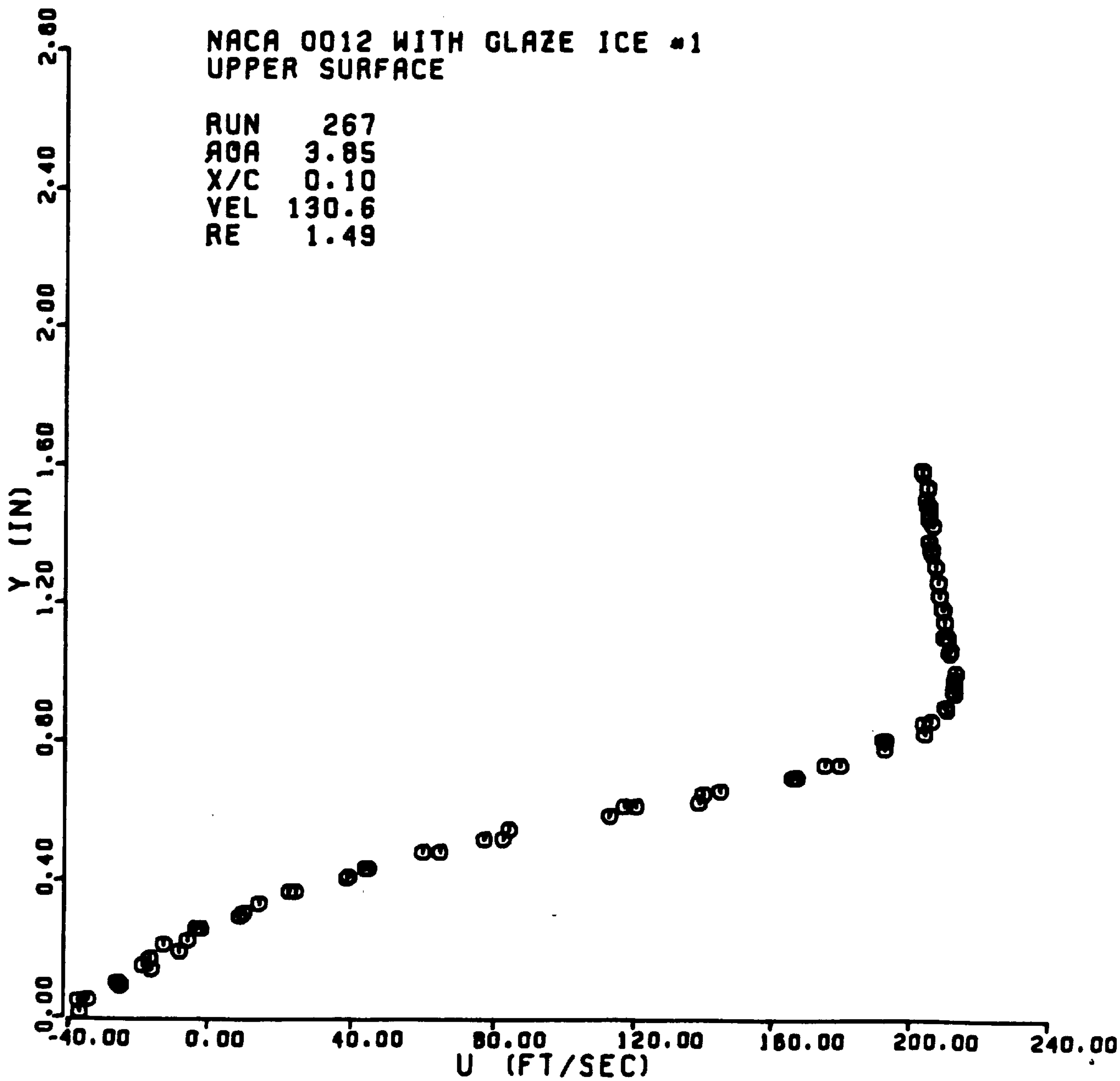
NACA 0012 WITH GLAZE ICE #1
UPPER SURFACE
RUN 267
AOA 3.85
X/C 0.10
VEL 130.6
RE 1.49
Y (IN)
0.00
0.40
0.80
1.20
1.60
2.00
2.40
2.80
-40.00
0.00
40.00
80.00
120.00
160.00
200.00
240.00
U (FT/SEC)

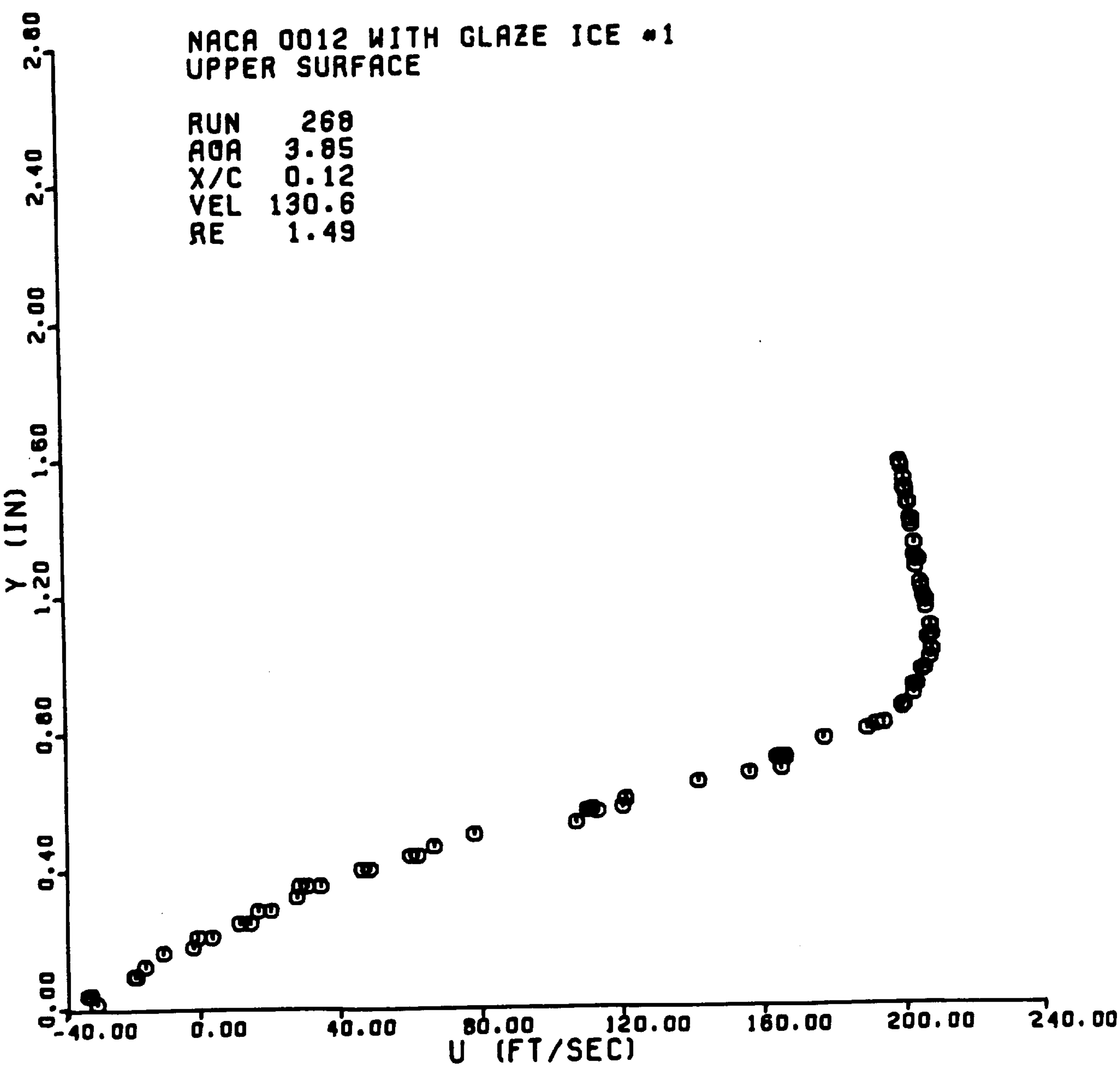
NACA 0012 WITH GLAZE ICE #1
UPPER SURFACE
RUN 268
AOA 3.85
X/C 0.12
VEL 130.6
RE 1.49
Y (IN)
U (FT/SEC)
0.00
0.40
0.80
1.20
1.60
2.00
2.40
2.80
-40.00
0.00
40.00
80.00
120.00
160.00
200.00
240.00

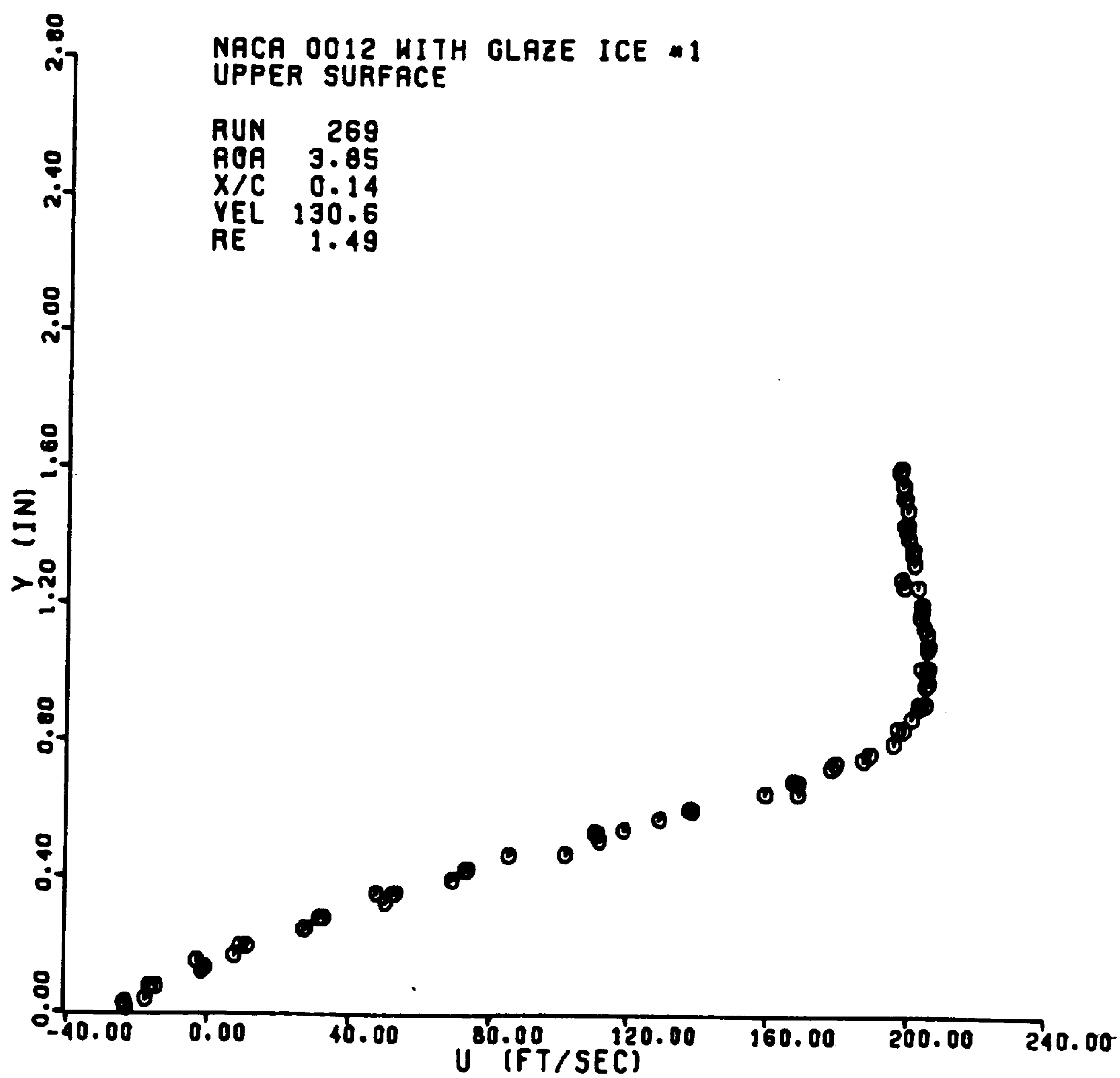
NACA 0012 WITH GLAZE ICE #1
UPPER SURFACE
RUN 269
AOA 3.85
X/C 0.14
VEL 130.6
RE 1.49
Y (IN)
U (FT/SEC)
-40.00
0.00
40.00
80.00
120.00
160.00
200.00
240.00
0.00
0.40
0.80
1.20
1.60
2.00
2.40
2.80

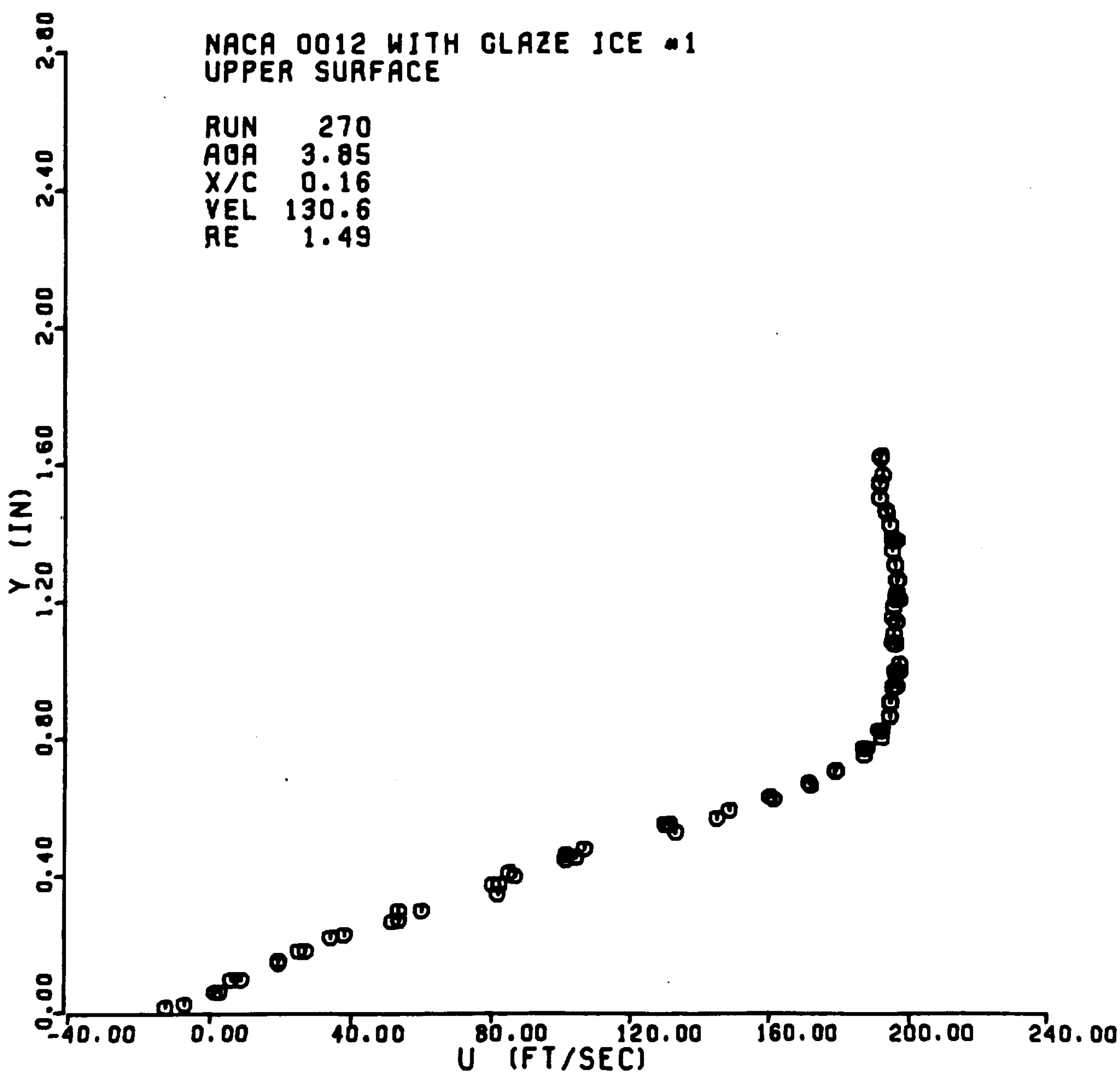

NACA 0012 WITH GLAZE ICE #1
UPPER SURFACE
RUN 270
AOA 3.85
X/C 0.16
VEL 130.6
RE 1.49
Y (IN)
0.00
0.40
0.80
1.20
1.60
2.00
2.40
2.80
-40.00
0.00
40.00
80.00
120.00
160.00
200.00
240.00
U (FT/SEC)

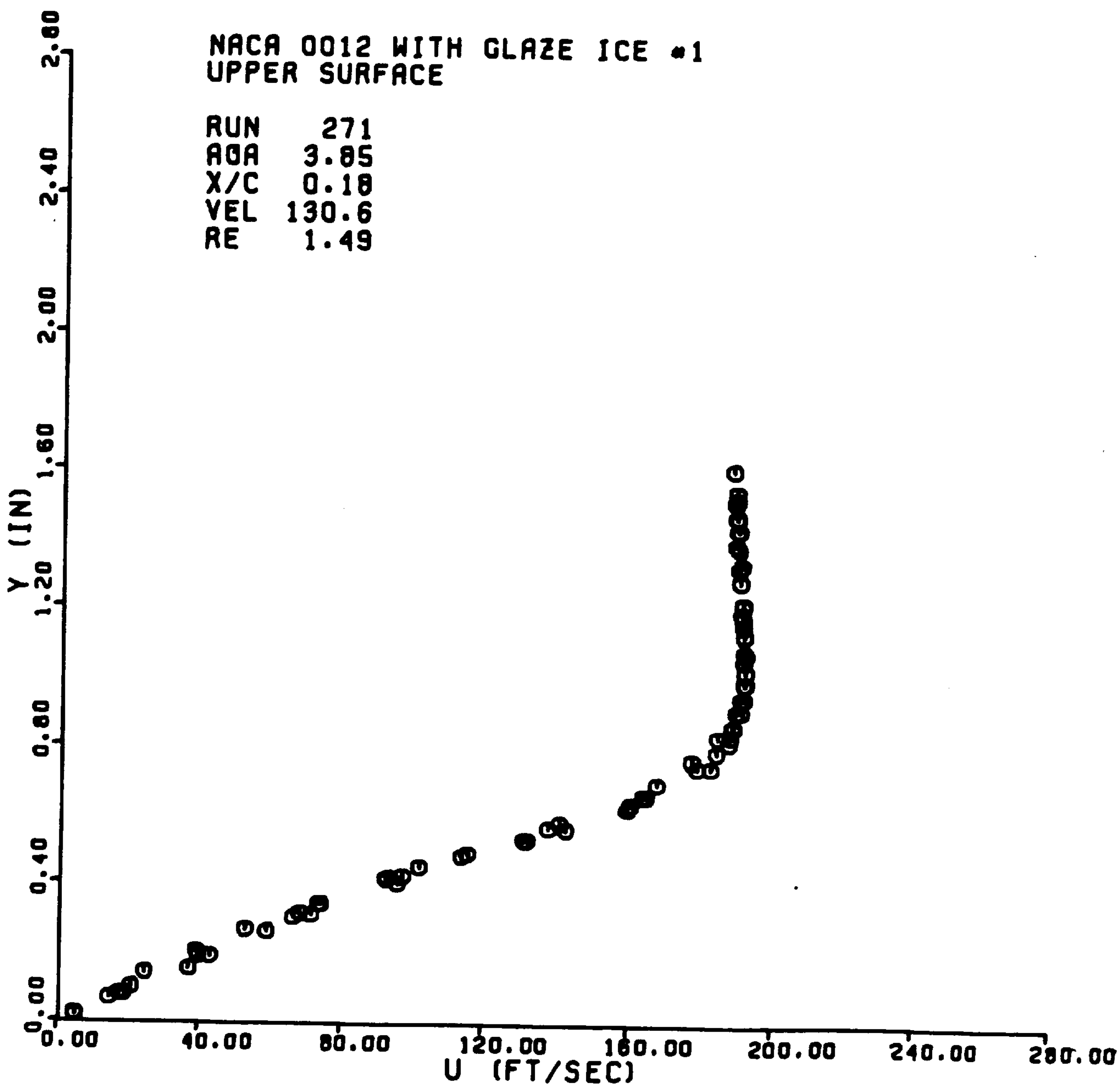
NACA 0012 WITH GLAZE ICE #1
UPPER SURFACE
RUN 271
AOA 3.85
X/C 0.18
VEL 130.6
RE 1.49
Y (IN)
0.00
0.40
0.80
1.20
1.60
2.00
2.40
2.80
0.00
40.00
80.00
120.00
160.00
200.00
240.00
280.00
U (FT/SEC)

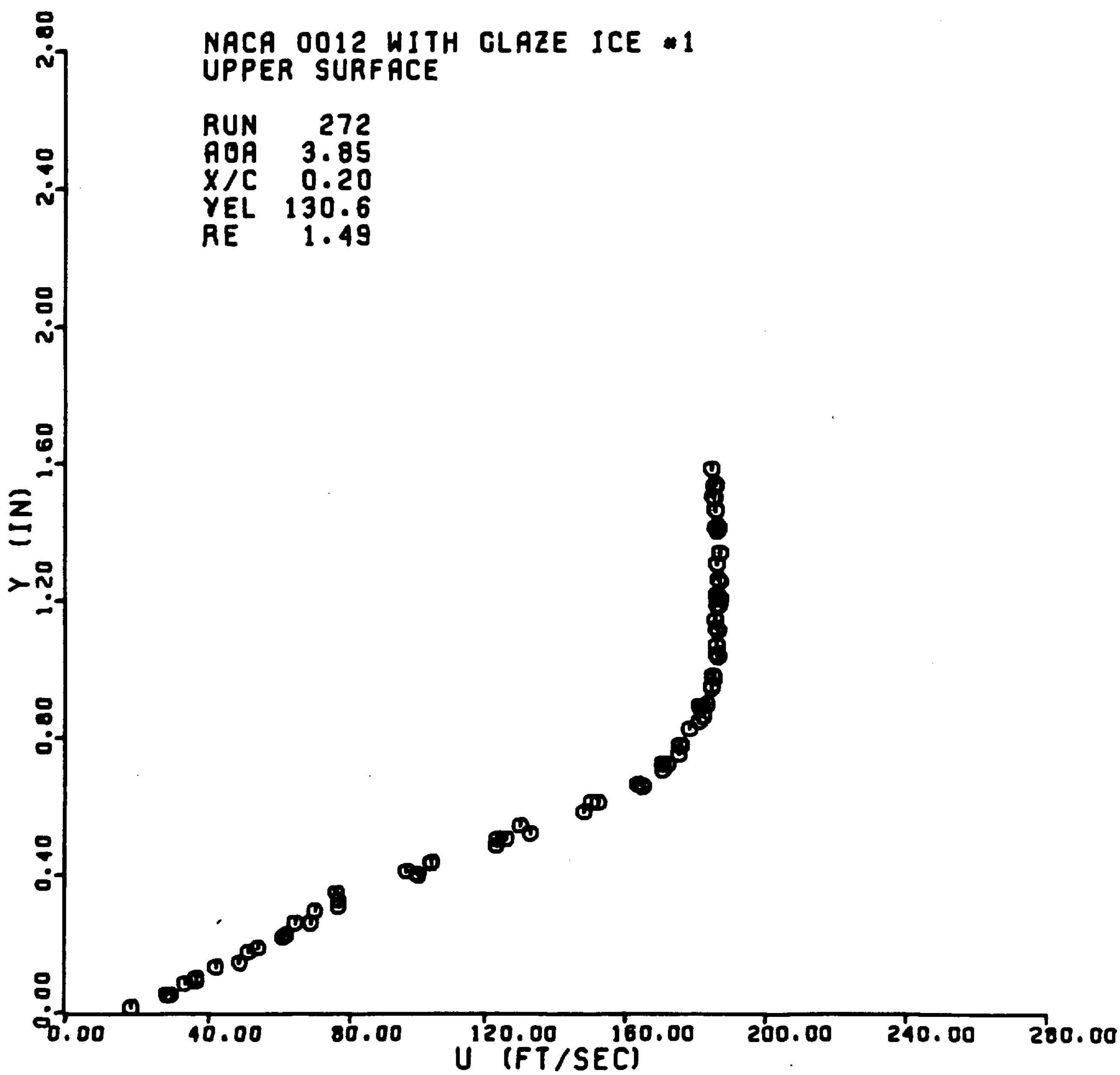
NACA 0012 WITH GLAZE ICE #1
UPPER SURFACE
RUN 272
AOA 3.85
X/C 0.20
VEL 130.6
RE 1.49
Y (IN)
0.00
0.40
0.80
1.20
1.60
2.00
2.40
2.80
0.00
40.00
80.00
120.00
160.00
200.00
240.00
280.00
U (FT/SEC)

-4

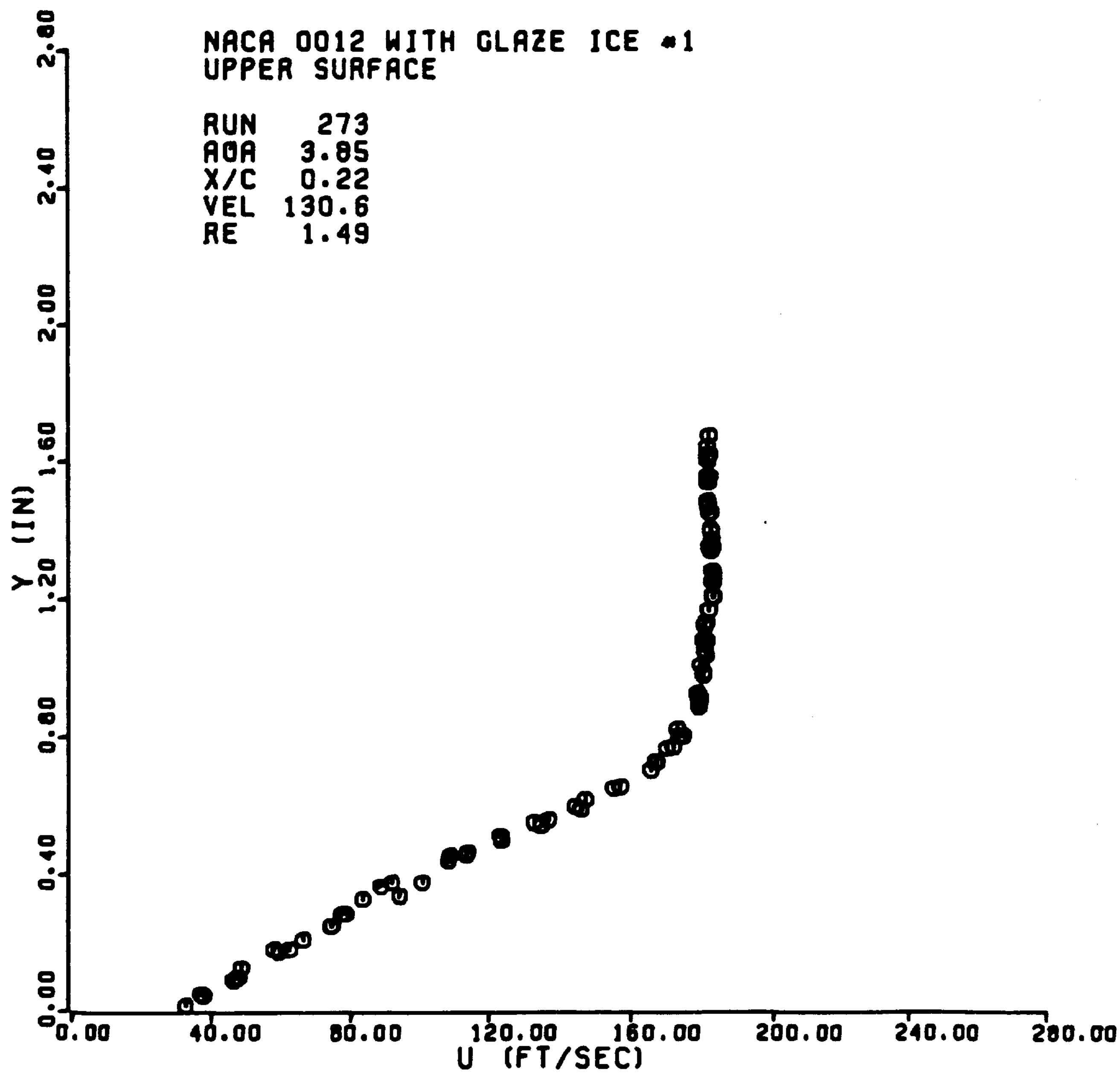

NACA 0012 WITH GLAZE ICE #1
UPPER SURFACE
RUN 273
AOA 3.85
X/C 0.22
VEL 130.6
RE 1.49
Y (IN)
0.00
0.40
0.80
1.20
1.60
2.00
2.40
2.80
U (FT/SEC)
0.00
40.00
80.00
120.00
160.00
200.00
240.00
280.00

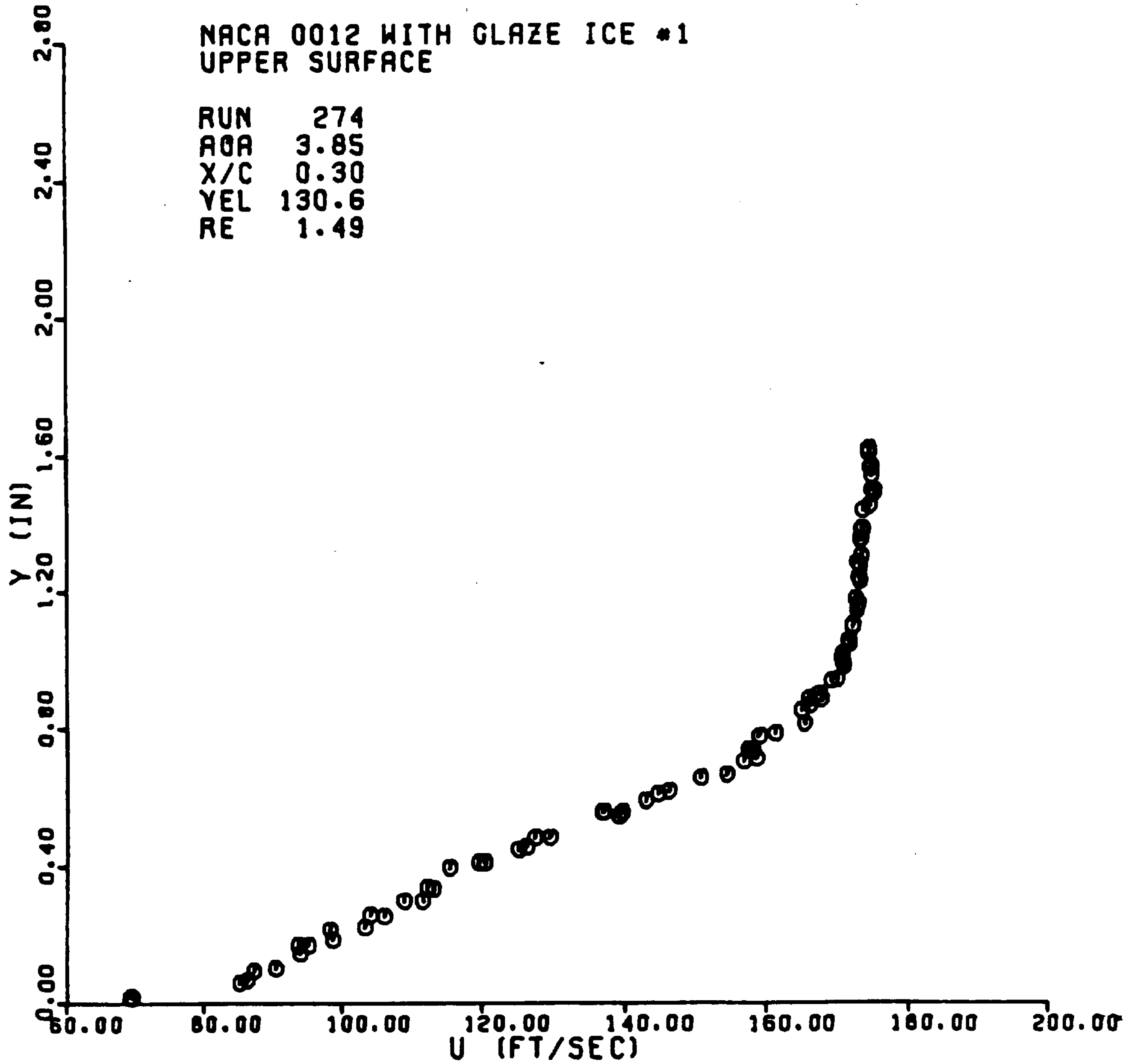
NACA 0012 WITH GLAZE ICE #1
UPPER SURFACE
RUN 274
AOA 3.85
X/C 0.30
VEL 130.6
RE 1.49
Y (IN)
0.00
0.40
0.80
1.20
1.60
2.00
2.40
2.80
60.00
80.00
100.00
120.00
140.00
160.00
180.00
200.00
U (FT/SEC)

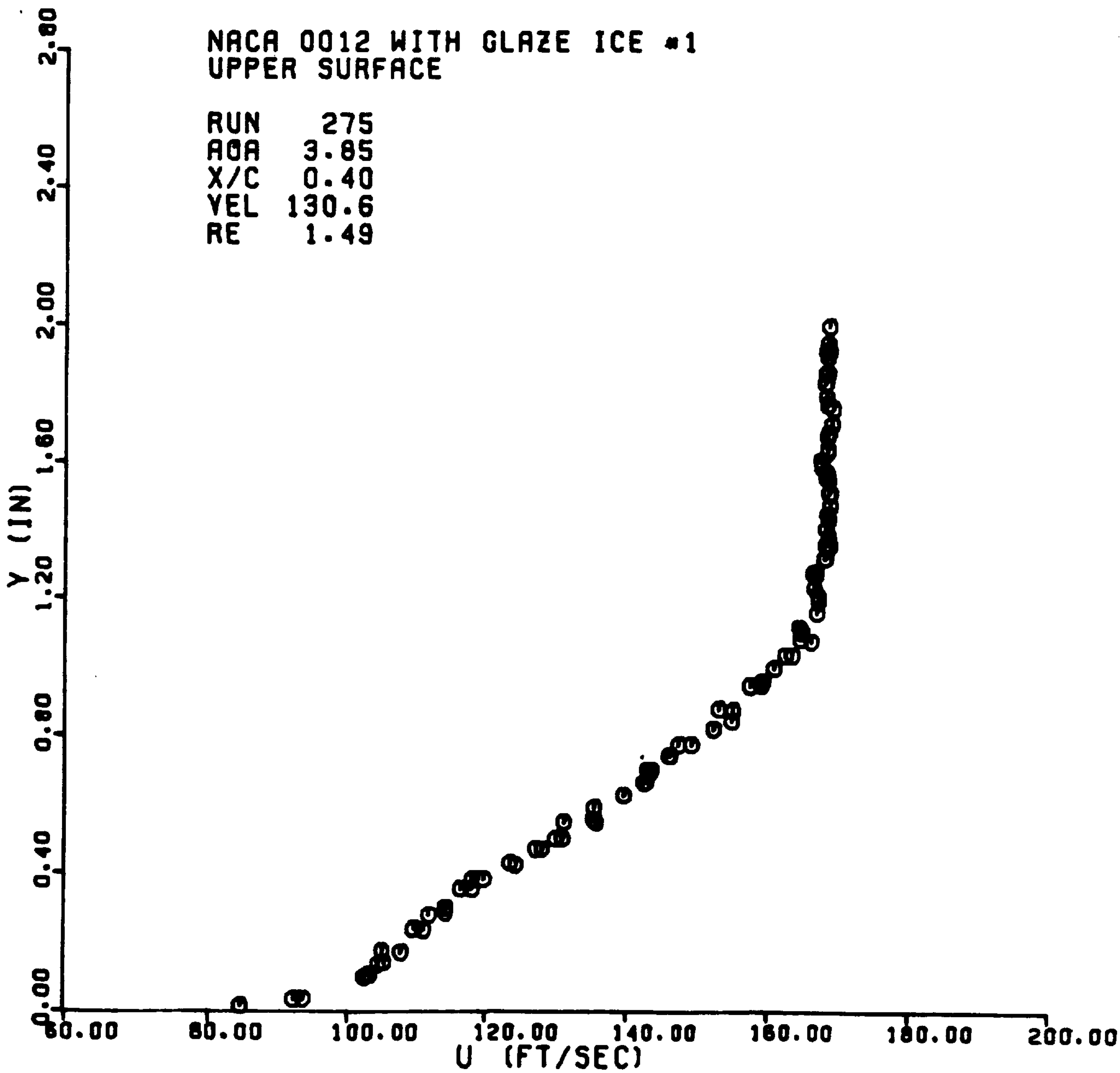

NACA 0012 WITH GLAZE ICE #1
UPPER SURFACE
RUN 275
AOA 3.85
X/C 0.40
VEL 130.6
RE 1.49
Y (IN)
2.80
2.40
2.00
1.60
1.20
0.80
0.40
0.00
60.00
80.00
100.00
120.00
140.00
160.00
180.00
200.00
U (FT/SEC)

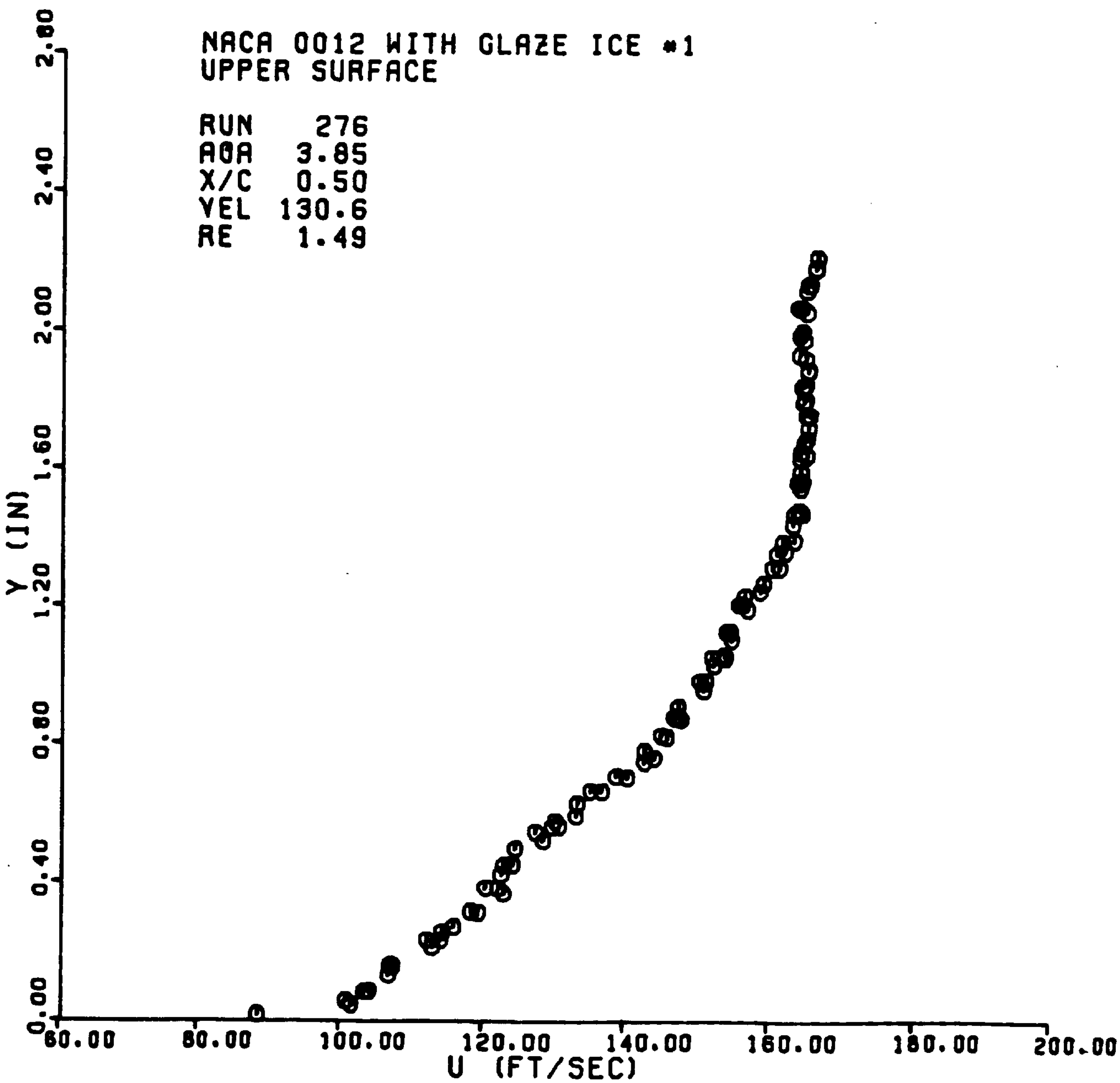
NACA 0012 WITH GLAZE ICE #1
UPPER SURFACE
RUN 276
AOA 3.85
X/C 0.50
VEL 130.6
RE 1.49
Y (IN)
0.00
0.40
0.80
1.20
1.60
2.00
2.40
2.80
60.00
80.00
100.00
120.00
140.00
160.00
180.00
200.00
U (FT/SEC)

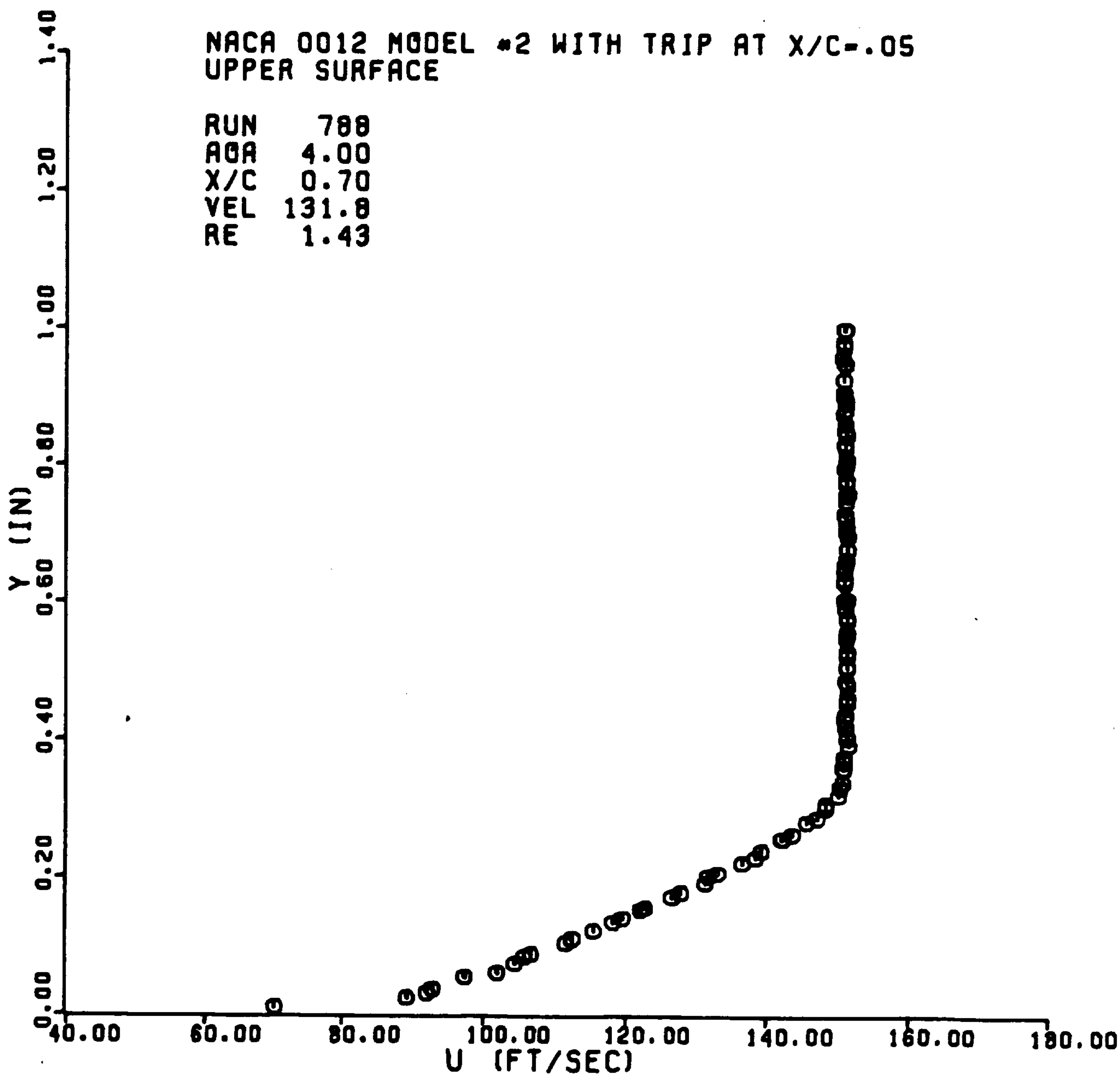

NACA 0012 MODEL #2 WITH TRIP AT X/C=.05
UPPER SURFACE
RUN 788
AOA 4.00
X/C 0.70
VEL 131.8
RE 1.43
Y (IN)
0.00
0.20
0.40
0.60
0.80
1.00
1.20
1.40
40.00
60.00
80.00
100.00
120.00
140.00
160.00
180.00
U (FT/SEC)

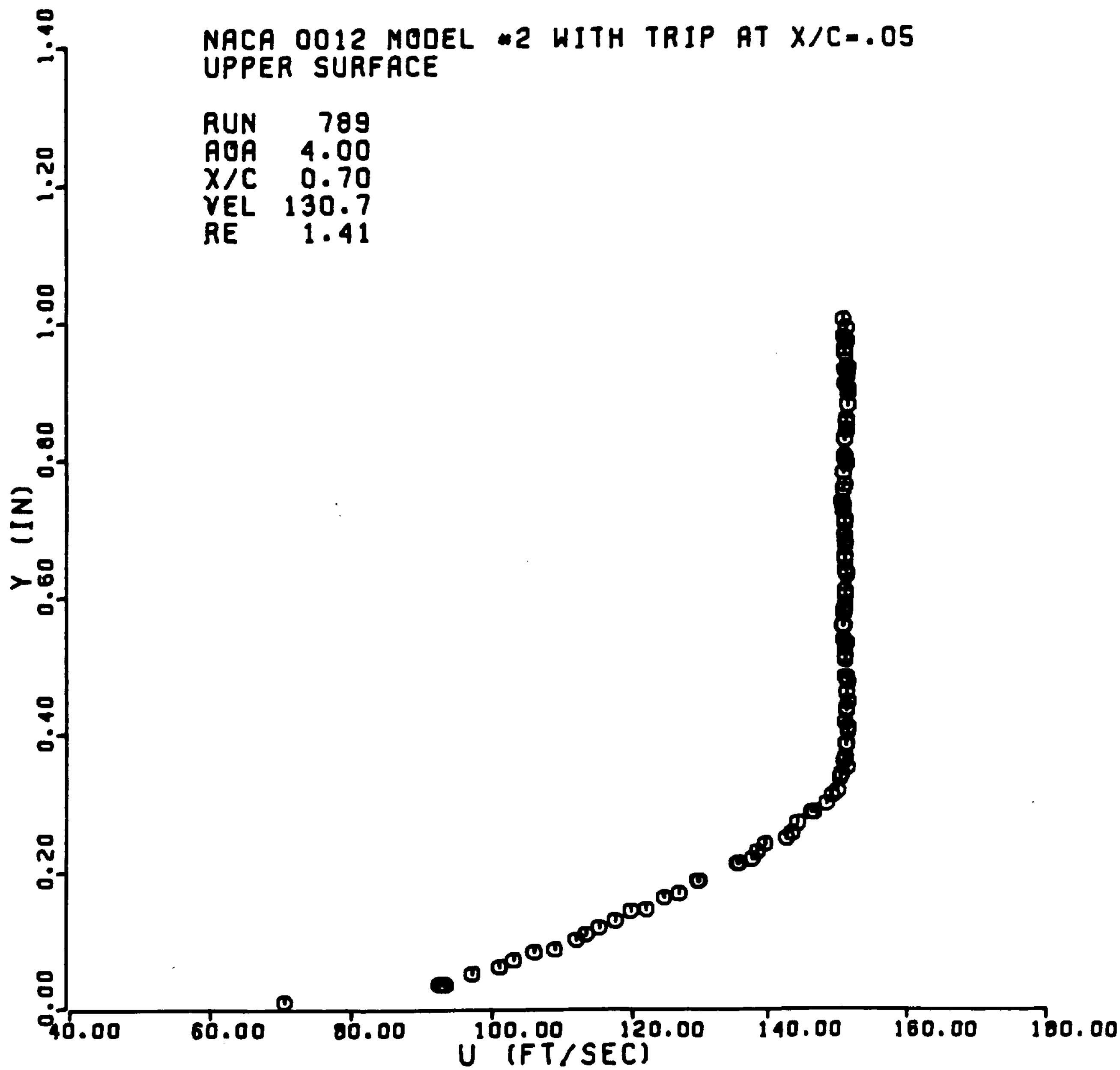

NACA 0012 MODEL *2 WITH TRIP AT X/C=.05
UPPER SURFACE
RUN 789
AOA 4.00
X/C 0.70
VEL 130.7
RE 1.41
Y (IN)
0.00
0.20
0.40
0.60
0.80
1.00
1.20
1.40
40.00
60.00
80.00
100.00
120.00
140.00
160.00
180.00
U (FT/SEC)

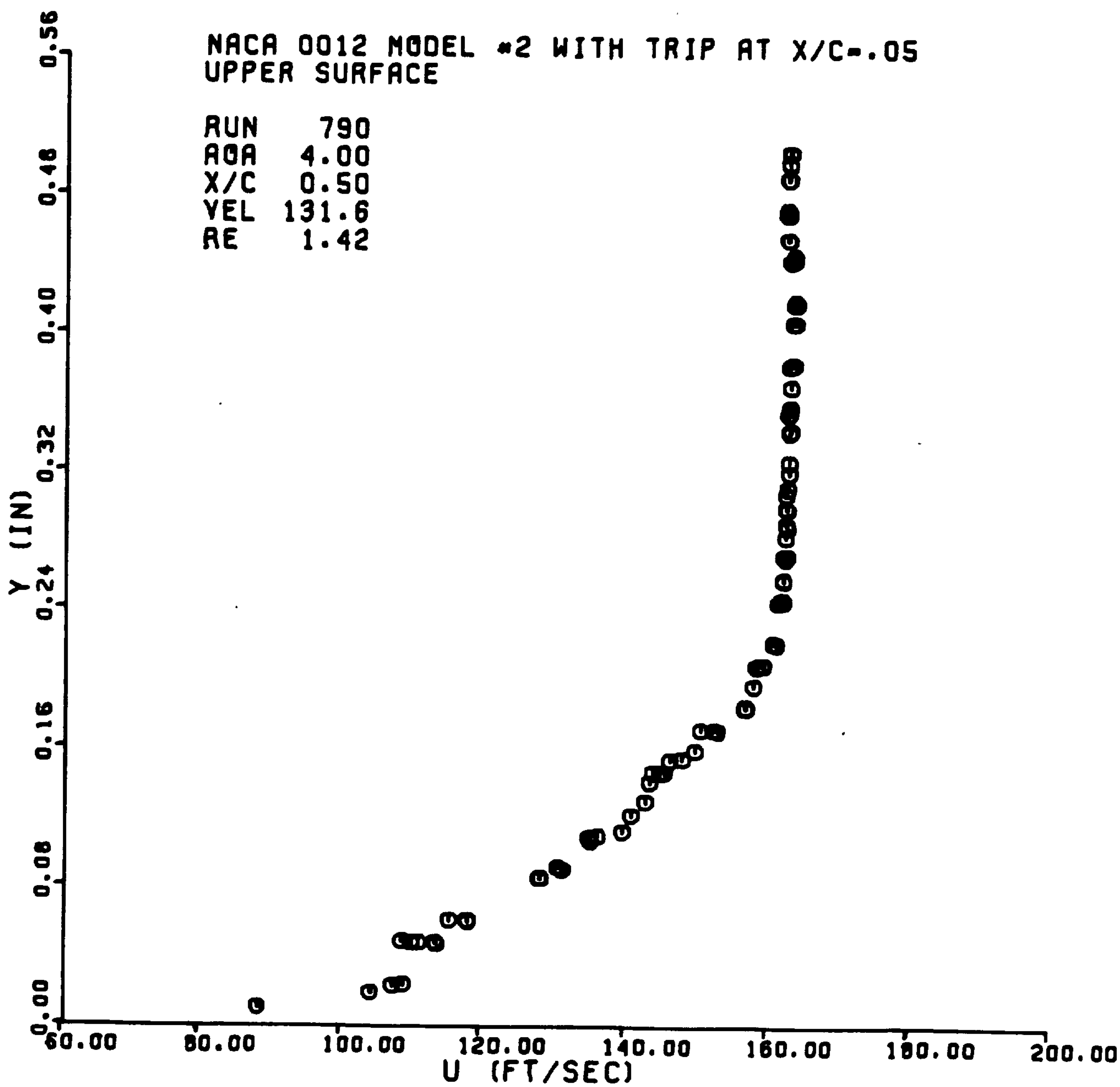
NACA 0012 MODEL #2 WITH TRIP AT X/C=.05
UPPER SURFACE
RUN 790
AOA 4.00
X/C 0.50
VEL 131.6
RE 1.42
Y (IN)
0.00
0.08
0.16
0.24
0.32
0.40
0.48
0.56
60.00
80.00
100.00
120.00
140.00
160.00
180.00
200.00
U (FT/SEC)

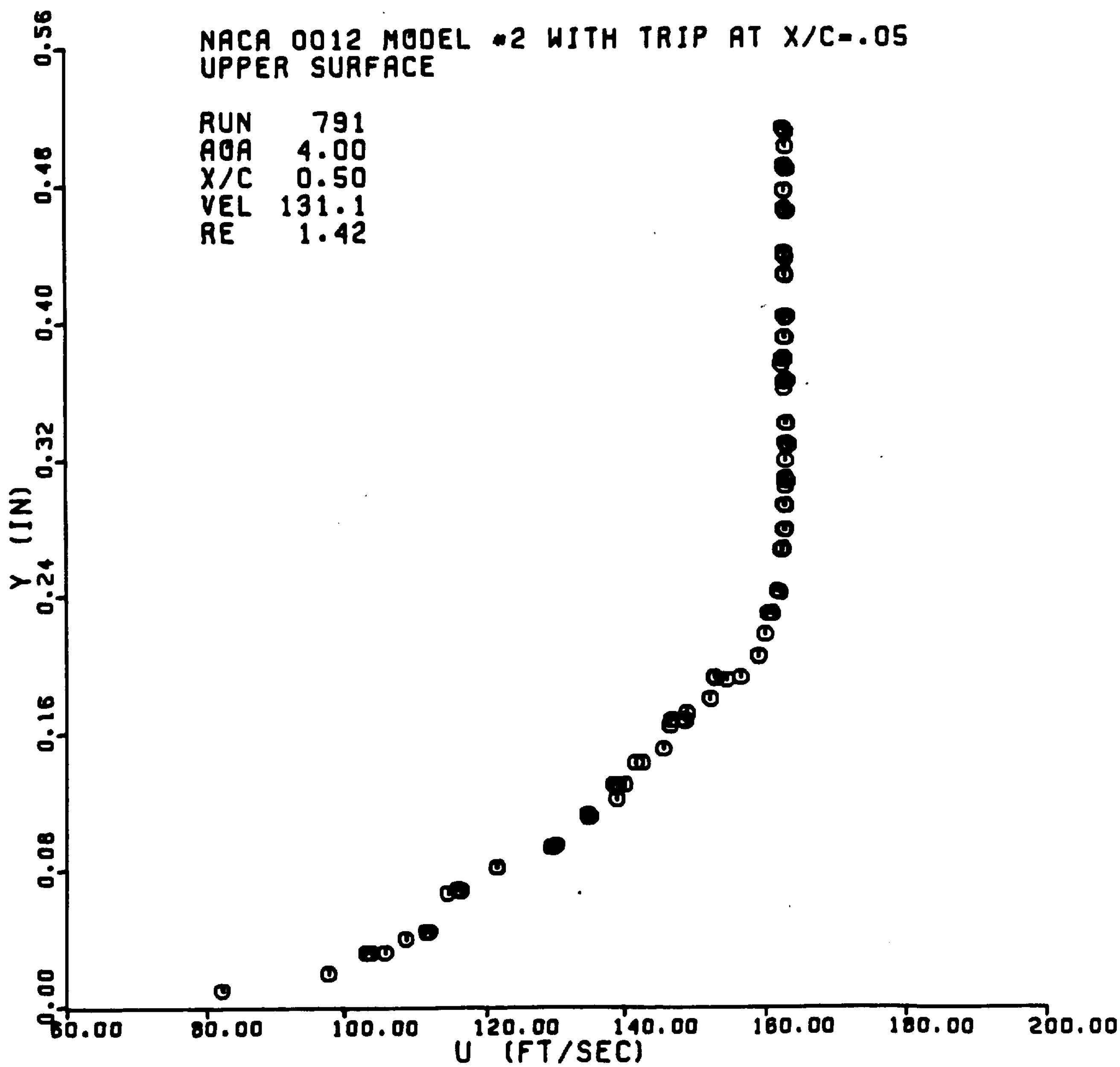
NACA 0012 MODEL #2 WITH TRIP AT X/C=.05
UPPER SURFACE
RUN 791
AOA 4.00
X/C 0.50
VEL 131.1
RE 1.42
Y (IN)
0.00
0.08
0.16
0.24
0.32
0.40
0.48
0.56
60.00
80.00
100.00
120.00
140.00
160.00
180.00
200.00
U (FT/SEC)

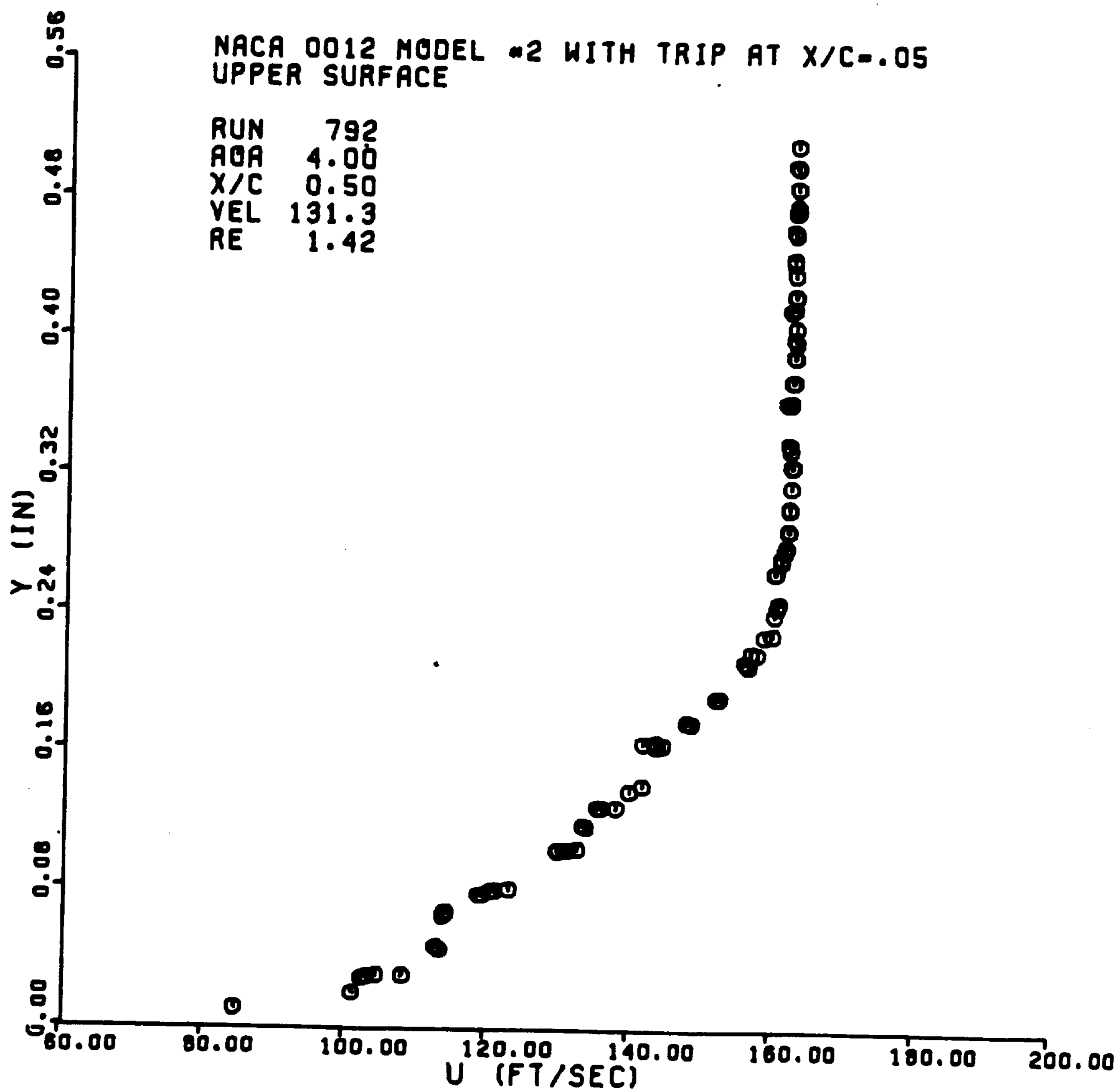
NACA 0012 MODEL #2 WITH TRIP AT X/C=.05
UPPER SURFACE
RUN 792
AOA 4.00
X/C 0.50
VEL 131.3
RE 1.42
Y (IN)
0.00
0.08
0.16
0.24
0.32
0.40
0.48
0.56
60.00
80.00
100.00
120.00
140.00
160.00
180.00
200.00
U (FT/SEC)

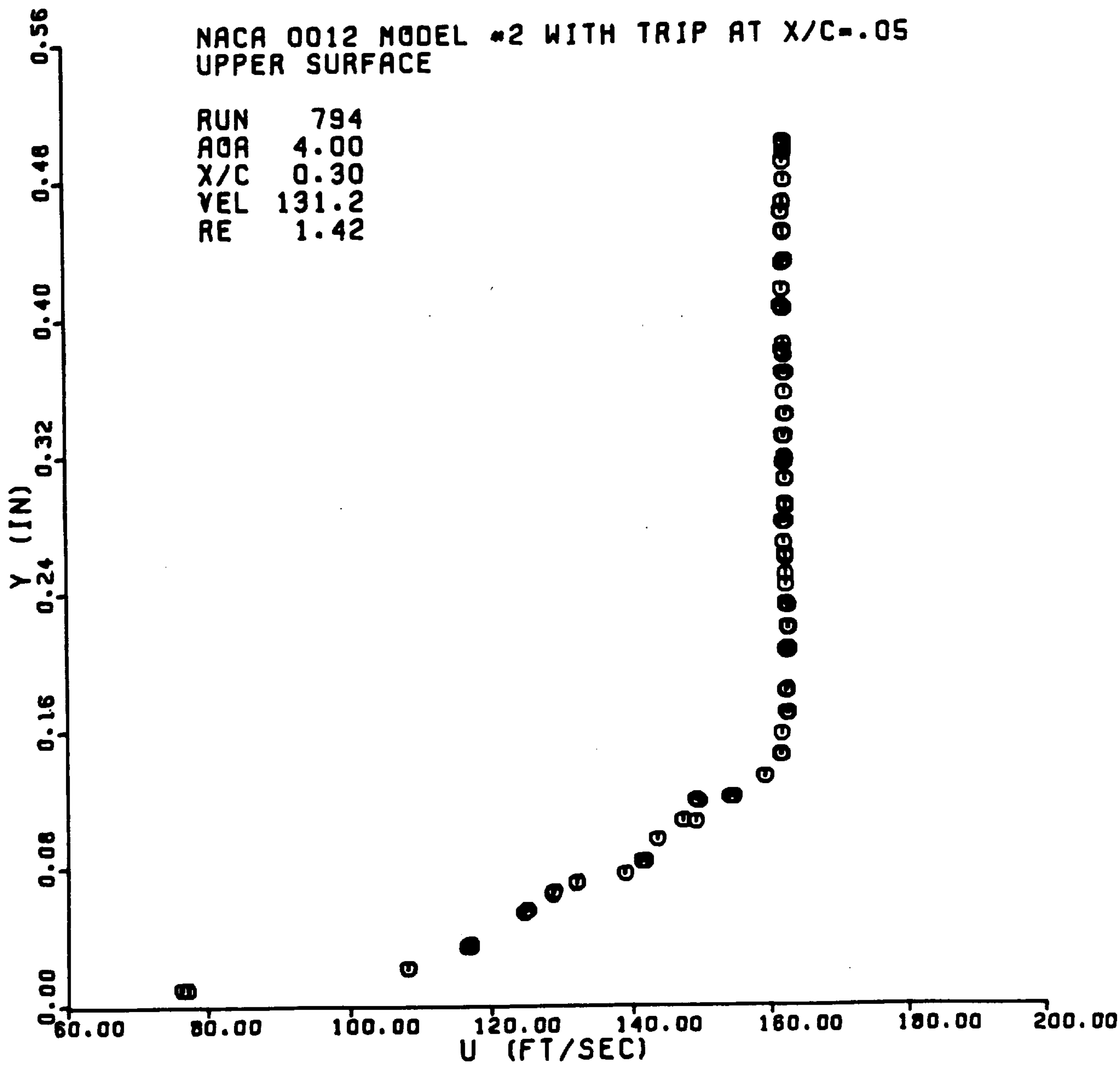

NACA 0012 MODEL *2 WITH TRIP AT X/C=.05
UPPER SURFACE
RUN 794
AOA 4.00
X/C 0.30
VEL 131.2
RE 1.42
Y (IN)
0.00
0.08
0.16
0.24
0.32
0.40
0.48
0.56
U (FT/SEC)
60.00
80.00
100.00
120.00
140.00
160.00
180.00
200.00

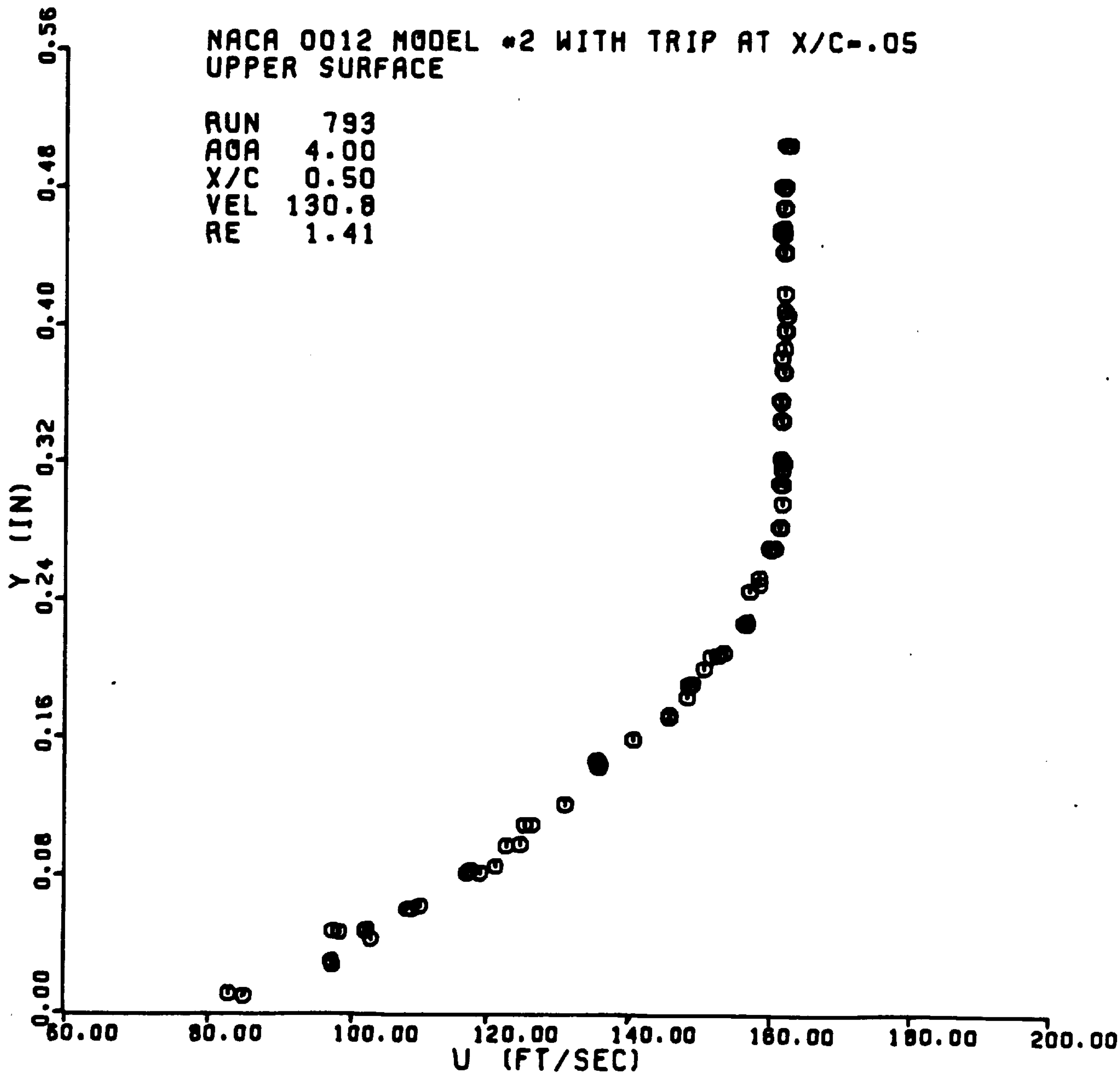
NACA 0012 MODEL #2 WITH TRIP AT X/C=.05
UPPER SURFACE
RUN 793
AOA 4.00
X/C 0.50
VEL 130.8
RE 1.41
Y (IN)
0.00
0.08
0.16
0.24
0.32
0.40
0.48
0.56
60.00
80.00
100.00
120.00
140.00
160.00
180.00
200.00
U (FT/SEC)

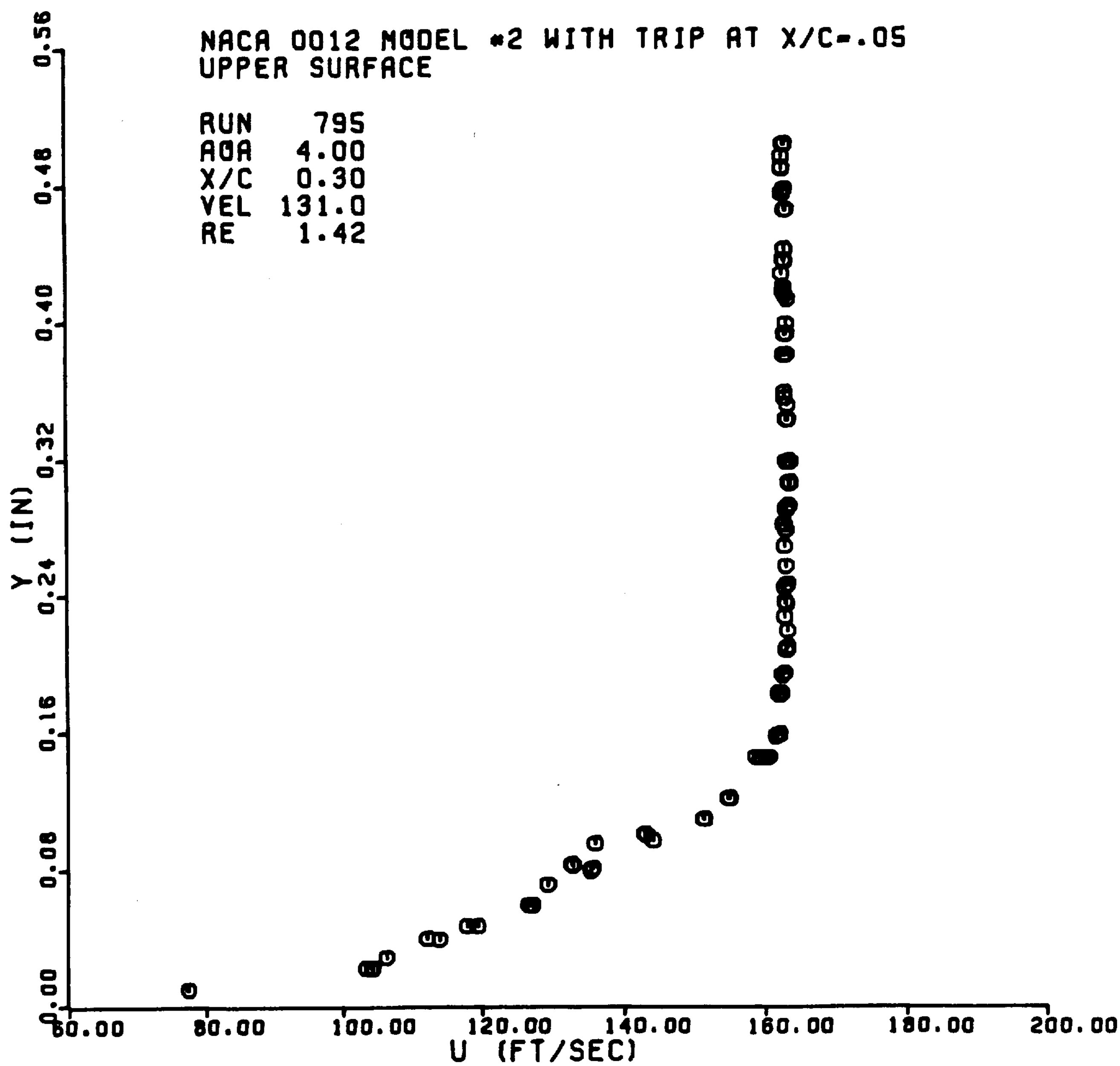
NACA 0012 MODEL #2 WITH TRIP AT X/C=.05
UPPER SURFACE
RUN 795
AOA 4.00
X/C 0.30
VEL 131.0
RE 1.42
Y (IN)
0.00
0.08
0.16
0.24
0.32
0.40
0.48
0.56
60.00
80.00
100.00
120.00
140.00
160.00
180.00
200.00
U (FT/SEC)

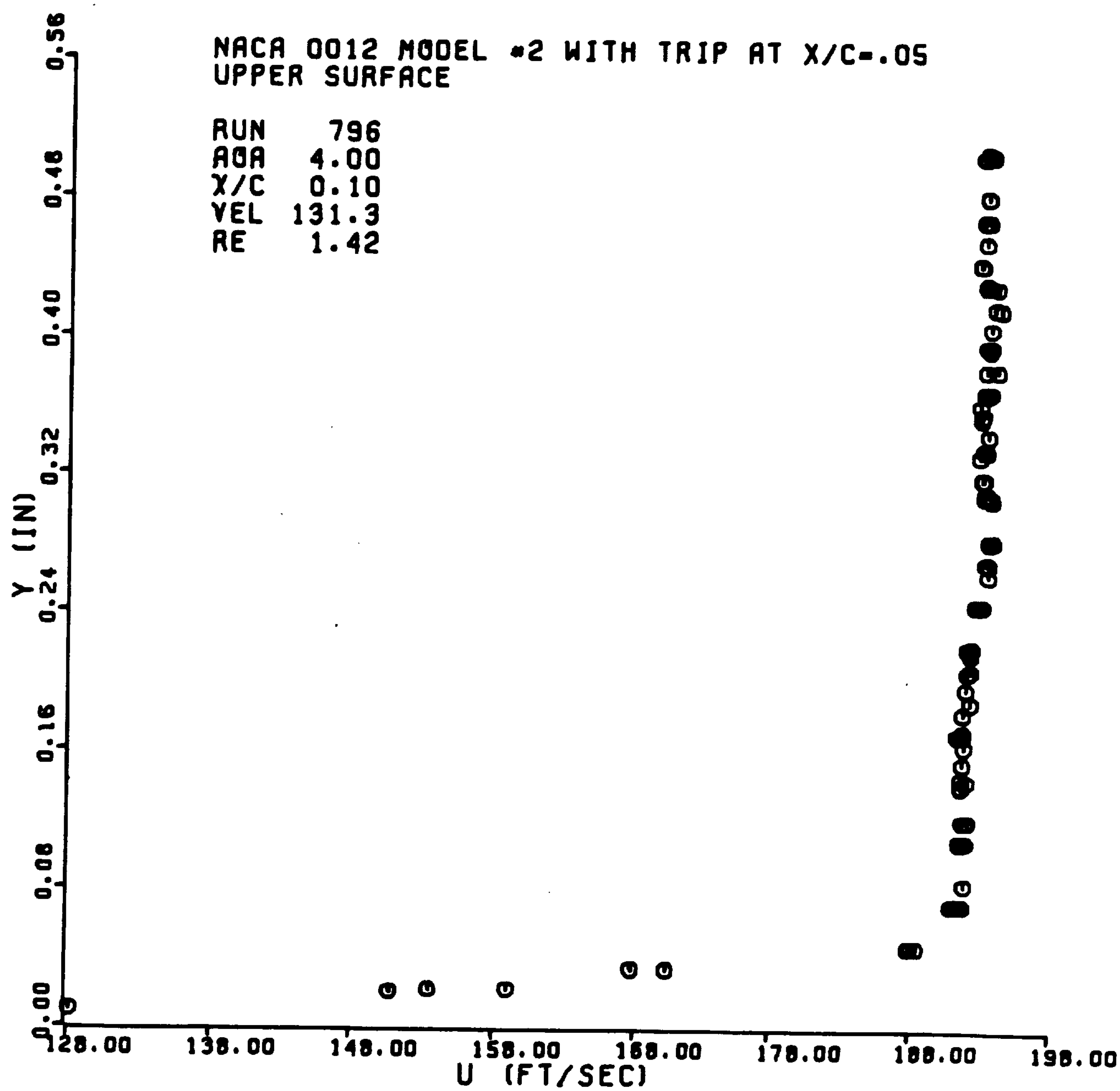
NACA 0012 MODEL #2 WITH TRIP AT X/C=.05
UPPER SURFACE
RUN 796
AOA 4.00
X/C 0.10
VEL 131.3
RE 1.42
Y (IN)
0.00
0.08
0.16
0.24
0.32
0.40
0.48
0.56
128.00
138.00
148.00
158.00
168.00
178.00
188.00
198.00
U (FT/SEC)

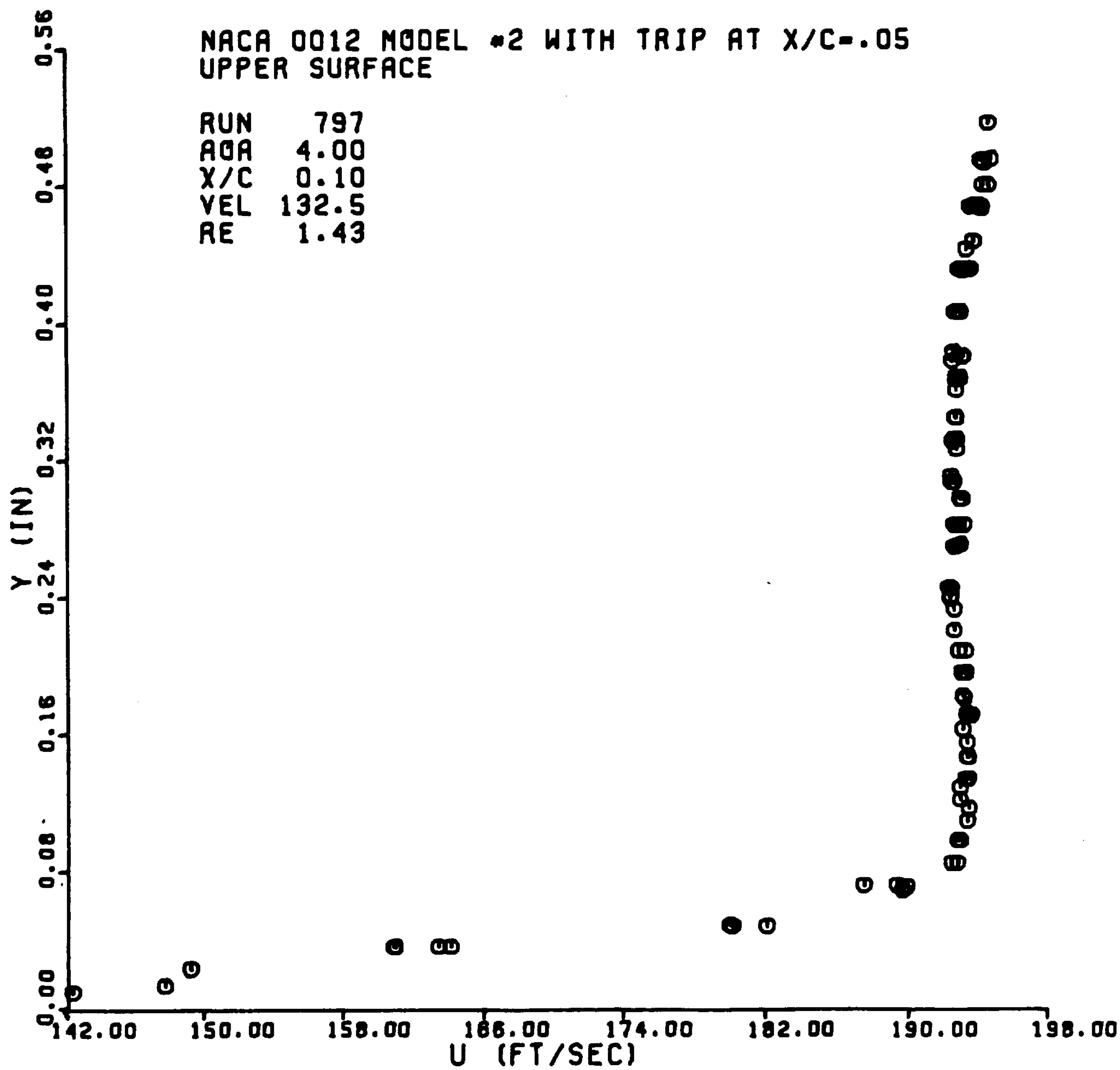
NACA 0012 MODEL #2 WITH TRIP AT X/C=.05
UPPER SURFACE
RUN 797
AOA 4.00
X/C 0.10
VEL 132.5
RE 1.43
Y (IN)
0.00
0.08
0.16
0.24
0.32
0.40
0.48
0.56
U (FT/SEC)
142.00
150.00
158.00
166.00
174.00
182.00
190.00
198.00

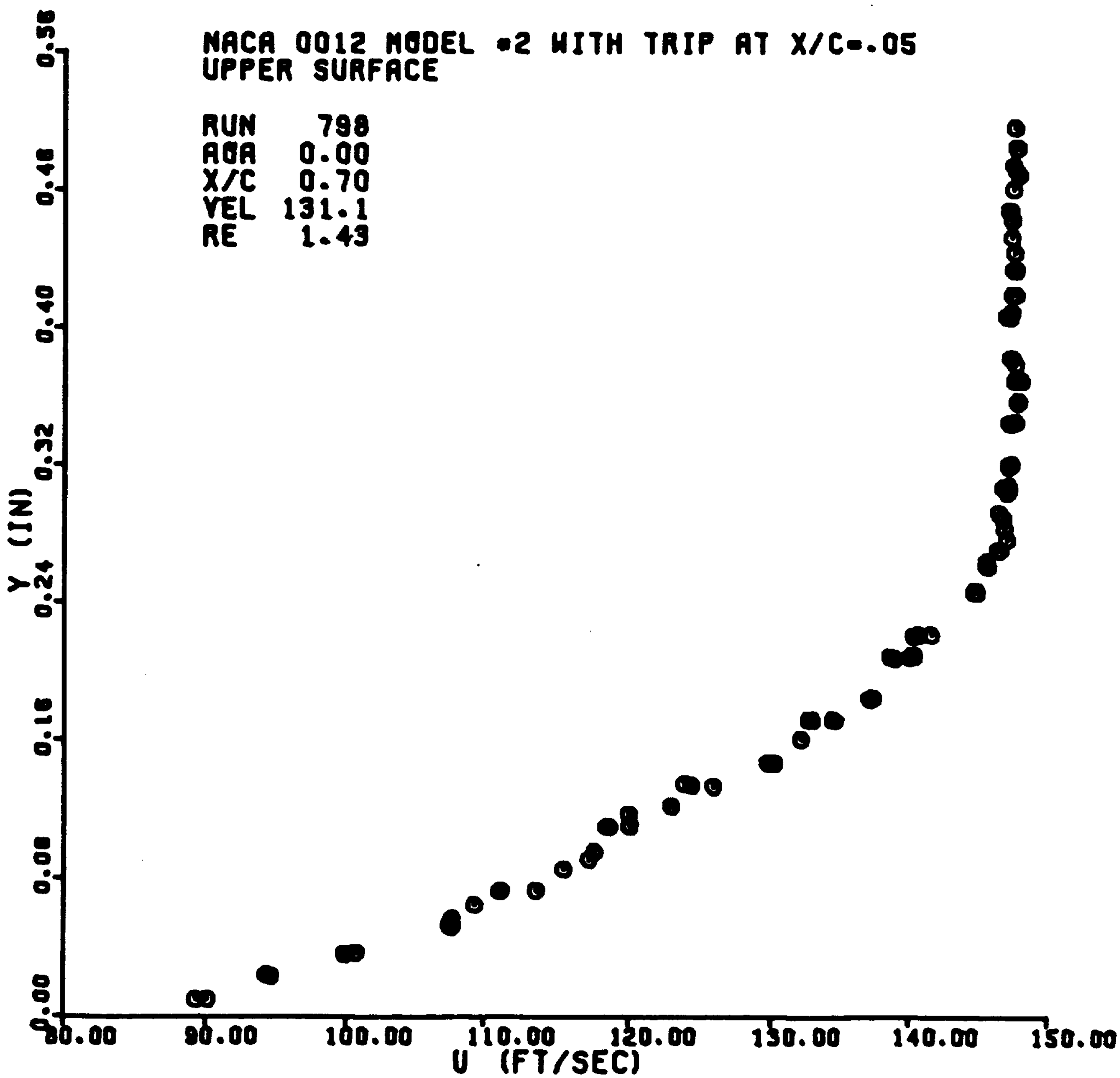
NACA 0012 MODEL #2 WITH TRIP AT X/C=.05
UPPER SURFACE
RUN 798
AOA 0.00
X/C 0.70
VEL 131.1
RE 1.43
Y (IN)
0.00
0.08
0.16
0.24
0.32
0.40
0.48
0.56
U (FT/SEC)
80.00
90.00
100.00
110.00
120.00
130.00
140.00
150.00

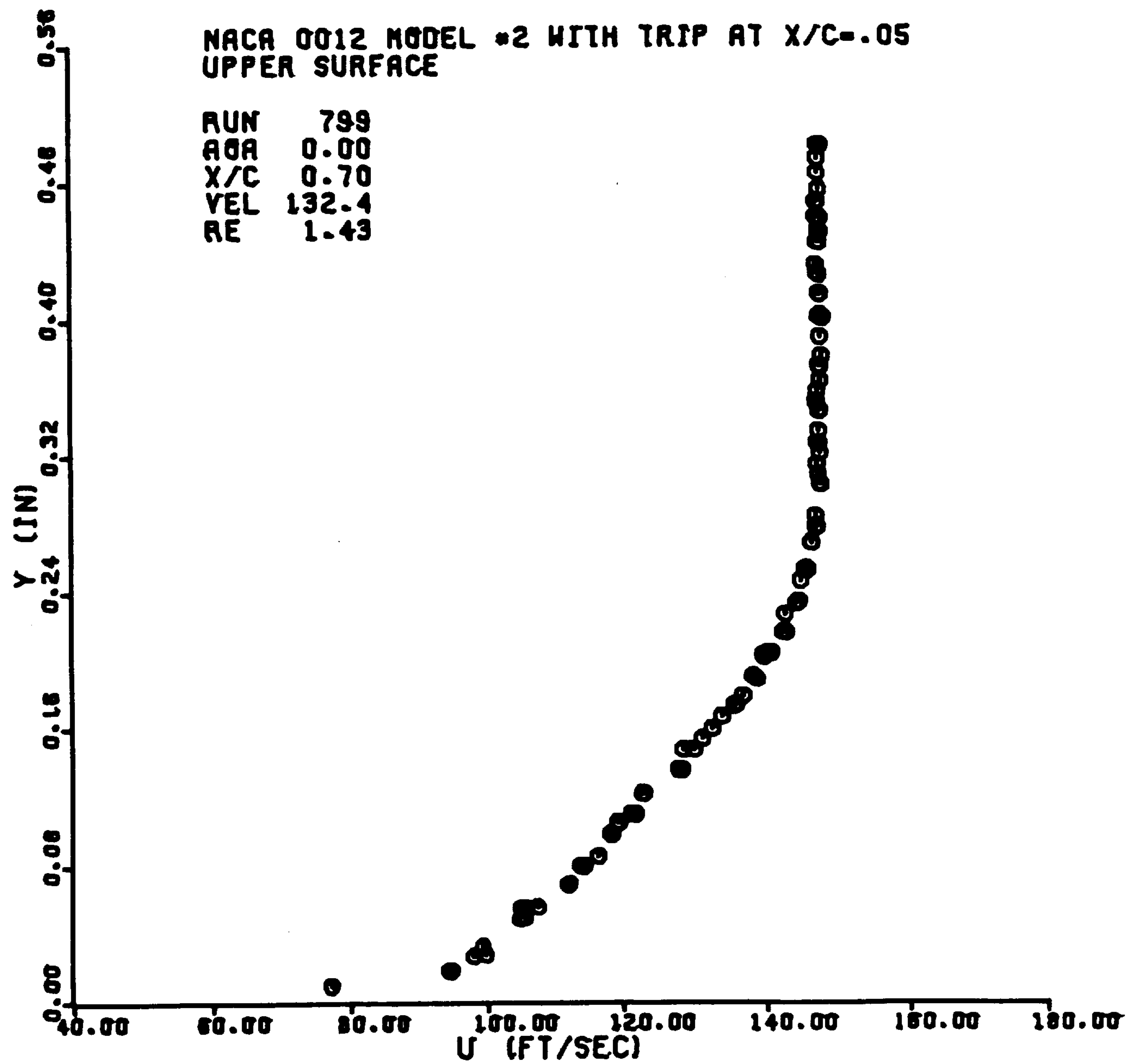
NACA 0012 MODEL *2 WITH TRIP AT X/C=.05
UPPER SURFACE
RUN 799
AOA 0.00
X/C 0.70
VEL 132.4
RE 1.43
Y (IN)
0.00
0.08
0.16
0.24
0.32
0.40
0.48
0.56
40.00
60.00
80.00
100.00
120.00
140.00
160.00
180.00
U (FT/SEC)

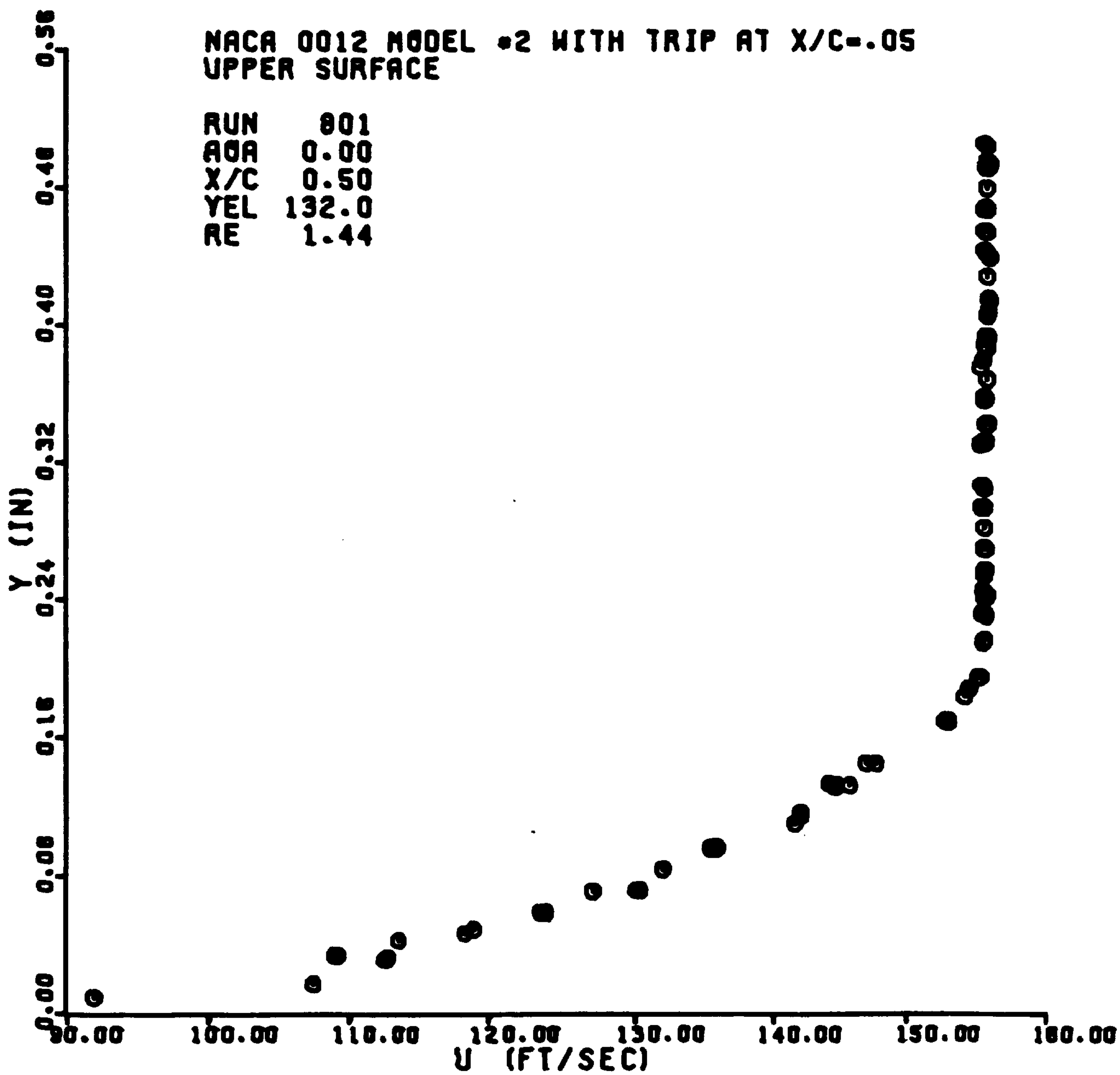
NACA 0012 MODEL #2 WITH TRIP AT X/C=.05
UPPER SURFACE
RUN 801
AOA 0.00
X/C 0.50
VEL 132.0
RE 1.44
Y (IN)
0.00
0.08
0.16
0.24
0.32
0.40
0.48
0.56
90.00
100.00
110.00
120.00
130.00
140.00
150.00
160.00
U (FT/SEC)

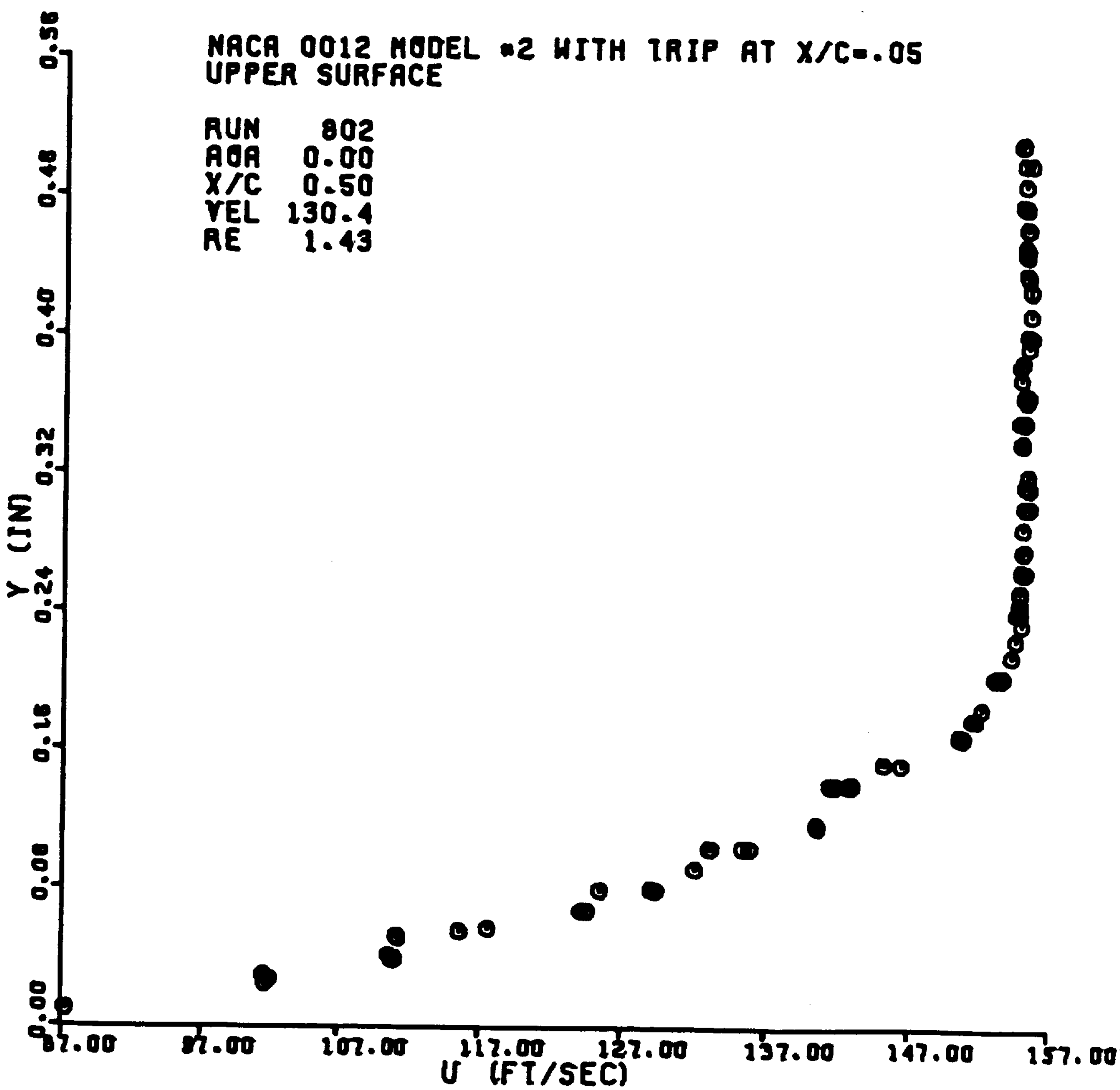
NACA 0012 MODEL #2 WITH TRIP AT X/C=.05
UPPER SURFACE
RUN 802
AOA 0.00
X/C 0.50
VEL 130.4
RE 1.43
Y (IN)
0.00
0.08
0.16
0.24
0.32
0.40
0.48
0.56
87.00
97.00
107.00
117.00
127.00
137.00
147.00
157.00
U (FT/SEC)

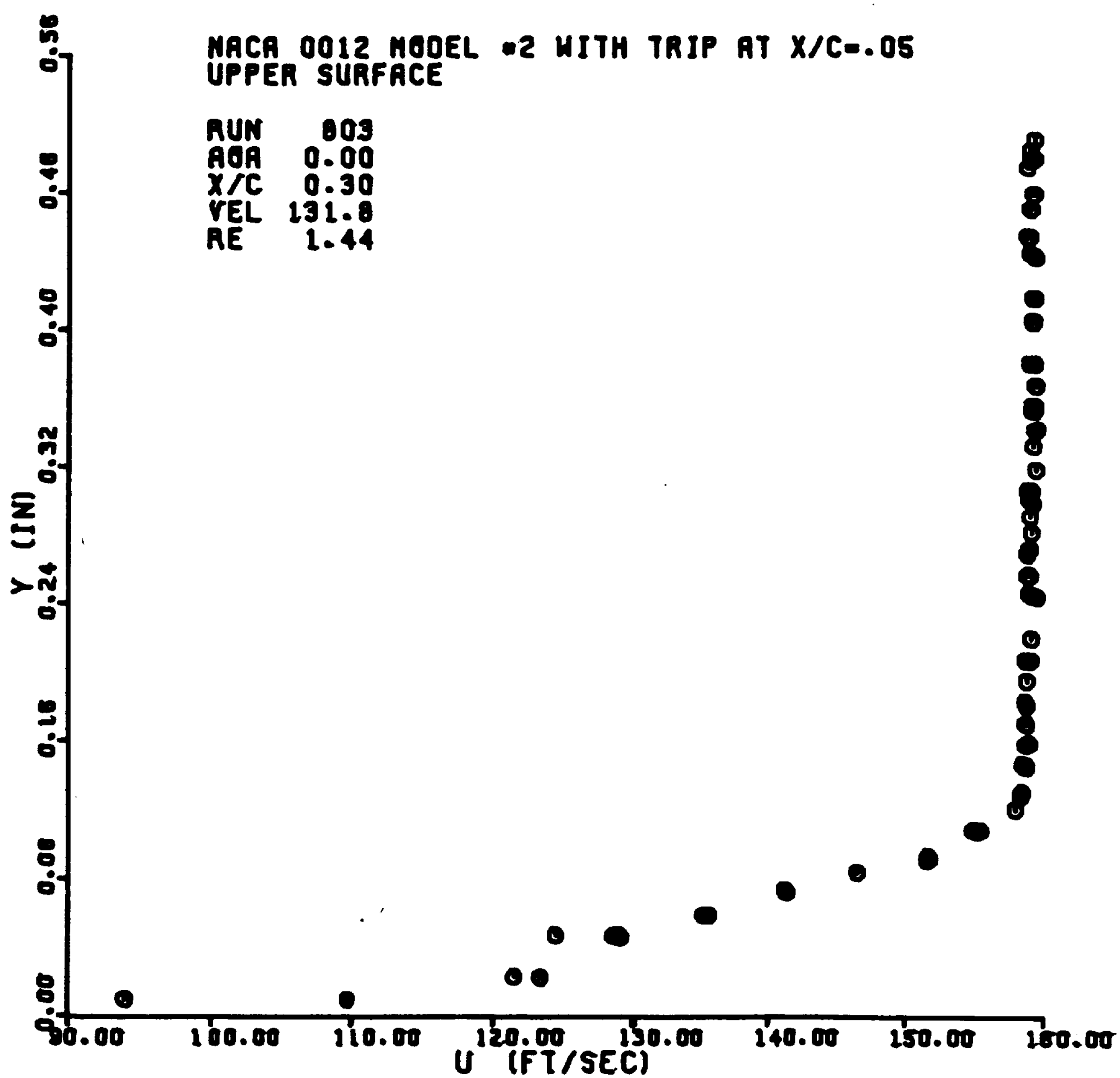

NACA 0012 MODEL #2 WITH TRIP AT X/C=.05
UPPER SURFACE
RUN 803
AOA 0.00
X/C 0.30
VEL 131.8
RE 1.44
Y (IN)
0.00
0.08
0.16
0.24
0.32
0.40
0.48
0.56
90.00
100.00
110.00
120.00
130.00
140.00
150.00
160.00
U (FT/SEC)

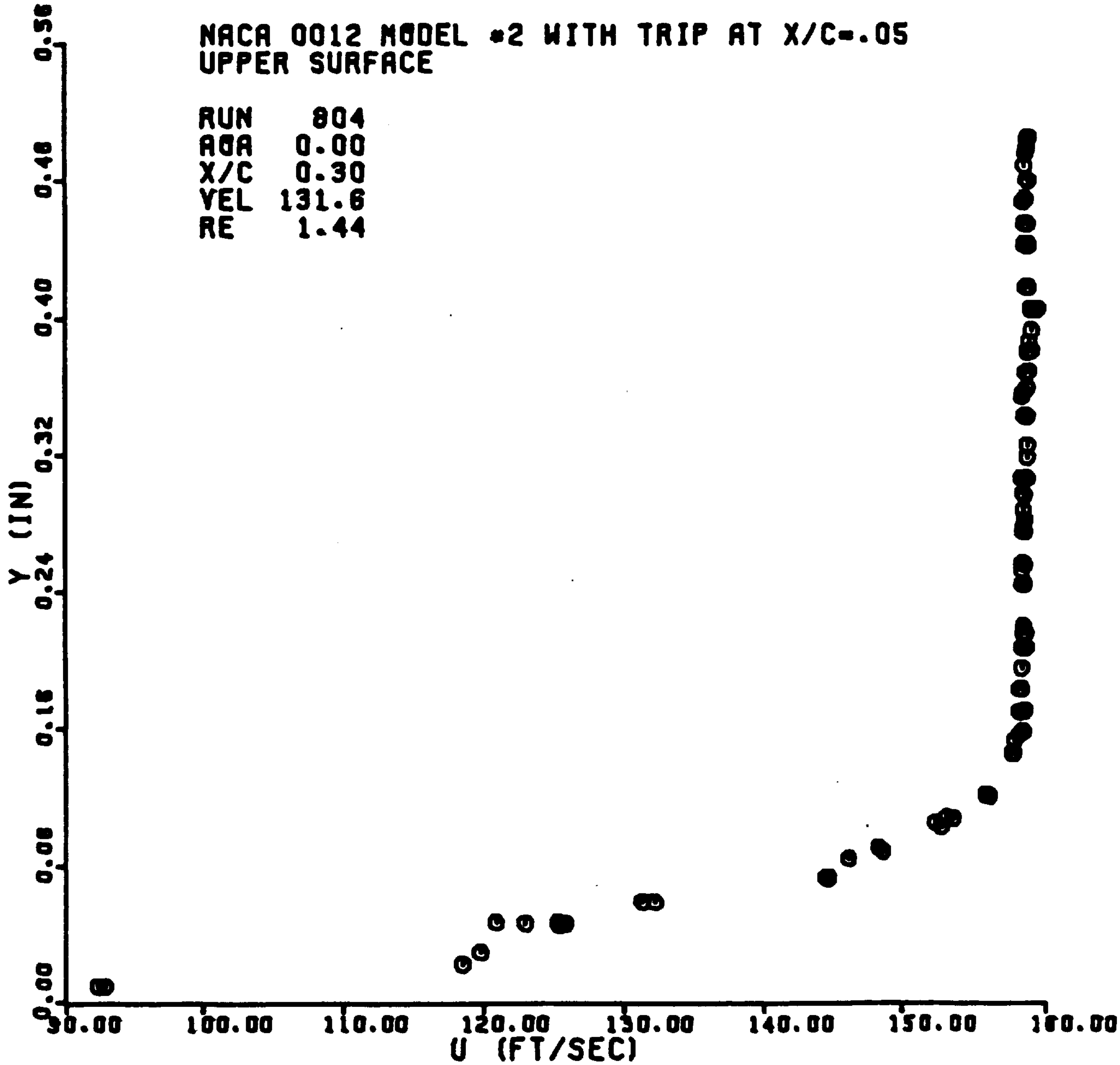

NACA 0012 MODEL #2 WITH TRIP AT X/C=.05
UPPER SURFACE
RUN 804
AOA 0.00
X/C 0.30
VEL 131.6
RE 1.44
Y (IN)
0.00
0.08
0.16
0.24
0.32
0.40
0.48
0.56
U (FT/SEC)
90.00
100.00
110.00
120.00
130.00
140.00
150.00
160.00

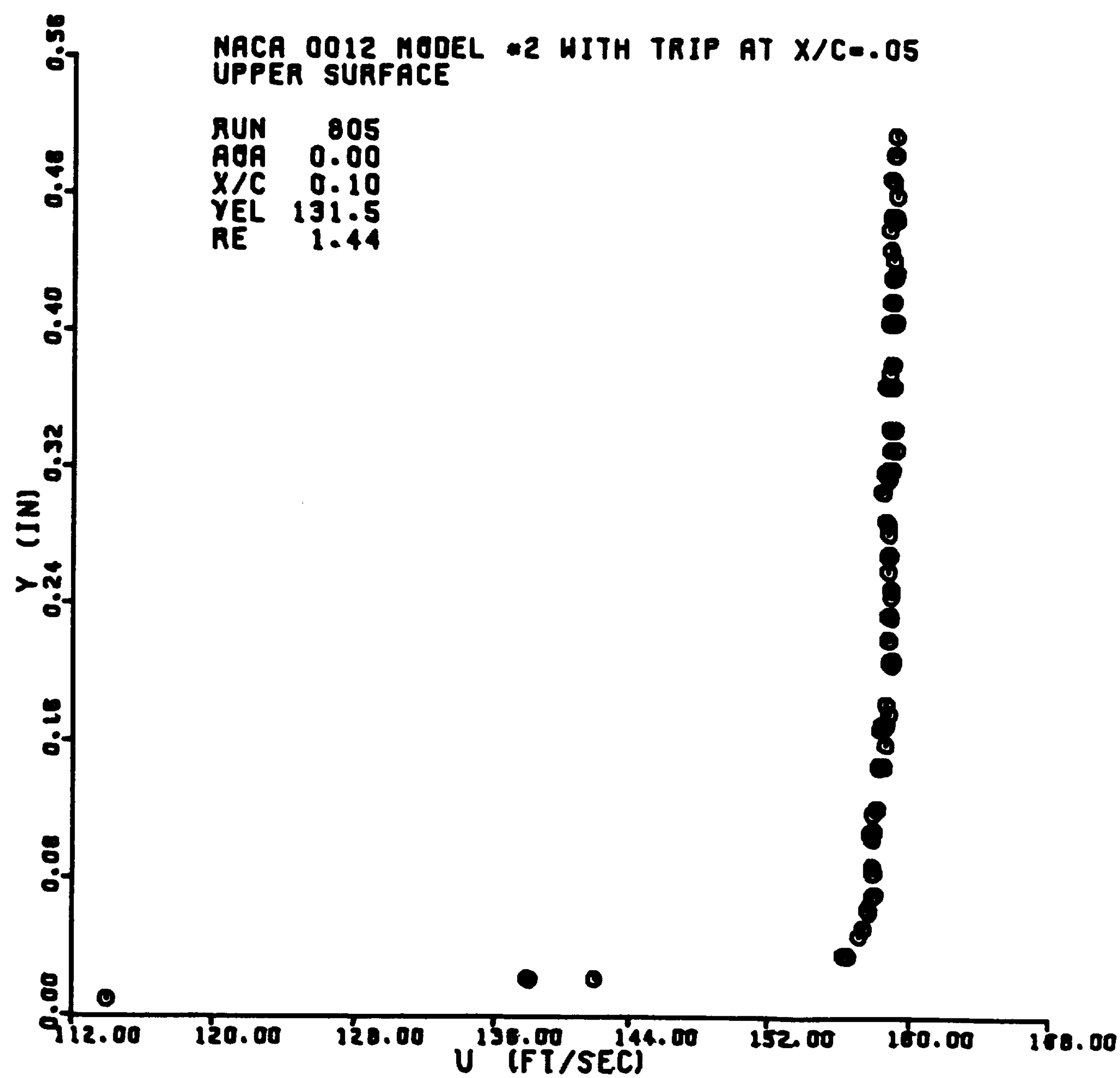
NACA 0012 MODEL #2 WITH TRIP AT X/C=.05
UPPER SURFACE
RUN 805
AOA 0.00
X/C 0.10
VEL 131.5
RE 1.44
Y (IN)
0.00
0.08
0.16
0.24
0.32
0.40
0.48
0.56
112.00
120.00
128.00
136.00
144.00
152.00
160.00
168.00
U (FT/SEC)

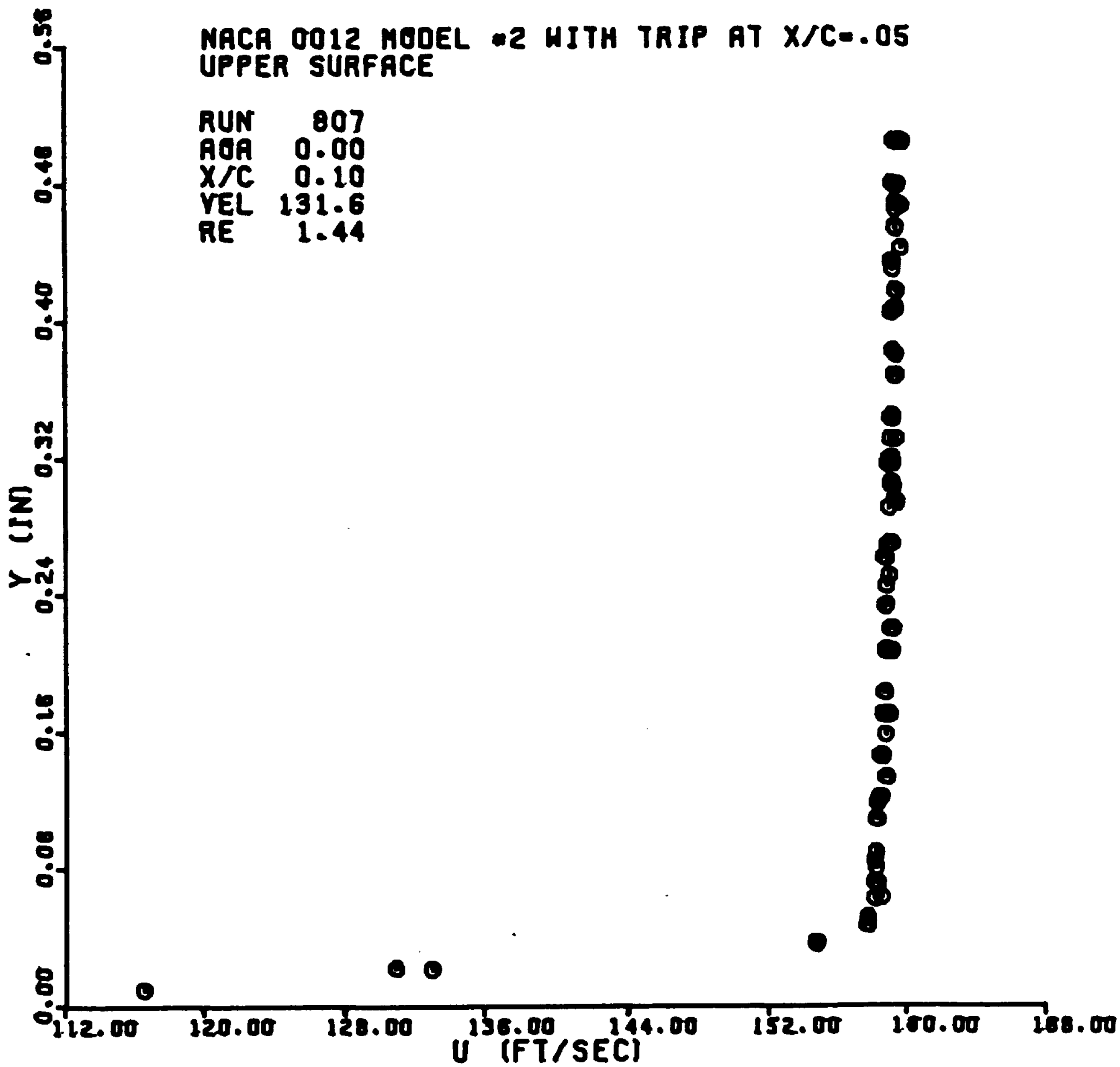
NACA 0012 MODEL #2 WITH TRIP AT X/C=.05
UPPER SURFACE
RUN 807
AOA 0.00
X/C 0.10
VEL 131.6
RE 1.44
Y (IN)
0.00
0.08
0.16
0.24
0.32
0.40
0.48
0.56
U (FT/SEC)
112.00
120.00
128.00
136.00
144.00
152.00
160.00
168.00

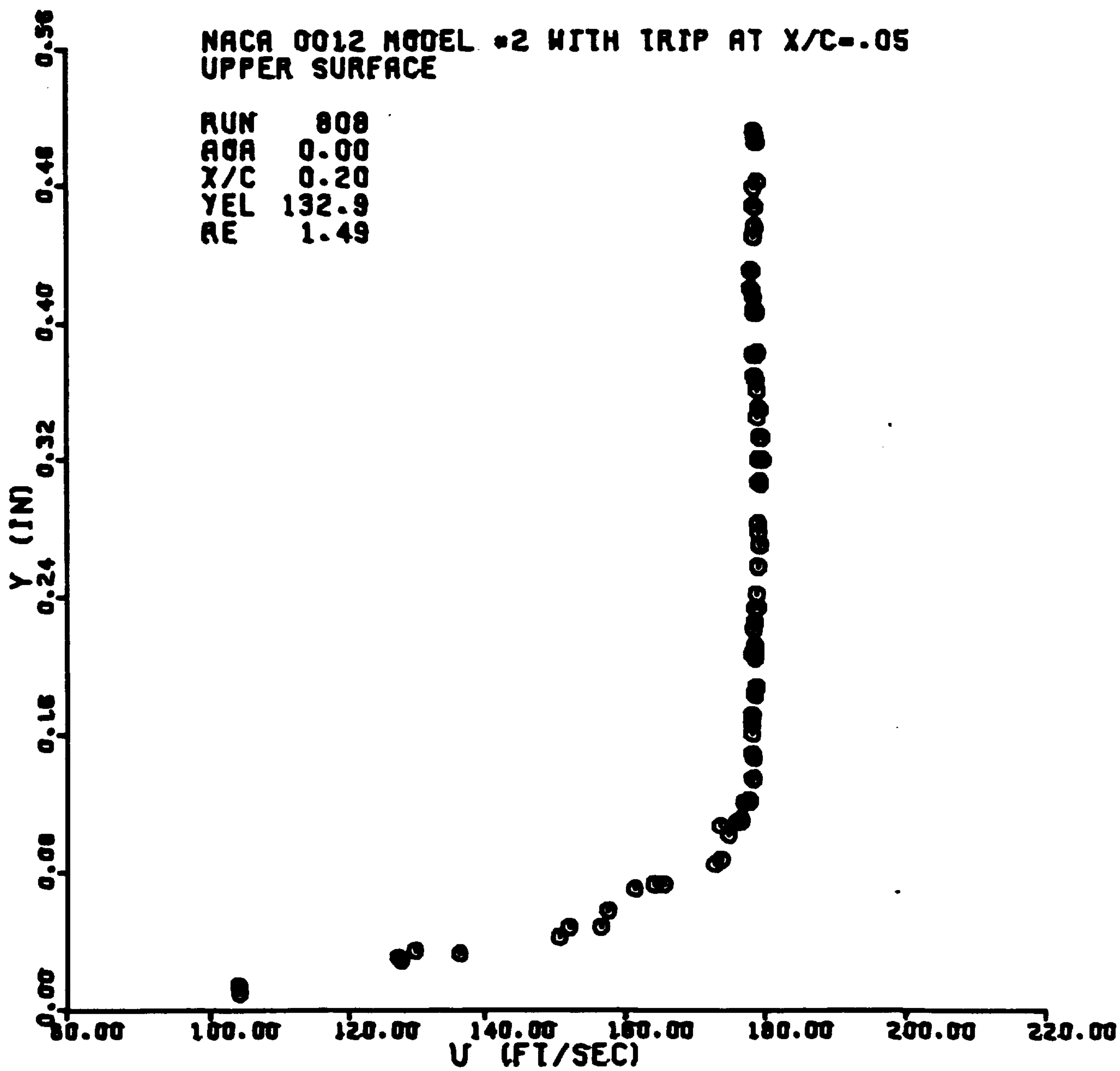

NACA 0012 MODEL #2 WITH TRIP AT X/C=.05
UPPER SURFACE
RUN 808
AOA 0.00
X/C 0.20
YEL 132.9
RE 1.49
Y (IN)
0.00
0.08
0.16
0.24
0.32
0.40
0.48
0.56
80.00
100.00
120.00
140.00
160.00
180.00
200.00
220.00
U (FT/SEC)

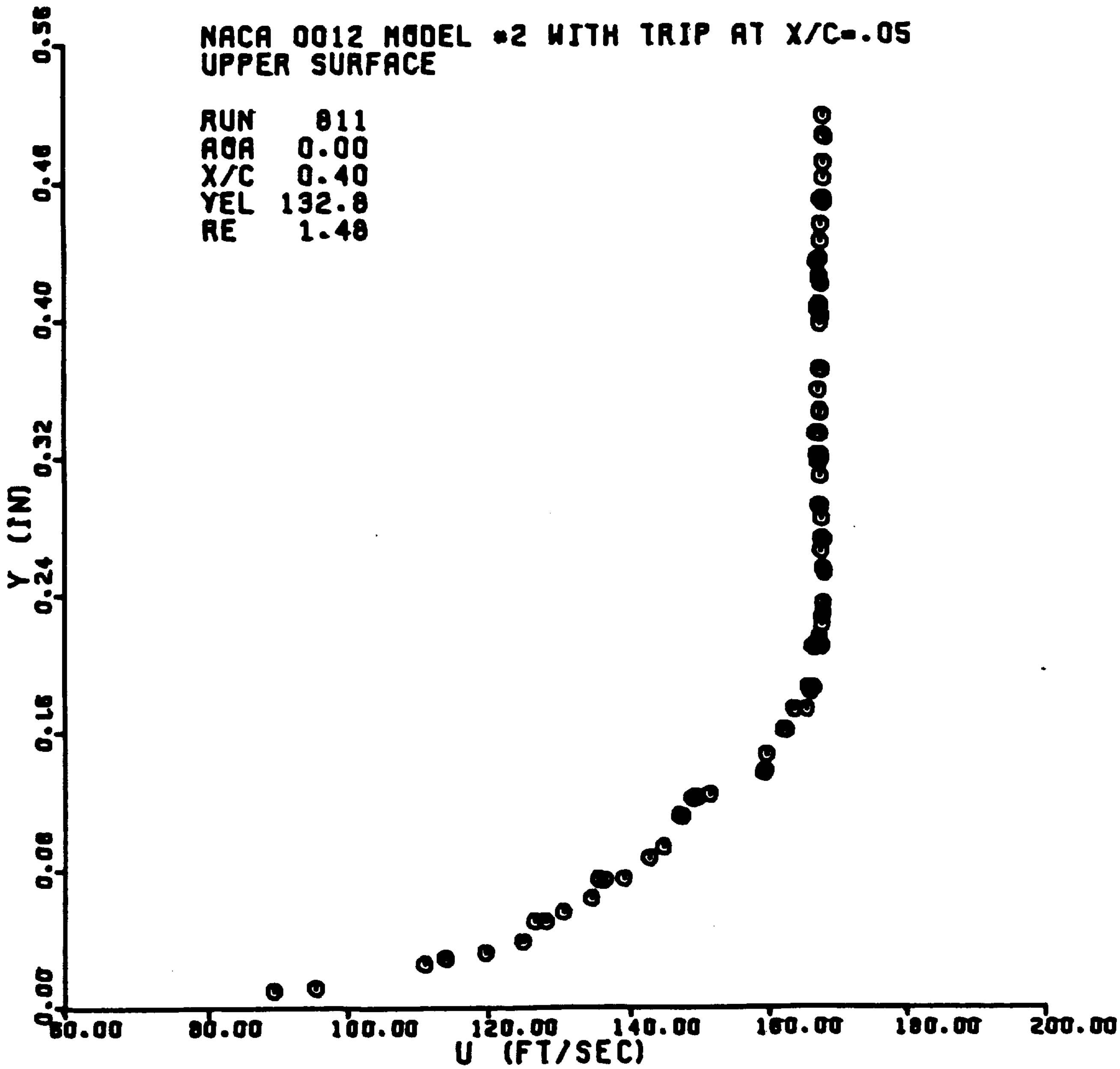
NACA 0012 MODEL #2 WITH TRIP AT X/C=.05
UPPER SURFACE
RUN 811
AOA 0.00
X/C 0.40
VEL 132.8
RE 1.48
Y (IN)
0.00
0.08
0.16
0.24
0.32
0.40
0.48
0.56
60.00
80.00
100.00
120.00
140.00
160.00
180.00
200.00
U (FT/SEC)

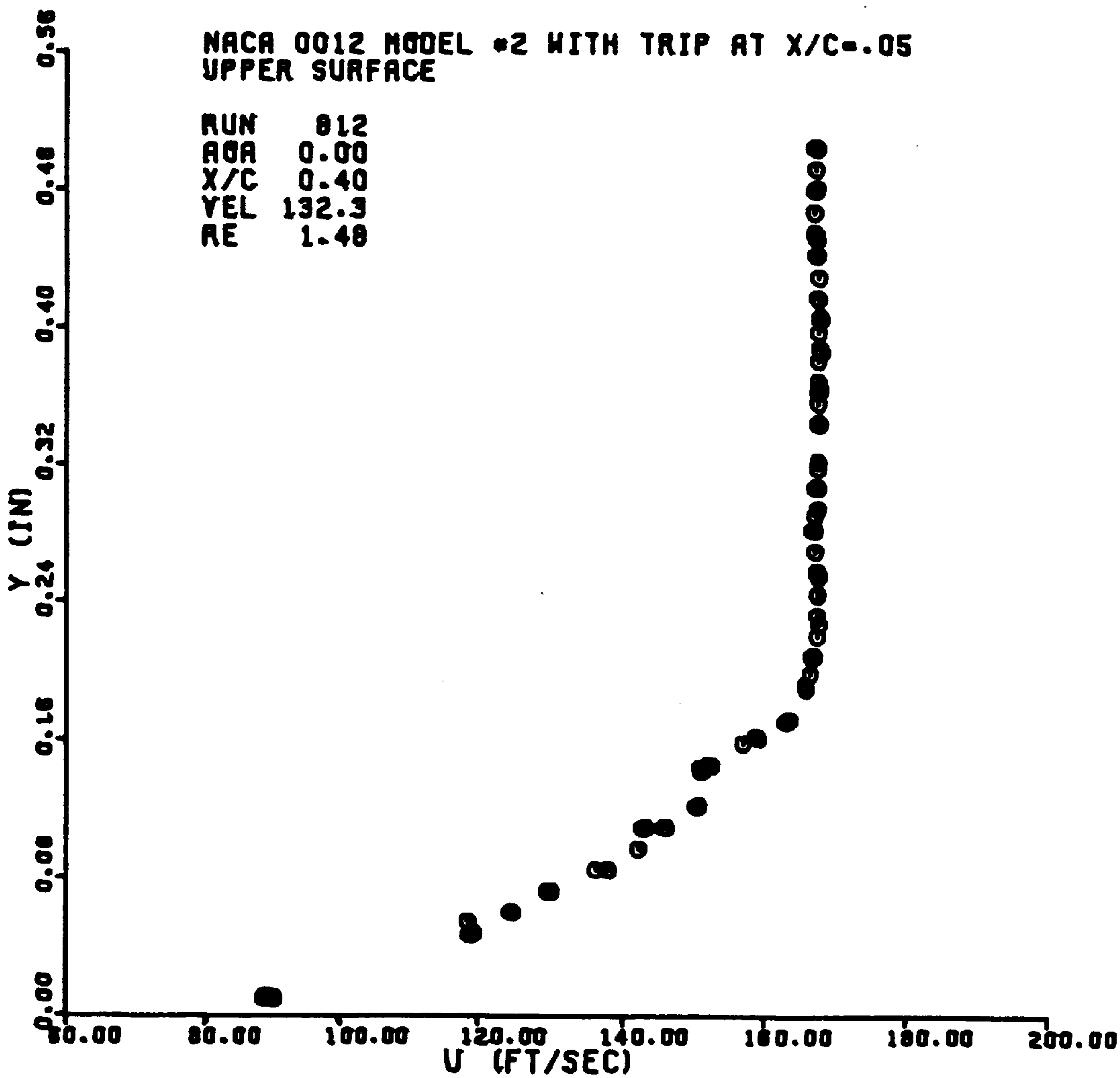
NACA 0012 MODEL #2 WITH TRIP AT X/C=.05
UPPER SURFACE
RUN 812
AOA 0.00
X/C 0.40
VEL 132.3
RE 1.48
Y (IN)
0.00
0.08
0.16
0.24
0.32
0.40
0.48
0.56
60.00
80.00
100.00
120.00
140.00
160.00
180.00
200.00
U (FT/SEC)

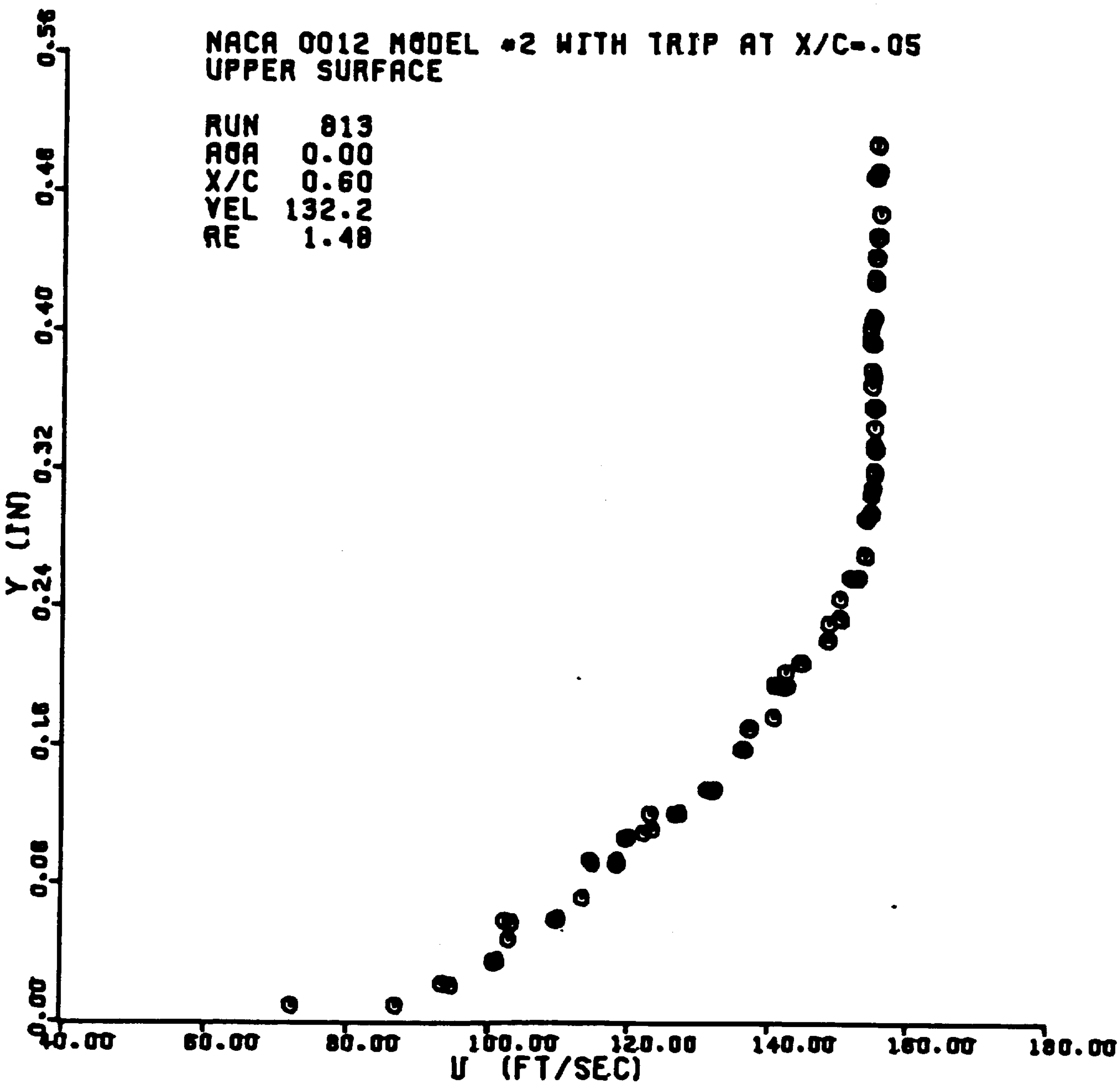

NACA 0012 MODEL #2 WITH TRIP AT X/C=.05
UPPER SURFACE
RUN 813
AOA 0.00
X/C 0.60
VEL 132.2
RE 1.48
Y (IN)
0.00
0.08
0.16
0.24
0.32
0.40
0.48
0.56
40.00
60.00
80.00
100.00
120.00
140.00
160.00
180.00
U (FT/SEC)